Molecular Mechanism and Application of Somatic Cell Cloning in Mammals

Edited by

Marcin Samiec and Maria Skrzyszowska

www.mdpi.com/journal/ijms

MDPI

Molecular Mechanism and Application of Somatic Cell Cloning in Mammals

Molecular Mechanism and Application of Somatic Cell Cloning in Mammals

Editors

Marcin Samiec
Maria Skrzyszowska

MDPI

Editors

Marcin Samiec
Department of Reproductive
Biotechnology and
Cryoconservation
National Research Institute of
Animal Production
Balice near Kraków
Poland

Maria Skrzyszowska
Department of Reproductive
Biotechnology and
Cryoconservation
National Research Institute of
Animal Production
Balice near Kraków
Poland

This is a reprint of articles from the Special Issue published online in the open access journal *International Journal of Molecular Sciences* (ISSN 1422-0067) (available at: www.mdpi.com/journal/ ijms/special_issues/Somatic_Cell_Cloning).

For citation purposes, cite each article independently as indicated on the article page online and as indicated below:

LastName, A.A.; LastName, B.B.; LastName, C.C. Article Title. *Journal Name* **Year**, *Volume Number*, Page Range.

Contents

About the Editors

Marcin Samiec

Prof. Dr. Marcin Samiec is a biotechnologist and embryologist with long-term and broad experience. He is employed as a Senior Scientist (Professor) at the Department of Reproductive Biotechnology and Cryoconservation of the National Research Institute of Animal Production in Balice near Kraków, Poland. His areas of expertise and interest include: (1) reproductive biology and biotechnology in different mammalian species (especially pigs, goats, cattle, rabbits and horses); (2) assisted reproductive technologies (ARTs) (experimental and applied embryology); (3) intra- and interspecies somatic cell cloning by somatic cell nuclear transfer (SCNT); (4) transgenic research; (5) parthenogenetic activation of oocytes (methods and molecular mechanisms of oocyte activation); (6) in vitro embryo production (IVP): in vitro oocyte maturation (IVM), in vitro fertilization (IVF), intracytoplasmic sperm injection (ICSI), and in vitro embryo culture (IVC); (7) stem cell research; (8) epigenetic and molecular aspects of embryonic development: epigenetics in developmental biology, epigenetic modulation of nuclear donor cells (somatic cells, stem cells), SCNT-derived oocytes or cloned embryos; (9) unravelling the transcriptomic and proteomic profiles in nuclear donor cell lines (somatic and stem cell lines) and nuclear recipient oocytes; (10) the ART-mediated programs of ex situ biodiversity conservation to protect and maintain the genetic resources of wild-living and domesticated mammalian species. He is the author and ad hoc reviewer of many research articles published in high-impact journals indexed in the JCR, WoS and Scopus databases. He is also the author of several patents granted for biotechnological/embryological inventions (indexed in the WoS database).

Maria Skrzyszowska

Prof. Dr. Maria Skrzyszowska is an embryologist with many years of experience. She is employed as a Senior Scientist (Professor) at Department of Reproductive Biotechnology and Cryoconservation of National Research Institute of Animal Production in Balice near Kraków, Poland. She is a specialist in the fields of: (1) animal reproduction biotechnology; (2) somatic cell cloning in different mammalian species; (3) embryonic cell cloning in different mammalian species, including embryo bisection methods; (4) in vitro embryo production; (5) in vitro oocyte maturation and ICSI-mediated in vitro fertilization; (6) transgenesis; (7) modern strategies to assess the molecular quality of somatic cell lines and female gametes for the purposes of advanced ARTs. She is the author or co-author of many research articles published in high-impact journals indexed in JCR, WoS and Scopus databases and several patents for embryological inventions (indexed in WoS database).

Preface to "Molecular Mechanism and Application of Somatic Cell Cloning in Mammals"

The paramount goal of the current book (in the form of a scientific monograph) is to comprehensively provide the state of the art and research highlights of the molecular factors and their biological networks determining the effectiveness of SCNT-mediated cloning from the perspective of mechanistic insights into genomic, epigenomic, transcriptomic and proteomic landscapes specific for nuclear donor cells, nuclear recipient oocytes and nuclear-transferred embryos. Widely unravelling the multi-faceted mechanisms underlying inter-genomic, inter-epigenomic, inter-transcriptomic and inter-proteomic crosstalk between the above-indicated factors might be a pivotal stimulus triggering the augmentation of in vitro and in vivo molecular capabilities of donor cell nuclei to be epigenetically reprogrammed in SCNT-derived oocytes, embryos, fetuses and offspring. In turn, this would enable scientists to increase the applicability of SCNT-based assisted reproductive technologies (ARTs) to a broad spectrum of research areas and interdisciplinary fields such as: (1) experimental and applied embryology; (2) biotechnology; (3) transgenics; (4) biomedicine; (5) biopharmacy; and (6) practical activities designed to develop and optimize the ex vivo and in vivo models focused on recognizing the etiopathogenesis, phenotypic and genotypic backgrounds of human and other mammalian hereditary or acquired diseases.

<div align="right">

Marcin Samiec and Maria Skrzyszowska
Editors

</div>

Editorial

Molecular Mechanism and Application of Somatic Cell Cloning in Mammals—Past, Present and Future

Marcin Samiec

Department of Reproductive Biotechnology and Cryoconservation, National Research Institute of Animal Production, Krakowska 1 Street, 32-083 Balice, Poland; marcin.samiec@iz.edu.pl

Thus far, nearly 25 mammalian species have been cloned by intra- or interspecies somatic cell nuclear transfer (SCNT). Among them, non-transgenic and transgenic representatives of such domesticated and wild-living animals that have been propagated and/or multiplied by intraspecific or interspecific SCNT-based cloning are:

- Pigs (*Sus scrofa domesticus*) [1,2];
- Sheep (*Ovis aries*) [3,4];
- Goats (*Capra aegagrus hircus*) [5,6];
- Cattle (*Bos taurus taurus*) [7–9];
- Horses (*Equus ferus caballus*) [10];
- Mules (equine hybrids: *Equus asinus* × *Equus ferus caballus*) [11];
- Dromedary camels (*Camelus dromedarius*) [12];
- Bactrian camels (*Camelus bactrianus ferus*) [13];
- Water buffalos (*Bubalus bubalis*) [14];
- Rabbits (*Oryctolagus cuniculus*) [15];
- Domestic cats (*Felis silvestris catus*) [16];
- Domestic dogs (*Canis lupus familiaris*) [17];
- Mice (*Mus musculus musculus*) [18];
- Rats (*Rattus norvegicus domestica*) [19];
- Ferrets (*Mustela putorius furo*) [20];
- Mouflon (*Ovis aries/ammon musimon*) [21];
- Gaur (*Bos gaurus*) [22];
- Red deer (*Cervus elaphus*) [23];
- Pyrenean ibex (bucardo; *Capra pyrenaica pyrenaica*) [24];
- African wild cat (*Felis silvestris lybica*) [25];
- Sand cat (*Felis margarita margarita*) [26];
- Gray wolf (*Canis lupus lupus*) [27];
- Coyote (*Canis latrans*) [28];
- Cynomolgus monkey/macaque (*Macaca fascicularis*) [29].

Despite the above-indicated abundant variety of SCNT-derived mammalian species, the effectiveness of SCNT-based cloning remains immensely or considerably low and oscillates between 0.1% and 5%, while estimating the outcomes of offspring born in relation to the total numbers of nuclear-transferred oocytes [30,31]. For this reason, at the present stage of investigations, extensive efforts are being undertaken to achieve considerable scientific breakthroughs, which would enable researchers to not only tremendously increase the ex vivo and in vivo developmental competences, but also to remarkably ameliorate the parameters related to the cytological, molecular and epigenetic qualities of SCNT-generated mammalian embryos. Only such a crucial turning point or a substantial research game changer would open up new possibilities for both improving the overall efficiency of SCNT-based cloning and, as a consequence, play an increasingly important role as an assisted reproductive technology (ART) which is characterized by a broad spectrum of applicability in embryology, biotechnology, transgenics and biomedicine [32,33].

It is beyond any doubt that the relatively or extremely low efficiency of mammalian SCNT-mediated cloning, including both its intra- and interspecies model, can only be improved by comprehensively recognizing molecular and epigenetic determinants and mechanisms affecting the developmental competences of SCNT-derived embryos [34]. A wide range of biological and molecular factors predestine and predominantly bias the biotechnological suitability of nuclear donor cells and nuclear recipient oocytes for SCNT-mediated ARTs. The extent of this suitability is measured and directly depends on the developmental capacity and quality parameters pinpointed for nuclear-transferred oocytes and corresponding somatic-cell-cloned embryos in different mammalian species [35]. The main impact on the development of cloned embryos is exerted by the type and provenance of nuclear donor cells [36–38]. In this context, an important role is played by the strategies used to artificially synchronize the mitotic cycle of nuclear donor cells expanded ex vivo at the G0/G1 stages [39,40]. Notably, the developmental outcomes of somatic-cell-cloned embryos are largely determined by the molecular quality parameters reflected in the incidence of apoptotic cell death and oxidative stress processes in the nuclear donor cells and SCNT-derived embryos cultured in vitro [40–43]. Additionally, it is worth highlighting that the developmental capability of cloned embryos is remarkably biased by the molecular quality of metaphase-II stage nuclear recipient oocytes, which largely depends on coordination between the processes of meiotic, cytoplasmic and epigenomic maturation [44–46]. Not without significance is the tremendous influence of the approaches applied to artificially activate the embryo-specific developmental program of SCNT-derived oocytes on the efficacy of propagating cloned embryos and their molecular quality [47–49]. Furthermore, the effectiveness of generating somatic-cell-cloned embryos results from the capabilities of donor cell nuclei to epigenetically reprogram their transcriptomic signatures in the cytoplasm of SCNT-derived oocytes and the blastomeres of corresponding cloned embryos [50,51]. In turn, the epigenomic reprogrammability of transcriptional activity within donor cell nuclei has been proven to be strongly affected by the molecular network of interrelations between nuclear and mitochondrial genomes that has been established during the early embryonic development of activated SCNT-derived oocytes [52–54]. Finally, as a consequence of applying a wide variety of methods focused on modulating/transforming the transcriptional activities of donor cell nuclear genomes by extrinsic epigenetic modifiers such as non-selective inhibitors of histone deacetylases (HDACi) and/or non-selective inhibitors of DNA methyltransferases (DNMTi), the enhanced capabilities of donor cell nuclei to correctly and faithfully reprogram their transcriptomic profiles in SCNT-derived embryos have been shown [31,55,56].

In summary, this Special Issue will publish research articles and comprehensive review papers aimed at highlighting the state of the art and mechanistic insights into precisely identifying and unravelling a wide array of genomic, epigenomic, transcriptomic and proteomic factors which cumulatively determine the molecular parameters which are of paramount importance for the quality of nuclear donor cells, nuclear recipient oocytes and SCNT-derived embryos. Thoroughly deciphering the multifaceted nature of all the aforementioned factors and insightful interpretation of the biological crosstalk between them can finally bias the augmentation of the overall efficiency of SCNT-based cloning. This is a preponderant condition indispensable for the practical implementation of SCNT-mediated ARTs to various research fields and interdisciplinary studies at the interface of experimental and applied embryology, biotechnology, transgenics, biomedicine, biopharmacology, the creation of animal models for etiopathogenesis and physiopathology of human diseases and the genetic rescue and/or resurrection of endangered/extinct mammalian species.

Conflicts of Interest: The author declares no conflict of interest. The author had no financial or other relationship with other people or organizations that might inappropriately influence this work. The funders had no role in the writing of the manuscript or in the decision to publish the results.

References

1. Onishi, A.; Iwamoto, M.; Akita, T.; Mikawa, S.; Takeda, K.; Awata, T.; Hanada, H.; Perry, A.C.F. Pig cloning by microinjection of fetal fibroblast nuclei. *Science* **2000**, *289*, 1188–1190. [CrossRef] [PubMed]
2. Zhao, H.; Li, Y.; Wiriyahdamrong, T.; Yuan, Z.; Qing, Y.; Li, H.; Xu, K.; Guo, J.; Jia, B.; Zhang, X.; et al. Improved production of GTKO/hCD55/hCD59 triple-gene-modified Diannan miniature pigs for xenotransplantation by recloning. *Transgenic Res.* **2020**, *29*, 369–379. [CrossRef]
3. Wilmut, I.; Schnieke, A.E.; McWhir, J.; Kind, A.J.; Campbell, K.H. Viable offspring derived from fetal and adult mammalian cells. *Nature* **1997**, *385*, 810–813. [CrossRef] [PubMed]
4. Deng, S.; Li, G.; Zhang, J.; Zhang, X.; Cui, M.; Guo, Y.; Liu, G.; Li, G.; Feng, J.; Lian, Z. Transgenic cloned sheep overexpressing ovine toll-like receptor 4. *Theriogenology* **2013**, *80*, 50–57. [CrossRef] [PubMed]
5. Keefer, C.L.; Keyston, R.; Lazaris, A.; Bhatia, B.; Begin, I.; Bilodeau, A.S.; Zhou, F.J.; Kafidi, N.; Wang, B.; Baldassarre, H.; et al. Production of cloned goats after nuclear transfer using adult somatic cells. *Biol. Reprod.* **2002**, *66*, 199–203. [CrossRef]
6. Feng, X.; Cao, S.; Wang, H.; Meng, C.; Li, J.; Jiang, J.; Qian, Y.; Su, L.; He, Q.; Zhang, Q. Production of transgenic dairy goat expressing human α-lactalbumin by somatic cell nuclear transfer. *Transgenic Res.* **2015**, *24*, 73–85. [CrossRef] [PubMed]
7. Guo, Y.; Li, H.; Wang, Y.; Yan, X.; Sheng, X.; Chang, D.; Qi, X.; Wang, X.; Liu, Y.; Li, J.; et al. Screening somatic cell nuclear transfer parameters for generation of transgenic cloned cattle with intragenomic integration of additional gene copies that encode bovine adipocyte-type fatty acid-binding protein (A-FABP). *Mol. Biol. Rep.* **2017**, *44*, 159–168. [CrossRef]
8. Hoshino, Y.; Hayashi, N.; Taniguchi, S.; Kobayashi, N.; Sakai, K.; Otani, T.; Iritani, A.; Saeki, K. Resurrection of a bull by cloning from organs frozen without cryoprotectant in a −80 °C freezer for a decade. *PLoS ONE* **2009**, *4*, e4142. [CrossRef]
9. Wang, M.; Sun, Z.; Yu, T.; Ding, F.; Li, L.; Wang, X.; Fu, M.; Wang, H.; Huang, J.; Li, N.; et al. Large-scale production of recombinant human lactoferrin from high-expression, marker-free transgenic cloned cows. *Sci. Rep.* **2017**, *7*, 10733. [CrossRef]
10. Hinrichs, K.; Choi, Y.H.; Varner, D.D.; Hartman, D.L. Production of cloned horse foals using roscovitine-treated donor cells and activation with sperm extract and/or ionomycin. *Reproduction* **2007**, *134*, 319–325. [CrossRef]
11. Woods, G.L.; White, K.L.; Vanderwall, D.K.; Li, G.P.; Aston, K.I.; Bunch, T.D.; Meerdo, L.N.; Pate, B.J. A mule cloned from fetal cells by nuclear transfer. *Science* **2003**, *301*, 1063. [CrossRef] [PubMed]
12. Moulavi, F.; Asadi-Moghadam, B.; Omidi, M.; Yarmohammadi, M.; Ozegovic, M.; Rastegar, A.; Hosseini, S.M. Pregnancy and calving rates of cloned dromedary camels produced by conventional and handmade cloning techniques and in vitro and in vivo matured oocytes. *Mol. Biotechnol.* **2020**, *62*, 433–442. [CrossRef] [PubMed]
13. Wani, N.A.; Vettical, B.S.; Hong, S.B. First cloned Bactrian camel (*Camelus bactrianus*) calf produced by interspecies somatic cell nuclear transfer: A step towards preserving the critically endangered wild Bactrian camels. *PLoS ONE* **2017**, *12*, e0177800. [CrossRef] [PubMed]
14. Madheshiya, P.K.; Sahare, A.A.; Jyotsana, B.; Singh, K.P.; Saini, M.; Raja, A.K.; Kaith, S.; Singla, S.K.; Chauhan, M.S.; Manik, R.S.; et al. Production of a cloned buffalo (*Bubalus bubalis*) calf from somatic cells isolated from urine. *Cell. Reprogram.* **2015**, *17*, 160–169. [CrossRef] [PubMed]
15. Li, S.; Guo, Y.; Shi, J.; Yin, C.; Xing, F.; Xu, L.; Zhang, C.; Liu, T.; Li, Y.; Li, H.; et al. Transgene expression of enhanced green fluorescent protein in cloned rabbits generated from in vitro-transfected adult fibroblasts. *Transgenic Res.* **2009**, *18*, 227–235. [CrossRef]
16. Song, S.H.; Lee, K.L.; Xu, L.; Joo, M.D.; Hwang, J.Y.; Oh, S.H.; Kong, I.K. Production of cloned cats using additional complimentary cytoplasm. *Anim. Reprod. Sci.* **2019**, *208*, 106125. [CrossRef]
17. Eun, K.; Hong, N.; Jeong, Y.W.; Park, M.G.; Hwang, S.U.; Jeong, Y.I.K.; Choi, E.J.; Olsson, P.O.; Hwang, W.S.; Hyun, S.H.; et al. Transcriptional activities of human elongation factor-1α and cytomegalovirus promoter in transgenic dogs generated by somatic cell nuclear transfer. *PLoS ONE* **2020**, *15*, e0233784. [CrossRef]
18. Azuma, R.; Miyamoto, K.; Oikawa, M.; Yamada, M.; Anzai, M. Combinational Treatment of Trichostatin A and Vitamin C Improves the Efficiency of Cloning Mice by Somatic Cell Nuclear Transfer. *J. Vis. Exp.* **2018**, *134*, 57036. [CrossRef]
19. Zhou, Q.; Renard, J.P.; Le Friec, G.; Brochard, V.; Beaujean, N.; Cherifi, Y.; Fraichard, A.; Cozzi, J. Generation of fertile cloned rats by regulating oocyte activation. *Science* **2003**, *302*, 1179. [CrossRef]
20. Li, Z.; Sun, X.; Chen, J.; Liu, X.; Wisely, S.M.; Zhou, Q.; Renard, J.P.; Leno, G.H.; Engelhardt, J.F. Cloned ferrets produced by somatic cell nuclear transfer. *Dev. Biol.* **2006**, *293*, 439–448. [CrossRef]
21. Loi, P.; Ptak, G.; Barboni, B.; Fulka, J., Jr.; Cappai, P.; Clinton, M. Genetic rescue of an endangered mammal by cross-species nuclear transfer using post-mortem somatic cells. *Nat. Biotechnol.* **2001**, *19*, 962–964. [CrossRef] [PubMed]
22. Srirattana, K.; Imsoonthornruksa, S.; Laowtammathron, C.; Sangmalee, A.; Tunwattana, W.; Thongprapai, T.; Chaimongkol, C.; Ketudat-Cairns, M.; Parnpai, R. Full-term development of gaur-bovine interspecies somatic cell nuclear transfer embryos: Effect of trichostatin A treatment. *Cell. Reprogram.* **2012**, *14*, 248–257. [CrossRef] [PubMed]
23. Berg, D.K.; Li, C.; Asher, G.; Wells, D.N.; Oback, B. Red deer cloned from antler stem cells and their differentiated progeny. *Biol. Reprod.* **2007**, *77*, 384–394. [CrossRef] [PubMed]

24. Folch, J.; Cocero, M.J.; Chesné, P.; Alabart, J.L.; Domínguez, V.; Cognié, Y.; Roche, A.; Fernández-Arias, A.; Martí, J.I.; Sánchez, P.; et al. First birth of an animal from an extinct subspecies (*Capra pyrenaica pyrenaica*) by cloning. *Theriogenology* **2009**, *71*, 1026–1034. [CrossRef] [PubMed]

25. Gómez, M.C.; Pope, C.E.; Giraldo, A.; Lyons, L.A.; Harris, R.F.; King, A.L.; Cole, A.; Godke, R.A.; Dresser, B.L. Birth of African Wildcat cloned kittens born from domestic cats. *Cloning Stem Cells* **2004**, *6*, 247–258. [CrossRef]

26. Gómez, M.C.; Pope, C.E.; Kutner, R.H.; Ricks, D.M.; Lyons, L.A.; Ruhe, M.; Dumas, C.; Lyons, J.; López, M.; Dresser, B.L.; et al. Nuclear transfer of sand cat cells into enucleated domestic cat oocytes is affected by cryopreservation of donor cells. *Cloning Stem Cells* **2008**, *10*, 469–483. [CrossRef]

27. Oh, H.J.; Kim, M.K.; Jang, G.; Kim, H.J.; Hong, S.G.; Park, J.E.; Park, K.; Park, C.; Sohn, S.H.; Kim, D.Y.; et al. Cloning endangered gray wolves (*Canis lupus*) from somatic cells collected postmortem. *Theriogenology* **2008**, *70*, 638–647. [CrossRef]

28. Hwang, I.; Jeong, Y.W.; Kim, J.J.; Lee, H.J.; Kang, M.; Park, K.B.; Park, J.H.; Kim, Y.W.; Kim, W.T.; Shin, T.; et al. Successful cloning of coyotes through interspecies somatic cell nuclear transfer using domestic dog oocytes. *Reprod. Fertil. Dev.* **2013**, *25*, 1142–1148. [CrossRef]

29. Liu, Z.; Cai, Y.; Wang, Y.; Nie, Y.; Zhang, C.; Xu, Y.; Zhang, X.; Lu, Y.; Wang, Z.; Poo, M.; et al. Cloning of Macaque Monkeys by Somatic Cell Nuclear Transfer. *Cell* **2018**, *172*, 881–887.e7. [CrossRef]

30. Glanzner, W.G.; de Macedo, M.P.; Gutierrez, K.; Bordignon, V. Enhancement of Chromatin and Epigenetic Reprogramming in Porcine SCNT Embryos-Progresses and Perspectives. *Front. Cell Dev. Biol.* **2022**, *10*, 940197. [CrossRef]

31. Srirattana, K.; Kaneda, M.; Parnpai, R. Strategies to Improve the Efficiency of Somatic Cell Nuclear Transfer. *Int. J. Mol. Sci.* **2022**, *23*, 1969. [CrossRef] [PubMed]

32. Song, S.; Lu, R.; Cheng, Y.; Zhang, T.; Gu, L.; Yu, K.; Zhou, M.; Li, D. Developmental analysis of reconstructed embryos of second-generation cloned transgenic goats. *Reprod. Domest. Anim.* **2022**, *57*, 473–480. [CrossRef] [PubMed]

33. Xu, K.; Zhang, X.; Liu, Z.; Ruan, J.; Xu, C.; Che, J.; Fan, Z.; Mu, Y.; Li, K. A transgene-free method for rapid and efficient generation of precisely edited pigs without monoclonal selection. *Sci. China Life. Sci.* **2022**, *65*, 1535–1546. [CrossRef]

34. Wang, X.; Qu, J.; Li, J.; He, H.; Liu, Z.; Huan, Y. Epigenetic Reprogramming During Somatic Cell Nuclear Transfer: Recent Progress and Future Directions. *Front. Genet.* **2020**, *11*, 205. [CrossRef]

35. Akagi, S.; Matsukawa, K.; Takahashi, S. Factors affecting the development of somatic cell nuclear transfer embryos in Cattle. *J. Reprod. Dev.* **2014**, *60*, 329–335. [CrossRef]

36. Zhai, Y.; Li, W.; Zhang, Z.; Cao, Y.; Wang, Z.; Zhang, S.; Li, Z. Epigenetic states of donor cells significantly affect the development of somatic cell nuclear transfer (SCNT) embryos in pigs. *Mol. Reprod. Dev.* **2018**, *85*, 26–37. [CrossRef] [PubMed]

37. Zhang, Y.T.; Yao, W.; Chai, M.J.; Liu, W.J.; Liu, Y.; Liu, Z.H.; Weng, X.G. Evaluation of porcine urine-derived cells as nuclei donor for somatic cell nuclear transfer. *J. Vet. Sci.* **2022**, *23*, e40. [CrossRef] [PubMed]

38. Son, Y.B.; Jeong, Y.I.; Jeong, Y.W.; Hossein, M.S.; Hwang, W.S. Impact of co-transfer of embryos produced by somatic cell nuclear transfer using two types of donor cells on pregnancy outcomes in dogs. *Anim. Biosci.* **2022**, *35*, 1360–1366. [CrossRef]

39. Nguyen, V.K.; Somfai, T.; Salamone, D.; Thu Huong, V.T.; Le Thi Nguyen, H.; Huu, Q.X.; Hoang, A.T.; Phan, H.T.; Thi Pham, Y.K.; Pham, L.D. Optimization of donor cell cycle synchrony, maturation media and embryo culture system for somatic cell nuclear transfer in the critically endangered Vietnamese İ pig. *Theriogenology* **2021**, *166*, 21–28. [CrossRef]

40. Yao, Y.; Yang, A.; Li, G.; Wu, H.; Deng, S.; Yang, H.; Ma, W.; Lv, D.; Fu, Y.; Ji, P.; et al. Melatonin promotes the development of sheep transgenic cloned embryos by protecting donor and recipient cells. *Cell Cycle* **2022**, *21*, 1360–1375. [CrossRef]

41. Kim, M.J.; Jung, B.D.; Park, C.K.; Cheong, H.T. Development of Porcine Somatic Cell Nuclear Transfer Embryos Following Treatment Time of Endoplasmic Reticulum Stress Inhibitor. *Dev. Reprod.* **2021**, *25*, 43–53. [CrossRef] [PubMed]

42. Samiec, M.; Skrzyszowska, M. Assessment of in vitro developmental capacity of porcine nuclear-transferred embryos reconstituted with cumulus oophorus cells undergoing vital diagnostics for apoptosis detection. *Ann. Anim. Sci.* **2013**, *13*, 513–529. [CrossRef]

43. Gao, W.; Yu, T.; Li, G.; Shu, W.; Jin, Y.; Zhang, M.; Yu, X. Antioxidant Activity and Anti-Apoptotic Effect of the Small Molecule Procyanidin B1 in Early Mouse Embryonic Development Produced by Somatic Cell Nuclear Transfer. *Molecules* **2021**, *26*, 6150. [CrossRef]

44. Li, R.; Wu, H.; Zhuo, W.W.; Mao, Q.F.; Lan, H.; Zhang, Y.; Hua, S. Astaxanthin Normalizes Epigenetic Modifications of Bovine Somatic Cell Cloned Embryos and Decreases the Generation of Lipid Peroxidation. *Reprod. Domest. Anim.* **2015**, *50*, 793–799. [CrossRef]

45. An, Q.; Peng, W.; Cheng, Y.; Lu, Z.; Zhou, C.; Zhang, Y.; Su, J. Melatonin supplementation during in vitro maturation of oocyte enhances subsequent development of bovine cloned embryos. *J. Cell. Physiol.* **2019**, *234*, 17370–17381. [CrossRef]

46. Meng, L.; Hu, H.; Liu, Z.; Zhang, L.; Zhuan, Q.; Li, X.; Fu, X.; Zhu, S.; Hou, Y. The Role of Ca^{2+} in Maturation and Reprogramming of Bovine Oocytes: A System Study of Low-Calcium Model. *Front. Cell Dev. Biol.* **2021**, *9*, 746237. [CrossRef] [PubMed]

47. Oh, H.J.; Lee, B.C.; Kim, M.K. Optimal Treatment of 6-Dimethylaminopurine Enhances the In Vivo Development of Canine Embryos by Rapid Initiation of DNA Synthesis. *Int. J. Mol. Sci.* **2021**, *22*, 7757. [CrossRef] [PubMed]

48. Samiec, M.; Skrzyszowska, M. Biological transcomplementary activation as a novel and effective strategy applied to the generation of porcine somatic cell cloned embryos. *Reprod. Biol.* **2014**, *14*, 128–139. [CrossRef]

49. Zhang, S.; Xiang, S.; Yang, J.; Shi, J.; Guan, X.; Jiang, J.; Wei, Y.; Luo, C.; Shi, D.; Lu, F. Optimization of parthenogenetic activation of rabbit oocytes and development of rabbit embryo by somatic cell nuclear transfer. *Reprod. Domest. Anim.* **2019**, *54*, 258–269. [CrossRef]
50. Brochard, V.; Beaujean, N. Somatic Reprograming by Nuclear Transfer. *Methods Mol. Biol.* **2021**, *2214*, 109123. [CrossRef]
51. Zhao, L.; Long, C.; Zhao, G.; Su, J.; Ren, J.; Sun, W.; Wang, Z.; Zhang, J.; Liu, M.; Hao, C.; et al. Reprogramming barriers in bovine cells nuclear transfer revealed by single-cell RNA-seq analysis. *J. Cell. Mol. Med.* **2022**, *26*, 4792–4804. [CrossRef] [PubMed]
52. Bebbere, D.; Ulbrich, S.E.; Giller, K.; Zakhartchenko, V.; Reichenbach, H.D.; Reichenbach, M.; Verma, P.J.; Wolf, E.; Ledda, S.; Hiendleder, S. Mitochondrial DNA Depletion in Granulosa Cell Derived Nuclear Transfer Tissues. *Front. Cell Dev. Biol.* **2021**, *9*, 664099. [CrossRef] [PubMed]
53. Yan, Z.H.; Zhou, Y.Y.; Fu, J.; Jiao, F.; Zhao, L.W.; Guan, P.F.; Huang, S.Z.; Zeng, Y.T.; Zeng, F. Donor-host mitochondrial compatibility improves efficiency of bovine somatic cell nuclear transfer. *BMC Dev. Biol.* **2010**, *10*, 31. [CrossRef] [PubMed]
54. Srirattana, K.; St John, J.C. Additional mitochondrial DNA influences the interactions between the nuclear and mitochondrial genomes in a bovine embryo model of nuclear transfer. *Sci. Rep.* **2018**, *8*, 7246. [CrossRef]
55. Samiec, M.; Skrzyszowska, M. Intrinsic and extrinsic molecular determinants or modulators for epigenetic remodeling and reprogramming of somatic cell-derived genome in mammalian nuclear-transferred oocytes and resultant embryos. *Pol. J. Vet. Sci.* **2018**, *21*, 217–227. [CrossRef] [PubMed]
56. Li, Y.; Sun, Q. Epigenetic manipulation to improve mouse SCNT embryonic development. *Front. Genet.* **2022**, *13*, 932867. [CrossRef]

Review

Extranuclear Inheritance of Mitochondrial Genome and Epigenetic Reprogrammability of Chromosomal Telomeres in Somatic Cell Cloning of Mammals

Marcin Samiec * and **Maria Skrzyszowska**

Department of Reproductive Biotechnology and Cryoconservation, National Research Institute of Animal Production, 32-083 Kraków, Poland; maria.skrzyszowska@iz.edu.pl
* Correspondence: marcin.samiec@iz.edu.pl

Abstract: The effectiveness of somatic cell nuclear transfer (SCNT) in mammals seems to be still characterized by the disappointingly low rates of cloned embryos, fetuses, and progeny generated. These rates are measured in relation to the numbers of nuclear-transferred oocytes and can vary depending on the technique applied to the reconstruction of enucleated oocytes. The SCNT efficiency is also largely affected by the capability of donor nuclei to be epigenetically reprogrammed in a cytoplasm of reconstructed oocytes. The epigenetic reprogrammability of donor nuclei in SCNT-derived embryos appears to be biased, to a great extent, by the extranuclear (cytoplasmic) inheritance of mitochondrial DNA (mtDNA) fractions originating from donor cells. A high frequency of mtDNA heteroplasmy occurrence can lead to disturbances in the intergenomic crosstalk between mitochondrial and nuclear compartments during the early embryogenesis of SCNT-derived embryos. These disturbances can give rise to incorrect and incomplete epigenetic reprogramming of donor nuclei in mammalian cloned embryos. The dwindling reprogrammability of donor nuclei in the blastomeres of SCNT-derived embryos can also be impacted by impaired epigenetic rearrangements within terminal ends of donor cell-descended chromosomes (i.e., telomeres). Therefore, dysfunctions in epigenetic reprogramming of donor nuclei can contribute to the enhanced attrition of telomeres. This accelerates the processes of epigenomic aging and replicative senescence in the cells forming various tissues and organs of cloned fetuses and progeny. For all the above-mentioned reasons, the current paper aims to overview the state of the art in not only molecular mechanisms underlying intergenomic communication between nuclear and mtDNA molecules in cloned embryos but also intrinsic determinants affecting unfaithful epigenetic reprogrammability of telomeres. The latter is related to their abrasion within somatic cell-inherited chromosomes.

Keywords: cloned mammalian embryo; SCNT-derived progeny; mtDNA; nuclear–mitochondrial interaction; epigenetic reprogrammability; telomere shortening/attrition

1. Biotechnological Possibilities of Applying the Techniques of Somatic Cell Nuclear Transfer (SCNT) to Produce Cloned Mammalian Species

The somatic cell cloning technique is a method of embryonic genome engineering. Unlike animal transgenesis, it involves micromanipulation not of individual nuclear DNA genes but of the whole nuclear and/or mitochondrial genome of both interphase nuclear donor somatic cells and female germ cells (in vitro- or in vivo-matured oocytes arrested at metaphase II), which are used as recipients of exogenous genetic material. Of all mammalian cloning techniques, somatic cell cloning can result in producing the largest numbers of genetically identical individuals that are designated as clones. In the somatic cell cloning of mammals, nuclear donor cells are available in practically unlimited quantities. Tissue samples obtained by biopsy from adult animals or fetuses are composed of hundreds of thousands cells, which can be further multiplied/expanded in vitro. Furthermore, when

cloning certain adult animals, tissue may be biopsied repeatedly to produce identical clones every time [1–7].

Animal cloning by somatic cell nuclear transfer (SCNT), which avoids the sexual reproduction pathway, offers the opportunity to obtain monogenetic offspring derived not only from adult animals of high genetic merit but also from genetically transformed (transgenic) specimens. Over the last 24 years, intra- and interspecies cloning via SCNT resulted in a fairly large number of transgenic and non-transgenic offspring, not only in various species or infertile interspecific hybrids (bastards) of domesticated animals, such as

(1) cattle [8–14];
(2) goats [6,15–20];
(3) sheep [21–26];
(4) pigs [27–41];
(5) equids—domestic horses [42–46] and mules [47];
(6) water buffaloes—Chinese swamp buffaloes [48,49] and Indian river/riverine buffaloes [50–53];
(7) one-humped or dromedary camels [7,54–56];
(8) two-humped or Bactrian camels [57];
(9) domestic cats [58–63];
(10) domestic dogs [64–71];
(11) polecat-ferrets [72];
(12) rabbits [73–78];
(13) mice [79–84];
(14) rats [85]; but also in several species of endangered or non-endangered wild mammals, such as
(15) gaur [86,87];
(16) mouflon [88];
(17) European red deer [89];
(18) African wild cat [90];
(19) Arabian sand cat [91];
(20) Eurasian gray wolf [92,93];
(21) coyote or prairie wolf [94];
(22) cynomolgus monkey, also known as Java macaque, crab-eating macaque, or long-tailed macaque—a catarrhine monkey from the family *Cercopithecidae* [95]; and even in the extinct subspecies of the Spanish/Iberian ibex:
(23) Pyrenean ibex, a wild goat known as bucardo [96].

Explanation of the mechanisms underlying intergenomic communication between nuclear and mitochondrial DNA molecules in cloned embryos and recognition/identification of the determinants affecting aberrant epigenetic reprogrammability of chromosomal telomeres will be suitable and reliable for resolving or reducing the imperfections in the generation of cloned embryos, conceptuses, and offspring by using SCNT technology. Moreover, the development of efficient strategies applied to the cryopreservation of nuclear donor somatic cells, nuclear-transferred oocytes reconstructed with somatic cells, and somatic cell-cloned embryos seems to be an inevitable progressive step contributing to the expedition of future large-scale attempts aimed to more successfully produce and multiply mammalian cloned offspring. The latter seems to be a sine qua non condition that allows one to more efficiently use SCNT-based assisted reproductive technology not only for transgenic, biotechnological, biomedical, and biopharmaceutical research but also for the ex situ conservation of biodiversity in both anthropogenic (agricultural) and non-anthropogenic (wild) ecosystems.

2. Dependence of Epigenetic Mechanisms Underlying Somatic Cell Nuclear Reprogramming and Intergenomic Communication between Nuclear and Mitochondrial DNA Fractions in Cloned Embryos on Various Approaches to Reconstruction of Enucleated Oocytes

In the reconstruction of enucleated oocytes (cytoplasts/ooplasts) by SCNT, the original genetic material is replaced with the somatic cell-inherited nuclear genome. Different approaches to SCNT are used to generate nuclear-transferred oocytes, i.e., oocytes reconstructed with somatic cell nuclei and the resultant cloned embryos (Table 1). The most common procedure is a relatively low-invasive method of SCNT based on the fusion of cytoplast–nuclear donor cell couplets that is induced by electric pulses [34,97–101] (Table 1). An alternative reconstruction method is a much more invasive microsurgical procedure, in which whole nuclear donor cells [102,103] or somatic-cell-derived karyoplasts [29,44,82,104,105] are microinjected directly into the cytoplasm of enucleated oocytes (Table 1). The karyoplast is a live membrane-bound structure formed as a result of mechanically induced lysis of the whole somatic cell. It contains the interphase cell nucleus or metaphase chromosomes that are surrounded only by a thin layer of the perinuclear cytoplasm (the so-called perikaryon) [27,105–108].

Whatever the method used, the reconstruction of ooplasts results in the combination and mingling (hybridization) of cytoplasmic environments of the ooplast and intact somatic cell or karyoplast isolated from the whole nuclear donor cell. As a result, a nuclear–cytoplasmic/nuclear–ooplasmic hybrid (i.e., cloned cybrid) is formed. This hybrid cell, formed by the hybridization of cytoplasmic microenvironments of the cells derived from two different developmental lines: gametogenic (germinal) and somatogenic (somatic), is referred to as a reconstructed or reconstituted oocyte or cybrid cloned zygote. As the mitotic cycle of nuclear donor somatic cells (artificially arrested at the G0 phase) is characterized by "latent" transcriptional activity, inhibited proliferative growth, and a slower metabolism of all organelles, the meiotic cycle of nuclear recipient oocytes also undergoes transient and reversible arresting at the metaphase II (MII) stage. At this stage of meiosis, the processes of advanced transcriptional suppression of genomic DNA take place as a result of attaining nuclear and ooplasmic maturity states. Proper coordination of the cytophysiological state of somatic cells or the karyoplasts isolated from them, and of the cytophysiological state of ooplasts during the reconstruction of cloned cybrids, results from the hybridization of the cytoplasmic environments of nuclear donor cells at the G0 phase of mitosis and of enucleated nuclear recipient oocytes at the MII stage of meiosis [27,98,101,109,110].

Techniques of enucleated oocyte reconstruction may largely affect molecular mechanisms of nuclear chromatin rearrangement, which include both its structural remodeling and epigenetic reprogramming of genomic DNA [99,102,104,107,111–113]. Hybridizing the cytoplasmic environment of two cells at different stages of the division cycle interferes with the cell cycle controlling mechanisms and carries the risk of abnormalities further into the development of the cybrid cloned zygote. However, not only does the proper selection of the cytophysiological states of somatic cells/karyoplasts and ooplasts during the reconstruction of cloned cybrids reduce genomic instability, rendering the genome less vulnerable to mutations, but it also reduces the degree of asynchrony in nuclear–cytoplasmic interactions and decreases the frequency of abnormal epigenome-dependent rearrangements of exogenous nuclear chromatin [114–120].

Table 1. Comparative characterization of the approaches to reconstruction of enucleated mammalian oocytes at the biotechnical, cytological, molecular, and epigenetic levels.

Method Used for Reconstruction of Enucleated Metaphase II-Stage Oocytes	Characterization at the Biotechnical and Cytological Levels	Characterization at the Molecular Level	Characterization at the Epigenetic Level
Electrofusion of ooplast–somatic cell couplets	Relatively low invasiveness of the method: - the generated electrostatic field interferes with ultrastructure and functions of the oolemma of nuclear recipient cells and the plasmalemma of nuclear donor cells through: ● transient formation in the plasma membrane phospholipid bilayer of micropores (microchannels) that facilitate fusion of ooplast–somatic cell complexes and are the pathway for passive intracellular transport of calcium ions under the conditions of simultaneous fusion and electrical activation (F / A) of reconstituted oocytes	Relatively high probability of the occurrence in the obtained clonal cybrids of: - cellular mtDNA heteroplasmy; - abnormal nuclear–cytoplasmic interactions; - abnormal intergenomic communication between allogeneic nuclear DNA, somatic cell-inherited mtDNA molecules, and mtDNA molecules of ooplasmic origin	Relatively high probability of the occurrence of abnormalities in: - structural and epigenetic remodeling of nuclear chromatin; - epigenetic reprogramming of transcriptional activity of the nuclear genome, including rearrangement of telomeres of somatic cell chromosomes in the reconstructed oocytes and in cloned embryos that develop as a result of their activation
Direct intraooplasmic microinjection of whole somatic cells	High invasiveness of the method: - interferes with the ultrastructure of the plasmalemma and the membrane and cytoskeleton of enucleated oocytes through: ● direct microsurgical transfer and deposition in their ooplasm of tiny (small-diameter) somatic cells displaying intact integrity of the plasma membrane	Relatively high probability of the occurrence in the obtained clonal cybrids of: - cellular mtDNA heteroplasmy; - abnormal nuclear–cytoplasmic interactions; - abnormal intergenomic communication between allogeneic nuclear DNA, somatic cell-inherited mtDNA molecules, and mtDNA molecules of ooplasmic origin	Relatively high probability of the occurrence of abnormalities in: - structural and epigenetic remodeling of nuclear chromatin; - epigenetic reprogramming of transcriptional activity of the nuclear genome, including rearrangement of telomeres of somatic cell chromosomes in the reconstructed oocytes and in cloned embryos that develop as a result of their activation
Direct intraooplasmic microinjection of karyoplasts	The highest invasiveness of the method: - interferes with the ultrastructure of the plasmalemma and the membrane and cytoskeleton of nuclear donor cells through: ● their mechanically induced cytolysis to isolate karyoplasts - interferes with the ultrastructure of the plasmalemma and the membrane and cytoskeleton of enucleated oocytes through: ● direct microsurgical transfer and deposition in their ooplasm of karyoplasts	Relatively low probability of the occurrence in the obtained clonal cybrids of: - cellular mtDNA heteroplasmy; - abnormal nuclear–cytoplasmic interactions; - abnormal intergenomic communication between allogeneic nuclear DNA, somatic cell-inherited mtDNA molecules, and mtDNA molecules of ooplasmic origin	Relatively low probability of the occurrence of abnormalities in: - structural and epigenetic remodeling of nuclear chromatin; - epigenetic reprogramming of transcriptional activity of the nuclear genome, including rearrangement of telomeres of somatic cell chromosomes in the reconstructed oocytes and in cloned embryos that develop as a result of their activation

In contrast to electrofusion, intraooplasmic microinjection of karyoplasts allows for the selective removal of a large part of the cytoplasm of nuclear donor cells, thus enabling relative thinning of the remnants of the somatic cell cytoplasm in a cytosolic microenvironment of the ooplast and early zygote. The direct consequence of this is that the adverse effect of cytoplasmic components of the somatic cell on remodeling and reprogramming of the transferred somatic cell nucleus, and thereby on the development of the reconstituted embryo, is avoided. Where nuclei of relatively small-diameter somatic cells are transplanted (e.g., cumulus oophorus cells, mural granulosa cells, and serum-starved fibroblast cells), the method of choice is the intraooplasmic microinjection of karyoplasts or whole nuclear donor cells [80,98,102–104,112,121,122]. Taking into account the above-mentioned finding, the in vitro developmental potential of cloned pig embryos that had been reconstructed by direct intraooplasmic microinjection of somatic cell-descended karyoplasts or whole tiny somatic cells was shown to be relatively higher in relation to cloned embryos produced by the electrofusion of somatic cell–ooplast couplets [29,102,107]. The small diameter of the above types of somatic cells is the reason for a considerably reduced contact surface area with the plasmalemma of enucleated oocytes (oolemma), which reduces the percentage of fused ooplast–nuclear donor cell complexes. In turn, the direct microinjection of karyoplasts or whole small-diameter somatic cells into the cytoplasm of enucleated oocytes avoids technical problems (resulting from inadequate adhesion of plasma membranes), which have the greatest limiting effect on the efficiency of electrofusion of nuclear donor cells with cytoplasts [102–104,122].

The direct microinjection of somatic cell nuclei into the cytoplasm of enucleated oocytes has the added advantage of being the "cleanest" of all nuclear transplantation methods. It requires no physicochemical transducers, which often have adverse effects by reducing the in vitro developmental potential of mammalian cloned embryos. For the cell electrofusion technique, all components of the donor cell (both nuclear and cytoplasmic components: organelles and cytoskeletal elements) become an integral part of the oocyte. In contrast, for intraooplasmic microinjection of karyoplasts, plasmalemma and the vast majority of the cytoplasmic material of the nuclear donor cell is rejected following cell lysis. Therefore, only trace amounts of residual cytoplasm, in the form of a narrow rim of membrane-bound protoplasm around the cell nucleus, are introduced as a small karyoplast into the enucleated oocyte. This is of prime importance in some studies that examine nuclear–cytoplasmic interactions in mammalian cloned cybrids [29,44,81,82,104,107,111,122].

The basic paradigm underlying the somatic cell cloning of mammals is the scientific thesis that the donor cell nucleus has to be completely reprogrammed epigenetically by specific factors of the oocyte's origin in order to support the development of the cybrid cloned zygote to term. A considerable portion of the protein nucleoplasmic (karyolymphatic) factors and cytosolic factors of the somatic cell, which are engaged directly or indirectly in the mechanisms underlying epigenetic reprogramming of donor cell genome, is associated with nuclear chromatin. The qualitative and quantitative composition of these factors within the somatic cell changes together with progressing cytodifferentiation. When the whole donor cell is fused with the enucleated oocyte, those specific factors of somatic cell are also transferred into the cytoplasm of the nuclear recipient oocyte. As a result of this, they may block the endogenous oocyte factors from supporting proper remodeling and reprogramming the epigenetic profile, which is characteristic of a foreign nucleus of a terminally differentiated somatic cell, toward an epigenetic status typical of the nucleus of totipotent stem cells such as the zygote [28,102,123–127]. Exogenous nucleoplasmic and cytoplasmic factors derived from the nuclear donor cell, which are responsible for modulating the epigenetic status of genomic DNA, are incorporated together with oocyte mRNA transcripts and proteins, into the remodeled nucleus of the somatic cell (the so-called pseudo-pronucleus). The pseudo-pronucleus is formed following artificial activation of the embryonic developmental program of the reconstructed oocyte [1,128–137]. In turn, an overabundance of the somatic cell-derived agents modulating the epigenetic

profile of the donor nucleus may remarkably reduce the concentration and activity of the oocyte's epigenetic factors. Thus, it may diminish the incidence of complete epigenetic reprogramming of transcriptional activity of the somatic cell nucleus in the developing cloned embryo [112,132–141].

3. Inheritance of the Mitochondrial Genome and Intergenomic Communication between Mitochondrial and Nuclear DNA Fractions during the Development of Cloned Embryos

The increased competence of the oocyte cytoplasm for epigenetic remodeling and reprogramming the somatic cell-inherited nuclear and mitochondrial genomes in cybrid cloned zygotes is a sine qua non condition for correctly inducing the developmental program specific for mammalian SCNT embryos [142–154].

Mitochondria are semiautonomous organelles that contain their own genetic material in the form of double-stranded (α-helix) circular DNA molecules (mtDNAs) of about 16,300–16,500 base pairs (bp). The mitochondrial DNA encodes 13 proteins, 22 tRNAs, and 2 rRNAs. Up to 95% of proteins, which are the products of the cytoplasmic translation system encoded by nuclear DNA, are involved in biogenesis and cytophysiological functions of mitochondria [155–157]. The copy number of mitochondrial genome in a typical mammalian somatic cell is approximately 2–5×10^3, whereas the number of mtDNA molecules in a meiotically matured (MII-stage) oocyte is about 1.6×10^5 in mice, 2.5×10^5 in cattle, 3–5×10^5 in pigs, and 3–8×10^5 in humans. The number of mitochondria in the somatic cell averages 1×10^3, and one organelle harbors between 1 and 10 mtDNA molecules. In turn, a single mitochondrion in the meiotically matured oocyte contains from one to two copies of the mitochondrial genome, which confirms that the abundance of the intraooplasmic population of these organelles is generally equivalent to the total pool of mtDNA molecules of an unfertilized mammalian oocyte [106,139,158,159].

In the procedure of cloning by SCNT, mitochondria of nuclear donor cells are transplanted with the nuclear genetic apparatus into the cytoplasm of enucleated recipient oocytes. Irrespective of the method used for the reconstruction of enucleated oocytes (Table 1), this step of the SCNT procedure always results in the conjunction and mingling (hybridization) of cytoplasmic environments of the ooplast and somatic cell or karyoplast. After its intraooplasmic microinjection, the karyoplast may also be a source of mitochondria (mitochondrial genome) of heteroplasmic origin. Therefore, a reconstructed cloned embryo, which from a cytological viewpoint is a cytoplasmic hybrid (cybrid), harbors the mitochondrial genome of both maternal (oocyte's) and exogenous origin (i.e., introduced together with the nuclear donor cell) [107,111,160–162]. In cloned embryos, fetuses, and offspring, mitochondria are primarily inherited with ooplasmic material. In turn, probably during the first few mitotic cleavage divisions, mitochondria derived from nuclear donor cells are rapidly eliminated from the cytoplasm of embryonic cells at the anaphase stage. The removal of somatic cell-inherited mitochondria largely depends on the polyubiquitination of specific protein substrates. For that reason, the presence of the somatogenic mitochondrial genome in the cells of cloned blastocysts is difficult to detect by genetic engineering techniques [133,158,163,164]. As a consequence, the uniparental inheritance of extranuclear genetic information in dividing cybrid cloned zygotes is regulated by the biodegradation of ubiquitin-labeled mitochondrial proteins (including ribonucleoproteins) and the nucleolysis of mtDNA molecules that are deprived of histones and non-histone proteins. The proteolytic degradation of mitochondria of heteroplasmic (allogeneic) origin is catalyzed by a complex proteasomal system in each blastomere of cloned embryos. This system is characterized by a Svedberg sedimentation coefficient of 26 and designated as a 26S proteasome. The mechanism of nucleolytic biodestruction of all the somatic-cell-derived mtDNA copies is determined by normal function of the intracellular lysosomal cycle, which is related to the exocytosis of endosomal vesicles. The ultimate outcome of this reaction is the removal from embryonic cells of the exogenous mtDNA fractions, which had previously been subjected to internucleosomal fragmentation into short oligonucleotide segments. The preimplantation-stage selective segregation of the mitochondrial genome

stemming from nuclear donor cells that is indirectly induced by the anaphase-promoting complex/cyclosome (APC/C) gradually leads to the establishment of cellular mtDNA homoplasmy in cloned embryos reconstituted with somatic cell nuclei. It is noteworthy that APC/C undergoes the heterodimerization with cyclin-dependent kinase cdc20 and is an integral part of the polysubunit enzymatic complex of ubiquitin ligase. Only occasionally could the lasting hybridization of allogeneic mtDNA copies (the so-called mtDNA heteroplasmy) be identified in the pre- and postnatal period of ontogenetic development of mammalian cloned specimens. This phenomenon of intracellular mtDNA heteroplasmy resulted from synergism/complementarity in the intergenomic communication between mtDNA molecules inherited with both nuclear donor cell cytoplasm and nuclear recipient cell ooplasm [155,165–168].

There are several species-specific epigenetic factors present in the oocyte cytoplasm that may contribute to nuclear–cytoplasmic incompatibilities either immediately after somatic cell nuclear transfer or at later stages of cloned embryo development [105,136,169,170]. In turn, this potential lack of coordination in the interactions of nuclear and cytosolic factors of cybrid cloned zygotes is probably one of the reasons for the limited practical application of the somatic cell cloning technique. It has been demonstrated that maternally inherited mtDNA molecules accumulated in the mitochondrial reservoirs of the oocyte cytosol play an important role in nuclear–ooplasmic asynchrony. This asynchrony involves incompatibilities in both the epigenetic modifications of the somatic genome supporting the developmental program of reconstituted cybrids and a lack of synergy in the molecular mechanisms controlling the karyokinesis and cytokinesis restriction points. These restriction points related to the anaphase segregation of somatic cell-derived chromosomes and asymmetrical telophase division of the cloned cybrid (nuclear–ooplasmic hybrid) that encompasses the expulsion of the pseudo-polar body into perivitelline space are collectively responsible for coordinated pseudomeiotic to mitotic cycle transition following activation of the reconstituted oocyte [134,156].

Moreover, the presence of an oocyte-derived mitochondrial genetic apparatus has been shown to influence the implantation of cloned embryos in the endometrium of a recipient female's uteri. For that reason, the deleterious effect, on the preimplantation development of cloned embryos, of heterogeneous mtDNA sources as a result of possible mitochondrial heteroplasmy in the reconstituted nuclear–cytoplasmic hybrids should not be discounted [139,160,161,169]. That is why the production of nuclear-transferred embryos, fetuses, and offspring with a precisely defined profile of nucleotide sequences in regulatory or coding segments of the nuclear and/or mitochondrial genome seems to be valuable tool. This tool can be suitable for experimentally dissecting the effects of not only nuclear and cytoplasmic genetic/epigenetic components but also the intrauterine environment of recipient females on embryonic, fetal, and postnatal development of cloned specimens [2,155,158,171].

Therefore, in the hybrid cytoplasmic environment of cloned zygotes, genetically different fractions of mitochondrial DNA of maternal (oocyte's) origin were found to coexist with those derived from the cytoplasm of allogeneic somatic cells. Although this extranuclear (mitochondrial) genetic apparatus of cloned nuclear–ooplasmic hybrids contains small (approximately 0.01%) amounts of a cell's genetic information, this mtDNA-dependent genetic information is completely different from information recorded in the nucleotide sequences of nuclear DNA. The latter provides approximately 99.99% of the cellular genome. In this respect, nuclear transplantation of allogeneic somatic cells into enucleated recipient oocytes (where nuclear donor cells and oocytes are derived from genetically different animals of the same species) gives rise to generating nuclear–cytoplasmic hybrids, which are characterized by heterogeneous mtDNA copies. In view of the fact that such heteroplasmic cloned cybrids develop into embryos with cellular mtDNA heteroplasmy, this may lead to apparent genotypic and phenotypic identity/compatibility of the cloned offspring (only in terms of traits determined by nuclear genome-dependent inheritance). Such cloned offspring exhibits a degree of variation/incompatibility with regard to phenotypic traits

determined by cytoplasmic (extranuclear) inheritance. The latter is dependent on the mitochondrial genotype known as the mitotype [105,157,159,160,167].

Different possible patterns/scenarios of extranuclear (cytoplasmic) inheritance of mtDNA fractions have been presented (see Figure 1 (for intraspecies cloning by SCNT) [2,158,165,172], Figure 2 (for interspecies SCNT using nuclear donor cells and recipient oocytes derived from closely related mammalian species) [163,170,171,173,174], and Figure 3 (for interspecies SCNT using nuclear donor cells and recipient oocytes derived from phylogenetically distant mammalian species) [162,164,175,176]).

The "ideal" clone can be generated only in a situation where the nuclei of its own (autogeneic) somatic cells are transferred into enucleated recipient oocytes. Put another way, such a cloned specimen can be produced when nuclear donor cells and oocytes originate from genetically identical individuals of a mammalian species, i.e., from mono-sexual (female) individuals. It is necessary to stress that completely homoplasmic cybrid cloned zygotes can only be created from the oocytes reconstructed in such a manner. The latter are characterized by homogeneous fractions of mtDNA molecules. The artificial activation of such nuclear–cytoplasmic hybrids results in the development of cloned embryos displaying cellular mtDNA homoplasmy. This naturally results in complete genotypic and phenotypic identity/compatibility of somatic cell-cloned fetuses and the resultant offspring. Taking into consideration the previously mentioned findings, only in the case of mammalian cloned females does the mitotype exhibit a homogeneous pattern of coding and regulatory sequences in all mtDNA copies of the somatic and germ cell lines. This condition can only be met assuming that during ontogenesis, the mitochondrial genome will not undergo spontaneous point mutations or those induced by reactive oxygen species [2,42,106,133,166,168,172,177].

Among the reasons for genetic diversification between the cloned specimens generated (somatic clones) and individuals subjected to somatic cell cloning (i.e., donors of somatic cells for SCNT procedure), mention should be made of the effect of mitochondrial (extranuclear/extrachromosomal) inheritance and the impact of intrauterine environment of recipient females receiving cloned embryos. Extranuclear inheritance of genetic material results from the microsurgical, random introduction of foreign mtDNA copies with the nuclear donor cell cytoplasm into the cytoplasmic environment of recipient oocyte. The mismatch of the mitochondrial genome molecules of maternal (oocyte's) origin and of somatogenic (nuclear donor cell) origin, i.e., mtDNA heteroplasmy, leads to inter-specimen diversification within the mitotype. This results in intra-population and inter-population genetic and phenotypic variability dependent on the mitochondrial genome [134,155–157,161]. The phenotypic differences between somatic clones and specimens undergoing SCNT are also contributed by different morphological, anatomotopographical, histological, physiological, endocrinological, embryotrophic, and immunological considerations associated with the reproductive system of recipient surrogates. Moreover, transplacental leakage of leukocyte and erythroblast mitochondria from the blood stream of recipient surrogates to the blood stream of cloned fetuses is often observed. This type of leukocyte–erythroblast chimerism results both from mtDNA heteroplasmy in peripheral blood cells and from genetic mosaicism within subpopulations of nucleated hematopoietic cells (i.e., hematopoietic karyocytes). Such chimerism may also have a certain effect on differences in the mitotype of cloned progeny [139,160,165,169].
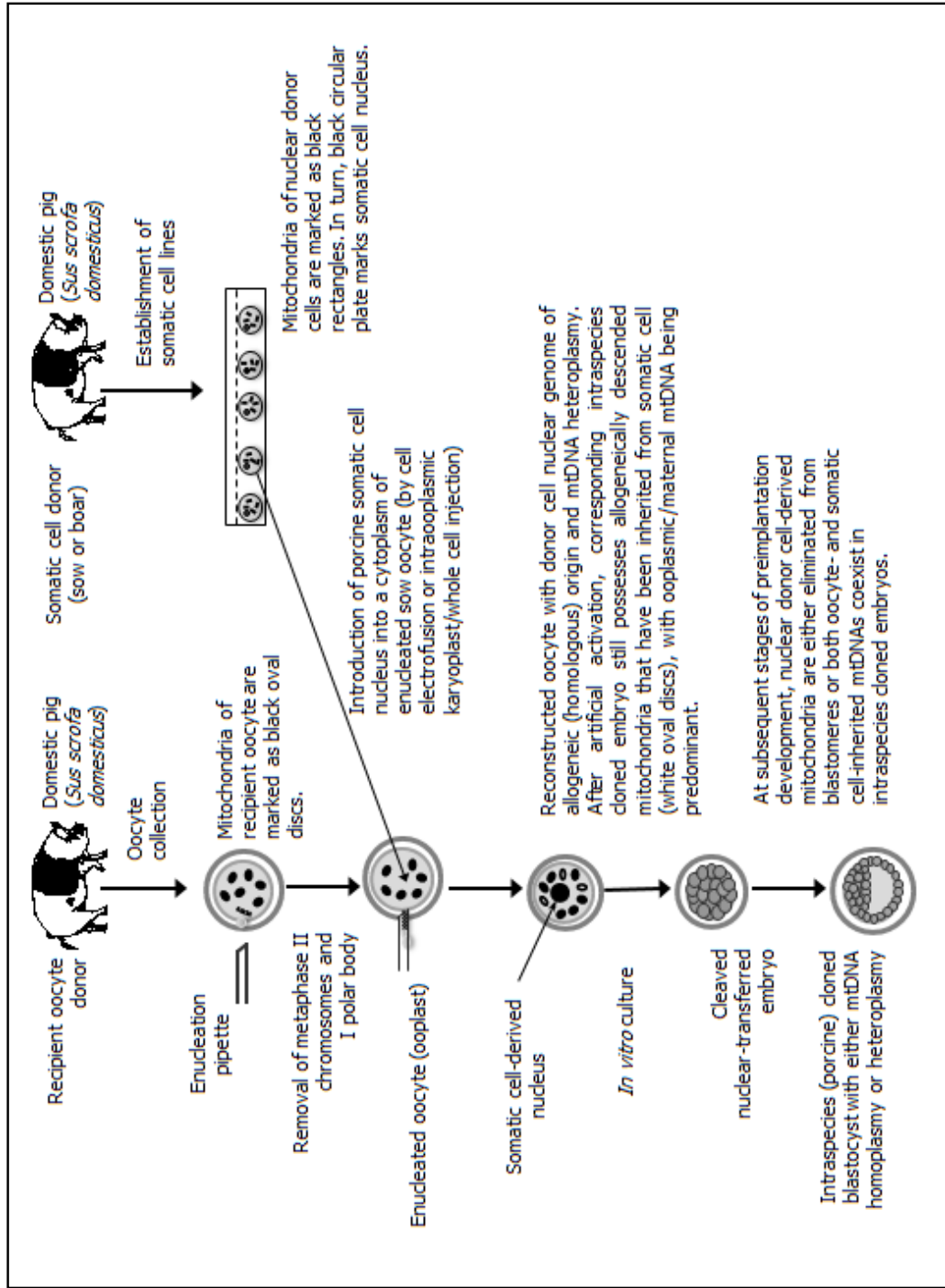
Figure 1. Intraspecies somatic cell cloning, in which the inheritance of allogeneic (homologous) mtDNAs stemming from genetically different nuclear recipient oocytes and nuclear donor cells is still incompletely recognized during preimplantation development of nuclear-transferred pig embryos. In the vast majority of intraspecies (porcine) cloned embryos, mitochondrial genome primarily arises from the nuclear recipient oocytes, whereas in their other counterparts, mtDNA copies appear to be inherited heteroplasmically (i.e., both from nuclear donor cells and from recipient ooplasm).
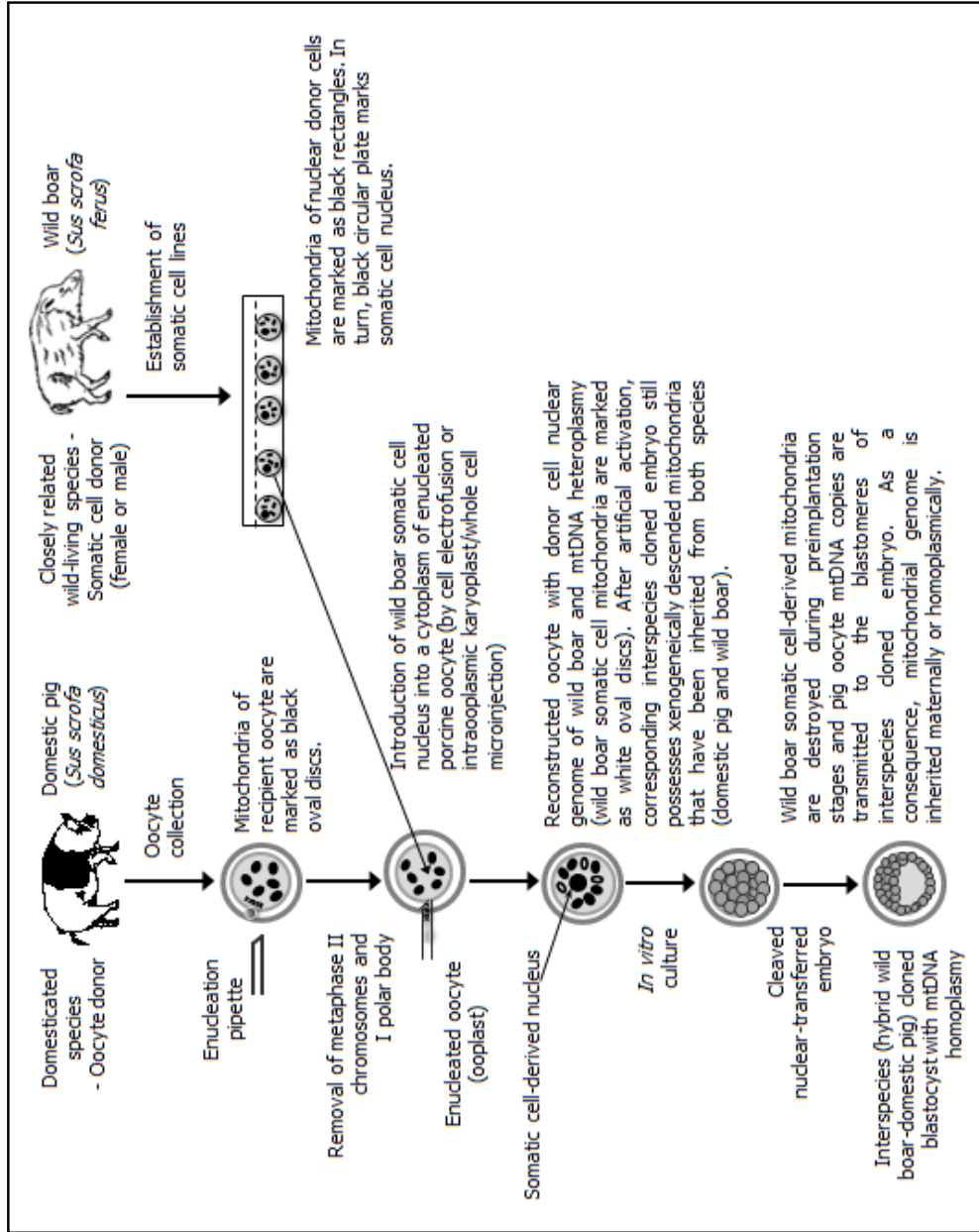
Figure 2. Interspecies (intrafamily and intragenus) somatic cell cloning, in which nuclear donor cells and recipient oocytes are recovered from phylogenetically consanguineous species (i.e., wild boar and domestic pig, respectively). Porcine oocyte-derived mitochondrial DNA (mtDNA) is inherited predominantly during preimplantation development of interspecies (wild boar→pig) cloned embryos, leading to intracellular mtDNA homoplasmy at the blastocyst stage.
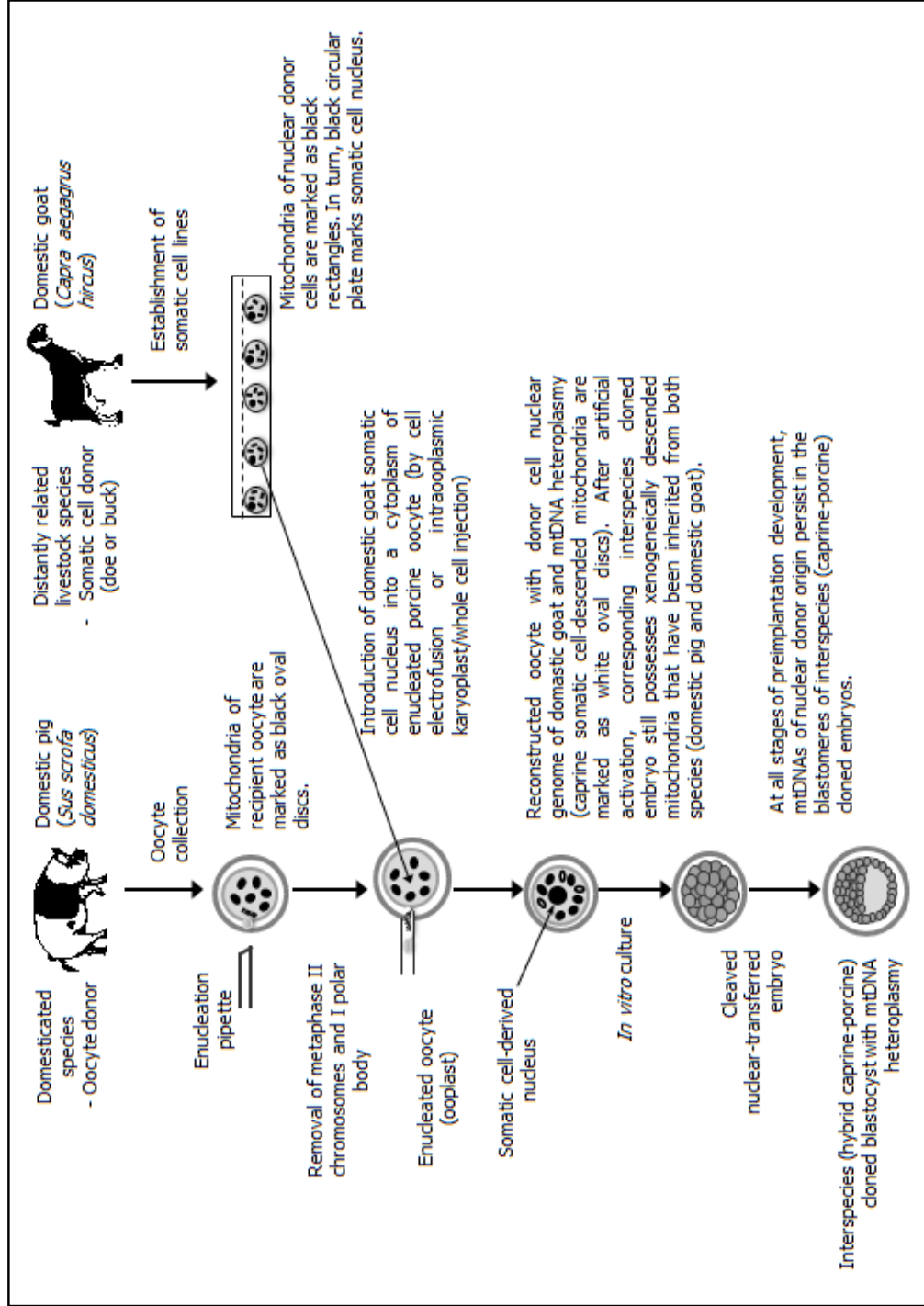
Figure 3. Interspecies (interfamily and intergenus) somatic cell cloning, in which nuclear donor cells and recipient oocytes are recovered from phylogenetically non-consanguineous species (i.e., domestic goat and domestic pig, respectively). Xenogeneic (heterologous) mitochondria that have been inherited from caprine nuclear donor cells and porcine recipient oocytes coexist during preimplantation development of interspecies (goat→pig) cloned embryos, leading to intracellular mtDNA heteroplasmy at the blastocyst stage.

4. Epigenetic Reprogramming of Telomeres in Chromosomes Inherited from Somatic Cell Nuclei throughout Development of Cloned Embryos, Fetuses, and Progeny

One of the essential prerequisites for epigenetic reprogramming of the cellular memory dependent on somatic cell-derived nuclear genome (nuclear DNA; nDNA) in the ontogenesis of mammals produced by SCNT is the structural–functional rearrangement of nuclear chromatin. The latter is associated with conformational changes in the length of terminal ends of chromosomes known as telomeres [178–182]. In turn, epigenomic biochemical alterations within telomeric chromatin are related to the biocatalytic activity of the telomerase enzyme [3,183–185]. One unresolved problem is the "epigenetic age" of cloned animals, which seems to be correlated to the length of terminal DNA fragments, i.e., the telomeres [186–189]. The telomeres are deoxyribonucleoprotein structures involved in the stabilization of the structure and conformation of nuclear chromatin during the division period of the mitotic cell cycle. This is necessary for the replication of mutation-free genomic DNA and karyokinetic segregation of chromosomes [190–192]. The replication of linear DNA in eukaryotic nuclear chromatin encounters the problem that the 5′-end of the lagging strand cannot replicate, as there is no space for the replication initiating RNA primer. An RNA primer is synthesized on the lagging strand template by primase or RNA polymerase, whose role is played by DNA polymerase α. This creates the risk that somatic cell chromosomes will shorten with every replication round, thus losing genetic information. In mammalian somatic cells, the classical α isoform of DNA polymerase is not capable of semiconservative replication of the 5′-end synthesized in fragments of the DNA chain, whose replication is delayed in relation to the 3′-end of the continuously copied leading strand [182,193]. As a result, in each cell division cycle, unreplicated telomere DNA sequences are gradually lost. For this reason, telomere length is a specific "physiological mitotic clock" of the cell. The shortening of chromosome telomeric regions is positively correlated with the number of cell divisions. Therefore, when the telomere length reaches a critical restriction/control point in a karyokinetically active somatic cell, this is signalized by the loss of nuclear chromatin stability, which is epigenetically programmed in the spatial structure/configuration and telomere functions. This is also signalized by triggering replicative senescence in the cell [187,194–196]. The characteristics of cells that undergo progressive replicative senescence include a considerable increase in diameter and a flattened shape caused by a drastic increase in cytosol volume. All of the above-mentioned epigenetic, genetic, physiological, morphological, and ultrastructural transformations, which occur in aging cells, lead in the first place to a rapid slowdown of both intracellular anabolic processes and the kinetics of mitotic divisions. At a later stage, these transformations bring about the irreversible inhibition of metabolic and proliferative activity. As a consequence of single doubling in the population of mammalian adult dermal fibroblasts cultured in vitro, telomere length decreases by about 48 DNA nucleotide pairs [180,183,188,197,198].

Telomerase is a ribonucleoprotein enzyme complex that displays the total activities of RNA reverse transcriptase and DNA integrase only in germ and embryonic cells, while its partial activity is observed in fetal somatic cells undergoing tissue-specific cytodifferentiation. However, the biocatalytic activity of this enzyme completely ceases in terminally differentiated somatic cells of adult specimens [184,185,193,199]. The function of telomerase is to restore the primary length of DNA telomeres by reverse transcription of its own RNA template. This gives rise to the de novo synthesis (reduplication) of tandem repeats within noncoding telomere DNA sequences (5′-TTAGGG-3′) that were lost as a result of terminating either consecutive mitotic and meiotic divisions of gametogenic (germinal) cells or mitotic cycles of blastomeres, leading to consecutive cleavage divisions of embryos. In the last phase of semiconservative DNA replication, the 3′-end of the leading strand extends beyond the 5′-end of the lagging strand. Telomerase contains an RNA molecule that is partially complementary to the tandem repeat of the short 5′-TTAGGG-3′ sequence at the 3′-end of the leading DNA strand, thus elongating the leading strand of telomeric DNA region using RNA as the template. Next, the enzyme detaches and

binds to a new telomeric end to extend the leading DNA strand. The extension process may occur hundreds of times before telomerase finally dissociates. Then, the extended, replicated leading strand serves as a template for replication of the 5′-end of the lagging strand that is catalyzed by DNA polymerase α. These two processes, where the 5′-ends of DNA are shortened during basic semiconservative replication and subsequently elongated due to telomerase activity, are mutually balanced, whereby the total chromosomal length remains more or less the same [180,192,199,200]. In contrast, a lack of telomerase activity and, as a consequence, a lack of elongating the temporally and spatially restricted length of nuclear DNA telomeric sequences are epigenomically determined factors specific for adult somatic cells that provide a source of nuclear donors for the SCNT procedure. These factors limit the survival rate, proliferative activity, and the number of division cycles of a cell before the cell reaches the critical point of the maximum telomere shortening. The latter is simultaneously the mitotic control point that signals the initiation and irreversibility of the replicative senescence of terminally differentiated somatic cells [188,190,195,201].

The problem of telomere shortening/attrition and replicative senescence of somatic cells was observed in chromosomes of Dolly the sheep, the first cloned mammal [114,178,189,196]. The telomeres in the chromosomes of Dolly the cloned ewe (at the age of 3 years) were much shorter than the telomeres in the chromosomes of control animals, which were of the same age and were born through natural reproduction. Moreover, the telomere length in Dolly's chromosomes was similar to that in the chromosomes of a 6-year-old sheep, which was used as a donor of somatic cells for the cloning procedure. At the time of molecular analysis of telomeres, Dolly was 3 years old, and her epigenetic age corresponded to the actual age of a 9-year-old sheep. Put differently, Dolly's somatic cells were epigenetically older by 6 years than herself. Born on 5 July 1996, Dolly the sheep lived above 6.5 years and was euthanized on 14 February 2003 after being diagnosed with a malignant lung cancer known as Jaagsiekte (ovine pulmonary adenocarcinoma). The etiologic agent of this chronic, contagious, and fatal lung cancer in sheep is Jaagsiekte sheep retrovirus (JSRV), which is responsible for the oncogenic transformation of bronchial exocrine epithelial cells, i.e., type II pneumocytes and bronchiolar club (Clara) cells. By 2000, Dolly produced a total of 6 lambs (including twins and triplets). Therefore, the cloned ewe was reproductively sound and displayed high fertility and prolificacy, which means that her reproductive capacity upon reaching sexual and breeding maturity was not impaired. However, in 2001, the hind legs of 5-year-old Dolly exhibited the first symptoms of an autoimmune chronic degenerative joint disease (osteoarthritis), namely rheumatoid arthritis. It should be noted that this disease is relatively frequent in different breeds of sheep, but generally, it does not affect animals younger than 10 years of age. Two questions arise: Could Dolly live 6–9 years less than the expected lifespan of 12–15 years (which is the average lifespan of Finn Dorset sheep, represented by the somatic cell donor ewe in the SCNT procedure)? As a result of somatic cell cloning, did she exhibit rapidly progressing symptoms of premature (anatomical and physiological) aging of the entire body or of some of its parts, tissues, and organs? The results of experiments performed to determine the telomeric age of Dolly the sheep suggest that animals cloned by transferring adult somatic cell nucleus into the enucleated oocyte are epigenetically compromised. For this reason, they have a genetic age of a specimen playing the role of somatic cell donor for SCNT. This means that at birth, they are epigenetically and genetically much older than their real-time birth date [178,184,189,196]. However, the evidence for cloned sheep was not reflected in the studies focused on the analyses of chromosomes isolated from somatic cells derived from cloned cattle. A study by Lanza et al. [194] on the chromosomes of cloned calves produced by using long-term cultured fibroblast cells for SCNT showed that the telomere length of these young animals is even slightly greater than that of control animals, despite the fact that the chromosomes of nuclear donor cells were almost completely depleted of telomeres. These analyses confirmed that the terminal ends of chromosomes are efficiently resynthesized in blastomeres of bovine cloned embryos, with a contribution from highly active telomerases. Analogously, Tian et al. [179] demonstrated that telomere length in chromosomes of four live (about 15.4 kbp) and six dead cloned calves (about 15.9 kbp) that had been generated using dermal fibroblast cells or cumulus cells derived from a 13-year-old cow not only did not differ

considerably from the telomere length characteristic of control chromosomes (about 14.7 kbp) but also significantly exceeded (by about 3–3.5 kbp) the telomere length in chromosomes of the aging cow (about 12.4 kbp), which served as the donor of somatic cells for SCNT-based cloning. Finally, Kato et al. [202] provided evidence that in cloned cattle, the telomere length is shortened only in the tissues matching those from the biopsy specimens of which the primary cell cultures were established. In turn, the latter provided the somatic cell lines that were nuclear donors used for SCNT procedures.

Telomere length in chromosomes of the dermal fibroblast cells originating from six transgenic cloned pigs matched the telomere length of the chromosomes of dermal fibroblast cells originating from control animals of the same age and produced by natural reproduction. In turn, two cloned piglets that died 3 to 7 days after birth displayed the same length of terminal ends of chromosomes as the telomeres of chromosomes in fetuses at the third trimester of pregnancy [185]. The terminal restriction fragment (TRF) assay of genomic DNA isolated from the cells stemming from the biopsy specimens retrieved from different organs/tissues of cloned fetuses (gonads, heart, liver, lungs, kidneys, and skin) has confirmed that telomere length in chromosomes remains constant in all the cell lines arising from cytodifferentiation that takes place throughout fetogenesis. The reason for this is the high efficiency of restoring the primary length of terminal chromosome ends via the active telomerase isoform throughout the interphase replication cycle of nuclear DNA in differentiating somatic cells that occupy new tissue niches and are engaged in multi-stage histo- and organogenesis processes. During the postnatal period, telomeres are gradually shortened with each mitotic division of somatic cells, and the reduction of telomere length is tissue-specific. This reflects inhibition of the biocatalytic activity of telomerase in differentiated lines of somatic cells derived from skin tissue explants and various internal organs harvested from gilts and boars both before and after attainment of sexual maturity [180,181,185,192,198].

5. Comprehensive Summary and Future Goals

Cloning by SCNT is currently used in assisted reproductive technologies (ARTs) of many mammalian species, including various species of farm animals. The application of this technology in experimental embryology and in molecular population genetics is of great importance for livestock breeding.

Somatic cell cloning as a method of asexual reproduction offers the opportunity for production and/or multiplication of monogenetic and monosexual progeny of high breeding worth, whose genotypic and phenotypic identity with progenitor donor of transcriptional mitochondrial and nuclear apparatus of the somatic cell only concerns genomic DNA. Animals produced by SCNT differ in phenotypic traits determined by the random segregation of oocyte-derived/maternal and somatic cell-derived/somatogenic mitochondrial genome (mtDNA) as a result of cytoplasmic (extranuclear) inheritance of genetic material [106,133,159,161]. Nevertheless, the particularly high application value of somatic cell cloning technology is related to the possibility of generating genotypically and phenotypically identical transgenic animals, i.e., animals with transformed nuclear genomes that are valuable due to the expression product of modified genes [4,28,38,203]. The yield of recombinant transgenic protein synthesis by genetically transformed cloned specimens is, to a certain extent, dependent on the effect of heteroplasmic sources of mitochondrial genotype (mitotype) on the transcriptional activity profile of modified nuclear DNA genes. This correlation may be negative with a high coefficient of heritability and regressive repeatability of a given quantitative and qualitative trait resulting from the transgenization of a breeding herd [2,133,158]. Therefore, an important problem in the production and multiplication of transgenic cloned specimens (the so-called clonal founder animals) is to generate offspring with an identical mitochondrial genome. These offspring carry only homoplasmic copies of mtDNA derived either from recipient oocytes or from somatic donor cells of genetically modified nuclei. Not without significance is the effect of inheritance of extranuclear genetic information that is accumulated in mitochondrial reservoirs of both somatic (somatogenic)

and germinal (gametogenic) cell lines on the transcriptional activity of quantitative trait loci (QTLs). The latter encompass loci for such traits of transgenic cloned specimens as reproductive traits (e.g., fertility and prolificacy), productive traits, including meatiness (e.g., loin eye area, contents of striated muscle tissue, intramuscular and intermuscular connective tissue, adipose tissue in different carcass, and half-carcass cuts) and milk yield traits (e.g., volume of milk synthesis, and milk secretion and ejection per day and per lactation period) [2,4,106,108,136,157,159,203]. In turn, genetic determinants of prolificacy or fertility traits from the heteroplasmic or homoplasmic pattern of mitochondrial genome segregation may influence the processes of intergenerational transmission of the transgene in germ cell lines of the descendant generations of cloned animals with the transformed nuclear genotype. On the one hand, a negative or positive genetic correlation between milk yield or dressing percentage traits (inherited with genomic DNA) and the transcriptional activity profile of mitochondrial DNA genes may be responsible for different extents or patterns of tissue-specific or organ-specific expression of xenogeneic (e.g., human) gene constructs in transgenic cloned animals. The expression extents or patterns of these gene constructs may be characterized by the inhibition or onset of their transcriptional suppression. On the other hand, the above-mentioned negative or positive correlation may also affect the expression profile of xenogeneic gene constructs (transgenes) in different cells, tissues, and organs of genetically modified cloned specimens. This profile of transcriptional activity of the transgenes integrated with the nuclear genome may be homogenous or heterogeneous, resulting in the induction or absence of transgenic mosaicism/chimerism in cloned animals [4,5,136,158,168,169]. The xenogeneic expressive gene constructs that have been incorporated into genomic DNA of cells localized in different tissues and organs of transgenic cloned animals can encode, for example, recombinant human therapeutic proteins. The synthesis and exo- or endocrine secretion of these proteins can be targeted at secretory cells of the mammary gland or smooth and striated muscle tissue found in all the corporeal organs, organ systems, and parts of farm animals [35,139,204–207].

Intergenomic communication between mitochondrial DNA and the transgene stably integrated with nuclear DNA may also create differences in the efficiency of transgenesis, which induces targeted mutagenesis, i.e., monoallelic deletion or the insertional inactivation of the gene coding for myostatin. Myostatin is a muscle-tissue-specific hormonal protein that paracrinally inhibits the gain (hypetrophy and hyperplasia) of skeletal and smooth muscles [18,208]. The presence of one or two knockout alleles of the myostatin gene or the presence of one or two posttranscriptionally silenced mRNA copies encoded by the myostatin gene in heterozygous or homozygous transgenic cloned beef cattle increases meatiness in cows and bulls. This results from the hypertrophy and hyperplasia of not only striated but also smooth muscle tissue [18,204].

The attractiveness of SCNT-based cloning of transgenic mammals, including various species of domesticated animals, is decided by the applicability of the hormonal or enzymatic product of the modified gene expression. This applicability first of all determines the scale and scope of the research. Although the first cloned mammal was a sheep, research targeted at the somatic cell cloning of other livestock species had a much wider span. The mammary glands (udders) of transgenic cloned cows [11,12,14,206,209,210], transgenic cloned sheep [23,24], and transgenic cloned goats [17,19] may become live bioreactors for producing humanized milk, easy-to-digest milk, or milk containing recombinant human therapeutic proteins (biopharmaceuticals or nutraceuticals). The latter may find clinical application in the treatment of patients afflicted with genetically determined diseases [12,211–213].

Compared to other ARTs in mammals (including livestock species), the efficiency of somatic cell cloning in domesticated animals, which is measured by the percentage of offspring born in relation to the number of reconstructed oocytes, remains low and oscillates between 0.3% and 2% on average. Nonetheless, the biotechnological possibilities of the somatic cell cloning in different mammalian species is far ahead of our understanding of the biological determinants, in particular the molecular and epigenetic aspects, of this

method [108,132,192,203]. Yet, the biological foundations that have been laid for embryonic genome engineering of domesticated animals, especially over the last 24 years, made feasible the development of an innovative technology of in vitro embryo production using the somatic cell cloning procedure, which may meet the requirements for application in laboratories or, in some cases, only for limited practical purposes [127,214,215]. The assisted reproductive technology that encompasses SCNT could be used on a larger practical scale only after the efficiency of somatic cell cloning in various mammalian species, including livestock, is increased to match the efficiency of in vitro fertilization (IVF) or artificial insemination (AI) as part of multiple ovulation and embryo transfer (MOET) programs in cattle. However, due to the relatively high incidence of lethal or sublethal developmental anomalies or anatomo-histological defects in cloned fetuses and progeny, it is not possible to use the somatic cell cloning of farm animals on a commercial scale, at least at the present level of sophistication of the relevant research performed in Europe and the world. Furthermore, it is also worth noting that the elaboration and optimization of efficient approaches applied to cryopreserving nuclear donor somatic cells, nuclear-transferred oocytes reconstructed with somatic cells, and somatic cell-cloned embryos appear to be important milestones that can help cryogenically protect these valuable types of biological materials. This can bring the investigators closer to the perspective of progression in the outcome of producing mammalian SCNT progeny. In turn, future large-scale attempts undertaken to more successfully generate mammalian cloned offspring can expedite their practical use for the purposes of not only agricultural, transgenic, biotechnological, biomedical, and biopharmaceutical research fields but also ex situ conservation of biological diversity in different anthropogenic and unspoiled natural ecosystems.

To sum up, it seems that after making the transition from basic to applied research, the techniques for intra- and interspecies somatic cell cloning of mammals could contribute to (1) the conservation of genetic resources and the establishment of the genetic reserves of threatened mammalian species and breeds, (2) the restoration and multiplication of the subpopulations of endangered or vulnerable wild and domesticated species of mammals in order to maintain biodiversity and to increase the level of intra-population and inter-specimen genetic variability, and (3) revival ("resurrection") and reintroduction into the wild of extinct, free-living species of mammals. Moreover, the practically applied research into the cloning of domesticated animals could serve to achieve other tangible benefits, including (4) the improvement of the breeding (genetic) and productive value of different farm animal breeds, e.g., increasing their milk and meat yields and reproductive ability (prolificacy and fertility), and (5) the implementation of basic research into interdisciplinary sciences aimed at the generation of animal biotechnological (transgenic) products for the biomedical, biopharmaceutical, nutraceutical, and food technology industries. One classic example of this is the permanent and highly heritable targeted transgenization of the mammary glands of domesticated species of small and large ruminants (i.e., sheep, goats, and cattle, respectively) and their use as animal bioreactors for producing humanized milk or milk containing recombinant human therapeutic proteins such as biopharmaceuticals and nutraceuticals.

Abbreviations

AI	Artificial insemination
APC/C	Anaphase-promoting complex/cyclosome
ARTs	Assisted reproductive technologies
IVF	In vitro fertilization
JSRV	Jaagsiekte sheep retrovirus
MII	Metaphase II
MOET	Multiple ovulation and embryo transfer
mtDNA	Mitochondrial DNA
nDNA	Nuclear DNA
QTLs	Quantitative trait loci
SCNT	Somatic cell nuclear transfer

References

1. Gao, R.; Wang, C.; Gao, Y.; Xiu, W.; Chen, J.; Kou, X.; Zhao, Y.; Liao, Y.; Bai, D.; Qiao, Z.; et al. Inhibition of aberrant DNA re-methylation improves post-implantation development of somatic cell nuclear transfer embryos. *Cell Stem Cell* **2018**, *23*, 426–435.e5. [CrossRef]
2. Liu, H.J.; Xue, J.; Li, K.; Ying, Z.Z.; Zheng, Z.; Wang, R. Improvement of the nuclear transfer efficiency by using the same genetic background of recipient oocytes as the somatic donor cells in goats. *Cell Biol. Int.* **2012**, *36*, 555–560. [CrossRef]
3. Liu, H.J.; Peng, H.; Hu, C.C.; Li, X.Y.; Zhang, J.L.; Zheng, Z.; Zhang, W.C. Effects of donor cells' sex on nuclear transfer efficiency and telomere lengths of cloned goats. *Reprod. Domest. Anim.* **2016**, *51*, 789–794. [CrossRef] [PubMed]
4. Samiec, M.; Skrzyszowska, M. Transgenic mammalian species, generated by somatic cell cloning, in biomedicine, biopharmaceutical industry and human nutrition/dietetics—recent achievements. *Pol. J. Vet. Sci.* **2011**, *14*, 317–328. [CrossRef] [PubMed]
5. Samiec, M.; Skrzyszowska, M. The possibilities of practical application of transgenic mammalian species generated by somatic cell cloning in pharmacology, veterinary medicine and xenotransplantology. *Pol. J. Vet. Sci.* **2011**, *14*, 329–340. [CrossRef]
6. Gavin, W.; Buzzell, N.; Blash, S.; Chen, L.; Hawkins, N.; Miner, K.; Pollock, D.; Porter, C.; Bonzo, D.; Meade, H. Generation of goats by nuclear transfer: A retrospective analysis of a commercial operation (1998–2010). *Transgenic Res.* **2020**, *29*, 443–459. [CrossRef]
7. Moulavi, F.; Asadi-Moghadam, B.; Omidi, M.; Yarmohammadi, M.; Ozegovic, M.; Rastegar, A.; Hosseini, S.M. Pregnancy and calving rates of cloned dromedary camels produced by conventional and handmade cloning techniques and in vitro and in vivo matured oocytes. *Mol. Biotechnol.* **2020**, *62*, 433–442. [CrossRef] [PubMed]
8. Forsberg, E.J.; Strelchenko, N.S.; Augenstein, M.L.; Betthauser, J.M.; Childs, L.A.; Eilertsen, K.J.; Enos, J.M.; Forsythe, T.M.; Golueke, P.J.; Koppang, R.W.; et al. Production of cloned cattle from in vitro systems. *Biol. Reprod.* **2002**, *67*, 327–333. [CrossRef]
9. Green, A.L.; Wells, D.N.; Oback, B. Cattle cloned from increasingly differentiated muscle cells. *Biol. Reprod.* **2007**, *77*, 395–406. [CrossRef]
10. Hoshino, Y.; Hayashi, N.; Taniguchi, S.; Kobayashi, N.; Sakai, K.; Otani, T.; Iritani, A.; Saeki, K. Resurrection of a bull by cloning from organs frozen without cryoprotectant in a −80 °C freezer for a decade. *PLoS ONE* **2009**, *4*, e4142. [CrossRef]
11. Liu, X.; Wang, Y.; Guo, W.; Chang, B.; Liu, J.; Guo, Z.; Quan, F.; Zhang, Y. Zinc-finger nickase-mediated insertion of the lysostaphin gene into the beta-casein locus in cloned cows. *Nat. Commun.* **2013**, *4*, 2565. [CrossRef]
12. Luo, Y.; Wang, Y.; Liu, J.; Lan, H.; Shao, M.; Yu, Y.; Quan, F.; Zhang, Y. Production of transgenic cattle highly expressing human serum albumin in milk by phiC31 integrase-mediated gene delivery. *Transgenic Res.* **2015**, *24*, 875–883. [CrossRef]
13. Wang, M.; Sun, Z.; Yu, T.; Ding, F.; Li, L.; Wang, X.; Fu, M.; Wang, H.; Huang, J.; Li, N.; et al. Large-scale production of recombinant human lactoferrin from high-expression, marker-free transgenic cloned cows. *Sci. Rep.* **2017**, *7*, 10733. [CrossRef]
14. Wang, Y.; Ding, F.; Wang, T.; Liu, W.; Lindquist, S.; Hernell, O.; Wang, J.; Li, J.; Li, L.; Zhao, Y.; et al. Purification and characterization of recombinant human bile salt-stimulated lipase expressed in milk of transgenic cloned cows. *PLoS ONE* **2017**, *12*, e0176864. [CrossRef] [PubMed]
15. Keefer, C.L.; Keyston, R.; Lazaris, A.; Bhatia, B.; Begin, I.; Bilodeau, A.S.; Zhou, F.J.; Kafidi, N.; Wang, B.; Baldassarre, H.; et al. Production of cloned goats after nuclear transfer using adult somatic cells. *Biol. Reprod.* **2002**, *66*, 199–203. [CrossRef] [PubMed]
16. Lan, G.C.; Chang, Z.L.; Luo, M.J.; Jiang, Y.L.; Han, D.; Wu, Y.G.; Han, Z.B.; Ma, S.F.; Tan, J.H. Production of cloned goats by nuclear transfer of cumulus cells and long-term cultured fetal fibroblast cells into abattoir-derived oocytes. *Mol. Reprod. Dev.* **2006**, *73*, 834–840. [CrossRef]
17. Meng, L.; Wan, Y.; Sun, Y.; Zhang, Y.; Wang, Z.; Song, Y.; Wang, F. Generation of five human lactoferrin transgenic cloned goats using fibroblast cells and their methylation status of putative differential methylation regions of *IGF2R* and *H19* imprinted genes. *PLoS ONE* **2013**, *8*, e77798. [CrossRef]
18. Zhou, Z.R.; Zhong, B.S.; Jia, R.X.; Wan, Y.J.; Zhang, Y.L.; Fan, Y.X.; Wang, L.Z.; You, J.H.; Wang, Z.Y.; Wang, F. Production of myostatin-targeted goat by nuclear transfer from cultured adult somatic cells. *Theriogenology* **2013**, *79*, 225–233. [CrossRef] [PubMed]

19. Feng, X.; Cao, S.; Wang, H.; Meng, C.; Li, J.; Jiang, J.; Qian, Y.; Su, L.; He, Q.; Zhang, Q. Production of transgenic dairy goat expressing human α-lactalbumin by somatic cell nuclear transfer. *Transgenic Res.* **2015**, *24*, 73–85. [CrossRef] [PubMed]

20. He, Z.; Lu, R.; Zhang, T.; Jiang, L.; Zhou, M.; Wu, D.; Cheng, Y. A novel recombinant human plasminogen activator: Efficient expression and hereditary stability in transgenic goats and in vitro thrombolytic bioactivity in the milk of transgenic goats. *PLoS ONE* **2018**, *13*, e0201788. [CrossRef] [PubMed]

21. McCreath, K.J.; Howcroft, J.; Campbell, K.H.S.; Colman, A.; Schnieke, A.E.; Kind, A.J. Production of gene targeted sheep by nuclear transfer from cultured somatic cells. *Nature* **2000**, *405*, 1066–1069. [CrossRef]

22. Loi, P.; Clinton, M.; Barboni, B.; Fulka, J., Jr.; Cappai, P.; Feil, R.; Moor, R.M.; Ptak, G. Nuclei of nonviable ovine somatic cells develop into lambs after nuclear transplantation. *Biol. Reprod.* **2002**, *67*, 126–132. [CrossRef] [PubMed]

23. Deng, S.; Li, G.; Zhang, J.; Zhang, X.; Cui, M.; Guo, Y.; Liu, G.; Li, G.; Feng, J.; Lian, Z. Transgenic cloned sheep overexpressing ovine toll-like receptor 4. *Theriogenology* **2013**, *80*, 50–57. [CrossRef]

24. Zhang, P.; Liu, P.; Dou, H.; Chen, L.; Chen, L.; Lin, L.; Tan, P.; Vajta, G.; Gao, J.; Du, Y.; et al. Handmade cloned transgenic sheep rich in omega-3 fatty acids. *PLoS ONE* **2013**, *8*, e55941. [CrossRef]

25. Yang, C.; Shang, X.; Cheng, L.; Yang, L.; Liu, X.; Bai, C.; Wei, Z.; Hua, J.; Li, G. DNMT 1 maintains hypermethylation of CAG promoter specific region and prevents expression of exogenous gene in fat-1 transgenic sheep. *PLoS ONE* **2017**, *12*, e0171442. [CrossRef] [PubMed]

26. Yuan, Y.; Liu, R.; Zhang, X.; Zhang, J.; Zheng, Z.; Huang, C.; Cao, G.; Liu, H.; Zhang, X. Effects of recipient oocyte source, number of transferred embryos and season on somatic cell nuclear transfer efficiency in sheep. *Reprod. Domest. Anim.* **2019**, *54*, 1443–1448. [CrossRef]

27. Onishi, A.; Iwamoto, M.; Akita, T.; Mikawa, S.; Takeda, K.; Awata, T.; Hanada, H.; Perry, A.C.F. Pig cloning by microinjection of fetal fibroblast nuclei. *Science* **2000**, *289*, 1188–1190. [CrossRef]

28. Lee, G.S.; Kim, H.S.; Hyun, S.H.; Lee, S.H.; Jeon, H.Y.; Nam, D.H.; Jeong, Y.W.; Kim, S.; Kim, J.H.; Han, J.Y.; et al. Production of transgenic cloned piglets from genetically transformed fetal fibroblasts selected by green fluorescent protein. *Theriogenology* **2005**, *63*, 973–991. [CrossRef] [PubMed]

29. Watanabe, S.; Iwamoto, M.; Suzuki, S.I.; Fuchimoto, D.; Honma, D.; Nagai, T.; Hashimoto, M.; Yazaki, S.; Sato, M.; Onishi, A. A novel method for the production of transgenic cloned pigs: Electroporation-mediated gene transfer to non-cultured cells and subsequent selection with puromycin. *Biol. Reprod.* **2005**, *72*, 309–315. [CrossRef]

30. Brunetti, D.; Perota, A.; Lagutina, I.; Colleoni, S.; Duchi, R.; Calabrese, F.; Seveso, M.; Cozzi, E.; Lazzari, G.; Lucchini, F.; et al. Transgene expression of green fluorescent protein and germ line transmission in cloned pigs derived from in vitro transfected adult fibroblasts. *Cloning Stem Cells* **2008**, *10*, 409–419. [CrossRef] [PubMed]

31. Deng, W.; Yang, D.; Zhao, B.; Ouyang, Z.; Song, J.; Fan, N.; Liu, Z.; Zhao, Y.; Wu, Q.; Nashun, B.; et al. Use of the 2A peptide for generation of multi-transgenic pigs through a single round of nuclear transfer. *PLoS ONE* **2011**, *6*, e19986. [CrossRef]

32. Richter, A.; Kurome, M.; Kessler, B.; Zakhartchenko, V.; Klymiuk, N.; Nagashima, H.; Wolf, E.; Wuensch, A. Potential of primary kidney cells for somatic cell nuclear transfer mediated transgenesis in pig. *BMC Biotechnol.* **2012**, *12*, 84. [CrossRef] [PubMed]

33. Kurome, M.; Geistlinger, L.; Kessler, B.; Zakhartchenko, V.; Klymiuk, N.; Wuensch, A.; Richter, A.; Baehr, A.; Kraehe, K.; Burkhardt, K.; et al. Factors influencing the efficiency of generating genetically engineered pigs by nuclear transfer: Multi-factorial analysis of a large data set. *BMC Biotechnol.* **2013**, *13*, 43. [CrossRef] [PubMed]

34. Li, Z.; He, X.; Chen, L.; Shi, J.; Zhou, R.; Xu, W.; Liu, D.; Wu, Z. Bone marrow mesenchymal stem cells are an attractive donor cell type for production of cloned pigs as well as genetically modified cloned pigs by somatic cell nuclear transfer. *Cell. Reprogram.* **2013**, *15*, 459–470. [CrossRef]

35. Ju, H.; Zhang, J.; Bai, L.; Mu, Y.; Du, Y.; Yang, W.; Li, Y.; Sheng, A.; Li, K. The transgenic cloned pig population with integrated and controllable GH expression that has higher feed efficiency and meat production. *Sci. Rep.* **2015**, *5*, 10152. [CrossRef] [PubMed]

36. Lu, D.; Liu, S.; Shang, S.; Wu, F.; Wen, X.; Li, Z.; Li, Y.; Hu, X.; Zhao, Y.; Li, Q.; et al. Production of transgenic-cloned pigs expressing large quantities of recombinant human lysozyme in milk. *PLoS ONE* **2015**, *10*, e0123551. [CrossRef] [PubMed]

37. Ozawa, M.; Himaki, T.; Ookutsu, S.; Mizobe, Y.; Ogawa, J.; Miyoshi, K.; Yabuki, A.; Fan, J.; Yoshida, M. Production of cloned miniature pigs expressing high levels of human apolipoprotein(a) in plasma. *PLoS ONE* **2015**, *10*, e0132155. [CrossRef]

38. Ma, J.; Li, Q.; Li, Y.; Wen, X.; Li, Z.; Zhang, Z.; Zhang, J.; Yu, Z.; Li, N. Expression of recombinant human α-lactalbumin in milk of transgenic cloned pigs is sufficient to enhance intestinal growth and weight gain of suckling piglets. *Gene* **2016**, *584*, 7–16. [CrossRef] [PubMed]

39. Kwon, D.J.; Kim, D.H.; Hwang, I.S.; Kim, D.E.; Kim, H.J.; Kim, J.S.; Lee, K.; Im, G.S.; Lee, J.W.; Hwang, S. Generation of α-1,3-galactosyltransferase knocked-out transgenic cloned pigs with knocked-in five human genes. *Transgenic Res.* **2017**, *26*, 153–163. [CrossRef]

40. Huang, J.; Wang, A.; Huang, C.; Sun, Y.; Song, B.; Zhou, R.; Li, L. Generation of marker-free *pbd-2* knock-in pigs using the CRISPR/Cas9 and Cre/loxP systems. *Genes* **2020**, *11*, 951. [CrossRef]

41. Zhao, H.; Li, Y.; Wiriyahdamrong, T.; Yuan, Z.; Qing, Y.; Li, H.; Xu, K.; Guo, J.; Jia, B.; Zhang, X.; et al. Improved production of GTKO/hCD55/hCD59 triple-gene-modified *Diannan* miniature pigs for xenotransplantation by recloning. *Transgenic Res.* **2020**, *29*, 369–379. [CrossRef]

42. Galli, C.; Lagutina, I.; Crotti, G.; Colleoni, S.; Turini, P.; Ponderato, N.; Duchi, R.; Lazzari, G. Pregnancy: A cloned horse born to its dam twin. *Nature* **2003**, *424*, 635. [CrossRef]

43. Lagutina, I.; Lazzari, G.; Duchi, R.; Colleoni, S.; Ponderato, N.; Turini, P.; Crotti, G.; Galli, C. Somatic cell nuclear transfer in horses: Effect of oocyte morphology, embryo reconstruction method and donor cell type. *Reproduction* **2005**, *130*, 559–567. [CrossRef]

44. Hinrichs, K.; Choi, Y.H.; Love, C.C.; Chung, Y.G.; Varner, D.D. Production of horse foals via direct injection of roscovitine-treated donor cells and activation by injection of sperm extract. *Reproduction* **2006**, *131*, 1063–1072. [CrossRef] [PubMed]

45. Hinrichs, K.; Choi, Y.H.; Varner, D.D.; Hartman, D.L. Production of cloned horse foals using roscovitine-treated donor cells and activation with sperm extract and/or ionomycin. *Reproduction* **2007**, *134*, 319–325. [CrossRef] [PubMed]

46. Olivera, R.; Moro, L.N.; Jordan, R.; Pallarols, N.; Guglielminetti, A.; Luzzani, C.; Miriuka, S.G.; Vichera, G. Bone marrow mesenchymal stem cells as nuclear donors improve viability and health of cloned horses. *Stem Cells Cloning* **2018**, *11*, 13–22. [CrossRef]

47. Woods, G.L.; White, K.L.; Vanderwall, D.K.; Li, G.P.; Aston, K.I.; Bunch, T.D.; Meerdo, L.N.; Pate, B.J. A mule cloned from fetal cells by nuclear transfer. *Science* **2003**, *301*, 1063. [CrossRef]

48. Shi, D.; Lu, F.; Wei, Y.; Cui, K.; Yang, S.; Wei, J.; Liu, Q. Buffalos (*Bubalus bubalis*) cloned by nuclear transfer of somatic cells. *Biol. Reprod.* **2007**, *77*, 285–291. [CrossRef] [PubMed]

49. Lu, F.; Luo, C.; Li, N.; Liu, Q.; Wei, Y.; Deng, H.; Wang, X.; Li, X.; Jiang, J.; Deng, Y.; et al. Efficient generation of transgenic buffalos (*Bubalus bubalis*) by nuclear transfer of fetal fibroblasts expressing enhanced green fluorescent protein. *Sci. Rep.* **2018**, *8*, 6967. [CrossRef]

50. Yang, B.Z.; Yang, C.Y.; Li, R.C.; Qin, G.S.; Zhang, X.F.; Pang, C.Y.; Chen, M.T.; Huang, F.X.; Li, Z.; Zheng, H.Y.; et al. An inter-subspecies cloned buffalo (*Bubalus bubalis*) obtained by transferring of cryopreserved embryos via somatic cell nuclear transfer. *Reprod. Domest. Anim.* **2010**, *45*, e21–e25. [CrossRef]

51. Madheshiya, P.K.; Sahare, A.A.; Jyotsana, B.; Singh, K.P.; Saini, M.; Raja, A.K.; Kaith, S.; Singla, S.K.; Chauhan, M.S.; Manik, R.S.; et al. Production of a cloned buffalo (*Bubalus bubalis*) calf from somatic cells isolated from urine. *Cell. Reprogram.* **2015**, *17*, 160–169. [CrossRef]

52. Saini, M.; Selokar, N.L.; Palta, P.; Chauhan, M.S.; Manik, R.S.; Singla, S.K. An update: Reproductive handmade cloning of water buffalo (*Bubalus bubalis*). *Anim. Reprod. Sci.* **2018**, *197*, 1–9. [CrossRef] [PubMed]

53. Selokar, N.L.; Sharma, P.; Saini, M.; Sheoran, S.; Rajendran, R.; Kumar, D.; Sharma, R.K.; Motiani, R.K.; Kumar, P.; Jerome, A.; et al. Successful cloning of a superior buffalo bull. *Sci. Rep.* **2019**, *9*, 11366. [CrossRef]

54. Wani, N.A.; Wernery, U.; Hassan, F.A.; Wernery, R.; Skidmore, J.A. Production of the first cloned camel by somatic cell nuclear transfer. *Biol. Reprod.* **2010**, *82*, 373–379. [CrossRef] [PubMed]

55. Wani, N.A.; Hong, S.B. Source, treatment and type of nuclear donor cells influences in vitro and in vivo development of embryos cloned by somatic cell nuclear transfer in camel (*Camelus dromedarius*). *Theriogenology* **2018**, *106*, 186–191. [CrossRef]

56. Wani, N.A.; Hong, S.; Vettical, B.S. Cytoplast source influences development of somatic cell nuclear transfer (SCNT) embryos in vitro but not their development to term after transfer to synchronized recipients in dromedary camels (*Camelus dromedarius*). *Theriogenology* **2018**, *118*, 137–143. [CrossRef] [PubMed]

57. Wani, N.A.; Vettical, B.S.; Hong, S.B. First cloned Bactrian camel (*Camelus bactrianus*) calf produced by interspecies somatic cell nuclear transfer: A step towards preserving the critically endangered wild Bactrian camels. *PLoS ONE* **2017**, *12*, e0177800. [CrossRef] [PubMed]

58. Shin, T.; Kraemer, D.; Pryor, J.; Liu, L.; Rugila, J.; Howe, I.; Buck, S.; Murphy, K.; Westhusin, M. A cat cloned by nuclear transplantation. *Nature* **2002**, *415*, 859. [CrossRef]

59. Choi, E.G.; Yin, X.J.; Lee, H.S.; Kim, L.H.; Shin, H.D.; Kim, N.H.; Kong, I.K. Reproductive fertility of cloned male cats derived from adult somatic cell nuclear transfer. *Cloning Stem Cells* **2007**, *9*, 281–290. [CrossRef] [PubMed]

60. Yin, X.J.; Lee, H.S.; Lee, Y.H.; Seo, Y.I.; Jeon, S.J.; Choi, E.G.; Cho, S.J.; Cho, S.G.; Min, W.; Kang, S.K.; et al. Cats cloned from fetal and adult somatic cells by nuclear transfer. *Reproduction* **2005**, *129*, 245–249. [CrossRef] [PubMed]

61. Yin, X.J.; Lee, H.S.; Yu, X.F.; Kim, L.H.; Shin, H.D.; Cho, S.J.; Choi, E.G.; Kong, I.K. Production of second-generation cloned cats by somatic cell nuclear transfer. *Theriogenology* **2008**, *69*, 1001–1006. [CrossRef]

62. Yin, X.J.; Lee, H.S.; Yu, X.F.; Choi, E.; Koo, B.C.; Kwon, M.S.; Lee, Y.S.; Cho, S.J.; Jin, G.Z.; Kim, L.H.; et al. Generation of cloned transgenic cats expressing red fluorescence protein. *Biol. Reprod.* **2008**, *78*, 425–431. [CrossRef]

63. Song, S.H.; Lee, K.L.; Xu, L.; Joo, M.D.; Hwang, J.Y.; Oh, S.H.; Kong, I.K. Production of cloned cats using additional complimentary cytoplasm. *Anim. Reprod. Sci.* **2019**, *208*, 106125. [CrossRef]

64. Lee, B.C.; Kim, M.K.; Jang, G.; Oh, H.J.; Yuda, F.; Kim, H.J.; Shamim, M.H.; Kim, J.J.; Kang, S.K.; Schatten, G.; et al. Dogs cloned from adult somatic cells. *Nature* **2005**, *436*, 641. [CrossRef]

65. Jang, G.; Kim, M.K.; Oh, H.J.; Hossein, M.S.; Fibrianto, Y.H.; Hong, S.G.; Park, J.E.; Kim, J.J.; Kim, H.J.; Kang, S.K.; et al. Birth of viable female dogs produced by somatic cell nuclear transfer. *Theriogenology* **2007**, *67*, 941–947. [CrossRef] [PubMed]

66. Jang, G.; Oh, H.J.; Kim, M.K.; Fibrianto, Y.H.; Hossein, M.S.; Kim, H.J.; Kim, J.J.; Hong, S.G.; Park, J.E.; Kang, S.K.; et al. Improvement of canine somatic cell nuclear transfer procedure. *Theriogenology* **2008**, *69*, 146–154. [CrossRef] [PubMed]

67. Jang, G.; Hong, S.G.; Oh, H.J.; Kim, M.K.; Park, J.E.; Kim, H.J.; Kim, D.Y.; Lee, B.C. A cloned toy poodle produced from somatic cells derived from an aged female dog. *Theriogenology* **2008**, *69*, 556–563. [CrossRef] [PubMed]

68. Hong, S.G.; Jang, G.; Kim, M.K.; Oh, H.J.; Park, J.E.; Kang, J.T.; Koo, O.J.; Kim, D.Y.; Lee, B.C. Dogs cloned from fetal fibroblasts by nuclear transfer. *Anim. Reprod. Sci.* **2009**, *115*, 334–339. [CrossRef]

69. Hossein, M.S.; Jeong, Y.W.; Park, S.W.; Kim, J.J.; Lee, E.; Ko, K.H.; Kim, H.S.; Kim, Y.W.; Hyun, S.H.; Shin, T.; et al. Cloning Missy: Obtaining multiple offspring of a specific canine genotype by somatic cell nuclear transfer. *Cloning Stem Cells* **2009**, *11*, 123–130. [CrossRef]

70. Ock, S.A.; Choi, I.; Im, G.S.; Yoo, J.G. Whole blood transcriptome analysis for lifelong monitoring in elite sniffer dogs produced by somatic cell nuclear transfer. *Cell. Reprogram.* **2019**, *21*, 301–313. [CrossRef] [PubMed]

71. Eun, K.; Hong, N.; Jeong, Y.W.; Park, M.G.; Hwang, S.U.; Jeong, Y.I.K.; Choi, E.J.; Olsson, P.O.; Hwang, W.S.; Hyun, S.H.; et al. Transcriptional activities of human elongation factor-1α and cytomegalovirus promoter in transgenic dogs generated by somatic cell nuclear transfer. *PLoS ONE* **2020**, *15*, e0233784. [CrossRef] [PubMed]

72. Li, Z.; Sun, X.; Chen, J.; Liu, X.; Wisely, S.M.; Zhou, Q.; Renard, J.P.; Leno, G.H.; Engelhardt, J.F. Cloned ferrets produced by somatic cell nuclear transfer. *Dev. Biol.* **2006**, *293*, 439–448. [CrossRef]

73. Chesné, P.; Adenot, P.G.; Viglietta, C.; Baratte, M.; Boulanger, L.; Renard, J.P. Cloned rabbits produced by nuclear transfer from adult somatic cells. *Nat. Biotechnol.* **2002**, *20*, 366–369. [CrossRef]

74. Skrzyszowska, M.; Smorąg, Z.; Słomski, R.; Kątska-Książkiewicz, L.; Kalak, R.; Michalak, E.; Wielgus, K.; Lehmann, J.; Lipiński, D.; Szalata, M.; et al. Generation of transgenic rabbits by the novel technique of chimeric somatic cell cloning. *Biol. Reprod.* **2006**, *74*, 1114–1120. [CrossRef] [PubMed]

75. Li, S.; Chen, X.; Fang, Z.; Shi, J.; Sheng, H.Z. Rabbits generated from fibroblasts through nuclear transfer. *Reproduction* **2006**, *131*, 1085–1090. [CrossRef]

76. Li, S.; Guo, Y.; Shi, J.; Yin, C.; Xing, F.; Xu, L.; Zhang, C.; Liu, T.; Li, Y.; Li, H.; et al. Transgene expression of enhanced green fluorescent protein in cloned rabbits generated from in vitro-transfected adult fibroblasts. *Transgenic Res.* **2009**, *18*, 227–235. [CrossRef] [PubMed]

77. Meng, Q.; Polgar, Z.; Liu, J.; Dinnyes, A. Live birth of somatic cell-cloned rabbits following trichostatin A treatment and cotransfer of parthenogenetic embryos. *Cloning Stem Cells* **2009**, *11*, 203–208. [CrossRef]

78. Yin, M.; Jiang, W.; Fang, Z.; Kong, P.; Xing, F.; Li, Y.; Chen, X.; Li, S. Generation of hypoxanthine phosphoribosyltransferase gene knockout rabbits by homologous recombination and gene trapping through somatic cell nuclear transfer. *Sci. Rep.* **2015**, *5*, 16023. [CrossRef] [PubMed]

79. Ono, Y.; Shimozawa, N.; Ito, M.; Kono, T. Cloned mice from fetal fibroblast cells arrested at metaphase by a serial nuclear transfer. *Biol. Reprod.* **2001**, *64*, 44–50. [CrossRef]

80. Wakayama, T.; Perry, A.C.; Zuccotti, M.; Johnson, K.R.; Yanagimachi, R. Full-term development of mice from enucleated oocytes injected with cumulus cell nuclei. *Nature* **1998**, *394*, 369–374. [CrossRef]

81. Wakayama, S.; Ohta, H.; Hikichi, T.; Mizutani, E.; Iwaki, T.; Kanagawa, O.; Wakayama, T. Production of healthy cloned mice from bodies frozen at −20 °C for 16 years. *Proc. Natl. Acad. Sci. USA* **2008**, *105*, 17318–17322. [CrossRef]

82. Mizutani, E.; Oikawa, M.; Kassai, H.; Inoue, K.; Shiura, H.; Hirasawa, R.; Kamimura, S.; Matoba, S.; Ogonuki, N.; Nagatomo, H.; et al. Generation of cloned mice from adult neurons by direct nuclear transfer. *Biol. Reprod.* **2015**, *92*, 81. [CrossRef]

83. Tanabe, Y.; Kuwayama, H.; Wakayama, S.; Nagatomo, H.; Ooga, M.; Kamimura, S.; Kishigami, S.; Wakayama, T. Production of cloned mice using oocytes derived from ICR-outbred strain. *Reproduction* **2017**, *154*, 859–866. [CrossRef]

84. Azuma, R.; Miyamoto, K.; Oikawa, M.; Yamada, M.; Anzai, M. Combinational treatment of trichostatin A and vitamin C improves the efficiency of cloning mice by somatic cell nuclear transfer. *J. Vis. Exp.* **2018**, *134*, 57036. [CrossRef]

85. Zhou, Q.; Renard, J.P.; Le Friec, G.; Brochard, V.; Beaujean, N.; Cherifi, Y.; Fraichard, A.; Cozzi, J. Generation of fertile cloned rats by regulating oocyte activation. *Science* **2003**, *302*, 1179. [CrossRef]

86. Lanza, R.P.; Cibelli, J.B.; Diaz, F.; Moraes, C.T.; Farin, P.W.; Farin, C.E.; Hammer, C.J.; West, M.D.; Damiani, P. Cloning of an endangered species (*Bos gaurus*) using interspecies nuclear transfer. *Cloning* **2000**, *2*, 79–90. [CrossRef] [PubMed]

87. Srirattana, K.; Imsoonthornruksa, S.; Laowtammathron, C.; Sangmalee, A.; Tunwattana, W.; Thongprapai, T.; Chaimongkol, C.; Ketudat-Cairns, M.; Parnpai, R. Full-term development of gaur-bovine interspecies somatic cell nuclear transfer embryos: Effect of trichostatin a treatment. *Cell. Reprogram.* **2012**, *14*, 248–257. [CrossRef] [PubMed]

88. Loi, P.; Ptak, G.; Barboni, B.; Fulka, J., Jr.; Cappai, P.; Clinton, M. Genetic rescue of an endangered mammal by cross-species nuclear transfer using *post-mortem* somatic cells. *Nat. Biotechnol.* **2001**, *19*, 962–964. [CrossRef]

89. Berg, D.K.; Li, C.; Asher, G.; Wells, D.N.; Oback, B. Red deer cloned from antler stem cells and their differentiated progeny. *Biol. Reprod.* **2007**, *77*, 384–394. [CrossRef] [PubMed]

90. Gómez, M.C.; Pope, C.E.; Giraldo, A.; Lyons, L.A.; Harris, R.F.; King, A.L.; Cole, A.; Godke, R.A.; Dresser, B.L. Birth of African Wildcat cloned kittens born from domestic cats. *Cloning Stem Cells* **2004**, *6*, 247–258. [CrossRef]

91. Gómez, M.C.; Pope, C.E.; Kutner, R.H.; Ricks, D.M.; Lyons, L.A.; Ruhe, M.; Dumas, C.; Lyons, J.; López, M.; Dresser, B.L.; et al. Nuclear transfer of sand cat cells into enucleated domestic cat oocytes is affected by cryopreservation of donor cells. *Cloning Stem Cells* **2008**, *10*, 469–483. [CrossRef]

92. Kim, M.K.; Jang, G.; Oh, H.J.; Yuda, F.; Kim, H.J.; Hwang, W.S.; Hossein, M.S.; Kim, J.J.; Shin, N.S.; Kang, S.K.; et al. Endangered wolves cloned from adult somatic cells. *Cloning Stem Cells* **2007**, *9*, 130–137. [CrossRef] [PubMed]

93. Oh, H.J.; Kim, M.K.; Jang, G.; Kim, H.J.; Hong, S.G.; Park, J.E.; Park, K.; Park, C.; Sohn, S.H.; Kim, D.Y.; et al. Cloning endangered gray wolves (*Canis lupus*) from somatic cells collected postmortem. *Theriogenology* **2008**, *70*, 638–647. [CrossRef] [PubMed]

94. Hwang, I.; Jeong, Y.W.; Kim, J.J.; Lee, H.J.; Kang, M.; Park, K.B.; Park, J.H.; Kim, Y.W.; Kim, W.T.; Shin, T.; et al. Successful cloning of coyotes through interspecies somatic cell nuclear transfer using domestic dog oocytes. *Reprod. Fertil. Dev.* **2013**, *25*, 1142–1148. [CrossRef]

95. Liu, Z.; Cai, Y.; Wang, Y.; Nie, Y.; Zhang, C.; Xu, Y.; Zhang, X.; Lu, Y.; Wang, Z.; Poo, M.; et al. Cloning of macaque monkeys by somatic cell nuclear transfer. *Cell* **2018**, *172*, 881–887.e7. [CrossRef] [PubMed]

96. Folch, J.; Cocero, M.J.; Chesné, P.; Alabart, J.L.; Domínguez, V.; Cognié, Y.; Roche, A.; Fernández-Arias, A.; Martí, J.I.; Sánchez, P.; et al. First birth of an animal from an extinct subspecies (*Capra pyrenaica pyrenaica*) by cloning. *Theriogenology* **2009**, *71*, 1026–1034. [CrossRef]

97. Niemann, H.; Wrenzycki, C.; Lucas-Hahn, A.; Brambrink, T.; Kues, W.A.; Carnwath, J.W. Gene expression patterns in bovine in vitro-produced and nuclear transfer-derived embryos and their implications for early development. *Cloning Stem Cells* **2002**, *4*, 29–38. [CrossRef]

98. Kurome, M.; Fujimura, T.; Murakami, H.; Takahagi, Y.; Wako, N.; Ochiai, T.; Miyazaki, K.; Nagashima, H. Comparison of electro-fusion and intracytoplasmic nuclear injection methods in pig cloning. *Cloning Stem Cells* **2003**, *5*, 367–378. [CrossRef] [PubMed]

99. Martinez-Diaz, M.A.; Che, L.; Albornoz, M.; Seneda, M.M.; Collis, D.; Coutinho, A.R.; El-Beirouthi, N.; Laurin, D.; Zhao, X.; Bordignon, V. Pre- and postimplantation development of swine-cloned embryos derived from fibroblasts and bone marrow cells after inhibition of histone deacetylases. *Cell. Reprogram.* **2010**, *12*, 85–94. [CrossRef] [PubMed]

100. Samiec, M.; Opiela, J.; Lipiński, D.; Romanek, J. Trichostatin A-mediated epigenetic transformation of adult bone marrow-derived mesenchymal stem cells biases the in vitro developmental capability, quality, and pluripotency extent of porcine cloned embryos. *Biomed. Res. Int.* **2015**, *2015*, 814686. [CrossRef]

101. Samiec, M.; Romanek, J.; Lipiński, D.; Opiela, J. Expression of pluripotency-related genes is highly dependent on trichostatin A-assisted epigenomic modulation of porcine mesenchymal stem cells analysed for apoptosis and subsequently used for generating cloned embryos. *Anim. Sci. J.* **2019**, *90*, 1127–1141. [CrossRef] [PubMed]

102. Lee, J.W.; Wu, S.C.; Tian, X.C.; Barber, M.; Hoagland, T.; Riesen, J.; Lee, K.H.; Tu, C.F.; Cheng, W.T.K.; Yang, X. Production of cloned pigs by whole-cell intracytoplasmic microinjection. *Biol. Reprod.* **2003**, *69*, 995–1001. [CrossRef]

103. Jiang, M.X.; Yang, C.X.; Zhang, L.S.; Zheng, Y.L.; Liu, S.Z.; Sun, Q.Y.; Chen, D.Y. The effects of chemical enucleation combined with whole cell intracytoplasmic injection on panda-rabbit interspecies nuclear transfer. *Zygote* **2004**, *12*, 315–320. [CrossRef] [PubMed]

104. Kawano, K.; Kato, Y.; Tsunoda, Y. Comparison of in vitro development of porcine nuclear-transferred oocytes receiving fetal somatic cells by injection and fusion methods. *Cloning Stem Cells* **2004**, *6*, 67–72. [CrossRef] [PubMed]

105. Samiec, M.; Skrzyszowska, M. Biological transcomplementary activation as a novel and effective strategy applied to the generation of porcine somatic cell cloned embryos. *Reprod. Biol.* **2014**, *14*, 128–139. [CrossRef]

106. Samiec, M. The role of mitochondrial genome (mtDNA) in somatic and embryo cloning of mammals. A review. *J. Anim. Feed Sci.* **2005**, *14*, 213–233. [CrossRef]

107. Samiec, M.; Skrzyszowska, M. Microsurgical nuclear transfer by intraooplasmic karyoplast injection as an alternative embryo reconstruction method in somatic cloning of pigs and other mammal species; application value of the method and its technical advantages: A review. *Czech J. Anim. Sci.* **2005**, *50*, 235–242. [CrossRef]

108. Samiec, M.; Skrzyszowska, M. Intrinsic and extrinsic molecular determinants or modulators for epigenetic remodeling and reprogramming of somatic cell-derived genome in mammalian nuclear-transferred oocytes and resultant embryos. *Pol. J. Vet. Sci.* **2018**, *21*, 217–227. [PubMed]

109. Lacham-Kaplan, O.; Diamente, M.; Pushett, D.; Lewis, I.; Trounson, A. Developmental competence of nuclear transfer cow oocytes after direct injection of fetal fibroblast nuclei. *Cloning* **2000**, *2*, 55–62. [CrossRef]

110. Galli, C.; Lagutina, I.; Vassiliev, I.; Duchi, R.; Lazzari, G. Comparison of microinjection (piezo-electric) and cell fusion for nuclear transfer success with different cell types in cattle. *Cloning Stem Cells* **2002**, *4*, 189–196. [CrossRef]

111. Samiec, M.; Skrzyszowska, M. Molecular conditions of the cell nucleus remodelling/reprogramming process and nuclear-transferred embryo development in the intraooplasmic karyoplast injection technique: A review. *Czech J. Anim. Sci.* **2005**, *50*, 185–195. [CrossRef]

112. Samiec, M.; Skrzyszowska, M. Assessment of in vitro developmental capacity of porcine nuclear-transferred embryos reconstituted with cumulus oophorus cells undergoing vital diagnostics for apoptosis detection. *Ann. Anim. Sci.* **2013**, *13*, 513–529. [CrossRef]

113. Skrzyszowska, M.; Karasiewicz, J.; Bednarczyk, M.; Samiec, M.; Smorąg, Z.; Waś, B.; Guszkiewicz, A.; Korwin-Kossakowski, M.; Górniewska, M.; Szablisty, E.; et al. Generation of cloned and chimeric embryos/offspring using the new methods of animal biotechnology. *Reprod. Biol.* **2006**, *6* (Suppl. 1), 119–135.

114. Wilmut, I.; Beaujean, N.; de Sousa, P.A.; Dinnyes, A.; King, T.J.; Paterson, L.A.; Wells, D.N.; Young, L.E. Somatic cell nuclear transfer. *Nature* **2002**, *419*, 583–586. [CrossRef]

115. Dean, W.; Santos, F.; Reik, W. Epigenetic reprogramming in early mammalian development and following somatic nuclear transfer. *Semin. Cell Dev. Biol.* **2003**, *14*, 93–100. [CrossRef]

116. Kang, Y.K.; Yeo, S.; Kim, S.H.; Koo, D.B.; Park, J.S.; Wee, G.; Han, J.S.; Oh, K.B.; Lee, K.K.; Han, Y.M. Precise recapitulation of methylation change in early cloned embryos. *Mol. Reprod. Dev.* **2003**, *66*, 32–37. [CrossRef]

117. Beaujean, N.; Taylor, J.; Gardner, J.; Wilmut, I.; Meehan, R.; Young, L. Effect of limited DNA methylation reprogramming in the normal sheep embryo on somatic cell nuclear transfer. *Biol. Reprod.* **2004**, *71*, 185–193. [CrossRef] [PubMed]

118. Samiec, M.; Skrzyszowska, M.; Bochenek, M. In vitro development of porcine nuclear-transferred embryos derived from fibroblast cells analysed cytometrically for apoptosis incidence and accuracy of cell cycle synchronization at the G0/G1 stages. *Ann. Anim. Sci.* **2013**, *13*, 735–752. [CrossRef]

119. Samiec, M.; Skrzyszowska, M.; Opiela, J. Creation of cloned pig embryos using contact-inhibited or serum-starved fibroblast cells analysed *intra vitam* for apoptosis occurrence. *Ann. Anim. Sci.* **2013**, *13*, 275–293. [CrossRef]

120. Opiela, J.; Samiec, M.; Romanek, J. In vitro development and cytological quality of inter-species (porcine→bovine) cloned embryos are affected by trichostatin A-dependent epigenomic modulation of adult mesenchymal stem cells. *Theriogenology* **2017**, *97*, 27–33. [CrossRef]

121. Cheong, H.T.; Ikeda, K.; Martinez Diaz, M.A.; Katagiri, S.; Takahashi, Y. Development of reconstituted pig embryos by nuclear transfer of cultured cumulus cells. *Reprod. Fertil. Dev.* **2000**, *12*, 15–20. [CrossRef] [PubMed]

122. Roh, S.; Hwang, W.S. In vitro development of porcine parthenogenetic and cloned embryos: Comparison of oocyte-activating techniques, various culture systems and nuclear transfer methods. *Reprod. Fertil. Dev.* **2002**, *14*, 93–99. [CrossRef]

123. Cezar, G.G.; Bartolomei, M.S.; Forsberg, E.J.; First, N.L.; Bishop, M.D.; Eilertsen, K.J. Genome-wide epigenetic alterations in cloned bovine fetuses. *Biol. Reprod.* **2003**, *68*, 1009–1014. [CrossRef]

124. Lee, J.; Inoue, K.; Ono, R.; Ogonuki, N.; Kohda, T.; Kaneko-Ishino, T.; Ogura, A.; Ishino, F. Erasing genomic imprinting memory in mouse clone embryos produced from day 11.5 primordial germ cells. *Development* **2003**, *129*, 1807–1817.

125. Shi, W.; Zakhartchenko, V.; Wolf, E. Epigenetic reprogramming in mammalian nuclear transfer. *Differentiation* **2003**, *71*, 91–113. [CrossRef] [PubMed]

126. Seki, Y.; Hayashi, K.; Itoh, K.; Mizugaki, M.; Saitou, M.; Matsui, Y. Extensive and orderly reprogramming of genome-wide chromatin modifications associated with specification and early development of germ cells in mice. *Dev. Biol.* **2005**, *278*, 440–458. [CrossRef] [PubMed]

127. Jin, L.; Guo, Q.; Zhang, G.L.; Xing, X.X.; Xuan, M.F.; Luo, Q.R.; Luo, Z.B.; Wang, J.X.; Yin, X.J.; Kang, J.D. The histone deacetylase inhibitor, CI994, improves nuclear reprogramming and in vitro developmental potential of cloned pig embryos. *Cell. Reprogram.* **2018**, *20*, 205–213. [CrossRef] [PubMed]

128. Campbell, K.H.; Alberio, R. Reprogramming the genome: Role of the cell cycle. *Reprod. Suppl.* **2003**, *61*, 477–494. [CrossRef]

129. Bang, J.I.; Yoo, J.G.; Park, M.R.; Shin, T.S.; Cho, B.W.; Lee, H.G.; Kim, B.W.; Kang, T.Y.; Kong, I.K.; Kim, J.H.; et al. The effects of artificial activation timing on the development of SCNT-derived embryos and newborn piglets. *Reprod. Biol.* **2013**, *13*, 127–132. [CrossRef]

130. Rybouchkin, A.; Kato, Y.; Tsunoda, Y. Role of histone acetylation in reprogramming of somatic nuclei following nuclear transfer. *Biol. Reprod.* **2006**, *74*, 1083–1089. [CrossRef]

131. Nashun, B.; Hill, P.W.; Hajkova, P. Reprogramming of cell fate: Epigenetic memory and the erasure of memories past. *EMBO J.* **2015**, *34*, 1296–1308. [CrossRef]

132. Saini, M.; Selokar, N.L. Approaches used to improve epigenetic reprogramming in buffalo cloned embryos. *Indian J. Med. Res.* **2018**, *148*, S115–S119. [PubMed]

133. Samiec, M. The effect of mitochondrial genome on architectural remodeling and epigenetic reprogramming of donor cell nuclei in mammalian nuclear transfer-derived embryos. *J. Anim. Feed Sci.* **2005**, *14*, 393–422. [CrossRef]

134. Srirattana, K.; Matsukawa, K.; Akagi, S.; Tasai, M.; Tagami, T.; Nirasawa, K.; Nagai, T.; Kanai, Y.; Parnpai, R.; Takeda, K. Constant transmission of mitochondrial DNA in intergeneric cloned embryos reconstructed from swamp buffalo fibroblasts and bovine ooplasm. *Anim. Sci. J.* **2011**, *82*, 236–243. [CrossRef] [PubMed]

135. Narbonne, P.; Miyamoto, K.; Gurdon, J.B. Reprogramming and development in nuclear transfer embryos and in interspecific systems. *Curr. Opin. Genet. Dev.* **2012**, *22*, 450–458. [CrossRef] [PubMed]

136. Takeda, K. Functional consequences of mitochondrial mismatch in reconstituted embryos and offspring. *J. Reprod. Dev.* **2019**, *65*, 485–489. [CrossRef]

137. Mann, M.R.W.; Chung, Y.G.; Nolen, L.D.; Verona, R.I.; Latham, K.E.; Bartolomei, M.S. Disruption of imprinted gene methylation and expression in cloned preimplantation stage mouse embryos. *Biol. Reprod.* **2003**, *69*, 902–914. [CrossRef]

138. Mann, M.R.W.; Lee, S.S.; Doherty, A.S.; Verona, R.I.; Nolen, L.D.; Schultz, R.M.; Bartolomei, M.S. Selective loss of imprinting in the placenta following preimplantation development in culture. *Development* **2004**, *131*, 3727–3735. [CrossRef]

139. Czernik, M.; Anzalone, D.A.; Palazzese, L.; Oikawa, M.; Loi, P. Somatic cell nuclear transfer: Failures, successes and the challenges ahead. *Int. J. Dev. Biol.* **2019**, *63*, 123–130. [CrossRef]

140. Lai, L.; Tao, T.; Macháty, Z.; Kühholzer, B.; Sun, Q.Y.; Park, K.W.; Day, B.N.; Prather, R.S. Feasibility of producing porcine nuclear transfer embryos by using G2/M-stage fetal fibroblasts as donors. *Biol. Reprod.* **2001**, *65*, 1558–1564. [CrossRef]

141. Lai, L.; Park, K.W.; Cheong, H.T.; Kühholzer, B.; Samuel, M.; Bonk, A.; Im, G.S.; Rieke, A.; Day, B.N.; Murphy, C.N.; et al. Transgenic pig expressing the enhanced green fluorescent protein produced by nuclear transfer using colchicine-treated fibroblasts as donor cells. *Mol. Reprod. Dev.* **2002**, *62*, 300–306. [CrossRef] [PubMed]

142. Lorthongpanich, C.; Solter, D.; Lim, C.Y. Nuclear reprogramming in zygotes. *Int. J. Dev. Biol.* **2010**, *54*, 1631–1640. [CrossRef] [PubMed]

143. Esteves, T.C.; Balbach, S.T.; Pfeiffer, M.J.; Araúzo-Bravo, M.J.; Klein, D.C.; Sinn, M.; Boiani, M. Somatic cell nuclear reprogramming of mouse oocytes endures beyond reproductive decline. *Aging Cell* **2011**, *10*, 80–95. [CrossRef] [PubMed]

144. Kungulovski, G.; Jeltsch, A. Epigenome editing: State of the art, concepts, and perspectives. *Trends Genet.* **2016**, *32*, 101–113. [CrossRef] [PubMed]

145. Eilertsen, K.J.; Power, R.A.; Harkins, L.L.; Misica, P. Targeting cellular memory to reprogram the epigenome, restore potential, and improve somatic cell nuclear transfer. *Anim. Reprod. Sci.* **2007**, *98*, 129–146. [CrossRef]

146. Whitworth, K.M.; Prather, R.S. Somatic cell nuclear transfer efficiency: How can it be improved through nuclear remodeling and reprogramming? *Mol. Reprod. Dev.* **2010**, *77*, 1001–1015. [CrossRef]

147. Mason, K.; Liu, Z.; Aguirre-Lavin, T.; Beaujean, N. Chromatin and epigenetic modifications during early mammalian development. *Anim. Reprod. Sci.* **2012**, *134*, 45–55. [CrossRef] [PubMed]

148. Armstrong, L.M.; Lako, W.; Dean, W.; Stojkovic, M. Epigenetic modification is central to genome reprogramming in somatic cell nuclear transfer. *Stem Cells* **2006**, *24*, 805–814. [CrossRef] [PubMed]

149. Corry, G.N.; Tanasijevic, B.; Barry, E.R.; Krueger, W.; Rasmussen, T.P. Epigenetic regulatory mechanisms during preimplantation development. *Birth Defects Res. C Embryo Today* **2009**, *87*, 297–313. [CrossRef] [PubMed]

150. Prather, R.S.; Ross, J.W.; Isom, S.C.; Green, J.A. Transcriptional, posttranscriptional and epigenetic control of porcine oocyte maturation and embryogenesis. *Soc. Reprod. Fertil. Suppl.* **2009**, *66*, 165–176.

151. Reik, W. Stability and flexibility of epigenetic gene regulation in mammalian development. *Nature* **2007**, *447*, 425–432. [CrossRef]

152. Yang, X.; Smith, S.L.; Tian, X.C.; Lewin, H.A.; Renard, J.P.; Wakayama, T. Nuclear reprogramming of cloned embryos and its implications for therapeutic cloning. *Nat. Genet.* **2007**, *39*, 295–302. [CrossRef] [PubMed]

153. Buganim, Y.; Faddah, D.A.; Jaenisch, R. Mechanisms and models of somatic cell reprogramming. *Nat. Rev. Genet.* **2013**, *14*, 427–439. [CrossRef]

154. Rodriguez-Osorio, N.; Urrego, R.; Cibelli, J.B.; Eilertsen, K.; Memili, E. Reprogramming mammalian somatic cells. *Theriogenology* **2012**, *78*, 1869–1886. [CrossRef] [PubMed]

155. Bowles, E.J.; Campbell, K.H.; St. John, J.C. Nuclear transfer: Preservation of a nuclear genome at the expense of its associated mtDNA genome(s). *Curr. Top. Dev. Biol.* **2007**, *77*, 251–290. [PubMed]

156. Lagutina, I.; Fulka, H.; Brevini, T.A.; Antonini, S.; Brunetti, D.; Colleoni, S.; Gandolfi, F.; Lazzari, G.; Fulka, J., Jr.; Galli, C. Development, embryonic genome activity and mitochondrial characteristics of bovine-pig inter-family nuclear transfer embryos. *Reproduction* **2010**, *140*, 273–285. [CrossRef]

157. St. John, J.C.; Srirattana, K.; Tsai, T.S.; Sun, X. The mitochondrial genome: How it drives fertility. *Reprod. Fertil. Dev.* **2017**, *30*, 118–139. [CrossRef]

158. Hiendleder, S. Mitochondrial DNA inheritance after SCNT. *Adv. Exp. Med. Biol.* **2007**, *591*, 103–116.

159. Takeda, K. Mitochondrial DNA transmission and confounding mitochondrial influences in cloned cattle and pigs. *Reprod. Med. Biol.* **2013**, *12*, 47–55. [CrossRef]

160. Burgstaller, J.P.; Schinogl, P.; Dinnyes, A.; Müller, M.; Steinborn, R. Mitochondrial DNA heteroplasmy in ovine fetuses and sheep cloned by somatic cell nuclear transfer. *BMC Dev. Biol.* **2007**, *7*, 141. [CrossRef] [PubMed]

161. Hua, S.; Lu, C.; Song, Y.; Li, R.; Liu, X.; Quan, F.; Wang, Y.; Liu, J.; Su, F.; Zhang, Y. High levels of mitochondrial heteroplasmy modify the development of ovine-bovine interspecies nuclear transferred embryos. *Reprod. Fertil. Dev.* **2012**, *24*, 501–509. [CrossRef]

162. Huang, X.; Song, L.; Zhan, Z.; Gu, H.; Feng, H.; Li, Y. Factors affecting mouse somatic cell nuclear reprogramming by rabbit ooplasms. *Cell. Reprogram.* **2017**, *19*, 344–353. [CrossRef] [PubMed]

163. Sansinena, M.J.; Lynn, J.; Bondioli, K.R.; Denniston, R.S.; Godke, R.A. Ooplasm transfer and interspecies somatic cell nuclear transfer: Heteroplasmy, pattern of mitochondrial migration and effect on embryo development. *Zygote* **2011**, *19*, 147–156. [CrossRef]

164. Kwon, D.; Koo, O.J.; Kim, M.J.; Jang, G.; Lee, B.C. Nuclear-mitochondrial incompatibility in interorder rhesus monkey-cow embryos derived from somatic cell nuclear transfer. *Primates* **2016**, *57*, 471–478. [CrossRef]

165. Takeda, K.; Kaneyama, K.; Tasai, M.; Akagi, S.; Takahashi, S.; Yonai, M.; Kojima, T.; Onishi, A.; Tagami, T.; Nirasawa, K.; et al. Characterization of a donor mitochondrial DNA transmission bottleneck in nuclear transfer derived cow lineages. *Mol. Reprod. Dev.* **2008**, *75*, 759–765. [CrossRef] [PubMed]

166. Yan, Z.H.; Zhou, Y.Y.; Fu, J.; Jiao, F.; Zhao, L.W.; Guan, P.F.; Huang, S.Z.; Zeng, Y.T.; Zeng, F. Donor-host mitochondrial compatibility improves efficiency of bovine somatic cell nuclear transfer. *BMC Dev. Biol.* **2010**, *10*, 31. [CrossRef]

167. Yan, H.; Yan, Z.; Ma, Q.; Jiao, F.; Huang, S.; Zeng, F.; Zeng, Y. Association between mitochondrial DNA haplotype compatibility and increased efficiency of bovine intersubspecies cloning. *J. Genet. Genom.* **2011**, *38*, 21–28. [CrossRef] [PubMed]

168. Srirattana, K.; St. John, J.C. Manipulating the mitochondrial genome to enhance cattle embryo development. *G3 (Bethesda)* **2017**, *7*, 2065–2080. [CrossRef] [PubMed]

169. Hiendleder, S.; Prelle, K.; Brüggerhoff, K.; Reichenbach, H.D.; Wenigerkind, H.; Bebbere, D.; Stojkovic, M.; Müller, S.; Brem, G.; Zakhartchenko, V.; et al. Nuclear-cytoplasmic interactions affect in utero developmental capacity, phenotype, and cellular metabolism of bovine nuclear transfer fetuses. *Biol. Reprod.* **2004**, *70*, 1196–1205. [CrossRef]

170. Ma, L.B.; Yang, L.; Hua, S.; Cao, J.W.; Li, J.X.; Zhang, Y. Development in vitro and mitochondrial fate of interspecies cloned embryos. *Reprod. Domest. Anim.* **2008**, *43*, 279–285. [CrossRef]

171. Imsoonthornruksa, S.; Srirattana, K.; Phewsoi, W.; Tunwattana, W.; Parnpai, R.; Ketudat-Cairns, M. Segregation of donor cell mitochondrial DNA in gaur-bovine interspecies somatic cell nuclear transfer embryos, fetuses and an offspring. *Mitochondrion* **2012**, *12*, 506–513. [CrossRef]

172. Choi, Y.H.; Ritthaler, J.; Hinrichs, H. Production of a mitochondrial-DNA identical cloned foal using oocytes recovered from immature follicles of selected mares. *Theriogenology* **2014**, *82*, 411–417. [CrossRef] [PubMed]

173. Gómez, M.C.; Pope, C.E.; Ricks, D.M.; Lyons, J.; Dumas, C.; Dresser, B.L. Cloning endangered felids using heterospecific donor oocytes and interspecies embryo transfer. *Reprod. Fertil. Dev.* **2009**, *21*, 76–82. [CrossRef] [PubMed]

174. Magalhães, L.C.; Cortez, J.V.; Bhat, M.H.; Sampaio, A.C.N.P.C.; Freitas, J.L.S.; Duarte, J.M.B.; Melo, L.M.; Freitas, V.J.F. In vitro development and mitochondrial gene expression in brown brocket deer (*Mazama gouazoubira*) embryos obtained by interspecific somatic cell nuclear transfer. *Cell Reprogram.* **2020**, *22*, 208–216. [CrossRef]

175. Yamochi, T.; Kida, Y.; Oh, N.; Ohta, S.; Amano, T.; Anzai, M.; Kato, H.; Kishigami, S.; Mitani, T.; Matsumoto, K.; et al. Development of interspecies cloned embryos reconstructed with rabbit (*Oryctolagus cuniculus*) oocytes and cynomolgus monkey (*Macaca fascicularis*) fibroblast cell nuclei. *Zygote* **2013**, *21*, 358–366. [CrossRef]

176. Amarnath, D.; Choi, I.; Moawad, A.R.; Wakayama, T.; Campbell, K.H. Nuclear-cytoplasmic incompatibility and inefficient development of pig-mouse cytoplasmic hybrid embryos. *Reproduction* **2011**, *142*, 295–307. [CrossRef]

177. Lee, J.H.; Peters, A.; Fisher, P.; Bowles, E.J.; St. John, J.C.; Campbell, K.H. Generation of mtDNA homoplasmic cloned lambs. *Cell. Reprogram.* **2010**, *12*, 347–355. [CrossRef]

178. Shiels, P.G.; Kind, A.J.; Campbell, K.H.S.; Waddington, D.; Wilmut, I.; Colman, A.; Schnieke, A.E. Analysis of telomere lengths in cloned sheep. *Nature* **1999**, *399*, 316–317. [CrossRef]

179. Tian, X.C.; Xu, J.; Yang, X. Normal telomere lengths found in cloned cattle. *Nat. Genet.* **2000**, *26*, 272–273. [CrossRef]

180. Jeon, H.Y.; Hyun, S.H.; Lee, G.S.; Kim, H.S.; Kim, S.; Jeong, Y.W.; Kang, S.K.; Lee, B.C.; Han, J.Y.; Ahn, C.; et al. The analysis of telomere length and telomerase activity in cloned pigs and cows. *Mol. Reprod. Dev.* **2005**, *71*, 315–320. [CrossRef] [PubMed]

181. Kurome, M.; Hisatomi, H.; Matsumoto, S.; Tomii, R.; Ueno, S.; Hiruma, K.; Saito, H.; Nakamura, K.; Okumura, K.; Matsumoto, M.; et al. Production efficiency and telomere length of the cloned pigs following serial somatic cell nuclear transfer. *J. Reprod. Dev.* **2008**, *54*, 254–258. [CrossRef]

182. Gomes, N.M.; Ryder, O.A.; Houck, M.L.; Charter, S.J.; Walker, W.; Forsyth, N.R.; Austad, S.N.; Venditti, C.; Pagel, M.; Shay, J.W.; et al. Comparative biology of mammalian telomeres: Hypotheses on ancestral states and the roles of telomeres in longevity determination. *Aging Cell* **2011**, *10*, 761–768. [CrossRef]

183. Xu, J.; Yang, X. Telomerase activity in early bovine embryos derived from parthenogenetic activation and nuclear transfer. *Biol. Reprod.* **2001**, *64*, 770–774. [CrossRef]

184. Cui, W.; Wylie, D.; Aslam, S.; Dinnyes, A.; King, T.; Wilmut, I.; Clark, A.J. Telomerase-immortalized sheep fibroblasts can be reprogrammed by nuclear transfer to undergo early development. *Biol. Reprod.* **2003**, *69*, 15–21. [CrossRef]

185. Jiang, L.; Carter, D.B.; Xu, J.; Yang, X.; Prather, R.S.; Tian, X.C. Telomere lengths in cloned transgenic pigs. *Biol. Reprod.* **2004**, *70*, 1589–1593. [CrossRef]

186. Miyashita, N.; Shiga, K.; Yonai, M.; Kaneyama, K.; Kobayashi, S.; Kojima, T.; Goto, Y.; Kishi, M.; Aso, H.; Suzuki, T.; et al. Remarkable differences in telomere lengths among cloned cattle derived from different cell types. *Biol. Reprod.* **2002**, *66*, 1649–1655. [CrossRef]

187. Kishigami, S.; Wakayama, S.; Hosoi, Y.; Iritani, A.; Wakayama, T. Somatic cell nuclear transfer: Infinite reproduction of a unique diploid genome. *Exp. Cell Res.* **2008**, *314*, 1945–1950. [CrossRef] [PubMed]

188. Le, R.; Kou, Z.; Jiang, Y.; Li, M.; Huang, B.; Liu, W.; Li, H.; Kou, X.; He, W.; Rudolph, K.L.; et al. Enhanced telomere rejuvenation in pluripotent cells reprogrammed via nuclear transfer relative to induced pluripotent stem cells. *Cell Stem Cell* **2014**, *14*, 27–39. [CrossRef] [PubMed]

189. Huili, J.; Haosheng, L.; Dengke, P. Epigenetic reprogramming by somatic cell nuclear transfer: Questions and potential solutions. *Yi Chuan* **2014**, *36*, 1211–1218. [PubMed]

190. Bekaert, S.; Derradji, H.; Baatout, S. Telomere biology in mammalian germ cells and during development. *Dev. Biol.* **2004**, *274*, 15–30. [CrossRef] [PubMed]

191. Schaetzlein, S.; Rudolph, K.L. Telomere length regulation during cloning, embryogenesis and ageing. *Reprod. Fertil. Dev.* **2005**, *17*, 85–96. [CrossRef]

192. Kong, Q.; Ji, G.; Xie, B.; Li, J.; Mao, J.; Wang, J.; Liu, S.; Liu, L.; Liu, Z. Telomere elongation facilitated by trichostatin A in cloned embryos and pigs by somatic cell nuclear transfer. *Stem Cell Rev.* **2014**, *10*, 399–407. [CrossRef] [PubMed]

193. Betts, D.H.; Perrault, S.; Harrington, L.; King, W.A. Quantitative analysis of telomerase activity and telomere length in domestic animal clones. *Methods Mol. Biol.* **2006**, *325*, 149–180.

194. Lanza, R.P.; Cibelli, J.B.; Blackwell, C.; Cristofalo, V.J.; Francis, M.K.; Baerlocher, G.M.; Mak, J.; Schertzer, M.; Chavez, E.A.; Sawyer, N.; et al. Extension of cell life-span and telomere length in animals cloned from senescent somatic cells. *Science* **2000**, *288*, 665–669. [CrossRef] [PubMed]

195. Kühholzer-Cabot, B.; Brem, G. Aging of animals produced by somatic cell nuclear transfer. *Exp. Gerontol.* **2002**, *37*, 1317–1323. [CrossRef]

196. Burgstaller, J.P.; Brem, G. Aging of cloned animals: A mini-review. *Gerontology* **2017**, *63*, 417–425. [CrossRef]

197. Kim, H.M.; Cho, Y.S.; Kim, H.; Jho, S.; Son, B.; Choi, J.Y.; Kim, S.; Lee, B.C.; Bhak, J.; Jang, G. Whole genome comparison of donor and cloned dogs. *Sci. Rep.* **2013**, *3*, 2998. [CrossRef]

198. Jeon, H.Y.; Jeong, Y.W.; Kim, Y.W.; Jeong, Y.I.; Hossein, S.M.; Yang, H.; Hyun, S.H.; Jeung, E.B.; Hwang, W.S. Senescence is accelerated through donor cell specificity in cloned pigs. *Int. J. Mol. Med.* **2012**, *30*, 383–391. [CrossRef] [PubMed]

199. Dang-Nguyen, T.Q.; Haraguchi, S.; Akagi, S.; Somfai, T.; Kaneda, M.; Watanabe, S.; Kikuchi, K.; Tajima, A.; Nagai, T. Telomere elongation during morula-to-blastocyst transition in cloned porcine embryos. *Cell. Reprogram.* **2012**, *14*, 514–519. [CrossRef]

200. Betts, D.; Bordignon, V.; Hill, J.; Winger, Q.; Westhusin, M.; Smith, L.; King, W. Reprogramming of telomerase activity and rebuilding of telomere length in cloned cattle. *Proc. Natl. Acad. Sci. USA* **2001**, *98*, 1077–1082. [CrossRef]

201. Imsoonthornruksa, S.; Sangmalee, A.; Srirattana, K.; Parnpai, R.; Ketudat-Cairns, M. Development of intergeneric and intrageneric somatic cell nuclear transfer (SCNT) cat embryos and the determination of telomere length in cloned offspring. *Cell. Reprogram.* **2012**, *14*, 79–87. [CrossRef]

202. Kato, Y.; Tani, T.; Tsunoda, Y. Cloning of calves from various somatic cell types of male and female adult, newborn and fetal cows. *J. Reprod. Fertil.* **2000**, *120*, 231–237. [CrossRef] [PubMed]

203. Samiec, M.; Skrzyszowska, M. Can reprogramming of overall epigenetic memory and specific parental genomic imprinting memory within donor cell-inherited nuclear genome be a major hindrance for the somatic cell cloning of mammals?—A review. *Ann. Anim. Sci.* **2018**, *18*, 623–638. [CrossRef]

204. Tessanne, K.; Golding, M.C.; Long, C.R.; Peoples, M.D.; Hannon, G.; Westhusin, M.E. Production of transgenic calves expressing an shRNA targeting myostatin. *Mol. Reprod. Dev.* **2012**, *79*, 176–185. [CrossRef] [PubMed]

205. Wang, Y.; Zhao, S.; Bai, L.; Fan, J.; Liu, E. Expression systems and species used for transgenic animal bioreactors. *Biomed Res. Int.* **2013**, *2013*, 580463. [CrossRef]

206. Lu, D.; Liu, S.; Ding, F.; Wang, H.; Li, J.; Li, L.; Dai, Y.; Li, N. Large-scale production of functional human lysozyme from marker-free transgenic cloned cows. *Sci. Rep.* **2016**, *6*, 22947. [CrossRef]

207. Guo, Y.; Li, H.; Wang, Y.; Yan, X.; Sheng, X.; Chang, D.; Qi, X.; Wang, X.; Liu, Y.; Li, J.; et al. Screening somatic cell nuclear transfer parameters for generation of transgenic cloned cattle with intragenomic integration of additional gene copies that encode bovine adipocyte-type fatty acid-binding protein (A-FABP). *Mol. Biol. Rep.* **2017**, *44*, 159–168. [CrossRef]

208. Proudfoot, C.; Carlson, D.F.; Huddart, R.; Long, C.R.; Pryor, J.H.; King, T.J.; Lillico, S.G.; Mileham, A.J.; McLaren, D.G.; Whitelaw, C.B.; et al. Genome edited sheep and cattle. *Transgenic Res.* **2015**, *24*, 147–153. [CrossRef]

209. Yang, B.; Wang, J.; Tang, B.; Liu, Y.; Guo, C.; Yang, P.; Yu, T.; Li, R.; Zhao, J.; Zhang, L.; et al. Characterization of bioactive recombinant human lysozyme expressed in milk of cloned transgenic cattle. *PLoS ONE* **2011**, *6*, e17593. [CrossRef] [PubMed]

210. Wang, J.; Yang, P.; Tang, B.; Sun, X.; Zhang, R.; Guo, C.; Gong, G.; Liu, Y.; Li, R.; Zhang, L.; et al. Expression and characterization of bioactive recombinant human α-lactalbumin in the milk of transgenic cloned cows. *J. Dairy Sci.* **2008**, *91*, 4466–4476. [CrossRef]

211. Jang, G.; Bhuiyan, M.M.; Jeon, H.Y.; Ko, K.H.; Park, H.J.; Kim, M.K.; Kim, J.J.; Kang, S.K.; Lee, B.C.; Hwang, W.S. An approach for producing transgenic cloned cows by nuclear transfer of cells transfected with human alpha 1-antitrypsin gene. *Theriogenology* **2006**, *65*, 1800–1812. [CrossRef]

212. Salamone, D.; Barañao, L.; Santos, C.; Bussmann, L.; Artuso, J.; Werning, C.; Prync, A.; Carbonetto, C.; Dabsys, S.; Munar, C.; et al. High level expression of bioactive recombinant human growth hormone in the milk of a cloned transgenic cow. *J. Biotechnol.* **2006**, *124*, 469–472. [CrossRef]

213. Monzani, P.S.; Sangalli, J.R.; De Bem, T.H.; Bressan, F.F.; Fantinato-Neto, P.; Pimentel, J.R.; Birgel-Junior, E.H.; Fontes, A.M.; Covas, D.T.; Meirelles, F.V. Breeding of transgenic cattle for human coagulation factor IX by a combination of lentiviral system and cloning. *Genet. Mol. Res.* **2013**, *12*, 3675–3688. [CrossRef] [PubMed]

214. Loi, P.; Iuso, D.; Czernik, M.; Ogura, A. A new, dynamic era for somatic cell nuclear transfer? *Trends Biotechnol.* **2016**, *34*, 791–797. [CrossRef] [PubMed]

215. Niemann, H. Epigenetic reprogramming in mammalian species after SCNT-based cloning. *Theriogenology* **2016**, *86*, 80–90. [CrossRef] [PubMed]

Review

Generating Cloned Goats by Somatic Cell Nuclear Transfer—Molecular Determinants and Application to Transgenics and Biomedicine

Maria Skrzyszowska *,† [ID] **and Marcin Samiec** *,† [ID]

Department of Reproductive Biotechnology and Cryoconservation, National Research Institute of Animal Production, Krakowska 1 Street, 32-083 Balice n. Kraków, Poland
* Correspondence: maria.skrzyszowska@iz.edu.pl (M.S.); marcin.samiec@iz.edu.pl (M.S.)
† These authors contributed equally to the preparation of this paper.

Abstract: The domestic goat (*Capra aegagrus hircus*), a mammalian species with high genetic merit for production of milk and meat, can be a tremendously valuable tool for transgenic research. This research is focused on the production and multiplication of genetically engineered or genome-edited cloned specimens by applying somatic cell nuclear transfer (SCNT), which is a dynamically developing assisted reproductive technology (ART). The efficiency of generating the SCNT-derived embryos, conceptuses, and progeny in goats was found to be determined by a variety of factors controlling the biological, molecular, and epigenetic events. On the one hand, the pivotal objective of our paper was to demonstrate the progress and the state-of-the-art achievements related to the innovative and highly efficient solutions used for the creation of transgenic cloned does and bucks. On the other hand, this review seeks to highlight not only current goals and obstacles but also future challenges to be faced by the approaches applied to propagate genetically modified SCNT-derived goats for the purposes of pharmacology, biomedicine, nutritional biotechnology, the agri-food industry, and modern livestock breeding.

1. Introduction

One of the most rapidly developing strategies for reproductive biotechnology in mammals, including farm livestock species, is cloning by somatic cell nuclear transfer (SCNT) (Figure 1).

It is beyond any doubt that the attractiveness of cloning techniques results from their potential to generate and multiply transgenic animals, which are valuable due to the expression of modified genes (Figure 1). Furthermore, this attractiveness also depends, to a lesser degree, on the possibility to replicate individuals with excellent, highly heritable breeding (genetic) and performance traits, which may shorten the generation interval and increase the rate of breeding progress. However, the aforementioned areas of research are being explored on a limited scale due to the high costs associated with the cloning procedure resulting from the low efficiency of the method. It is beyond any doubt that the widespread use of cloning methods will be possible once efficacy and repeatable results are guaranteed [1–4].

The main reason for low pre- and postimplantation developmental potential and poor quality of SCNT-derived embryos is the abnormal adaptation of the transferred somatic cell nuclei to the biochemical conditions of the oocyte cytoplasmic microenvironment, i.e., their incomplete or improper remodeling and reprogramming in the cytoplasm of nuclear-transferred oocytes. The latter also gives rise to the relatively high incidence of congenital malformations (anatomo-, histo-, and physiopathological changes) in cloned fetuses and

offspring. This calls for studies aimed at the precise determination of the conditions that facilitate epigenetic reprogramming in the nuclear donor cell genome during the pre- and postimplantation development of SCNT-generated embryos and fetuses of different mammalian species, including the domestic goat [5–10]. Promising results were achieved by investigations that focused on the use of extrinsic nonselective agents for stimulating the epigenetically regulated transcriptional activity of genomic DNA in both nuclear donor somatic cells and SCNT-cloned embryos [11–15].
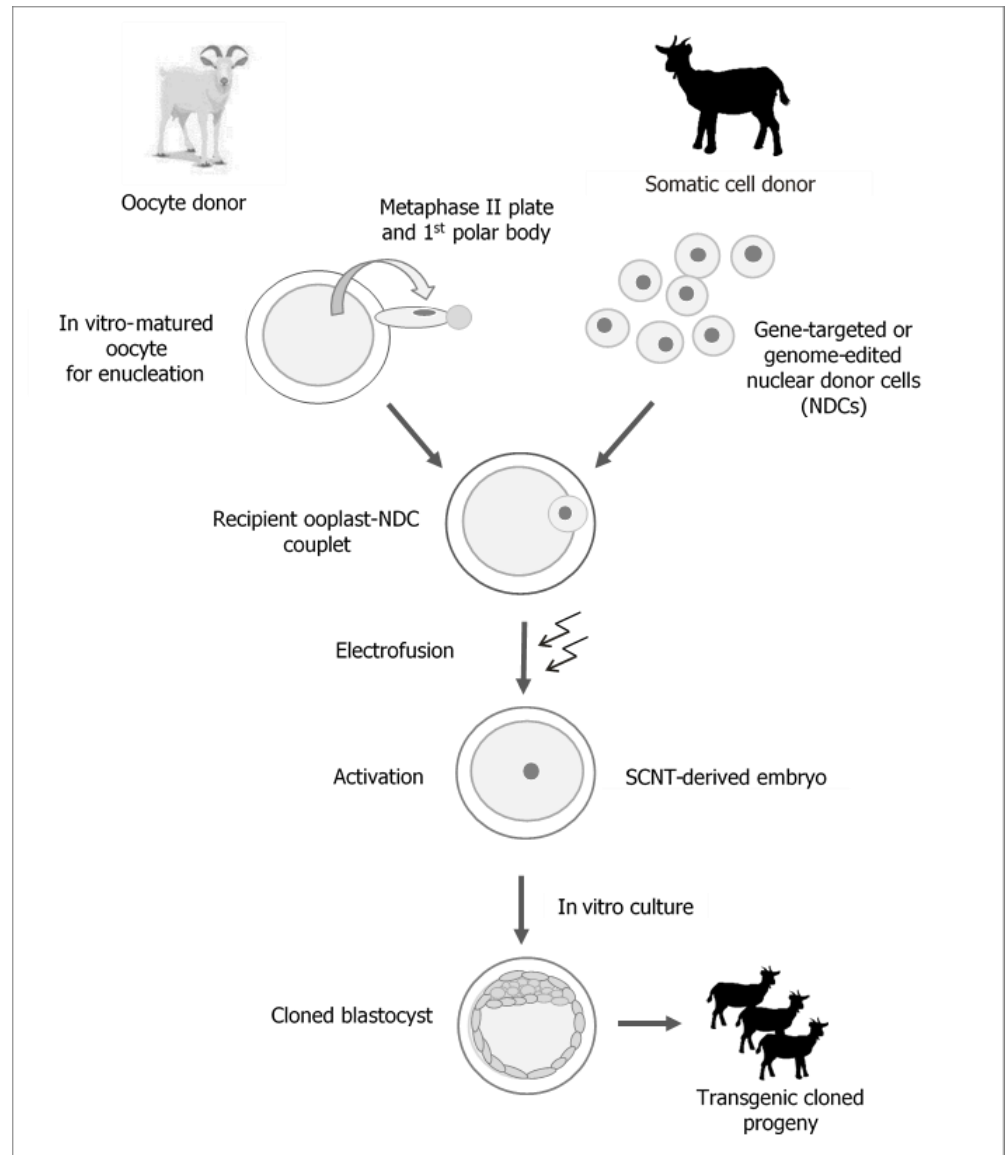
Figure 1. Generation of transgenic cloned goats by somatic cell nuclear transfer (SCNT).

2. Key Issues Related to Biological, Molecular, and Epigenetic Determinants Affecting the Efficacy of Somatic Cell Cloning in Goats

The provenance of somatic cells is a factor that can have a significant impact on cloning efficiency in goats. Relatively few types of nuclear donor cells have been tested for their suitability for the production of cloned embryos, fetuses, and/or offspring in this livestock species. Those that have been tested include cells stemming from several types of tissues collected from both caprine fetuses and adult animals of both sexes and of different ages. Among the nuclear donor cells (NDCs) used for SCNT procedures, mention should be made of: (1) in vitro cultured (transgenic or nontransgenic) fetal dermal fibroblasts [12,16–22];

(2) juvenile and adult dermal fibroblasts [14,23–26]; (3) mural granulosa cells isolated from antral ovarian follicles [18,27]; (4) cumulus oophorus cells [18,27,28].

Special consideration should be given to the use of pituicytes, i.e., endocrine cells originating from the anterior pituitary (also known as adenohypophysis) of postpubertal bucks, as a source of nuclear donors for SCNT in goats [29]. To date, this cerebral tissue-specific type of endocrine cell, which synthesizes and secretes tropic hormones, has not been used for SCNT in other species of farm and laboratory animals. It has been postulated, however, that artificial (ectopic) control of metabolic and secretory activities of the endocrine compartment in all lobes of the pituitary gland of livestock species might be feasible through genetic modification (transfection) of pituicytes at the in vitro culture level. In turn, utilizing genetically transformed pituitary-derived glandular cells, which are characterized by inducible expression of recombinant human hormonal proteins or polypeptides, for the generation of transgenic specimens of different mammalian species by somatic cell cloning opens up a variety of new application opportunities. The latter encompass the production of transgenic animal bioreactors, which provide xenogeneic (human) tropic hormones in cytosol extracts (homogenates) of pituicytes or in blood plasma. These hormones are indispensable for the clinical application of therapies for many human monogenic diseases, which induce endocrine-mediated congenital malformations. The transfer of caprine SCNT embryos that had been reconstructed with pituicytes into the reproductive tract of hormonally synchronized recipient females resulted in the birth of a cloned male kid. The results of these experiments confirmed that even the nuclear genome of terminally differentiated somatic cells such as pituicytes can successfully undergo the complete processes of epigenetic remodeling and reprogramming in pre- and postimplantation cloned goat embryos [29].

Deng et al. [30] examined the methylation profile and expression level of the *Xist* (X-inactive specific transcript) gene in the cells of SCNT embryos and in ear fibroblast cells, lung-derived cells, and cerebral cells collected from deceased cloned goats. The methylation profile observed for the *Xist* gene, which is transcribed into a noncoding mRNA molecule, i.e., a transcript that does not exhibit translational activity, was higher in 8-blastomere-stage SCNT embryos as compared to their in vitro-fertilized embryo counterparts generated by intracytoplasmic sperm injection (ICSI). Moreover, an increased methylation profile of the *Xist* gene was observed in the cells stemming from explants representing tissues/organs such as conchal skin, lungs, and brain, isolated postmortem from dead 3-day-old cloned female kids in relation to naturally bred specimens. While for ear skin-derived tissue bioptates originating from live cloned does, and for lung and brain tissue samples retrieved from dead cloned kids, the methylation profile of 5′-cytidine-3′-monophopshate-5′-guanosine-3′ (CpG) islands within the differentially methylated regions/imprinting control regions (DMRs/ICRs) of the *Xist* gene remained unchanged. Therefore, the transcriptional activity of the *Xist* gene diminished remarkably in the lungs and brain of dead cloned does, resulting in a lack of inactivation recognized for one of the X chromosomes (either of paternal or of maternal origin) in the cells of the previously indicated organs. In turn, a significant increase in *Xist* gene expression was shown in the ear-derived cutaneous fibroblast cells of live cloned does. This contributed to the normal inactivation of one of the two X chromosomes in these specimens. It is evident from this study that an increased incidence of hypermethylation and transcriptional suppression of the *Xist* gene, and thus no inactivation of one of the two X chromosomes, or in other words, active initiation of enhanced transcriptional activity (i.e., biallelic overexpression) of the genes localized in the loci of the paternal and maternal X chromosomes occurred in caprine SCNT-derived female fetuses. For these reasons, the aforementioned processes, which were also identified in the tissue explants recovered from 3-day-old dead cloned does, are found to arise from incomplete and aberrant reprogramming and were highlighted as a result of the epigenetically determined transcriptional activity of the somatic cell nuclear genome in cloned goat embryos [30].

Incomplete or incorrect epigenetic reprogramming of epigenetic memory, which is encoded in extragenic covalent modifications of the somatic cell nuclear genome, was found to be one of the main factors decreasing the efficiency of somatic cell cloning in mammals, including the domestic goat. Reductions in this efficiency are reflected in the weakened in vitro and/or in vivo developmental potential of SCNT-derived embryos [7,8,31]. Methylation of cytosine residues in CpG islands/dinucleotides is a widely explored/recognized modification of the somatic cell nuclear genome in cloned embryos [6,9,10,32]. Han et al. [33] demonstrated that enzymatic activity of ten-eleven translocation methylcytosine dioxygenase 3 (TET3) is a key molecular mechanism underlying active DNA demethylation in preimplantation goat embryos created by somatic cell cloning. Knocking out the *TET3* gene led to the inhibition of active (i.e., DNA replication-independent) demethylation of 5-methylcytosine (5-mC) residues in 2-blastomere-stage cloned goat embryos. As a consequence, this brought about the downregulation of the expression of the pluripotency-related *Nanog* gene in the inner cell mass (ICM) compartment of the generated blastocysts. In turn, overexpression of the *TET3* gene that had been induced by transgenization of in vitro cultured somatic cells resulted in: (1) abundant demethylation of DNA 5-mC residues; (2) declined quantitative profile of 5-mC moieties; (3) increased incidence of 5-hydroxymethylcytosine residues; (4) intensified transcriptional activity of crucial pluripotency-related genes. Furthermore, the use of genetically transformed somatic cells displaying overexpression of the *TET3* gene—as nuclear donors for the reconstruction of caprine enucleated oocytes—contributed to an enhancement in the extent of active demethylation of 5-mC residues within somatic cell-inherited nuclear DNA. The latter perpetuated hypomethylation of the somatic cell-derived genome in cleaved SCNT embryos, subsequently triggering remarkable improvements in their in vitro and in vivo developmental capabilities. It follows that overexpression of the *TET3* gene in NDCs significantly ameliorates the efficacy of somatic cell cloning in goats.

The developmental potential of the mammalian SCNT embryos, including their caprine representatives, which inherit the somatic cell nuclear genome as a result of the reconstruction of enucleated oocytes, is highly dependent on the level of epigenetic modifications within DNA and chromatin-derived histones of the NDCs undergoing long-term in vitro culture [34–36]. One of the strategies to reverse advanced alterations in the pattern of epigenetic covalent modifications within somatic cell nuclei, which encompass rapid DNA methylation and a decrease in the quantitative profile of histone protein acetylation, appears to be the exposure of NDCs, SCNT-derived oocytes, and corresponding embryos to reversible agents inhibiting biocatalytic activity of DNA methyltransferases (DNMTs) and/or histone deacetylases (HDACs). The use of nonselective or selective promoters of epigenetically determined transcriptional activity of genomic DNA in both in vitro cultured NDCs and cloned embryos is supposed to be an approach that allows for proper reprogramming of somatic cell nuclei [7,12,14]. Exogenously modulating the epigenetic memory profile of genomic DNA appears to contribute to successfully reversing the "transcriptional clock" of a differentiated somatic cell nucleus to the status of a cell nucleus characteristic of a totipotent or pluripotent embryonic cell. As a consequence, such efforts induce the restoration of the expression pattern that is seen in genes that are inevitable in the initiation and progress of the developmental program of SCNT-derived embryos [37,38]. This results in a reduction in the methylation degree of DNA cytosine residues and an increase in the acetylation of nuclear chromatin histone proteins [39,40]. In turn, the previously specified processes were shown to bring about recapitulation and perpetuation of the correct and faithful profiles of transcriptional activities observed both for the genes indispensable to induce and maintain the totipotency/pluripotency states and for the genes encoding enzymes responsible for endogenous epigenetic modifications during pre- and postimplantation embryogenesis. The totipotency/pluripotency-related genes encompass those that encode such proteins as: e.g., octamer-binding transcription factor 3/4 (Oct3/4), the homeobox-containing transcription factor Nanog, whose name stems from the Celtic/Irish mythical word Tír na nÓg (i.e., The Land of the Ever-Young), DNA-

binding proto-oncogenic/oncogenic transcription factor c-Myc, sex-determining region Y (SRY)-box 2 transcription factor (Sox2), Krüppel-like factor 4 (Klf4), reduced expression protein 1 (Rex1), and caudal-type homeobox protein 2 (Cdx2). The epigenetic modifier genes involve those that encode such enzymatic proteins as: e.g., DNA methyltransferase type 1 (DNMT1), DNA methyltransferase type 3a (DNMT3a), DNA methyltransferase type 3b (DNMT3b), histone deacetylase type 1 (HDAC1), histone deacetylase type 2 (HDAC2), histone methyltransferase (HMT), and histone acetyltransferase (HAT) [3,41,42]. In the wake of recent research, innovative and highly efficient methods were developed to modulate the epigenetic memory profile of mammalian SCNT embryos, including their caprine counterparts. These methods are focused on applying exogenous nonselective HDAC inhibitors (such as trichostatin A, valproic acid, and scriptaid) and/or nonselective DNMT inhibitors (such as 5-aza-2′-deoxycytidine) or selective inhibitors lysine K4 demethylases specific for histones H3 within the nucleosomal core of nuclear chromatin (such as trans-2-phenylcyclopropylamine (tranylcypromine; 2-PCPA)). The aforementioned strategies may considerably modify the epigenetically determined reprogramming of the somatic cell nuclear genome in SCNT-derived embryos. The final results of these innovative solutions turn out to be significant enhancements of the pre- and/or postimplantation developmental competence and an improvement in the molecular quality of cloned embryos in mammals, including the domestic goat [12–14,42–44].

3. Species-Specific Advantages of the Goat That Increase the Potential for Its Practical Application in Transgenics, Biopharmacy, Biomedicine, and Biotechnology

The domestic goat (*Capra aegagrus hircus*), a species with a tremendously high biodiversity of breeds showing relatively high milk and/or meat yield, may serve as an excellent research subject for SCNT-mediated production of transgenic bioreactor specimens. These caprine genetically engineered bioreactors of foreign species-descended (xenogeneic) biopreparations can provide recombinant human therapeutic proteins that are designated as biopharmaceuticals or nutraceuticals (Table 1), together with physiological secretions (e.g., milk) and excreta (e.g., urine). Moreover, somatic cell cloning in this livestock species seems to be a reliable, feasible, and powerful tool for generating and/or multiplying specimens (does and bucks) that display genetically modified parameters of meatiness and intramuscular adipose tissue content (Table 1). Increasing the efficiency of producing purified xenogeneic biopharmaceuticals or bionutraceuticals derived from the mammary glands (udders) of transgenic goats would thus allow them to be phased into the biopharmaceutical industry [24,45]. Another tangible benefit of producing transgenic cloned goats, which appears to be especially valuable for the xenogeneic product of the transgenic expression of exogenous DNA (directed at the mammary glands or resulting in higher meatiness), is the relatively short species-specific generation interval. The latter allows for increasing the rate of genetic progress in the breeding of founder does and bucks [24,25]. Yet another advantage of this small ruminant species is the low susceptibility of dairy and meat goats to infection with pathological prions (PrP^Sc) that cause scrapie in sheep [27,46,47]. Transgenic goats may serve as optimal bioreactors to produce human therapeutic proteins for various agroeconomic reasons. Compared to the breeding of transgenic cows, these animals are more easily farmed, their natural and biotechnologically assisted reproduction can be more rapidly controlled, and they are much cheaper to keep as compared to large ruminants. Relative to their body size, they have fairly large udders with a predominance of glandular tissue over fibrous parenchyma, which makes this small ruminant species genetically predisposed to a high production potential of colostrum and milk. The possible consequence of these anatomo-physiological advantages in goats is the high performance of transgenic doe herds in terms of lactogenic synthesis and secretion of recombinant human therapeutic proteins (biopharmaceuticals or nutraceuticals) by alveolar mammary epithelial cells. These caprine cells provide udder-derived secretion with a genetically modified qualitative and quantitative composition [24,48,49].

Table 1. Targets and effects of genetic modification in transgenic cloned goats.

Target of Genetic Modification	Strategy of Genetic Modification	Method of Somatic Cell Transfection	Genotypic Effect of Genetic Modification	Phenotypic Effect of Genetic Modification	Reference
Mammary gland (udder)	Gene targeting (HR-mediated targeted mutagenesis)	Electroporation	- HR-induced disruption of caprine the *BLG* gene by: • either its monoallelic knockout • or knock-in of the *hLA* gene construct into the *BLG* exon	- Functionally inactivating the caprine *BLG* gene - Targeted expression of the *hLA* gene in the lactogenic cells of udder-based bioreactors - Synthesis of upgraded or humanized milk without allergenic (BLG-triggered) properties	[21]
		Lipofection	- HR-dependent targeted incorporation of *hLF* cDNA into the nuclear genome (under the control of the goat β-casein gene promoter)	- Mammary gland-specific monoallelic expression of the *hLF* gene - Udder-mediated synthesis of upgraded or humanized milk - Production of genetically engineered milk (GEM) characterized by a broad spectrum of hLF-induced immunotherapeutic properties - GEM properties determined by antimicrobial, immunomodulatory, anti-inflammatory, and anticancer attributes of hLF	[50,51]
	TALEN-mediated gene editing	Electroporation	- TALEN-dependent targeted insertion of *hLF* cDNA at *BLG* locus resulting in: • biallelic knock-in of the *hLF* coding sequence into the *BLG* exon	-Targeted expression of the *hLF* gene in udder-based bioreactors - Synthesis of hLF-enriched or humanized milk - Production of GEM displaying immunotherapeutic properties	[22]
Skeletal muscles	Gene targeting (HR-mediated targeted mutagenesis)	Lipofection	- Monoallelic knockout (semi-deficiency) of the *MSTN* gene in SCNT-derived progeny	- Inducing hyperplasia and hypertrophy of striated muscle cells -Remarkably gaining skeletal muscle mass and augmenting meatiness by genetically transforming the muscular system of heterozygous ($MSTN^{+/-}$) transgenic cloned offspring	[25]
	CRISPR/Cas9-mediated gene editing	Electroporation	- Monoallelic knockout (semi-deficiency) of the *MSTN* gene in SCNT-derived progeny	- Expression of cellular hyperplasia and hypertrophy in genome-edited (GE) skeletal muscle tissue of heterozygous ($MSTN^{+/-}$) transgenic cloned offspring	[52]
		Nucleofection	- Biallelic knockout (deficiency) of the *MSTN* gene in SCNT-derived progeny	- Expression of myofiber hyperplasia and hypertrophy in GE muscular system of homozygous ($MSTN^{-/-}$) transgenic cloned offspring	[53]
	TALEN-mediated gene editing	Electroporation	- Monoallelically knocking out the *MSTN* gene - Biallelically knocking out the *MSTN* gene in SCNT-derived progeny	- Triggering hyperplasia and hypertrophy of skeletal myocytes in the GE muscular system of: • either heterozygous ($MSTN^{+/-}$) transgenic cloned offspring • or their homozygous ($MSTN^{-/-}$) counterparts	[54]
		Electroporation	- Monoallelic knockout of the *MSTN* gene ($MSTN^{+/-}$) in NDCs - Biallelic knockout of the *MSTN* gene ($MSTN^{-/-}$) in NDCs	- Onset of the mono- or biallelically transcriptionally silencing *MSTN* gene in isozygous GE NDCs - Failure in the generation of GE cloned progeny exhibiting phenotypes determined by *MSTN* mono- or biallelic deletion	[52]

The first transgenic cloned kids were generated from the nuclear-transferred embryos reconstructed with caprine somatic cells that had been previously transfected in vitro with relatively simple gene constructs. These gene constructs contained no genomic sequences of the regions encoding structural transgenes, but were composed of the exon segments of genes encoding selectable marker proteins, e.g., *PGKneo* fusion genes. The aforementioned fusion genes are comprised of murine phosphoglycerate kinase (*PGK*) promoters and neomycin phosphotransferase (*neo*) genes. The *neo* gene determines resistance to selective aminoglycoside antibiotic designated as geneticin disulphate (G418 sulphate). In the study

by Zou et al. [19], in vitro cultured fetal fibroblasts provided a source of transgenic NDCs for SCNT-based cloning in goats. The transgenic NDCs were created by their transfection with a gene construct that only contained the *neo* gene. The above-mentioned study resulted in the production of five genetically modified kids. In turn, Keefer et al. [17] and Baldassarre et al. [27,46] used the in vitro lipofection approach to transfect fetal fibroblasts with a more complex plasmid gene construct (*CEeGFP*). The *CEeGFP*-fusion gene was composed of: (1) the enhanced green fluorescent protein (*eGFP*)-reporter gene driven by the human elongation factor-1α promoter and cytomegalovirus enhancer and (2) the *neo* gene under the control of the simian virus-40 (*SV-40*) promoter. Following the transfer of genetically transformed cloned embryos into the reproductive tracts of recipient surrogates, one cloned doe showing the expression of the *eGFP*-reporter transgene was produced.

Transgenic animals with the high transcriptional activity profiles (diagnosed in vivo) of a xenogeneic gene may be subsequently multiplied by somatic cell cloning. This is particularly justified when biopharmaceuticals stemming from these animals may find widespread application in the treatment of patients suffering from various single-gene heritable disorders. When transgenic biopharmaceuticals obtain certification for application in humans, somatic cell cloning of genetically modified specimens will allow, at least in theory, for the maintenance of homogeneity of the drugs extracted from natural secretions and excretions (milk, urine) of the successive generations of cloned animals. This technology was successfully used by the American biotechnology company GTC Biotherapeutics (formerly Genzyme Transgenics Corporation), which generated transgenic goats exhibiting monoallelic expression of recombinant human antithrombin III gene (*rhAT*) in their mammary glands (udders). The production of transgenic cloned goats was based on the use of a standard intrapronuclear microinjection into the zygotes of cDNA constructs containing the goat β-casein gene promoter. In the performed experiments, genetically modified fibroblast cell lines were established from fetuses obtained by mating nontransgenic does with a genetically modified founder buck. This buck displayed transcriptional activity of the *rhAT* gene that was directed into the mammary gland (udder). Clonal lines of transgenic fetal fibroblast cells served as a source of nuclear donors in the somatic cell cloning procedure, which resulted in a total of eight genetically engineered SCNT-derived female kids [16,45]. The findings of Cheng et al. [28] represent another example of applying the somatic cell cloning technique for multiplying populations of genetically transformed specimens. In this case, enucleated oocytes were reconstructed by SCNT with the use of in vitro cultured fibroblast cell lines collected from dermal tissue explants of a transgenic goat displaying ubiquitous expression of recombinant human erythropoietin (rhEPO). After surgical transfer of the cloned embryos into the reproductive tracts of hormonally synchronized recipient does, two genetically modified kids were born. The SCNT-derived offspring were characterized by mammary gland-specific expression of xenogeneic rhEPO protein.

4. Transgenic Cloned Goats as Bioreactors That Produce Recombinant Human Therapeutic Proteins

The nuclear transfer of in vitro-transfected somatic cells increases the probability of producing nonmosaic transgenic offspring, which have an exogenous gene construct incorporated into the primordial germ cell line. Such specimens, which are identified as nonchimeric with regard to the genetic transformation of gametogenic and somatic cells, retain their full capacity to transmit phenotypically and molecularly diagnosed transgene expression to the secretory epithelial cells (lactocytes) in the mammary glands of the next generation of kids [49,55,56]. An outstanding example is found in the findings of Baguisi et al. [45]. High-level expression of the *rhAT* gene detected in the udder lactogenic cells of three cloned does, which were produced from SCNT embryos reconstructed with transgenic fetal fibroblasts, was also reflected in the very high phenotypic value of this genetically modified trait in the milk samples. Over a 33-day lactation induced at 2 months of age, the milk yield of these genetically engineered does reached approximately 160 mL. Additionally, the rhAT concentration in the collected milk was maintained at a level

of as much as 5.8 g/L (20.5 U/mL was observed for the enzymatic activity of purified biopharmaceutical) at day 5 and 3.7 g/L (14.6 U/mL for the biocatalytic activity) by day 9 of lactation. At such high concentrations of recombinant therapeutic proteins in milk, large-sized herds of transgenic goats could easily yield 300 kg of extracted (purified) biopharmaceutical product per year. Combining somatic cell cloning technology with hormonal induction of early lactation in prepubertal transgenic does will shorten the time needed to obtain the transgene expression product by as much as 8 to 9 months from the time of cell line transfection to the secretion of the genetically engineered protein biopreparation into milk [20,45]. On the one hand, the volume of these retrieved milk samples is sufficient for estimating the recombinant protein yield. On the other hand, taking into account even a relatively low quantitative profile of translational activity identified for transgene-transcribed mRNA (as measured by milligram quantities of therapeutic protein per 1 mL of milk), this amount of milk can be used for multiple clinical tests of the pharmacokinetic, hormonal, and enzymatic activity of the produced biopharmaceuticals.

Special consideration should be given to the broad international commercialization of the first biopharmaceutical in 2006–2009, designated as ATryn®, by GTC Biotherapeutics. The basic active biochemical component of this pharmacological biopreparation is rhAT, which was recovered from the milk synthesized and secreted by the udders of transgenic cloned specimens of a large livestock species, the domestic goat [47,57,58]. This is a milestone in the practical, commercial-scale implementation of the first biopharmaceutical product of modern mammalian reproductive biotechnology based on embryonic genome engineering technologies such as transgenesis and somatic cell cloning of farm animals. It is worth pointing out here that ATryn® is the world's first drug to be provided by mammary gland-based bioreactors of genetically engineered cloned goats that exhibit highly efficient and organ-specific mono- or biallelic expression of the *rhAT* transgene. This biopharmaceutical was originally granted a marketing authorization by the European Medicines Agency (EMA) in 2006 for use in the biopharmaceutical and medical sector of the European Union, followed by certification from the United States Food and Drug Administration (FDA or USFDA) in 2009 for marketing in the biopharmaceutical and biomedical sector in the USA and Canada [1,59]. At this stage, ATryn® is widely used in biomedical programs/therapeutic platforms for the treatment of hereditary AT deficiency in hospitalized medical patients [60,61].

Another example of the practical application of the mammary glands of genetically transformed cloned goats as bioreactors to synthesize human therapeutic proteins or so-called humanized milk is found in the study by Zhu et al. [21]. This investigation was aimed at ameliorating allergic reactions and inflammatory responses to β-lactoglobulin (BLG) protein (Table 1). As a major whey protein with potential allergenic effect, BLG occurs in the milk of all even-toed mammals (*Artiodactyla*), including the domestic goat. It has no allergenic properties in human milk. The presence of this protein in caprine milk considerably limits, to a high degree, the consumption of this lactogenesis-derived product despite its high nutritive value and health-promoting benefits. Using conventional homologous recombination, the above-mentioned investigators were the first to functionally inactivate a single copy of the *BLG* gene, either through *BLG* gene knockout or through *hLA* (human α-lactalbumin) gene knock-in into the nuclear genome of in vitro cultured fetal fibroblast cells. These cells subsequently provided a source of nuclear donors for reconstructing enucleated doe oocytes in the somatic cell cloning procedure. The ultimate outcome of this research was the birth of three SCNT-derived kids, among which mono-allelic knockout of the targeted *BLG* gene was confirmed in two specimens (Table 1) [21].

In turn, Yuan et al. [22] used the strategy of somatic cell cloning to generate transgenic goats whose udders were bioreactors that synthesized humanized milk containing pharmaceutical or nutraceutical immune glycoprotein, known as recombinant human lactoferrin (hLF). Genetically transformed fetal fibroblasts provided the source of nuclear donor cells for the reconstruction of enucleated oocytes by somatic cell cloning. The genome of nuclear donor cells had been previously edited by inserting *hLF* cDNA into the *BLG* locus, i.e., by

replacing the *BLG* gene with the *hLF* gene. Editing the nuclear genome of fetal fibroblast cells had been mediated by transcription activator-like effector nucleases (TALENs). The efficiency of the targeted mutagenesis observed for the *BLG* gene oscillated at the level of approximately 10%. The results of investigations by Yuan et al. [22] confirmed that the combination of TALEN-based genome editing with the SCNT strategy gave rise to biallelic inactivation of the *BLG* gene through the knock-in of *hLF* exons into the genomic DNA of cloned goats whose mammary glands were targeted by programmed genetic transformation to produce recombinant hLF (Table 1). Transgenically encoded qualitative and quantitative modification of the biochemical composition of caprine milk that subsequently brought about the production of humanized milk in the udders of SCNT-derived goats appears to ameliorate its allergenicity. Diminishing the capability of the milk provided by genetically engineered bioreactors to trigger acute allergic reactions in humans is simultaneously reflected in enriching the goat milk with the valuable multipotent protein designated as LF. This immune glycoprotein, apart from physiologically regulating the dynamic homeostasis of the metabolism of iron cations, is characterized by several other desirable immunotherapeutic properties, including antimicrobial (antibacterial, mycostatic, and antiviral), immunomodulatory, anti-inflammatory, and anticancer abilities (Table 1) [22,24,56].

It is also noteworthy that Zhang et al. [50] reported the effective integration of the recombinant *hLF* gene with the xenogeneic host genome as a result of genetically transforming the caprine fetal fibroblast cells under in vitro culture conditions. The genetically transformed fetal fibroblasts were subsequently used to generate transgenic kids (does) with the *hLF* gene in ear skin tissue samples by somatic cell cloning (Table 1). Out of the six transgenic cloned kids produced, three does died during the perinatal period due to severe bronchopulmonary dysplasia in underdeveloped lungs and acute hypoxemic respiratory failure. The epigenetic analysis of tissue explants collected postmortem from the lungs of perished transgenic does revealed hypermethylation of CpG islands/dinucleotides within the DMR/ICR domain of the gene encoding insulin-like growth factor 2 receptor (IGF2R). For that reason, the maternal allele of the *IGF2R* gene was found to be transcriptionally overactive/upregulated due to enhanced methylation of cytosine residues in the DMR/ICR-associated intron sequence, while its paternal counterpart was shown to be transcriptionally silenced due to the occurrence of parent-of-origin and allele-specific methylation imprint. As a result, the overexpression of mRNA transcribed by the maternal allele of the *IGF2R* gene that had undergone aberrant genomic imprinting was identified in the cell samples of postmortem isolated lung tissue explants stemming from the cloned kids [50].

In summary, imprinted genes are an important epigenomic regulator of anatomo-histological growth and development and physiological maturation of the lungs. In turn, aberrant or incomplete reprogramming of the epigenetically determined transcriptional activity of DNA, which underlies abnormal (i.e., increased) methylation of cytosine moieties within DMR/ICR-related intron sequences of the imprinted maternal allele of the *IGF2R* gene, determines the monoallelic overexpression of this gene exprimed from the maternal genome in the lungs of cloned fetuses. The latter appears to be one of the main lethal factors positively correlated with etiopathogenesis of lung hypoplasia and acute pulmonary insufficiency in neonatal transgenic cloned kids [50].

5. Transgenic Cloned Goats as a Source of Valuable Meat for Humans

Attempts to create and multiply transgenic cloned goats may provide a research basis for the SCNT-mediated generation of genetically engineered specimens (bucks and does) that exhibit genotypic and phenotypic modifications related to increased carcass meatiness and decreased intramuscular fatness. These animals could serve as a valuable research model for expanding our knowledge of the importance of myostatin, e.g., in the context of the quality and taste of the meat from individuals displaying superior gains in muscle tissue and myofiber size. Myostatin, encoded by the *MSTN* gene, is a hormonal inhibitory

polypeptide that inhibits/downregulates the growth, differentiation, maturation, and development of skeletal muscles in mammals. Research shows that functional inactivation of the *MSTN* gene using gene targeting (targeted mutagenesis) or genome editing techniques contributes to increase skeletal muscle mass while diminishing the content of intramuscular adipose tissue and reducing genetically determined or diet-induced obesity. This has the beneficial effects of increased meat yield, fattening performance, and dressing percentage in genetically modified males and females generated by SCNT-based cloning. These effects are evoked by cellular hyperplasia (proliferation) and hypertrophy (enlargement) of striated muscle tissue (Table 1). The hyperplasia and hypertrophy of striated muscle cells (i.e., skeletal sarcocytes known as syncytial myocytes) are synergistically triggered as a result of the following:

– Expediting differentiation of the predominant multipotent muscle stem cells (i.e., satellite cells) and their myogenic progenitor cell derivatives into primary myoblasts;
– Accelerating the proliferative growth of mononucleated myoblasts;
– Facilitating cyto- and histophysiological maturation of genetically engineered skeletal muscle tissue by syncytial fusion of myoblasts and their conversion (transformation) into myotubes and the resultant multinucleated myofibers;
– Enlargement of muscle fibers;
– Extension of myofiber lengths and individual sarcomere lengths in whole muscle fibers;
– Increase in both myofibrillar volume and myofiber number [25,62,63].

It is beyond any doubt that SCNT-derived goats that are characterized by *MSTN* gene silencing (Table 1) [25] represent a powerful, reliable, and feasible tool for investigations targeted at nutritional physiology, food technology, dietetics, nutrigenomics, nutriepigenomics, nutritranscriptomics, nutriproteomics, and human nutrition metabolomics and metabonomics. Myostatin gene knockout (*MSTN*-KO) in goats (Table 1) [25,62,64] and sheep [63,65] was investigated in several research centers. However, as a result of the low efficacy of homologous recombination (HR)-mediated targeted mutagenesis, short-hairpin RNA-mediated gene targeting, and zinc-finger nuclease (ZFN)-mediated genome editing, only a few studies resulted in successful *MSTN* gene knockdown in ex vivo expanded caprine juvenile cutaneous fibroblasts [25], ovine fetal myoblasts [63], or ovine fetal cutaneous fibroblasts [65].

In recent years, other noteworthy solutions have been applied to genome editing and have been subsequently adapted to ARTs. These were then applied in combination to cloning goats using SCNT. These solutions are aimed at strategies based on the use of TALENs or the clustered regularly interspaced short palindromic repeat/CRISPR-associated endonuclease type 9 (CRISPR/Cas9)-assisted system. The progress achieved in developing and optimizing the techniques of targeted knockout of specific gene loci is promising. Therefore, these techniques are increasingly utilized for precise genome editing, allowing for the genome of mammals, including the domestic goat, to be modified with relative ease [66–71]. Ni et al. [53] were the first to demonstrate that CRISPR/Cas9-mediated genome editing can induce accurate mono- or biallelic mutations in the *MSTN* gene of caprine fetal fibroblast cells. The clonal lines of these NDCs that exhibit biallelic *MSTN*-KO were used in a SCNT procedure, resulting in three live-born cloned kids, all of which carried a biallelic mutation in the form of double inactivation of the *MSTN* gene's loci (Table 1).

In turn, Yu et al. [54] showed that TALEN-based genetic transformation leads to the successful inhibition of *MSTN* gene expression in gene-edited cloned goats (Table 1). Moreover, the outcome of both TALEN- and CRISPR/Cas9-mediated systems that were applied to edit the nuclear genome of SCNT-derived Alpas breed cashmere goats (Table 1) was evaluated by Zhang et al. [52]. The efficiency of triggering *MSTN*-KO was compared at many levels of pre- and postimplantation development of transgenic cloned embryos. The rates of both electro-transfecting/electroporating the somatic cells and cutting exon 1 within the *MSTN* gene were found to be higher for the CRISPR/Cas9-assisted strategy of genome

editing than for its TALEN-mediated counterpart. Nevertheless, the genome-wide off-target effects were shown to be more frequent for the CRISPR/Cas9-mediated system than for the TALEN-mediated system. Furthermore, for CRISPR/Cas9-based genome editing, the incidence of effectively inducing targeted biallelic mutagenesis of the *MSTN* gene increased over eight times as compared to TALEN-based genome editing. In turn, caprine SCNT embryos that had been reconstructed with TALEN-mediated transgenic NDCs reached the 8-blastomere stage more quickly and their cleavage activity was significantly higher as compared to SCNT embryos derived from CRISPR/Cas9-mediated gene-edited NDCs. However, cloned kids were produced, following the surgical transfer of SCNT embryos into recipient does, that stemmed from NDCs that were genetically modified only using the CRISPR/Cas9-assisted technique (Table 1). This ultimately suggests that the high yield of generating targeted modifications of the *MSTN* gene (*MSTN*-KO) was achieved using CRISPR/Cas9-mediated genome editing [52].

To summarize, the study by Zhang et al. [52] proved that, although the TALEN-dependent genome transformation strategy has a certain advantage over the CRISPR/Cas9-dependent system, the latter offers significant benefits related to the precision programmed editing of the genes (Table 1). This makes this system a powerful and high-performance genetic engineering tool for livestock breeding practice and, in particular, in the fields of agri-food biotechnology and human food technology (nutritechnology) based on a meat diet [52,68–71].

6. Conclusions and Future Goals

Although the efficiency of somatic cell cloning in goats remains relatively low, further studies are necessary because modern ART has important implications in the fields of goat breeding, the transgenics of this mammalian species, agri-food biotechnology, biomedicine, and biopharmacy.

An increase in the efficiency of somatic cell cloning techniques in the domestic goat can be brought about by further intensive research into improving both developmental competence and the parameters related to the molecular and epigenetic quality of SCNT-derived embryos. The latter can be achieved by efforts aimed at using nonselective or selective inhibitors of DNMTs and HDACs, which would in turn lead to enhancements in the reprogrammability of the epigenetic memory profile within genomic DNA of NDCs, nuclear-transferred oocytes, and the corresponding caprine cloned embryos. This is a sine qua non condition for the practical use of SCNT-based cloning, and thus for the production of genetically transformed goats for the purposes of human nutrition technology based on a meat diet. The main focus of the aforementioned efforts is the successful SCNT-mediated creation and multiplication of transgenic does and bucks with enhanced meat yields due to cellular hyperplasia and hypertrophy within skeletal muscle tissue. This is also a basic requirement for the effective propagation of genetically engineered or genome-edited does for the biopharmaceutical and nutraceutical industry. An ideal example of this is the generation of transgenic goats whose udders serve as bioreactors for recombinant human therapeutic proteins or biochemically humanized milk.

Author Contributions: Conceptualization, M.S. (Maria Skrzyszowska) and M.S. (Marcin Samiec); Writing—original draft, M.S. (Maria Skrzyszowska) and M.S. (Marcin Samiec); Writing—review and editing, M.S. (Marcin Samiec); Supervision and funding acquisition, M.S. (Marcin Samiec); Tabular and graphic documentation, M.S. (Marcin Samiec) and M.S. (Maria Skrzyszowska). All authors have read and agreed to the published version of the manuscript.

Institutional Review Board Statement: Not applicable.

Informed Consent Statement: Not applicable.

Data Availability Statement: Not applicable.

Conflicts of Interest: The authors declare no conflict of interest.

Abbreviations

ART	Assisted reproductive technology
BLG	β-lactoglobulin
Cas9	CRISPR-associated endonuclease type 9
Cdx2	A product transcribed from proto-oncogene/oncogene encoding caudal-type homeobox protein 2 that represents the family of intestinal epithelium/adenocarcinoma-specific and DNA-binding homeodomain transcription factors inevitable in intestinal organogenesis
c-Myc	Avian myelocytomatosis viral oncogene homolog encoding a DNA-binding proto-oncogenic/oncogenic transcription factor
CpG	5′-Cytidine-3′-monophopshate-5′-guanosine-3′
CRISPR	Clustered regularly interspaced short palindromic repeat
DMR	Differentially methylated region
DNMT	DNA methyltransferase
eGFP	Enhanced green fluorescent protein
GE	Genome-edited
GEM	Genetically engineered milk
HAT	Histone acetyltransferase
HDAC	Histone deacetylase
HMT	Histone methyltransferase
hLA	Human α-lactalbumin
hLF	Human lactoferrin
HR	Homologous recombination
ICM	Inner cell mass
ICR	Imprinting control region
ICSI	Intracytoplasmic sperm injection
IGF2R	Insulin-like growth factor 2 receptor
Klf4	Krüppel-like factor 4 (also called gut-enriched Krüppel-like factor or GKLF); an evolutionarily conserved zinc finger-containing transcription factor that regulates diverse cellular processes such as cell growth, proliferation, differentiation, apoptosis, and somatic cell reprogramming
5-mC	5-Methylcytosine
MSTN	Myostatin
MSTN-KO	Myostatin gene knockout
Nanog	Homeobox-containing transcription factor whose name stems from the Celtic/Irish mythical word Tír na nÓg (i.e., Tir Na Nog; The Land of the Ever-Young)
NDC	Nuclear donor cell
Oct3/4	Octamer-binding transcription factor 3/4 (also designated as POU5F1); a member of the family of POU (Pit-Oct-Unc)-domain and homeodomain transcription factors
2-PCPA	Trans-2-phenylcyclopropylamine; Tranylcypromine
PGKneo	Neomycin phosphoglycerol kinase; Neomycin glycerol phosphotransferase
Rex1	Reduced expression gene 1 encoding a DNA-binding transcription factor known as reduced expression protein 1 or zinc finger protein 42 homolog
rhAT	Recombinant human antithrombin III
rhEPO	Recombinant human erythropoietin
SCNT	Somatic cell nuclear transfer
Sox2	Sex-determining region Y (SRY)-box 2; a member of the high mobility group (HMG)-box family of DNA-binding transcription factors
SV-40	Simian virus-40
TALEN	Transcription activator-like effector nuclease
TET3	Ten-eleven translocation 3 protein; TET 5-methylcytosine dioxygenase 3
Xist	X-inactive specific transcript
ZFN	Zinc-finger nuclease

References

1. Samiec, M.; Skrzyszowska, M. Transgenic mammalian species, generated by somatic cell cloning, in biomedicine, biopharmaceutical industry and human nutrition/dietetics—Recent achievements. *Pol. J. Vet. Sci.* **2011**, *14*, 317–328. [CrossRef]
2. Samiec, M.; Skrzyszowska, M. The possibilities of practical application of transgenic mammalian species generated by somatic cell cloning in pharmacology, veterinary medicine and xenotransplantology. *Pol. J. Vet. Sci.* **2011**, *14*, 329–340. [CrossRef]
3. Hall, V.; Hinrichs, K.; Lazzari, G.; Betts, D.H.; Hyttel, P. Early embryonic development, assisted reproductive technologies, and pluripotent stem cell biology in domestic mammals. *Vet. J.* **2013**, *197*, 128–142. [CrossRef]
4. Skrzyszowska, M.; Samiec, M. Generation of monogenetic cattle by different techniques of embryonic cell and somatic cell cloning—Their application to biotechnological, agricultural, nutritional, biomedical and transgenic research—A review. *Ann. Anim. Sci.* **2021**, *21*, 1–15.
5. Martins, L.T.; Neto, S.G.; Tavares, K.C.; Calderón, C.E.; Aguiar, L.H.; Lazzarotto, C.R.; Ongaratto, F.L.; Rodrigues, V.H.; Carneiro Ide, S.; Rossetto, R.; et al. Developmental outcome and related abnormalities in goats: Comparison between somatic cell nuclear transfer- and *in vivo*-derived concepti during pregnancy through term. *Cell. Reprogram.* **2016**, *18*, 264–279. [CrossRef] [PubMed]
6. Samiec, M.; Skrzyszowska, M. Can reprogramming of overall epigenetic memory and specific parental genomic imprinting memory within donor cell-inherited nuclear genome be a major hindrance for the somatic cell cloning of mammals?—A review. *Ann. Anim. Sci.* **2018**, *18*, 623–638. [CrossRef]
7. Samiec, M.; Skrzyszowska, M. Intrinsic and extrinsic molecular determinants or modulators for epigenetic remodeling and reprogramming of somatic cell-derived genome in mammalian nuclear-transferred oocytes and resultant embryos. *Pol. J. Vet. Sci.* **2018**, *21*, 217–227. [PubMed]
8. Yang, M.; Perisse, I.; Fan, Z.; Regouski, M.; Meyer-Ficca, M.; Polejaeva, I.A. Increased pregnancy losses following serial somatic cell nuclear transfer in goats. *Reprod. Fertil. Dev.* **2018**, *30*, 1443–1453. [CrossRef] [PubMed]
9. Deng, M.; Liu, Z.; Chen, B.; Wan, Y.; Yang, H.; Zhang, Y.; Cai, Y.; Zhou, J.; Wang, F. Aberrant DNA and histone methylation during zygotic genome activation in goat cloned embryos. *Theriogenology* **2020**, *148*, 27–36. [CrossRef] [PubMed]
10. Deng, M.; Zhang, G.; Cai, Y.; Liu, Z.; Zhang, Y.; Meng, F.; Wang, F.; Wan, Y. DNA methylation dynamics during zygotic genome activation in goat. *Theriogenology* **2020**, *156*, 144–154. [CrossRef] [PubMed]
11. Iager, A.E.; Ragina, N.P.; Ross, P.J.; Beyhan, Z.; Cunniff, K.; Rodriguez, R.M.; Cibelli, J.B. Trichostatin A improves histone acetylation in bovine somatic cell nuclear transfer early embryos. *Cloning Stem Cells* **2008**, *10*, 371–379. [CrossRef]
12. Mao, T.; Han, C.; Deng, R.; Wei, B.; Meng, P.; Luo, Y.; Zhang, Y. Treating donor cells with 2-PCPA corrects aberrant histone H3K4 dimethylation and improves cloned goat embryo development. *Syst. Biol. Reprod. Med.* **2018**, *64*, 174–182. [CrossRef]
13. Samiec, M.; Romanek, J.; Lipiński, D.; Opiela, J. Expression of pluripotency-related genes is highly dependent on trichostatin A-assisted epigenomic modulation of porcine mesenchymal stem cells analysed for apoptosis and subsequently used for generating cloned embryos. *Anim. Sci. J.* **2019**, *90*, 1127–1141. [CrossRef]
14. Skrzyszowska, M.; Samiec, M. Enhancement of in vitro developmental outcome of cloned goat embryos after epigenetic modulation of somatic cell-inherited nuclear genome with trichostatin A. *Ann. Anim. Sci.* **2020**, *20*, 97–108. [CrossRef]
15. Wiater, J.; Samiec, M.; Skrzyszowska, M.; Lipiński, D. Trichostatin A-assisted epigenomic modulation affects the expression profiles of not only recombinant human α1,2-fucosyltransferase and α-galactosidase A enzymes but also Galα1→3Gal epitopes in porcine bi-transgenic adult cutaneous fibroblast cells. *Int. J. Mol. Sci.* **2021**, *22*, 1386. [CrossRef]
16. Reggio, B.C.; James, A.N.; Green, H.L.; Gavin, W.G.; Behboodi, E.; Echelard, Y.; Godke, R.A. Cloned transgenic offspring resulting from somatic cell nuclear transfer in the goat: Oocytes derived from both follicle-stimulating hormone-stimulated and nonstimulated abattoir-derived ovaries. *Biol. Reprod.* **2001**, *65*, 1528–1533. [CrossRef]
17. Keefer, C.L.; Baldassarre, H.; Keyston, R.; Wang, B.; Bhatia, B.; Bilodeau, A.S.; Zhou, J.F.; Leduc, M.; Downey, B.R.; Lazaris, A.; et al. Generation of dwarf goat (*Capra hircus*) clones following nuclear transfer with transfected and nontransfected fetal fibroblasts and in vitro-matured oocytes. *Biol. Reprod.* **2001**, *64*, 849–856. [CrossRef]
18. Keefer, C.L.; Keyston, R.; Lazaris, A.; Bhatia, B.; Begin, I.; Bilodeau, A.S.; Zhou, F.J.; Kafidi, N.; Wang, B.; Baldassarre, H.; et al. Production of cloned goats after nuclear transfer using adult somatic cells. *Biol. Reprod.* **2002**, *66*, 199–203. [CrossRef]
19. Zou, X.; Wang, Y.; Cheng, Y.; Yang, Y.; Ju, H.; Tang, H.; Shen, Y.; Mu, Z.; Xu, S.; Du, M. Generation of cloned goats (*Capra hircus*) from transfected foetal fibroblast cells, the effect of donor cell cycle. *Mol. Reprod. Dev.* **2002**, *61*, 164–172. [CrossRef]
20. Baldassarre, H.; Wang, B.; Pierson, J.; Neveu, N.; Lapointe, J.; Cote, F.; Kafidi, N.; Keefer, C.L.; Lazaris, A.; Karatzas, C.N. Prepubertal propagation of transgenic cloned goats by laparoscopic ovum pick-up and in vitro embryo production. *Cloning Stem Cells* **2004**, *6*, 25–29. [CrossRef]
21. Zhu, H.; Hu, L.; Liu, J.; Chen, H.; Cui, C.; Song, Y.; Jin, Y.; Zhang, Y. Generation of β-lactoglobulin-modified transgenic goats by homologous recombination. *FEBS J.* **2016**, *283*, 4600–4613. [CrossRef]
22. Yuan, Y.G.; Song, S.Z.; Zhu, M.M.; He, Z.Y.; Lu, R.; Zhang, T.; Mi, F.; Wang, J.Y.; Cheng, Y. Human lactoferrin efficiently targeted into caprine beta-lactoglobulin locus with transcription activator-like effector nucleases. *Asian Australas. J. Anim. Sci.* **2017**, *30*, 1175–1182. [CrossRef]
23. Behboodi, E.; Memili, E.; Melican, D.T.; Destrempes, M.M.; Overton, S.A.; Williams, J.L.; Flanagan, P.A.; Butler, R.E.; Liem, H.; Chen, L.H.; et al. Viable transgenic goats derived from skin cells. *Transgenic Res.* **2004**, *13*, 215–224. [CrossRef] [PubMed]

24. Wan, Y.J.; Zhang, Y.L.; Zhou, Z.R.; Jia, R.X.; Li, M.; Song, H.; Wang, Z.Y.; Wang, L.Z.; Zhang, G.M.; You, J.H.; et al. Efficiency of donor cell preparation and recipient oocyte source for production of transgenic cloned dairy goats harboring human lactoferrin. *Theriogenology* **2012**, *78*, 583–592. [CrossRef] [PubMed]

25. Zhou, Z.R.; Zhong, B.S.; Jia, R.X.; Wan, Y.J.; Zhang, Y.L.; Fan, Y.X.; Wang, L.Z.; You, J.H.; Wang, Z.Y.; Wang, F. Production of myostatin-targeted goat by nuclear transfer from cultured adult somatic cells. *Theriogenology* **2013**, *79*, 225–233. [CrossRef] [PubMed]

26. Kumar, D.; Sarkhel, B.C. Differential expression pattern of key regulatory developmental genes in pre-implant zona free cloned vs in vitro fertilized goat embryos. *Gene Expr. Patterns* **2017**, *25*, 118–123. [CrossRef] [PubMed]

27. Baldassarre, H.; Wang, B.; Kafidi, N.; Keefer, C.L.; Lazaris, A.; Karatzas, C.N. Advances in the production and propagation of transgenic goats using laparoscopic ovum pick-up and in vitro embryo production technologies. *Theriogenology* **2002**, *57*, 275–284. [CrossRef]

28. Cheng, Y.; Wang, Y.G.; Luo, J.P.; Shen, Y.; Yang, Y.F.; Ju, H.M.; Zou, X.G.; Xu, S.F.; Lao, W.D.; Du, M. Cloned goats produced from the somatic cells of an adult transgenic goat. *Sheng Wu Gong Cheng Xue Bao (Chin. J. Biotechnol.)* **2002**, *18*, 79–83. (In Chinese)

29. Ohkoshi, K.; Takahashi, S.; Koyama, S.; Akagi, S.; Adachi, N.; Furusawa, T.; Fujimoto, J.; Takeda, K.; Kubo, M.; Izaike, Y.; et al. In vitro oocyte culture and somatic cell nuclear transfer used to produce a live-born cloned goat. *Cloning Stem Cells* **2003**, *5*, 109–115. [CrossRef]

30. Deng, M.; Liu, Z.; Ren, C.; An, S.; Wan, Y.; Wang, F. Highly methylated *Xist* in SCNT embryos was retained in deceased cloned female goats. *Reprod. Fertil. Dev.* **2019**, *31*, 855–866. [CrossRef]

31. Wang, F.; Kou, Z.; Zhang, Y.; Gao, S. Dynamic reprogramming of histone acetylation and methylation in the first cell cycle of cloned mouse embryos. *Biol. Reprod.* **2007**, *77*, 1007–1016. [CrossRef]

32. Deng, M.; Ren, C.; Liu, Z.; Zhang, G.; Wang, F.; Wan, Y. Epigenetic status of *H19-Igf2* imprinted genes and loss of 5-hydroxymethylcytosine in the brain of cloned goats. *Cell. Reprogram.* **2017**, *19*, 199–207. [CrossRef]

33. Han, C.; Deng, R.; Mao, T.; Luo, Y.; Wei, B.; Meng, P.; Zhao, L.; Zhang, Q.; Quan, F.; Liu, J.; et al. Overexpression of *Tet3* in donor cells enhances goat somatic cell nuclear transfer efficiency. *FEBS J.* **2018**, *285*, 2708–2723. [CrossRef]

34. Yang, F.; Hao, R.; Kessler, B.; Brem, G.; Wolf, E.; Zakhartchenko, V. Rabbit somatic cell cloning: Effects of donor cell type, histone acetylation status and chimeric embryo complementation. *Reproduction* **2007**, *133*, 219–230. [CrossRef]

35. Yamanaka, K.; Sugimura, S.; Wakai, T.; Kawahara, M.; Sato, E. Acetylation level of histone H3 in early embryonic stages affects subsequent development of miniature pig somatic cell nuclear transfer embryos. *J. Reprod. Dev.* **2009**, *55*, 638–644. [CrossRef]

36. Wan, Y.; Deng, M.; Zhang, G.; Ren, C.; Zhang, H.; Zhang, Y.; Wang, L.; Wang, F. Abnormal expression of DNA methyltransferases and genomic imprinting in cloned goat fibroblasts. *Cell Biol. Int.* **2016**, *40*, 74–82. [CrossRef]

37. Xiong, X.; Lan, D.; Li, J.; Zhong, J.; Zi, X.; Ma, L.; Wang, Y. Zebularine and scriptaid significantly improve epigenetic reprogramming of yak fibroblasts and cloning efficiency. *Cell. Reprogram.* **2013**, *15*, 293–300. [CrossRef]

38. Xiong, X.R.; Li, J.; Fu, M.; Gao, C.; Wang, Y.; Zhong, J.C. Oocyte extract improves epigenetic reprogramming of yak fibroblast cells and cloned embryo development. *Theriogenology* **2013**, *79*, 462–469. [CrossRef]

39. Zhang, Y.; Li, J.; Villemoes, K.; Pedersen, A.M.; Purup, S.; Vajta, G. An epigenetic modifier results in improved in vitro blastocyst production after somatic cell nuclear transfer. *Cloning Stem Cells* **2007**, *9*, 357–363. [CrossRef]

40. Wang, Y.S.; Xiong, X.R.; An, Z.X.; Wang, L.J.; Liu, J.; Quan, F.S.; Hua, S.; Zhang, Y. Production of cloned calves by combination treatment of both donor cells and early cloned embryos with 5-aza-2'-deoxycytidine and trichostatin A. *Theriogenology* **2011**, *75*, 819–825. [CrossRef]

41. Dutta, R.; Malakar, D.; Khate, K.; Sahu, S.; Akshey, Y.; Mukesh, M. A comparative study on efficiency of adult fibroblast, putative embryonic stem cell and lymphocyte as donor cells for production of handmade cloned embryos in goat and characterization of putative ntES cells obtained from these embryos. *Theriogenology* **2011**, *76*, 851–863. [CrossRef]

42. Gómez, M.C.; Biancardi, M.N.; Jenkins, J.A.; Dumas, C.; Galiguis, J.; Wang, G.; Earle Pope, C. Scriptaid and 5-aza-2'deoxycytidine enhanced expression of pluripotent genes and in vitro developmental competence in interspecies black-footed cat cloned embryos. *Reprod. Domest. Anim.* **2012**, *47*, 130–135. [CrossRef] [PubMed]

43. Zhao, J.; Hao, Y.; Ross, J.W.; Spate, L.D.; Walters, E.M.; Samuel, M.S.; Rieke, A.; Murphy, C.N.; Prather, R.S. Histone deacetylase inhibitors improve in vitro and in vivo developmental competence of somatic cell nuclear transfer porcine embryos. *Cell. Reprogram.* **2010**, *12*, 75–83. [CrossRef] [PubMed]

44. Kim, Y.J.; Ahn, K.S.; Kim, M.; Shim, H. Comparison of potency between histone deacetylase inhibitors trichostatin A and valproic acid on enhancing in vitro development of porcine somatic cell nuclear transfer embryos. *In Vitro Cell. Dev. Biol. Anim.* **2011**, *47*, 283–289. [CrossRef] [PubMed]

45. Baguisi, A.; Behboodi, E.; Melican, D.T.; Pollock, J.S.; Destrempes, M.M.; Cammuso, C.; Williams, J.L.; Nims, S.D.; Porter, C.A.; Midura, P.; et al. Production of goats by somatic cell nuclear transfer. *Nat. Biotechnol.* **1999**, *17*, 456–461. [CrossRef]

46. Baldassarre, H.; Keefer, C.; Wang, B.; Lazaris, A.; Karatzas, C.N. Nuclear transfer in goats using in vitro matured oocytes recovered by laparoscopic ovum pick-up. *Cloning Stem Cells* **2003**, *5*, 279–285. [CrossRef] [PubMed]

47. An, L.; Yang, L.; Huang, Y.; Cheng, Y.; Du, F. Generating goat mammary gland bioreactors for producing recombinant proteins by gene targeting. *Methods Mol. Biol.* **2019**, *1874*, 391–401. [PubMed]

48. Lu, R.; Zhang, T.; Wu, D.; He, Z.; Jiang, L.; Zhou, M.; Cheng, Y. Production of functional human CuZn-SOD and EC-SOD in bitransgenic cloned goat milk. *Transgenic Res.* **2018**, *27*, 343–354. [CrossRef]

49. Gash, K.K.; Yang, M.; Fan, Z.; Regouski, M.; Rutigliano, H.M.; Polejaeva, I.A. Assessment of microchimerism following somatic cell nuclear transfer and natural pregnancies in goats. *J. Anim. Sci.* **2019**, *97*, 3786–3794. [CrossRef]

50. Zhang, Y.L.; Zhang, G.M.; Wan, Y.J.; Jia, R.X.; Li, P.Z.; Han, L.; Wang, F.; Huang, M.R. Identification of transgenic cloned dairy goats harboring human lactoferrin and methylation status of the imprinted gene *IGF2R* in their lungs. *Genet. Mol. Res.* **2015**, *14*, 11099–11108. [CrossRef]

51. Meng, L.; Wan, Y.; Sun, Y.; Zhang, Y.; Wang, Z.; Song, Y.; Wang, F. Generation of five human lactoferrin transgenic cloned goats using fibroblast cells and their methylation status of putative differential methylation regions of *IGF2R* and *H19* imprinted genes. *PLoS ONE* **2013**, *8*, e77798. [CrossRef]

52. Zhang, J.; Liu, J.; Yang, W.; Cui, M.; Dai, B.; Dong, Y.; Yang, J.; Zhang, X.; Liu, D.; Liang, H.; et al. Comparison of gene editing efficiencies of CRISPR/Cas9 and TALEN for generation of *MSTN* knock-out cashmere goats. *Theriogenology* **2019**, *132*, 1–11. [CrossRef]

53. Ni, W.; Qiao, J.; Hu, S.; Zhao, X.; Regouski, M.; Yang, M.; Polejaeva, I.A.; Chen, C. Efficient gene knockout in goats using CRISPR/Cas9 system. *PLoS ONE* **2014**, *9*, e106718. [CrossRef]

54. Yu, B.; Lu, R.; Yuan, Y.; Zhang, T.; Song, S.; Qi, Z.; Shao, B.; Zhu, M.; Mi, F.; Cheng, Y. Efficient TALEN-mediated myostatin gene editing in goats. *BMC Dev. Biol.* **2016**, *16*, 26. [CrossRef]

55. Baldassarre, H.; Wang, B.; Kafidi, N.; Gauthier, M.; Neveu, N.; Lapointe, J.; Sneek, L.; Leduc, M.; Duguay, F.; Zhou, J.F.; et al. Production of transgenic goats by pronuclear microinjection of in vitro produced zygotes derived from oocytes recovered by laparoscopy. *Theriogenology* **2003**, *59*, 831–839. [CrossRef]

56. Zhang, T.; Yuan, Y.; Lu, R.; Xu, S.; Zhou, M.; Yuan, T.; Lu, Y.; Yan, K.; Cheng, Y. The goat β-casein/CMV chimeric promoter drives the expression of hLF in transgenic goats produced by cell transgene microinjection. *Int. J. Mol. Med.* **2019**, *44*, 2057–2064. [CrossRef]

57. Echelard, Y.; Ziomek, C.A.; Meade, H.M. Production of recombinant therapeutic proteins in the milk of transgenic animals. *BioPharm Int.* **2006**, *19*, 36–46.

58. Niemann, H.; Kues, W.A. Transgenic farm animals: An update. *Reprod. Fertil. Dev.* **2007**, *19*, 762–770. [CrossRef]

59. Shepelev, M.V.; Kalinichenko, S.V.; Deykin, A.V.; Korobko, I.V. Production of recombinant proteins in the milk of transgenic animals: Current state and prospects. *Acta Nat.* **2018**, *10*, 40–47. [CrossRef]

60. Echelard, Y.; Meade, H.M.; Ziomek, C.A. The first biopharmaceutical from transgenic animals: ATryn®. In *Modern Biopharmaceuticals: Design, Development and Optimization*; Knäblein, J., Ed.; WILEY-VCH Verlag GmbH & Co. KGaA: Weinheim, Germany, 2005; Chapter 11; pp. 995–1020, Print ISBN: 9783527311842, Online ISBN: 9783527620982, ISBN 9783527311842. [CrossRef]

61. Patnaik, M.M.; Moll, S. Inherited antithrombin deficiency: A review. *Haemophilia* **2008**, *14*, 1229–1239. [CrossRef]

62. Wang, X.; Yu, H.; Lei, A.; Zhou, J.; Zeng, W.; Zhu, H.; Dong, Z.; Niu, Y.; Shi, B.; Cai, B.; et al. Generation of gene-modified goats targeting *MSTN* and *FGF5* via zygote injection of CRISPR/Cas9 system. *Sci. Rep.* **2015**, *5*, 13878. [CrossRef] [PubMed]

63. Liu, C.; Li, W.; Zhang, X.; Zhang, N.; He, S.; Huang, J.; Ge, Y.; Liu, M. Knockdown of endogenous myostatin promotes sheep myoblast proliferation. *In Vitro Cell. Dev. Biol. Anim.* **2014**, *50*, 94–102. [CrossRef] [PubMed]

64. Petersen, B.; Niemann, H. Molecular scissors and their application in genetically modified farm animals. *Transgenic Res.* **2015**, *24*, 381–396. [CrossRef] [PubMed]

65. Zhang, C.; Wang, L.; Ren, G.; Li, Z.; Ren, C.; Zhang, T.; Xu, K.; Zhang, Z. Targeted disruption of the sheep *MSTN* gene by engineered zinc-finger nucleases. *Mol. Biol. Rep.* **2014**, *41*, 209–215. [CrossRef]

66. Miller, J.C.; Tan, S.; Qiao, G.; Barlow, K.A.; Wang, J.; Xia, D.F.; Meng, X.; Paschon, D.E.; Leung, E.; Hinkley, S.J.; et al. A TALE nuclease architecture for efficient genome editing. *Nat. Biotechnol.* **2011**, *29*, 143–148. [CrossRef]

67. Frock, R.L.; Hu, J.; Meyers, R.M.; Ho, Y.J.; Kii, E.; Alt, F.W. Genome-wide detection of DNA double-stranded breaks induced by engineered nucleases. *Nat. Biotechnol.* **2015**, *33*, 179–186. [CrossRef]

68. Hu, J.H.; Davis, K.M.; Liu, D.R. Chemical biology approaches to genome editing: Understanding, controlling, and delivering programmable nucleases. *Cell Chem. Biol.* **2016**, *23*, 57–73. [CrossRef]

69. Hao, F.; Yan, W.; Li, X.; Wang, H.; Wang, Y.; Hu, X.; Liu, X.; Liang, H.; Liu, D. Generation of cashmere goats carrying an *EDAR* gene mutant using CRISPR-Cas9-mediated genome editing. *Int. J. Biol. Sci.* **2018**, *14*, 427–436. [CrossRef]

70. Fan, Z.; Yang, M.; Regouski, M.; Polejaeva, I.A. Gene knockouts in goats using CRISPR/Cas9 system and somatic cell nuclear transfer. *Methods Mol. Biol.* **2019**, *1874*, 373–390.

71. Kalds, P.; Zhou, S.; Cai, B.; Liu, J.; Wang, Y.; Petersen, B.; Sonstegard, T.; Wang, X.; Chen, Y. Sheep and goat genome engineering: From random transgenesis to the CRISPR era. *Front. Genet.* **2019**, *10*, 750. [CrossRef]

The Relative Abundances of Human Leukocyte Antigen-E, α-Galactosidase A and α-Gal Antigenic Determinants Are Biased by Trichostatin A-Dependent Epigenetic Transformation of Triple-Transgenic Pig-Derived Dermal Fibroblast Cells

Marcin Samiec [1,*] , Jerzy Wiater [2,*] , Kamil Wartalski [2] , Maria Skrzyszowska [1] , Monika Trzcińska [1] , Daniel Lipiński [3] , Jacek Jura [1] , Zdzisław Smorąg [1] , Ryszard Słomski [3,4] and Małgorzata Duda [5]

1   Department of Reproductive Biotechnology and Cryoconservation, National Research Institute of Animal Production, Krakowska 1 Street, 32-083 Balice, Poland
2   Department of Histology, Jagiellonian University Medical College, Kopernika 7 Street, 31-034 Kraków, Poland
3   Department of Biochemistry and Biotechnology, Poznań University of Life Sciences, Dojazd 11 Street, 60-647 Poznań, Poland
4   Institute of Human Genetics, Polish Academy of Sciences, Strzeszyńska 32 Street, 60-479 Poznań, Poland
5   Department of Endocrinology, Institute of Zoology and Biomedical Research, Faculty of Biology, Jagiellonian University in Krakow, Gronostajowa 9 Street, 30-387 Kraków, Poland
*   Correspondence: marcin.samiec@iz.edu.pl (M.S.); jerzy.wiater@uj.edu.pl (J.W.)

Abstract: The present study sought to establish the mitotically stable adult cutaneous fibroblast cell (ACFC) lines stemming from h*FUT2*×h*GLA*×*HLA-E* triple-transgenic pigs followed by trichostatin A (TSA)-assisted epigenetically modulating the reprogrammability of the transgenes permanently incorporated into the host genome and subsequent comprehensive analysis of molecular signatures related to proteomically profiling the generated ACFC lines. The results of Western blot and immunofluorescence analyses have proved that the profiles of relative abundance (RA) noticed for both recombinant human α-galactosidase A (rhα-Gal A) and human leukocyte antigen-E (HLA-E) underwent significant upregulations in tri-transgenic (3×TG) ACFCs subjected to TSA-mediated epigenetic transformation as compared to not only their TSA-unexposed counterparts but also TSA-treated and untreated non-transgenic (nTG) cells. The RT-qPCR-based analysis of porcine tri-genetically engineered ACFCs revealed stable expression of mRNA fractions transcribed from h*FUT2*, h*GLA* and *HLA-E* transgenes as compared to a lack of such transcriptional activities in non-transgenic ACFC variants. Furthermore, although TSA-based epigenomic modulation has given rise to a remarkable increase in the expression levels of Galα1→3Gal (α-Gal) epitopes that have been determined by lectin blotting analysis, their semi-quantitative profiles have dwindled profoundly in both TSA-exposed and unexposed 3×TG ACFCs as compared to their nTG counterparts. In conclusion, thoroughly exploring proteomic signatures in such epigenetically modulated ex vivo models devised on h*FUT2*×h*GLA*×*HLA-E* triple-transgenic ACFCs that display augmented reprogrammability of translational activities of two mRNA transcripts coding for rhα-Gal A and HLA-E proteins might provide a completely novel and powerful research tool for the panel of further studies. The objective of these future studies should be to multiply the tri-transgenic pigs with the aid of somatic cell nuclear transfer (SCNT)-based cloning for the purposes of both xenografting the porcine cutaneous bioprostheses and dermoplasty-mediated surgical treatments in human patients.

Keywords: swine; trichostatin A; epigenetic transformation; ex vivo model; tri-genetically modified; ACFC line; HLA-E; rhα-Gal A; rhα1,2-FT; α-Gal antigenic determinant; porcine skin xenograft

1. Introduction

At the present stage of investigations in the fields of transplantation medicine and immunology, swine tissues and organs may be an alternative to their human counterparts.

This is a highlight of research in an era of huge shortages of tissues and organs for allotransplantation, also taking into account a deficiency of allogeneic dermo-epidermal grafts in reconstructive medicine of the human integumentary system and dermoplasty-based therapies targeted at cutaneous/subcutaneous tissue engineering. The choice of pigs as donors of xenografts is not accidental. Firstly, anatomohistological and anatomo-topographical biocompatibility of porcine tissues, organs and organ systems with their human counterparts determines, to a large extent, closely related physiological sufficiency of organs in these two mammalian species. Secondly, the genetic similarity between humans and domestic pigs is very high, reaching a level oscillating around 96%. Thirdly, *Sus scrofa domesticus* taxon is characterized by tremendously efficient outcomes noticed for species-specific fertility and prolificacy, which makes this livestock species relatively easy to breed [1–5]. Nonetheless, a lack of taxonomic consanguinity occurring between humans and pigs results in the appearance of interspecies immunophysiological incompatibility that largely limits and even prevents completely surgical treatments aimed at xenografting and xenogeneic tissue engineering. This interspecies immunological hindrance is triggered by the presence of a plasmalemma-anchored oligosaccharide moieties of glycoproteins and glycolipids, i.e., Galα(1,3)Galβ(1,4)GlcNAc-R that are designated as the α-Gal antigenic determinants or Galα1→3Gal epitopes on the surface of a vast majority of porcine cells (especially those forming vascular endothelium) [6]. The Galα1→3Gal epitope is common in mammals, but humans and apes have lost this structure through evolution [3,7]. Humans and apes produce natural antibodies against the Galα1→3Gal epitope. Unfortunately, the binding of these antibodies to the Galα1→3Gal epitope leads to hyperacute rejection (HAR) or acute humoral and cellular rejection of porcine xenografts [8–10]. The efforts undertaken to overcome the porcine→human immunological obstacle gave rise to the generation of transgenic pigs exhibiting a reduced or completely abrogated expression of the Galα1→3Gal epitopes [11]. The Galα1→3Gal epitopes can be removed from the surface of porcine cells by stably incorporating the h*FUT2* and h*GLA* gene constructs that is mediated by their intrapronuclear microinjection into porcine fertilized ova (zygotes) [4]. The h*FUT2* gene encodes the enzyme termed as α1,2-fucosyltransferase (H-transferase; α1,2-FT), which is responsible for the formation of the H structure, the core of the system of blood groups AB0 in humans. The action of α1,2-FT blocks the synthesis of the Galα1→3Gal epitope, while promoting the formation of the H structure, which is neutral for the human immune system [12]. The h*GLA* gene encodes human α-galactosidase A (α-Gal A), an enzyme that biocatalyzes the reaction directed to cleave terminal D-galactose residues from the Galα1→3Gal epitope. Deprivation of the Galα1→3Gal epitope of the terminal D-galactose molecules remarkably attenuates its xenoreactivity. This structure becomes undetectable by specific antibodies [13]. Another pivotal problem is the interspecies (porcine→human) immunological incompatibility that arises from phylogenetic divergence and subsequently brings about the species-specific variability at the level of major histocompatibility complex (MHC) proteins. To overcome this limitation, transgenic pigs expressing the *HLA-E* gene are indispensable. The effectiveness of this genetic modification has been proven by research confirming that the presence of human leukocyte antigen-E (HLA-E) molecules in porcine endothelial cells protects them against attack by human NK (natural killer) lymphocytes [14]. Pigs displaying the expression of the *HLA-E* transgene have been successfully created with the aid of intrapronuclear microinjection of the zygotes [15].

It is noteworthy that the applied genetic modification does not always result in a satisfactory (sufficiently high) level of expression of the transgenes integrated with the nuclear host genome. One of the ways to increase the expression of foreign (xenogeneic) genes introduced into the genomic DNA of recipient cells appears to be their epigenetic transformation applying non-specific inhibitors of histone deacetylases (HDACi). Our previous study [16] proved, for the first time, that the use of non-selective HDACi designated as trichostatin A (TSA) for the epigenomic modulation of porcine h*FUT2*×h*GLA* bi-transgenic adult cutaneous fibroblast cells (ACFCs) has contributed to improved reprogrammability followed by increased translational activities identified for mRNA transcripts

synthesized from h*FUT2* and h*GLA* transgenes. Moreover, the action of TSA as a non-specific epigenetic modifier has been reflected in the augmented expression of pivotal genes coding for structural, enzymatic and other functional proteins indispensable for the biosynthesis and bioaccumulation of the Galα1→3Gal antigenic determinants. However, TSA has been shown to simultaneously enhance the expression of the incorporated h*FUT2*×h*GLA* gene constructs more strongly, so that the extent of Galα1→3Gal epitope silencing estimated for TSA-treated double-transgenic ACFCs was considerably higher than that noticed for TSA-untreated non-transgenic cells. Therefore, the TSA-mediated approach to epigenomically modulate the bi-genetically engineered variant of ACFC lines turned out to be beneficial, since it caused a remarkably diminished incidence of Galα1→3Gal epitopes in this ACFC type [16]. The molecular mechanisms underlying the capabilities of transgenes to epigenetically reprogram their transcriptional activities are complex. They involve amplifying the extent of lysine acetylation (i.e., hyperacetylation) within histones forming chromatin-derived nucleosomal cores. In our previously devised model of bi-transgenic ACFCs [16], hyperacetylation seemed to result from alleviation of biocatalytic functions of HDACs by TSA. A TSA-prompted decline in histone deacetylation may also affect other processes, such as the demethylation of DNA cytosine residues, incurring their intensification. A broad spectrum of non-specific HDACi, including TSA, and/or non-specific inhibitors of DNA methyltransferases (DNMTi) and/or selective inhibitors of histone methyltransferases (HMTi) have been formerly utilized in the strategies aimed to epigenomically modulate nuclear recipient oocytes [17–19], nuclear donor cells [20–23] and activated nuclear-transferred oocytes in pigs and other mammalian species [24–26]. These strategies have been developed to predominantly facilitate/refine the reprogramming of epigenomic memory and subsequently enhance the transcriptional activity of donor cell nuclear genomes in mammalian cloned embryos propagated by somatic cell nuclear transfer (SCNT) [27–31].

Taking into consideration all the aforementioned findings, h*FUT2*×h*GLA*×*HLA-E* tri-transgenic ACFC lines also needed to be tested separately by designing their models of the ex vivo migration and expansion under the conditions of TSA-dependent epigenetic transformation. In the current investigation, on the one hand, we have decided to unravel proteomic signatures related to relative abundances (RAs) estimated for HLA-E, rhα-Gal A and rhα1,2-FT in porcine triple-transgenic ACFCs undergoing TSA-assisted epigenomic modulation. On the other hand, the present study sought to decipher semi-quantitative profiles of α-Gal epitopes at the glycoprotein level. This research is the first to comprehensively assess the TSA-expedited enhancement of capabilities of transgene-encoded transcripts to epigenomically reprogram their translational activities in the ex vivo models elaborated to explore proteomic and glycoproteomic profiles in porcine h*FUT2*×h*GLA*×*HLA-E* tri-genetically engineered ACFC lines.

2. Results

2.1. Western Blot Analysis of the RA Pinpointed for HLA-E, rhα1,2-FT and rhα-Gal A Proteins in the Ex Vivo-Expanded Porcine Triple- and Non-Transgenic ACFCs Undergoing or Not Undergoing TSA-Mediated Epigenetic Transformation

In vitro proliferating ACFC lines exposed and not exposed to TSA (TSA$^+$ and TSA$^-$, respectively) were established from dermal explants that had been recovered post-mortem from either h*FUT2*×h*GLA*×*HLA-E* triple-transgenic pigs or their non-transgenic counterparts served as a control group (CTR nTG). Western blot analysis of total protein samples revealed the presence of rhα1,2-FT, rhα-Gal A and HLA-E proteins in all the tri-transgenic samples (Figure 1A). For the TSA$^-$ control group, a weak positive signal stemming from all the analyzed proteins was noticed, but it was shown to be unremarkable. In contrast, Western blot analysis of total protein samples derived from TSA$^+$ ACFCs confirmed the occurrence of clear positive signals for not only rhα1,2-FT but also rhα-Gal A and HLA-E. Signal intensities of analyzed proteins were normalized to β-actin, which was used as a loading control. The semi-quantitative analysis of Western blot strongly supported our findings. Indeed, the relative expression of the HLA-E and rhα-Gal A proteins has been

proven to significantly increase (at least $p < 0.05$) in TSA-treated tri-genetically modified ACFCs as compared to the relevant samples originating from TSA-untreated $3 \times$TG cells (Figure 1B–D). In turn, we did not observe significant differences in the relative expression of rhα1,2-FT between total protein samples derived from TSA$^+$ and TSA$^-$ triple-transgenic ACFCs. Interestingly, a clear positive signal was also identified for not only α1,2-FT and α-Gal A enzymes but also swine homolog of the HLA-E (shHLA-E) protein in TSA$^+$ ACFCs stemming from CTR nTG pigs. This result has been confirmed both qualitatively and semi-quantitatively (at least $p < 0.05$) (Figure 1B–D). It is noteworthy that pigs are characterized by the lack of α-Gal A protein expression, which arises from species-specific silencing both alleles of p*GLA* gene. Taking this finding into consideration, the epigenetic alterations resulting from the conditions of either in vitro culture or TSA-assisted epigenomic modulation seem to trigger, to some extent, the onset of transcriptional and translational activities for p*GLA* alleles and their transcribed mRNAs in the ex vivo-expanded porcine CTR nTG ACFCs.
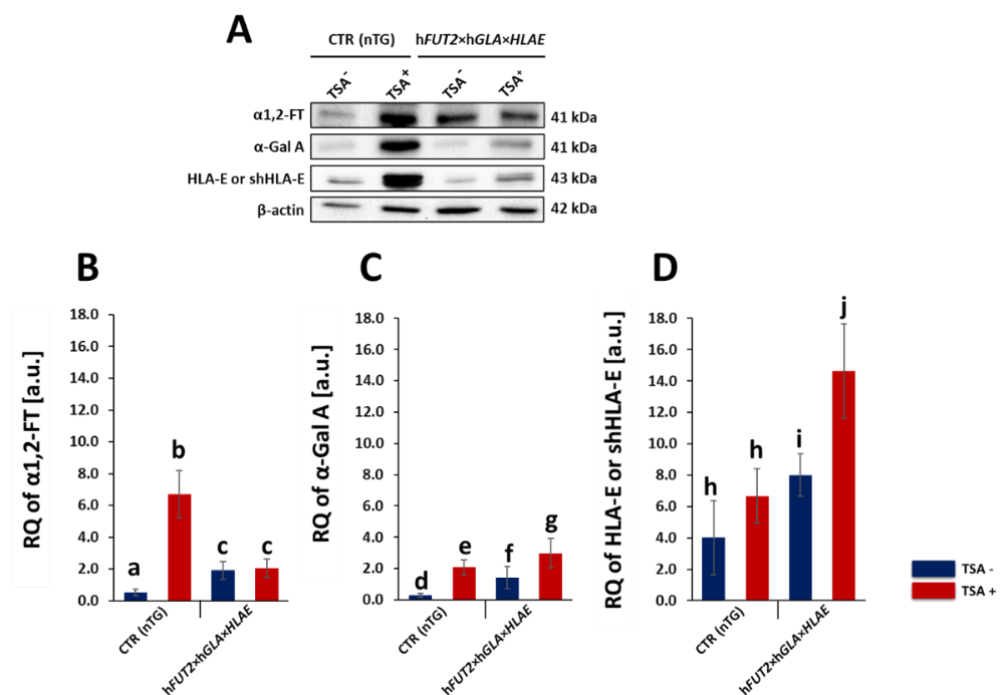
Figure 1. Western blot analysis of the relative expression of human α1,2-fucosyltransferase (α1,2-FT), α-galactosidase A (α-Gal A) and human leukocyte antigen-E (HLA-E) proteins in porcine triple-transgenic and non-transgenic ACFCs epigenetically transformed or not transformed with trichostatin A (TSA$^+$ and TSA$^-$, respectively). Representative blots of the expression of α1,2-FT, α-Gal A and HLA-E proteins in the ACFC samples derived from epigenomically modified (TSA$^+$) and non-modified (TSA$^-$) groups—panel (**A**). The samples stemming from non-transgenic pigs served as a control group (CTR nTG)—panel (**A**). β-Actin provided a loading control for all the analyzed samples. The results of relative expression (in arbitrary units) of α1,2-FT, α-Gal A and HLA-E or swine homolog of HLA-E (shHLA-E) are shown in panels (**B–D**), respectively. The relative optical density (ROD) from three separate analyses of at least three animals for each variant is expressed as mean. The bar graphs show the mean $\pm$ SEM. Statistics: one-way ANOVA and Newman–Keuls post hoc test. The bars marked with different letters vary significantly; values denoted as a-b, b-c, e-g: $p < 0.01$; a-c, d-e, e-g, f-g, h-i, h-j, i-j: $p < 0.05$.

2.2. RT-qPCR-Mediated Confirmation of Stability in the Expression Profiles Pinpointed for hFUT2, hGLA and HLA-E mRNA Transcripts in the Ex Vivo-Expanded Porcine Triple-Transgenic ACFCs Subjected or Not Subjected to TSA-Assisted Epigenetic Transformation

To ascertain the stability of transgene-encoded transcripts in porcine h*FUT2*$\times$h*GLA*$\times$*HLA-E* triple-transgenic ACFCs that either did or did not undergo TSA-dependent epigenetic

transformation (TSA− and TSA+, respectively), the RT-qPCR analysis was performed to detect the quantitative expression profiles noticed for h*FUT2* mRNA, h*GLA* mRNA and *HLA-E* mRNA. The obtained results confirmed a significant upregulation of all three investigated human genes in porcine tri-transgenic ACFCs originating from the TSA− group ($p < 0.001$) (Figure 2A). In turn, estimating the relative quantities that were identified for h*FUT2*, h*GLA* and *HLA-E* transcripts in porcine triple-transgenic ACFCs stemming from the TSA+ group indicated a much smaller upward trend as compared to the control non-transgenic group (CTR nTG), but this augmentation also turned out to be statistically significant ($p < 0.001$) (Figure 2B).
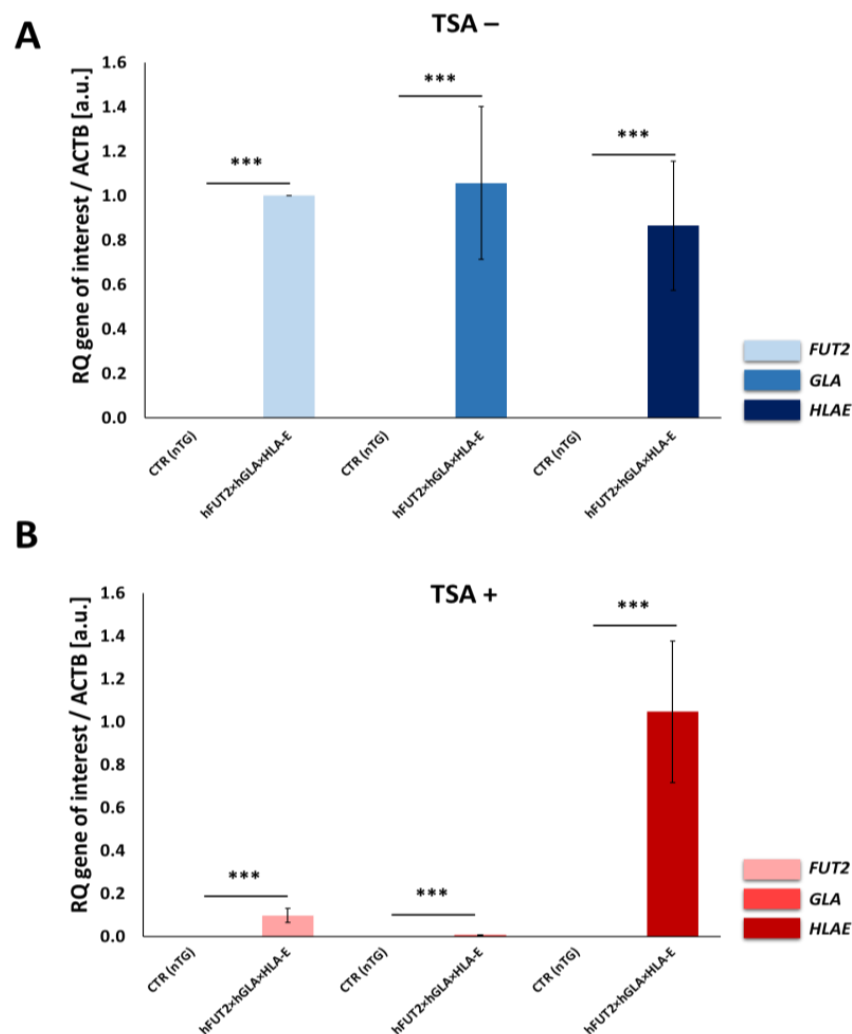
Figure 2. RT-qPCR analysis of the relative expression of human genes: h*FUT2*, h*GLA* and *HLA-E* in porcine triple-transgenic (3×TG) ACFCs epigenetically not transformed (**A**) or transformed (**B**) with trichostatin A (TSA− and TSA+, respectively). The p*ACTB* gene encoding porcine β-actin was used as endogenous reference gene. The bar graphs show the mean ± SEM. Statistics: one-way ANOVA and Newman–Keuls post hoc test. The bars marked with different letters vary significantly; values denoted as *** $p < 0.001$. The numbers of biological replicates (i.e., numbers of 3×TG and CTR nTG pigs serving as independent biological donors) ≥ 3. Number of technical replicates = 3 (within each biological replicate).

2.3. Immunofluorescence Localization of HLA-E, rhα1,2-FT and rhα-Gal A in the Ex Vivo-Expanded Porcine Triple- and Non-Transgenic ACFCs Epigenetically Transformed or Not Transformed by TSA Treatment

The localization of the HLA-E, rhα1,2-FT and rhα-Gal A proteins was examined by immunofluorescence staining of TSA-treated (TSA⁺) and untreated (TSA⁻) ACFCs derived

from h*FUT2*×h*GLA*×*HLA-E* triple-transgenic (Figure 3) and non-transgenic (Figure 4) pigs used as a control group (CTR nTG).

Figure 3. Immunofluorescence analysis of ex vivo-expanded porcine ACFCs epigenomically modulated (TSA+) (**b**,**d**,**f**) and not modulated with trichostatin A (TSA−) (**a**,**c**,**e**). Representative microphotographs of immunofluorescence localization of human leukocyte antigen-E (HLA-E; (**a**,**b**)), recombinant human α1,2-fucosyltransferase (rhα1,2-FT; (**c**,**d**)) and α-galactosidase A (rhα-Gal A; (**e**,**f**)) in ACFCs originating from h*FUT2*×h*GLA*×*HLA-E* triple-transgenic pigs. Immunofluorescent staining with Alexa Fluor 488- or Cy3-labelled secondary antibodies (green and red fluorescence, respectively) and DAPI counterstaining (blue fluorescence). Scale bars represent 100 μm. Immunoreaction was performed on ex vivo proliferating porcine ACFCs derived from at least three pigs of each experimental group. The immunofluorescence signal arisen from rhα1,2-FT was distributed in the perinuclear region of all the analyzed ACFCs from each variant. The MHC representative termed as HLA-E and rhα-Gal A enzyme were homogeneously located in whole cytoplasm of all the analyzed ACFCs. The TSA⁺ ACFCs were characterized by largely intensified signal estimated for both HLA-E and rhα-Gal A proteins (**b**,**f**), but not for rhα1,2-FT (**d**) as compared to their TSA⁻ cell counterparts (**a**,**c**,**e**).
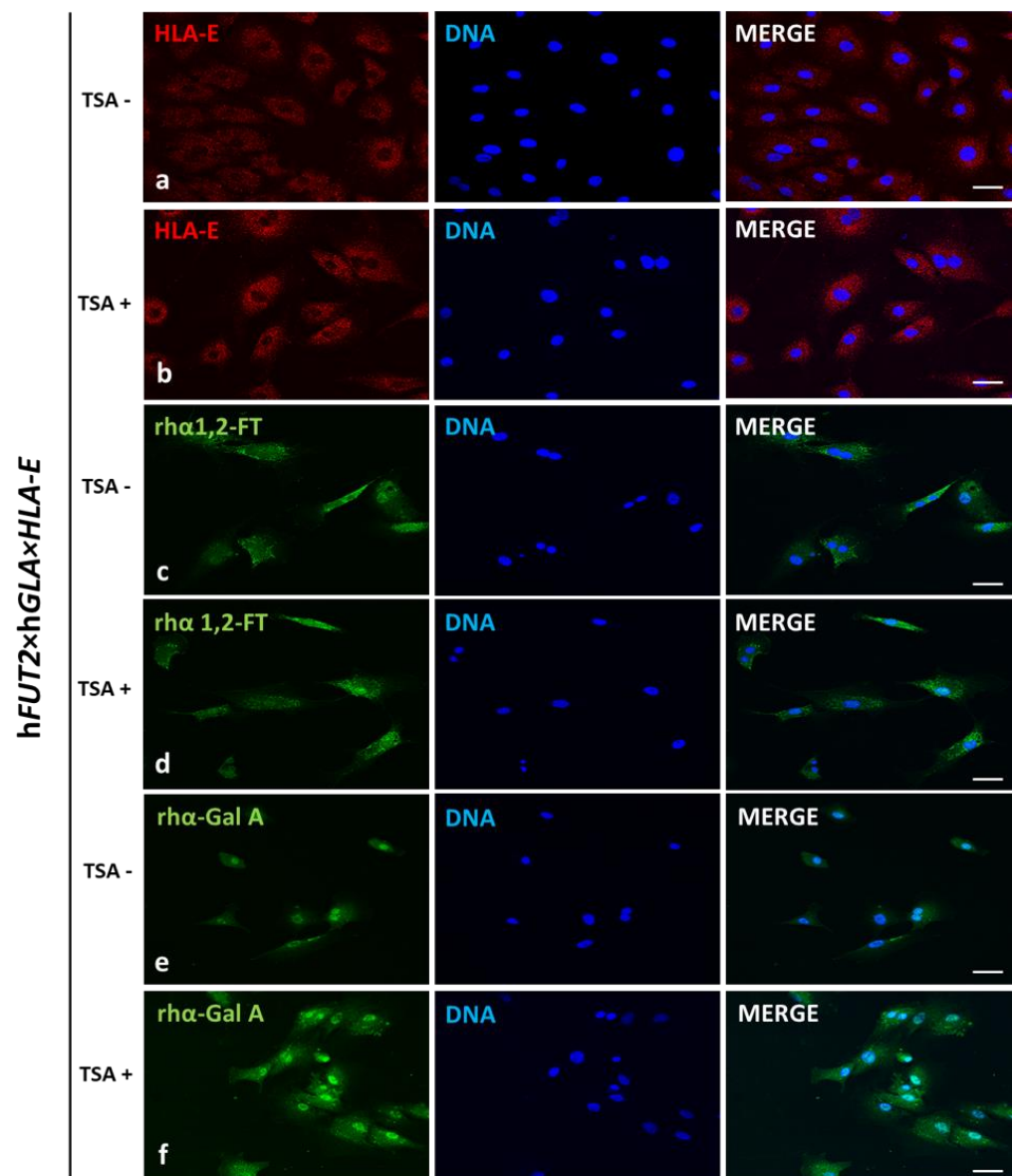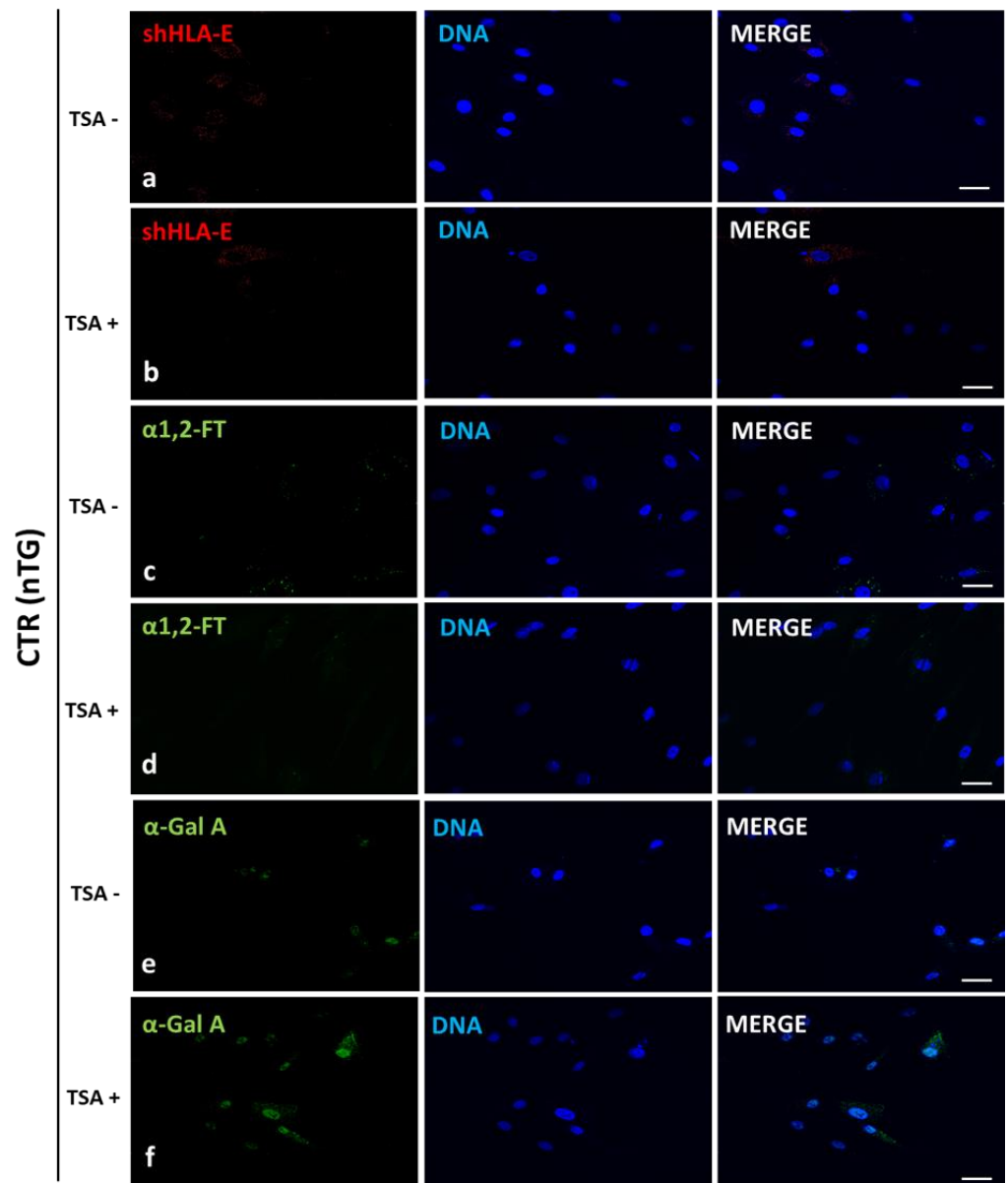
Figure 4. Immunofluorescence analysis of the ex vivo-expanded porcine ACFCs epigenomically modulated (TSA+) (**b**,**d**,**f**) and not modulated with trichostatin A (TSA−) (**a**,**c**,**e**). Representative microphotographs of immunofluorescence localization of swine homolog of human leukocyte antigen-E (shHLA-E; (**a**,**b**)), α1,2-fucosyltransferase (α1,2-FT; (**c**,**d**)) and α-galactosidase A (α-Gal A; (**e**,**f**)) in ACFCs stemming from non-transgenic pigs (CTR nTG). Immunofluorescent staining with Alexa Fluor 488- or Cy3-labelled secondary antibodies (green and red fluorescence, respectively) and DAPI counterstaining (blue fluorescence). Scale bars represent 100 μm. Immunoreaction was performed on ex vivo proliferating porcine ACFCs derived from at least three pigs of each experimental group. TSA⁺ ACFCs displayed more highly intensified signals identified for not only shHLA-E but also α1,2-FT and α-Gal A proteins in control non-transgenic (CTR nTG) ACFCs (**b**,**d**,**f**). No positive signals originating from either shHLA-E representative of MHC or α1,2-FT and α-Gal A enzymes were observed in the TSA⁻ CTR nTG group (**a**,**c**,**e**).

The positive immunofluorescence signals descended from HLA-E and rhα-Gal A were found to be dispersed homogenously and intensively detectable in the whole cytoplasm of h*FUT2*×h*GLA*×*HLA-E* triple-transgenic ACFCs (Figure 3). In turn, the signal identified for rhα1,2-FT was mainly distributed in small perinuclear clusters in tri-genetically engineered ACFCs. Remarkably stronger immunofluorescence signals were observed for both HLA-

E and rhα-Gal A proteins in TSA$^+$ ACFCs (Figure 3b,f). Interestingly, no differences in rhα1,2-FT-derived immunofluorescence signal intensity took place between ACFCs exposed to TSA (TSA$^+$) and their cell counterparts not exposed to this HDACi (TSA$^-$) (Figure 3c,d). Moreover, a weak immunofluorescence signal stemming from all the analyzed proteins was noticed for control non-transgenic (CTR nTG) ACFCs subjected to TSA-based epigenetic transformation (Figure 4b,d,f). However, in TSA$^-$ CTR nTG ACFCs, swine homolog of HLA-E and α1,2-FT enzyme were shown to be scarcely detectable by immunofluorescence, whereas no positive signal descended from intrinsic species-specific α-Gal A enzyme was identified (Figure 4).

2.4. Lectin Blotting Analysis of Galα1→3Gal Epitope Expression at the Protein Level in the Ex Vivo-Expanded Porcine Triple- and Non-Transgenic ACFCs Subjected or Not Subjected to TSA-Dependent Epigenetic Transformation

The expression profile of Galα1→3Gal epitopes at the total protein level was estimated by lectin blot analysis using horseradish peroxidase (HRP)-conjugated isolectin GS I-B$_4$. The results of our study confirmed that significantly decreased expression of Galα1→3Gal epitopes was identified in h*FUT2*×h*GLA*×*HLA-E* tri-transgenic (3×TG) ACFCs as compared to their CTR nTG cell counterparts. In turn, for both groups (CTR nTG and 3×TG), the RA noticed for Galα1→3Gal antigenic determinants was proven to increase significantly in protein samples derived from ex vivo proliferating ACFCs epigenetically transformed with TSA (TSA$^+$; Figure 5A). β-Actin served as a loading control protein. The semi-quantitative analysis of protein samples extracted from TSA-unmodulated (TSA$^-$) and modulated (TSA$^+$) tri-genetically modified ACFCs positively verified these observations. The significantly lowest RA estimated for Galα1→3Gal epitopes was identified in TSA-untransformed ACFCs originating from h*FUT2*×h*GLA*×*HLA-E* triple-transgenic pigs, indicating the occurrence of statistical variability in relation to the TSA$^-$ CTR nTG ($p < 0.05$) and TSA$^+$ CTR nTG groups ($p < 0.05$). The semi-quantitative profile of Galα1→3Gal epitopes in ACFCs stemming from the TSA$^+$ 3×TG group was significantly higher ($p < 0.05$) than that pinpointed for ACFCs assigned to the TSA$^-$ 3×TG group, but it was shown to be still lower than that recognized for both CTR nTG groups ($p < 0.05$) (Figure 5B).
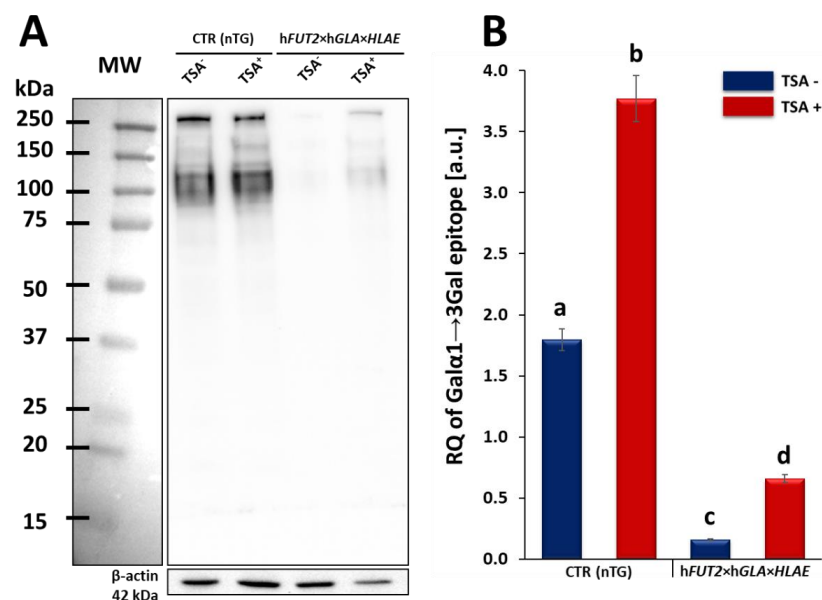
Figure 5. Lectin blot analysis of Galα1→3Gal epitope expression at the protein level in the ex vivo-expanded porcine h*FUT2*×h*GLA*×*HLA-E* tri-transgenic (3×TG) and control non-transgenic (CTR nTG) ACFCs epigenetically transformed (TSA$^+$) or not transformed with trichostatin A (TSA$^-$). (**A**) Representative lectin blots of the expression of Galα1→3Gal (α-Gal) epitopes in TSA$^-$ and TSA$^+$

ex vivoproliferating ACFCs established from dermal tissue explants stemming from CTR nTG and 3×TG pigs. MW indicates the molecular weight of protein standards (Precision Plus Protein™ Dual Color Standards, Bio-Rad). Each band represents a glycosylated protein containing the Galα1→3Gal antigenic determinant. β-Actin provided a loading control for all the analyzed samples. (**B**) The semi-quantitative analysis of relative expression pinpointed for Galα1→3Gal epitopes (in arbitrary units). Relative optical density (ROD) from three separate analyses of at least three animals for each variant is expressed as mean. Graph bar shows the mean ± SEM. Statistics: one-way ANOVA and Newman–Keuls post hoc test. The bars marked with different letters vary significantly. Values denoted as a-b: $p < 0.01$; a-c, a-d, b-c, b-d, c-d: $p < 0.05$. It is worth highlighting that the semi-quantitative profile of Galα1→3Gal epitopes dwindled significantly in TSA-untransformed and transformed ACFCs stemming from h*FUT2*×h*GLA*×*HLA-E* triple-transgenic pigs as compared to the TSA-unexposed and exposed ACFCs originating from CTR nTG specimens. Nonetheless, the protein samples isolated from TSA-unmodulated 3×TG ACFCs exhibited the significantly lowest relative abundance (RA) noticed for Galα1→3Gal epitopes. Taking into consideration both tri-genetically modified and non-modified ACFCs, RAs estimated for Galα1→3Gal antigenic determinants increased significantly in protein samples derived from TSA$^+$ cells as compared to those recognized for their protein counterparts extracted from TSA$^-$ cells. However, the level of α-Gal epitopes pinpointed for TSA-modulated 3×TG ACFCs was still profoundly lower than the semi-quantitative profiles of α-Gal antigenic determinants observed in TSA-modulated and unmodulated CTR nTG ACFCs.

3. Discussion

The use of swine tissues and organs seems to be a response to the current shortage of organs for allogeneic transplantation in humans, considering also a paucity of human dermo-integumentary allografts. However, due to hyperacute rejection, which is the main obstacle in pig-to-human xenotransplantation, genetically modified pigs need to be propagated and multiplied [4]. Currently, many methods of genetic modification are available. At first, they encompass the generation of homozygous pigs lacking the gene coding for α1,3-galactosyltransferase (α1,3-GT) for the purpose of depletion of anti-pig antibodies [11]. Secondly, removal of the Galα1→3Gal epitopes using genetically engineered enzymes is taken into account, ending at the production of pigs transgenic for some graft-protective proteins [32–35].

In our current study, we applied Western blotting and immunofluorescence staining with confocal microscopy to assess the effect of TSA-triggered epigenetic modulation both on the overexpression of HLA-E, rhα1,2-FT and rhα-Gal A proteins and on the RA of Galα1→3Gal antigenic determinants in porcine h*FUT2*×h*GLA*×*HLA-E* tri-transgenic ACFC lines as compared to their non-transgenic counterparts. Since genetically modified pigs have been successfully generated to avoid hyperacute rejection of tissue/organ xenografts [12,13,36], we have decided to conduct the next panel of research, in which we discuss this aspect in regard to the ex vivo models based on the mitotically stable triple-transgenic ACFCs undergoing TSA-prompted epigenetic transformation followed by profound examination of molecular signatures dependent on proteomic and glycoproteomic profiles. The results of Western blot and immunofluorescence analyses revealed considerable enhancements in the expression of rhα-Gal A and HLA-E but not rhα1,2-FT in TSA-modulated tri-genetically engineered ACFCs as compared to their cell counterparts not modulated by TSA treatment. Furthermore, immunofluorescence staining with antibodies against HLA-E, rhα1,2-FT and rhα-Gal A has provided strong evidence that TSA-assisted epigenetic transformation leads to a significant increase in the expression levels estimated for HLA-E and rhα-Gal A but not for rhα1,2-FT in triple-transgenic ACFC lines. Our previous study [16] has confirmed that the semi-quantitative profiles of both rhα-Gal A and rhα1,2-FT were characterized by remarkable augmentation in porcine h*FUT2*×h*GLA* bi-transgenic ACFCs subjected to TSA-mediated epigenomic modulation. In turn, lectin blotting analysis has demonstrated a similar decrease in the RAs pinpointed for Galα1→3Gal epitopes in TSA-modified triple-transgenic ACFCs as those recognized for α-Gal antigenic determinants in the TSA-modulated double-transgenic ACFC coun-

terparts [16]. For those reasons, it can be assumed that the lack of a profound influence of TSA-induced epigenetic modification on the RA noticed for rhα1,2-FT in tri-genetically engineered ACFCs does not relieve the capability of this enzyme to abrogate the expression of the Galα1→3Gal epitopes. It is also possible that TSA-facilitated amelioration of the semi-quantitative profiles of rhα-Gal A alone had the remarkable effect of reducing the molecular levels of α-Gal antigenic determinants. Another study has proved that the biocatalytic activity of only human α-Gal A alone alleviated the relative abundance of Galα1→3Gal epitopes by 78%, and the co-expression of human α1,2-FT and α-Gal A enzymes diminished the quantitative profile of α-Gal antigenic determinants to a negligible level on the surface of porcine genetically modified aortic endothelial cells subjected to SV40-mediated immortalization [37]. The study by Wiater et al. [38], in which confocal microscopy and lectin blotting analyses were accomplished to molecularly evaluate the proteomic and glycoproteomic signatures occurring in liver-derived tissue explants originating from h*FUT2*×h*GLA* double-transgenic pigs, has shown that the co-expression of human α-Gal A and α1,2-FT enzymes has led to a decline in RAs of Galα1→3Gal epitopes by 62% (as has been proven on the basis of intensity of fluorescence) and by 47% (as has been proven on the basis of blotting), respectively. The failure to completely suppress the expression of Galα1→3Gal antigenic determinants in the above-indicated studies seems to arise from low molecular levels of rhα1,2-FT and rhα-Gal A enzymes. Therefore, the use of TSA-assisted epigenomic modulation of genetically engineered cells to enhance the relative expression of these enzymatic proteins appears to be a powerful tool suitable for the solution to this problem. However, taking into consideration the fact that the impacts of TSA-dependent epigenetic transformation of porcine tri-transgenic ACFCs have been exerted not only on the semi-quantitative profiles of rhα-Gal A and HLA-E proteins but also on the RAs recognized for Galα1→3Gal epitopes, these results are consistent with our previous study aimed at exploring the ex vivo models designed on porcine bi-transgenic ACFCs [16]. In turn, the present investigation has confirmed that TSA-evoked epigenomic modulation did not considerably affect the molecular signatures related to the semi-quantitative profiles identified for rhα1,2-FT enzyme. This finding can be scientifically justified by the overall existing expression of the aforementioned enzymatic protein in porcine tri-transgenic ACFCs, which turned out to be robustly lower than that noticed for porcine bi-transgenic ACFCs that have been proteomically and glycoproteomically evaluated in our former research [16]. Nevertheless, lectin blotting analysis revealed the considerably diminished relative abundance detected for Galα1→3Gal epitopes in both TSA-unmodulated and modulated porcine triple-transgenic ACFCs as compared to their non-transgenic cell counterparts.

The presence of α-Gal antigenic determinants is not the only hindrance in pig-to-human xenotransplantation. In this context, a pivotal role is also played by the immunological incompatibility between porcine and human tissues at the level of the MHC proteins. As a consequence, it was indispensable to generate and multiply the genetically modified pigs expressing HLA-E [15,36]. As one of the predominant members of the family involving MHC proteins, HLA-E has been allotted to a class Ib representatives of non-classical MHC molecules together with two additional members of this family, designated as HLA-F and HLA-G. Importantly, HLA-E occurs ubiquitously in all nucleated cells at relatively low levels, although it is expressed most abundantly in endothelial cells and various types of immune cells [39–42]. In addition, HLA-E is a major ligand for the inhibitory receptor of NK cells, which is termed as CD94/NKG2A [14,41,43], and the capacity of HLA-E to suppress macrophage-mediated cytotoxicity has been demonstrated [44,45]. Taking into account all these unique properties of HLA-E, our primary goal of great importance was to create such ex vivo h*FUT2*×h*GLA*×*HLA-E* tri-genetically engineered models of mitotically stable porcine ACFC lines, in which the semi-quantitative profiles estimated for HLA-E representative of MHC proteins were sustainably perpetuated at sufficiently high levels. For these reasons, the extensive efforts undertaken in the current research to perform the TSA-dependent epigenetic transformation of these triple-transgenic ACFCs have been

proven to be a reliable and feasible strategy for the desirable achievement of a tremendously remarkable amelioration of relative abundance pinpointed for HLA-E protein. This TSA-expedited overexpression of HLA-E has been ascertained not only with respect to its molecular levels identified for TSA-untransformed 3×TG ACFCs but also, to an even more noticeable extent, with respect to semi-quantitatively profiling the swine homolog of HLA-E recognized for TSA-unmodulated and modulated non-transgenic cell counterparts.

Our current investigation provided, for the first time, clear evidence of a differentiable extent/advancement for the TSA-mediated augmentation of the capabilities of mRNA molecules transcribed from *HLA-E*, h*GLA* and h*FUT2* transgenes to epigenomically reprogram their translational activities in the ex vivo models designed on porcine tri-genetically engineered ACFCs. The TSA-dependent epigenetic transformation of h*FUT2*×h*GLA*×*HLA-E* triple-transgenic ACFCs has been also found to incur the enhancement of translational reprogrammability of mRNA transcripts synthesized not only from extrinsic (xenogeneic) genes but also from the own intrinsic genes within host nuclear DNA. Furthermore, no research has ever demonstrated the simultaneous overabundance of rhα-Gal A and HLA-E proteins followed by strong attenuation of semi-quantitative profiles identified for Galα1→3Gal antigenic determinants in porcine tri-transgenic ACFCs that have been epigenomically modulated by their exposure to a representative of potent non-selective HDACi, termed as trichostatin A. Nonetheless, TSA-assisted epigenetic transformation did not considerably affect the RAs of rhα-1,2-FT in 3×TG ACFC lines. Despite this fact, TSA-based epigenomic modulation did not relieve the biocatalytic capability of the rhα-1,2-FT enzyme to diminish the semi-quantitative profile of α-Gal epitopes. On the one hand, this finding can deliver an insightful interpretation of and meaningful justification for a sufficiently large and significant TSA-assisted impact on the expression levels estimated for rhα-Gal A. On the other hand, it can implement/incorporate new scientific knowledge and mechanistic insights into either the predominant role played by the enzymatic activity of rhα-Gal A or its possible synergistic cooperation with overabundant HLA-E proteins and strong inter-proteomic crosstalk between rhα-Gal A and HLA-E molecules. This intermolecular communication can be directed at pleiotropically and more efficiently prompting the tremendously alleviated expression of Galα1→3Gal antigenic determinants in h*FUT2*×h*GLA*×*HLA-E* triple-transgenic ACFCs. Furthermore, it is worth highlighting that, regardless of the molecular scenario by which the TSA-mediated epigenetic transformation of porcine tri-genetically modified ACFCs triggers the augmentation of the semi-quantitative profiles of α-Gal epitopes, the incidence of Galα1→3Gal antigenic determinants dwindled profoundly in both TSA-modulated and unmodulated h*FUT2*×h*GLA*×*HLA-E* tri-transgenic ACFCs exhibiting overexpression of rhα-Gal A and HLA-E proteins as compared to their non-transgenic cell counterparts.

In summary, these ex vivo models of mitotically stable and TSA-modulated h*FUT2*×h*GLA*×*HLA-E* triple-transgenic ACFCs, whose molecular signatures encompass not only downregulated glycoproteomic profiles of Galα1→3Gal antigenic determinants but also upregulated RAs of recombinant human immune enzymes (rhα-Gal A, rhα1,2-FT) and MHC representative (HLA-E), have been profoundly explored and might provide a completely new source of and powerful tool for highly reprogrammable (epigenomically dedifferentiable) nuclear donor cells for further studies. To the best of our knowledge, no research has ever been conducted to ascertain the suitability of such strongly reprogrammable h*FUT2*×h*GLA*×*HLA-E* tri-transgenic models of ACFC lines for future investigations targeted at multiplying tri-genetically modified pigs by SCNT-mediated cloning. The goals of these investigations might be focused on the use of the above-indicated tri-transgenic ACFC models, which are characterized by a genetically engineered diminished interspecies (porcine→human) immunological barrier, for the efforts undertaken to propagate and multiply cloned embryos, conceptuses and progeny by SCNT. These novel models of the ex vivo migrating and expanding triple-transgenic ACFC lines that exhibit TSA-facilitated epigenomic plasticity reflected in enhanced translational activities of desirable transgene-encoded transcripts might be a prerequisite for performing efficient preclinical

and clinical trials aimed at the pig-to-human transplantation of dermo-epidermal xenografts conceptualized on the basis of porcine $3 \times$ TG ACFCs undergoing TSA-dependent epigenetic transformation. The swine cutaneous bioprostheses or substitutes of human skin, which are comprised of TSA-modulated porcine tri-genetically engineered ACFC lines, appear to be characterized by considerably diminished inter-species histophysiological and immunopathological incompatibility and shortened porcine→human immunogenetic distance. All these previously mentioned attributes might give rise to the amelioration of the capabilities of TSA-exposed porcine h*FUT2*×h*GLA*×*HLA-E* triple-transgenic ACFCs to cytophysiologically promote, perpetuate and expedite the kinetics of the ex vivo migration and proliferation of human cutaneous keratinocytes in hybrid (porcine→human) dermo-epidermal bioprostheses. Designing such skin bioprostheses based on porcine tri-transgenic ACFC xenografting seems to be profoundly reliable and feasible for preclinical and clinical studies focused on reconstructive surgery related to regenerative medicine treatments and dermoplasty-mediated tissue engineering of human integumentary system. A scarcity of allogeneic dermo-epidermal transplants in reconstructive and regenerative medicine triggers a necessity for creating transgenic animal models, including swine models, characterized by high histo- and anatomophysiological homology with the human dermo-integumentary system and genetically engineered attenuated interspecies immunological barrier. Such genetically modified swine models could provide biocompatible materials for developing desirable hybrid (porcine→human) or completely xenogeneic dermo-epidermal bioprostheses based on the ex vivo migration and expansion of multiple-transgenic ACFC lines. The latter could play a helping stimulatory function for the extracorporeal in situ proliferation of human and/or porcine epidermal keratinocytes. The aforementioned tools designed on swine ex vivo models of h*FUT2*×h*GLA*×*HLA-E* tri-transgenic ACFCs might be targeted at the future pre- and clinical trials undertaken to utilize the porcine tri-genetically engineered ACFC-based bioprostheses for the replacement or removal of: (1) hereditary anatomo- and histopathological changes within the human dermo-integumentary system; (2) malignant and non-malignant skin tumors; (3) surgical or burn skin wounds and scars or skin injuries; and (4) senescence-related alterations within the cutaneous and subcutaneous tissue compartments.

4. Materials and Methods

4.1. Establishment and TSA-Dependent Epigenetic Transformation of the Ex Vivo-Expanded ACFC Lines Stemming from Triple- and Non-Transgenic Pigs

The ACFC lines were established according to the protocols described in our previous studies [16,46]. In our current investigation, ACFCs derived from h*FUT2*×h*GLA*×*HLA-E* triple-transgenic pigs ($n \geq 3$), which had been generated by the crossbreeding of h*FUT2*×h*GLA* double-transgenic pigs [47] with *HLA-E* single-transgenic specimens [36], were used. ACFCs originating from non-transgenic pigs served as a control group (CTR nTG; $n \geq 3$). All animal procedures that were accomplished in the research by Hryhorowicz et al. [36] and Zeyland et al. [47] were conducted in accordance with the European Directive 2010/63/EU and approved by the Second Local Ethics Committee in Kraków, Poland (permission 1181/2015 from 21 May 2015). All ACFC lines were cultured in DMEM/F12 (1:1) (Sigma-Aldrich, St. Louis, MO, USA) enriched with 15% FBS (Sigma-Aldrich) and 1% penicillin/streptomycin cocktail (Sigma-Aldrich) in a CO_2 incubator under stabilized conditions as follows: a temperature of +38.5 °C, 5% CO_2 and relative humidity of air atmosphere ranging from 90 to 95%. For Western and Lectin blot analyses, cells were cultured in T-25 flasks of up to 2–3 passages, but for immunofluorescence, cells in the second passage were seeded onto sterile coverslips in 6-well plates. Immediately after the ex vivo-expanded ACFC lines reached approximately 85% of confluence, their epigenetic transformation was prompted by supplementation of the culture medium with 50 nM of TSA (Sigma-Aldrich). Both tri-transgenic and non-transgenic ACFCs were epigenomically modulated by treatment with TSA for 24 h. The effect of TSA-mediated epigenetic transformation on not only relative quantities of h*FUT2*, h*GLA* and *HLA-E* mRNA transcripts but also abundance

profiles of adequate transgenically biosynthesized proteins and Galα1→3Gal epitopes was determined in the ex vivo-expanded ACFC lines originating from 3×TG (n ≥ 3) pigs. The ACFCs derived from non-transgenic (nTG; n ≥ 3) pigs provided TSA$^+$ and TSA$^−$ control groups. All the cell cultures were independently triplicated.

4.2. Total RNA Isolation, cDNA Synthesis and Reverse Transcription

Total RNA was extracted from either TSA-modulated or unmodulated h*FUT2*×h*GLA*× *HLA-E* triple-transgenic ACFCs and their non-transgenic cell counterparts. Total cellular RNA was isolated using the Total RNA Mini Plus Kit (A&A Biotechnology, Gdańsk, Poland) according to the manufacturer's protocol. The quantity and quality of the total RNA were ascertained by measuring the absorbance at the detection wavelengths λ equal to 260 nm and 280 nm with a NanoDrop™ Lite Spectrophotometer (Thermo Scientific, Wilmington, DE, USA). Moreover, RNA samples were electrophoresed on a 1% (*w/v*) denaturing agarose gel to verify the RNA quality and stored frozen at −80 °C. First-strand cDNA was prepared by reverse transcription (RT) using 1 mg of total RNA, random primers and a High-Capacity cDNA Reverse Transcription Kit (Applied Biosystems, Foster City, CA, USA) according to the manufacturer's protocol. The 20-mL total reaction volume contained random primers, dNTP mix, RNAse inhibitor and Multi Scribe Reverse Transcriptase. RT was performed in a T100 Thermal Cycler (Bio-Rad, Hercules, CA, USA) according to the following thermal profile: (1) 25 °C for 10 min, (2) 37 °C for 120 min and (3) 85 °C for 5 min. Genomic DNA amplification contamination was checked using control experiments, in which reverse transcriptase was omitted during the RT step. The samples were kept at −20 °C until further analysis.

4.3. Real-Time Quantitative Polymerase Chain Reaction (RT-qPCR)

The RT-qPCR was performed according to the manufacturer's protocol. To quantitatively assess the transcriptional activities identified for each analyzed transgene (i.e., h*FUT2*, h*GLA* and *HLA-E*), the RT-qPCR reactions were successfully initiated and subsequently completed for each sample using a reaction mix prepared as follows: 1× SYBR Select Master Mix (Thermo Fisher Scientific), 2 μL of forward and reverse primers (1 μM each) and 4 μL of 20× diluted cDNA in a final volume of 15 μL. A no-RT control run was conducted with DNase-digested RNA to verify that the digestion was successful and sufficient for selected samples. The amplification protocol included an initial preheating at 50 °C for 2 min, initial denaturation at 95 °C for 10 min and 40 cycles of amplification (15 s at 95 °C and 60 s at 60 °C). A melting curve analysis was achieved at the end of each run. The RT-qPCR was carried out with a CFX96 Touch Real-Time PCR Detection System (Bio-Rad). The sequences of all the RT-qPCR primers are presented in Table 1.

Table 1. Primers used for RT-qPCR.

Gene	F/R	Primer Sequence (5′→3′)	T$_m$ (°C)	Reference
h*FUT2*	F	ATGTCGGAGGAGCACGCGG	55.9	[12]
	R	CCACGGTGTAGCCTCCTGTCC	55.4	[12]
h*GLA*	F	GGGGAGGGGTTTTATGCGATGGAG	51.8	[13]
	R	CTGGCTCTTCCTGGCAGTCA	51.8	[13]
HLA-E	F	TTCCGAGTGAATCTGCGGAC	51.8	[36]
	R	AGGCGAACTGTTCATACCCG	53.8	[36]
p*ACTB*	F	CAAAGCCAACCGTGAGAAGA	53.8	[36]
	R	GTACCCCTCGTAGATGGGCA	53.0	[36]

Alterations in the quantitative profiles (i.e., relative quantities; RQs) noticed for adequate mRNA transcripts that had been triggered by the TSA-mediated epigenomic modulation of ex vivo-expanded h*FUT2*×h*GLA*×*HLA-E* triple-transgenic and non-transgenic ACFC lines were rendered as a ratio of target gene versus reference *ACTB* gene (coding for β-actin) in relation to expression in control samples using the method developed and optimized by Pfaffl [48] according to the following equation:

$$Ratio = \frac{\left(E_{target}\right)^{nCt} \ Target^{(control-sample)}}{\left(E_{reference}\right)^{nCt} \ Reference^{(control-sample)}} \tag{1}$$

In the above-indicated algorithmic formulation, the mathematical designation *E* denotes the amplification efficiency, whereas the *nCt* symbol is assigned to the number of RT-qPCR cycles needed for the signal to exceed a predetermined threshold value. To minimize the error associated with the differences in the quantity of applied template, the analyses were run in triplicate (at least three biological replicates and three technical replicates within each biological replicate), and the results were averaged.

4.4. Total Protein Extraction and Western or Lectin Blot Analyses Accomplished to Ascertain the Semi-Quantitative Profiles Pinpointed for α1,2-FT, α-Gal A and HLA-E/shHLA-E Proteins or Galα1→3Gal Epitopes at the Glycoprotein Levels in the Ex Vivo-Expanded Triple- and Non-Transgenic ACFCs

Total protein was extracted from harvested ACFCs using radioimmunoprecipitation assay lysis buffer (RIPA buffer, Thermo Fisher Scientific, Waltham, MA, USA) containing 1% proteinase inhibitor cocktail (RIPA+PI; Bioshop Inc., Burlington, ON, Canada). After treatment with TSA, cells were washed twice with ice-cold PBS, then 300 μL of RIPA+PI was added per flask, and cells were harvested with cell scrapers. The samples were subsequently sonicated and centrifuged at 13,200 rpm for 15 min at +4 °C, and supernatant was collected. Protein concentration was estimated with microassay DC™ Protein Assay (Bio-Rad Laboratories, Hercules, CA, USA) using bovine serum albumin (BSA) as a standard. Protein samples were stored at −80 °C for further analyses.

For sodium dodecyl-sulphate (SDS)-polyacrylamide gel electrophoresis (PAGE), protein samples were diluted in 2× Laemmli Sample Buffer (Bio-Rad Laboratories, Hercules, CA, USA) containing β-mercaptoethanol and denatured at 99.5 °C per 5 min. Electrophoresis was performed with 5% stacking and 10% resolving polyacrylamide gels. Each lane was loaded with 20 μg of protein. Then, proteins were electro-transferred onto a poly(vinylidene fluoride) (PVDF) membrane (Immobilon-P; Merck, Darmstadt, Germany) at a constant amperage of 250 mA for 120 min.

For immunoblotting membranes, after several washes in TBS, they were blocked for 1 h in 5% non-fat milk in TBST (Tris buffer saline with 0.1% *v*/*v* Tween20; Bioshop Inc.). Subsequently, the membranes were rinsed several times in TBST and incubated overnight at +4 °C with the following primary antibodies: against HLA-E (diluted 1:1000 in TBST; mouse monoclonal antibodies, ab11820, Abcam, Cambridge, UK), human α1,2-FT (diluted 1:1000 in TBST; rabbit polyclonal antibodies, ab198712, Abcam) and human α-Gal A (diluted 1:1000 in TBST; rabbit polyclonal antibodies, PA5-27349, ThermoFisher Scientific, Waltham, MA, USA). β-Actin served as a loading control protein (diluted 1:2000 in TBST; mouse monoclonal antibodies, ab8224, Abcam). Then, membranes were washed several times in TBST and incubated with goat anti-rabbit or goat anti-mouse HRP-conjugated secondary antibodies (ThermoFisher Scientific, Waltham, MA, USA) at a dilution of 1:6000 in TBST for 1 h at room temperature.

For lectin blotting, membranes were blocked for 30 min in 1% BSA (Bioshop Inc.) in TBST. Then, membranes were washed three times in DPBS containing Ca^{2+}/Mg^{2+} ions (Gibco® ThermoFisher Scientific, Waltham, MA, USA) followed by TBS. In the next step, membranes were incubated overnight at +4 °C with isolectin GS I-B$_4$ labelled with HRP (L5391, Sigma-Aldrich) diluted 1:2000 in DPBS. Finally, membranes were washed in TBS buffer.

For both Western blotting and lectin blotting, protein bands were detected by chemiluminescence using Clarity™ Western ECL Blotting Substrate (Bio-Rad Laboratories, Hercules, CA, USA) and visualized with the ChemiDoc™ XRS+ Imaging System (Bio-Rad Laboratories, Hercules, CA, USA). Protein bands were quantified using the Image Lab™ 2.0 Software (Bio-Rad Laboratories, Hercules, CA, USA). Semi-quantitative analysis was performed for three separately repeated experiments for each control and experimental group and normalized on β-actin (reference protein)-related signal. This indicates that at least three biological replicates originated from at least three independent 3×TG and nTG pigs. Subsequently, each of these biological replicates was run in three technical replicates in either one Western blot assay or one lectin blot assay. Each analysis was calculated as follows:

$$Relative\ expression = \frac{signal_{SAMPLE}}{signal_{REFERENCE\ PROTEIN}} \tag{2}$$

Subsequently, the results encompassing the relative expression of the HLA-E, rhα1,2-FT and rhα-Gal A enzymes were shown as a mean ± SEM.

4.5. Immunofluorescence Staining of the Ex Vivo-Expanded Triple- and Non-Transgenic ACFCs Epigenomically Modulated or Not Modulated by Their Exposure to TSA

Immediately after TSA-assisted epigenetic transformation, tri-genetically modified or non-modified ACFCs were washed with sterile PBS and fixed with 4% paraformaldehyde for 10 min at room temperature. After several washes in PBS, cells were blocked in 5% normal goat serum (NGS) in PBST (PBS containing 0.1% Triton X-100) for 30 min. Cells were then incubated overnight at +4 °C in a humidified chamber with the following primary antibodies (the same as those for Western blot) against HLA-E (diluted 1:300 in PBST), human α1,2-FT (diluted 1:150 in PBST) and human α-Gal A (diluted 1:200 in PBST). In the next step, cells were washed several times in PBST and incubated with goat anti-rabbit Alexa Fluor 488-conjugated or goat anti-mouse Cy3-conjugated secondary antibodies (diluted 1:500 in PBST; ThermoFisher Scientific, Waltham, MA, USA) for 1 h at room temperature. After final washes, ACFCs were mounted in Fluoroshield with 4′,6-diamidino-2-phenylindole (DAPI) mounting medium (F6057, Sigma-Aldrich, St. Louis, MO, USA). All the experiments were independently replicated thrice, which denotes that at least three biological replicates were collected from at least three independent 3×TG and nTG pigs. Each of these biological replicates was run in three technical replicates in a single immunoreaction assay. Fluorescently labelled ACFCs were examined as described in Section 4.6.

4.6. Confocal Microscope Analyses of the Ex Vivo-Expanded Triple- and Non-Transgenic ACFCs Undergoing or Not Undergoing TSA-Based Epigenetic Transformation

Fluorescently labelled cells were examined by confocal microscope Olympus FluoView 1200 on inverted stand IX83 (Olympus, Tokyo, Japan). A magnification objective of 40 times (NA = 0.95) was used, and diode laser (473 nm), diode laser (543 nm) and diode laser (405 nm) were applied to excite green (Alexa Fluor 488), red (Cy3) and blue (DAPI) fluorescence, respectively.

4.7. Statistical Analysis

For each TSA-transformed and -untransformed ACFC variant stemming from tri-genetically engineered (n ≥ 3) and non-engineered pigs (n ≥ 3) and for all analyses, three replications were performed. Quantitative data were expressed as the mean ± standard error of the mean (SEM) and examined using the Shapiro–Wilks *W* test for normality. Comparisons between the appropriate means were achieved by one-way analysis of variance (ANOVA) followed by Newman–Keuls post hoc test for multiple ranges. All statistical analyses were carried out using Statistica 13 Software (StatSoft Inc., Tulsa, OK, USA). Sta-

tistical significance was marked by letters at the appropriate charts. The bars that were marked with different letters vary significantly.

5. Conclusions

The current research creates, for the first time, strong scientific foundations that empirically justify the highly elevated epigenetic reprogrammability of porcine h*FUT2*×h*GLA*×*HLA-E* tri-genetically modified ACFC lines due to their TSA-dependent epigenomic modulation. This has been clearly proven by proteomically profiling in such completely novel ex vivo models designed on the triple-transgenic cells. The comprehensive deciphering of molecular signatures in these tri-transgenic ACFCs has remarkably confirmed the TSA-mediated augmentation of the RAs noticed for rhα-Gal A and HLA-E proteins, which arises from enhanced translational activities of mRNA transcripts undergoing stable synthesis from h*GLA* and *HLA-E* transgenes. The TSA-facilitated scenarios of increased expression levels identified for rhα-Gal A and HLA-E proteins simultaneously brought about a decline in the semi-quantitative profiles of Galα1→3Gal antigenic determinants recognized at the glycoprotein levels, as has been compared to the ex vivo non-transgenic models of ACFC lines. For these reasons, the present study has been targeted at thoroughly estimating the semi-quantitative profiles of α-Gal epitopes at the glycoprotein level, which have been successfully downregulated by the synergistic interplay and reciprocal cooperation of overabundant protein products translated from genetically engineered mRNA transcripts of overexpressed h*GLA*, *HLA-E* and h*FUT2* transgenes in tri-genetically modified ACFCs subjected to TSA-mediated epigenetic transformation.

Abbreviations

3×TG	Triple-transgenic; tri-transgenic
ACFC	Adult cutaneous fibroblast cell
ACTB	β-Actin
α-Gal	Galα1→3Gal antigenic determinant (epitope)
α1,3-GT	α1,3-galactosyltransferase
CTR nTG	Control non-transgenic

DNMTi	Inhibitors of DNA methyltransferases
HAR	Hyperacute rejection
HDACi	Inhibitors of histone deacetylases
HLA-E	Human leukocyte antigen-E
MHC	Major histocompatibility complex
NK	Natural killer
RA	Relative abundance
rhα1,2-FT	Recombinant human α1,2-fucosyltransferase
rhα-Gal A	Recombinant human α-galactosidase A
RT-qPCR	Reverse transcription-quantitative polymerase chain reaction
SCNT	Somatic cell nuclear transfer
shHLA-E	Swine homolog of human leukocyte antigen-E
TSA	Trichostatin A

References

1. Niemann, H.P. The production of multi-transgenic pigs: Update and perspectives for xenotransplantation. *Transgenic Res.* **2016**, *25*, 361–374. [CrossRef] [PubMed]
2. Cooper, D.K.; Gollackner, B.; Sachs, D.H. Will the pig solve the transplantation backlog? *Annu. Rev. Med.* **2002**, *53*, 133–147. [CrossRef] [PubMed]
3. Galili, U.; Shohet, S.B.; Kobrin, E.; Stults, C.L.; Macher, B.A. Man, apes, and Old World monkeys differ from other mammals in the expression of alpha-galactosyl epitopes on nucleated cells. *J. Biol. Chem.* **1988**, *263*, 17755–17762. [CrossRef]
4. Hryhorowicz, M.; Zeyland, J.; Słomski, R.; Lipiński, D. Genetically Modified Pigs as Organ Donors for Xenotransplantation. *Mol. Biotechnol.* **2017**, *59*, 435–444. [CrossRef]
5. Whyte, J.J.; Prather, R.S. Genetic modifications of pigs for medicine and agriculture. *Mol. Reprod. Dev.* **2011**, *78*, 879–891. [CrossRef] [PubMed]
6. Galili, U.; Rachmilewitz, E.A.; Peleg, A.; Flechner, I. A unique natural human IgG antibody with anti-a-galactosyl specificity. *J. Exp. Med.* **1984**, *160*, 1519–1531. [CrossRef] [PubMed]
7. Cooper, D.K.; Koren, E.; Oriol, R. Genetically engineered pigs. *Lancet* **1993**, *342*, 682–683. [CrossRef]
8. Cooper, D.K.C.; Ekser, B.; Tector, A.J. Immunobiological barriers to xenotransplantation. *Int. J. Surg.* **2015**, *23*, 211–216. [CrossRef] [PubMed]
9. Cooper, D.K.; Dou, K.F.; Tao, K.S.; Yang, Z.X.; Tector, A.J.; Ekser, B. Pig liver xenotransplantation: A review of progress toward the clinic. *Transplantation* **2016**, *100*, 2039–2047. [CrossRef] [PubMed]
10. Lu, T.; Yang, B.; Wang, R.; Qin, C. Xenotransplantation: Current status in preclinical research. *Front. Immunol.* **2020**, *10*, 3060. [CrossRef]
11. Hryhorowicz, M.; Lipiński, D.; Hryhorowicz, S.; Nowak-Terpiłowska, A.; Ryczek, N.; Zeyland, J. Application of Genetically Engineered Pigs in Biomedical Research. *Genes* **2020**, *11*, 670. [CrossRef] [PubMed]
12. Lipiński, D.; Jura, J.; Zeyland, J.; Juzwa, W.; Mały, E.; Kalak, R.; Bochenek, M.; Pławski, A.; Szalata, M.; Smorąg, Z.; et al. Production of transgenic pigs expressing human a1,2-fucosyltransferase to avoid humoral xenograft rejection. *Med. Weter.* **2010**, *66*, 316–322.
13. Zeyland, J.; Gawrońska, B.; Juzwa, W.; Jura, J.; Nowak, A.; Słomski, R.; Smorąg, Z.; Szalata, M.; Woźniak, A.; Lipiński, D. Transgenic pigs designed to express human α-galactosidase to avoid humoral xenograft rejection. *J. Appl. Genet.* **2013**, *54*, 293–303. [CrossRef] [PubMed]
14. Lilienfeld, B.G.; Crew, M.D.; Forte, P.; Baumann, B.C.; Seebach, J.D. Transgenic expression of HLA-E single chain trimer protects porcine endothelial cells against human natural killer cell-mediated cytotoxicity. *Xenotransplantation* **2007**, *14*, 126–134. [CrossRef]
15. Boksa, M.; Zeyland, J.; Słomski, R.; Lipiński, D. Immune modulation in xenotransplantation. *Arch. Immunol. Ther. Exp.* **2015**, *63*, 181–192. [CrossRef] [PubMed]
16. Wiater, J.; Samiec, M.; Skrzyszowska, M.; Lipiński, D. Trichostatin A-Assisted Epigenomic Modulation Affects the Expression Profiles of Not Only Recombinant Human α1,2-Fucosyltransferase and α-Galactosidase A Enzymes But Also Galα1$\rightarrow$3Gal Epitopes in Porcine Bi-Transgenic Adult Cutaneous Fibroblast Cells. *Int. J. Mol. Sci.* **2021**, *22*, 1386. [CrossRef] [PubMed]
17. Wang, H.; Cui, W.; Meng, C.; Zhang, J.; Li, Y.; Qian, Y.; Xing, G.; Zhao, D.; Cao, S. MC1568 Enhances Histone Acetylation During Oocyte Meiosis and Improves Development of Somatic Cell Nuclear Transfer Embryos in Pig. *Cell. Reprogram.* **2018**, *20*, 55–65. [CrossRef] [PubMed]
18. Samiec, M.; Skrzyszowska, M. High developmental capability of porcine cloned embryos following trichostatin A-dependent epigenomic transformation during in vitro maturation of oocytes pre-exposed to *R*-roscovitine. *Anim. Sci. Pap. Rep.* **2012**, *30*, 383–393.
19. Gupta, M.K.; Heo, Y.T.; Kim, D.K.; Lee, H.T.; Uhm, S.J. 5-Azacytidine improves the meiotic maturation and subsequent in vitro development of pig oocytes. *Anim. Reprod. Sci.* **2019**, *208*, 106118. [CrossRef] [PubMed]

20. Diao, Y.F.; Naruse, K.J.; Han, R.X.; Li, X.X.; Oqani, R.K.; Lin, T.; Jin, D.I. Treatment of fetal fibroblasts with DNA methylation inhibitors and/or histone deacetylase inhibitors improves the development of porcine nuclear transfer-derived embryos. *Anim. Reprod. Sci.* **2013**, *141*, 164–171. [CrossRef]

21. Samiec, M.; Romanek, J.; Lipiński, D.; Opiela, J. Expression of pluripotency-related genes is highly dependent on trichostatin A-assisted epigenomic modulation of porcine mesenchymal stem cells analysed for apoptosis and subsequently used for generating cloned embryos. *Anim. Sci. J.* **2019**, *90*, 1127–1141. [CrossRef] [PubMed]

22. No, J.G.; Hur, T.Y.; Zhao, M.; Lee, S.; Choi, M.K.; Nam, Y.S.; Yeom, D.H.; Im, G.S.; Kim, D.H. Scriptaid improves the reprogramming of donor cells and enhances canine-porcine interspecies embryo development. *Reprod. Biol.* **2018**, *18*, 18–26. [CrossRef] [PubMed]

23. Guo, Z.; Lv, L.; Liu, D.; Fu, B. Effects of trichostatin A on pig SCNT blastocyst formation rate and cell number: A meta-analysis. *Res. Vet. Sci.* **2018**, *117*, 161–166. [CrossRef] [PubMed]

24. Cao, Z.; Hong, R.; Ding, B.; Zuo, X.; Li, H.; Ding, J.; Li, Y.; Huang, W.; Zhang, Y. TSA and BIX-01294 Induced Normal DNA and Histone Methylation and Increased Protein Expression in Porcine Somatic Cell Nuclear Transfer Embryos. *PLoS ONE* **2017**, *12*, e0169092. [CrossRef] [PubMed]

25. Skrzyszowska, M.; Samiec, M. Enhancement of Developmental Outcome of Cloned Goat Embryos After Epigenetic Modulation of Somatic Cell-Inherited Nuclear Genome with Trichostatin A. *Ann. Anim. Sci.* **2020**, *20*, 97–108. [CrossRef]

26. Jin, L.; Zhu, H.Y.; Guo, Q.; Li, X.C.; Zhang, Y.C.; Zhang, G.L.; Xing, X.X.; Xuan, M.F.; Luo, Q.R.; Yin, X.J.; et al. PCI-24781 can improve in vitro and in vivo developmental capacity of pig somatic cell nuclear transfer embryos. *Biotechnol. Lett.* **2016**, *38*, 1433–1441. [CrossRef]

27. Srirattana, K.; Kaneda, M.; Parnpai, R. Strategies to Improve the Efficiency of Somatic Cell Nuclear Transfer. *Int. J. Mol. Sci.* **2022**, *23*, 1969. [CrossRef] [PubMed]

28. Samiec, M.; Opiela, J.; Lipiński, D.; Romanek, J. Trichostatin A-mediated epigenetic transformation of adult bone marrow-derived mesenchymal stem cells biases the in vitro developmental capability, quality, and pluripotency extent of porcine cloned embryos. *BioMed Res. Int.* **2015**, *2015*, 814686. [CrossRef] [PubMed]

29. Yang, G.; Zhang, L.; Liu, W.; Qiao, Z.; Shen, S.; Zhu, Q.; Gao, R.; Wang, M.; Wang, M.; Li, C.; et al. Dux-Mediated Corrections of Aberrant H3K9ac during 2-Cell Genome Activation Optimize Efficiency of Somatic Cell Nuclear Transfer. *Cell Stem Cell* **2021**, *28*, 150–163.e5. [CrossRef] [PubMed]

30. Silva, C.G.D.; Martins, C.F.; Bessler, H.C.; da Fonseca Neto, Á.M.; Cardoso, T.C.; Franco, M.M.; Mendonça, A.D.S.; Leme, L.O.; Borges, J.R.J.; Malaquias, J.V.; et al. Use of trichostatin A alters the expression of *HDAC3* and *KAT2* and improves in vitro development of bovine embryos cloned using less methylated mesenchymal stem cells. *Reprod. Domest. Anim.* **2019**, *54*, 289–299. [CrossRef] [PubMed]

31. Sun, J.; Cui, K.; Li, Z.; Gao, B.; Jiang, J.; Liu, Q.; Huang, B.; Shi, D. Histone hyperacetylation may improve the preimplantation development and epigenetic status of cloned embryos. *Reprod. Biol.* **2020**, *20*, 237–246. [CrossRef] [PubMed]

32. Pierson, R.N., III. Antibody-mediated xenograft injury: Mechanisms and protective strategies. *Transpl. Immunol.* **2009**, *21*, 65–69. [CrossRef] [PubMed]

33. Weiss, E.H.; Lilienfeld, B.G.; Müller, S.; Müller, E.; Herbach, N.; Kessler, B.; Wanke, R.; Schwinzer, R.; Seebach, J.D.; Wolf, E.; et al. HLA-E/human b2-microglobulin transgenic pigs: Protection against xenogeneic human anti-pig natural killer cell cytotoxicity. *Transplantation* **2009**, *87*, 35–43. [CrossRef] [PubMed]

34. Crew, M.D.; Cannon, M.J.; Phanavanh, B.; Garcia-Borges, C.N. An HLA-E single trimer inhibits human NK cell reactivity towards porcine cells. *Mol. Immunol.* **2005**, *42*, 1205–1214. [CrossRef] [PubMed]

35. Forte, P.; Baumann, B.C.; Weiss, E.H.; Seebach, J.D. HLA-E expression on porcine cells: Protection from human NK cytotoxicity depends on peptide loading. *Am. J. Transplant.* **2005**, *5*, 2085–2093. [CrossRef]

36. Hryhorowicz, M.; Zeyland, J.; Nowak-Terpiłowska, A.; Jura, J.; Juzwa, W.; Słomski, R.; Bocianowski, J.; Smorąg, Z.; Woźniak, A.; Lipiński, D. Characterization of Three Generations of Transgenic Pigs Expressing the *HLA-E* Gene. *Ann. Anim. Sci.* **2018**, *18*, 919–935. [CrossRef]

37. Jia, Y.; Ren, H.; Gao, X.; Ji, S.; Yang, J.; Liu, Z.; Li, S.; Zhang, Y. Expression of human alpha-galactosidase and alpha1,2-fucosyltransferase genes modifies the cell surface Galalpha1,3Gal antigen and confers resistance to human serum-mediated cytolysis. *Chin. Med. Sci. J. Chung-Kuo I Hsueh K'o Hsueh Tsa Chih* **2004**, *19*, 31–37.

38. Wiater, J.; Karasiński, J.; Słomski, R.; Smorąg, Z.; Wartalski, K.; Gajda, B.; Jura, J.; Romek, M. The effect of recombinant human alpha-1,2-fucosyltransferase and alpha-galactosidase A on the reduction of alpha-gal expression in the liver of transgenic pigs. *Folia Biol.* **2020**, *68*, 121–133. [CrossRef]

39. Kochan, G.; Escors, D.; Breckpot, K.; Guerro-Setas, D. Role of non-classical MHC class I molecules in cancer immunosuppression. *Oncoimmunology* **2013**, *2*, e26491. [CrossRef] [PubMed]

40. Kraemer, T.; Blasczyk, R.; Bade-Doeding, C. HLA-E: A novel player for histocompatibility. *J. Immunol. Res.* **2014**, *2014*, 352160. [CrossRef] [PubMed]

41. Lee, N.; Llano, M.; Carretero, M.; Ishitani, A.; Navarro, F.; López-Botet, M.; Geraghty, D.E. HLA-E is a major ligand for the natural killer inhibitory receptor CD94/NKG2A. *Proc. Natl. Acad. Sci. USA* **1998**, *95*, 5199–5204. [CrossRef] [PubMed]

42. Coupel, S.; Moreau, A.; Hamidou, M.; Horejsi, V.; Soulillou, J.P.; Charreau, B. Expression and release of soluble HLA-E is an immunoregulatory feature of endothelial cell activation. *Blood* **2007**, *109*, 2806–2814. [CrossRef] [PubMed]

43. Matsunami, K.; Miyagawa, S.; Nakai, R.; Yamada, M.; Shirakura, R. Modulation of the leader peptide sequence of the *HLA-E* gene up-regulates its expression and down-regulates natural killer cell-mediated swine endothelial cell lysis. *Transplantation* **2002**, *73*, 1582–1589. [CrossRef]

44. Maeda, A.; Kawamura, T.; Ueno, T.; Usui, N.; Eguchi, H.; Miyagawa, S. The suppression of inflammatory macrophage-mediated cytotoxicity and proinflammatory cytokine production by transgenic expression of HLA-E. *Transpl. Immunol.* **2013**, *29*, 76–81. [CrossRef] [PubMed]

45. Esquivel, E.L.; Maeda, A.; Eguchi, H.; Asada, M.; Sugiyama, M.; Manabe, C.; Sakai, R.; Matsuura, R.; Nakahata, K.; Okuyama, H.; et al. Suppression of human macrophage-mediated cytotoxicity by transgenic swine endothelial cell expression of HLA-G. *Transpl. Immunol.* **2015**, *32*, 109–115. [CrossRef]

46. Wiater, J.; Samiec, M.; Wartalski, K.; Smorąg, Z.; Jura, J.; Słomski, R.; Skrzyszowska, M.; Romek, M. Characterization of Mono- and Bi-Transgenic Pig-Derived Epidermal Keratinocytes Expressing Human *FUT2* and *GLA* Genes—In Vitro Studies. *Int. J. Mol. Sci.* **2021**, *22*, 9683. [CrossRef]

47. Zeyland, J.; Woźniak, A.; Gawrońska, B.; Juzwa, W.; Jura, J.; Nowak, A.; Słomski, R.; Smorąg, Z.; Szalata, M.; Mazurek, U.; et al. Double transgenic pigs with combined expression of human α1,2-fucosyltransferase and α-galactosidase designed to avoid hyperacute xenograft rejection. *Arch. Immunol. Ther. Exp.* **2014**, *62*, 411–422. [CrossRef]

48. Pfaffl, M.W. A new mathematical model for relative quantification in real-time RT-PCR. *Nucleic Acids Res.* **2001**, *29*, e45. [CrossRef]

Article

Characterization of Mono- and Bi-Transgenic Pig-Derived Epidermal Keratinocytes Expressing Human *FUT2* and *GLA* Genes—In Vitro Studies

Jerzy Wiater [1], Marcin Samiec [2,*], Kamil Wartalski [1], Zdzisław Smorąg [21], Jacek Jura [2], Ryszard Słomski [3,4], Maria Skrzyszowska [2] and Marek Romek [5,*]

[1] Department of Histology, Jagiellonian University Medical College, Kopernika 7 Street, 31-034 Kraków, Poland; jerzy.wiater@uj.edu.pl (J.W.); kamil.wartalski@uj.edu.pl (K.W.)

[2] Department of Reproductive Biotechnology and Cryoconservation, National Research Institute of Animal Production, Krakowska 1 Street, 32-083 Balice near Kraków, Poland; zdzislaw.smorag@iz.edu.pl (Z.S.); jacek.jura@iz.edu.pl (J.J.); maria.skrzyszowska@iz.edu.pl (M.S.)

[3] Institute of Human Genetics, Polish Academy of Sciences, Strzeszyńska 32 Street, 60-479 Poznań, Poland; slomski@up.poznan.pl

[4] Department of Biochemistry and Biotechnology, Poznań University of Life Sciences, Dojazd 11 Street, 60-647 Poznań, Poland

[5] Department of Cell Biology and Imaging, Institute of Zoology and Biomedical Research, Jagiellonian University in Kraków, Gronostajowa 9 Street, 30-387 Kraków, Poland

* Correspondence: marcin.samiec@iz.edu.pl (M.S.); marek.romek@uj.edu.pl (M.R.)

Abstract: Pig-to-human xenotransplantation seems to be the response to the contemporary shortage of tissue/organ donors. Unfortunately, the phylogenetic distance between pig and human implies hyperacute xenograft rejection. In this study, we tested the hypothesis that combining expression of human α1,2-fucosyltransferase (h*FUT2*) and α-galactosidase A (h*GLA*) genes would allow for removal of this obstacle in porcine transgenic epidermal keratinocytes (PEKs). We sought to determine not only the expression profiles of recombinant human α1,2-fucosyltransferase (rhα1,2-FT) and α-galactosidase A (rhα-Gal A) proteins, but also the relative abundance (RA) of Galα1→3Gal epitopes in the PEKs stemming from not only h*FUT2* or h*GLA* single-transgenic and h*FUT2*×h*GLA* double-transgenic pigs. Our confocal microscopy and Western blotting analyses revealed that both rhα1,2-FT and rhα-Gal A enzymes were overabundantly expressed in respective transgenic PEK lines. Moreover, the semiquantitative levels of Galα1→3Gal epitope that were assessed by lectin fluorescence and lectin blotting were found to be significantly diminished in each variant of genetically modified PEK line as compared to those observed in the control nontransgenic PEKs. Notably, the bi-transgenic PEKs were characterized by significantly lessened (but still detectable) RAs of Galα1→3Gal epitopes as compared to those identified for both types of mono-transgenic PEK lines. Additionally, our current investigation showed that the coexpression of two protective transgenes gave rise to enhanced abrogation of Galα→3Gal epitopes in h*FUT2*×h*GLA* double-transgenic PEKs. To summarize, detailed estimation of semiquantitative profiles for human α-1,2-FT and α-Gal A proteins followed by identification of the extent of abrogating the abundance of Galα1→3Gal epitopes in the ex vivo expanded PEKs stemming from mono- and bi-transgenic pigs were found to be a sine qua non condition for efficiently ex situ protecting stable lines of skin-derived somatic cells inevitable in further studies. The latter is due to be focused on determining epigenomic reprogrammability of single- or double-transgenic cell nuclei inherited from adult cutaneous keratinocytes in porcine nuclear-transferred oocytes and corresponding cloned embryos. To our knowledge, this concept was shown to represent a completely new approach designed to generate and multiply genetically transformed pigs by somatic cell cloning for the needs of reconstructive medicine and dermoplasty-mediated tissue engineering of human integumentary system.

Keywords: genetically modified pig; epidermal keratinocyte; human α-1,2-fucosyltransferase; human α-galactosidase A; Galα1→3Gal epitope

1. Introduction

Nowadays, the use of the porcine cells, tissues, and organs seems to be the response to the contemporary scarcity of organs for transplantation. Porcine organs display a vast variety of anatomo-histological and physiological similarities to their human counterparts. Furthermore, the extent of genetic identity between these two mammalian species oscillates at a level of approximately 96% [1–5]. Pigs are characterized by high rates of fertility and prolificacy, which reflects in both enhanced breeding potential and rapid gain of specimen-specific body mass in this livestock species displaying relatively low or negligible incidence of time- and cost-consuming production.

Unfortunately, the phylogenetic distance between pigs and humans implies complex immune response, leading to either hyperacute rejection (HAR) or acute humoral and cellular rejection of porcine xenografts [6–8]. The HAR is an immediate reaction of human immune system to the high frequency of occurrence noticed for Galα1→3Gal epitopes undergoing expression on the external surface of porcine cells' plasmalemma compartments. The biogenesis of Galα1→3Gal antigenic determinants is enzymatically catalyzed by α1,3-galactosyltransferase (α1,3-GT), which is encoded by *GGTA1* gene. The α1,3-GT enzyme displays the capability to biocatalyse the biochemical reactions of transferring galactose moieties from uridine 5′-diphosphogalactose (UDP-Gal) residues followed by α1→3 glycosidic binding these monosaccharide molecules to glycoproteins or glycosphingolipids containing terminal Galβ1→4GlcNAc-R residues [9,10]. Therefore, genetically engineering triggering the simultaneous coexpression of recombinant human α1,2-fucosyltransferase (rhα1,2-FT) and α-galactosidase A (rhα-Gal A) enzymes, which are encoded by h*FUT2* and h*GLA* transgenes, appears to be a promising approach to overcome the HAR of porcine cell, tissue, and organ xenotransplants [11,12]. Both endogenous porcine α1,3-GT and the transgenically expressed rhα1,2-FT utilize *N*-acetyllactosamine (LacNAc) residues for the purposes of their biocatalytic activities. However, human α1,2-FT occurs in the *cis* compartment of the Golgi apparatus and acts earlier than porcine endogenous α1,3-GT, which is present in the *trans* compartment of this organelle. As oligosaccharide moves through the Golgi apparatus, it is primarily fucosylated by rhα1,2-FT, whereby it cannot accept the terminal galactose residue in the subsequent reaction biocatalysed by α1,3-GT. This strategy is based on the competition of these two enzymes acting on the same substrate during oligosaccharide processing within transgenic cells [12,13]. In turn, the rhα-Gal A enzyme is responsible for the cleavage of terminal *D*-galactose moieties [14]. Zeyland et al. [15] reported successfully generating and multiplying the double-transgenic pigs displaying robust and ubiquitous expression of enzymatic rhα1,2-FT and rhα-Gal A immunoproteins for the first time. These investigators also demonstrated considerably dwindling the incidence of α-Gal antigenic determinants on the extracellular surface of porcine cutaneous fibroblast's plasma membranes. However, the effect of genetically engineered modification of the aforementioned immunoenzymes may vary among different cell types due to their specific glycosylation patterns. To our knowledge, no research has ever been conducted to comprehensively estimate not only the concomitant semiquantitative profiles (RAs) of enzymatic rhα1,2-FT and rhα-Gal A immunoproteins, but also enhanced abrogation of Galα1→3Gal epitopes in the extracorporeally proliferating PEK lines that were previously established from dermal explants of the h*FUT2*×h*GLA* bi-transgenic pigs.

The ex vivo expanding and cryogenically protecting mono- and bi-transgenic adult epidermal cells (keratinocytes) that were thoroughly characterized by recognizing proteomic signatures related to semiquantifying not only led to the overabundance of rhα1,2-FT and/or rhα-Gal A enzymes, but also augmented downregulation of Galα1→3Gal antigenic determinants, which seem to be indispensable to subsequently investigating the suitability of PEKs for producing genetically engineered cloned pigs by somatic cell nuclear transfer (SCNT). The use of somatic cell cloning for multiplication of genetically transformed pigs, whose skin (including all its principal layers such as epidermis, dermis, and hypodermis) displays robust and ubiquitous expression profiles of rhα1,2-FT and rhα-Gal A proteins and, concomitantly, diminished RA of Galα1→3Gal epitopes, appears to be reliable and feasible

strategy required to design different models of porcine dermo-epidermal bioprostheses or substitutes of human skin. The latter are intended for minimally invasive procedures of surgically repairing damaged or injured human skin by xenotransplanting porcine cutaneous grafts. These procedures are inevitable not only in regenerative medicine and tissue engineering of human dermo-integumentary system, but also in dermoplasty based on reconstructive surgery, which is mediated by xenogeneic skin grafting. The aforementioned tools of modern plastic surgery and reconstructive medicine are focused on applying the porcine genetically engineered skin bioprostheses to replacement or removal of: (1) congenital malformations of human dermo-integumentary system; (2) dermodysplastic lesions triggered by postoperative (surgical) skin wounds and scars or skin burn wounds and scars or accidental and inflicted skin injuries; (3) precancerous (premalignant) skin lesions in patients afflicted with e.g., precancerous keratosis; (4) cancerous skin tumors (malignant neoplasms) designated as metastatic cancers; (5) noncancerous oncogenic skin alterations resulting in the formation of benign (nonmalignant) tumors; and (6) degenerative changes in aging skin.

Cumulatively, it is beyond any doubt that a variety of comprehensive approaches used to determine the proteomic profile of permanent and homogenous cell lines of PEKs, which were successfully established from primary cultures stemming from skin-derived bioptates of mono- and bi-transgenic pigs, were applied for the first time. These approaches were accomplished to ex situ cryopreserve the reservoirs providing epigenetically reprogrammable nuclear donor epidermal cells (NDECs) for future studies aimed at cloning multigenetically transformed pigs by SCNT. To the best of our knowledge, the conceptualization of utilizing porcine single- or double-transgenic cutaneous keratinocytes as a source of terminally differentiated NDECs for efforts undertaken to generate somatic cell-cloned embryos, fetuses, and progeny in mammals was not yet developed. So far, the only sources of nuclear donor cells derived from dermo-integumentary system of adult mammalian specimens that were used for creation of cloned embryos, conceptuses, and offspring in mice originate from multipotent hair follicle bulge-derived epithelial stem cells and partially differentiated nonbulge keratinocyte progenitor cells, i.e., transit amplifying cells isolated from the basal layer of the epidermis and the upper outer root sheath of the hair follicles [16]. Therefore, attempts, which are targeted at exploring the capabilities of genetically modified cell nuclei inherited from adult epidermal keratinocytes to be epigenetically reprogrammed in porcine SCNT-derived oocytes and resultant embryos, are found to be a completely new strategy elaborated for the purpose of somatic cell cloning of pigs and other mammalian species.

2. Results

2.1. Fluorescent Immunolocalization of Recombinant Human α1,2-Fucosyltransferase (rhα1,2-FT) and α-Galactosidase A (rhα-Gal A) Enzymes in the Ex Vivo-Expanded Single- and Double-Transgenic PEKs

The regions of localization noticed for rhα1,2-FT and rhα-Gal A enzymes were determined by immunofluorescence staining of the in vitro cultured PEKs stemming from h*FUT2* or h*GLA* mono-transgenic (Figure 1), h*FUT2*×h*GLA* bi-transgenic (Figure 1), and nontransgenic (Figure 2) pigs served as a control group (CTR nTG). The positive rhα1,2-FT-derived immunofluorescence signal was predominantly confined to the perinuclear area in PEKs originating from h*FUT2* single-transgenic (Figure 1a) and h*FUT2*×h*GLA* double-transgenic (Figure 1c) cell lines. In turn, homogenously dispersed regions associated with fluorescently immunostaining the rhα-Gal A molecules were found to occur in whole cytoplasm of both transgenic PEK variants as follows: h*GLA* (Figure 1b) and h*FUT2*×h*GLA* (Figure 1d). But, in the porcine CTR nTG keratinocytes, we did not identify any positive signal descended from either extrinsic rhα1,2-FT or intrinsic species-specific α1,2-FT (Figure 2a), whereas the incidental locations related to immunofluorescently tagging the α-Gal A proteins were shown to be scarcely detectable (Figure 2b).
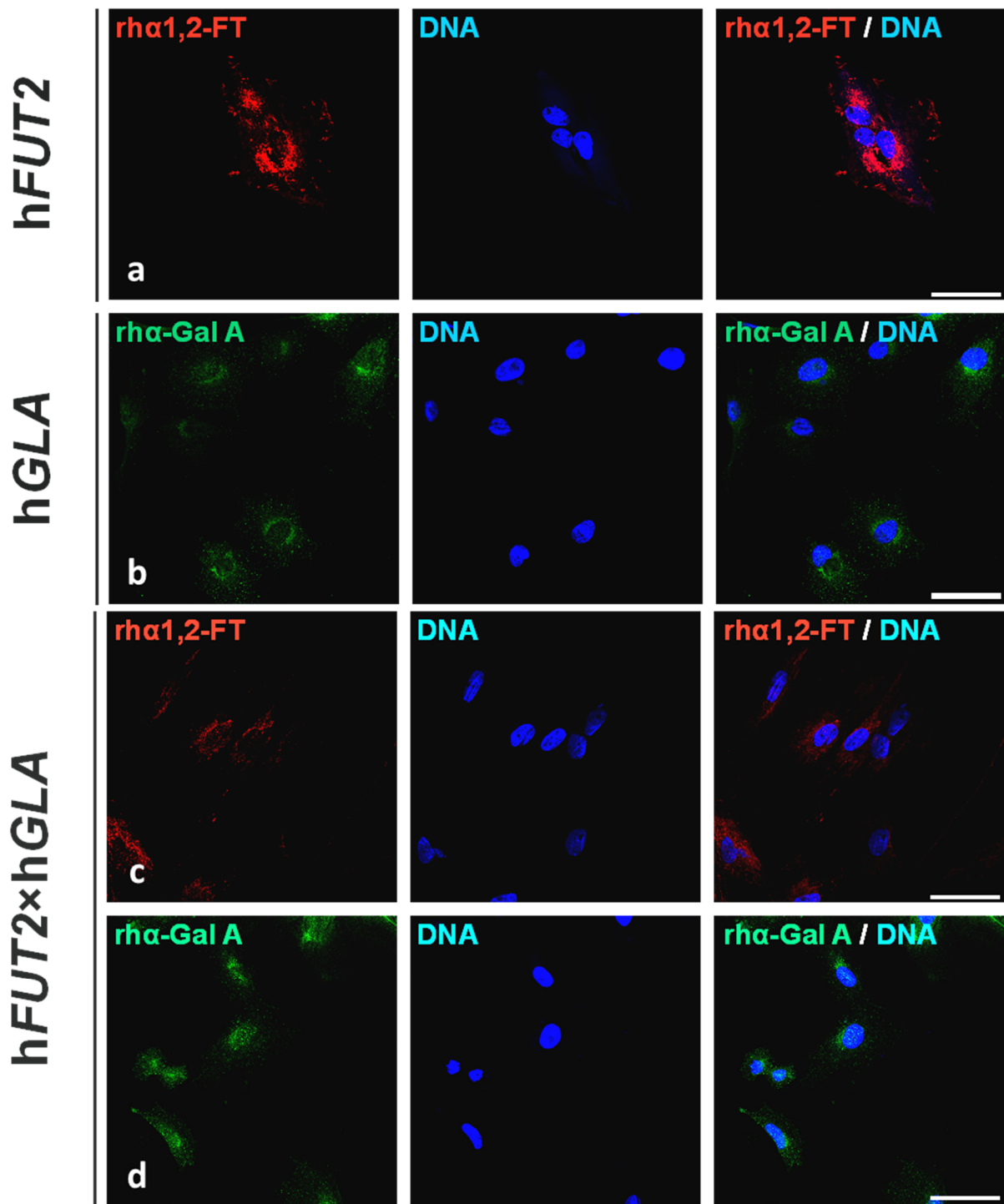
Figure 1. Immunofluorescence analysis of ex vivo-expanded PEKs originating from different variants of genetically engineered pigs detailed as: h*FUT2* mono-transgenic (**a**), h*GLA* mono-transgenic (**b**) and h*FUT2*×h*GLA* bi-transgenic (**c,d**). Representative microphotographs depicting immunofluorescent detection of rhα1,2-FT-related (**a,c**) and rhα-Gal A-related (**b,d**) locations recognized in single- and double-transgenic PEKs, respectively. Immunostaining with aid of red Cy3 fluorochrome-tagged or green Alexa Fluor 488 fluorochrome-tagged secondary antibodies and blue fluorescent nuclear counterdyeing with use of 4′,6-diamidino-2-phenylindole (DAPI). Scale bars represent 50 μm. Centers of immunofluorescently labelling the rhα1,2-FT enzymes were primarily localized in the perinuclear region of all analyzed cells (**a,c**). rhα-Gal A-descended signaling points were found to be homogeneously distributed in whole cytoplasm of diagnosed cells from each transgenic variant (**b,d**).
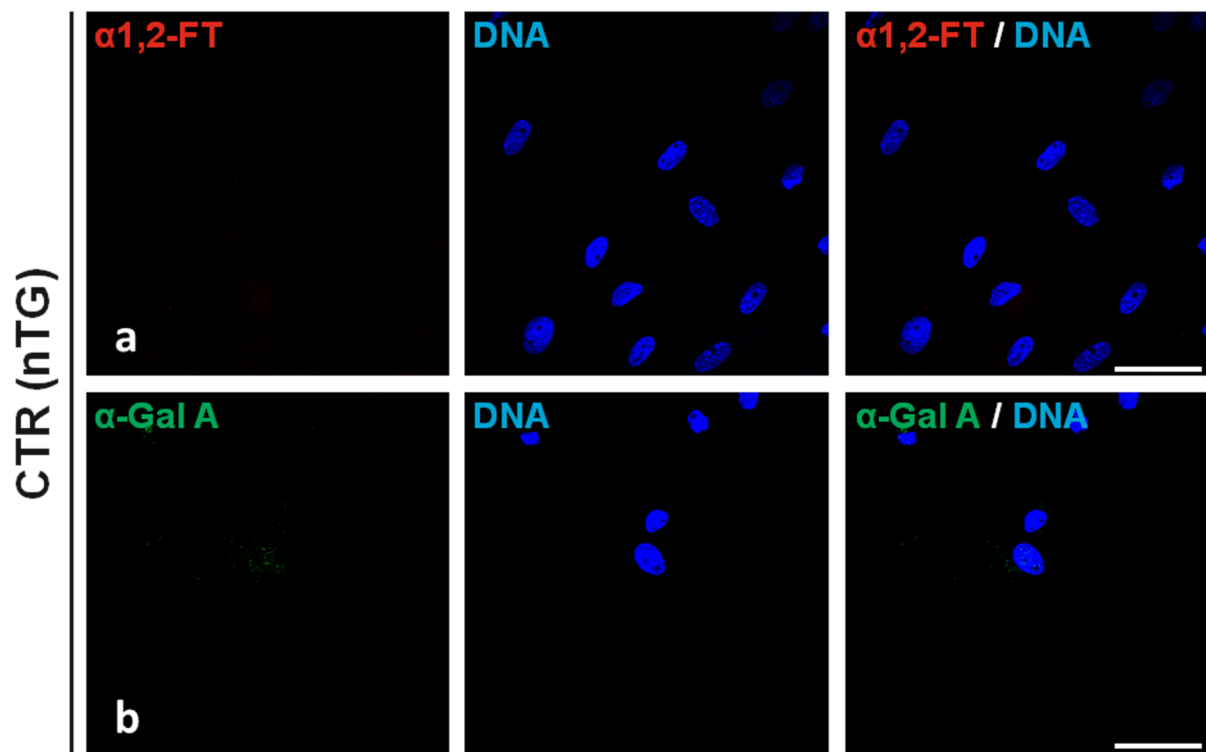
Figure 2. Immunofluorescence analysis of ex vivo-expanded PEKs stemming from control nontransgenic pigs (CTR nTG). Representative microphotographs depicting the immunofluorescent detection of α1,2-FT-related (**a**) and α-Gal A-related (**b**) locations identified in nontransgenic PEKs. Immunostaining with red Cy3 fluorochrome-tagged or green Alexa Fluor 488 fluorochrome-tagged secondary antibodies and blue fluorescent nuclear counterdyeing with the use of 4′,6-diamidino-2-phenylindole (DAPI). Scale bars represent 100 μm. No positive signaling points descended from either xenogeneic rhα1,2-FT or endogenous species-specific α1,2-FT were recognized (**a**), while sporadic incidence of hardly detectable spots correlated with immunofluorescently labelling the α-Gal A enzymes was noticed (**b**).

2.2. Western Blot-Mediated Determination of the Relative Expression Specific for Recombinant Human α1,2-Fucosyltransferase (rhα1,2-FT) and α-Galactosidase A (rhα-Gal A) Enzymes in the Ex Vivo-Expanded Single- and Double-Transgenic PEKs

To carry out Western blot analysis, the total protein samples were isolated from the in vitro cultured PEKs stemming not only from h*FUT2* mono-transgenic, h*GLA* mono-transgenic, and h*FUT2*×h*GLA* bi-transgenic, but also from control nontransgenic (CTR nTG) pigs. Western blot analysis of total protein extracts descended from the ex vivo proliferating PEKs confirmed the occurrence of rhα1,2-FT and rhα-Gal A enzymes in all the corresponding transgenic samples (Figure 3a–c). In the CTR nTG group (Figure 3d), we identified a weak positive signal for intrinsic species-specific α1,2-FT and barely detectable signal for intrinsic α-Gal A. Pigs are characterized by the lack of α-Gal A protein expression, which stems from species-specific silencing both alleles of p*GLA* gene. Taking this into consideration, the epigenetic alterations resulting from the in vitro culture conditions seem to trigger, to a very limited extent, onset of transcriptional and translational activities for p*GLA* alleles and their transcribed mRNAs in the negligible pools of the ex vivo expanded porcine CTR nTG keratinocytes. Signal intensities of the analyzed proteins (rhα1,2-FT and rhα-Gal A) were normalized to β-actin, which provides a loading control. The semiquantitative analysis of Western blot clearly proved that the relative abundances (RAs) estimated for both tested enzymes were considered to be significantly augmented (at least $p < 0.01$) in the total protein samples from each transgenic variant of PEKs as compared to the RA determined for CTR nTG group (Figure 3e,f).
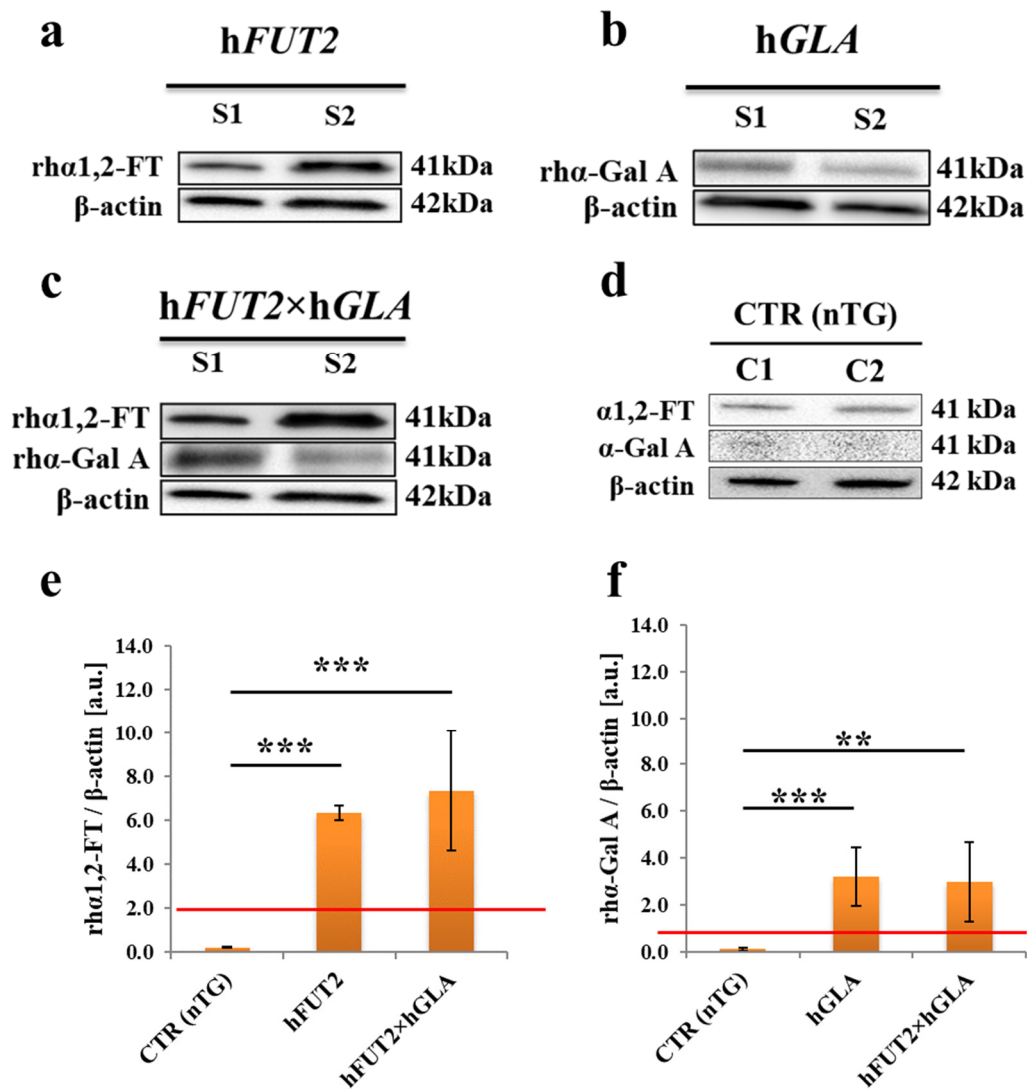
Figure 3. Western blot-mediated estimation of the semiquantitative profiles noticed for expression of recombinant human α1,2-fucosyltransferase (rhα1,2-FT) and α-galactosidase A (rhα-Gal A) enzymes in total protein samples extracted from the ex vivo-expanded control nontransgenic (CTR nTG) PEKs and their cell counterparts stemming from h*FUT2* and h*GLA* single-transgenic pigs and h*FUT2*×h*GLA* double-transgenic specimens. Representative blots corresponding to expression of rhα1,2-FT and rhα-Gal A enzymes in total protein samples that were isolated from PEKs stemming from h*FUT2* mono-transgenic (**a**), h*GLA* mono-transgenic (**b**), h*FUT2*×h*GLA* bi-transgenic (**c**) and CTR nTG pigs (**d**). β-Actin provides a loading control for all analyzed protein samples. Results of the semiquantitatively analyzing the relative abundances (RAs) determined for rhα1,2-FT and rhα-Gal A enzymes (in arbitrary units) were presented in panels (**e**,**f**), respectively. Bar graphs show mean ± standard error of mean (SEM) of relative optical density (ROD) descended from three separate analyses of three animals for each variant. Red line is taken as the cut-off value 1.0. Statistics: one-way analysis of variance (ANOVA) followed by Tukey's honestly significant difference (HSD) post hoc test. Values that are denoted as ** and *** indicate incidence of statistically significant differences between experimental groups with a probability of occurring random errors at the levels of $p < 0.01$ and $p < 0.001$, respectively.

2.3. Lectin GS I-B$_4$-Mediated Fluorocytochemically Detecting the Expression Profiles of Galα1→3 Gal Epitope in the Ex Vivo-Expanded Single-, Double- and Nontransgenic PEKs

The expression levels noticed for Galα1→3Gal antigenic determinants were identified in the in vitro cultured PEKs by their tagging with Alexa Fluor 647-conjugated lectin GS I-B$_4$. Figure 4 depicts the panels of microphotographs, in which the occurrence of Galα1→3Gal epitopes was fluorocytochemically confirmed in extracorporeally proliferating PEKs derived from control nontransgenic (CTR nTG; Figure 4a), h*FUT2* or h*GLA* mono-transgenic

(Figure 4b,c, respectively) and h*FUT2*×h*GLA* bi-transgenic pigs (Figure 4d). The Alexa Fluor 647/lectin GS I-B$_4$ conjugates strongly labelled Galα1→3Gal antigenic determinants in the intracellular compartments, cytoskeleton, membrane skeleton and plasmalemma of the PEKs stemming from the CTR nTG group (Figure 4a). In contrast, the PEKs that originated from not only h*FUT2* and h*GLA* mono-transgenic pigs (Figure 4b,c, respectively) but also h*FUT2*×h*GLA* bi-transgenic pigs (Figure 4d) were characterized by the incidences of lectin GS I-B$_4$-assisted fluorocytochemically recognizing the Galα1→3Gal epitopes that were shown to be remarkably lower than that observed in the CTR nTG group.
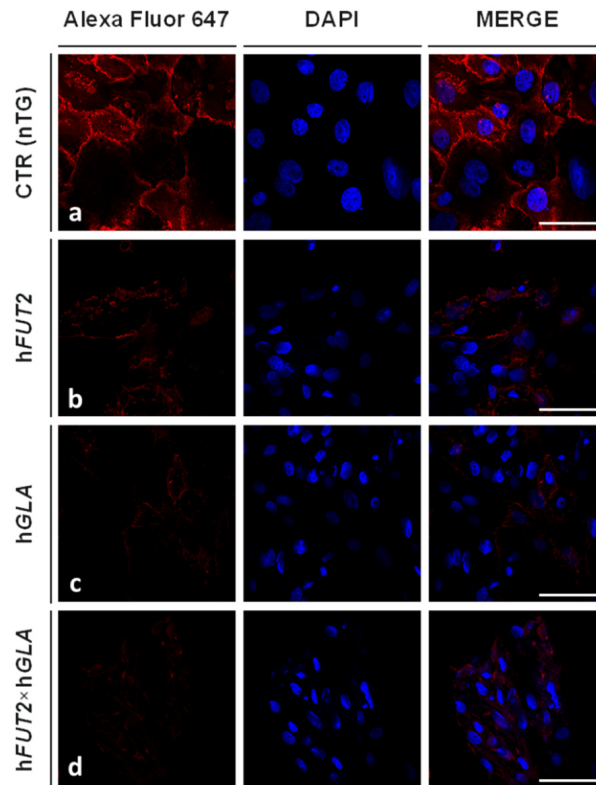
Figure 4. Lectin fluorescence analysis of expression profiles specific for Galα1→3Gal epitopes in ex vivo-expanded PEKs stemming either from genetically nontransformed pigs designated as CTR nTG group (**a**) or from different types of genetically transformed pigs as follows: h*FUT2* mono-transgenic (**b**), h*GLA* mono-transgenic (**c**) and h*FUT2*×h*GLA* bi-transgenic (**d**). Representative microphotographs depicting incidences of fluorocytochemically recognizing lectin GS I-B$_4$-labelled Galα1→3Gal antigenic determinants localized in intracellular compartments and plasma membranes of PEKs from each experimental variant specified as: CTR nTG (**a**), h*FUT2* single-transgenic (**b**), h*GLA* single-transgenic (**c**), and h*FUT2*×h*GLA* double-transgenic (**d**). The lectin fluorescence analysis was accomplished by using Alexa Fluor 647-conjugated lectin GS I-B$_4$ (highly specific red fluorocytochemical tagging of Galα1→3Gal antigenic determinants) and 4′,6-diamidino-2-phenylindole (DAPI) counterstain (blue dyeing of the cell nuclei). Scale bars represent 100 μm.

Semi-quantitatively analyzing the fluorescence intensity (FI) of Alexa Fluor 647 dye (Figure 5) revealed that the expression levels estimated for lectin GS I-B$_4$-tagged Galα1→3Gal epitopes were found to significantly wane in the PEKs of each transgenic variant as compared to their CTR nTG cell counterparts ($p < 0.01$). However, intergroup variability in the extents of Alexa Fluor 647-descended FI was not statistically proven among different types of genetically engineered PEK lines ($p \geq 0.05$).
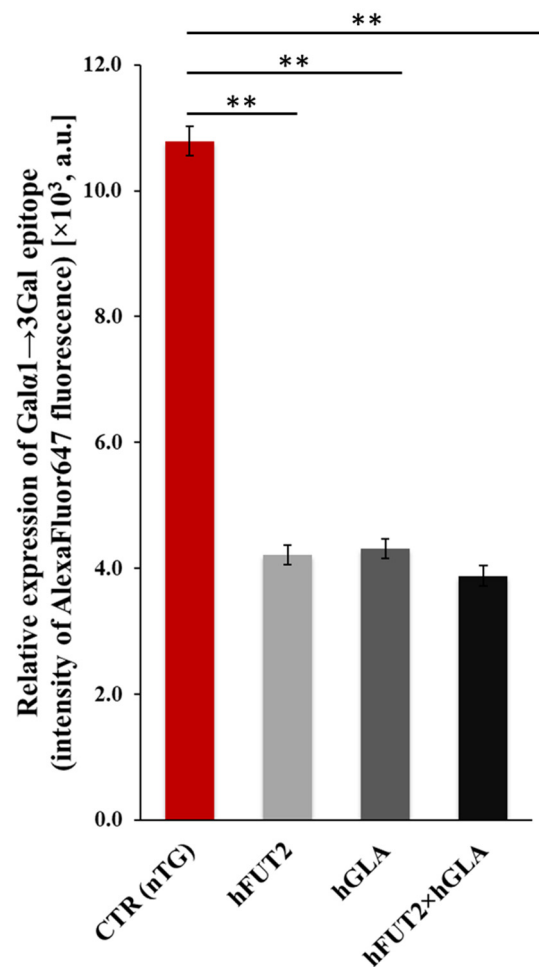
Figure 5. Semiquantitative analysis of fluorescence intensity of Alexa Fluor 647 dye for detecting expression of lectin GS I-B$_4$-tagged Galα1→3Gal epitopes in the ex vivo-expanded PEKs stemming from control nontransgenic (CTR nTG) pigs and all the three types of transgenic specimens (h*FUT2*, h*GLA* and h*FUT2*×h*GLA*). For each variant, at least 70 regions of interest (ROI) of each field of view (*n* = 9) obtained from 5 animals were measured. Results on graph are presented in arbitrary units in form of exponential notation (×10^3). Bars show mean ± standard error of the mean (SEM). Statistics: one-way analysis of variance (ANOVA) followed by Tukey's honestly significant difference (HSD) post hoc test. Values that are denoted as ** indicate occurrence of statistically significant differences between experimental groups (*p* < 0.01). Relative expression of Galα1→3Gal epitope in all the tested cell samples (from each transgenic variant) were found to dwindle significantly as compared to that of CTR nTG group. PEKs derived from h*FUT2*×h*GLA* bi-transgenic pigs exhibited lowest expression of Galα1→3Gal antigenic determinants. Nonetheless, this expression level did not vary significantly from those identified in the h*FUT2* and h*GLA* mono-transgenic variants of PEKs (*p* ≥ 0.05).

2.4. Lectin Blotting Analysis of Galα1→3Gal Epitope Expression at the Protein Level in the Ex Vivo-Expanded Single-, Double- and Nontransgenic PEKs

By using horseradish peroxidase (HRP)-conjugated isolectin GS I-B$_4$, lectin blot analysis was performed to estimate the relative abundance (RA) of Galα1→3Gal antigenic determinants at the total protein level. The occurrence of Galα1→3Gal epitopes in all analyzed protein samples, including those isolated from control nontransgenic (CTR nTG) PEKs and their cell counterparts originating from h*FUT2* and h*GLA* mono-transgenic pigs and h*FUT2*×h*GLA* bi-transgenic specimens (Figure 6a). In turn, β-Actin provides a loading control. The semiquantitative analysis of RAs determined for Galα1→3Gal epitope revealed the presence of statistically significant intergroup variability between the samples descended from CTR nTG keratinocytes and their equivalents derived from all

types of genetically modified (h*FUT2*, h*GLA* and h*FUT2*×h*GLA*) PEKs (Figure 6b). The semiquantitative profile noticed for the expression of Galα1→3Gal antigenic determinants was shown to be reduced, to the largest extent, in the h*FUT2*×h*GLA* double-transgenic PEKs as compared to that of the CTR nTG group ($p < 0.01$; Figure 6b). However, the RA of Galα1→3Gal epitope observed for the h*FUT2*×h*GLA* bi-transgenic cells was found to be significantly lower than those identified in both h*FUT2* and h*GLA* mono-transgenic keratinocytes ($p < 0.05$; Figure 6b).

Figure 6. Analyzing semiquantitative profiles of Galα1→3Gal epitope expression by lectin blotting of protein samples isolated from ex vivo-expanded control nontransgenic (CTR nTG) PEKs and their cell

counterparts stemming from h*FUT2* and h*GLA* single-transgenic pigs and h*FUT2*×h*GLA* double-transgenic specimens. (**a**): representative lectin blots corresponding to expression of Galα1→3Gal antigenic determinants in total protein samples that were extracted from PEKs originating from CTR nTG, mono- (h*FUT2*, h*GLA*) and bi-transgenic (h*FUT2*×h*GLA*) 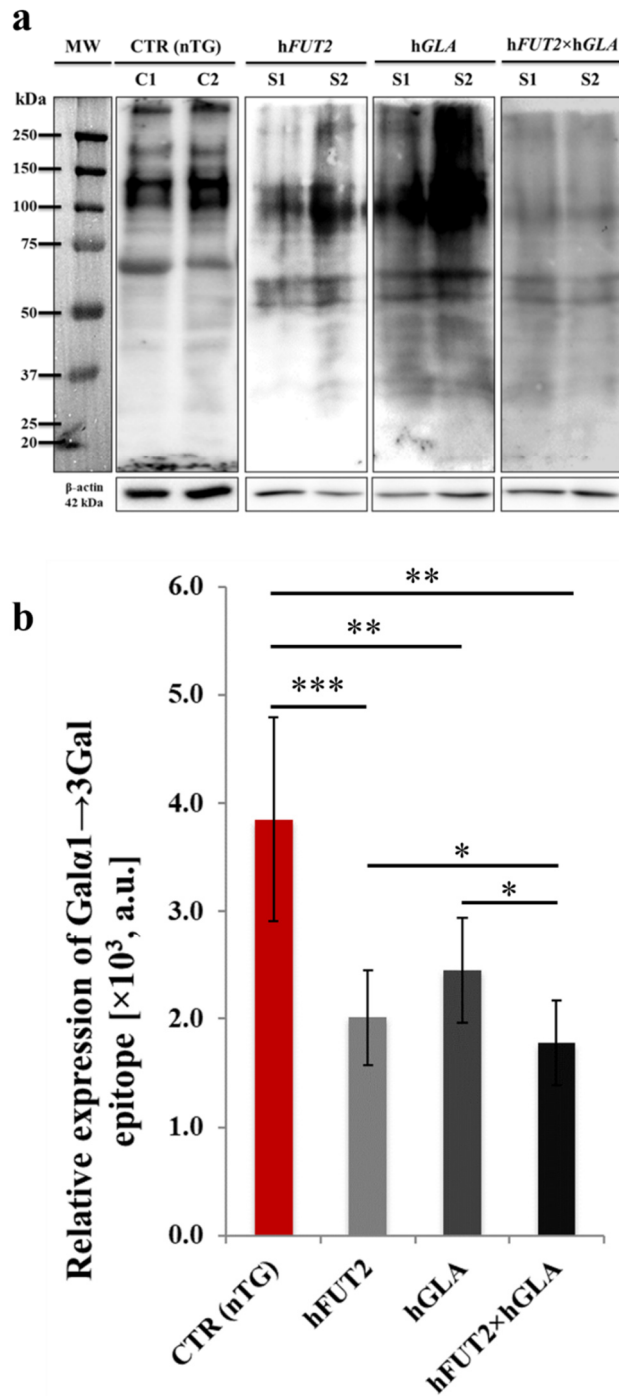pigs. MW indicates molecular weight of protein standards. Control 1, control 2, sample 1, and sample 2 were designated as C1, C2, S1, and S2, respectively. Each band represents a glycosylated protein containing the Galα1→3Gal epitope. β-Actin served as a loading control for all analyzed protein samples. (**b**): semiquantitatively analyzing the relative abundances (RAs) estimated for Galα1→3Gal epitopes (in arbitrary units). Relative optical density (ROD) from three separate analyses of at least three animals for each variant is expressed as mean. Graph bar shows mean ± standard error of the mean (SEM). Statistics: one-way analysis of variance (ANOVA) followed by Tukey's honestly significant difference (HSD) post hoc test. Values that are denoted as *, ** and *** indicate incidence of statistically significant differences between experimental groups with a probability of occurring random errors at levels of $p < 0.05$, $p < 0.01$, and $p < 0.001$, respectively. Relative expression recognized for Galα1→3Gal antigenic determinants was proven to be perpetuated at significantly diminished extents in all types/models of transgenic PEKs (h*FUT2*, h*GLA* and h*FUT2*×h*GLA*) as compared to that of the CTR nTG group. Definitely lowest RA of Galα1→3Gal epitopes was determined for total protein samples derived from h*FUT2*×h*GLA* bi-transgenic keratinocytes. This RA was also considered to recede significantly in relation to the protein samples descended from h*FUT2* and h*GLA* mono-transgenic PEKs, which have turned out to vary only unremarkably from each other.

3. Discussion

Genetically modified pigs could become, in the near future, a tremendously valuable source of xenogeneic cells, tissues, or organs for transplantation into humans. In compliance with the above-mentioned finding, the efforts attempted to apply the PEK-mediated xenografting could provide research highlight and pivotal complement to the preclinical and clinical treatments that are targeted at cell/tissue engineering, regenerative medicine, and reconstructive surgery of skin defects caused by a variety of factors. At the present stage, the strategies undertaken to use the human keratinocyte-based cutaneous bioprostheses for personalized medicine are of a great importance, which is reflected in expanding the scale and scope of clinical significance for different dermoplasty-related therapies. Cell cultures of oral and epidermal keratinocytes have gained high popularity in surgical treatments of maxillofacial and oral cavities. The latter result especially from the loss of epithelial structures due to chemical or thermal burns, trauma, penetrating injuries in gunshot wounds, or various procedures of tumor ablation in the maxillofacial area [17–20].

In our current study, we focused on the effects of overexpression of rhα1,2-FT and rhα-Gal A proteins on the levels of Galα1→3Gal epitopes in the extracorporeally expanded PEKs derived from mono- and bi-transgenic pigs. Our lectinfluorescence and lectinblotting analyses revealed the considerable diminishments in the RAs noticed for Galα1→3Gal antigenic determinants in the PEK lines of each transgenic variant (h*FUT2*, h*GLA* and h*FUT2*×h*GLA*) as compared to that of ex vivo expanded PEKs stemming from nontransgenic pigs. Moreover, taking into consideration the double-transgenic PEKs, the semiquantitative profiles of Galα1→3Gal epitopes dwindled remarkably in relation to both their single-transgenic cell counterparts. Therefore, the results of this investigation clearly indicated that constitutive coexpression of cooperating enzymes such as rhα1,2-FT and rhα-Gal A turns out to be more efficient in biocatalytic removal of the Galα1→3Gal antigenic determinants from PEK plasma membranes than separate transgenically induced functional activities of either rhα1,2-FT or rhα-Gal A enzymatic proteins translated from single h*FUT2* or h*GLA* mRNA transcripts. Furthermore, these results are consistent with our previous research focused on the liver tissues of genetically engineered pigs displaying the same genotypes [21]. Our data also support beyond any doubt emerging findings and a strong evidence that multiple-transgenic pig models are required to successfully eliminate the major xenoantigen to prolong the survival of cells, tissues and organs after pig-to-human transplantation [22–30]. Further, mono-transgenic pigs, which provided a

source of dermal explants for efficiently establishing PEK lines in our current study, were previously generated by intrapronuclear microinjection of porcine in vivo-fertilized zygotes with linearized gene constructs. The latter were composed of porcine cytomegalovirus (*CMV*) promoters and h*FUT2* or h*GLA* exon sequences [15,22,31]. In turn, h*FUT2*×h*GLA* bi-transgenic pigs were produced by subsequently interbreeding the h*FUT2* and h*GLA* mono-transgenic specimens. For those reasons, there is a risk that the expression levels of the introduced genes can tend to be decreased with the next generations of genetically engineered pigs, until they will were completely silenced. These phenomena were proven to occur frequently in the progeny derived from transgenic animals [22,31,32]. Kong et al. [33] showed that transgene expression is strongly related to gene copy number and methylation capacity in transgenic pigs. Moreover, random integration of a single gene construct or multiple gene constructs on the chromosomes also bring about suppressing the transcriptional activities of transgenes [34–36]. In turn, Folger et al. [37] found that foreign DNA that was randomly introduced into the nuclear genome leads to tandem integration of multiple transgene copies, most often designated as the so-called concatamers or series of linked transgene molecules. Such linkage results from homologous recombination between exogenous DNA molecules. But, more importantly, Kong et al. [33] also demonstrated that the number of integrated gene copies may vary depending on the type of tissue tested. This directly suggests that the use of intrapronuclear microinjection of gene constructs into the zygotes does not allow to accurately determine the number of gene copies inserted/incorporated into the genome of a given animal. Also, a slight increase in the copy number of the introduced gene due to homologous recombination between the transgene molecules in tandem repeats cannot be excluded [34–36]. Thus, it seems to be indispensable to check the gene copy number at each stage of generating transgenic animals. Zeyland et al. [15,31] and Lipiński et al. [22] confirmed that, taking into account the h*FUT2* transgene, the average integration was maintained at the level of 3 gene copies, while, considering the h*GLA* transgene, it was perpetuated at the level of 16 copies, both for mono- and bi-transgenic pigs. However, the above-mentioned studies were performed only on ear skin-derived fibroblasts originating from transgenic piglets and encompassed only DNA and/or RNA analyzes with the aid of RT-PCR and/or Southern blot hybridization. The present research was targeted at analyzing the expression of protein products for mRNA molecules transcribed from h*FUT2* and h*GLA* genes in the in vitro cultured PEKs stemming both from h*FUT2* or h*GLA* mono-transgenic pigs and from h*FUT2*×h*GLA* bi-transgenic pigs. Nonetheless, the immunofluorescence analyses that were accomplished with the use of antibodies against human α1,2-FT and α-Gal A proved the presence of these enzymes in PEKs derived from all the types/models of transgenic pigs. The signal was clear and specific for each of the analyzed transgenic variants. Western blot analysis supported the observations from the immunofluorescence reaction. A strongly positive signal in the form of specific bands was observed for each of the tested immunoproteins in the samples originating from all transgenic variants. On the other hand, semiquantitative analysis enabled to finally confirm the expression of the diagnosed proteins in the samples stemming from all the types of transgenic PEKs as compared to that of the CTR nTG group. Notably, slight (statistically nonsignificant) differences in the RAs of rhα1,2-FT and rhα-Gal were identified in keratinocytes derived from single-transgenic pigs (h*FUT2*, h*GLA*) and their bi-transgenic (h*FUT2*×h*GLA*) counterparts.

The panel of the current studies aimed at estimating the expression of the Galα1→3Gal epitopes with the use of fluorescently labelled isolectin GS I-B$_4$ did not show unequivocally an additive effect of both enzymes (rhα1,2-FT and rhα-Gal) in porcine keratinocytes. In spite of the important fact that levels estimated for the relative expression of Galα1→3Gal antigenic determinants pivotally dropped in h*FUT2*×h*GLA* double-transgenic PEKs as compared to that identified in their nontransgenic cell counterparts, the inconsiderably declined expression profiles of these epitopes were recognized for bi-transgenic keratinocytes (fold change oscillating at the level of 2.78) in relation to their h*FUT2* and h*GLA* mono-transgenic cell equivalents. The additive effect of rhα1,2-FT and rhα-Gal A proteins was demonstrated

only by the Eastern blot method using HRP-labelled isolectin GS I-B$_4$. Houndebine et al. [34] and Zeyland et al. [15] also did not observe a clear synergistic effect of both enzymes. In our present investigation, the lack of a clearly additive effect of rhα1,2-FT and rhα-Gal A proteins may be because the analyzed keratinocytes stemmed from heterozygous pigs. The obtained results are consistent with the study by Zeyland et al. [15], in which researchers also sought to examine the pigs heterozygous for h*FUT2* and h*GLA* genes. The aforementioned researchers concluded that investigations targeted at generating and multiplying homozygous pigs are inevitable to verify the cumulative effect of these genes. Nevertheless, the results achieved in our current study and the literature data have justified the requirement of the use of pigs expressing both the rhα1,2-FT and rhα-Gal A, which seems to be the most promising solution for the experimental, preclinical, and clinical strategies attempted to carry out surgical treatments targeted at pig-to-human transplanting cell, tissue, or organ xenografts. The present investigation is another step towards recognizing mechanisms that underlie the phylogenetic (interspecies) immune barrier between pigs and humans. Finally, the achievements resulting from the current study and accessible literature data proved that a variety of approaches to genetic engineering are indispensable to be linked/combined each other to generate poly-transgenic pigs exhibiting stable incorporation of xenogeneic/heterologous genes into their nuclear genomes. This is a sine qua non condition for overcoming taxonomic (pig-to-human) hindrance to efficient surgical treatments encompassing xenotransplantation of cells, tissues, or organs.

4. Materials and Methods

4.1. Postmortem Collection of Skin Tissue Explants from Single-, Double- and Nontransgenic Pigs

All analyses were conducted on porcine dermal tissue bioptates that were postmortem recovered from not only h*FUT2* and h*GLA* mono-genetically engineered specimens but also their h*FUT2*×h*GLA* bi-transgenic and nontransgenic counterparts. All sampling and material procedures were carried out according to the protocols thoroughly described in our previous study [21]. In our current investigation, a total of 20 skin tissue samples derived from 10 mono-transgenic pigs (h*FUT2*, *n* = 5; h*GLA*, *n* = 5), 5 bi-transgenic pigs (h*FUT2*×h*GLA*, *n* = 5) and 5 nontransgenic pigs of Polish Large White breed (served as a control group) were utilized. Genetically transformed pigs were designed to display the robust and ubiquitous expression of either such recombinant human immuno-enzymes as: only rhα1,2-FT or rhα-Gal A (mono-transgenic animal models) or both rhα1,2-FT and rhα-Gal A (bi-transgenic animal models) [15,22]. Dermal tissue explants were retrieved from 12- to 18-month-old (i.e., postpubertal) animals at a body weight ranging from 150 to 200 kg. All animal procedures that were used in the studies by Zeyland et al. [15] and Wiater et al. [21] were performed in accordance with the European Directive 2010/63/EU and approved by the Second Local Ethics Committee in Kraków, Poland (Permission 1181/2015 from 21 May 2015). Collected dermal tissue bioptates were deposited into ice-cold transporting buffer, which was comprised of Ca^{2+}- and Mg^{2+}-free phosphate-buffered saline (PBS) solution (pH = 7.4; Biomed, Lublin, Poland) and supplemented with 3% (*v/v*) penicilin/streptomycin cocktail (Gibco^{TM}; Thermo Fisher Scientific, Waltham, MA, USA) and 0.25 µg/mL amphotericin B (Gibco^{TM}; Thermo Fisher Scientific). Antibiotically and antimycotically protected skin tissue samples were subsequently transported on wet ice into laboratory within 4 h.

4.2. Establishment of the Ex Vivo-Expanded Epidermal Keratinocytes Stemming from Skin Tissue Samples of Single-, Double- and Nontransgenic Pigs

The dermal tissue explants were rinsed thrice in sterile calcium/magnesium cation-deprived PBS (pH = 7.4; Biomed) supplemented with 3% (*v/v*) penicilin/streptomycin cocktail (Gibco^{TM}; Thermo Fisher Scientific, Waltham, MA, USA) and 0.25 µg/mL amphotericin B (Gibco^{TM}; Thermo Fisher Scientific). Afterwards, dermal tissue samples were carefully dissected and minced followed by 2-h enzymatic digestion of epidermal pieces with the aid of sterile 0.2% collagenase (Sigma–Aldrich; St. Louis, MO, USA) in PBS

(Biomed) at a temperature of +37 °C. The cell suspensions were subsequently filtered through a 70-μm nylon cell strainers and washed in PBS (Biomed), followed by their triple centrifugation at $200\times g$ for 5 min. In the next step, porcine epidermal keratinocytes (PEKs) were subcultured in Dulbecco's Modified Eagle's Medium/Nutrient Ham's Mixture F-12 (DMEM/F-12) (1:1) (Gibco[TM]; Thermo Fisher Scientific) enriched with 5% fetal bovine serum (FBS; Gibco[TM], Thermo Fisher Scientific), 1% penicillin/streptomycin cocktail (Gibco[TM]; Thermo Fisher Scientific) and 0.1% amphotericin B (Gibco[TM]; Thermo Fisher Scientific). All the homogenous sub-cultures of mitotically stable PEK lines were maintained in CO_2 Incubator (Galaxy 170R, New Brunswick, NJ, USA) for 7 days at 37 °C in a 100% water-saturated atmosphere of 5% CO_2 and 95% air. Medium intended for the ex vivo expanding the PEKs was replenished every 3 days. For immunofluorescence and lectin staining, the cells were plated into 8-well microscopic chamber slides (LabTek[TM] CC2 Nunc; Thermo Fisher Scientific) and then perpetuated under such proliferative and adherent subculture conditions until they reach a subconfluence at the level of approximately 85%.

4.3. Immunofluorescence Dyeing of the Ex Vivo-Expanded Single-, Double- and Nontransgenic PEKs

The PEKs were washed with ice-cold PBS (Biomed) and fixed with cold 4% paraformaldehyde (PFA; Sigma–Aldrich) in PBS for 10 min. After several washes in PBS (Biomed), they were blocked in 5% normal goat serum in PBST (phosphate-buffered saline with the addition of 0.1% v/v Triton X-100; Bioshop Inc., Burlington, VT, Canada) for 30 min. The PEKs were subsequently incubated overnight at +4 °C in a humidified chamber with the appropriate primary antibodies (i.e., rabbit polyclonal immunoglobulins isotype G; IgGs) against: human α1,2-FT (diluted 1:150 in PBST; ab198712, Abcam, Cambridge, UK) and human α-Gal A (diluted 1:200 in PBST; PA5-27349, Thermo Fisher Scientific, Waltham, MA, USA). Afterwards, the cells were rinsed repeatedly in PBST followed by 1-h exposure to either goat anti-rabbit Cy3-tagged secondary antibodies, i.e., IgGs against human α1,2-FT (diluted 1:600 in PBST; Jackson ImmunoResearch Laboratories, Inc., West Grove, Chester County, PA, USA) or goat anti-rabbit Alexa Fluor 488-tagged secondary antibodies, i.e., IgGs against human α-Gal A (diluted 1:600 in PBST; Thermo Fisher Scientific) at room temperature. In the next step, the cell sections that were previously washed several times were counterstained with 4′,6-diamidino-2-phenylindole (DAPI) in Fluoroshield Antifade Mounting Medium (F6057, Sigma-Aldrich), whose unique formula enables to retain prolonged fluorescence not only by preventing rapid photobleaching (fading) of Cy3 and Alexa Fluor 488 fluorochromes, but also by minimizing the blinking-mediated phenomena resulting from extended lifetime and long-term excitation of previously mentioned fluorescent dyes. Finally, fluorescently tagged cells were mounted onto precleaned glass microscope slides under coverslips, and then evaluated as was described in paragraph "*4.5. Confocal Microscope Analyses of the Ex Vivo-Expanded Single-, Double- and Nontransgenic PEKs*".

4.4. Lectin-Mediated Labelling of Galα1→3Gal Epitopes in the Ex Vivo-Expanded Single-, Double- and Nontransgenic PEKs

The localization of Galα1→3Gal antigenic determinants and subsequent comparative assessment of their semiquantitative expression profiles (RAs) in the PEKs from both CTR nTG group and each transgenic variant (h*FUT2*, h*GLA* and h*FUT2*×h*GLA*) were accomplished by using Alexa Fluor 647 fluorochrome-conjugated lectin/isolectin GS I-B$_4$ displaying a strict specificity and strong affinity for terminal αGal residues. The isolectin GS I-B$_4$ is a member representing the family of tetrameric phytohemagglutinins that were isolated from the seeds of the tropical African legume shrub *Griffonia simplicifolia* (I32450, Molecular Probes, Invitrogen[TM], Thermo Fisher Scientific). The PEKs were rinsed with ice-cold PBS (Biomed) and then fixed with cold 4% PFA (Sigma-Aldrich) in PBS for 10 min. Following serial PBS-mediated washes, they were blocked in 1% bovine serum albumin (BSA; Bioshop Inc., Burlington, VT, Canada) in PBST for 1 h. After repeatedly rinsing with PBS, the PEKs underwent the overnight exposure to isolectin GS I-B$_4$ (diluted 1:200 in DPBS) at +4 °C in a dark humidified chamber. Finally, cells were washed thrice in PBS followed by mounting in DAPI-supplemented Fluoroshield Medium (comprised of antifade reagent

with antiphotobleaching and anti-blinking properties that allow for perpetuating and extending the lifetime of Alexa Fluor 647 fluorochrome-derived fluorescent signals). After the fluorescently tagged PEKs of various genetically engineered models (h*FUT2*, h*GLA* and h*FUT2*×h*GLA*) and their nontransgenic counterparts were successfully coverslipped, they were subjected to comparative estimation of RAs noticed for Galα1→3Gal epitopes according to the protocol thoroughly described in paragraph "*4.5. Confocal Microscope Analyses of the Ex Vivo-Expanded Single-, Double- and Nontransgenic PEKs*".

4.5. Confocal Microscope Analyses of the Ex Vivo-Expanded Single-, Double- and Nontransgenic PEKs

Fluorescently labelled cells were assessed by using laser scanning confocal microscope Olympus FluoView 1200 on inverted stand IX83 (Olympus, Tokyo, Japan). Forty-times magnification objective (NA = 0.95) was used, and diode laser (473 nm), diode laser (543 nm), diode laser (635 nm) and diode laser (405 nm) were applied to excite green (Alexa Fluor 488), red (Cy3), far-red (Alexa Fluor 647) and blue (DAPI) fluorescence, respectively. Relative intensities of fluorescence were quantified in each, randomly chosen region of interest (ROI) using ImageJ version 1.46r software (National Institutes of Health, Bethesda, MD, USA) in a greyscale of 256 levels [38,39]. Both for each variant of genetically modified PEKs (h*FUT2*, h*GLA* and h*FUT2*×h*GLA*) and for CTR nTG PEKs, three sections were sampled by 70 ROI.

4.6. Total Protein Extraction and Western or Lectin Blot Analyses Accomplished to Determine RAs Estimated for rhα1,2-FT and rhα-Gal A Enzymes or Galα1→3Gal Epitopes at the Protein Levels in the Ex Vivo-Expanded Single-, Double- and Nontransgenic PEKs

Total protein was extracted from the in vitro proliferating and detached PEKs of all the transgenic types/models (h*FUT2*, h*GLA* and h*FUT2*×h*GLA*) and their nontransgenic cell counterparts by using radioimmunoprecipitation assay lysis buffer (RIPA buffer; Thermo Fisher Scientific) containing 1% of proteinase inhibitor cocktail (RIPA+PI; Bioshop Inc., Burlington, VT, Canada). Following the first passage, the PEKs were cultured in T-25 flasks for 7 days to reach a total confluence. Afterwards, the cells were rinsed twice in ice-cold PBS (Biomed) and then 300 μL of RIPA+PI was added per single culture flask, followed by harvesting the PEKs with the use of cell scrapers. In the next step, cell lysates were sonicated and centrifuged at 14,000× *g* for 15 min at +4 °C, followed by collection of supernatants. Protein concentration was determined with the aid of microassay DC™ Protein Assay (Bio-Rad Laboratories, Hercules, CA, USA) using BSA (Sigma–Aldrich) as a standard. Protein samples were stored at –80 °C for subsequent analyses.

For sodium dodecyl-sulphate (SDS)-polyacrylamide gel electrophoresis (SDS-PAGE), protein samples were diluted in 2× Laemmli Sample Buffer (Bio-Rad Laboratories) containing 5% β-mercaptoethanol and denatured at 100 °C per 5 min. Then, the proteins were separated in SDS-PAGE using 5% stacking and 10% resolving gels. Molecular weights of the analyzed proteins were estimated with reference to standard proteins (Precision Plus Dual Color Protein Standard; Bio-Rad Laboratories). For immunoblotting and lectin blotting, proteins were electro-transferred onto a poly(vinylidene fluoride) (PVDF) membrane (Immobilon-P; Merck, Darmstadt, Germany) at constant amperage of 250 mA for 120 min.

Taking into account the immunoblotting, membranes were blocked for 1 h in 5% non-fat milk in TBST (Tris-buffered saline with 0.1% *v/v* Tween20; Bioshop Inc.) and, after several rinses with TBST, incubated overnight at +4 °C with the following primary antibodies (the same as those for immunofluorescent labelling): rabbit polyclonal IgGs against human α1,2-FT (diluted 1:1000 in TBST; ab198712, Abcam) and rabbit polyclonal IgGs against human α-Gal A (diluted 1:1000 in TBST; PA5-27349, Thermo Fisher Scientific). β-Actin was used as a reference protein (mouse monoclonal IgG designated as anti-β-actin, diluted 1:2000 in TBST; ab8224, Abcam). Afterwards, membranes were washed several times in TBST followed by 1-h incubation with appropriate HRP-conjugated secondary antibodies (i.e., goat anti-rabbit IgGs against human α1,2-FT and goat anti-mouse IgGs against β-actin; Thermo Fisher Scientific), each at a dilution of 1:6000 in TBST, at room temperature [40].

Taking into consideration the lectin blotting, membranes were blocked for 30 min in 1% BSA in TBST (Bioshop Inc.). After several washes in Ca^{2+}- and Mg^{2+}-enriched Dulbecco's phosphate-buffered saline (DPBS; Gibco, Thermo Fisher Scientific), followed by rinsing with TBS (Bioshop Inc.), membranes were subjected to overnight incubation with HRP-labelled isolectin GS I-B$_4$ (L5391; Sigma-Aldrich) at a dilution of 1:2000 in DPBS and, then, underwent a terminal washing in TBS.

Finally, all the protein bands were detected by chemiluminescence using Clarity^{TM} Western ECL Blotting Substrate (Bio-Rad Laboratories) and visualized with the ChemiDoc^{TM} XRS+ Imaging System (Bio-Rad Laboratories). Protein bands were semiquantified using the Image Lab^{TM} 2.0 Software (Bio-Rad Laboratories) by measurement of their relative optical densities (RODs). Following detection of the bands related to the analyzed protein samples, membranes were stripped and reprobed with anti-β-actin antibody for loading control (i.e., reference) protein.

4.7. Statistical Analysis

For each variant/model of genetically engineered and nonengineered PEKs and for all the analyses carried out, three repeats were performed. Semiquantitative data were expressed in the form of the mean ± standard error of the mean (SEM) and subjected to statistical estimation by using the Shapiro–Wilks *W* test for normality to determine whether a variable that is presumed to cause a change in another variable is normally distributed in a population. The accomplishments of comparatively analyzing between the assigned means ± SEMs were mediated by one-way analysis of variance (ANOVA) and subsequent Tukey's honestly significant difference (HSD) post hoc test. The incidences of statistically significant intergroup variability with the probabilities of occurring random errors at the levels of $p < 0.05$, $p < 0.01$, and $p < 0.001$ were denoted as follows: single superscript asterisks (*), double superscript asterisks (**), and triple superscript asterisks (***), respectively.

5. Conclusions

The efforts targeted at establishing and cryogenically protecting stable and homogenous cell lines of single- and double-transgenic PEKs that are characterized by not only ameliorated expression levels of rhα-1,2-FT and/or rhα-Gal A proteins, but also lessened/attenuated semiquantitative profiles of Galα1→3Gal epitopes were efficiently undertaken for the first time. To the best of our knowledge, the current investigation is also the first to thoroughly and simultaneously specify the RAs noticed for extrinsic rhα1,2-FT and rhα-Gal A immune-related enzymes followed by augmented decline in the levels of Galα1→3Gal antigenic determinants among the ex vivo-expanded PEK lines that were successfully generated and clonally multiplied from cutaneous bioptates stemming from h*FUT2*×h*GLA* bi-transgenic pigs.

The aforementioned strategies will enable us to carry out further studies focused on cloning the genetically engineered pigs by SCNT for the needs of clinical research designed to develop and optimize the negligibly intrusive and nontraumatic procedures of regenerative medicine and reconstructive surgery of human dermo-integumentary system. The latter encompass dermoplasty-based therapies aimed either at repairing the injuries in human cutaneous and subcutaneous tissues or at minimizing and eliminating the impairments in human skin integrity by porcine mono- and/or bi-genetically modified dermo-epidermal xenotransplants. Collectively, the concept of using single- or double-transgenic epidermal keratinocytes as a source of adult donor cells for SCNT represents an entirely novel approach both in pigs and in other mammalian species.

Author Contributions: Conceptualization, J.W., M.S. (Marcin Samiec), Z.S., M.R. and R.S.; analysis of data and their interpretation, J.W., M.S. (Marcin Samiec), M.R. and M.S. (Maria Skrzyszowska); performance of experiments and preparation of results, J.W., M.S. (Marcin Samiec), K.W., Z.S., J.J., M.S. (Maria Skrzyszowska) and R.S.; writing the article—original draft, J.W., M.S. (Marcin Samiec) and M.R.; writing the article—review and editing, M.S. (Marcin Samiec), J.W. and M.R.; supervision and funding acquisition, Z.S. and M.S. (Marcin Samiec); graphic and photographic documentation, J.W. and K.W. All authors have read and agreed to the published version of the manuscript.

Institutional Review Board Statement: Not applicable.

Informed Consent Statement: Not applicable.

Data Availability Statement: Not applicable.

Conflicts of Interest: The authors declare no conflict of interest. The funders had no role in the design of the study; in the collection, analyses, or interpretation of data; in the writing of the manuscript, or in the decision to publish the results.

Abbreviations

HAR	Hyperacute rejection
HRP	Horseradish peroxidase
LacNAc	*N*-Acetyllactosamine
NDECs	Nuclear donor epidermal cells
rhα1,2-FT	Recombinant human α1,2-fucosyltransferase
rhα-Gal A	Recombinant human α-galactosidase A
α1,3-GT	α1,3-Galactosyltransferase
PEKs	Porcine epidermal keratinocytes
RA	Relative abundance
SCNT	Somatic cell nuclear transfer
UDP-Gal	Uridine 5′-diphosphogalactose; Galactose-uridine-5′-diphosphate; UDP-α-D-galactose

References

1. Niemann, H.P. The production of multi-transgenic pigs: Update and perspectives for xenotransplantation. *Transgenic Res.* **2016**, *25*, 361–374. [CrossRef] [PubMed]
2. Cooper, D.K.; Gollackner, B.; Sachs, D.H. Will the pig solve the transplantation backlog? *Annu. Rev. Med.* **2002**, *53*, 133–147. [CrossRef] [PubMed]
3. Galili, U.; Shohet, S.B.; Kobrin, E.; Stults, C.L.; Macher, B.A. Man, apes, and Old World monkeys differ from other mammals in the expression of alpha-galactosyl epitopes on nucleated cells. *J. Biol. Chem.* **1988**, *263*, 17755–17762. [CrossRef]
4. Hryhorowicz, M.; Zeyland, J.; Słomski, R.; Lipiński, D. Genetically modified pigs as organ donors for xenotransplantation. *Mol. Biotechnol.* **2017**, *59*, 435–444. [CrossRef] [PubMed]
5. Whyte, J.J.; Prather, R.S. Genetic modifications of pigs for medicine and agriculture. *Mol. Reprod. Dev.* **2011**, *78*, 879–891. [CrossRef] [PubMed]
6. Cooper, D.K.C.; Ekser, B.; Tector, A.J. Immunobiological barriers to xenotransplantation. *Int. J. Surg.* **2015**, *23*, 211–216. [CrossRef]
7. Cooper, D.K.; Dou, K.F.; Tao, K.S.; Yang, Z.X.; Tector, A.J.; Ekser, B. Pig liver xenotransplantation: A review of progress toward the clinic. *Transplantation* **2016**, *100*, 2039–2047. [CrossRef] [PubMed]
8. Lu, T.; Yang, B.; Wang, R.; Qin, C. Xenotransplantation: Current status in preclinical research. *Front. Immunol.* **2020**, *10*, 3060. [CrossRef]
9. Sandrin, M.S.; McKenzie, I.F. Gal alpha (1,3)Gal, the major xenoantigen(s) recognised in pigs by human natural antibodies. *Immunol. Rev.* **1994**, *141*, 169–190. [CrossRef]
10. Blanken, W.M.; van den Eijnden, D.H. Biosynthesis of terminal Gal α1→3Galβ1→4GlcNAc-R oligosaccharide sequences on glycoconjugates. Purification and acceptor specificity of a UDP-Gal: *N*-acetyllactosaminide α1→3-galactosyltransferase from calf thymus. *J. Biol. Chem.* **1985**, *260*, 12927–12934. [CrossRef]
11. Osman, N.; McKenzie, I.F.; Ostenried, K.; Ioannou, Y.A.; Desnick, R.J.; Sandrin, M.S. Combined transgenic expression of alpha-galactosidase and alpha1,2-fucosyltransferase leads to optimal reduction in the major xenoepitope Galalpha(1,3)Gal. *Proc. Natl. Acad. Sci. USA* **1997**, *94*, 14677–14682. [CrossRef]
12. Varki, A. Factors controlling the glycosylation potential of the Golgi apparatus. *Trends Cell Biol.* **1998**, *8*, 34–40. [CrossRef]
13. Hartel-Schenk, S.; Minnifield, N.; Reutter, W.; Hanski, C.; Bauer, C.; Morré, D.J. Distribution of glycosyltransferases among Golgi apparatus subfractions from liver and hepatomas of the rat. *Biochim. Biophys. Acta* **1991**, *1115*, 108–122. [CrossRef]
14. Luo, Y.; Wen, J.; Luo, C.; Cummings, R.D.; Cooper, D.K.C. Pig xenogeneic antigen modification with green coffee bean α-galactosidase. *Xenotransplantation* **1999**, *6*, 238–248. [CrossRef] [PubMed]
15. Zeyland, J.; Woźniak, A.; Gawrońska, B.; Juzwa, W.; Jura, J.; Nowak, A.; Słomski, R.; Smorąg, Z.; Szalata, M.; Mazurek, U.; et al. Double transgenic pigs with combined expression of human α1,2-fucosyltransferase and α-galactosidase designed to avoid hyperacute xenograft rejection. *Arch. Immunol. Ther. Exp.* **2014**, *62*, 411–422. [CrossRef] [PubMed]

16. Li, J.; Greco, V.; Guasch, G.; Fuchs, E.; Mombaerts, P. Mice cloned from skin cells. *Proc. Natl. Acad. Sci. USA* **2007**, *104*, 2738–2743. [CrossRef] [PubMed]

17. Izumi, K.; Feinberg, S.E. Skin and oral mucosal substitutes. *Oral Maxillofac. Surg. Clin. N. Am.* **2002**, *14*, 61–71. [CrossRef]

18. Izumi, K.; Takacs, G.; Terashi, H.; Feinberg, S.E. *Ex vivo* development of a composite human oral mucosal equivalent. *J. Oral Maxillofac. Surg.* **1999**, *57*, 571–577. [CrossRef]

19. Wanichpakorn, S.; Kedjarune-Laggat, U. Primary cell culture from human oral tissue: Gingival keratinocytes, gingival fibroblasts and periodontal ligament fibroblasts. *Songklanakarin J. Sci. Technol.* **2010**, *32*, 327–331.

20. Xu, H.; Wan, H.; Sandor, M.; Qi, S.; Ervin, F.; Harper, J.R.; Silverman, R.P.; McQuillan, D.J. Host response to human acellular dermal matrix transplantation in a primate model of abdominal wall repair. *Tissue Eng. Part A* **2008**, *14*, 2009–2019. [CrossRef]

21. Wiater, J.; Karasiński, J.; Słomski, R.; Smorąg, Z.; Wartalski, K.; Gajda, B.; Jura, J.; Romek, M. The effect of recombinant human alpha-1,2-fucosyltransferase and alpha-galactosidase A on the reduction of alpha-gal expression in the liver of transgenic pigs. *Folia Biol.* **2020**, *68*, 121–133. [CrossRef]

22. Lipinski, D.; Jura, J.; Zeyland, J.; Juzwa, W.; Mały, E.; Kalak, R.; Bochenek, M.; Plawski, A.; Szalata, M.; Smorag, Z.; et al. Production of transgenic pigs expressing human a1,2-fucosyltransferase to avoid humoral xenograft rejection. *Med. Weter.* **2010**, *66*, 316–322.

23. Ramirez, P.; Montoya, M.J.; Ríos, A.; García Palenciano, C.; Majado, M.; Chávez, R.; Muñoz, A.; Fernández, O.M.; Sánchez, A.; Segura, B.; et al. Prevention of hyperacute rejection in a model of orthotopic liver xenotransplantation from pig to baboon using polytransgenic pig livers (CD55, CD59, and H-transferase). *Transplant. Proc.* **2005**, *37*, 4103–4106. [CrossRef] [PubMed]

24. Lutz, A.J.; Li, P.; Estrada, J.L.; Sidner, R.A.; Chihara, R.K.; Downey, S.M.; Burlak, C.; Wang, Z.Y.; Reyes, L.M.; Ivary, B.; et al. Double knockout pigs deficient in N-glycolylneuraminic acid and Galactose α-1,3-Galactose reduce the humoral barrier to xenotransplantation. *Xenotransplantation* **2013**, *20*, 27–35. [CrossRef] [PubMed]

25. Sahara, H.; Watanabe, H.; Pomposelli, T.; Yamada, K. Lung xenotransplantation. *Curr. Opin. Organ Transplant.* **2017**, *22*, 541–548. [CrossRef]

26. Klymiuk, N.; Aigner, B.; Brem, G.; Wolf, E. Genetic modification of pigs as organ donors for xenotransplantation. *Mol. Reprod. Dev.* **2010**, *77*, 209–221. [CrossRef]

27. Bottino, R.; Wijkstrom, M.; van der Windt, D.J.; Hara, H.; Ezzelarab, M.; Murase, N.; Bertera, S.; He, J.; Phelps, C.; Ayares, D.; et al. Pig-to-monkey islet xenotransplantation using multi-transgenic pigs. *Am. J. Transplant.* **2014**, *14*, 2275–2287. [CrossRef]

28. Kong, S.; Ruan, J.; Xin, L.; Fan, J.; Xia, J.; Liu, Z.; Mu, Y.; Yang, S.; Li, K. Multi-transgenic minipig models exhibiting potential for hepatic insulin resistance and pancreatic apoptosis. *Mol. Med. Rep.* **2016**, *13*, 669–680. [CrossRef]

29. Kwon, D.J.; Kim, D.H.; Hwang, I.S.; Kim, D.E.; Kim, H.J.; Kim, J.S.; Lee, K.; Im, G.S.; Lee, J.W.; Hwang, S. Generation of α-1,3-galactosyltransferase knocked-out transgenic cloned pigs with knocked-in five human genes. *Transgenic Res.* **2017**, *26*, 153–163. [CrossRef]

30. Fischer, K.; Kraner-Scheiber, S.; Petersen, B.; Rieblinger, B.; Buermann, A.; Flisikowska, T.; Flisikowski, K.; Christan, S.; Edlinger, M.; Baars, W.; et al. Efficient production of multi-modified pigs for xenotransplantation by 'combineering', gene stacking and gene editing. *Sci. Rep.* **2016**, *6*, 29081. [CrossRef]

31. Zeyland, J.; Gawrońska, B.; Juzwa, W.; Jura, J.; Nowak, A.; Słomski, R.; Smorąg, Z.; Szalata, M.; Woźniak, A.; Lipiński, D. Transgenic pigs designed to express human α-galactosidase to avoid humoral xenograft rejection. *J. Appl. Genet.* **2013**, *54*, 293–303. [CrossRef]

32. Haruyama, N.; Cho, A.; Kulkarni, A.B. Overview: Engineering transgenic constructs and mice. *Curr. Protoc. Cell Biol.* **2009**, *42*, 19.10.1–19.10.9. [CrossRef]

33. Kong, Q.; Wu, M.; Huan, Y.; Zhang, L.; Liu, H.; Bou, G.; Luo, Y.; Mu, Y.; Liu, Z. Transgene expression is associated with copy number and cytomegalovirus promoter methylation in transgenic pigs. *PLoS ONE* **2009**, *4*, e6679. [CrossRef]

34. Houdebine, L.M. Use of transgenic animals to improve human health and animal production. *Reprod. Domest. Anim.* **2005**, *40*, 269–281. [CrossRef] [PubMed]

35. Clark, A.J.; Bissinger, P.; Bullock, D.W.; Damak, S.; Wallace, R.; Whitelaw, C.B.A.; Yull, F. Chromosomal position effects and the modulation of transgene expression. *Reprod. Fertil. Dev.* **1994**, *6*, 589–594. [CrossRef]

36. Garrick, D.; Fiering, S.; Martin, D.I.K.; Whitelaw, E. Repeat-induced gene silencing in mammals. *Nat. Genet.* **1998**, *18*, 56–59. [CrossRef] [PubMed]

37. Folger, K.R.; Wong, E.A.; Wahl, G.; Capecchi, M.R. Patterns of integration of DNA microinjected into cultured mammalian cells: Evidence for homologous recombination between injected plasmid DNA molecules. *Mol. Cell. Biol.* **1982**, *2*, 1372–1387. [CrossRef] [PubMed]

38. Gajda, B.; Romek, M.; Grad, I.; Krzysztofowicz, E.; Bryla, M.; Smorag, Z. Lipid content and cryotolerance of porcine embryos cultured with phenazine ethosulfate. *Cryo Lett.* **2011**, *32*, 349–357. [CrossRef]

39. Romek, M.; Gajda, B.; Krzysztofowicz, E.; Kucia, M.; Uzarowska, A.; Smorag, Z. Improved quality of porcine embryos cultured with hyaluronan due to the modification of the mitochondrial membrane potential and reactive oxygen species level. *Theriogenology* **2017**, *102*, 1–9. [CrossRef]

40. Wiater, J.; Samiec, M.; Skrzyszowska, M.; Lipiński, D. Trichostatin A-Assisted Epigenomic Modulation Affects the Expression Profiles of not only Recombinant Human α1,2-Fucosyltransferase and α-Galactosidase a Enzymes but also Galα1$\rightarrow$3Gal Epitopes in Porcine Bi-Transgenic Adult Cutaneous Fibroblast Cells. *Int. J. Mol. Sci.* **2021**, *22*, 1386. [CrossRef]

Article

Anabolic Steroids-Driven Regulation of Porcine Ovarian Putative Stem Cells Favors the Onset of Their Neoplastic Transformation

Gabriela Gorczyca [1,†] , **Kamil Wartalski** [2,†] , **Jerzy Wiater** [2] , **Marcin Samiec** [3,*] , **Zbigniew Tabarowski** [4] and **Małgorzata Duda** [1,*]

1   Department of Endocrinology, Faculty of Biology, Institute of Zoology and Biomedical Research, Jagiellonian University in Krakow, Gronostajowa 9 Street, 30-387 Krakow, Poland; gabriela.gorczyca@uj.edu.pl
2   Department of Histology, Faculty of Medicine, Jagiellonian University Medical College, Kopernika 7 Street, 31-034 Krakow, Poland; kamil.wartalski@uj.edu.pl (K.W.); jerzy.wiater@uj.edu.pl (J.W.)
3   Department of Reproductive Biotechnology and Cryoconservation, National Research Institute of Animal Production, Krakowska 1 Street, 32-083 Balice near Kraków, Poland
4   Department of Experimental Hematology, Faculty of Biology, Institute of Zoology and Biomedical Research, Jagiellonian University in Krakow, Gronostajowa 9 Street, 30-387 Krakow, Poland; zbigniew.tabarowski@uj.edu.pl
*   Correspondence: marcin.samiec@iz.edu.pl (M.S.); maja.duda@uj.edu.pl (M.D.)
†   These authors contributed equally to this work.

Abstract: Nandrolone (Ndn) and boldenone (Bdn), the synthetic testosterone analogues with strong anabolic effects, despite being recognized as potentially carcinogenic compounds, are commonly abused by athletes and bodybuilders, which includes women, worldwide. This study tested the hypothesis that different doses of Ndn and Bdn can initiate neoplastic transformation of porcine ovarian putative stem cells (poPSCs). Immunomagnetically isolated poPSCs were expanded ex vivo in the presence of Ndn or Bdn, for 7 and 14 days. Results show that pharmacological doses of both Ndn and Bdn, already after 7 days of poPSCs culture, caused a significant increase of selected, stemness-related markers of cancer cells: CD44 and CD133. Notably, Ndn also negatively affected poPSCs growth not only by suppressing their proliferation and mitochondrial respiration but also by inducing apoptosis. This observation shows, for the first time, that chronic exposure to Ndn or Bdn represents a precondition that might enhance risk of poPSCs neoplastic transformation. These studies carried out to accomplish detailed molecular characterization of the ex vivo expanded poPSCs and their potentially cancerous derivatives (PCDs) might be helpful to determine their suitability as nuclear donor cells (NDCs) for further investigations focused on cloning by somatic cell nuclear transfer (SCNT). Such investigations might also be indispensable to estimate the capabilities of nuclear genomes inherited from poPSCs and their PCDs to be epigenetically reprogrammed (dedifferentiated) in cloned pig embryos generated by SCNT. This might open up new possibilities for biomedical research aimed at more comprehensively recognizing genetic and epigenetic mechanisms underlying not only tumorigenesis but also reversal/retardation of pro-tumorigenic intracellular events.

Keywords: pig; ovary; putative stem cells; nandrolone; boldenone; neoplastic transformation

1. Introduction

Individual tumors consist of mixed cell populations that differ in function, morphology, and molecular signatures. Of these, only a small subset of tumor cells is capable to initiate and sustain tumor growth. These cells were termed cancer stem cells (CSCs) [1,2]. On the basis of functional and molecular analysis of CSCs isolated from many organs, it was confirmed that they display stem cell-like characteristics. These are self-renewal, multi-lineage differentiation and expression of stemness-related markers [3,4]. Some of these features have been even confirmed by the analysis of single cells [5]. Based on the

above, it is believed that CSCs may play a crucial role in disease recurrence after treatment and remission. Similar to ESCs and ASCs, CSCs express markers that are not expressed by normal somatic cells and are thus thought to contribute towards a 'stemness' phenotype. Various specific markers (clusters of differentiation), including CD44 and CD133, have been employed for the isolation and characterization of ovarian CSCs from ovarian cancer cell lines and patients' tumors [6–9]. Importantly, CD44 and CD133 are the most widely used markers in CSCs research and they are also therapeutic targets in cancers [10].

Cluster of differentiation 44 (CD44), a transmembrane glycoprotein, is expressed normally by both fetal and adult hematopoietic stem cells. Upon binding to hyaluronic acid (HA), its primary ligand, CD44, mediates cell division, migration, adhesion, and signaling [11]. CD44 is highly expressed in many types of cancers including breast, prostate, and ovarian cancers [12,13]. Zhang et al. [14] have shown that ovarian cancer initiating cells (OCICs) express both CD44 and CD117. In turn, Bourguignon et al. [15] proved the dependence between CD44 receptor and pluripotency proteins, mainly NANOG, in human ovarian cancer cells line. Binding to HA, CD44 receptor promotes association of the NANOG protein with CD44, followed by NANOG activation and expression of pluripotent stem cell regulators, e.g., Rex1 and Sox2. Thus, CD44 supports the differentiation and proliferation of neoplastic cells [15]. CD133, another transmembrane glycoprotein, is normally expressed in hematopoietic stem cells, endothelial progenitor cells, and neuronal and glial stem cells [16]. CD133 is involved in cell growth and development [17]. Almost all tumor types, including ovarian ones, can be detected on the basis of CD133 expression. Interestingly, in ovarian tumors both epitopes, i.e., CD133-1 and CD133-2, have been detected [18]. What is more, CD133 is highly specific for rare and phenotypically distinct population of CSCs occurring in solid ovarian tumors [19]. Moreover, CD133-positive neoplastic cells have been found to display such stem cell-related attributes as self-renewal, differentiation, and tumor formation in the NOD-SCID mouse model. After injection into immune-compromised mice, CD133-positive neoplastic cells also exhibit chemo- and radio-resistance [20], which makes CD133 a potential anti-cancer therapeutic target [21].

Anabolic androgenic steroids (AAS) are substances synthesized from testosterone or one of its derivatives, with anabolic or androgenic properties, depending on the target tissue [22,23]. AAS exert their effects by binding to androgen receptors (ARs), thus mimicking or blocking their action, by altering endogenous hormone levels or by modifying hormone receptor turn over [24]. Importantly, the International Agency for Research on Cancer classified AAS to the group of potentially carcinogenic compounds for humans. These compounds may exert both genotoxic and cytotoxic effects, which can lead to the formation of a tumor [25]. AAS, including nandrolone (Ndn) and boldenone (Bdn), are rapidly becoming a widespread group of drugs used both clinically and illicitly. The illicit use of AAS is diffused among adolescents and bodybuilders because of their anabolic proprieties and their capacity to increase tolerance to exercise. Moreover, despite the regulations (The European Community banned the use of anabolics in Europe by means of laws 96/22/EC and 96/23/EC), these compounds are still widely used in fodder for farm animals, and their metabolites end up in the environment with their urine. Ndn is an androgen receptor agonist but also a potent progestogen [26]. In medicine, it is used in convalescence after debilitating diseases and to improve the body structure and physical condition of the body [27,28]. It is also known that the pharmacological dose of Ndn slows down cell growth, inhibits mitochondrial respiration, inhibits respiratory chain complexes I and III, and increases the production of mitochondrial reactive oxygen species (ROS). Whereas chronic administration of Ndn favors the maintenance of stem cells in various tissues but may increase the risk of their neoplastic transformation [29]. Bdn is also a dehydrated testosterone analog [26] and an androgen receptor agonist [28]. Bdn is frequently abused because it increases appetite, protein synthesis, nitrogen retention, and also stimulates the release of erythropoietin in the kidneys [30]. Although, the positive and deleterious effects promoted by AAS are well documented, none of the studies have

focused on their effects on mechanisms responsible for the initiation of stem cells' possible neoplastic transformation.

Among various animal experimental models, pigs share many similarities with humans in the form of organ size, physiology, and functioning [31]. The limited ethical dilemmas and importantly, successful isolation of putative stem cells from the ovarian cortex (poPSCs) [32–34], make pigs the valuable experimental model for not only preclinical assessment for stem cell therapy but also for the purposes of somatic cell nuclear transfer (SCNT)-based cloning in mammals. The efforts undertaken to use poPSCs, which have been subjected to extrinsic anabolic steroid-dependent oncogenic transformation (carcinogenesis), as a completely new source of nuclear donor cells (NDCs) for future research focused on SCNT, have not yet been accomplished. The results of the studies that sought to examine the suitability of malignant neoplastic cells derived from cerebellum-specific medulloblastoma [35] and breast cancer [36] as the sources of NDCs, successfully promoting the in vitro and/or early in vivo development of murine cloned embryos, have already confirmed the improvements in epigenetic reprogrammability of such NDCs following reconstruction and activation of SCNT-derived mouse oocytes. Furthermore, investigations by Li et al. [35] and Shao et al. [36] have proved that NDCs stemming from metastatic cancers have irreversibly lost their pro-oncogenic genotypic attributes and pro-cancerous phenotypic traits due to efficient epigenetic reprogramming of their nuclear genomes in murine SCNT-derived oocytes and corresponding embryos. The identifying capabilities of cancerous tumor-derived NDCs to be epigenetically reprogrammed into normal (i.e., noncancerous) cell types could give rise to the development of a general strategy reliable and feasible for assessing the contribution of genetic and epigenetic factors to not only tumorigenesis but also cessation of pro-cancerous scenario of molecular pathways followed by onset and subsequent recapitulation of anti-oncogenic transformation. Thus, exploring the extent of epigenomic plasticity and reprogrammability that determine the incidence of reversal (abrogation) and cessation (suppression) of molecular events leading to pro-cancerous conversion of poPSCs, whose nuclear genomes have been used for generating porcine SCNT-derived embryos, seems to be an especially attractive research problem. Solving this problem might contribute to the increase in the efficiency of somatic cell cloning in pigs and other mammalian species.

To the best of our knowledge, no studies about anabolic steroid-triggered immortalization of poPSCs via the activation of molecular pathways related to neoplastic transformation (neoplasia) have been reported so far. To meet this goal, we examined: (1) possible interactions of AAS with the AR in poPSCs and (2) amount and location of the most widely-used markers of CSCs: CD44 and CD133, both at mRNA and protein levels, after exposure to different doses of Ndn and Bdn in vitro. Additionally, we tested the effect of selected AAS on proliferation, viability, incidence of apoptotic events, and modulation of mitochondrial oxidative metabolism of poPSCs.

2. Results

2.1. poPSCs Cultured In Vitro with or without the Presence of Boldenone and Nandrolone Express the Androgen Receptor

Androgen receptor showed a specific nuclear localization (Figure 1) in both poPSCs cultured without anabolic steroid addition (line A) and in those cultured for 14 days with the addition of Bdn (line B) or Ndn (line C). The intense green color (white arrows) from the Alexa488 fluorochrome, which coincides with the blue signal from DAPI in the cell nucleus, indicates the nuclear localization of AR in poPSCs. The results indicate that these anabolic steroids do not disturb AR expression in poPSCs. They also provide an indirect demonstration that both nandrolone and boldenone bind to ARs and induce their activation, thus exerting the biological effects in poPSCs. After a 14-Day in vitro culture of poPSCs in the presence of nandrolone, a statistically significant (* $p < 0.05$) increase in ARs expression was observed. While the 14-Day exposure of poPSCs to boldenone caused a slight decrease in AR expression, it was not a statistically significant change.
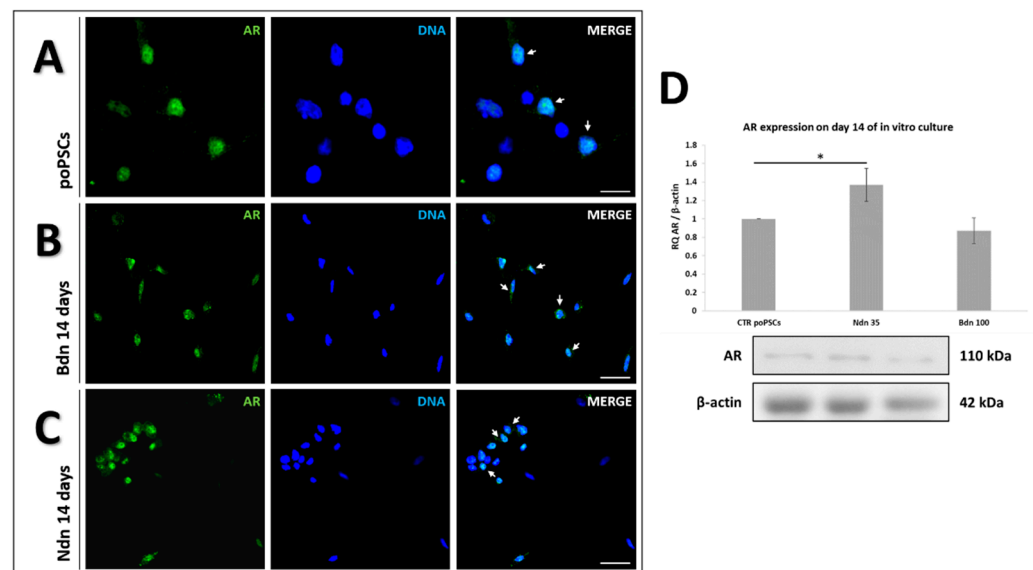
Figure 1. The presence and localization of AR in poPSCs cultured without the addition of anabolic steroids (**A**) and in poPSCs cultured for 14 days in the presence of boldenone at a dose of 100 μM (**B**) and nandrolone at a dose of 35 μM (**C**). Green signal-AlexaFluor 488 fluorescent dye, blue signal–DAPI; scale bars represent 50 μm in A and 100 μm in B and C. The immunofluorescence staining was repeated thrice; the figure shows the best representative micrographs selected from 3 replicates. Expression of AR at the level of total protein after 14-Day culture in the presence of nandrolone and boldenone (**D**). The graphs depict the relative abundances (RAs) noticed for AR obtained from measurements of the optical density of the bands representing a specific signal. Results represent the mean with $n = 3 \pm$ standard deviation (SD). Statistical analysis: homogeneity of variance—Levene's test, normality of distribution-Shapiro–Wilk test, one-way ANOVA, Tukey's post-hoc test, * $p < 0.05$.

2.2. Nandrolone and Boldenone Affect the Proliferation of poPCS after 14-Day In Vitro Culture

In order to test the effect of Ndn and Bdn on cell proliferation, poPSCs were treated for 14 days with these drugs at concentrations ranging from 15 to 35 μM and 60 to 140 μM for Ndn and Bdn, respectively. Lysates from poPSCs cultured in the presence of various concentrations of AAS were tested for the expression level of the PCNA proliferation marker against poPSCs cultured without these steroids. Figure 2 shows the results noticed for relative expression of proliferating cell nuclear antigen (PCNA), which is normalized to the reference protein of β-actin. Based on this, the treatment with 35 μM of nandrolone was chosen, since it caused a marked inhibition of cell growth still preserving cell viability. In turn, 100 μM of boldenone induced the opposite effect—a significant increase in the proliferation of poPSCs; thereby this dose was selected for further experiments.

2.3. Boldenone and Nandrolone Influence on poPSCs Viability, Cytotoxicity, and Apoptotic Activity

To further understand how the selected doses of both anabolic steroids (35 μM for nandrolone and 100 μM for boldenone) impact the viability, cytotoxicity, and caspase activation-related events in poPSCs during 14 days of their culture, the ApoTox-Glo triplex assay was performed.

Both nandrolone and boldenone have been found to insignificantly bias the viability and cytotoxicity among ex vivo-expanded poPSCs. In turn, 14-Day exposure of poPSCs to 35 μM of nandrolone induced their apoptosis (* $p < 0.05$) (Figure 3).
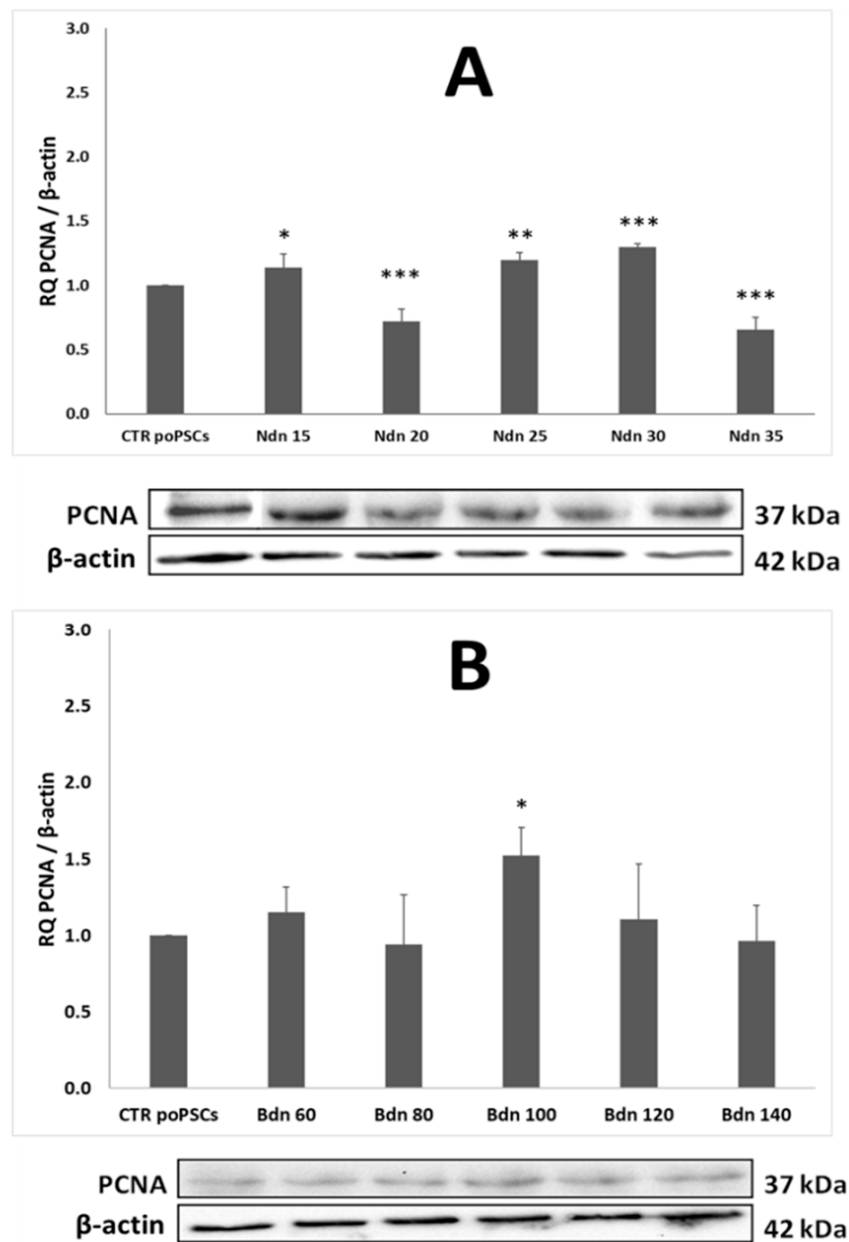
Figure 2. PCNA proliferation marker expression at the level of total protein isolated from poPSCs grown at different concentrations of nandrolone (**A**) and boldenone (**B**). The graphs show the relative content of PCNA protein obtained from measurements of the optical density of the bands representing a specific signal. Results represent the mean with $n = 5 \pm$ standard deviation (SD). Statistical analysis: homogeneity of variance—Levene's test, normality of distribution—Shapiro–Wilk test, one-way ANOVA, and Duncan's post-hoc test: part of the differences on the level of PCNA expression was statistically significant as follows: * $p < 0.05$; ** $p < 0.01$; *** $p < 0.001$. N 15-N 35: applied doses of nandrolone in concentrations ranging from 15 μM to 35 μM; B 60-B 140: doses of boldenone used in concentrations ranging from 60 μM to 140 μM, CTR poPSCs-control culture without the addition of anabolic steroids.
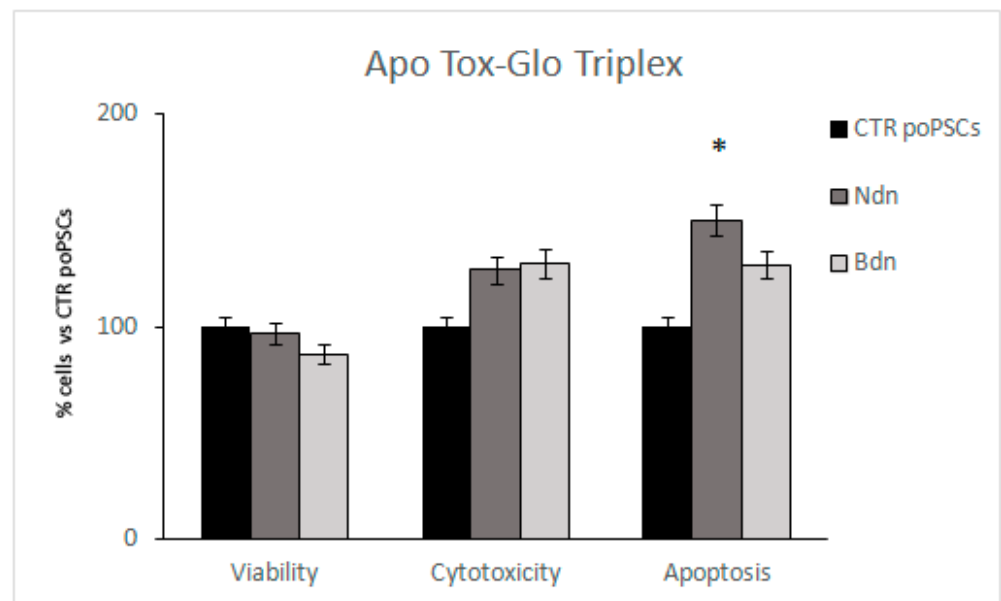
Figure 3. The effect of 14-Day treatment of poPSCs with either 35 µM of nandrolone or 100 µM of boldenone on cellular viability, cytotoxicity, and apoptotic cell death (estimated by ApoTox-Glo Triplex Assay). Results were expressed as percentages with the poPSCs control values (CTR) taken as 100%. The results represent the mean with $n = 5 \pm$ standard deviation (SD). Statistical analysis: homogeneity of variance—Levene's test, normality of distribution—Shapiro–Wilk test, one-way ANOVA, Tukey's post-hoc test, * $p < 0.05$.

2.4. Nandrolone and Boldenone Trigger the Expression of Selected Cancer Stem Cells Markers: CD44 and CD133

In poPSCs cultured with nandrolone supplementation, an increase in the abundance of CD44 protein (** $p < 0.01$) was observed after 7 days of treatment. Next, a decrease to the value found in control poPSCs cultures was noted (Figure 4B). The profile of CD133 protein abundance in poPSCs cultured under the influence of nandrolone was very similar. After 7 days of poPSCs-nandrolone treatment, increase in CD133 abundance (* $p < 0.05$) was observed. Prolonged treatment of poPSCs with nandrolone for up to 14 days decreased the CD133 protein abundance to the value found in the poPSCs control cultures (Figure 4D).

A slightly different situation was observed in poPSCs cultured under the influence of boldenone. CD44 protein abundance significantly increased (* $p < 0.05$) in poPSCs cultured in vitro for 14 days in the presence of boldenone, while 7 days of exposure to boldenone induced its statistically insignificant increase (Figure 4A) when compared to that in the corresponding poPSCs control cultures. In turn, CD133 protein abundance was markedly increased in poPSCs cultured in the presence of boldenone for both 7- and 14-days (* $p < 0.05$ and *** $p < 0.001$, respectively) when compared to the poPSCs from control cultures (Figure 4C).

Analysis of cancer stem cells marker genes, CD44 and PROM1, by real time PCR showed their significant upregulation in both nandrolone or boldenone treated poPSCs, after 7 or 14 days of culture. CD44 mRNA expression in poPSCs cultured for 7 days in the presence of nandrolone was three times higher compared to the control cultures (** $p < 0.01$) (Figure 5B). After 14 days of nandrolone treatment, CD44 mRNA expression markedly increased (** $p < 0.01$) in comparison with the control cultures (Figure 5B). PROM1 mRNA expression in poPSCs cultured for 7 days in the presence of nandrolone was nearly three times higher (** $p < 0.01$) than that in the control poPSCs (Figure 5D). The expression of PROM1 mRNA after 14 days of poPSCs culture in the presence of nandrolone was unchanged compared to the 7-day nandrolone-exposed poPSCs cultures.
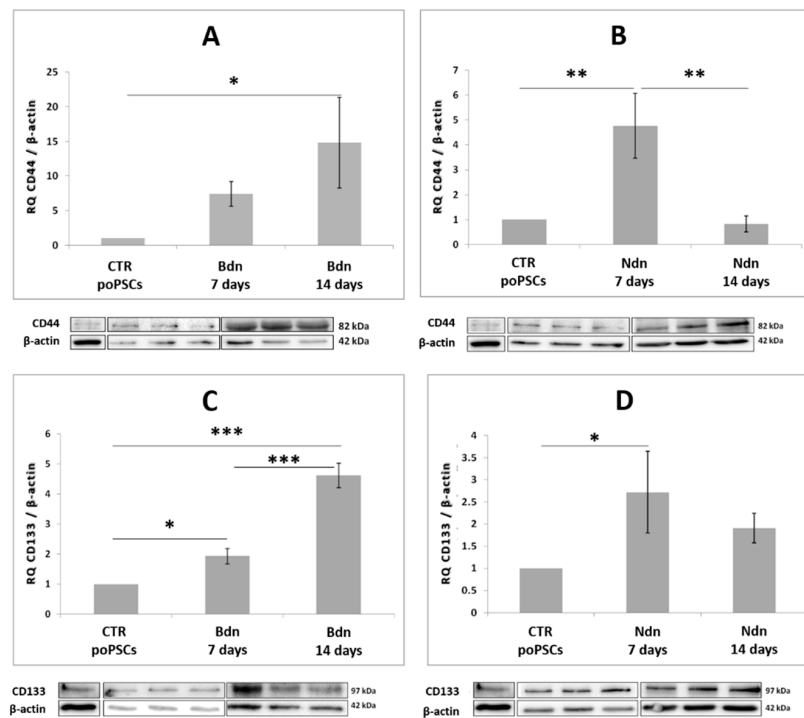
Figure 4. Expression of the protein markers CSCs: CD44 (**A**,**B**) and CD133 (**C**,**D**) at the level of total protein on day 7 and 14 of culture in the presence of boldenone (**A**,**C**) and nandrolone (**B**,**D**). The graphs show the relative content of CD44 and CD133 proteins obtained from measurements of the optical density of the bands representing a specific signal. Results represent the mean with $n = 5 \pm$ standard deviation (SD). Statistical analysis: homogeneity of variance—Levene's test, normality of distribution—Shapiro–Wilk test, one-way ANOVA, Tukey's post-hoc test, * $p < 0.05$; ** $p < 0.01$; *** $p < 0.001$.
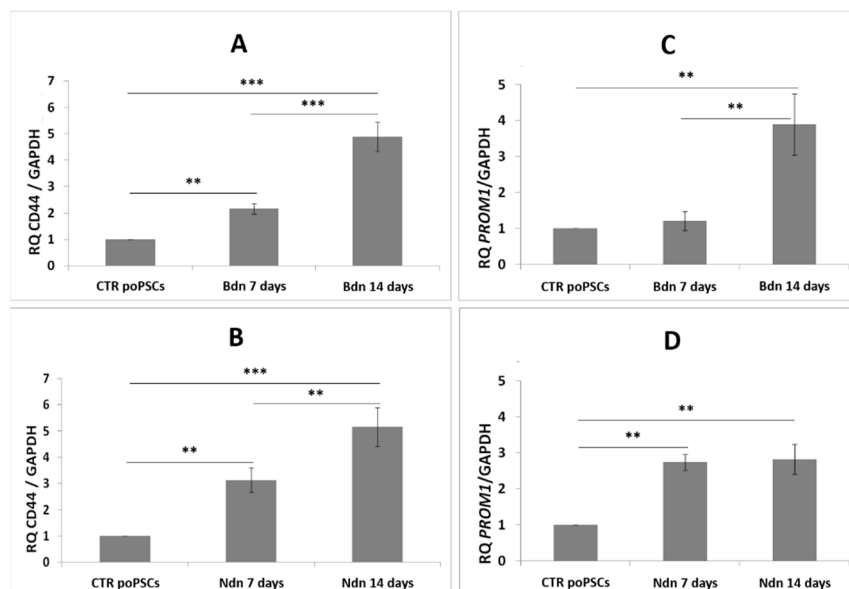
Figure 5. Expression of marker genes for CSCs: CD44 (**A**,**B**), PROM1 (**C**,**D**) at 7th and 14th day of culture in the presence of boldenone (**A**,**C**) and nandrolone (**B**,**D**) versus PSCs cultured without the addition of steroids at the transcript level as shown by RT-qPCR. The results ($2^{-\Delta\Delta Ct}$) are presented as mean values with $n = 3 \pm$ standard deviation (SD). Statistical analysis: homogeneity of variance— Levene's test, normality of distribution—Shapiro–Wilk test, one-way ANOVA and Tukey's post-hoc test, ** $p < 0.01$; *** $p < 0.001$.

The level of CD44 expression in poPSCs cultured for 7 days in the presence of Bdn was nearly two-fold higher than in the control poPSCs (** $p < 0.01$). In turn, in poPSCs cultured for 14 days in the presence of Bdn, the level of CD44 expression increased nearly five-fold when compared to that in poPSCs control cultures (*** $p < 0.001$) (Figure 5A). There were no statistically significant differences in the expression level of PROM1 in poPSCs cultured for 7 days in the presence of boldenone compared to the control cultures (Figure 5C). On the other hand, the level of PROM1 expression in poPSCs cultured for 14 days in the presence of boldenone increased approximately four times compared to the control (** $p < 0.01$) (Figure 5C).

After 14-days of PSCs culture under the Ndn and Bdn influence, immunofluorescence analysis of CD44 and CD133—surface markers identifying a subset of cancer stem cells—was performed. Control poPSCs (data not shown) demonstrated no staining for these markers, but after 14 days of culture in the presence of Bdn (Figure 6AC) or Ndn (Figure 6BD), the overall fluorescence intensity of CD44 and CD133 was markedly enhanced. The results of the IF analysis are consistent with those of the Western blot (WB) and quantitative real-time PCR analyses.
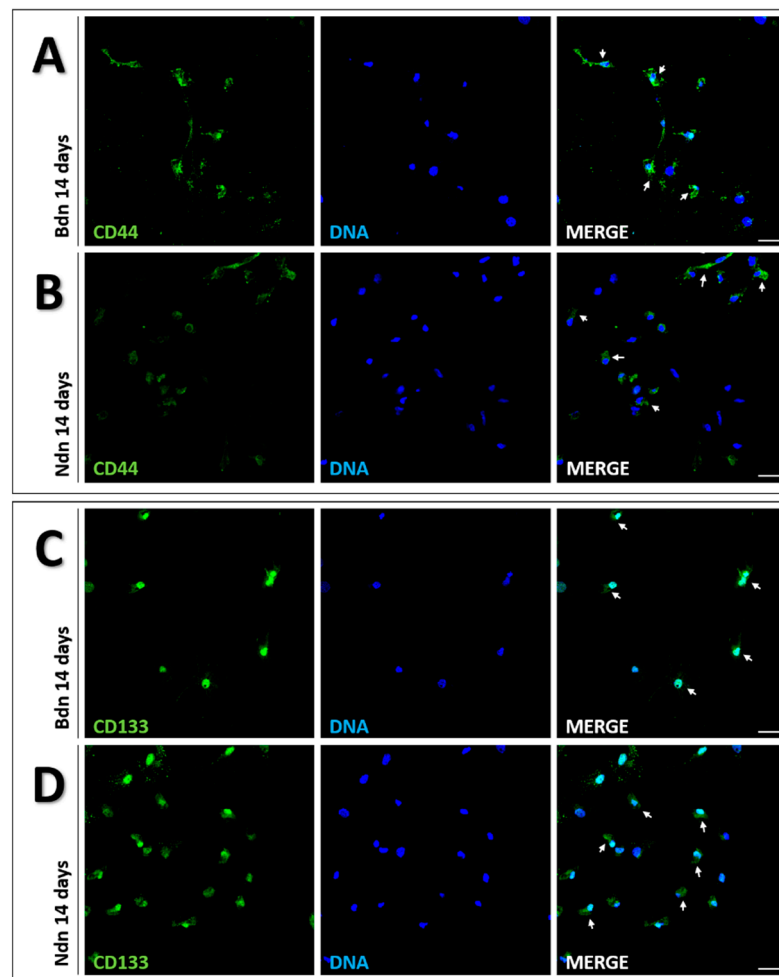
Figure 6. Immunofluorescent localization of CD44 (lines **A**,**B**) and CD133 (lines **C**,**D**) in poPSCs after 14 days of culture in the presence of boldenone at a dose of 100 μM (lines **A**,**C**) and nandrolone at a dose of 35 μM (lines **B**,**D**). Green signal—AlexaFluor 488 fluorescent dye, blue signal—DAPI, scale bars represent 100 μm. The immunofluorescence staining was repeated thrice; the figure shows the best representative micrographs selected from 3 replicates.

2.5. Oxygen Consumption in poPSCs after 7- and 14-Day In Vitro Culture in the Presence of Boldenone and Nandrolone

Since cell proliferation requires a bioenergetic support it was of interest whether nandrolone affected cell metabolism by impairing mitochondrial oxidative phosphorylation. To this aim, by using the Seahorse extracellular flux analyzer, mitochondrial oxygen consumption rate (OCR) and the extracellular acidification rate (ECAR) were simultaneously measured.

The Seahorse XF Cell Mito Stress Test showed that mitochondrial respiration (OCR) was significantly decreased in poPSCs cultured for 7 days in the presence of nandrolone compared to poPSCs cultured in the presence of boldenone or to control cultures (** $p < 0.01$ and *** $p < 0.001$, respectively) (Figure 7D). What is more, Ndn reduced the OCR level in the maximal respiration test (Figure 7A). Ndn significantly reduced also the OCR level in the spare respiratory capacity test (Figure 7B). The level of OCR in cells cultured for 7 days with the addition of nandrolone was four times lower than in the control and about three times lower compared to the boldenone test. It was also observed that after Ndn treatment, OCR level in non-mitochondrial oxygen consumption test was significantly decreased (** $p < 0.01$) (Figure 7C). The level of OCR in cells cultured for 7 days with the addition of nandrolone was about twice lower than in the control and about twice lower compared to the boldenone test. Interestingly, exposure to boldenone did not significantly affect the level of OCR relative to the control in any of the tests performed. The results obtained suggest that nandrolone may inhibit mitochondrial respiration and thus slowing poPSCs growth.
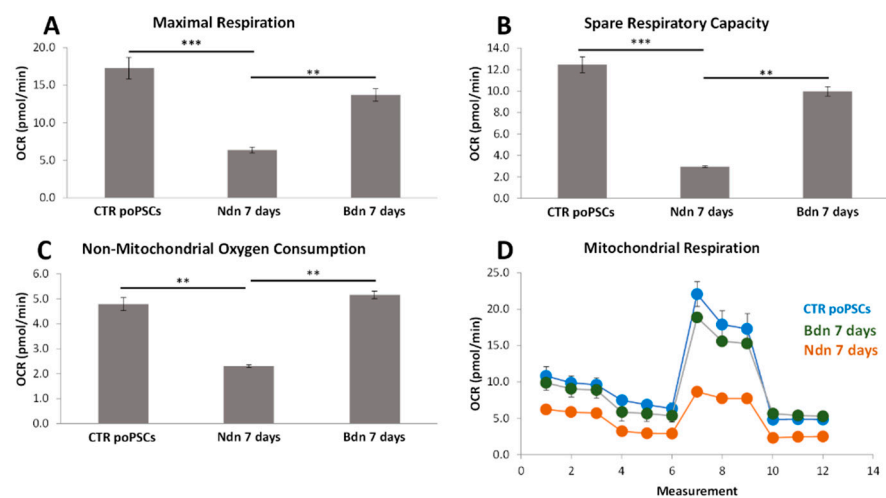
Figure 7. Seahorse XF Cell Mito Stress Test: The graphs show representative oxygen consumption rates (OCR) in mitochondrial respiration (**D**) broken down into maximal respiration (**A**), spare respiratory capacity (**B**), and non-mitochondrial oxygen consumption (**C**). Mitochondrial respiration was measured as OCR in poPSCs cultured for 7 days in the presence of nandrolone or boldenone. The obtained results were compared to the OCR level obtained on poPSCs cultured without the addition of these anabolic steroids (control). Results represent the mean with $n = 4 \pm$ standard deviation (SD). Statistical analysis: homogeneity of variance—Levene's test, normality of distribution—Shapiro–Wilk test, one-way ANOVA, Tukey's post-hoc test, ** $p < 0.01$; *** $p < 0.001$.

### 2.6. Nandrolone and Boldenone Affect the Expression and Phosphorylation of Proteins within the PI3K/Akt Pathway

After 14-days of poPSCs culture in the medium supplemented with nandrolone, the significant (** $p < 0.01$) decrease in the relative abundance (RA) of unphosphorylated Akt protein was observed (Figure 8B). In turn, the RA that has been determined for phosphorylated Akt (*p*-Akt) protein significantly increased (*** $p < 0.001$) after nandrolone treatment (Figure 8C). Simultaneously with the alterations identified for Akt, the significant

decrease of PI3K (** $p < 0.01$) protein expression was confirmed following nandrolone treatment (Figure 8A).
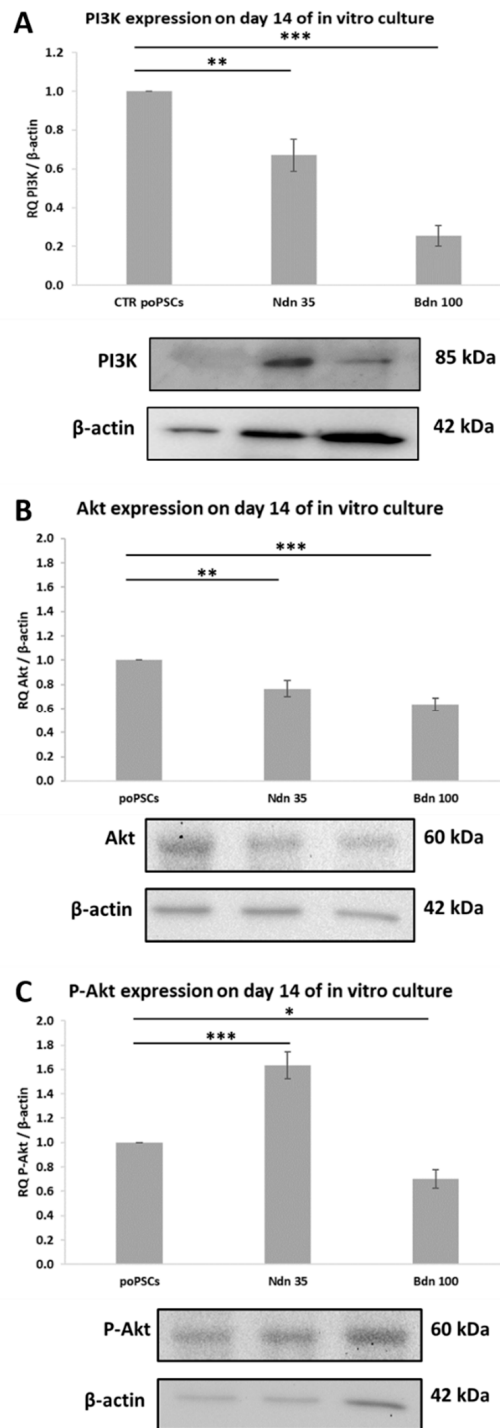
Figure 8. Expression of signaling pathway-related proteins: PI3K (**A**), Akt (**B**), and P-Akt (**C**) at the level of total protein after 14-Day culture in the presence of nandrolone and boldenone. The graphs depict the relative abundances (RAs) noticed for PI3K, Akt and P-Akt proteins obtained from measurements of the optical density of the bands representing a specific signal. Results represent the mean with $n = 3 \pm$ standard deviation (SD). Statistical analysis: homogeneity of variance—Levene's test, normality of distribution—Shapiro–Wilk test, one-way ANOVA, Tukey's post-hoc test, * $p < 0.05$; ** $p < 0.01$; *** $p < 0.001$.

As has been shown in Figure 8, significant diminishments in the expression and phosphorylation of investigated proteins engaged in the PI3K/Akt pathway (* $p < 0.05$ or *** $p < 0.001$ for P-Akt or Akt and PI3K, respectively) were noticed after 14-Day culture of poPSCs in the medium enriched with boldenone.

3. Discussion

Beyond the deleterious macro-effects mentioned above, testosterone-derived anabolic steroids may affect directly cellular functions, acting together with either genetic or epigenetic factors determining their toxic, mutagenic, genotoxic, and carcinogenic results. This is possible because AAS exert their actions by several different mechanisms: (i) they can modulate androgen receptor expression and as a consequence intracellular metabolism; (ii) they can affect directly the androgen receptor and thus its subsequent interaction with co-activators and transcriptional activity; (iii) they can interfere with the glucocorticoid receptor expression eliciting an anti-catabolic effect; and (iv) they can function by the activation of non-genomic pathways [37]. In this context, the first aim of this study was to investigate whether poPSCs possess AR receptors through which Ndn and Bdn can affect them. In control poPSCs cultures, specific nuclear localization of the AR receptor has been demonstrated. This paved the way for experiments studying the effects of anabolic steroids on them. After 14-days of poPSCs culture in the presence of both nandrolone and boldenone, the specific nuclear localization of AR was found using immunofluorescence. The presence of AR in stem cells including poPSCs is not unusual. At the transcript level, AR was confirmed for the first time in undifferentiated ESCs by Chang's team [38]. In turn, MSCs isolated from the bone marrow showing the AR receptor have already been used in regenerative medicine for the treatment of liver cirrhosis [39]. The AR receptors have also been found to regulate the progression of CSCs in various cancer types, including ovarian ones [40]. A study conducted by Chung et al. [41], using ovarian teratoma cells, provided evidence that ligand-independent AR functions in cancer stem/progenitor cells (CD133^{+} cells) facilitated ovarian teratoma cell growth. Moreover, Ling et al. [42] showed that AR expression promotes CSCs self-renewal through both classical androgen/AR activation and non-classical signaling pathways involving, inter alia, mTOR activation via the PI3K/Akt pathway. Based on the above-mentioned data and the results obtained in the current study, it might be possible that Ndn promotes the initiation of poPSCs neoplastic transformation by activating PI3K/Akt pathway. Our present investigation proved for the first time that a remarkable enhancement in Akt phosphorylation took place in nandrolone-treated poPSCs, whereas a declined semi-quantitative profile of Akt phosphorylation was recognized for boldenone-exposed poPSCs as compared to the control group of cell counterparts. Therefore, a decrease in the level of P-Akt that was markedly demonstrated after the use of boldenone suggests the inhibition of the PI3K/Akt pathway. In turn, an increase in Akt phosphorylation in nandrolone-treated poPSCs indicates an agonistic effect of this compound on the PI3K/Akt pathway. Interestingly, the qualitative and quantitative Western blot analysis showed that, in poPSCs treated with both nandrolone and boldenone, no increase in the protein level for PI3K was identified. A quite opposite effect of nandrolone was observed in MCF7 and MDA-MB-231 breast cancer cell lines, where nandrolone (at a concentration of 0.1 μM) inhibited their proliferation and migration by antagonizing the PI3K/Akt/NF-κB signaling pathway [43]. Masi et al. [43] provided the evidence that such nandrolone effect results from its binding to the membrane-bound receptor designated as oxo-eicosanoid receptor 1 (OXER1). OXER1 represents a novel link between androgens and their AR-independent action. Taking into consideration all the aforementioned findings, it should be stated that the activation of Akt under the influence of either hormones or testosterone-derived anabolic steroids is dose- and tissue-dependent. Moreover, it is worth highlighting that a broad spectrum of the non-classical and cell surface-dependent actions exerted by androgens are mediated by novel mARs, i.e., GPCRC6A, ZIP9/SLC39A9 and OXER1. Due to the fact that there is still not enough information regarding the molecular mechanisms underlying the intracellular events triggered by nandrolone and boldenone,

further in-depth studies are needed. Taking into account the results of the semi-quantitative analysis of WB, slight changes in the expression of the AR and a decrease in the expression of PI3K/Akt kinases prove that nandrolone and boldenone act pleiotropically, probably activating different signal transduction pathways. This finding seems to confirm the broad-spectrum and multifaceted Ndn- and Bdn-dependent effects, which can justify a necessity for carrying out another more-detailed studies targeted at the exploration of other signaling pathways such as, e.g., those related to ERK1/2.

Nandrolone and boldenone, apart from desired effects, when used in very high doses by extended treatment periods, also cause adverse effects [44]. The AAS concentrations used in the present study (35 µM of nandrolone and 100 µM of boldenone) were chosen firstly, based on existing literature data, which have shown that micro-molar but not nano-molar concentrations cause significant adverse effects in cultured cells [45–47] and secondly based on the results from assessment of PCNA level in poPSCs cultured in the presence of different doses of Ndn or Bdn. The results presented herein proved that two of the five doses used of Ndn, 20 µM and 35 µM, produced a statistically significant suppression of poPSCs proliferation. Interestingly, although both doses that had been established at the level of either 35 µM for nandrolone or 100 µM for boldenone did not affect the viability and cytotoxicity estimated for the ex vivo-expanded poPSCs undergoing exposure to nandrolone, the onset of the scenario related to apoptotic cell death has been confirmed. Based on this and literature data, dose of 35 µM was used for further experiments. On the other hand, the lowest dose of Bdn that increased the proliferation rate of poPSCs was 100 µM, which was also used for further in vitro experiments. These concentrations might mimic the supraphysiological doses used by AAS-users but should not be interpreted as the actual concentration the organism is exposed to. The exposure time used in the study (7- and 14-days) was chosen to mimic repeated, prolonged treatment. The data from this relatively long exposure of poPSCs cannot be directly transferred to years of AAS abuse but could shed light on the molecular processes triggered by Ndn and Bdn. The results from the assessment of PCNA level presented herein are supported by similar findings reported by some investigators [48]. Similar to boldenone, other anabolic steroid boldione more than doubled PCNA expression in bovine large luteal cells cultured for 48 h in its presence. The authors of this study believe that the use of boldione may be the cause of granulomas observed in slaughtered calves in northern Italy, where this steroid is still often used [48]. While the effects of boldenone on the female reproductive system are not fully understood, numerous pathological changes have been observed in males. Groot and Biolatti [49] tested a group of bulls, in which the boldenone derivative designated as 17-β-boldenone was detected in the urine. Cysts in the prostate gland and excessive secretion of the prostatic fluid were observed in 45% of the bulls. In 70% of cases, there were abnormalities in testicular development and degenerative changes in the sperm-forming epithelium [49]. Given that the male reproductive system is heavily regulated by AR activity, the disorders observed by Groot and Biolatti [49] may have resulted from the action of boldenone via AR. The presented study was aimed to check whether boldenone, also acting through the AR receptor expressed in the poPSC, may contribute to their neoplastic transformation. In turn, the second of the tested AAS, nandrolone, despite its own anabolic nature, negatively affected the proliferation of neural stem cells in rats [50]. Nandrolone reduced proliferation of these cells in both males and females by acting through the cyclin-dependent kinase inhibitor-p21. A much stronger effect was observed in pregnant females, which indicates the involvement of estrogens in the action of nandrolone [50]. It is suggested that the high level of circulating estrogen in the blood during pregnancy in rats enhanced the effect of nandrolone, although the mechanism of this phenomenon is unknown. This is suspected to be related to the activation of relevant receptors during proliferation of neural stem cells and/or influencing various downstream signaling molecules. In addition, their studies have shown that the decrease in proliferation rate under the influence of nandrolone can be inhibited by the AR antagonist designated as flutamide [50]. Consistent with these findings are the results of the investigations by Agriesti et al. [29], in which

the pharmacological dose of nandrolone significantly suppressed the proliferative activity of human hepatocarcinoma-derived cell lines (HepG2). A similar proliferation-inhibiting effect of nandrolone has been already reported on other cell lines such as the breast cancer cells [51] or rat Leydig R2C cells [52]. In turn, a quite opposite effect was documented by Chimento et al. [53]. Using the aforementioned rat Leydig R2C cell line, they showed that high doses of nandrolone administered together with peptide hormones like insulin-like growth factor-I (IGF-I), as it occurs in the doping practice, increased proliferation of rat Leydig R2C tumor cells via an estrogen-dependent mechanism. Taken together, the above presented data clearly indicate that the use of high doses of AAS causes an adverse effect; however, whether AAS enhance or significantly inhibit cell proliferation depends on the target site of action (i.e., whether they are somatic, stem, or cancer cells). In addition, the effect of their action directly depends what kind of molecular mechanism, estrogen- or androgen-dependent, they trigger.

Inhibiting cell proliferation or slowing down their growth are generally linked to the modification of the cell metabolism because of the lower energy needs. To analyze this, we evaluated the bioenergetic metabolic fluxes in poPSCs, both control ones and those exposed to Ndn and Bdn for a long-term, by the Seahorse methodology. As expected, the mitochondrial oxygen consumption rate appeared to be lower in cells treated with AAS. These results suggest that nandrolone by inhibition of mitochondrial respiration slows poPSCs growth. Consistent with this observation are results obtained by Agriesti et al. [29]. Using HepG2 cell lines, these investigators showed that Ndn not only repressed mitochondrial respiration but also inhibited the respiratory chain complexes I and III and enhanced mitochondrial reactive oxygen species (ROS) production. Importantly, as previously reported, the illicit use of AAS, including Ndn and Bdn, is associated with serious adverse effects, including cellular neoplasmic transformation. Since the AR is expressed in a diverse range of tissues, AAS might be implicated in induction of their tumorigenesis [54,55]. Several studies demonstrated the key role of the androgen signaling in the regulation of normal or cancer stem cells (CSCs) [56,57]. CSCs are a small subgroup of neoplastic cells which are characterized by high self-renewal, extensive proliferation, and strong tumorigenesis capacity. The latter feature causes CSCs to play an important role in the genesis of various cancers [58,59]. A recent study revealed the relationship between androgens and hepatic CSCs maintenance, demonstrating that androgens and AR participated in their regulation through the NANOG-related pathway, a potent positive regulator of CSCs stemness [60].

Cancer stem cells are mostly identified by virtue of the expression of specific cell surface markers. Of these, two should be highlighted: CD44 and CD133, which are the most widely used markers in CSCs research [10]. More particularly, the expression of CD44 and CD133 distinguishes a number of cancer-initiating cells [20,61–63]. In our current investigation, a chronic exposure of poPSCs to pharmacological doses of both Ndn and Bdn has been shown for the first time to trigger the expression of such clusters of differentiation as CD44 and CD133, which indicates the risk of occurrence of molecular events characteristic for the neoplastic transformation of poPSCs. An increased expression of CD44 and CD133 following AAS exposure is the evidence of a phenotype shift, from poPSCs, which constitute the heterogeneous population of MSCs, to CSCs. This is a strong support of the current hypotheses that suggests that tumors originate from cells that carried out a process of "malignant reprogramming" driven by genetic and epigenetic alterations. Since CD133 transcription is controlled by both histone modifications and promoter methylation, expression of CD133 in ovarian cancer can be directly regulated by epigenetic modifications. The results reported here are in line with the notion that CD133 characterizes the ovarian tumor initiating cell population [64]. A meta-analysis of the relationship between CD133 expression, prognosis, and clinical and pathological features of ovarian cancer showed that, unlike CD44, high CD133 expression correlates with a worse prognosis in patients [65]. Moreover, based on a number of emerging evidence, as well as the results obtained, it can be concluded that cancer stem cells can switch their

metabolic phenotypes in response to external stimuli for better survival [66]. Thanks to this, CSCs are more resistant to anti-tumor treatments than the non-stem cancer cells. Therefore, surviving CSCs might be responsible for metastasis and therapy resistance.

To sum up, our current investigation, which has been aimed at the development and optimization of the in vitro models for extrinsic anabolic steroid-dependent stimulation or modification applied to reprogram the molecular properties and cytophysiological functions of poPSCs, has proven that their exposure to either Ndn or Bdn brings about the enhancements in the expression of CSC-related markers. This may indicate that the approaches used for Ndn- or Bdn-assisted modulation of poPSCs are supposed to predominantly trigger their neoplastic transformation. On the one hand, molecular and epigenetic plasticity of isolated population of ovarian putative stem cells (oPSCs) offers a great opportunity for preclinical and clinical approaches targeted at ovarian cell/tissue engineering and surgical treatments based on regenerative and reconstructive medicine. These treatments can be mediated by oPSC-based auto-, iso-, allo-, or xenografting and are intended for infertile or sub-fertile female patients afflicted with ovary-specific dysfunctions/disorders such as polycystic ovary syndrome (PCOS). On the other hand, a variety of attributes related to augmented plasticity of oPSCs carry a considerable risk of initiating molecular pathways responsible for their oncogenic transformation (carcinogenesis).

4. Materials and Methods

4.1. Sample Collection and poPSCs Isolation

Porcine ovaries were collected from sexually immature Polish Landrace gilts (approximately weighing 60 to 70 kg and 5 to 6 months of age) at a local abattoir under veterinarian control within 10 min of slaughter. Next, they were placed in sterile ice-cold Dulbecco's modified phosphate-buffered saline (DPBS; pH 7.4, PAA The Cell Culture Company, Piscataway, NJ, USA) with the addition of antibiotics (Antibiotic/Antimycotic Solution; AASoln; 1% (*v/v*), PAA The Cell Culture Company) and taken to the laboratory within 1 h. After washing the experimental material twice using sterile DPBS, the ovarian cortex was separated from the ovarian cord with a scalpel and cut into uniform-size pieces of ~1 mm^3 with a tissue slicer. The obtained fragments of ovarian cortex were subjected to a 2-h enzymatic digestion procedure in a Liberase™ TH Research Grade solution (0.26 U/mL in PBS; Sigma-Aldrich, St. Louis, MO, USA) in an incubator at temperature 37 °C, with 150 rotations/min. Next, enzymatic digestion was terminated by adding an equal volume of cold DPBS (+4 °C). After that, the resulting suspension was filtered through 100-, 70-, and 40-μm nylon strainers. In the further step, the cells were washed several times in sterile DPBS and recovered by centrifugation (90× *g* for 10 min). poPSCs were isolated by an immunomagnetic method, modified, and described by us previously [67], using a monoclonal antibody–anti-human SSEA-4, conjugated to magnetic beads (EasySep™ hESC/hiPSC SSEA-4 Positive Selection Kit, StemCell™ Technologies, Vancouver, Canada). Next, the poPSCs were cultured in the maintenance medium (MM): DMEM/F12 medium (Sigma-Aldrich) supplemented with 2% B-27 (Thermo Fisher Scientific, Waltham, MA, USA) and 2 μL/mL SCF (Thermo Fisher Scientific). The prepared suspension of 3×10^3 cells/mL was seeded into the culture dishes. Cells for total protein or total RNA extraction after the experiment were cultured in six-well polystyrene plates (Nunc™, Thermo Fisher Scientific) coated with poly-*L*-lysine (Sigma-Aldrich). Cells for immunofluorescence studies were cultured on eight-cell Lab-Tek™ II-CC2 (Nunc™, Thermo Fisher Scientific) slides also coated with poly-*L*-lysine.

4.2. Evaluation of poPSCs Proliferation after 14-Day Exposure to Different Doses of Nandrolone or Boldenone

Following pre-culture, the medium was changed to fresh in 6-well plates (DMEM/F12 medium supplemented with 2% B-27 and 2 μL/mL SCF). For all in vitro experiments, Ndn (Sigma-Aldrich) and Bdn (Sigma-Aldrich) stocks were prepared in absolute dimethylsulfoxide (DMSO) and subsequently diluted in the culture medium. The final concentration

of DMSO was kept at <5 μL/mL. poPSCs were exposed to different concentrations of Ndn (0-control, 15, 20, 25, 30, and 35 μM/L) or Bdn (0-control, 60, 80, 100, 120, and 140 μM/L). Cells in the presence of AAS were grown in the same conditions as in pre-cultures for 14 days. Every two days, the medium was changed, maintaining the dose regimen of both test compounds, and the cells were passaged when they reached 80% confluence. After completion of the culture, total protein was isolated from the cells growing in each well for subsequent semi-quantitative analysis of the PCNA proliferation marker.

4.3. poPSC Culture in the Presence of Selected Doses of Nandrolone or Boldenone

After preculture, the medium was changed to fresh (DMEM/F12, 2% B-27, 2 μL/mL SCF). The plates and slides were then divided into two equal subgroups. The first subgroup was given a boldenone solution in DMSO so as to obtain a concentration of 100 μM in the medium, and the second subgroup received a nandrolone solution to obtain a concentration of 35 μM in the medium. The Ndn and Bdn concentrations for the experiment were selected based on both: literature data and the results of the previous proliferation test. Every two days, the medium was changed, maintaining the dosing pattern of both test compounds, and the cells were passaged when they reached 80% confluence. After completion of culture on day 7 and 14, total protein and total RNA were isolated from cells growing in 6-well plates, and cells growing on eight-chamber slides were fixed for immunofluorescence.

4.4. ApoTox-Glo Triplex Assay

For apoptosis, viability, and cytotoxicity assays, poPSCs that had been cultured under the conditions of Ndn or Bdn supplementation were analyzed using the ApoTox-Glo Triplex Assay (Promega GmbH, High-Tech-Park, Mannheim, Germany) according to the manufacturer's protocol. In brief, 20 μL of viability/cytotoxicity reagent mixture that was comprised of the permeable protease substrate known as glycylphenylalanyl-aminofluorocoumarin (GF-AFC) and a fluorogenic peptide substrate designated as bis-alanyl-alanyl-phenylalanyl-rhodamine 110 (bis-AAF-R110) was added to each well, and both of these compounds were shortly mixed by orbital shaking (at the parameters of 300 rpm and 30 s). The cells were subsequently incubated at 37 °C for 120 min in the presence of GF-AFC and bis-AAF-R110 reagent mixture. Fluorescence was measured at an excitation/absorption maximum wavelength of λ_{ex} equal to 400 nm and an emission maximum wavelength of λ_{em} equal to 505 nm (for assessment of cell viability) and $\lambda_{ex}/\lambda_{em}$ = 485 nm/520 nm (for evaluation of cytotoxicity) using a microplate spectrophotometer (Infinite M200; TECAN Group, Mannedorf, Switzerland). In the next step, 100 μL of Caspase-Glo 3/7 reagent was added to each well, and the samples were briefly mixed by orbital shaking (at the parameters of 300 rpm and 30 s) followed by incubation at room temperature (RT) for 120 min. Luminescence was quantitatively ascertained for 1 s according to the relevant protocol established for detection/determination of luminescence and its measurement was proportional to the amount of caspase activity present (Infinite M200, TECAN).

4.5. Immunofluorescence

Immunofluorescence, performed according to a technique developed and modified in our laboratory [67], was used to localize AR and cancer stem cells markers such as CD44 and CD133 in poPSCs incubated with steroids (boldenone and nadrolone). Additionally, PSCs cultured in the absence of steroids served as a control. After culture termination, cells were washed with PBS and fixed with cold 4% paraformaldehyde (PFA) in PBS for 10 min. After several washes with PBS, permeabilization of the cell membranes was performed by applying 0.1% Triton X-100 (Sigma-Aldrich) in Tris-buffered saline (TBS; pH 7.4). In the next step, nonspecific binding sites were blocked by an incubation with 5% normal goat serum (NGS, Sigma-Aldrich) in a humidified chamber for 40 min at room temperature. Then, NGS was removed, and the cells were incubated with the primary antibodies against the cancer stem cells markers CD44 (monoclonal mouse anti-CD44, ab6124, diluted 1:100, Abcam, Cambridge, UK) and CD133 (polyclonal rabbit anti-CD133, ab 19898, diluted 1:100,

Abcam, Cambridge, UK) and against the androgen receptor-AR (polyclonal rabbit anti-AR, sc-816, diluted 1:50, Santa Cruz Biotechnology, Dallas, TX, USA) overnight at 4 °C in a humidified chamber. Subsequently, the cells were washed several times with TBST (TBS þ 0.1% Tween 20, Sigma-Aldrich) and incubated with the appropriate secondary antibody, either Alexa Fluor 488-labeled goat anti-rabbit (for AR and CD133) or goat anti-mouse (for CD44) at a 1:500 dilution (Thermo Fisher Scientific) for 1 h at room temperature in a dark, humidified chamber. Negative controls included cells incubated with 5% NGS. Immuno-labeled cells were mounted in VectaShield® HardSet™ Mounting Medium with DAPI (Vector Laboratories, Burlingame, CA, USA), and they were analyzed with an OLYMPUS FV1200 FLUOVIEW scanning confocal laser microscope (parameters: OLYMPUS, Tokyo, Japan) under both 20× and 40× objective lenses.

4.6. Western Blot Analysis

Western blot analysis was performed according to a technique developed and modified in our laboratory [68]. Briefly, after termination of both poPSCs cultured in the presence of steroids for 7 or 14 days and poPSCs cultured without addition of steroids, they were washed twice with cold PBS. Next, total protein from all cultured cells samples was extracted using radioimmunoprecipitation assay buffer (RIPA; Thermo Scientific, Inc., Rockford, IL, USA) in the presence of protease inhibitor cocktail (Sigma-Aldrich). The suspension was then sonicated and centrifuged at $10,000 \times g$ for 20 min at 4 °C. The supernatant was collected and stored at −20 °C. The protein concentration was determined with the DC™ Protein Assay (Bio-Rad Protein Assay; Bio-Rad Laboratories GmbH, München, Germany) using bovine serum albumin (BSA, Sigma-Aldrich) as a standard. Aliquots of cell lysates containing 30 mg of protein were solubilized in a sample buffer consisting of 62.5 mM Tris-HCl pH 6.8, 2% SDS, 25% glycerol, 0.01% bromophenol blue, and 5% β-mercaptoethanol (Bio-Rad Laboratories) and denatured at 99.9 °C for 3 min. After denaturation, the samples were separated via 10% (for AR, CD44, CD133, Akt, P-Akt, and PI3K) or 12% (for PCNA) sodium dodecyl-sulphate (SDS)-polyacrylamide gel electrophoresis (SDS-PAGE) under reducing conditions. The separated proteins were transferred onto a poly(vinylidene fluoride) (PVDF) membrane using a wet blotter in Genie Transfer Buffer (20 mM Tris, 150 mM glycine in 20% methanol, pH 8.4) for 90 min at a constant amperage of 350 mA. Then, the membranes were blocked with 5% non-fat milk in TBST (Tris-buffered saline with 0.1% *v/v* Tween20; Bioshop Inc., Burlington, VT, Canada) for 30 min at room temperature with gentle shaking, and next they were treated (overnight at ~4 °C) with the primary antibodies. The same primary antibodies as those used for immunofluorescent labelling were utilized as follows: immunoglobulins isotype G (IgGs) raised against AR (at a 1:200 dilution), against CD44 (at a 1:500 dilution), and against CD133 (at a 1:500 dilution). Additionally, IgGs against a proliferation marker PCNA (at a 1:1000 dilution) and IgGs against signaling pathway-related proteins such as: Akt (at a 1:1000 dilution), P-Akt (at a 1:1000 dilution), and PI3K (at a 1:1000 dilution) (Cell Signaling Technology; Danvers, MA, USA) were used. β-Actin was used as an internal control (monoclonal mouse anti-β-actin, diluted 1:2000; Sigma-Aldrich). The membranes were washed and incubated with an appropriate horseradish peroxidase (HRP)-conjugated secondary antibody (goat anti-mouse IgG for β-actin, CD44, and PCNA or goat anti-rabbit IgG for AR, CD133, Akt, P-Akt, and PI3K, Vector Laboratories; diluted 1:1000) for 1 h at RT. Immunoreactive protein bands were detected by chemiluminescence using Clarity™ Western ECL Blotting Substrate (Bio-Rad Laboratories). The blots were visualized using the ChemiDoc™, and all bands were quantified using the Image Lab™ 2.0 Software (Bio-Rad Laboratories). Semi-quantitative analysis was performed for three separately repeated experiments for each control and experimental group.

4.7. Total RNA Isolation and cDNA Synthesis

Total RNA was extracted from both poPSCs cultured in the presence of steroids for 7 or 14 days and poPSCs cultured without addition of steroids. Total cellular RNA was

isolated using the EZ-10 Spin Column Total RNA Mini Preps Super Kit (Bio Basic Canada Inc.; Markham, ON, Canada) according to the manufacturer's protocol. The quantity and quality of the total RNA were ascertained by measuring the absorbance at 260 and 280 nm with a NanoDrop ND2000 Spectrophotometer (Thermo Fisher Scientific; Wilmington, DE, USA). Moreover, RNA samples were electrophoresed on a 1% (wt/vol) denaturing agarose gel to verify the RNA quality and stored frozen at $-80\,°C$. First-strand cDNA was prepared by reverse transcription (RT) using 1 mg of total RNA, random primers, and a High-Capacity cDNA Reverse Transcription Kit (Applied Biosystems; Foster City, CA, USA) according to the manufacturer's protocol. The 20-mL total reaction volume contained random primers, dNTP mix, RNAse inhibitor, and Multi Scribe Reverse Transcriptase. RT was performed in a Veriti Thermal Cycler (Applied Biosystems) according to the following thermal profile: (1) $25\,°C$ for 10 min, (2) $37\,°C$ for 120 min, and (3) $85\,°C$ for 5 min. Genomic DNA amplification contamination was checked using control experiments, in which reverse transcriptase was omitted during the RT step. The samples were kept at $-20\,°C$ until further analysis.

4.8. Quantitative Real-Time qPCR

The real-time PCR was performed according to the manufacturer's protocol. For quantitative analysis, the mRNA levels of the investigated genes CD44 and PROM1 (CD133) in each sample were assessed using the TaqMan Gene Expression Assay (Applied Biosystems; assay ID: CD44 ARTZ9RP and PROM1 ARRWE6T). The level of glyceraldehyde-3-phosphate dehydrogenase (GAPDH; Applied Biosystems; assay ID: Ss03373286_u1) was estimated as an internal control. All real-time PCR experiments were performed in duplicate [68]. Amplifications were performed with a StepOne™ Real-Time PCR System (Applied Biosystems) according to the recommended cycling program (2 min at $50\,°C$, 10 min at $95\,°C$, 40 cycles of 15 s at $95\,°C$, and 1 min at $60\,°C$). Amplification of contaminating genomic DNA was checked by control experiments in which reverse transcriptase was omitted during the RT step. Threshold cycles (Ct values) for the expression of the investigated gene were calculated using StepOne software. All samples were normalized to GAPDH ($\Delta\Delta$Ct value). The relative expression of the genes of interest was expressed as $2^{-\Delta\Delta Ct}$ [69].

4.9. Seahorse Analysis

The cellular bioenergetics were determined using the XFp analyser (Agilent; Boston, MA, USA) kindly provided by Perlan Technologies (Warsaw, Poland). All assays were programmed (designed) in XF data acquisition Wave 2.6.1 software (Agilent, Boston, MA, USA). In each experiment, 3 baseline measurements were taken prior to the addition of any compound/substrate/inhibitor, and at least 3 response measurements were taken after the addition of each compound. Oxygen Consumption Rate (OCR) and Extracellular Acidification Rate (ECAR) were reported as absolute rates (pM/min for OCR and mpH/min for ECAR). While sensor cartridges were hydrated (overnight) and calibrated (XF Calibrant), cell plates were incubated in a $37\,°C$ for 30 min prior to the start of an assay. All experiments were performed at $37\,°C$ in non-CO_2 conditions. Detailed protocols and their justification can be found at https://www.agilent.com/en/product/cell-analysis/how-torun-an-assay (accessed from June 2020 to May 2021). Additionally, detailed protocols were previously published [70–72].

Seahorse XF Measurement of ECAR and OCR Using Seahorse XF Cell Mito Stress Test

The pools/subpopulations of poPSCs, after 7- and 14-days of culture under Ndn or Bdn exposure were suspended in sterile (0.2-µm syringe strainer filtered) HBSS(+) w/o sodium bicarbonate (Gibco; Waltham, MA, USA) supplemented with 1 mM sodium pyruvate (Sigma–Aldrich, Saint Louis, MO, USA), 2 mM *L*-Glutamine (Sigma–Aldrich; Saint Louis, MO, USA), 10 mM *D*-glucose (Lonza Bioscience; Basel, Switzerland) and 5 mM HEPES (Sigma–Aldrich; Saint Louis, MO, USA) and adjusted to pH 7.4 with 0.1-N NaOH

(Sigma–Aldrich; Saint Louis, MO, USA). Buffer factor of assay media was validated prior to experiments and was equal to 2.9 mM/pH. Next, cells were plated (4×10^5 cells/well) in 180 μL on Agilent Seahorse 8-well XFp Cell Culture Miniplate and allowed to settle/adhere for 30 min at 37 °C. Real-time, noninvasive measurements of ECAR and OCR were obtained which correlated to acidification, mostly derived from glycolysis and mitochondrial function, respectively. Measurements were continued for 1 h and consisted of (i) a sample mixing time (each 1 min long) and (ii) a data acquisition period of 57 min. The latter consisted of 3 cycles with waiting time before each measurement lasting for 15 min.

4.10. Statistical Analysis

Statistical analysis was performed using Statistica 10.0 software (StatSoft, Inc.; Tulsa, OK, USA). For cell culture experiments, experiments were performed in quadruplicate ($n = 5$). Levene's test for homogeneity of variance, the Shapiro–Wilk test for normality and one-way ANOVA followed by Tukey's or Duncan's post-hoc test were used to assess differences between control and experimental cultures. Western blot and real-time PCR analyses were repeated three times (in duplicate). The data are expressed as the mean $\pm$ SEM. Statistical significance was established at * $p \leq 0.05$, ** $p \leq 0.01$, and *** $p \leq 0.001$.

5. Conclusions

The efforts undertaken in this study to comprehensively characterize molecular advantages of poPSCs and their potentially neoplastic cell derivatives are necessary to assess whether cell nuclei stemming from such NDCs will not fail to be epigenetically dedifferentiated in porcine SCNT-derived oocytes and resultant cloned embryos. It is noteworthy that these efforts have been conceptualized for the purpose of somatic cell cloning in pigs and different mammalian species for the first time. Furthermore, the approaches applied to sustainably ameliorate/repress pro-carcinogenic activity or eliminate oncogenicity (cancerogenicity) of ovarian MSC-like cells, the epigenomic memories and transcriptional profiles of which have been efficiently reprogrammed in porcine nuclear-transferred embryos, have not yet been devised. Therefore, optimizing these approaches is largely desirable for the needs of recognizing the suitability of ovarian putative stem cells that have undergone cancerous transformation to use them as NDCs for future studies aimed at SCNT in pigs and other mammalian species.

For the above-indicated reasons, thoroughly identifying factors that affect augmented epigenetic plasticity of the ovary-specific MSC-like cells and thereby enhanced reprogrammability of these NDCs in porcine nuclear-transferred embryos appears to be highly justified. As a consequence, this is of tremendous importance for the studies that attempt to improve the effectiveness of somatic cell cloning in pigs and a variety of mammalian species. The aforementioned scientific problems are also required to be widely resolved in order to remarkably increase the potential of practically using SCNT-based investigations for a broad spectrum of transgenic, biomedical, biopharmaceutical, and biotechnological research.

Author Contributions: Conceptualization, M.D., K.W. and M.S; Analysis of data and their interpretation, M.D., K.W., G.G., J.W. and M.S.; Performance of experiments and preparation of results, K.W., G.G., J.W. and M.D.; Writing the article—original draft, K.W., M.D. and M.S.; Writing the article—review and editing, K.W., M.D. and M.S.; Supervision and funding acquisition, M.D. and K.W.; Graphic and photographic documentation, K.W. and J.W.; Language correction of article, Z.T. and M.S. All authors have read and agreed to the published version of the manuscript.

Institutional Review Board Statement: Not applicable.

Informed Consent Statement: Not applicable.

Abbreviations

AAS	Anabolic androgenic steroids
AASoln	Antibiotic/antimycotic solution
Akt	A member of serine/threonine-specific protein kinase family (also known as protein kinase B; PKB) that plays a pivotal function in controlling the molecular balance between survival and death pathways in cells
AR	Androgen receptor
ASCs	Adult stem cells
Bdn	Boldenone
CSCs	Cancer stem cells
CD	Cluster of differentiation
ECAR	Extracellular acidification rate
ERK1/2	Extracellular signal-regulated protein kinases 1 and 2; also known as p44 mitogen-activated protein (MAP) kinase (a 44-kDa isoform of MAPK) and p42 mitogen-activated protein (MAP) kinase (a 42-kDa isoform of MAPK), respectively
ESCs	Embryonic stem cells
GPCRC6A	G protein-coupled receptor family C group 6 member A; a novel membrane androgen receptor (mAR) related to the extranuclear action of androgens
HA	Hyaluronic acid
HepG2	Human hepatocarcinoma-derived cell lines
IGF-I	Insulin-like growth factor-I
Klf-4	Krüppel-like factor-4 (also called gut-enriched Krüppel-like factor or GKLF); an evolutionarily conserved zinc finger-containing transcription factor that regulates diverse cellular processes such as cell growth, proliferation, differentiation, apoptosis, and somatic cell reprogramming
mARs	Novel membrane androgen receptors (unrelated to nuclear androgen receptors) that are engaged in a broad spectrum of non-classical, cell surface-initiated androgen actions
MSCs	Mesenchymal stem cells
mTOR	Mechanistic target of rapamycin (previously known as mammalian target of rapamycin) that represents a family of serine/threonine-specific protein kinases; mammalian target of rapamycin (mTOR) kinase that has been identified as a direct target of the rapamycin-FKBP12 (FK506-binding protein 12 kDa) complex; mTOR kinase is also designated as FK506-binding protein 12-rapamycin complex-associated protein 1 (FRAP1)
NANOG	Homeobox-containing transcription factor whose name stems from Celtic/Irish mythical word Tír na nÓg (i.e., Tir Na Nog; The Land of the Ever-Young)
NDCs	Nuclear donor cells
Ndn	Nandrolone
NF-κB	Nuclear factor-κB (nuclear factor kappa-light-chain-enhancer of activated B cells); a pleiotropic inducible transcription factor that occurs in almost all cell types and is the endpoint of a series of signal transduction events that are initiated by a vast array of stimuli related to many biological processes such as cytodifferentiation, cell growth, tumorigenesis, apoptosis, inflammation, and immunity
NOD-SCID	Non-obese diabetic/severe combined immunodeficient mouse model

OCICs	Ovarian cancer initiating cells
OCR	Oxygen consumption rate
Oct-4	Octamer-binding transcription factor-4 (also designated as POU5F1); a member of the family of POU (Pit-Oct-Unc)-domain and homeodomain transcription factors
oPSCs	Ovarian putative stem cells
OXER1	G protein-coupled oxo-eicosanoid receptor 1; a receptor of the arachidonic acid metabolite, i.e., 5-oxoeicosatetraenoic acid (5-oxoETE); known as a novel mAR involved in the rapid effects of androgens
PCDs	Potentially cancerous derivatives
PCNA	Proliferating cell nuclear antigen
PCOS	Polycystic ovary syndrome
PI3K	Phosphatidylinositol 3-kinase; a downstream kinase activated by receptor tyrosine kinases that generates a series of phosphorylated phosphoinositides, which recruit 3-phosphoinositide-dependent protein kinase-1 (PDPK1) activity to the plasma membrane, leading to activation of Akt
poPSCs	Porcine ovarian putative stem cells
RIPA	Radioimmunoprecipitation assay buffer
Rex1	Reduced expression gene 1 encoding a DNA-binding transcription factor known as reduced expression protein 1 or zinc finger protein 42 homolog
ROS	Reactive oxygen species
SCNT	Somatic cell nuclear transfer
Sox2	Sex-determining region Y (SRY)-box 2; a member of the high mobility group (HMG)-box family of DNA-binding transcription factors
ZIP9	Zinc transporter member 9; also designated as solute carrier family 39 member 9 (SLC39A9) or transmembrane zinc-influx transporter (Zrt)- and transmembrane iron-influx transporter (Irt)-like protein (ZIP) 9; represents both zinc (Zn^{2+})-iron (Fe^{2+}) permease (ZIP) family and a novel membrane androgen receptor (mAR) family related to the extranuclear action of androgens

References

1. Pardal, R.; Clarke, M.F.; Morrison, S.J. Applying the principles of stem-cell biology to cancer. *Nat. Rev. Cancer* **2003**, *3*, 895–902. [CrossRef]
2. Tysnes, B.B. Tumor-initiating and-propagating cells: Cells that we would to identify and control. *Neoplasia* **2010**, *12*, 506–515. [CrossRef]
3. Medema, J.P. Cancer stem cells: The challenges ahead. *Nat. Cell Biol.* **2013**, *15*, 338–344. [CrossRef]
4. Pattabiraman, D.R.; Weinberg, R.A. Tackling the cancer stem cells—What challenges do they pose? *Nat. Rev. Drug Discov.* **2014**, *13*, 497–512. [CrossRef] [PubMed]
5. Patel, A.P.; Tirosh, I.; Trombetta, J.J.; Shalek, A.K.; Gillespie, S.M.; Wakimoto, H.; Cahill, D.P.; Nahed, B.V.; Curry, W.T.; Martuza, R.L.; et al. Single-cell RNA-seq highlights intratumoral heterogeneity in primary glioblastoma. *Science* **2014**, *344*, 1396–1401. [CrossRef] [PubMed]
6. Alison, M.R.; Islam, S.; Wright, N.A. Stem cells in cancer: Instigators and propagators? *J. Cell Sci.* **2010**, *123*, 2357–2368. [CrossRef]
7. Foster, R.; Buckanovich, R.J.; Rueda, B.R. Ovarian cancer stem cells: Working towards the root of stemness. *Cancer Lett.* **2013**, *338*, 147–157. [CrossRef] [PubMed]
8. Garson, K.; Vanderhyden, B.C. Epithelial ovarian cancer stem cells: Underlying complexity of a simple paradigm. *Reproduction* **2015**, *149*, 59–70. [CrossRef]
9. Nozawa-Suzuki, N.; Nagasawa, H.; Ohnishi, K.; Morishige, K.I. The inhibitory effect of hypoxic cytotoxin on the expansion of cancer stem cells in ovarian cancer. *Biochem. Biophys. Res. Commun.* **2015**, *457*, 706–711. [CrossRef]
10. Zhao, W.; Li, Y.; Zhang, X. Stemness-related markers in cancer. *Cancer Transl. Med.* **2017**, *3*, 87–95.
11. Basakran, N.S. CD44 as a potential diagnostic tumor marker. *Saudi Med. J.* **2015**, *36*, 273–279. [CrossRef]
12. Palapattu, G.S.; Wu, C.; Silvers, C.R.; Martin, H.B.; Williams, K.; Salamone, L.; Bushnell, T.; Huang, L.; Yang, Q.; Huang, J. Selective expression of CD44, a putative prostate cancer stem cell marker, in neuroendocrine tumor cells of human prostate cancer. *Prostate* **2009**, *69*, 787–798. [CrossRef] [PubMed]
13. Orian-Rousseau, V. CD44, a therapeutic target for metastasising tumours. *Eur. J. Cancer* **2010**, *46*, 1271–1277. [CrossRef] [PubMed]
14. Zhang, S.; Balch, C.; Chan, M.W.; Lai, H.C.; Matei, D.; Schilder, J.M.; Yan, P.S.; Huang, T.H.M.; Nephew, K.P. Identification and characterization of ovarian cancer-initiating cells from primary human tumors. *Cancer Res.* **2008**, *68*, 4311–4320. [CrossRef]
15. Bourguignon, L.Y.; Peyrollier, K.; Xia, W.; Gilad, E. Hyaluronan-CD44 interaction activates stem cell marker Nanog, Stat-3-mediated MDR1 gene expression, and ankyrin-regulated multidrug efflux in breast and ovarian tumor cells. *J. Biol. Chem.* **2008**, *283*, 17635–17651. [CrossRef] [PubMed]

16. Handgretinger, R.; Gordon, P.R.; Leimig, T.; Chen, X.; Buhring, H.J.; Niethammer, D.; Kuci, S. Biology and plasticity of CD133+ hematopoietic stem cells. *Ann. N. Y. Acad. Sci.* **2003**, *996*, 141–151. [CrossRef]

17. Li, Z. CD133: A stem cell biomarker and beyond. *Exp. Hematol. Oncol.* **2013**, *2*, 17. [CrossRef] [PubMed]

18. Ferrandina, G.; Bonanno, G.; Pierelli, L.; Perillo, A.; Procoli, A.; Mariotti, A.; Corallo, M.; Martinelli, E.; Rutella, S.; Paglia, A.; et al. Expression of CD133-1 and CD133-2 in ovarian cancer. *Int. J. Gynecol. Cancer* **2008**, *18*, 506–514. [CrossRef]

19. Curley, M.D.; Therrien, V.A.; Cummings, C.L.; Sergent, P.A.; Koulouris, C.R.; Friel, A.M.; Roberts, D.J.; Seiden, M.V.; Scadden, D.T.; Rueda, B.R.; et al. CD133 expression defines a tumor initiating cell population in primary human ovarian cancer. *Stem Cells* **2009**, *27*, 2875–2883.

20. Singh, S.K.; Hawkins, C.; Clarke, I.D.; Squire, J.A.; Bayani, J.; Hide, T.; Henkelman, R.M.; Cusimano, M.D.; Dirks, P.B. Identification of human brain tumour initiating cells. *Nature* **2004**, *432*, 396–401. [CrossRef]

21. Skubitz, A.P.; Taras, E.P.; Boylan, K.L.; Waldron, N.N.; Oh, S.; Panoskaltsis-Mortari, A.; Vallera, D.A. Targeting CD133 in an in vivo ovarian cancer model reduces ovarian cancer progression. *Gynecol. Oncol.* **2013**, *130*, 579–587. [CrossRef] [PubMed]

22. Bahrke, M.S.; Yesalis, C.E. Abuse of anabolic androgenic steroids and related substances in sport and exercise. *Curr. Opin. Pharmacol.* **2004**, *4*, 614–620. [CrossRef]

23. Simão, V.A.; Berloffa Belardin, L.; Araujo Leite, G.A.; De Almeida Chuffa, L.G.; Camargo, I.C.C. Effects of different doses of nandrolone decanoate on estrous cycle and ovarian tissue of rats after treatment and recovery periods. *Int. J. Exp. Pathol.* **2015**, *96*, 338–349. [CrossRef] [PubMed]

24. Combarnous, Y.; Nguyen, T.M.D. Comparative overview of the mechanisms of action of hormones and endocrine disruptor compounds. *Toxics* **2019**, *7*, 5. [CrossRef]

25. Souza, J.P.; Cerqueira, E.D.M.M.; Meireles, J.R.C. Chromosome damage, apoptosis, and necrosis in exfoliated cells of oral mucosa from androgenic anabolic steroids users. *J. Toxicol. Environ. Health A* **2015**, *78*, 67–77. [CrossRef] [PubMed]

26. Elks, J.; Ganellin, C.R. *The Dictionary of Drugs: Chemical Data: Chemical Data, Structures and Bibliographies*, 1st ed.; Springer Science and Business Media: Berlin/Heidelberg, Germany, 1990; pp. 44, 209, 408, 410, 640, 660.

27. Handelsman, D.J. Androgen physiology, pharmacology and abuse. In *Endocrinology-E-Book: Adult and Pediatric*, 6th ed.; Jameson, J.L., De Groot, L.J., Eds.; Elsevier Health Sciences: Amsterdam, The Netherlands, 2010; pp. 2469–2498.

28. Llewellyn, W. Part III: Drug profiles. In *Anabolics*; Llewellyn, W., Ed.; Molecular Nutrition LLC: Jupiter, FL, USA, 2011; pp. 739–780.

29. Agriesti, F.; Tataranni, T.; Pacelli, C.; Scrima, R.; Laurenzana, I.; Ruggieri, V.; Cela, O.; Mazzoccoli, C.; Salerno, M.; Sessa, F.; et al. Nandrolone induces a stem cell-like phenotype in human hepatocarcinoma-derived cell line inhibiting mitochondrial respiratory activity. *Sci. Rep.* **2020**, *10*, 1–17. [CrossRef]

30. Forbes, G.B. The effect of anabolic steroids on lean body mass: The dose response curve. *Metabolism* **1985**, *34*, 571–573. [CrossRef]

31. Whyte, J.J.; Prather, R.S. Genetic modifications of pigs for medicine and agriculture. *Mol. Reprod. Dev.* **2011**, *78*, 879–891. [CrossRef]

32. Bui, H.T.; Van Thuan, N.; Kwon, D.N.; Choi, Y.J.; Kang, M.H.; Han, J.W.; Kim, T.; Kim, J.H. Identification and characterization of putative stem cells in the adult pig ovary. *Development* **2014**, *141*, 2235–2244. [CrossRef] [PubMed]

33. Wartalski, K.; Gorczyca, G.; Wiater, J.; Tabarowski, Z.; Palus-Chramiec, K.; Setkowicz, Z.; Duda, M. Efficient generation of neural-like cells from porcine ovarian putative stem cells–morphological characterization and evaluation of their electrophysiological properties. *Theriogenology* **2020**, *155*, 256–268. [CrossRef]

34. Wartalski, K.; Gorczyca, G.; Wiater, J.; Tabarowski, Z.; Duda, M. Porcine ovarian cortex-derived putative stem cells can differentiate into endothelial cells in vitro. *Histochem. Cell Biol.* **2021**, *156*, 349–362, online ahead of print. [CrossRef] [PubMed]

35. Li, L.; Connelly, M.C.; Wetmore, C.; Curran, T.; Morgan, J.I. Mouse embryos cloned from brain tumors. *Cancer Res.* **2003**, *63*, 2733–2736. [PubMed]

36. Shao, G.B.; Ding, H.M.; Gao, W.L.; Li, S.H.; Wu, C.F.; Xu, Y.X.; Liu, H.L. Effect of trychostatin A treatment on gene expression in cloned mouse embryos. *Theriogenology* **2009**, *71*, 1245–1252. [CrossRef]

37. Hampl, R.; Kubátová, J.; Stárka, L. Steroids and endocrine disruptors—History, recent state of art and open questions. *J. Steroid Biochem. Mol. Biol.* **2016**, *155*, 217–223. [CrossRef] [PubMed]

38. Chang, C.Y.; Hsuuw, Y.D.; Huang, F.J.; Shyr, C.R.; Chang, S.Y.; Huang, C.K.; Kang, H.Y.; Huang, K.E. Androgenic and antiandrogenic effects and expression of androgen receptor in mouse embryonic stem cells. *Fertil. Steril.* **2006**, *85*, 1195–1203. [CrossRef] [PubMed]

39. Huang, C.K.; Lee, S.O.; Lai, K.P.; Ma, W.L.; Lin, T.H.; Tsai, M.Y.; Luo, J.; Chang, C. Targeting androgen receptor in bone marrow mesenchymal stem cells leads to better transplantation therapy efficacy in liver cirrhosis. *Hepatology* **2013**, *57*, 1550–1563. [CrossRef] [PubMed]

40. Chung, W.M.; Chen, L.; Chang, W.C.; Su, S.Y.; Hung, Y.C.; Ma, W.L. Androgen/androgen receptor signaling in ovarian cancer: Molecular regulation and therapeutic potentials. *Int. J. Mol. Sci.* **2021**, *22*, 7748. [CrossRef]

41. Chung, W.M.; Chang, W.C.; Chen, L.; Lin, T.Y.; Chen, L.C.; Hung, Y.C.; Ma, W.L. Ligand-independent androgen receptors promote ovarian teratocarcinoma cell growth by stimulating self-renewal of cancer stem/progenitor cells. *Stem Cell Res.* **2014**, *13*, 24–35. [CrossRef]

42. Ling, K.; Jiang, L.; Liang, S.; Kwong, J.; Yang, L.; Li, Y.; Ping, Y.; Deng, Q.; Liang, Z. Nanog interaction with the androgen receptor signaling axis induce ovarian cancer stem cell regulation: Studies based on the CRISPR/Cas9 system. *J. Ovarian Res.* **2018**, *211*, 36. [CrossRef]

43. Masi, M.; Garattini, E.; Bolis, M.; Di Marino, D.; Maraccani, L.; Morelli, E.; Grolla, A.A.; Fagiani, F.; Corsini, E.; Travelli, C.; et al. OXER1 and RACK1-associated pathway: A promising drug target for breast cancer progression. *Oncogenesis* **2020**, *9*, 1–15. [CrossRef]

44. Goldman, A.; Basaria, S. Adverse health effects of androgen use. *Mol. Cell Endocrinol.* **2018**, *464*, 46–55. [CrossRef]

45. Estrada, M.; Varshney, A.; Ehrlich, B.E. Elevated testosterone induces apoptosis in neuronal cells. *J. Biol. Chem.* **2006**, *281*, 25492–25501. [CrossRef]

46. Zelleroth, S.; Nylander, E.; Nyberg, F.; Grönbladh, A.; Hallberg, M. Toxic impact of anabolic androgenic steroids in primary rat cortical cell cultures. *Neuroscience* **2019**, *397*, 172–183. [CrossRef]

47. Balgoma, D.; Zelleroth, S.; Grönbladh, A.; Hallberg, M.; Pettersson, C.; Hedeland, M. Anabolic androgenic steroids exert a selective remodeling of the plasma lipidome that mirrors the decrease of the de novo lipogenesis in the liver. *Metabolomics* **2020**, *16*, 1–13. [CrossRef] [PubMed]

48. Pregel, P.; Bollo, E.; Cannizzo, F.T.; Rampazzo, A.; Appino, S.; Biolatti, B. Effect of anabolics on bovine granulosa-luteal cell primary cultures. *Folia Histochem. Cytobiol.* **2007**, *45*, 265–271.

49. Groot, M.J.; Biolatti, B. Histopathological effects of boldenone in cattle. *J. Vet. Med. A Physiol. Pathol. Clin. Med.* **2004**, *51*, 58–63. [CrossRef] [PubMed]

50. Brännvall, K.; Bogdanovic, N.; Korhonen, L.; Lindholm, D. 19-Nortestosterone influences neural stem cell proliferation and neurogenesis in the rat brain. *Eur. J. Neurosci.* **2005**, *21*, 871–878. [CrossRef]

51. Cops, E.J.; Bianco-Miotto, T.; Moore, N.L.; Clarke, C.L.; Birrell, S.N.; Butler, L.M.; Tilley, W.D. Antiproliferative actions of the synthetic androgen, mibolerone, in breast cancer cells are mediated by both androgen and progesterone receptors. *J. Steroid Biochem. Mol. Biol.* **2008**, *110*, 236–243. [CrossRef]

52. Pomara, C.; Barone, R.; Marino Gammazza, A.; Sangiorgi, C.; Barone, F.; Pitruzzella, A.; Locorotondo, N.; Di Gaudio, F.; Salerno, M.; Maglietta, F.; et al. Effects of nandrolone stimulation on testosterone biosynthesis in leydig cells. *J. Cell Physiol.* **2016**, *231*, 1385–1391. [CrossRef]

53. Chimento, A.; Sirianni, R.; Zolea, F.; De Luca, A.; Lanzino, M.; Catalano, S.; Andò, S.; Pezzi, V. Nandrolone and stanozolol induce Leydig cell tumor proliferation through an estrogen-dependent mechanism involving IGF-I system. *J. Cell Physiol.* **2012**, *227*, 2079–2088. [CrossRef] [PubMed]

54. Giannitrapani, L.; Soresi, M.; La Spada, E.; Cervello, M.; D'alessandro, N.; Montalto, G. Sex hormones and risk of liver tumor. *Ann. N. Y. Acad. Sci.* **2006**, *1089*, 228–236. [CrossRef]

55. Schwingel, P.A.; Cotrim, H.P.; Salles, B.R.; Almeida, C.E.; dos Santos, C.R., Jr.; Nachef, B.; Andrade, A.R.; Zoppi, C.C. Anabolic-androgenic steroids: A possible new risk factor of toxicant-associated fatty liver disease. *Liver Int.* **2011**, *31*, 348–353. [CrossRef] [PubMed]

56. Kanda, T.; Jiang, X.; Yokosuka, O. Androgen receptor signaling in hepatocellular carcinoma and pancreatic cancers. *World J. Gastroenterol.* **2014**, *20*, 9229–9236.

57. Huang, C.K.; Luo, J.; Lee, S.O.; Chang, C. Concise review: Androgen receptor differential roles in stem/progenitor cells including prostate, embryonic, stromal, and hematopoietic lineages. *Stem Cells* **2014**, *32*, 2299–2308. [CrossRef] [PubMed]

58. Visvader, J.E.; Lindeman, G.J. Cancer stem cells in solid tumours: Accumulating evidence and unresolved questions. *Nat. Rev. Cancer* **2008**, *8*, 755–768. [CrossRef] [PubMed]

59. Visvader, J.E.; Lindeman, G.J. Cancer stem cells: Current status and evolving complexities. *Cell Stem Cell* **2012**, *10*, 717–728. [CrossRef] [PubMed]

60. Jiang, L.; Shan, J.; Shen, J.; Wang, Y.; Yan, P.; Liu, L.; Zhao, W.; Xu, Y.; Zhu, W.; Su, L.; et al. Androgen/androgen receptor axis maintains and promotes cancer cell stemness through direct activation of Nanog transcription in hepatocellular carcinoma. *Oncotarget* **2016**, *7*, 36814–36828. [CrossRef]

61. Olempska, M.; Eisenach, P.A.; Ammerpohl, O.; Ungefroren, H.; Fandrich, F.; Kalthoff, H. Detection of tumor stem cell markers in pancreatic carcinoma cell lines. *Hepatobiliary Pancreat. Dis. Int.* **2007**, *6*, 92–97.

62. Yin, S.; Li, J.; Hu, C.; Chen, X.; Yao, M.; Yan, M.; Jiang, G.; Ge, C.; Xie, H.; Wan, D.; et al. CD133 positive hepatocellular carcinoma cells possess high capacity for tumorigenicity. *Int. J. Cancer* **2007**, *120*, 1444–1450. [CrossRef]

63. Monzani, E.; Facchetti, F.; Galmozzi, E.; Corsini, E.; Benetti, A.; Cavazzin, C.; Gritti, A.; Piccinini, A.; Porro, D.; Santinami, M.; et al. Melanoma contains CD133 and ABCG2 positive cells with enhanced tumourigenic potential. *Eur. J. Cancer* **2007**, *43*, 935–946. [CrossRef]

64. Baba, T.; Convery, P.A.; Matsumura, N.; Whitaker, R.S.; Kondoh, E.; Perry, T.; Huang, Z.; Bentley, R.C.; Mori, S.; Fujii, S.; et al. Epigenetic regulation of CD133 and tumorigenicity of CD133+ ovarian cancer cells. *Oncogene.* **2009**, *28*, 209–218. [CrossRef] [PubMed]

65. Zhou, Q.; Chen, A.; Song, H.; Tao, J.; Yang, H.; Zuo, M. Prognostic value of cancer stem cell marker CD133 in ovarian cancer: A meta-analysis. *Int. J. Clin. Exp. Med.* **2015**, *8*, 3080–3088.

66. Jia, D.; Park, J.H.; Jung, K.H.; Levine, H.; Kaipparettu, B.A. Elucidating the metabolic plasticity of cancer: Mitochondrial reprogramming and hybrid metabolic states. *Cells* **2018**, *7*, 21. [CrossRef]

67. Wartalski, K.; Tabarowski, Z.; Duda, M. Magnetic isolation and characterization of porcine ovarian putative stem cells (PSCs): An in vitro study. *JFIV Reprod. Med. Genet.* **2016**, *4*, 191.
68. Gorczyca, G.; Wartalski, K.; Tabarowski, Z.; Duda, M. Effects of vinclozolin exposure on the expression and activity of SIRT1 and SIRT6 in the porcine ovary. *J. Physiol. Pharmacol.* **2019**, *70*, 153–165.
69. Livak, K.J.; Schmittgen, T.D. Analysis of relative gene expression data using real-time quantitative PCR and the 2 (-MC (T)) Method. *Methods* **2001**, *25*, 402–408. [CrossRef] [PubMed]
70. De Moura, M.B.; Van Houten, B. Bioenergetic analysis of intact mammalian cells using the Seahorse XF24 Extracellular Flux analyzer and a luciferase ATP assay. *Methods Mol. Biol.* **2014**, *1105*, 589–602.
71. Scrima, R.; Menga, M.; Pacelli, C.; Agriesti, F.; Cela, O.; Piccoli, C.; Cotoia, A.; De Gregorio, A.; Gefter, J.V.; Cinnella, G.; et al. Para-hydroxyphenylpyruvate inhibits the pro-inflammatory stimulation of macrophage preventing LPS-mediated nitro-oxidative unbalance and immunometabolic shift. *PLoS ONE* **2017**, *12*, e0188683.
72. Muller, B.; Lewis, N.; Adeniyi, T.; Leese, H.J.; Brison, D.R.; Sturmey, R.G. Application of extracellular flux analysis for determining mitochondrial function in mammalian oocytes and early embryos. *Sci. Rep.* **2019**, *9*, 1–14. [CrossRef]

Article

Brachygnathia Inferior in Cloned Dogs Is Possibly Correlated with Variants of Wnt Signaling Pathway Initiators

Yong-ho Choe [1,†], Tai-Young Hur [2,†], Sung-Lim Lee [1,3,*], Seunghoon Lee [2], Dajeong Lim [4], Bong-Hwan Choi [4], Haeyun Jeong [2], Jin-Gu No [2] and Sun A Ock [2,*]

1   Department of Theriogenology and Biotechnology, College of Veterinary Medicine,
     Gyeongsang National University, Jinju 52828, Korea; yhchoego@gmail.com
2   Animal Biotechnology Division, National Institute of Animal Science (NIAS), Rural Development
     Administration (RDA), 1500, Kongjwipatjwi-ro, Isero-myeon, Wanju 55365, Korea; tyohur@korea.kr (T.-Y.H.);
     sage@korea.kr (S.L.); ahzk111@gmail.com (H.J.); shrkftm@gmail.com (J.-G.N.)
3   Research Institute of Life Sciences, Gyeongsang National University, Jinju 52828, Korea
4   Division of Animal Genomics & Bioinformatics, NIAS, RDA, Kongjwipatjwi-ro, Isero-myeon,
     Wanju 55365, Korea; lim.dj@korea.kr (D.L.); bhchoi@korea.kr (B.-H.C.)
*   Correspondence: sllee@gnu.ac.kr (S.-L.L.); ocksa@korea.kr (S.A.O.)
†   These authors contributed equally to this work.

Abstract: Abnormalities in animals cloned via somatic cell nuclear transfer (SCNT) have been reported. In this study, to produce bomb-sniffing dogs, we successfully cloned four healthy dogs through SCNT using the same donor genome from the skin of a male German shepherd old dog. Veterinary diagnosis (X-ray/3D-CT imaging) revealed that two cloned dogs showed normal phenotypes, whereas the others showed abnormal shortening of the mandible (brachygnathia inferior) at 1 month after birth, even though they were cloned under the same conditions except for the oocyte source. Therefore, we aimed to determine the genetic cause of brachygnathia inferior in these cloned dogs. To determine the genetic defects related to brachygnathia inferior, we performed karyotyping and whole-genome sequencing (WGS) for identifying small genetic alterations in the genome, such as single-nucleotide variations or frameshifts. There were no chromosomal numerical abnormalities in all cloned dogs. However, WGS analysis revealed variants of Wnt signaling pathway initiators (WNT5B, DVL2, DACT1, ARRB2, FZD 4/8) and cadherin (CDH11, CDH1like) in cloned dogs with brachygnathia inferior. In conclusion, this study proposes that brachygnathia inferior in cloned dogs may be associated with variants in initiators and/or regulators of the Wnt/cadherin signaling pathway.

Keywords: cloned dog; brachygnathia inferior; whole-genome sequencing; Wnt signaling pathway

1. Introduction

Animal cloning is a useful technology in developmental biology and genetic studies and in the restoration of endangered species [1–3]. Since the first successful dog cloning was reported [1], cloning has been applied not only in the commercial breeding of companion dogs but also in the production of working dogs with various desirable abilities [4].

Dog cloning differs from cloning in other animals, such as sheep, cattle, and pigs, owing to the different reproductive processes, such as ovulation of oocytes at the metaphase I stage. Therefore, dog cloning is performed with in vivo-matured oocytes, after which cloned embryos are quickly transferred into the oviduct to overcome the inadequate in vitro culture systems [5,6]. The cloned offspring are expected to not only genetically but also phenotypically identical to the original donor dog [7]. However, abnormal phenotypes not present in the original dog may appear in the clones, and this is presumed to occur during developmental events. This phenomenon has been commonly reported and studied in detail in other animals [2,8,9], but minimally reported in cloned dogs.

Defects in cloned animals mainly include high or low birth weight, placental abnormalities, and pulmonary and cardiovascular disorders [3]. Brachygnathia inferior (also called underbite, overshot, parrot mouth, or prognathia), an osteogenesis imperfecta presenting as shortening of the mandible, is a common congenital anomaly in sheep and cattle [10,11]. However, brachygnathia inferior is very rarely found in dogs [12], and there have been no reports of brachygnathia inferior in cloned dogs.

In the present study, we identified that out of four dogs cloned under the same conditions, except for the oocytes, two exhibited abnormalities including brachygnathia inferior. To the best of our knowledge, this is the first attempt to detect and determine the causes of brachygnathia inferior in cloned dogs. Therefore, we aimed to determine the genetic cause of brachygnathia inferior in these cloned dogs. Genome sequencing is a powerful tool for discovering genes and genetic variants that cause a disease [13]. Whole-genome sequencing (WGS) can provide information on the entire DNA sequence of the genome of an individual and serve as a tool for determining the genomic variation that increases the risk for common and rare disorders. Using WGS and functional prediction tools, we identified the specific genes that were upregulated only in these abnormal cloned dogs and the signaling pathways associated with the phenotypic features of brachygnathia inferior. We revealed mutations in the initiators and/or modulators of two important signaling pathways related to brachygnathia inferior in the cloned dogs.

2. Results

2.1. Production of Cloned Dogs

A total of 89 nuclear transfer (NT) embryos were transferred to 10 surrogate mother dogs. The pregnancy rate was confirmed to be 20% (2 out of 10 dogs). Surrogate mother dogs (SMD), called SMD1 and SMD2, gave birth to one offspring (NT-1) by cesarean section (≈60 days of gestation) and five offspring (NT-2 to -6) by natural delivery, respectively (Figure S1A,B). Among the five offspring delivered by SMD2, three (NT-2, 3, and 4) survived, but two died: one was stillborn (NT-5), and the other died of hypothermia (NT-6) at one day after delivery (Figure 1). The cloning efficacy ratio, calculated from the number of live offspring per number of transferred embryos, was 5.6%.
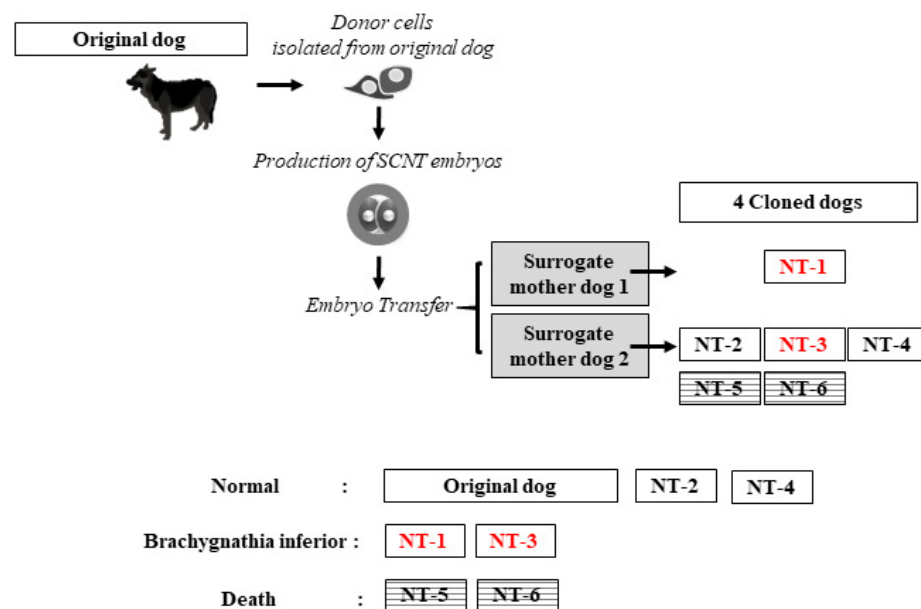

Figure 1. Schematic description of the dog cloning process via somatic cell nuclear transfer (SCNT), showing the descendant pedigree and phenotype of offspring. Donor cells were collected from a 5-year-old male German shepherd dog (original donor). NT refers to the cloned offspring produced via SCNT. Red colors (NT-1 and NT-2) were represented cloned dogs with brachygnathia inferior.

To evaluate the genetic identity of the offspring, we compared canine-specific polymorphic microsatellites between the cloned puppies and donor cells. As shown in Table 1, the cloned puppies and donor cells showed genetic homogeneity, confirming that the puppies were cloned from the original dog.

Table 1. Matching of microsatellite of between donor cells and cloned offspring.

Source	FH2537		FH3005		FH3372		FH3116		REN51C16		REN2770O5		FH2834		REN204K13		FH2097		FH2712		FH2998	
Donor cells	146	146	224	224	154	158	190	190	255	259	333	333	265	265	248	248	284	288	174	174	208	228
NT-1	146	146	224	224	154	158	190	190	255	259	333	333	265	265	248	248	284	288	174	174	208	228
NT-2	146	146	224	224	154	158	190	190	255	259	333	333	265	265	248	248	284	288	174	174	208	228
NT-3	146	146	224	224	154	158	190	190	255	259	333	333	265	265	248	248	284	288	174	174	208	228
NT-4	146	146	224	224	154	158	190	190	255	259	333	333	265	265	248	248	284	288	174	174	208	228

Donor cells used for nuclear transfer (NT); cloned offsprings (NT-1 to NT-4) were produced by NT.

2.2. Care and Feeding of Cloned Offspring

NT-1, the first cloned puppy, was fed by bottle because the surrogate mother did not care for her baby. During the artificial nursing period, slight pneumonia occurred, but was completely cured within one week. NT-2, -3, and -4, who were born by the same SMD2, were successfully breastfed by their SMD2. At the age of one month old, every puppy was stopped from milk feeding and fed commercial feed. The weight of all cloned puppies measured daily was in normal range, but the weight growth rates of NT-1 and -3 were lower than those of NT-2 and -4 until one month after birth (Figure S1C). Both NT-1 and -3 showed jaw abnormalities, such as open-bite malocclusion of the mandible, starting at one month after birth, especially NT-1 (Figure 2A). Further detailed analyses were performed to determine the cause.

2.3. Clinical Diagnosis of Brachygnathia Inferior

First, NT-1, which presented severe jaw abnormality, was subjected to veterinary pathological analysis. Complete blood count (CBC) and biochemical parameters were within the reference ranges, without significant differences. CBC values were similar between the donor dog and the cloned offspring (Table 2). There were no differences in biochemical parameters, such as creatinine, glucose, blood urea nitrogen (BUN), gamma-glutamyl transferase (GGT), albumin (ALB), total bilirubin (TB), total protein (TP), alanine aminotransferase (ALT), aspartate aminotransferase (AST), creatine kinase, cholesterol, and amylase levels, between the original dog and the clones (Table 3).
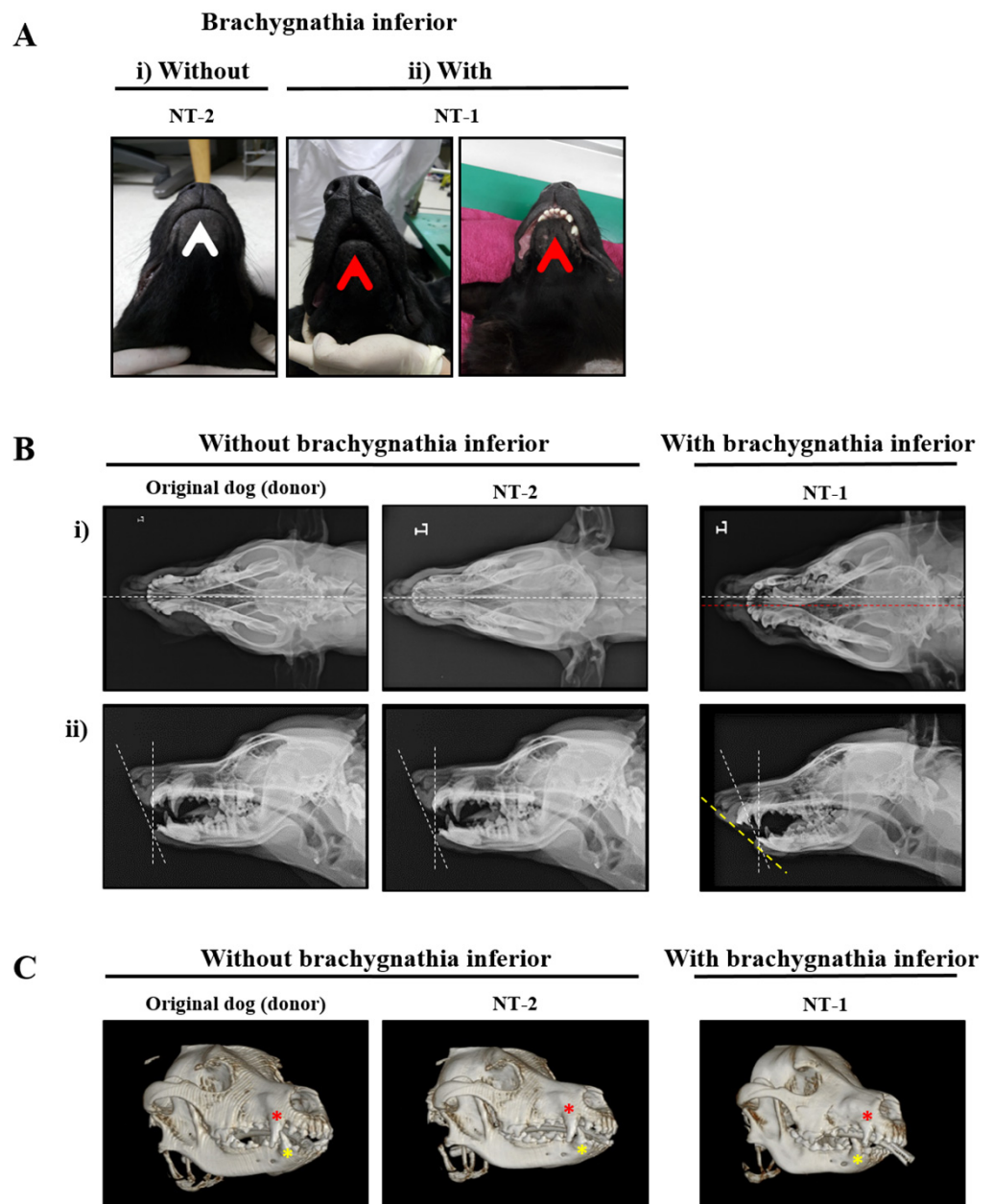
Figure 2. Clinical diagnosis of cloned dogs. (**A**) Visual inspection of mandibular malocclusion in the cloned dogs. (**i**) A cloned dog without brachygnathia inferior (NT-2); (**ii**) a cloned dog with brachygnathia inferior (NT-1). Arrows indicate the lower jaw with (red) and without (white) brachygnathia inferior. (**B**) Craniofacial radiographic images of the cloned dogs. Left column, the original dog as a control; central column, a cloned dog without brachygnathia inferior (NT-2); right column, a cloned dog with brachygnathia inferior (NT-1). (**i**,**ii**) are shown in the dorsoventral and lateral view of their craniofacial profile, respectively. White dotted lines in (**i**) indicate the central axis of the skull in the dorsoventral view of the craniofacial profile. The cross of white and yellow dotted lines in (**ii**) indicate the craniofacial angle between the maxilla and mandible. (**C**) Three-dimensional volume-rendered computed tomography images. Left, the original dog as a control; center, a cloned dog without brachygnathia inferior (NT-2); right, a cloned dog with brachygnathia inferior (NT-1). Red and yellow asterisks indicate the maxillary and mandible canines, respectively.

Table 2. The values of complete blood counts for original donor and cloned dogs.

Parameters (Unit)	Original Dog (Donor Cells)	Brachygnathia Inferior		
		without		with
		NT2	NT4	NT-1
RBC (10^{12}/L)	8.85	5.9	6.74	7.43
Hematocrit [Hct] (%)	56.7	37.7	41.2	48.1
Hemoglobin [Hb] (g/dL)	19.6	12.1	14.3	15.8
MCV (fL)	64.1	63.9	61.1	64.7
MCH (pg)	22.1	20.5	21.2	21.3
MCHC (g/dL)	34.6	32.1	34.7	32.8
PDW (%)	20.2	18.7	19.5	18.9
Reticulocyte (%)	0.2	1.8	0.5	1.1
Reticulocyte (10^3/uL)	18.6	108	30.3	81.7
WBC (10^9/L)	13.8	15.7	19.2	13.86
WBC-Neut (%)	70.6	56.9	64.6	60
WBC-Lymph (%)	15.3	29.5	24.9	25.2
WBC-Mono (%)	7.8	8.3	8.7	7
WBC-Eos (%)	6.2	5.2	1.7	7.8
WBC-Baso (%)	0.1	0.1	0.1	0
WBC-Neut (10^9/L)	9.75	8.94	12.4	8.32
WBC-Lymph (10^9/L)	2.11	4.63	4.76	3.49
WBC-Mono (10^9/L)	1.08	1.31	1.66	0.97
WBC-Eos (10^9/L)	0.85	0.81	0.33	1.08
WBC-Baso (10^9/L)	0.01	0.01	0.02	0
Platelet (10^9/L)	201	411	325	429
MPV (fL)		12.3	13.1	13.1
RDW (fL)		19.36	18.8	18.8
PCT (%)		0.5	0.56	0.56

RBC, red blood cell; MCV, mean corpuscular volume; MCH, mean corpuscular hemoglobin; MCHC, mean corpuscular hemoglobin concentration; PDW, platelet distribution width; WBC, white blood cell; MPV, mean platelet volume; RDW, red cell distribution width; PCT, plateletcrit.

Table 3. The values of blood chemistry parameters of original donor and cloned dogs.

Parameters (Unit)	Original Dog (Donor Cells)	Brachygnathia Inferior			
		without		with	
		NT2	NT4	NT-1	NT-3
Glucose (mg/dL)	68	31	104	62	90
BUN (mg/dL)	13	13	19	13	4
Creatinine (mg/dL)	1.2	1	0.7	1.1	0.3
BUN: Creatinine (Ratio)	11	13	25	11	12
Phosphorus-Inorganic (mg/dL)	3	8	8.7	5.7	8.3
Calcium (mg/dL)	10.8	11	9.9	10.9	11
Protein-Total (g/dL)	7.8	5.7	5	7.1	6.1
Albumin (g/dL)	4	2.9	2.7	3.4	2.9
Globulin (g/dL)	3.8	2.8	2.3	3.7	3.2
A/G ratio	1.1	1.1	1.2	0.9	0.9
ALT (U/L)	47	22	18	23	67
ALKP (U/L)	17	173	151	106	216
GGT (U/L)	0	0	2	0	8
Bilirubin-Total (mg/dL)	0.2	0.1	0.1	0.1	0.7
Cholesterol-Total (mg/dL)	191	119	171	170	237
Amylase (U/L)	727	539	299	863	323
Lipase (U/L)	341	331	352	322	93
Na+ (mmol/L)	153	150	147	151	140.9
K+ (mmol/L)	4.2	5	5.7	4.3	5.05

Table 3. *Cont.*

Parameters (Unit)	Original Dog (Donor Cells)	Brachygnathia Inferior			
		without		with	
		NT2	NT4	NT-1	NT-3
Na+:K+ (Ratio)	36	30	26	36	23.5
Cl$^-$ (mmol/L)	110	107	107	107	111.3
Osmorality	301	294	296	297	

BUN, blood urea nitrogen; A/G ratio, the ratio of albumin and globulin; ALT, alanine aminotransferase; ALKP, alkaline phosphatase; AST, aspartate aminotransferase; GGT, gamma-glutamyltransferase.

The cloned dogs were diagnosed by visual inspection and X-ray/computed tomography (CT) examinations. Mandibular malocclusion was observed in both NT-1 and -3, whereas NT-1 presented severe mandibular malocclusion. In the case of NT-1, malalignment of the central axis of the skull was confirmed in the dorsoventral view of the craniofacial radiograph (Figure 2B(i)). Additionally, the craniofacial angle between the maxilla and the mandible in the lateral view of the craniofacial region was measured by radiography (Figure 2B(ii)). NT-1 showed an increased craniofacial angle compared to the donor dog and NT-2. NT-1 showed normal teeth arrangement in terms of the number and order, but its tooth morphology was irregular and denser compared with that of the donor dog and NT-2. In NT-1, it was confirmed through three-dimensional CT images that the maxillary canines protruded to a greater extent than the mandibular canines (Figure 2C), unlike those in the donor dogs and NT-2. When the above findings were considered, NT-1 was diagnosed with typical brachygnathia inferior.

2.4. Chromosomal Aberrations in the Donor and Cloned Dogs

Karyotyping was performed to analyze chromosomal abnormalities in peripheral blood samples from all cloned dogs and the donor dog. All samples were read as normal diploids with 78 + XY (Figure 3). It was found that cloning did not induce chromosomal aberrations, observed as numerical and structural abnormalities, and thus brachygnathia inferior did not occur as a result of large-scale chromosomal aberrations.

Therefore, further studies were performed to identify the cause of brachygnathia inferior in the cloned dogs on the basis of single nucleotide variations (SNVs) or short insertions/deletions (indels).
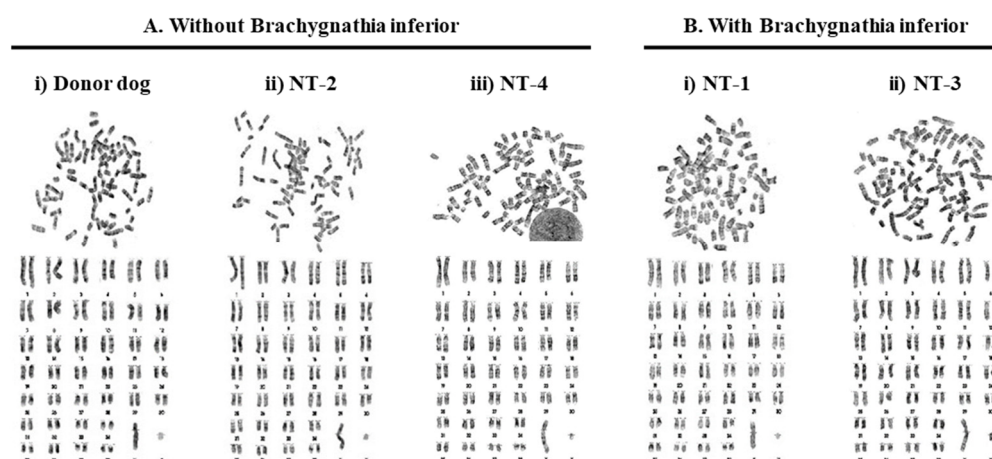
Figure 3. Karyotyping in cloned dogs. Karyotyping was performed using peripheral blood samples from the dogs. The normal diploid chromosome number for dogs is 78, with the autosomes acrocentric, whereas the X and Y chromosomes are the large and small submetacentric chromosomes, respectively. (**A**,**B**) Dogs with and without brachygnathia inferior, respectively. Aa and Ab represent the original dog (as control, donor) and the cloned dog, respectively. All dogs were male and had a normal number of chromosomes.

2.5. Identification and Validation of Candidate Genes for Brachygnathia Inferior by Whole-Genome Sequencing

WGS was performed for the donor dogs and cloned offspring, and high-quality sequence data were obtained. Data on variants were subjected to quality control, and the results are presented in Tables S1–S3. The circos plot of WGS confirmed the presence of genomic variations, including SNVs and indels, between the groups (Figure 4). Coexisting variants present in all animal subjects including the donor dog were filtered. Through Venn diagram analysis, we identified 10,112 variants in 3164 genes, including unique SNVs and indels, exclusively in the group with brachygnathia inferior (Figure 4B). These variants were located in the protein-coding and intergenic regions of the 3164 genes.

Next, we examined whether these 3164 genes have phenotype-related functions. To determine the biological characteristics of these candidate genes for brachygnathia inferior, we performed Gene Ontology (GO) analysis on biological processes using the DAVID database. Among the 3164 genes, 1471 genes were significantly enriched ($p < 0.001$), as shown in Figure 5A. The biological functions of these genes are mostly related to cellular and systemic developmental processes. Interestingly, out of the 1471 genes, 221 were involved in anatomical structure morphogenesis ($p = 0.000007$).

Furthermore, functional prediction was conducted for the 3164 candidate genes using the Protein Analysis Through Evolutionary Relationships (PANTHER) annotation system. Out of the 3164 candidate genes, 1913 were mapped on 110 pathways, and the top 10 pathways are presented in Figure 5B. The top four enriched pathways were identified as the Wnt (47%), cadherin (31%), integrin signaling (30%), and gonadotropin-releasing hormone receptor (27%) pathways.

A Venn diagram showing the overlapping of genes related to the four pathways revealed that the Wnt (Figure 5C(ii)) and cadherin (Figure 5C(iii)) signaling pathways had many shared genes, compared to the integrin (Figure 5C(i)) and gonadotropin (Figure 5C(iv)) signaling pathways. Thus, 50 candidate genes for brachygnathia inferior were extracted from the 1913 genes related to the Wnt/cadherin signaling pathway (Figure 5D, detailed in Table 4). Of these 50 genes, 30 were shared between the Wnt and cadherin signaling pathway.

Detailed information on mutations in 50 candidate genes for brachygnathia inferior is summarized as shown in Table 4. Especially, two uncharacterized proteins and six genes (CDH8, CDH12, PCDH9, CTNND2, PCDH9, and ENSCAFG00000023180) with more than 10 variations were identified. Thus, it is presumed that these specific variants in NT-1 and -3 cause alterations in genes related to the Wnt/cadherin signaling pathway, although the exact mechanism is unknown.

(**A**)
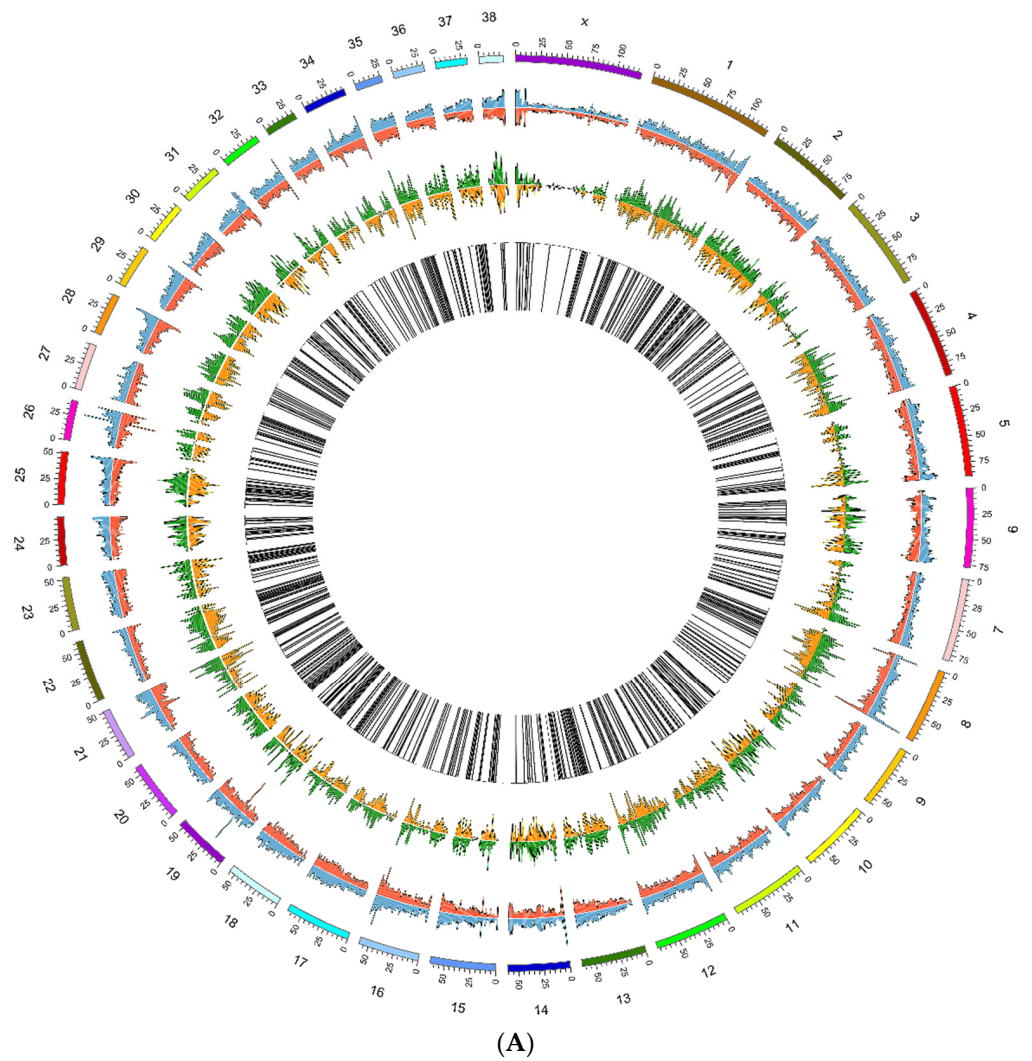
Brachygnathia inferior
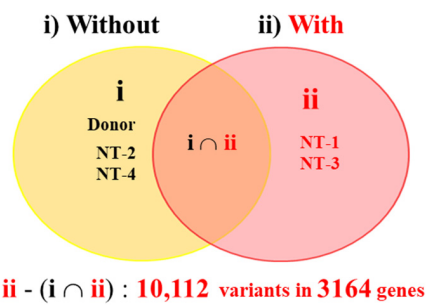
(**B**)

Figure 4. Comparative analysis of whole-genome sequences between the original dog (donor) and cloned dogs. (**A**) Circos plot comparing variants in genome sequence between the cloned dogs with (NT-1 and -3) and without brachygnathia inferior (original dog, NT-2 and -4). From the outside, each layer indicates reference chromosomes, the number of single-nucleotide variants (SNVs) (blue: normal, red: affected), and the number of insertions and deletions (indels) (green, normal; orange, affected). The black bar represents the differences between the normal and affected samples. (**B**) Venn diagram of specific variants between the dogs with (**ii**) and without (**i**) brachygnathia inferior.

Figure 5. Gene ontology (GO) term enrichment analysis and Protein Analysis Through Evolutionary Relationships (PANTHER, v.14.0, 1 January 2019, http://pantherdb.org). The 3164 genes with specific variants found in cloned dogs with brachygnathia inferior were included in these analyses. (**A**) Classification of 1471 genes according to the GO biological process using Database for Annotation, Visualization, and Integrated Discovery (DAVID, v.6.8, 1 January 2019, http://david.abcc.ncifcrf.gov). (**i,ii**) The categories and bar plots of the GO biological processes, respectively. The red lines in "a" represent GO categories that participate in the development process. The *p*-values of each process were converted to −log10 P to calculate the enrichment score. (**B**) Mapping of 1913 genes via PANTHER.

Relative gradient violet color represents the percentage of the enriched gene number relative to the total number of each pathway component gene. The bar plot displays the number of enriched genes. Venn diagrams in (**C,D**) represent the number of overlapping genes of the top-four most enriched pathways (**i–iv**) and the common and different gene list between the top-two gene pathways (**ii,iii**), respectively. (**i–iv**) Integrin (**i**), Wnt (**ii**) and cadherin (**iii**) signaling pathways, and the GnRH receptor pathway (**iv**).

2.6. Interactive Network Analysis of Candidate Genes for Brachygnathia Inferior

To elucidate how these candidate genes for brachygnathia inferior interact with each other, we predicted a protein–protein interaction network using the STRING database. We found 132 interaction edges with an enrichment *p*-value $< 10^{-15}$, as shown in Figure 6. A total of 50 candidate genes for brachygnathia inferior were confirmed to be related to the Wnt (yellow highlight)/cadherin (red highlight) signaling pathway. The network showed that the genes were closely interacting with each other, with WNT5B, ARRB2, CTNNA3, and CTNND2 at the center.

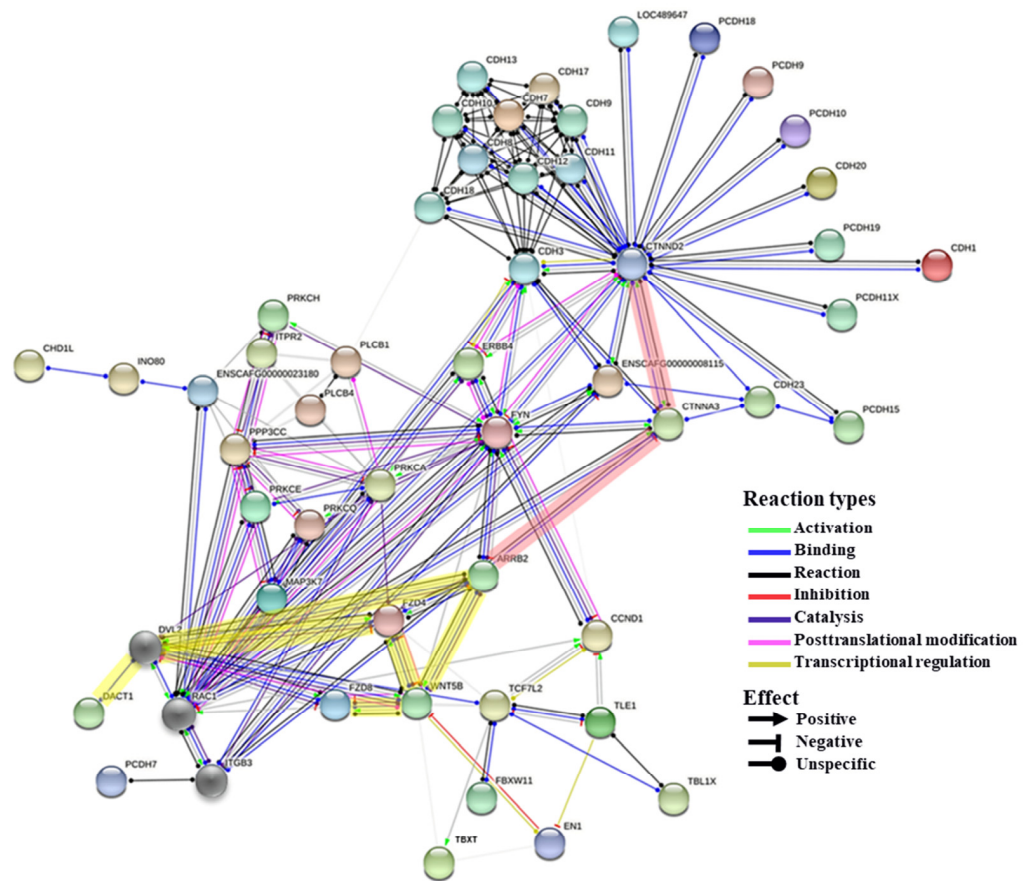**Figure 6.** Interactive network of candidate genes for brachygnathia inferior. Each edge indicates interaction between two genes. The interaction types and their effects are described in the figure. This analysis was performed using the Search Tool for the Retrieval of Interacting Genes/Proteins (STRING) database. Yellow and red letters indicate genes involved in the Wnt and cadherin pathways, respectively.

Table 4. Variants found in WNT/cadherin signaling pathway in cloned dogs with brachygnathia inferior.

#	Gene Symbol (Gene Name)	CHR	POS	REF	ALTS	Putative Impact	Genotype				
							Without Brachygnathia Inferior			With Brachygnathia Inferior	
							Original Dog	NT-2	NT-4	NT-1	NT-3
1	ARRB2 (arrestin beta 2)	5	31834580	T	G	+ MOD	0/0	0/0	0/0	0/1	0/1
2	CCND1 (G1/S-specific cyclin-D1)	18	48505585	G	T	MOD	0/0	0/0	0/0	0/1	0/1
			48511836	T	TG	MOD	0/1	0/1	0/1	1/1	1/1
3	CDH3 (cadherin 3)	5	80888237	C	G	MOD	0/0	0/0	0/0	0/1	0/1
			80917292	A	T	MOD	0/0	0/0	0/0	0/1	0/1
4	CDH7 (cadherin 7)	1	11751189	C	T	MOD	0/0	0/0	0/0	0/1	0/1
			11765372	CATATATATATATATATAT	C	MOD	0/1	0/1	0/1	1/1	1/1
5	CDH8 (cadherin 8)	5	86401758	A	T	MOD	0/0	0/0	0/0	0/1	0/1
			86708399	C	A	MOD	0/0	0/0	0/0	0/1	0/1
			86742629	C	T	MOD	0/0	0/0	0/0	0/1	0/1
			86745597	T	TATACAC	MOD	0/1	0/1	0/1	1/1	1/1
			87225311	T	A	MOD	0/0	0/0	0/0	0/1	0/1
			87225313	T	A	MOD	0/0	0/0	0/0	0/1	0/1
			85863919	A	T	MOD	0/0	0/0	0/0	0/1	0/1
			86114270	C	CT	MOD	0/1	0/1	0/1	1/1	1/1
			86222689	T	G	MOD	0/0	0/1	0/0	1/1	1/1
			86296806	C	G	MOD	0/1	0/1	0/1	1/1	1/1
			86390011	TACCCC	T	MOD	0/1	0/1	0/1	1/1	1/1

Variant Information

Table 4. *Cont.*

#	Gene Symbol (Gene Name)	CHR	Variant Information				Genotype				
			POS	REF	ALTS	Putative Impact	Without Brachygnathia Inferior			With Brachygnathia Inferior	
							Original Dog	NT-2	NT-4	NT-1	NT-3
6	CDH9 (cadherin 9)	4	78675775	A	T	MOD	0/0	0/0	0/0	0/1	0/1
			78830300	A	T	MOD	0/0	0/0	0/0	0/1	0/1
			78840862	T	C	MOD	0/0	0/0	0/0	0/1	0/1
			79012127	G	A	MOD	0/0	0/0	0/0	0/1	0/1
			81023137	T	G	MOD	0/0	0/0	0/0	0/1	0/1
			81051478	A	T	MOD	0/0	0/0	0/0	0/1	0/1
7	CDH10 (cadherin 10)	4	80613492	GTC	G	MOD	0/0	0/0	0/0	0/1	0/1
			80892138	GT	G	MOD	0/1	0/1	0/1	1/1	1/1
			80904036	A	T	MOD	0/0	0/0	0/0	0/1	0/1
8	CDH11 (cadherin 11)	5	84404903	AAGAG	AAGAGAG,A	MOD	0/0	0/0	0/0	0/2	0/2
			84473862	C	T	MOD	0/0	0/0	0/0	0/1	0/1
9	CDH12 (cadherin 12)	4	82754279	T	TATATATAG	MOD	0/1	0/1	0/1	1/1	1/1
			82856048	C	A	MOD	0/0	0/0	0/0	0/1	0/1
			82947779	G	A	MOD	0/0	0/0	0/0	0/1	0/1
			83011986	C	CGT	MOD	0/1	0/1	0/1	1/1	1/1
			83066202	G	T	MOD	0/0	0/0	0/0	0/1	0/1
			83101151	C	T	MOD	0/0	0/0	0/0	0/1	0/1
			81762398	T	A	MOD	0/0	0/0	0/0	0/1	0/1
			81811393	TTGAAA	T	MOD	0/1	0/1	0/1	1/1	1/1

Table 4. *Cont.*

#	CHR	Gene Symbol (Gene Name)	Variant Information				Genotype				
							Without Brachygnathia Inferior			With Brachygnathia Inferior	
			POS	REF	ALTS	Putative Impact	Original Dog	NT-2	NT-4	NT-1	NT-3
9	4	CDH12 (cadherin 12)	81895595	G	C	MOD	0/1	0/1	0/1	1/1	1/1
			81895601	C	A	MOD	0/1	0/1	0/1	1/1	1/1
			81934549	T	A	MOD	0/0	0/0	0/0	0/1	0/1
			81942964	A	C	MOD	0/0	0/0	0/0	0/1	0/1
			82120066	A	G	MOD	0/0	0/0	0/0	0/1	0/1
			82213787	AT	A	MOD	0/0	0/0	0/0	0/1	0/1
			82245479	C	CT	MOD	0/0	0/0	0/0	0/1	0/1
			82346773	T	G	MOD	0/1	0/1	0/1	1/1	1/1
			82391279	GT	G	MOD	0/0	0/0	0/0	0/1	0/1
			82427446	T	G	MOD	0/0	0/0	0/0	0/1	0/1
			82427448	T	G	MOD	0/0	0/0	0/0	0/1	0/1
			82567248	G	A	MOD	0/0	0/0	0/0	0/1	0/1
			82591151	C	T	MOD	0/0	0/0	0/0	0/1	0/1
			82672898	T	G	MOD	0/0	0/0	0/0	0/1	0/1
10	5	CDH13 (cadherin 13)	68789330	G	A	MOD	0/0	0/0	0/0	0/1	0/1
			69134746	GT	G	MOD	0/1	0/1	0/1	1/1	1/1
11	29	CDH17 (cadherin 17)	38980475	A	C	MOD	0/0	0/0	0/0	0/1	0/1
			38980931	C	T	MOD	0/0	0/0	0/0	0/1	0/1

Table 4. *Cont.*

| # | Gene Symbol (Gene Name) | CHR | Variant Information | | | | Genotype | | | | |
| | | | | | | | Without Brachygnathia Inferior | | | With Brachygnathia Inferior | |
			POS	REF	ALTS	Putative Impact	Original Dog	NT-2	NT-4	NT-1	NT-3
12	CDH18 (cadherin 18)	4	84572993	G	T	MOD	0/0	0/0	0/0	0/1	0/1
			84609771	A	C	MOD	0/0	0/0	0/0	0/1	0/1
			84777718	CT	C	MOD	0/1	0/1	0/1	1/1	1/1
			84815886	CT	C	MOD	0/0	0/0	0/0	0/1	0/1
			84845137	AT	A	MOD	0/1	0/1	0/1	1/1	1/1
			84917669	TTA	T,TTATA	MOD	0/2	0/2	0/2	2/2	2/2
			85340830	G	A	MOD	0/0	0/0	0/0	0/1	0/1
13	CDH19 (cadherin 19)	1	11213176	A	T	MOD	0/0	0/0	0/0	0/1	0/1
			11219146	T	C	MOD	0/0	0/0	0/0	0/1	0/1
			11302080	T	TA	MOD	0/1	0/1	0/1	1/1	1/1
14	CDH20 (cadherin 20)	1	15018520	CTTTTTTTTTTTTTT	C	MOD	0/0	0/0	0/0	0/1	0/1
			15026159	C	G	MOD	0/0	0/0	0/0	0/1	0/1
			15385740	C	T	MOD	0/0	0/0	0/0	0/1	0/1
			15397278	C	T	MOD	0/0	0/0	0/0	0/1	0/1
15	CDH23 (cadherin 23)	4	22217920	A	C	MOD	0/0	0/0	0/0	0/1	0/1
			22268845	G	A	MOD	0/0	0/0	0/0	0/1	0/1
			22296573	A	T	MOD	0/0	0/0	0/0	0/1	0/1
			22308343	G	C	MOD	0/0	0/0	0/0	0/1	0/1
			22521773	T	G	MOD	0/0	0/0	0/0	0/1	0/1

Table 4. *Cont.*

| | | | Variant Information | | | | Genotype | | | | |
| | | | | | | | Without Brachygnathia Inferior | | | With Brachygnathia Inferior | |
#	Gene Symbol (Gene Name)	CHR	POS	REF	ALTS	Putative Impact	Original Dog	NT-2	NT-4	NT-1	NT-3
16	CHD1L (chromodomain helicase DNA-binding protein 1-like)	17	57755822	A	C	MOD	0/0	0/0	0/0	0/1	0/1
			57801618	C	T	MOD	0/0	0/0	0/0	0/1	0/1
17	CTNND2 (catenin delta 2)	34	2587961	C	G	MOD	0/0	0/0	0/0	0/1	0/1
			2605251	C	CAG	MOD	0/1	0/1	0/1	1/1	1/1
			2683554	C	CT	MOD	0/1	0/1	0/1	1/1	1/1
			2729501	C	G	MOD	0/0	0/0	0/0	0/1	0/1
			2790163	CAG	C	MOD	0/0	0/0	0/0	0/1	0/1
			2887443	G	T	MOD	0/0	0/0	0/0	0/1	0/1
			2926914	GA	G	MOD	0/0	0/0	0/0	0/1	0/1
			3386604	T	TTTC	MOD	0/1	0/1	0/1	1/1	1/1
			1984298	C	A	MOD	0/0	0/0	0/0	0/1	0/1
			2045599	A	AG	MOD	0/1	0/1	0/1	1/1	1/1
			2211983	T	TACACAC	MOD	0/1	0/1	0/1	1/1	1/1
			2325817	T	A	MOD	0/0	0/0	0/0	0/1	0/1
			2340793	C	G	MOD	0/0	0/0	0/0	0/1	0/1
			2420433	T	A	MOD	0/1	0/1	0/1	1/1	1/1
			2420448	G	A	MOD	0/1	0/1	0/1	1/1	1/1

Table 4. *Cont.*

#	Gene Symbol (Gene Name)	CHR	Variant Information				Genotype				
			POS	REF	ALTS	Putative Impact	Without Brachygnathia Inferior			With Brachygnathia Inferior	
							Original Dog	NT-2	NT-4	NT-1	NT-3
18	DACT1 (Dishevelled binding antagonist of beta catenin 1)	8	33957483	G	A	HIGH	0/0	0/0	0/0	0/1	0/1
			33957480	C	T	LOW	0/0	0/0	0/0	0/1	0/1
19	EN1 (engrailed homeobox 1)	19	31181296	T	C	MOD	0/0	0/0	0/0	0/1	0/1
			31191156	TA	T	MOD	0/1	0/1	0/1	1/1	1/1
			19286254	T	G	MOD	0/0	0/0	0/0	0/1	0/1
20	ERBB4 (Erb-b2 receptor tyrosine kinase 4)	37	19629719	C	CT	MOD	0/1	0/1	0/1	1/1	1/1
			19767395	TTTC	T	MOD	0/1	0/1	0/1	1/1	1/1
			20133592	T	A	MOD	0/0	0/0	0/0	0/1	0/1
21	FBXW11 (F-box and WD repeat domain-containing 11)	4	40367311	CT	C	MOD	0/1	0/1	0/1	1/1	1/1
			40278734	T	TA	MOD	0/1	0/1	0/1	1/1	1/1
			40314614	C	T	MOD	0/0	0/0	0/0	0/1	0/1
22	FYN (tyrosine-protein kinase)	12	68231298	A	C	MOD	0/0	0/0	0/0	0/1	0/1
			68274356	T	TTA	MOD	0/1	0/1	0/1	1/1	1/1
23	FZD4 (frizzled class receptor 4)	21	12700289	G	T	MOD	0/0	0/0	0/0	0/1	0/1
24	FZD8 (frizzled class receptor 8)	2	1329228	T	G	MOD	0/0	0/0	0/0	0/1	0/1
			1333216	TA	T	MOD	0/0	0/0	0/0	0/1	0/1

Table 4. *Cont.*

#	Gene Symbol (Gene Name)	CHR	Variant Information				Genotype				
							Without Brachygnathia Inferior			With Brachygnathia Inferior	
			POS	REF	ALTS	Putative Impact	Original Dog	NT-2	NT-4	NT-1	NT-3
25	INO80 (INO80 complex ATPase subunit)	30	8165408	A	T	MOD	0/0	0/0	0/0	0/1	0/1
			8165412	A	T	MOD	0/0	0/0	0/0	0/1	0/1
			8165416	A	T	MOD	0/0	0/0	0/0	0/1	0/1
			8206520	TA	T	MOD	0/0	0/0	0/0	0/1	0/1
26	ITPR2 (inositol 1,4,5-trisphosphate receptor type 2)	27	20831508	A	AG	MOD	0/1	0/1	0/1	1/1	1/1
			20872227	A	C	MOD	0/0	0/0	0/0	0/1	0/1
27	MAP3K7 (mitogen-activated protein kinase kinase 7)	12	49749924	A	AT	MOD	0/0	0/0	0/0	0/1	0/1
			49769002	C	CT	MOD	0/1	0/1	0/1	1/1	1/1
			8973713	T	C	MOD	0/0	0/0	0/0	0/1	0/1
28	PCDH10 (protocadherin 10)	19	9008967	G	T	MOD	0/0	0/0	0/0	0/1	0/1
			9157583	C	T	MOD	0/0	0/0	0/0	0/1	0/1
29	PCDH11X (protocadherin-11 X-linked)	X	68666259	G	C	MOD	0/0	0/0	0/0	0/1	0/1
			68746381	G	A	MOD	0/0	0/0	0/0	0/1	0/1

Table 4. *Cont.*

| | | | Variant Information | | | | Genotype | | | | |
| | | | | | | | Without Brachygnathia Inferior | | | With Brachygnathia Inferior | |
#	Gene Symbol (Gene Name)	CHR	POS	REF	ALTS	Putative Impact	Original Dog	NT-2	NT-4	NT-1	NT-3
30	PCDH15 (protocadherin-related 15)	26	34702015	T	C	MOD	0/0	0/0	0/0	0/1	0/1
			35097300	T	G	MOD	0/0	0/0	0/0	0/1	0/1
			33646637	G	A	MOD	0/0	0/0	0/0	0/1	0/1
			33672867	T	G	MOD	0/0	0/0	0/0	0/1	0/1
			33672897	G	A	MOD	0/0	0/0	0/0	0/1	0/1
31	PCDH18 (protocadherin 18)	19	5101338	G	A	MOD	0/0	0/0	0/0	0/1	0/1
			5101376	G	A	MOD	0/0	0/0	0/0	0/1	0/1
			74412666	T	G	MOD	0/0	0/0	0/0	0/1	0/1
			74418677	G	A	MOD	0/0	0/0	0/0	0/1	0/1
32	PCDH19 (protocadherin 19)	X	74250517	C	T	MOD	0/0	0/0	0/0	0/1	0/1
			74256962	G	A	MOD	0/1	0/1	0/1	1/1	1/1
			74260225	G	A	MOD	0/0	0/0	0/0	0/1	0/1
33	PCDH7 (protocadherin 7)	3	80140770	TAAA	T	MOD	0/1	0/1	0/1	1/1	1/1
			80356304	G	GA	MOD	0/1	0/1	0/1	1/1	1/1
			79602331	T	TGA	MOD	0/1	0/1	0/1	1/1	1/1
			79874335	T	A	MOD	0/0	0/0	0/0	0/1	0/1
			79951643	G	A	MOD	0/0	0/0	0/0	0/1	0/1

Table 4. *Cont.*

#	Gene Symbol (Gene Name)	CHR	Variant Information				Genotype				
							Without Brachygnathia Inferior			With Brachygnathia Inferior	
			POS	REF	ALTS	Putative Impact	Original Dog	NT-2	NT-4	NT-1	NT-3
			22259657	CA	C	MOD	0/0	0/0	0/0	0/1	0/1
			22267695	C	T	MOD	0/0	0/0	0/0	0/1	0/1
			20900771	T	A	MOD	0/0	0/0	0/0	0/1	0/1
			21327589	T	TA	MOD	0/1	0/1	0/1	1/1	1/1
34	PCDH9 (protocadherin 9)	22	21447120	CAG	C	MOD	0/0	0/0	0/0	0/1	0/1
			21629025	T	A	MOD	0/0	0/0	0/0	0/1	0/1
			21682718	TA	T	MOD	0/0	0/0	0/0	0/1	0/1
			21741598	G	A	MOD	0/0	0/0	0/0	0/1	0/1
			21855444	T	G	MOD	0/0	0/0	0/0	0/1	0/1
			21977854	G	GA	MOD	0/1	0/1	0/1	1/1	1/1
			13687020	C	T	MOD	0/1	0/1	0/1	1/1	1/1
35	PLCB1 (phospholipase C beta 4)	24	13703533	CCCTCACACACA	C	MOD	0/1	0/1	0/1	1/1	1/1
			13506621	AT	A	MOD	0/0	0/0	0/0	0/1	0/1
			13545968	C	A	MOD	0/0	0/0	0/0	0/1	0/1
36	PLCB4 (phospholipase C beta 4)	24	13106067	G	A	MOD	0/0	0/0	0/0	0/1	0/1
			13222123	C	CT	MOD	0/1	0/1	0/1	1/1	1/1
37	PPP3CC (protein phosphatase 3 catalytic subunit gamma)	25	34764968	TA	T	MOD	0/0	0/0	0/0	0/1	0/1
			34812396	TA	T	MOD	0/0	0/0	0/0	0/1	0/1

Table 4. *Cont.*

#	Gene Symbol (Gene Name)	CHR	Variant Information				Genotype				
								Without Brachygnathia Inferior			With Brachygnathia Inferior	
			POS	REF	ALTS	Putative Impact	Original Dog	NT-2	NT-4	NT-1	NT-3
38	PRKCA (protein kinase C alpha)	9	13673919	T	C	MOD	0/0	0/0	0/0	0/1	0/1
			13871044	TAA	T,TA	MOD	0/1	0/1	0/1	0/2	1/2
			13872388	G	GC	MOD	0/1	0/1	0/1	1/1	1/1
			13906274	G	A	MOD	0/0	0/0	0/0	0/1	0/1
			13963246	G	GT	MOD	0/0	0/0	0/0	0/1	0/1
			13987502	GA	G	MOD	0/0	0/0	0/1	0/1	0/1
39	PRKCE (protein kinase C epsilon type)	10	48018924	G	GT	MOD	0/1	0/1	0/1	1/1	1/1
			48021663	G	A	MOD	0/0	0/0	0/0	0/1	0/1
			48362949	A	T	MOD	0/1	0/1	0/1	1/1	1/1
			48362950	A	T	MOD	0/1	0/1	0/1	1/1	1/1
			48362951	A	T	MOD	0/1	0/1	0/1	1/1	1/1
			48452967	A	T	MOD	0/0	0/0	0/0	0/1	0/1
40	PRKCH (protein kinase C epsilon)	8	36326004	A	T	MOD	0/0	0/0	0/0	0/1	0/1
			36445470	C	A	MOD	0/0	0/0	0/0	0/1	0/1
41	PRKCQ (protein kinase C theta)	2	29254232	C	T	MOD	0/0	0/0	0/0	0/1	0/1
			29254236	C	T	MOD	0/0	0/0	0/0	1/1	1/1
			29246453	C	CA	MOD	0/1	0/1	0/1	1/1	1/1
42	TBL1X (transducin beta like 1 X-linke)	X	6446386	T	C	MOD	0/0	0/0	0/0	0/1	0/1
			6446390	T	C	MOD	0/0	0/0	0/0	0/1	0/1

Table 4. *Cont.*

#	Gene Symbol (Gene Name)	CHR	Variant Information				Genotype				
							Without Brachygnathia Inferior			With Brachygnathia Inferior	
			POS	REF	ALTS	Putative Impact	Original Dog	NT-2	NT-4	NT-1	NT-3
43	TBXT (T-box transcription factor T)	1	53860297	T	G	MOD	0/0	0/0	0/0	0/1	0/1
			53860299	T	G	MOD	0/0	0/0	0/0	0/1	0/1
			53916908	G	C	MOD	0/0	0/0	0/0	0/1	0/1
			54140252	G	A	MOD	0/1	0/1	0/1	1/1	1/1
44	TCF7L2 (transcription factor 7 like 2)	28	23954797	A	C	MOD	0/0	0/0	0/0	0/1	0/1
			23973312	C	T	MOD	0/0	0/0	0/0	0/1	0/1
			24061992	C	T	MOD	0/0	0/0	0/0	0/1	0/1
45	TLE1 (TLE family member 1, transcriptional corepressor)	1	77969485	G	GT	MOD	0/1	0/1	0/1	1/1	1/1
			78272418	A	T	MOD	0/0	0/0	0/0	0/1	0/1
			77521907	A	AT	MOD	0/1	0/1	0/1	1/1	1/1
			77529973	CATAT	C	MOD	0/1	0/1	0/1	1/1	1/1
46	WNT5B (Wnt family member 5B)	27	43705981	A	T	MOD	0/0	0/0	0/0	0/1	0/1
			43718076	A	C	MOD	0/0	0/0	0/0	0/1	0/1
			44082433	CTTTTTT	C,CTTTTT	MOD	0/2	0/2	0/2	0/1	0/1
47	ENSCAFG0000008115	17	44366744	T	C	MOD	0/0	0/0	0/0	0/1	0/1
			44392169	C	A	MOD	0/0	0/0	0/0	0/1	0/1

Table 4. *Cont.*

#	Gene Symbol (Gene Name)	CHR	Variant Information				Genotype				
							Without Brachygnathia Inferior			With Brachygnathia Inferior	
			POS	REF	ALTS	Putative Impact	Original Dog	NT-2	NT-4	NT-1	NT-3
			17723198	C	CTCTG	MOD	0/1	0/1	0/1	1/1	1/1
			18058494	T	C	MOD	0/0	0/0	0/0	0/1	0/1
			18069599	CT	C	MOD	0/0	0/0	0/0	0/1	0/1
48	CTNNA3 (catenin alpha 3)	4	16891381	CA	C	MOD	0/1	0/1	0/1	1/1	1/1
			16989930	G	A	MOD	0/0	0/0	0/0	0/1	0/1
			16989932	A	T	MOD	0/0	0/0	0/0	0/1	0/1
			17291872	TA	T	MOD	0/0	0/0	0/0	0/1	0/1
			99421688	G	A	MOD	0/0	0/0	0/0	0/1	0/1
			99421696	G	A	MOD	0/0	0/0	0/0	0/1	0/1
			99421697	G	T	MOD	0/0	0/0	0/0	0/1	0/1
			99421711	G	C	MOD	0/0	0/0	0/0	0/1	0/1
			99421728	T	C	MOD	0/0	0/0	0/0	0/1	0/1
49	ENSCAFG00000023180	X	99421731	G	T	MOD	0/0	0/0	0/0	0/1	0/1
			99421735	C	T	MOD	0/0	0/0	0/0	0/1	0/1
			99421993	C	T	MOD	0/0	0/0	0/0	0/1	0/1
			99421995	C	T	MOD	0/0	0/0	0/0	0/1	0/1
			99422007	C	G	MOD	0/0	0/0	0/0	0/1	0/1
			99422009	A	C	MOD	0/0	0/0	0/0	0/1	0/1

Table 4. *Cont.*

#	Gene Symbol (Gene Name)	CHR	Variant Information				Genotype					
			POS	REF	ALTS	Putative Impact	Without Brachygnathia Inferior				With Brachygnathia Inferior	
							Original Dog	NT-2	NT-4	NT-1	NT-3	
50	LOC489647 (cadherin-1-like)	5	63556214	G	A	MOD	0/0	0/0	0/0	0/1	0/1	
			63556216	G	A	MOD	0/0	0/0	0/0	0/1	0/1	
			63556219	C	G	MOD	0/0	0/0	0/0	0/1	0/1	
			63556227	T	C	MOD	0/0	0/0	0/0	0/1	0/1	
			63556230	T	C	MOD	0/0	0/0	0/0	0/1	0/1	
			63556233	T	C	MOD	0/0	0/0	0/0	0/1	0/1	

CHR = chromosome, POS = position (genomic coordinate), REF = reference allele, ALT = alternative allele, [+] MOD = moderate.

3. Discussion

Many animals have been cloned via nucleus transfer from somatic cells to mature oocytes in vitro [14–18]. However, owing to inadequate in vitro culture conditions and different estrus cycles, dogs are typically cloned using surgically recovered mature oocytes in vivo [5,6]. Nevertheless, the cloned dogs were also found to have many abnormalities as in other cloned animals [19]. In cloned animals, the causes of these abnormalities include incomplete reprogramming and imprinting, as well as inappropriate culture environment [20–22]. However, the cause has not been clearly identified. We found brachygnathia inferior for the first time in cloned dogs and attempted to identify the cause through analysis of genetic signals involved in embryonic fate.

The efficiency of cloning, which is calculated from the number of viable offspring per transferred embryo, is known to be 5–15%, depending on the animal species [3]. The cloning efficiency of the first cloned sheep, Dolly, was 3.4%. In the present study, the 5.6% cloning efficiency was similar to that reported in previous studies. This efficiency value indicates that 95–85% of SCNT embryos died before reaching full term [23]. In addition, a high incidence of malformations, large offspring syndrome, placental defects, and brain defects, as well as pulmonary, renal, and cardiovascular failure were observed in the placenta, fetuses, and offspring in cloned animals [3,22]. Incomplete remodeling and abnormal epigenetic modification of somatic nucleic acids have been identified as the cause of these abnormalities [20–22]. In cloned dogs, cleft palate and abnormal external genitalia such as failure of preputial closure at the ventral distal part and persistent penile frenulum have been reported [19]. In the present study, although there were no abnormalities in hematological parameters and chromosome numbers among the four cloned dogs produced by SCNT under the same environmental conditions, brachygnathia inferior caused by growth failure of mandible occurred in two dogs, as determined by morphological observation, X-ray imaging, and CT diagnosis at 1 month after birth.

Craniofacial malformations, such as cleft palate and mandibular abnormalities, have been studied in many animals. Despite the relatively high incidence of these disorders, their genetic cause have not been studied in detail. In cattle, trisomy 17 and 22 [24,25], as well as mutations in GON4L [26], are related to brachygnathia inferior. In sheep, frameshift in OBSL1 has been shown to affect brachygnathia inferior [27], and mutations in COL1A1 and COL1A2 cause osteogenesis imperfecta [28]. In dogs, LINE-1 insertion within DLX6 induces cleft palate and mandibular abnormalities, as reported by a genome-wide association study in a canine model [29]. The skull shape of dogs is regulated by a missense mutation in BMP3 [30]. In the present study, WGS analysis revealed that cloned dogs with brachygnathia inferior had 10,112 SNVs and indels in 3164 genes, compared to normal dogs without brachygnathia inferior. Interestingly, two variants between BMP3 and PRKG3, n.5244256C>T and n.5248552A>G, were detected in cloned dogs with brachygnathia inferior. However, these two single-nucleotide variants were located in the intergenic region. It was difficult to evaluate their effect on mandibular abnormalities [31].

The Wnt signaling pathway is known to be involved in cell destiny, polarity, and migration during embryonic development and differentiation [32,33]. The major Wnt signaling pathways are divided into canonical pathways that start with the binding of Wnt ligands (WNT 1, WNT 3, WNT 7, etc.), Frizzled (Fzd) receptors, and low-density lipoprotein receptor-related protein (LRP) 5 or LRP6, as well as into non-canonical pathways that start with the binding of WNT5a class ligand and FZD receptor. The non-canonical Wnt pathway consists of two types: the planar cell polarity (PCP) pathway, related to cell polarity and migration, and the Wnt/Ca^{2+} pathway, which is involved in the activation of Ca^{2+}-dependent proteins (CaMK2, PKC, and calcium) related to cell differentiation, relocation, and adhesion. In both canonical and non-canonical Wnt signaling pathways, the cascade begins through the activation/induction of Dishevelled (Dsh) via the binding of Wnt and FZD [34–36]. In the present study, through Wnt/cadherin signaling network analysis in cloned dogs with brachygnathia inferior, we found that WNT5B interacted closely with FZD4, FZD8, DVL2, β-adrrestin2 (ARBB2), and DVL binding antagonist of β-catenin (DACT1) as negative

regulators of WNT signaling, and that these genes were closely related to initiators of canonical and non-canonical Wnt signaling pathways [37]. Pathogenic variants of these genes were also identified, including tumor or posterior malformation in FZD4 (c.74G>T), ARRB2 (c.287A>C), and DACT1 (c.1561-1G>A) in humans and mice [37–39].

In the β-catenin-independent pathway, the WNT5 subfamily, including WNT5a and WNT5b, which can combine with FZD4 or FZD8, is closely involved in osteogenesis, and disruption of the WNT5 subfamily leads to skeletal defects [40,41]. In osteoblastic cell lines, cadherin 11 (calcium-dependent adhesion, CDH 11) is implicated in bone development and maintenance [42]. E-cadherin (CDH1) interacts with catenin α-δ types in the cytoplasm, and their complexes are important for epithelial cell polarity and function [43]. Therefore, we propose that brachygnathia inferior in cloned dogs was affected by two pathways: (1) the non-canonical WNT pathway, such as activation by DVL2/ARRB2 or inhibition by DVL2/DACT1 after the binding of WNT5b to FZD4/FZD8, and (2) the catenin/cadherin pathway via the interaction of α/δ catenin (CTNNA3, CTNND2) and CDH by ARRB2. The involvement of the catenin/cadherin pathway is supported by the discovery of LOC489647 (cadherin-1-like) [44].

Although it is not possible to precisely estimate how the Wnt and cadherin signaling pathways are differentially expressed in dogs cloned under the same conditions, it is presumed that the use of oocytes recovered from different dogs affects the reprogramming of donor somatic cell nuclei from the original donor dog. This hypothesis is supported by previous reports that oocyte cytoplasm extracts such as ooplasmic factor can regulate the epigenetic reprogramming of somatic cell nuclei, such as the demethylation of histones [45,46].

4. Conclusions

This study revealed that brachygnathia inferior in cloned dogs was associated with variants in the initiators and/or regulators of the Wnt/cadherin signaling pathway, especially the non-canonical Wnt signaling pathway via WNT5b. Although the direct cause of the abnormalities in cloned dogs, such as brachygnathia inferior, could not be determined, it was presumed that the oocytes used for cloning altered the reprogramming of the donor somatic cells. In order for this hypothesis to be proven, further gene editing and epigenetic reprogramming error studies are necessary in order to identify abnormalities in cloned offspring. However, considering that dogs are companion animals, and not laboratory animals such as mice, future research for identifying the related genetic variants should utilize genetic samples from dogs with brachygnathia inferior that are naturally born.

5. Materials and Methods

5.1. Animals

All experiments were authorized by the Animal Center for Biomedical Experimentation at the National Institute of Animal Science of the Rural Development Administration (approval number 2015-143 on 21 May 2015) and followed animal care and use guidelines.

5.2. Cloning of Dogs

For dog cloning, somatic cell nuclear transfer (SCNT) and embryo transfer were performed according to a previously described protocol [6] with minor modifications, as shown in Figure 1. As donor cells, ear fibroblasts were collected from a 5-year-old male German shepherd dog (original donor) via ear skin biopsy after anesthesia. The original dog was diagnosed with a normal phenotype that was clinically healthy and without physical disabilities. Fibroblasts at the second to third passage were stored in LN_2 before use as donor cells in SCNT. Three days prior to SCNT, the cryopreserved cells were thawed and cultured at a seeding concentration of 5×10^4 cells per well in a 4-well dish. Cells at the second to third passage were used for the production of cloned embryos. After SCNT, the embryos were immediately surgically transferred into the oviduct of a surrogate mother

using a previously described method [6]. Pregnancy rates were determined by ultrasound diagnosis at ≈31 days after embryo transfer.

5.3. Microsatellite Analysis for Confirmation of Paternity

For confirmation of genetic identity, genomic DNA was extracted from the blood of four cloned dogs with a Wizard Genomic DNA Purification Kit (Promega, Madison, WI, USA) and from donor cells with PureLink™ Genomic DNA Mini Kit (Thermo Fisher Scientific, Carlsbad, CA, USA). Multiplex PCR was performed using the GeneAmp PCR system 9700 (ABI) using a previously reported method (Ko et al., 2019). PCR products were analyzed using a DNA sequencer (ABI 3730xl; Applied Biosystems, Foster City, CA, USA), and microsatellite analysis was conducted using GeneSMapper version 4 (ABI). Microsatellite markers, such as FH2537, FH3005, FH3372, FH3116, REN51C16, REN2770O5, FH2834, REN204K13, FH2097, FH2712, and FH2998, were selected according to previous studies [47,48].

5.4. Hematological and Biochemical Analysis of Blood

Blood samples were collected from each dog via jugular venipuncture. For complete blood count (CBC) measurement, blood samples were collected into EDTA-containing tubes, and leukocytes, erythrocytes, and thrombocyte were counted using an automated hematology cell counter (MS9-5V; Melet Schloesing Lab, Osny France). To assess kidney, liver, and heart functions, we performed blood chemistry analysis using a bench-top dry chemistry analyzer (Vettest 8008 Chemistry Analyzer; IDEXX Lab, Chalfont St Peter, United Kingdom), in which creatinine, glucose, blood urea nitrogen (BUN), gamma-glutamyl transferase (GGT), albumin, total bilirubin, total protein (TP), alanine aminotransferase (ALT), aspartate aminotransferase (AST), creatine kinase, cholesterol, and amylase levels were determined.

5.5. X-ray and CT Imaging

X-ray and CT imaging were performed using a two-channel multi-detector row CT scanner (Somatom Emotion, Siemens Medical System, Erlangen, Germany). For CT scanning, the animals were anesthetized by inhalation of 2% isoflurane, and CT was performed at 110 kV, 36 mAs, and 1 mm slice thickness. Datasets were transferred to a separate workstation, and the volume and size of the vertebral window by pediculectomy for each site were measured using the Lucion software (Infinitt Technology, Seoul, Korea).

5.6. Karyotype Analysis

For chromosome analysis, peripheral blood samples were added to RPMI media (1640; Gibco, Rockville, MD, USA) supplemented with FBS and phytohemagglutinin, and cultured overnight into CO_2 incubator at 37 °C. The blood cells were arrested in metaphase by adding 0.1 μg/mL of colcemid for 1 h, and then harvested using 0.25% trypsin/EDTA solution. The single-cell suspension was incubated in hypotonic solution buffer (0.075 M KCl) for 45 min and fixed with methanol-acetic acid (3:1). After fixation, condensed chromosomes were spread on pre-cleaned glass slides and stained with Giemsa solution. Karyotyping of cultured cells was performed using standard cytogenetic techniques, revealing a female chromosomal constitution of 2n = 78, XY.

5.7. Whole-Genome Sequencing, Sequence Mapping, and Variant Calling

Blood samples were collected from the normal phenotype group (original dog, NT-2, and NT-4) and the brachygnathia inferior group (NT-1 and NT-3), and genomic DNA was extracted using the TruSeq Nano DNA Sample Prep Kit (Illumina, San Diego, CA, USA). Whole-genome sequencing was performed using the Illumina HiSeq 2500 sequencing platform (Illumina, San Diego, CA, USA). Skewer software (v0.2.2) was used for adapter trimmer, and BWA (v0.7.15) were used for aligning the collected sequence data to the canine reference genome (CanFam 3.1). The Genome Analysis Toolkit (GATK, v2.3.9Lite)

was used for improvement of alignment errors and genotype calling and refining with default parameters. SNP-calling procedure was performed to discover SNPs using SAM tools (v.1.3.1). The detected SNPs were then annotated to functional categories using SnpEff software (v4.3a).

5.8. Predictive Functional and Interaction Analyses of Brachygnathia Inferior Candidate Genes

To validate the basic biological function of brachygnathia inferior candidate genes, we mapped a list of genes to the biological process (BP) of Gene Ontology (GO) in the DAVID database (v.6.8, accessed on 1 January 2019, http://david.abcc.ncifcrf.gov). Significantly enriched GOBP categories of brachygnathia inferior candidate genes were determined by the enrichment *p*-value. Signaling pathway enrichment analysis was performed using PANTHER pathway analysis tools (v.14.0, accessed on 1 January 2019, http://pantherdb. org). The signaling pathway of brachygnathia inferior candidate genes was determined by the number of genes mapped on each pathway and the percentage of enriched gene number against the total number of each pathway component genes.

To analyze the gene-to-gene functional correlation of brachygnathia inferior candidate genes, we constructed an interaction network using Search Tool for the Retrieval of Interacting Proteins (STRING, accessed on 1 January 2019, http://string-db.org).

Supplementary Materials: The following are available online at https://www.mdpi.com/article/10.3390/ijms23010475/s1.

Author Contributions: Conceptualization, manuscript writing, review, and editing, S.A.O.; project administration, funding acquisition, conceptualization, and veterinary treatment, T.-Y.H.; assembly of data, manuscript writing, and veterinary diagnosis, Y.-h.C. and S.-L.L.; dog cloning and veterinary treatment, S.L., H.J. and J.-G.N.; WGS analysis, D.L.; microsatellites for paternity test, B.-H.C. All authors have read and agreed to the published version of the manuscript.

Institutional Review Board Statement: All animal experiments were approved by the Animal Center for Biomedical Experimentation at the National Institute of Animal Science of the Rural Development Administration (approval number 2015-143).

Informed Consent Statement: Not applicable.

Data Availability Statement: The data presented in this study are available from the corresponding author on reasonable request.

Conflicts of Interest: The authors declare no conflict of interest.

Abbreviations

SCNT	Somatic cell nuclear transfer
CT	Computed tomography
WGS	Whole-genome sequencing
Wnt	Wingless-related integration site
DNA	Deoxyribonucleic acid
NT	Nuclear transfer
SMD	Surrogate mother dogs
CBC	Complete blood count
RBC	Red blood cell
MCV	Mean corpuscular volume
MCH	Mean corpuscular hemoglobin
MCHC	Mean corpuscular hemoglobin concentration
PDW	Platelet distribution width
WBC	White blood cell
MPV	Mean platelet volume

RDW	Red cell distribution width
PCT	Plateletcrit
BUN	Blood urea nitrogen
GGT	Gamma-glutamyl transferase
ALB	Albumin
TB	Total bilirubin
TP	Total protein
ALT	Alanine aminotransferase
AST	Aspartate aminotransferase
SNVs	Single nucleotide variations
Indels	Insertions/deletions
GO	Gene Ontology
PANTHER	Protein analysis through evolutionary relationships
DAVID	Database for annotation, visualization, and integrated discovery
GnRH	Gonadotropin-releasing hormone
STRING	Search tool for the retrieval of interacting genes/proteins
PCP	Planar cell polarity
FBS	Fetal bovine serum
BP	Biological process

References

1. Lee, B.C.; Kim, M.K.; Jang, G.; Oh, H.J.; Yuda, F.; Kim, H.J.; Shamim, M.H.; Kim, J.J.; Kang, S.K.; Schatten, G.; et al. Developmemtal technology: Dogs cloned from adult somatic cells. *Nature* **2005**, *436*, 641. [CrossRef] [PubMed]
2. Keefer, C.L.; Baldassarre, H.; Keyston, R.; Wang, B.; Bhatia, B.; Bilodeau, A.S.; Zhou, J.F.; Leduc, M.; Downey, B.R.; Lazaris, A.; et al. Generation of dwarf goat (*Capra hircus*) clones following nuclear transfer with transfected and nontransfected fetal fibroblasts and in vitro-matured oocytes. *Biol. Reprod.* **2001**, *64*, 849–856. [CrossRef] [PubMed]
3. Keefer, C.L. Artificial cloning of domestic animals. *Proc. Natl. Acad. Sci. USA* **2015**, *112*, 8874–8878. [CrossRef]
4. Kim, M.J.; Oh, H.J.; Hwang, S.Y.; Hur, T.Y.; Lee, B.C. Health and temperaments of cloned working dogs. *J. Vet. Sci.* **2018**, *19*, 585–591. [CrossRef]
5. Kim, M.J.; Oh, H.J.; Kim, G.A.; Setyawan, E.M.N.; Choi, Y.B.; Lee, S.H.; Petersen-Jones, S.M.; Ko, C.M.J.; Lee, B.C. Birth of clones of the world's first cloned dog. *Sci. Rep.* **2017**, *7*, 3–6. [CrossRef] [PubMed]
6. Lee, S.; Zhao, M.; No, J.; Nam, Y.; Im, G.S.; Hur, T.Y. Dog cloning with in vivo matured oocytes obtained using electric chemiluminescence immunoassay-predicted ovulation method. *PLoS ONE* **2017**, *12*, e0173735. [CrossRef]
7. Kim, H.M.; Cho, Y.S.; Kim, H.; Jho, S.; Son, B.; Choi, J.Y.; Kim, S.; Lee, B.C.; Bhak, J.; Jang, G. Whole genome comparison of donor and cloned dogs. *Sci. Rep.* **2013**, *3*, 1–4. [CrossRef]
8. De Sousa, P.A.; King, T.; Harkness, L.; Young, L.E.; Walker, S.K.; Wilmut, I. Evaluation of gestational deficiencies in cloned sheep fetuses and placentae. *Biol. Reprod.* **2001**, *65*, 23–30. [CrossRef] [PubMed]
9. Hill, J.R.; Burghardt, R.C.; Jones, K.; Long, C.R.; Looney, C.R.; Shin, T.; Spencer, T.E.; Thompson, J.A.; Winger, Q.A.; Westhusin, M.E. Evidence for placental abnormality as the major cause of mortality in first-trimester somatic cell cloned bovine fetuses. *Biol. Reprod.* **2000**, *63*, 1787–1794. [CrossRef]
10. Eriksen, T.; Ganter, M.; Distl, O.; Staszyk, C. Cranial morphology in the brachygnathic sheep. *BMC Vet. Res.* **2016**, *12*, 1–8. [CrossRef]
11. Shatab, M.S.; Kumar, N.; Singh, M.; Kumar, S.; Seckhon, M.S.; Dhindsa, S.S. Brachygnathia (parrot mouth) inferior calf in a murrah buffalo. *Buffalo Bull.* **2018**, *37*, 101–103.
12. Dierks, C.; Hoffmann, H.; Heinrich, F.; Hellige, M.; Hewicker-Trautwein, M.; Distl, O. Suspected X-linked facial dysmorphia and growth retardation in related labrador retriever puppies. *Vet. J.* **2017**, *220*, 48–50. [CrossRef]
13. Yin, R.; Kwoh, C.K.; Zheng, J. Whole genome sequencing analysis: Computational pipelines and workflows in bioinformatics. In *Encyclopedia of Bioinformatics and Computational Biology: ABC of Bioinformatics*; Shoba, R., Gribskov, M., Nakai, K., Christian, S., Eds.; Elsevier: Amsterdam, The Netherlands, 2018; Volume 3, pp. 176–183.
14. Wilmut, I.; Schnieke, A.E.; McWhir, J.; Kind, A.J.; Campbell, K.H.S. Viable offspring derived from fetal and adult mammalian cells. *Nature* **1997**, *385*, 810–813. [CrossRef]
15. Wakayama, T.; Perry, A.C.F.; Zuccotti, M.; Johnson, K.R.; Yanagimachi, R. Full-term development of mice from enucleated oocytes injected with cumulus cell nuclei. *Nature* **1998**, *394*, 369–374. [CrossRef] [PubMed]
16. Kato, Y.; Tani, T.; Sotomaru, Y.; Kurokawa, K.; Kato, J.Y.; Doguchi, H.; Yasue, H.; Tsunoda, Y. Eight calves cloned from somatic cells of a single adult. *Science* **1998**, *282*, 2095–2098. [CrossRef] [PubMed]
17. Baguisi, A.; Behboodi, E.; Melican, D.T.; Pollock, J.S.; Destrempes, M.M.; Cammuso, C.; Williams, J.L.; Nims, S.D.; Porter, C.A.; Midura, P.; et al. Production of goats by somatic cell nuclear transfer. *Nat. Biotechnol.* **1999**, *17*, 456–461. [CrossRef] [PubMed]
18. Polejaeva, I.A.; Chen, S.H.; Vaught, T.D.; Page, R.L.; Mullins, J.; Ball, S.; Dai, Y.; Boone, J.; Walker, S.; Ayares, D.L.; et al. Cloned pigs produced by nuclear transfer from adult somatic cells. *Nature* **2000**, *407*, 86–90. [CrossRef] [PubMed]

19. Kim, M.J.; Oh, H.J.; Kim, G.A.; Jo, Y.K.; Choi, J.; Kim, H.J.; Choi, H.Y.; Kim, H.W.; Choi, M.C.; Lee, B.C. Reduced birth weight, cleft palate and preputial abnormalities in a cloned dog. *Acta Vet. Scand.* **2014**, *56*, 18–21. [CrossRef]

20. Tanaka, S.; Oda, M.; Toyoshima, Y.; Wakayama, T.; Tanaka, M.; Hattori, N.; Yoshida, N.; Ohgane, J.; Yanagimachi, R.; Shiota, K. Placentomegaly in cloned mouse concepti caused by expansion of the spongiotrophoblast layer. *Biol. Reprod.* **2001**, *65*, 1813–1821. [CrossRef]

21. Dean, W.; Santos, F.; Stojkovic, M.; Zakhartchenko, V.; Walter, J.; Wolf, E.; Reik, W. Conservation of methylation reprogramming in mammalian development: Aberrant reprogramming in cloned embryos. *Proc. Natl. Acad. Sci. USA* **2001**, *98*, 13734–13738. [CrossRef]

22. Gouveia, C.; Huyser, C.; Egli, D.; Pepper, M.S. Lessons learned from somatic cell nuclear transfer. *Int. J. Mol. Sci.* **2020**, *21*, 2314. [CrossRef] [PubMed]

23. Yanagimachi, R. Cloning: Experience from the mouse and other animals. *Mol. Cell. Endocrinol.* **2002**, *187*, 241–248. [CrossRef]

24. Iannuzzi, L.; PiaDiMeo, G.; Leifsson, P.S.; Eggen, A.; Christensen, K. A case of trisomy 28 in cattle revealed by both banding and FISH-mapping techniques. *Hereditas* **2001**, *134*, 147–151. [CrossRef]

25. Mayr, B.; Krutzler, H.; Auer, H.; Schleger, W.; Sasshofer, K.; Glawischig, E. A viable calf with trisomy 22. *Cytogenet. Genome Res.* **1985**, *39*, 77–79. [CrossRef]

26. Schwarzenbacher, H.; Wurmser, C.; Flisikowski, K.; Misurova, L.; Jung, S.; Langenmayer, M.C.; Schnieke, A.; Knubben-Schweizer, G.; Fries, R.; Pausch, H. A frameshift mutation in GON4L is associated with proportionate dwarfism in Fleckvieh cattle. *Genet. Sel. Evol.* **2016**, *48*, 1–10. [CrossRef]

27. Woolley, S.A.; Hayes, S.E.; Shariflou, M.R.; Nicholas, F.W.; Willet, C.E.; O'Rourke, B.A.; Tammen, I. Molecular basis of a new ovine model for human 3M syndrome-2. *BMC Genet.* **2020**, *21*, 1–11. [CrossRef] [PubMed]

28. Thompson, K.G.; Piripi, S.A.; Dittmer, K.E. Inherited abnormalities of skeletal development in sheep. *Vet. J.* **2008**, *177*, 324–333. [CrossRef]

29. Wolf, Z.T.; Leslie, E.J.; Arzi, B.; Jayashankar, K.; Karmi, N.; Jia, Z.; Rowland, D.J.; Young, A.; Safra, N.; Sliskovic, S.; et al. A LINE-1 insertion in DLX6 is responsible for cleft palate and mandibular abnormalities in a canine model of pierre robin sequence. *PLoS Genet.* **2014**, *10*, e1004257. [CrossRef] [PubMed]

30. Schoenebeck, J.J.; Hutchinson, S.A.; Byers, A.; Beale, H.C.; Carrington, B.; Faden, D.L.; Rimbault, M.; Decker, B.; Kidd, J.M.; Sood, R.; et al. Variation of BMP3 contributes to dog breed skull diversity. *PLoS Genet.* **2012**, *8*, e1002849. [CrossRef]

31. Dashti, M.J.S.; Gamieldien, J. A practical guide to filtering and prioritizing genetic variants. *Biotechniques* **2017**, *62*, 18–30. [CrossRef]

32. Cadigan, K.M.; Nusse, R. Wnt signaling: A common theme in animal development. *Genes Dev.* **1997**, *11*, 3286–3305. [CrossRef]

33. Brault, V.; Moore, R.; Kutsch, S.; Ishibashi, M.; Rowitch, D.H.; McMahon, A.P.; Sommer, L.; Boussadia, O.; Kemler, R. Inactivation of the β-catenin gene by Wnt1-Cre-mediated deletion results in dramatic brain malformation and failure of craniofacial development. *Development* **2001**, *128*, 1253–1264. [CrossRef] [PubMed]

34. Acebron, S.P.; Niehrs, C. β-catenin-independent roles of Wnt/LRP6 signaling. *Trends Cell Biol.* **2016**, *26*, 956–967. [CrossRef]

35. Nusse, R.; Clevers, H. Wnt/β-catenin signaling, disease, and emerging therapeutic modalities. *Cell* **2017**, *169*, 985–999. [CrossRef]

36. Haseeb, M.; Pirzada, R.H.; Ain, Q.U.; Choi, S. Wnt signaling in the regulation of immune cell and cancer therapeutics. *Cells* **2019**, *8*, 1380. [CrossRef]

37. Bonnans, C.; Flacelière, M.; Grillet, F.; Dantec, C.; Desvignes, J.P.; Pannequin, J.; Severac, D.; Dubois, E.; Bibeau, F.; Escriou, V.; et al. Essential requirement for β-arrestin2 in mouse intestinal tumors with elevated Wnt signaling. *Proc. Natl. Acad. Sci. USA* **2012**, *109*, 3047–3052. [CrossRef]

38. Wen, J.; Chiang, Y.J.; Gao, C.; Xue, H.; Xu, J.; Ning, Y.; Hodes, R.J.; Gao, X.; Chen, Y.G. Loss of Dact1 disrupts planar cell polarity signaling by altering dishevelled activity and leads to posterior malformation in mice. *J. Biol. Chem.* **2010**, *285*, 11023–11030. [CrossRef]

39. Yin, X.; Xiang, T.; Li, L.L.; Su, X.; Shu, X.; Luo, X.; Huang, J.; Yuan, Y.; Peng, W.; Oberst, M.; et al. DACT1, an antagonist to Wnt/β-catenin signaling, suppresses tumor cell growth and is frequently silenced in breast cancer. *Breast Cancer Res.* **2013**, *15*, 1–12. [CrossRef]

40. Yang, Y.; Topol, L.; Lee, H.; Wu, J. Wnt5a and Wnt5b exhibit distinct activities in coordinating chondrocyte proliferation and differentiation. *Development* **2003**, *130*, 1003–1015. [CrossRef] [PubMed]

41. Suthon, S.; Perkins, R.S.; Bryja, V.; Miranda-Carboni, G.A.; Krum, S.A. WNT5B in physiology and disease. *Front. Cell Dev. Biol.* **2021**, *9*, 1–20. [CrossRef] [PubMed]

42. Kawaguchi, J.; Azuma, Y.; Hoshi, K.; Kii, I.; Takeshita, S.; Ohta, T.; Ozawa, H.; Takeichi, M.; Chisaka, O.; Kudo, A. Targeted disruption of cadherin-11 leads to a reduction in bone density in calvaria and long bone metaphyses. *J. Bone Miner. Res.* **2001**, *16*, 1265–1271. [CrossRef]

43. Aberle, H.; Schwartz, H.; Kemler, R. Cadherin-catenin complex: Protein interactions and their implications for cadherin function. *J. Cell. Biochem.* **1996**, *61*, 514–523. [CrossRef]

44. Hagman, R.; Rönnberg, E.; Pejler, G. Canine uterine bacterial infection induces upregulation of proteolysis-related genes and downregulation of homeobox and zinc finger factors. *PLoS ONE* **2009**, *4*, e8039. [CrossRef]

45. Hansis, C.; Barreto, G.; Maltry, N.; Niehrs, C. Nuclear reprogramming of human somatic cells by xenopus egg extract requires BRG1. *Curr. Biol.* **2004**, *14*, 1475–1480. [CrossRef]

46. Bui, H.T.; Wakayama, S.; Kishigami, S.; Kim, J.H.; Van Thuan, N.; Wakayama, T. The cytoplasm of mouse germinal vesicle stage oocytes can enhance somatic cell nuclear reprogramming. *Development* **2008**, *135*, 3935–3945. [CrossRef] [PubMed]
47. Ko, M.; Kwon, S. Genomic polymorphism analysis using microsatellites in the jeju dogs. *J. Life Sci.* **2019**, *29*, 637–644.
48. Kim, S.; Jang, H.; Kim, L.; Lim, D.; Lee, S.; Cho, Y.; Kim, T.; Seong, H.; Oh, S.; Choi, B. Paternity diagnosis using the multiplex PCR with microsatellite markers in dogs. *Reprod. Dev. Biol.* **2011**, *35*, 399–405.

Article

The Molecular Quality and Mitochondrial Activity of Porcine Cumulus–Oocyte Complexes Are Affected by Their Exposure to Three Endocrine-Active Compounds under 3D In Vitro Maturation Conditions

Gabriela Gorczyca [1] , Kamil Wartalski [2] , Marek Romek [3] , Marcin Samiec [4,*] and Małgorzata Duda [1,*]

[1] Department of Endocrinology, Institute of Zoology and Biomedical Research, Faculty of Biology, Jagiellonian University in Krakow, Gronostajowa 9 Street, 30-387 Krakow, Poland; gabriela.gorczyca@doctoral.uj.edu.pl

[2] Department of Histology, Jagiellonian University Medical College, Kopernika 7 Street, 31-034 Krakow, Poland; kamil.wartalski@uj.edu.pl

[3] Department of Cell Biology and Imaging, Institute of Zoology and Biomedical Research, Faculty of Biology, Jagiellonian University in Krakow, Gronostajowa 9 Street, 30-387 Krakow, Poland; marek.romek@uj.edu.pl

[4] Department of Reproductive Biotechnology and Cryoconservation, National Research Institute of Animal Production, Krakowska 1 Street, 32-083 Balice, Poland

* Correspondence: marcin.samiec@iz.edu.pl (M.S.); maja.duda@uj.edu.pl (M.D.)

Abstract: Thus far, the potential short- and long-term detrimental effects of a variety of environmental chemicals designated as endocrine-active compounds (EACs) have been found to interfere with histo- and anatomo-physiological functions of the reproductive system in humans and wildlife species. For those reasons, this study sought to examine whether selected EACs, which encompass the fungicide vinclozolin (Vnz), the androgenic anabolic steroid nandrolone (Ndn) and the immunosuppressant cyclosporin A (CsA), affect the developmental competence and molecular quality (MQ) of porcine cumulus–oocyte complexes (COCs) subjected to in vitro maturation (IVM) under 3D culture conditions. The COCs underwent 3D-IVM in the presence of Vnz, Ndn or CsA for 48 h. To explore whether the selected EACs induce internucleosomal DNA fragmentation in cumulus cells (CCs), TUNEL-assisted detection of late apoptotic cells was performed. Additionally, for the detailed evaluation of pro- and antiapoptotic pathways in COCs, apoptosis proteome profiler arrays were used. To determine changes in intracellular metabolism in COCs, comprehensive assessments of mitochondrial ultrastructure and activity were carried out. Moreover, the relative abundances (RAs) of mRNAs transcribed from genes that are involved in scavenging reactive oxygen species (ROS), such as *SIRT3* and *FOXO3*, and intramitochondrial bioenergetic balance, such as ATP synthase subunit (*ATP5A1*), were ascertained. Finally, to investigate the extent of progression of oocyte maturation, the intraooplasmic levels of cAMP and the RAs of mRNA transcripts encoding regulatory and biocatalytic subunits of a heterodimeric meiosis-promoting factor, termed cyclin B1 (*CCNB1*) and cyclin-dependent kinase 1 (*CDC2*), were also estimated. The obtained results provide, for the first time, strong evidence that both Vnz and Ndn decrease the developmental competence of oocytes and stimulate apoptosis processes in CCs. The present study is also the first to highlight that Vnz accelerates the maturation process in immature oocytes due to both increased ROS production and the augmented RA of the *CCNB1* gene. Furthermore, Vnz was proven to trigger proapoptotic events in CCs by prompting the activity of the FOXO3 transcription factor, which regulates the mitochondrial apoptosis pathway. In turn, Ndn was shown to inhibit oocyte maturation by inducing molecular events that ultimately lead to an increase in the intraooplasmic cAMP concentration. However, due to the simultaneous enhancement of the expression of TNF-β and HSP27 proteins in CCs, Ndn might be responsible for the onset of their neoplastic transformation. Finally, our current investigation is the first to clearly demonstrate that although CsA did not interfere with the nuclear and cytoplasmic maturation of oocytes, by inducing mitophagy in CCs, it disrupted oocyte metabolism, consequently attenuating the parameters related to the MQ of COCs. Summing up, Vnz, Ndn and CsA reduced not only the processes of growth and

IVM but also the MQ of porcine COCs, which might make them unsuitable for assisted reproductive technologies (ARTs) such as in vitro fertilization by either gamete co-incubation or intracytoplasmic sperm injection (ICSI) and cloning by somatic cell nuclear transfer (SCNT).

---

1. Introduction

The presence of various industrial contaminants, pesticides and fungicides in the environment and the frequent abuse of anabolic steroids or hormonal replacement therapy drugs have led to the scientific interest in a group of chemicals called endocrine-active compounds (EACs) or endocrine-disrupting chemicals (EDCs) [1]. EACs/EDCs disturb the normal function of endocrine glands and the hormonal balance of organisms by imposing biological effects, e.g., by binding with receptors for endogenous hormones. Not without significance is the high bioaccumulation of these compounds in plant and animal tissues, which indirectly, through their consumption, may influence organisms and people of both sexes [2]. Among potent EACs/EDCs, mention should be made of: (1) a commonly used dicarboximide fungicide designated as vinclozolin (Vnz); (2) a member of the androgenic anabolic steroid (AAS) family, known as nandrolone (Ndn); and (3) a representative of immunosuppressants termed cyclosporin A (CsA).

Vnz is a component of anti-gray mold preparations used in the protection of crops of fruits and vegetables. Two major ring-opened metabolites of Vnz were detected in rodent physiological fluids and tissue extracts following in vivo exposure [3]. Since Vnz possesses anti-androgenic activity in both fish and mammals [4–6], exposure to it during the gonadal sex determination period promotes a transgenerational increase in pregnancy abnormalities and female adult-onset malformations in reproductive organs [7,8]. Our previous studies have shown that vinclozolin at an environmentally relevant concentration might contribute to the amplification and propagation of apoptotic cell death in the granulosa layer, leading to the rapid removal of atretic follicles in the porcine ovary. Additionally, it seems possible that vinclozolin activates nongenomic signaling pathways, directly modifying the androgen receptor action [9–12].

Another interesting group of EACs is AASs, which encompass biochemical substances synthesized from testosterone or one of their derivatives. Depending on the target tissue, AASs exhibit anabolic or androgenic effects [13,14]. AASs are clinically indicated, for example, for the treatment of chronic obstructive pulmonary disease, for the treatment of hepatic or renal failure and in conditions of either acquired immunodeficiency syndrome (AIDS) or carcinogenesis, tumor progression and metastasis [15–17]. AASs are also recommended for androgen replacement therapy after menopause [18,19]. A cause for concern is the increasing illegal use of AASs by athletes and amateurs [20–23]. This is unfortunately directly caused by the dissemination of the image of strong bodies as the model for the ideal posture in mass communication media [24]. Usually, AASs are administered at supra-physiological doses [25], which are 5-fold to 29-fold higher than the dose recommended for hormonal replacement therapy. Because of the abusive use of AASs by women, numerous side effects, such as atrophy of the breasts, aggressiveness and menstrual irregularity, were found [26,27]. The observed alterations were dose- and time-dependent [28]. Moreover, in women abusing AASs, abnormal gonadal function, such as precocious/accelerated or delayed puberty, anovulation or luteal phase deficiency, may occur [25]. Unfortunately, some of these changes are irreversible even after cessation of AAS administration [29]. As a further matter, AASs, despite regulations (the European Community banned the use of anabolic substances in Europe by means of laws 96/22/EC and 96/23/EC), are still used for anabolic purposes in industrial livestock breeding [30]. Among AAS derivatives, Ndn is the most used injectable steroid [31]. Ndn, acting through androgen receptors, has a strong

anabolic and weak androgenic effect [32]. Additionally, Ndn is a strong progestogen [32]. In medicine, Ndn is used in convalescence after debilitating diseases and to improve the physical condition of the body [14,33]. It is also known that the pharmacological dose of Ndn slows cell growth, inhibits mitochondrial respiration, inhibits respiratory chain complexes I and III, and increases the production of mitochondrial reactive oxygen species (ROS). Chronic administration of Ndn favors the maintenance of stem cells in various tissues, but it may simultaneously increase the risk of their neoplastic transformation [34,35]. Several recent research results also indicate that Ndn negatively affects the functioning of the female reproductive system [36–39].

CsA is a cyclic peptide produced by fungi belonging to the species *Tolypocladium inflatum* [40]. Due to its natural immunosuppressive properties, CsA is used in transplant medicine. Most often, it is administered orally; it is absorbed in the intestines and is metabolized in the liver by cytochrome P450 enzymes [41]. The mechanism of action of CsA is based on the blocking of the early stages of T cell activation. This results in a delay in antibody production and macrophage activation [42], which reduces the risk of graft rejection [43]. Due to its ability to interact with membrane proteins, CsA is one of the most used compounds in studies targeting the exploration of mitochondrial function [44]. In canine cardiomyocytes, CsA has been shown to protect mitochondria by blocking the opening of mitochondrial permeability transition pores (mPTPs). Opening even a single mPTP can cause depolarization of the mitochondrial membrane and vacuolization of the mitochondria; it is one of the signals that activate the processes of programmed cell death [45]. Additionally, CsA has been found to increase the membrane potential of mitochondria [46]. Studies aiming to analyze CsA-mediated effects on ovulation processes in rats have demonstrated that CsA triggers a decline in the quantity of mature antral ovarian follicles displaying the ability to ovulate and, consequently, a reduction in the assumed number of ovulated oocytes [47]. In turn, exposure of pregnant mice to CsA at doses of 20 and 30 mg/kg reduced the possibility of embryo implantation [48]. Although the harmful impacts of EACs on female reproductive parameters have already been extensively recognized, only a few studies have focused on the elucidation of the mechanisms underlying the actions of the above-mentioned EACs that are exerted on oocytes and the surrounding cumulus cells (CCs) [49,50].

Oocyte maturation is the culmination of an extended period of their growth and development within the ovarian follicle. Fully grown oocytes become competent to undergo three synergistic processes of maturation: nuclear, epigenomic and cytoplasmic, which should be initiated and completed synchronously. Whereas nuclear maturation encompasses the release of oocytes from dictyotene (i.e., germinal vesicle/GV stage)-related meiotic arrest and the progression of meiosis from prophase I to metaphase II (MII) [51,52], their epigenomic counterpart depends on the onset, progression and termination of epigenetic covalent modifications in terms of the extent of methylation within genomic DNA cytosine residues and associated alterations in deacetylation and methylation/demethylation profiles within histone lysine and arginine moieties of chromatin nucleosomal cores [53–55]. In turn, cytoplasmic maturation involves the accumulation of mRNA, proteins and nutrients and the redistribution of organelles that are cumulatively indispensable to attain meiotic competence, efficiently finalize meiotic maturation and finally render MII-stage oocytes able to either be successfully fertilized under in vivo or in vitro conditions [56–60] or be effectively subjected to the procedures of cloning by somatic cell nuclear transfer (SCNT) [61–63].

It is noteworthy that the occurrence of morphologically, ultrastructurally and cytophysiologically normal ovarian follicle-derived compartments composed of CCs that are characterized by high molecular quality seems to be extremely important for the faithful progression and termination of oocyte maturation [64–66]. Intrafollicular compartments composed of CCs and oocytes have been found to reciprocally cooperate in order to bi-directionally exchange small molecules (e.g., adenosine triphosphate (ATP), cyclic adenosine 3′,5′-monophosphate (cAMP) and calcium ions), which takes place through gap

junctions [67,68]. The proper molecular function of CCs allows for maintaining oocyte meiotic arrest, followed by participation in meiosis resumption, and supports ooplasmic maturation. This bi-directional interplay between oocyte- and CC-specific intraovarian compartments is crucial for perpetuating not only synergistic interrelations but also proper coordination of the molecular network necessary for transcriptional and proteomic crosstalk between intrafollicular female gamete- and cumulus oophorus-committed niches [69].

Another pivotal factor on which the adequate growth and maturation of oocytes directly depend is their mitochondrial bioenergetic reserve capacity [70,71]. On the one hand, the mitochondria represent the powerhouse of each cell, and therefore, they are designated as so-called bioaccumulators or intracellular deposits of bioenergy arising from ATP synthesis [72,73]. On the other hand, these organelles are also responsible for not only regulating oxidation–reduction (redox) reactions but also retaining Ca^{2+} homeostasis and controlling apoptosis processes [74,75].

Taking into account the modern strategies of assisted reproductive technologies (ARTs) and in vitro embryo production (IVP), the absence of mitochondrion-deficient cells and the intracellular imbalance of mitochondrial compartments, followed by the lack of chronic cytophysiological failures/insufficiencies of mitochondria, have been shown to play a key role in the determination of high parameters of efficiency for the processes of in vitro maturation (IVM), in vitro fertilization (IVF), SCNT-mediated reconstruction of enucleated oocytes and preimplantation development of embryos generated by IVF or SCNT-based cloning [76–81]. For those reasons, the high incidence of perturbations in the quantity and function of mitochondria in oocytes may reduce their quality and subsequently compromise embryonic development [82–84]. Therefore, it is so important to thoroughly accomplish the molecular characterization of intracellular niches committed to/occupied by mitochondria and comprehensively unravel the transcriptional and proteomic alterations leading to intramitochondrial dysfunctions and disturbances in intermitochondrial communication following the exposure of oocytes to the selected EACs. If such exposure to ectopic or environmental endocrine disruptors induces ultrastructural damage and cytophysiological incompetence of mitochondria, it may contribute to the rapid diminishment of oocyte quality and consequently to the depletion of the intraovarian reserve of female gametes and the progressive scarcity of meiotically competent oocytes retaining enhanced fertilizability [85–89] or capability to be reconstructed by SCNT [90–92].

In light of the above, our research hypothesis assumed that in porcine cumulus oocyte–complexes (COCs), Vnz, Ndn and CsA adversely affect the processes of growth and IVM, which might make them unsuitable for ARTs such as standard IVF by gamete co-incubation or microsurgical IVF by intracytoplasmic sperm injection (ICSI) and SCNT-based cloning. Thus, the aim of this study was to investigate the impacts of the selected EACs on parameters associated with the molecular quality of COCs subjected to the IVM procedure with the use of a three-dimensional (3D) culture model. A multi-faceted assessment of the molecular quality of 3D-IVM-generated COCs was carried out by estimating their transcriptional and proteomic profiles based on the induction of intracellular pro- and antiapoptotic pathways. To the best of our knowledge, the current investigation is the first to holistically demonstrate and exhaustively track the Vnz-, Ndn- and CsA-dependent mechanisms by which these endocrine disruptors can evoke rapid and robust alterations in transcriptional and proteomic signatures in porcine 3D-IVM-derived oocytes. The present research also provides, for the first time, a collective demonstration that genome- and proteome-wide scales of these alterations induce the strong multipath propagation of apoptotic cell death-related signals, irreversibly leading to a drastic attenuation of the molecular quality of pig oocytes subjected to extracorporeal meiotic maturation in the 3D model. Additionally, changes in the molecular quality of COCs undergoing IVM under 3D culture conditions were confirmed by identifying not only alterations in the cytosolic levels of cAMP but also the occurrence of ultrastructural transformations and late-apoptotic symptoms of internucleosomal DNA fragmentation in TUNEL-positive oocytes and surrounding CCs. Moreover, the current investigation sought to evaluate in detail

the Vnz-, Ndn- and CsA-mediated effects exerted on COCs' mitochondrial compartments, which were reflected in increases in: (1) defects in mitochondrion-specific morphology; (2) dysfunctions detected in mitochondrial activity and intraorganelle cytometabolic balance; (3) impairments in the distribution of mitochondria and interorganelle signal transduction (i.e., organelle interactions) between mitochondrial compartments; (4) disturbances in ATP production; and (5) dysregulations in the expression of mitophagy-related markers.

2. Results

2.1. Vinclozolin and Nandrolone Accelerate Apoptosis of Cumulus Cells

A TUNEL analysis was performed to examine genomic DNA fragmentation as an indicator of late apoptosis in porcine COCs exposed to Vnz, Ndn or CsA during IVM under 3D culture conditions (Figure 1). The presence of apoptotic cells (white arrows in panel A of Figure 1) was observed in the CCs stemming from COCs that represent all three experimental groups. However, the number of TUNEL-positive CCs increased significantly after exposure to Ndn (4.5% ± 0.97%) and Vnz (3.67% ± 0.41%). Compared to the control (CTR) group (1.79% ± 0.19%), these differences were statistically significant ($p < 0.05$ and $p < 0.01$, respectively) (Figure 1B).
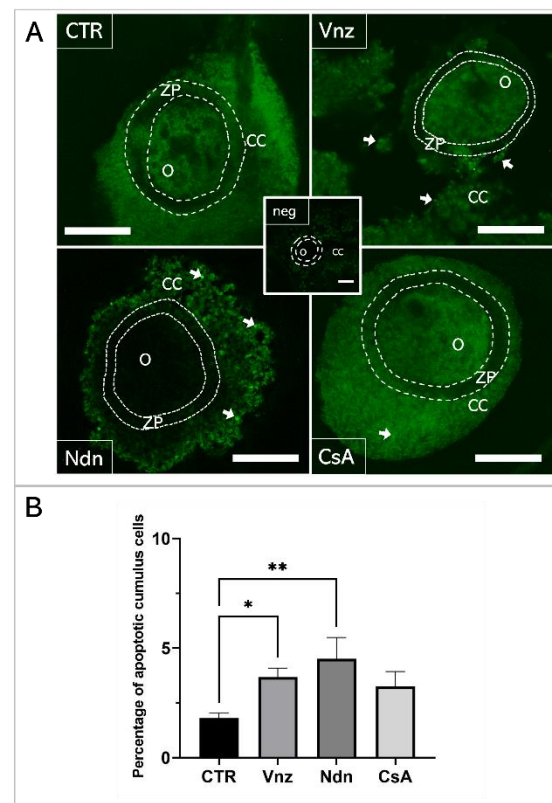
Figure 1. (**A**): TUNEL assay-mediated identification of the localization of late-apoptotic cells in porcine COCs subjected to the IVM procedure using a 3D culture model (alginate capsules). Representative images of COCs stemming from control (CTR) and experimental groups of 3D-IVM: in the presence of vinclozolin (Vnz), nandrolone (Ndn) or cyclosporin A (CsA). The contours of the oocytes are marked with dashed lines. White arrows indicate TUNEL-positive late-apoptotic cumulus cells (CCs) that fluoresced in bright green. A negative control was performed without active terminal deoxynucleotidyl transferase (TdT) enzyme (neg). O: oocyte; ZP: zona pellucida. All scale bars represent 100 μm (magnification 40×). (**B**): The results of the semi-quantitative TUNEL analysis. The results represent the mean value with $n = 9 \pm$ standard deviation (SD) for all experimental groups. Statistical analysis: homogeneity of variance—Brown–Forsythe test; normality of distribution—Bartlett's test and one-way ANOVA followed by Dunnett's post hoc test, * $p < 0.05$, ** $p < 0.01$.

2.2. Analysis of the Apoptosis Mechanism in 3D-IVM-Generated Cumulus–Oocyte Complexes Treated with the Selected Endocrine Disruptors

To thoroughly unravel the molecular nature of the increased incidence of programmed cell death in COCs subjected to Vnz, Ndn or CsA treatment, the Human Apoptosis Antibody Array kit was used to analyze the profiles of expression of apoptosis-related proteins. The obtained data showed that there were remarkable enhancements in the expression profiles of caspase-3 (CTR 10.9 ± 3.30, Vnz 22.9 ± 1.90, Ndn 22.8 ± 1.18, CsA 22.3 ± 1.02), tumor necrosis factor-β (TNF-β) (CTR 18.5 ± 0.91, Vnz 26.1 ± 0.42, Ndn 31.9 ± 0.27, CsA 28.8 ± 2.02), heat shock protein (HSP) 27 (CTR 2.4 ± 0.14, Vnz 6.9 ± 0.13, Ndn 15.2 ± 0.24, CsA 13.2 ± 1.68) and livin (CTR 7.0 ± 0.32, Vnz 32.8 ± 1.09, Ndn 11.6 ± 3.60, CsA 22.1 ± 1.42) (Figure 2A–D) in COCs derived from all of the experimental groups compared to CTR, while the expression levels of Bcl-2 and Bcl-w proteins were either downregulated in COCs derived from Ndn (4.7 ± 1.36 and 7.0 ± 0.84 respectively) and CsA (3.1 ± 0.14 and 5.3 ± 0.61 respectively) experimental groups or showed no significant impact ($p = 0.69$), as was observed for COCs derived from the Vnz group (5.7 ± 0.38 and 9.4 ± 2.30, respectively) (Figure 2E,F). Furthermore, the protein array analysis revealed that both Vnz (23.8 ± 1.68, 29.4 ± 5.62, 36.8 ± 4.01), Ndn (20.7 ± 0.87, 23.1 ± 1.48, 36.7 ± 3.55) and CsA (19.9 ± 0.81, 22.7 ± 1.42, 37.1 ± 0.05) brought about significant increases in p53, BIM and cytochrome c protein levels in COCs during the 3D-IVM procedure (Figure 3A,C,D). A statistically significant increase in the expression of Bad protein after exposure to Vnz (35.6 ± 4.39) or Ndn (28.0 ± 5.80) was also found, whereas the exposure of COCs to CsA (12.7 ± 1.59) gave rise to a decrease in the expression of this protein (Figure 3B). Thus, the observed enhancement of BIM protein expression with the simultaneous inhibition of Bcl-2 expression, which were accompanied by an increase in cytochrome c release from mitochondria, provides strong evidence for the predominant activation of the mitochondrial pathway of apoptotic cell death in the 3D-IVM-produced COCs undergoing treatment with the selected EACs.

2.3. Gene Expression of Main Apoptosis and Autophagy Mediators

Because the main executioner caspase, caspase-3, was mediated by both Vnz, Ndn and CsA in the protein array analysis, we next examined whether exposure of COCs to selected EACs during 3D-IVM also triggered the modification of caspase-3 expression at the gene level. According to the results acquired using the antibody array, we performed qRT-PCR to detect the expression of *CASP3* mRNA. The obtained results confirmed the significant upregulation of the *CASP3* gene in porcine COCs exposed to Vnz (1.4 ± 0.80) and Ndn (2.8 ± 0.27) during IVM under 3D culture conditions (Figure 4A).

Additionally, considering the finality/irreversibility of apoptosis induction and its consequences for proper oocyte maturation, it was beyond any doubt that these findings must be verified by exploring whether the selected EACs could promote cell survival in the autophagy process via potential interconnections between the apoptotic and autophagy-dependent pathways. For those reasons, qRT-PCR analysis for a pivotal biomarker of autophagy, the *LC3* gene (*MAP1LC3A*), was performed. Quantitatively estimating the relative abundance (RA) of mRNA transcribed from the *MAP1LC3A* gene proved a statistically significant increase ($p < 0.0001$) in the rates of RA of *LC3* transcripts among COCs subjected to 3D-IVM in the presence of CsA (6.9 ± 2.24) as compared to the CTR group. In turn, the quantitative profiles that were identified for *LC3* transcripts in COCs undergoing 3D-IVM and simultaneous treatment with either Vnz (2.2 ± 0.66) or Ndn (2.3 ± 0.12) trended upwards as compared to the control group, but this augmentation did not turn out to be statistically significant ($p = 0.51$ and $p = 0.42$, respectively) (Figure 4B).
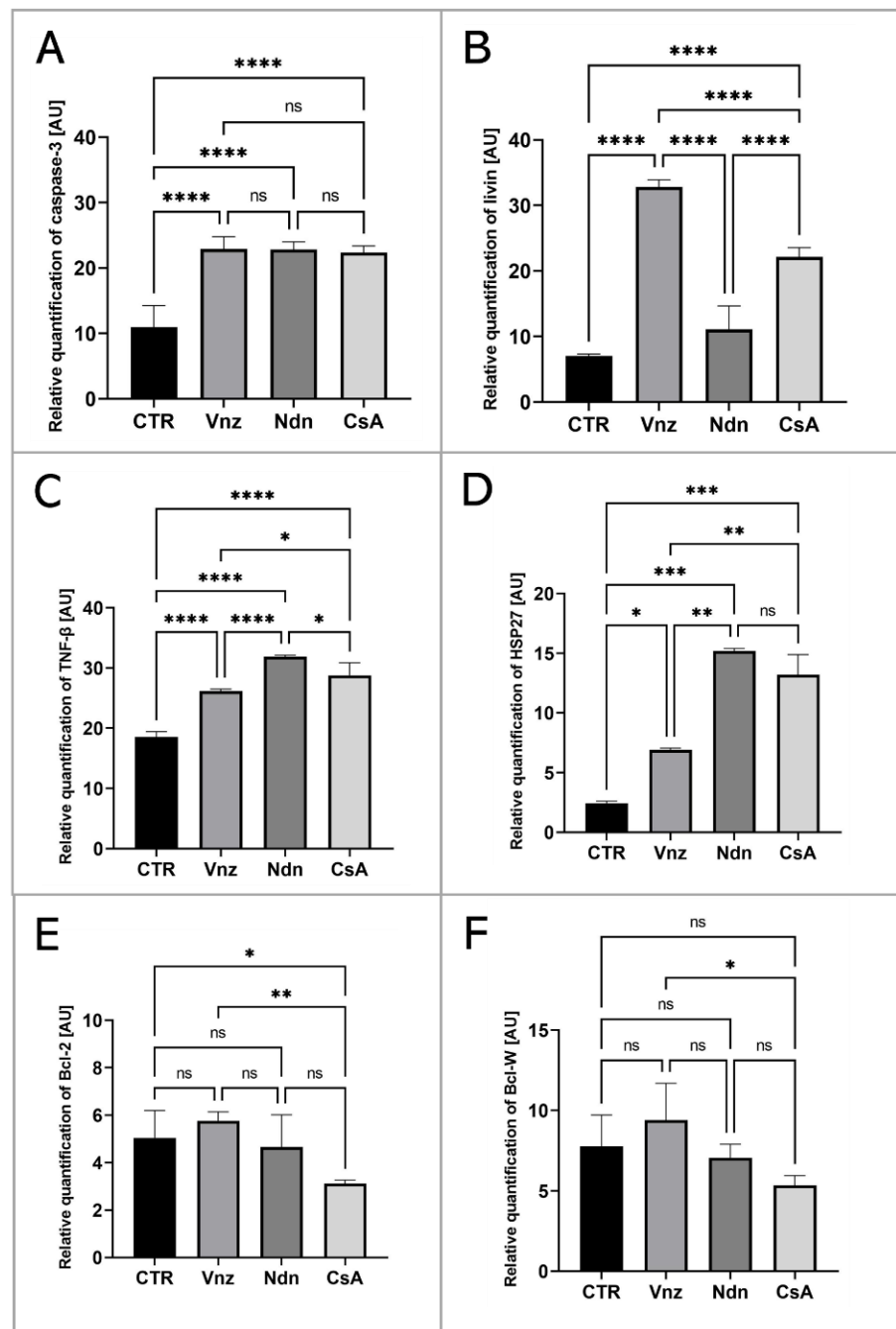
Figure 2. Apoptosis array analysis at the level of total protein in porcine COCs subjected to the IVM procedure using a 3D culture model (alginate capsules) in control cultures (CTR) or in experimental cultures: in the presence of vinclozolin (Vnz), nandrolone (Ndn) or cyclosporin A (CsA). The graphs show the relative content of caspase 3 (**A**), livin (**B**), TNF-β (**C**), HSP27 (**D**), Bcl-2 (**E**) and Bcl-w (**F**) proteins obtained from measurements of the optical density of the spots representing a specific signal after normalization against the positive control. Results represent the mean with $n = 5 \pm$ standard deviation (SD); each "n" consisted of 200 COCs. Statistical analysis: homogeneity of variance—Brown–Forsythe test; normality of distribution—Bartlett's test and one-way ANOVA followed by Dunnett's post hoc test, * $p < 0.05$, ** $p < 0.01$, *** $p < 0.001$, **** $p < 0.0001$; ns-non—significant.
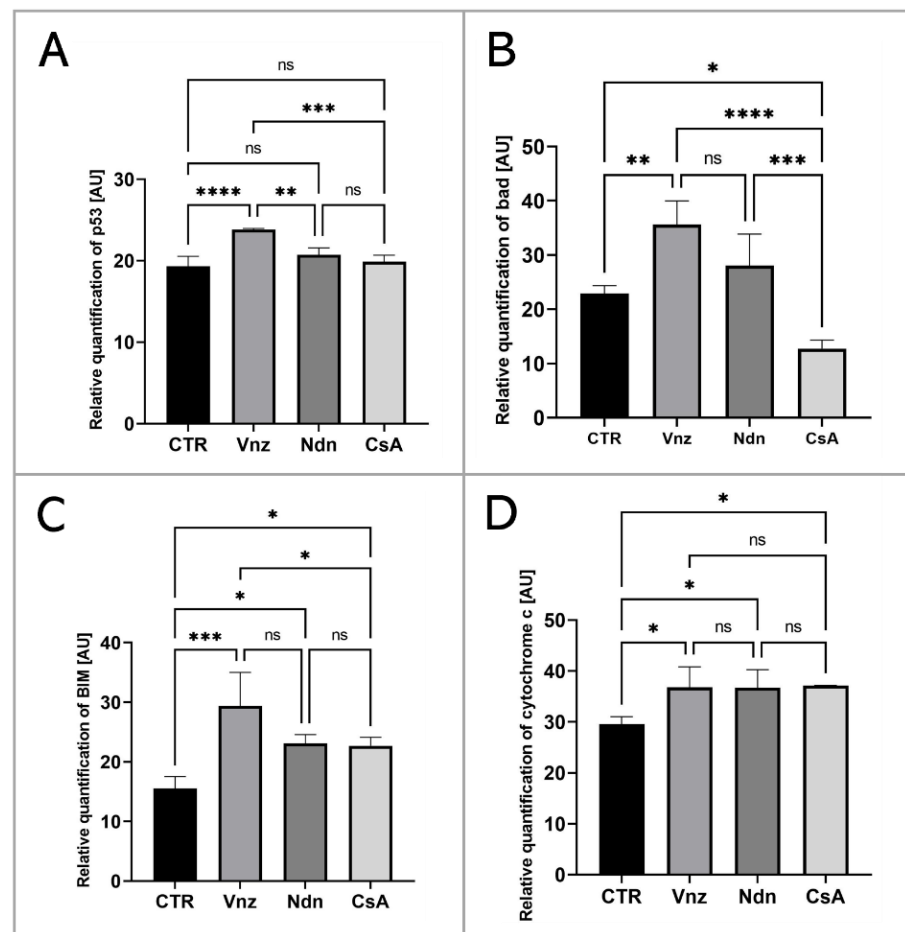
Figure 3. Analysis of the expression of proteins involved in the activation of the mitochondrial pathway of apoptosis at the level of total protein (apoptosis antibody array k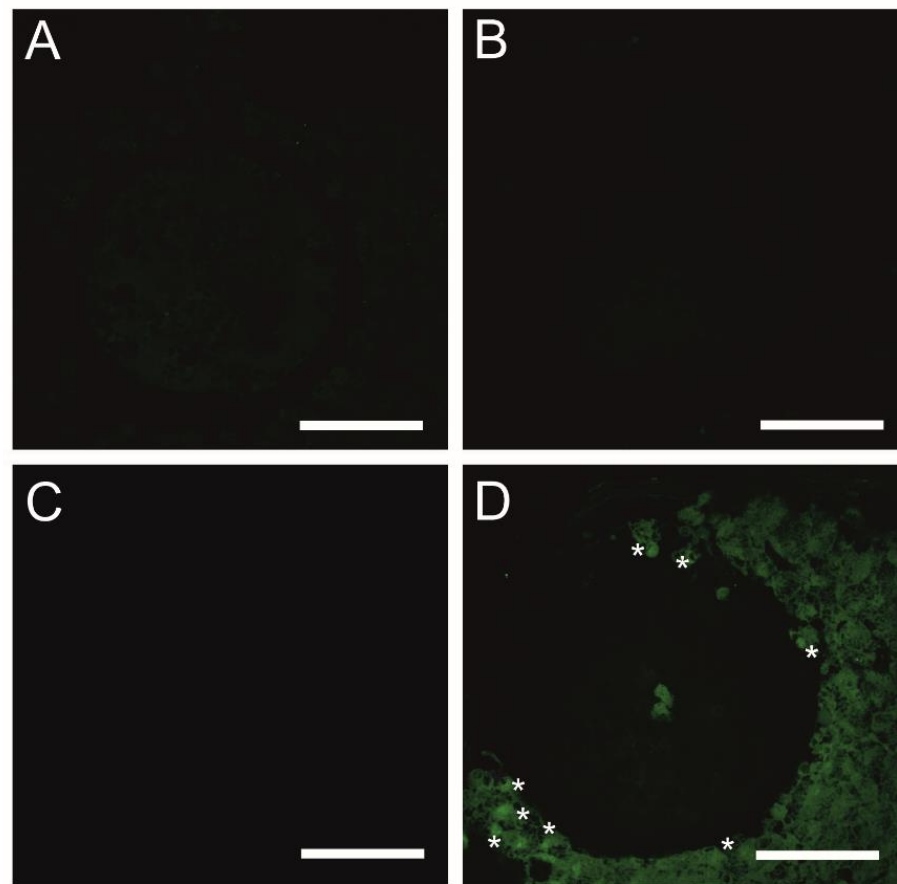it) in porcine COCs subjected to the IVM procedure using a 3D culture model (alginate capsules) in control cultures (CTR) or in experimental cultures: in the presence of vinclozolin (Vnz), nandrolone (Ndn) or cyclosporin A (CsA). The graphs show the relative content of p53 (**A**), bad (**B**), BIM (**C**) and cytochrome c (**D**) proteins obtained from measurements of the optical density of the spots representing a specific signal after normalization against the positive control. Results represent the mean with $n = 5 \pm$ standard deviation (SD); each "*n*" consisted of 200 COCs. Statistical analysis: homogeneity of variance—Brown–Forsythe test; normality of distribution—Bartlett's test and one-way ANOVA followed by Dunnett's post hoc test, * $p < 0.05$, ** $p < 0.01$, *** $p < 0.001$, **** $p < 0.0001$; ns—nonsignificant.

The results obtained by quantitatively estimating *LC3* mRNA expression were confirmed by COC ultrastructure analysis (TEM). Numerous late autophagosomes (LAs) were found to occur in the cytoplasm of 3D-IVM-produced oocytes exposed to CsA. LAs contained partially or completely degraded organelle material, which was characterized by a higher electron density than the cytoplasm surrounding the autophagosome. The aforementioned material was most frequently recognizable as mitochondria and peroxisomes (Figure 4C). A lot of early autophagosomes (EAs) were also found to contain ultrastructurally intact cytoplasm that seemed to be identical to the surrounding cytoplasm (Figure 4D). It is noteworthy that the presence of EAs was shown in the cytoplasm of 3D-IVM-generated oocytes derived from Vnz- or Ndn-treated groups.
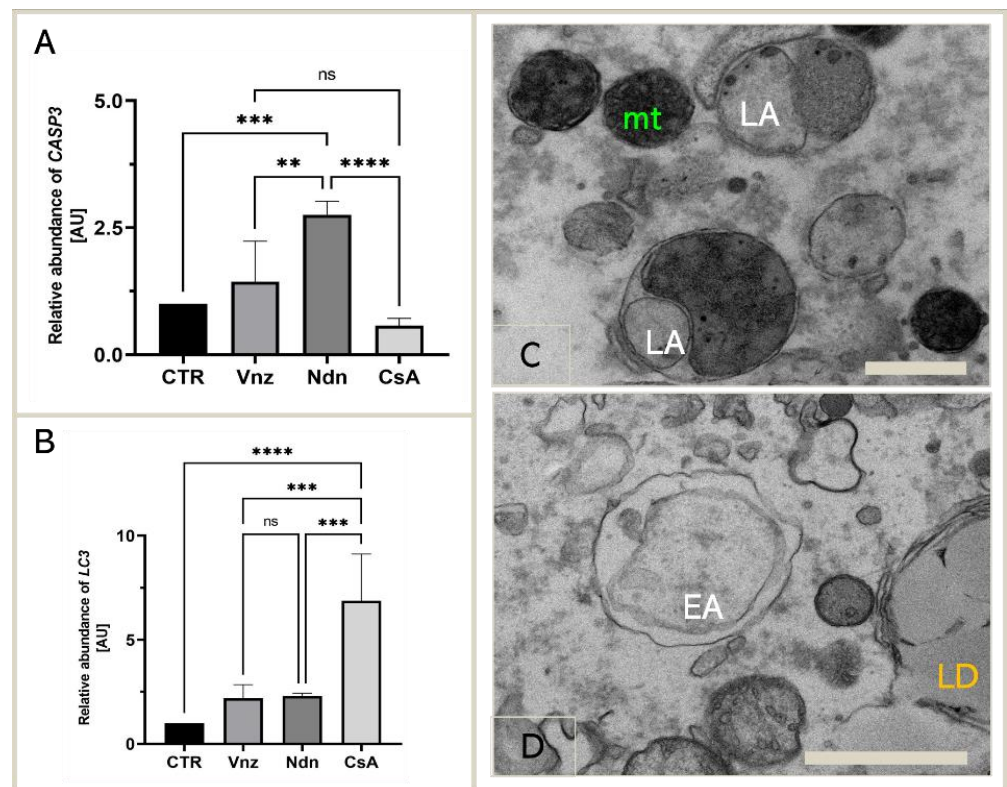
Figure 4. Expression of genes coding for apoptosis and autophagy mediators: CASP3 (**A**) and LC3 (**B**) in porcine COCs subjected to the IVM procedure using a 3D culture model (alginate capsules) in control cultures (CTR) or in experimental cultures: in the presence of vinclozolin (Vnz), nandrolone (Ndn) or cyclosporin A (CsA), shown by RT-qPCR at the transcript level. The results are presented as mean values with $n = 5 \pm$ standard deviation (SD); each "n" consisted of 50 COCs. Statistical analysis: homogeneity of variance—Brown–Forsythe test; normality of distribution—Bartlett's test and one-way ANOVA followed by Dunnett's post hoc test, ** $p < 0.01$, *** $p < 0.001$, **** $p < 0.0001$; ns— nonsignificant. (**C**): The ultrastructure of late autophagosome (LA) in oocytes maturing in vitro in the presence of CsA; scale bars represent 400 nm. (**D**): The ultrastructure of early autophagosome (EA) in oocytes maturing in vitro in the presence of Ndn; scale bars represent 900 nm. mt: mitochondria; LD: lipid droplets.

2.4. Cyclosporin A Induces Mitophagy in COCs Undergoing IVM under 3D Culture Conditions

As presented in Figure 5A, the fluorescent image of COCs in the CTR shows that mitophagy was not detected, whereas mitophagy was identified in COCs exposed to CsA during IVM under 3D culture conditions. The identification of mitophagy was reflected in the fusion of lysosomes and the mitochondria (Figure 5D). In COCs treated with Vnz and Ndn, there was no colocalization of mitochondria and lysosomes, which remarkably confirms the lack of mitophagy induction (Figure 5B,C).

Figure 5. Detection of mitophagy in porcine COCs subjected to the IVM procedure using a 3D culture model (alginate capsules) in control cultures (**A**) or in experimental cultures: in the presence of vinclozolin (**B**), nandrolone (**C**) or cyclosporin A (**D**). White asterisks indicate colocalization of lysosome and mitochondrion. Scale bars represent 50 μm (magnification 40×).

2.5. Analysis of Cellular Metabolism in 3D-IVM-Generated COCs Treated with the Selected Endocrine Disruptors

To assess the effects of the selected EACs on cellular metabolism in 3D-IVM-derived COCs, the analysis of mitochondria distribution and activity in both CCs and oocytes was performed. Comprehensive efforts were also undertaken to evaluate mitochondrial ultrastructure and explore vital mitochondrial activity in oocytes undergoing exposure to the selected EACs during 3D-IVM. Moreover, quantitative estimation of the transcriptional activities of a panel of genes that encode the ATP synthase subunit (*ATP5A1*) and are involved in the process of scavenging free radicals (*SIRT3* and *FOXO3*) was performed. Additionally, measurements aimed at ascertaining the intracytoplasmic levels of glutathione (GSH) were made.

2.5.1. Analysis of the Distribution and Ultrastructure of Mitochondria in COCs Subjected to 3D-IVM in the Presence of Selected EACs

MitoTracker™ Orange CM-H2TMRos (MtOR) fluorescence staining was used to both visualize the distribution of mitochondria (mt) in CCs and analyze the mitochondrial membrane potential. The results obtained from the fluorescence signal analysis for MtOR detection were compared with the results of the mt ultrastructure analysis using the transmission electron microscope (TEM) (Figure 6).
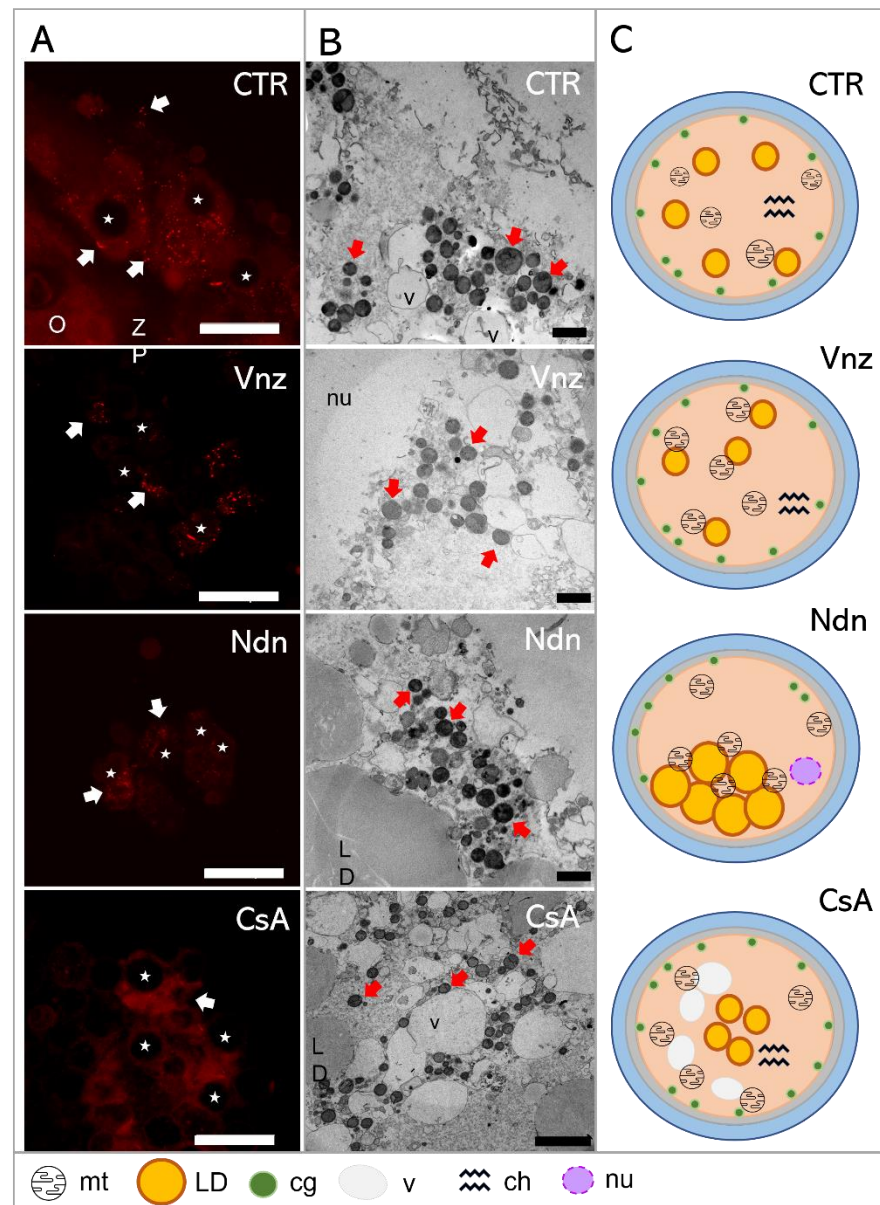
Figure 6. (**A**): Representative images of MitoTracker Orange CM-H2TMRos-positive mitochondrial distribution in porcine CCs subjected to the IVM procedure using a 3D culture model (alginate capsules) in control cultures (CTR) or in experimental cultures: in the presence of vinclozolin (Vnz), nandrolone (Ndn) or cyclosporin A (CsA). (**B**): Transmission electron micrographs of ultrastructure in porcine oocytes subjected to the IVM procedure using a 3D culture model in CTR or in the presence of Vnz, Ndn or CsA. (**C**): A diagram summarizing the results of the ultrastructure analysis of the oocyte and the distribution of organelles in their ooplasm after the completion of 3D-IVM in the presence of selected EACs. O—oocyte; ZP—zona pellucida; LD—lipid droplets; v—vacuole; cg—cortical granules; nu—nucleus; red arrows—mitochondria; stars—nuclei of CCs. Scale bars represent 1000 nm. MtOR magnification 60×.

Based on the observed strong intensity of the fluorescence reaction, high activities of mitochondria in both the cumulus cells and oocyte-specific compartments were confirmed among the 3D-IVM-produced COCs derived from the CTR group (Figure 6A). Generally, the mitochondria of the CCs representing the CTR group were evenly distributed (homogenously dispersed) throughout the cytoplasm. However, in CCs directly adjacent to the oocyte, polar localization of these organelles was found. A vast majority of mt were focused in the pole adjacent to the oocyte, in which mt were concentrated close to the

zona pellucida and in the immediate proximity of numerous lipid droplets (Figure 6B). This provides strong evidence for the occurrence of both a cytophysiological network of reciprocal interrelations and functional cooperation between CCs and oocytes and the exchange of substances indispensable to achieve the developmental competence of oocytes (Figure 6C).

In COCs undergoing 3D-IVM in the presence of Vnz, the most intense fluorescence signals for MtOR were found as compared to the other experimental groups and CTR (Figure 6A). In the vast majority of CCs, mitochondria were characterized by perinuclear location; however, in a few cases, mitochondria were focused similarly to those from the control group—at the pole facing the oocyte. Ultrastructural analysis of oocytes from the Vnz group revealed the central location of mostly round mitochondria with a bright matrix (Figure 6B,C).

Among 3D-IVM-derived COCs exposed to Ndn, a significantly weaker fluorescence signal for MtOR was found, which proves the lower activity of mt (Figure 6A). In cumulus cells, mitochondria were located unevenly in the form of single clusters within the cytoplasm. The oocyte mitochondria were small and round with a dark matrix. They were also unevenly distributed between the large lipid droplets (Figure 6B,C).

Porcine COCs subjected to the 3D-IVM procedure in the presence of CsA displayed an even, strong fluorescence signal for MtOR in the cytoplasm of cumulus cells, which proves their high activity (Figure 6A). The distribution of mt in CCs adjacent to the oocyte was polar: i.e., mt were concentrated on the pole facing the oocyte. Ultrastructural analysis of oocytes originating from the CsA group revealed an even, subcortical distribution of mt, which colocalized with numerous vacuoles. The mitochondria were round with a single mitochondrial crest (Figure 6B,C).

2.5.2. The Live Cell-Based Analysis of Mitochondrial Activity in 3D-IVM-Derived COCs Treated with the Selected Endocrine Disruptors

To measure the mitochondrial activity in live cells, the COCs were subjected to the IVM procedure with Seahorse XFp PDL Cell Culture Miniplates under the influence of selected EACs. The Seahorse XF Cell Mito Stress Test was used to analyze ATP production and proton leak in COCs from both CTR and experimental groups (Vnz, Ndn and CsA). In all experimental groups, there was a decline in the level of ATP production (Figure 7A) as compared to CTR (43.0 ± 8.52). The highest decrease was observed in the subpopulations of 3D-IVM-generated COCs exposed to Ndn (3.8 ± 2.98; $p < 0.0001$). At the same level of statistical significance (17.4 ± 1.41; $p < 0.0001$), a diminishment in ATP production was observed for COCs subjected to 3D-IVM in the presence of CsA. In turn, porcine COCs that underwent 3D-IVM and simultaneous Vnz (31.3 ± 3.58) treatment exhibited a reduction in ATP biosynthesis as compared to CTR at a significance level of $p < 0.01$.

A high increase in proton leak (Figure 7B) was found in COCs undergoing 3D-IVM in the presence of Vnz (11.8 ± 1.36). Compared to the control group, this difference was statistically significant ($p < 0.001$). The extent of proton leak in porcine COCs subjected to 3D-IVM and simultaneously exposed to either Ndn (3.1 ± 0.78) or CsA ($3.2 \pm \underline{0}.73$) was proven to be 2-fold lower than that estimated for the CTR group (8.1 ± 1.25). This decline turned out to be statistically significant ($p < 0.0001$).

To confirm whether and to what extent the selected EACs bias the efficiency of the ATP synthesis process, the quantitative profile of mRNA transcribed from the *ATP5A1* gene encoding for the ATP catalytic synthase subunit was examined. The results are depicted in Figure 7C. Quantitatively analyzing the RA identified for *ATP5A1* mRNA revealed its 7-fold increase in 3D-IVM-produced COCs treated with Vnz (6.7 ± 2.28) as compared to CTR. This intergroup variability was statistically significant ($p < 0.0001$). In contrast, there were no statistically significant differences ($p = 0.63$ and $p = 0.24$) in the levels of *ATP5A1* mRNA expression in 3D-IVM-derived COCs cultured under the conditions of either Ndn (2.1 ± 0.46) or CsA (2.7 ± 0.81) treatments as compared to the EAC-untreated group.
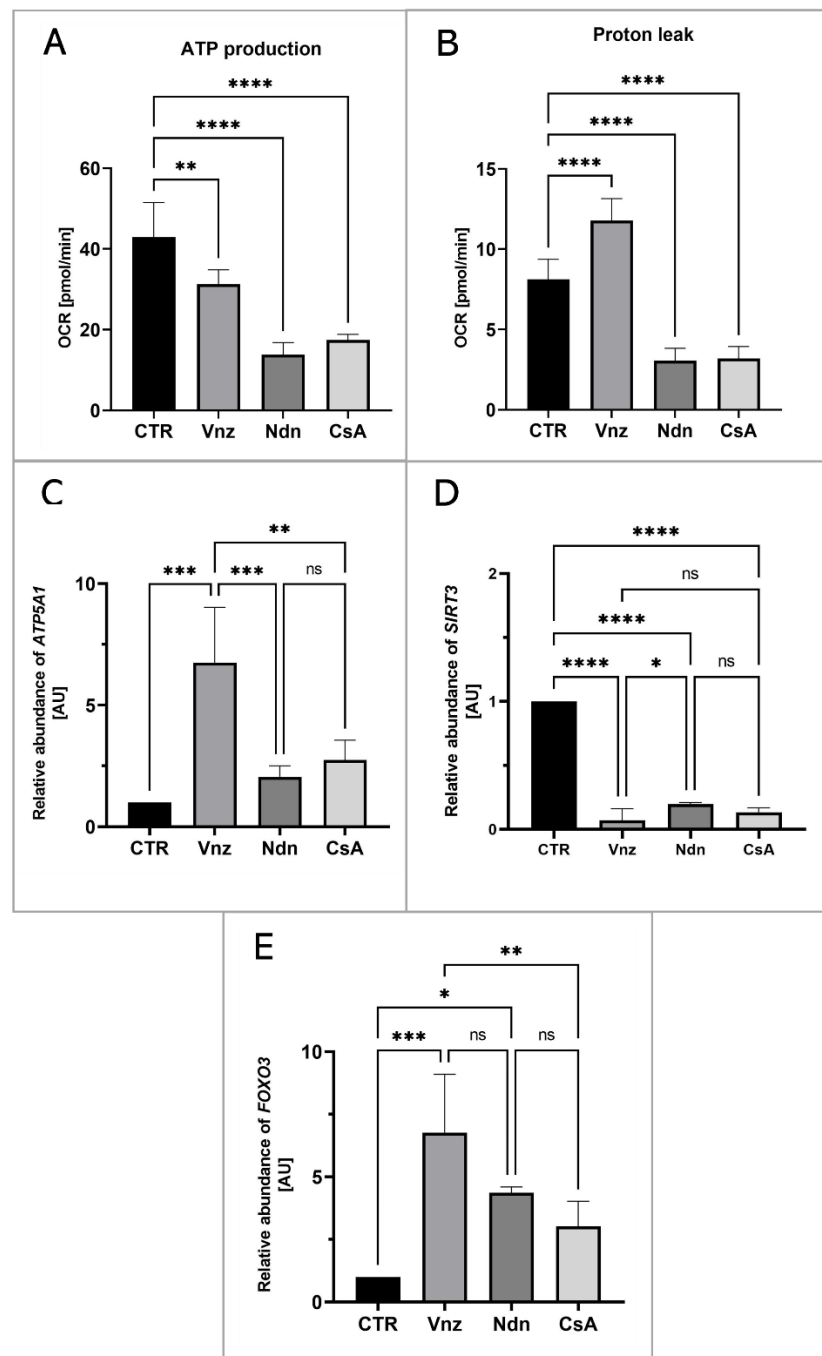
Figure 7. The live cell-based analysis of mitochondrial activity in porcine COCs subjected to the IVM procedure using a 3D culture model (alginate capsules) in control cultures (CTR) or in experimental cultures: in the presence of vinclozolin (Vnz), nandrolone (Ndn) or cyclosporin A (CsA). (**A**): ATP synthesis level analysis performed with the aid of Seahorse XF Cell Mito Stress Test; (**B**): proton leak analysis performed with the aid of Seahorse XF Cell Mito Stress Test; the results represent the mean value with $n = 5 \pm$ standard deviation (SD), and each "n" consisted of 12 COCs. Statistical analysis: homogeneity of variance—Brown–Forsythe test; normality of distribution—Bartlett's test and one-way ANOVA followed by Dunnett's post hoc test, ** $p < 0.01$, **** $p < 0.0001$. (**C–E**): Quantitative profiles for expression of *ATP5A1*, *SIRT3* and *FOXO3* genes, shown by RT-qPCR at the transcript level. The results represent the mean value with $n = 5 \pm$ standard deviation (SD), and each "n" consisted of 50 COCs. Statistical analysis: homogeneity of variance—Brown–Forsythe test; normality of distribution—Bartlett's test and one-way ANOVA followed by Dunnett's post hoc test, * $p < 0.05$, ** $p < 0.01$, *** $p < 0.001$, **** $p < 0.0001$; ns—nonsignificant.

Additionally, in order to assess whether the selected EACs used in the presented studies activate the cell's defense mechanisms against ROS, the rates of RA observed for mRNA transcripts that are synthesized from genes involved in scavenging ROS were estimated. The following genes were selected for the analyses: (1) *SIRT3* encoding the sirtuin 3 protein, which is localized in mitochondria and is responsible for the elimination of ROS, and (2) *FOXO3* encoding the FOXO transcription factor, which, together with sirtuin 3, contributes to enhancing the antioxidative activity of mitochondria. As is depicted in Figure 7D, the analysis of the mRNA expression level for the *SIRT3* gene revealed its nearly 10-fold decrease in all experimental groups (Vnz 0.1 ± 0.09, Ndn 0.2 ± 0.01, CsA 0.1 ± 0.03) as compared to the CTR counterpart. This difference was shown to be statistically significant ($p < 0.0001$). In contrast, the analysis of the mRNA level quantified for the *FOXO3* gene (Figure 7E) showed its increase in all experimental groups as compared to CTR. In COCs subjected to 3D-IVM in the presence of Vnz, this increase was 7 times higher (6.8 ± 2.34) than in CTR. The difference was statistically significant ($p < 0.001$). In 3D-IVM-generated COCs treated with Ndn, the determined mRNA level was 5 times higher (4.4 ± 0.23) than in CTR, and the difference between these values turned out to be statistically significant ($p < 0.01$). In COCs undergoing exposure to CsA (3.0 ± 1.00) during 3D-IVM, the observed increase in the quantitative profile of *FOXO3* transcripts was statistically insignificant ($p = 0.17$).

2.5.3. Quantitative Analysis of Intracytoplasmic Glutathione Concentration in 3D-IVM-Generated COCs Treated with the Selected Endocrine Disruptors

To assess the influence of the selected EACs on the COCs' intracytoplasmic concentration of glutathione (GSH), its abundance in the isolated total protein was measured. Based on the obtained results, a decrease in the GSH intracytoplasmic concentration was recognized in all experimental groups as compared to the level of 1.7 ± 0.24 µM/mL estimated for the CTR group. In COCs subjected to 3D-IVM in the presence of Vnz, Ndn and CsA, the GSH concentrations reached levels as follows: 0.4 ± 0.09 µM/mL, 0.3 ± 0.16 µM/mL and 0.2 ± 0.02 µM/mL. The differences between the experimental and CTR groups were found to be statistically significant ($p < 0.0001$) (Figure 8A).
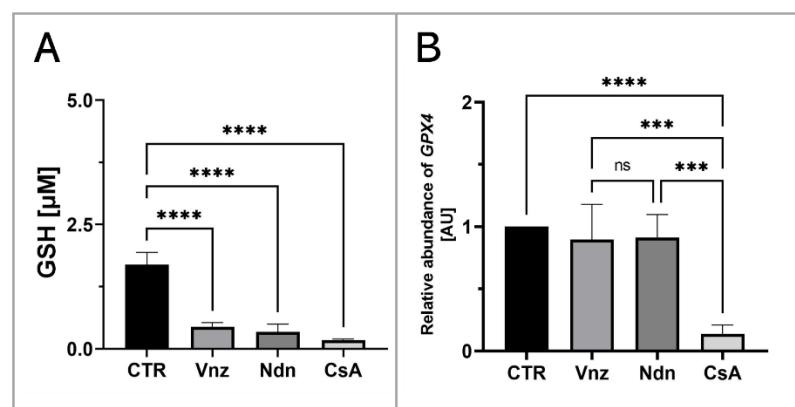
Figure 8. Quantitative analysis of intracytoplasmic glutathione concentration (**A**) and *GPX4* gene (**B**) shown by RT-qPCR at the transcript level in porcine COCs subjected to the IVM procedure using a 3D culture model (alginate capsules) in control cultures (CTR) or in experimental cultures: in the presence of vinclozolin (Vnz), nandrolone (Ndn) or cyclosporin A (CsA). The results are presented as mean values with $n = 5 \pm$ standard deviation (SD), and each "*n*" consisted of 50 COCs. Statistical analysis: homogeneity of variance—Brown–Forsythe test; normality of distribution—Bartlett's test and one-way ANOVA followed by Dunnett's post hoc test, *** $p < 0.001$, **** $p < 0.0001$; ns—nonsignificant.

Additionally, to examine whether the observed decrease in the intracytoplasmic concentration of GSH might be a result of the intensive process of eliminating ROS, the rate of RA was estimated for mRNA transcribed from the *GPX4* gene encoding glutathione

peroxidase 4, which is responsible for the reduction of, among others, lipid peroxides. Ascertaining the quantitative profile of *GPX4* transcripts confirmed their almost 10-fold decrease (0.1 ± 0.07) in 3D-IVM-derived COCs exposed to CsA as compared to CTR. This diminishment turned out to be statistically significant ($p < 0.0001$). No statistically significant changes ($p = 0.83$ and $p = 0.9$) in the levels of mRNA transcripts identified for the *GPX4* gene were shown in the subpopulations of COCs undergoing 3D-IVM in the presence of Vnz (0.9 ± 0.28) or Ndn (0.9 ± 0.18) (Figure 8B).

2.6. Analyzing the Extent of Meiosis/Maturation Progression in Oocytes Treated with the Selected Endocrine Disruptors during IVM Procedure under 3D Culture Conditions

In order to assess the influence of the selected EACs on the oocyte maturation process, the RAs of mRNA molecules that were biosynthesized as a result of transcriptional activities of genes encoding regulatory and biocatalytic subunits of a heterodimeric meiosis/maturation-promoting factor, designated as *CCNB1* (cyclin B1) and *CDC2* (cyclin-dependent kinase 1), were ascertained. The quantification of mRNA expression for the *CCNB1* gene showed its almost 15-fold increase in COCs subjected to 3D-IVM in the presence of Vnz (14.1 ± 4.59) as compared to the CTR group. This intergroup variability was statistically significant ($p < 0.0001$). In turn, no statistically significant changes ($p = 0.99$ and $p = 0.93$) within the quantitative profiles of mRNA transcripts identified for the *CCNB1* gene were observed in 3D-IVM-derived COCs exposed to Ndn (0.7 ± 0.31) or CsA (undetectable) (Figure 9A). Interestingly, quantitatively analyzing the RA of *CDC2* mRNAs revealed their significant decrease in all experimental groups (Vnz = 0.002 ± 0.002, Ndn = 0.6 ± 0.14, CsA = 0.012 ± 0.003) as compared to CTR ($p < 0.0001$) (Figure 9B).
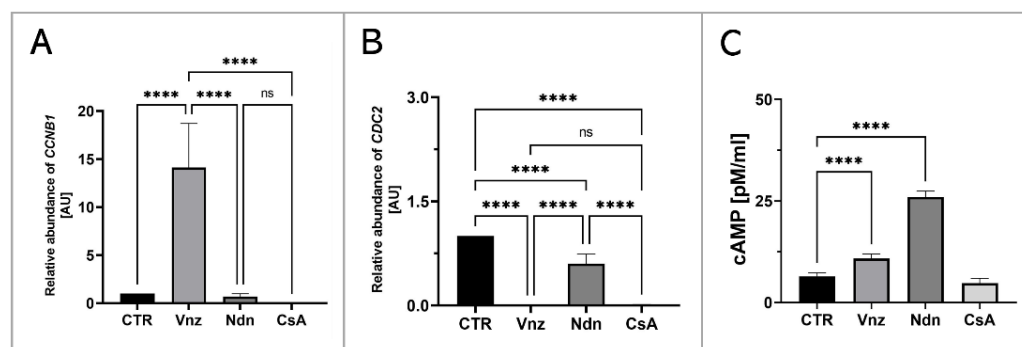
Figure 9. Analysis of the extent of meiosis/maturation progression in porcine COCs subjected to the IVM procedure using a 3D culture model (alginate capsules) in control cultures (CTR) or in experimental cultures: in the presence of vinclozolin (Vnz), nandrolone (Ndn) or cyclosporin A (CsA). (**A**,**B**): Quantitative profiles estimated for expression of *CCNB1* and *CDC2* genes, shown by RT-qPCR at the transcript level. The results are presented as mean values with $n = 5 \pm$ standard deviation (SD), and each "n" consisted of 50 COCs. (**C**): Analysis of intracytoplasmic cAMP concentration. Statistical analysis: homogeneity of variance—Brown–Forsythe test; normality of distribution—Bartlett's test and one-way ANOVA followed by Dunnett's post hoc test, **** $p < 0.0001$; ns—nonsignificant.

Additionally, to assess the effect of the selected EACs on the level of 3′,5′-cyclic AMP (cAMP), its concentration in the isolated total protein was determined using protein extracts stemming from the 3D-IVM-generated COCs (Figure 9C). Based on the obtained results, the highest concentration of cAMP of 26 ± 1.43 pM/mL was found in 3D-IVM-derived COCs cultured in the presence of Ndn. There was a statistically significant difference ($p < 0.0001$) in the measured cAMP concentrations between Ndn-treated and untreated (6.4 ± 0.88 pM/mL) subpopulations of COCs undergoing 3D-IVM. In COCs cultured in the 3D-IVM model and simultaneously treated with Vnz, a cAMP concentration of 10.8 ± 1.12 pM/mL was estimated. The difference in the measured cAMP levels between Vnz and CTR groups was statistically significant ($p < 0.0001$). Exposure of porcine COCs to CsA during 3D-IVM did not cause the occurrence of statistically significant changes

(p = 0.054) in the level of cAMP (4.7 $\pm$ 1.12 pM/mL) as compared to CsA-unexposed subpopulations of COCs.

3. Discussion

So far, the direct consequences of long-term exposure to the EACs/EDCs tested in the current study, which might lead to the disturbed regulation of mammalian oocyte maturation, have not been precisely recognized. The research undertaken by our team allowed us to obtain completely new information about the possible negative impacts of the selected endocrine disruptors (Vnz, Ndn and CsA) on the quality of oocytes, which determines the reproductive success of females dependent on efficiently terminating meiotic maturation under not only in vivo physiological conditions but also ex vivo conditions associated with experimental and applied embryology and ART strategies, including the IVM procedure. The concentration of Vnz in the aquatic environment obviously directly influences the fish living there. This is especially true of the disrupted development of their reproductive system. Taking this finding into consideration, decreased egg production and progressive degeneration of oocytes have been found in females of the *Pimephales promelas* species [93]. In turn, in *Oryzias latipes*, the termination of oogenesis at its early stages (i.e., pre-vitellogenesis and initial stages of vitellogenesis) was proven by the results of investigations by Kiparissis et al. [5]. As a consequence of the increased concentration of Vnz in the aquatic environment, both augmented concentration of testosterone in blood plasma and a reduction in ovarian weight in relation to the total body weight in adult *Pimephales promelas* females were shown by Makynen et al. [94]. Of particular interest, an increased bioconcentration of this fungicide in the tissues of females was observed compared to males of this species, which may be related to the different contents of lipids in the two sexes. In mammals, the influence of Vnz on the development and functioning of the female and male reproductive systems has also been confirmed. For example, administration of Vnz to pregnant female rats triggered developmental disorders of the reproductive system in male and female embryos, which was a transgenerational effect. In male rats, an increased incidence of apoptosis in spermatogonia, together with lower sperm counts and diminished motility, was identified [95]. On the other hand, in female rats, Vnz determined the course of pregnancy in subsequent generations (anemia of pregnant animals and intrauterine hemorrhage). There was also progressive feminization of male embryos and masculinization of female ones [96]. As for the direct negative impact of Vnz on the human body, a negative correlation has been demonstrated between the high concentrations of pesticides, including Vnz (3000 g/ha of arable land) in surface waters, and the reduced quality of oocytes in women living in the northern part of France in Picardy [97].

Our present investigations carried out on 3D-IVM-derived COCs treated with Vnz show, for the first time, that Vnz induces the apoptosis of cumulus cells by enhancing the expression of p53, Bad and caspase 3 proteins, which gives rise to the internucleosomal biodestruction of the nuclear genome. These findings are supported by observations obtained previously with the use of whole porcine follicles exposed to Vnz [10]. The p53 protein directly activates the transcription of the *FOXO3* gene in response to DNA damage and brings about the promotion and progression of apoptotic cell death [98]. This is consistent with the results achieved in our study, which were confirmed by the increased RA of *FOXO3* mRNA in COCs maturing in the presence of Vnz. In turn, FOXO3 is responsible for the induction of apoptosis through interactions with the BIM protein, which is associated with the mitochondrial pathway of apoptosis [99]. Research undertaken by Obexer et al. [100] and Hagenbuchner et al. [101] demonstrated that intramitochondrial accumulation of ROS in human neuroblastoma cells contributes to the fusion of FOXO3 with the BIM protein, which, in turn, evokes mPTP opening and subsequently cytochrome c leakage. This mechanism also appears to be prompted in response to the action of Vnz in CCs. The intensified occurrence of late-apoptotic symptoms in CCs correlates with a decreased fertilization rate and, consequently, attenuated quality of human IVF-

derived embryos [102]. The use of protein microarrays showed a significant increase in the expression of the livin protein, which belongs to the family of proteins that inhibit apoptosis [103]. Its action is based on blocking the extrinsic apoptotic pathway, regulated by the Fas/FasL pathway [104] and TNF-β [103]. The p53 protein, which imitates the function of a transcription factor for the receptors involved, is also engaged in the activation of this pathway [105]. Enhanced expression of livin in 3D-IVM-generated COCs exposed to Vnz, which was identified in our current study, may indicate the onset of cell defense mechanisms against apoptosis caused by the action of this fungicide.

The analysis aimed at examining the influence of Vnz on mitochondria revealed that this endocrine disruptor induced the augmentation of the quantitative profile of mRNA transcribed from the *ATP5A1* gene encoding the ATP synthase subunit. This result is also reflected in the level of ATP produced and in the intensity of MtOR staining. The significant increase in the level of proton leak seems to be interesting, which indicates damage to the mitochondrial membrane [106] and is associated with the generation of ROS [107]. The loss of integrity within the ultrastructure of the mitochondrial membrane leads to a decrease in the membrane potential and, consequently, to the dwindling of ATP levels [108]. Elevated ROS concentration is one of the factors that promote the necrosis process in murine embryonic fibroblasts [109,110], and as has been shown in our previous studies [11], Vnz can also induce pro-necrotic alterations in granulosa cells in porcine ovarian follicles. Additionally, a high level of ROS in the oocyte initiates germinal vesicle breakdown (GVBD); however, the extrusion of the polar body into perivitelline space is blocked [111]. Immediately before GVBD, there is a sudden increase in ATP levels [112], which was observed during the Seahorse XFp analysis. On the other hand, an elevated concentration of cyclin B accelerates the disintegration of the germinal vesicle due to premature activation of MPF [113]. All of these findings provide strong evidence that treatment of porcine COCs with Vnz results in a considerable diminishment of their molecular quality by promoting proapoptotic changes in CCs and expediting GVBD processes within oocytes.

A panel of the presented studies focused on the 3D-IVM of COCs undergoing exposure to Ndn indicated the rapid increase in the intraooplasmic cAMP concentration. Perpetuation of a high intracytosolic concentration of cAMP is a pivotal biomarker of the inhibition of the process of nuclear maturation of the oocyte, which arises from blocking the resumption of meiosis I [114,115]. The analysis of the oocyte ultrastructure revealed the accumulation of large (>3 μm) lipid droplets (LDs) in the oocyte, which are irregularly distributed in the cytoplasm. Even though the presence of many LDs is one of the factors determining the increased developmental competence of the oocyte [70,116], the occurrence of intracytoplasmic lipid droplets exhibiting such morphology and distribution is characteristic of immature oocytes [117]. The extensive and nonspecific storage of lipid droplets in the cytoplasm of oocytes subjected to 3D-IVM in the presence of Ndn could explain the observed low level of ATP synthesis in COCs. Taking into account the enhanced intraooplasmic accumulation of LDs and the corresponding decline in mitochondrial activity that were proven in our current investigation, the results of the studies by He et al. [118], in which LD accumulation in response to intramitochondrial metabolic quiescence was identified, seem to be particularly interesting. Moreover, oocytes grown in melatonin-supplemented medium also displayed intracytoplasmic accumulation of LDs at one pole [118]. The authors of the research undertaken to empirically explore the molecular nature of human hepatocarcinoma-derived cell lines (HepG2) hypothesized that nandrolone, by inhibiting complex III (i.e., cytochrome complex) in the respiratory/electron transport chain, brings about the promotion of intracellular antioxidative events. These events give rise to the rapid elimination of ROS in HepG2 cells [34]. In turn, the drastically dwindling of the concentration of ROS that arises from their scavenging promotes the dormancy of healthy or cancerous stem cells [34]. For that reason, additional extensive studies should be performed to confirm whether such a mechanism is activated in oocytes during their IVM. Moreover, it appears to be of great importance to examine the relationship between β-oxidation of fatty acids and glucose metabolism in COCs.

A panel of TUNEL-based investigations demonstrated that the highest percentage of late-apoptotic cumulus cells occurred in COCs subjected to 3D-IVM in the presence of nandrolone. The results obtained with the use of protein microarrays confirmed the proapoptotic effect of Ndn. Ndn has been shown to enhance the expression of caspase 3 at both mRNA and protein levels. These findings are consistent with those achieved in the study by Bordbar et al. [119], in which the induction of apoptosis in granulosa cells stemming from primary follicles was observed in rats treated with Ndn. Additionally, exposure to Ndn was found to decrease blood levels of LH, FSH, estrogens and progesterone. Moreover, the protein microarray-mediated analysis revealed that the expression of cytochrome c increases rapidly in COCs cultured in the 3D-IVM model associated with Ndn treatment. Thus, long exposure of COCs to Ndn triggers damage to the mitochondria. Therefore, the level of ATP synthesis is sharply reduced, as was evidenced by the declined RA of mRNA transcripts synthesized from the *ATP5A1* gene coding for the ATP synthase subunit. A similar negative effect of Ndn on ATP synthesis was recognized in HepG2 cells and nerve cells in the research by Agriesti et al. [34] and Carteri et al. [120], respectively. In contrast, other investigators discovered the existence of a positive correlation between increased ATP levels and high in vitro developmental competence of bovine and human oocytes [121,122]. In turn, biodegradation of mitochondria, elevated ROS concentration and diminished ATP production accelerate follicular atresia and contribute to the premature extinction of ovarian function in women under the age of 40 years [123].

Especially interesting results achieved within the framework of the present exploration are those identifying an increase in the expression of TNF-β (α-lymphotoxin) and HSP27 proteins in COCs undergoing 3D-IVM and simultaneous exposure to Ndn. The cell synthesizes HSP27 in response to stressors triggering apoptosis [124], as was also supported by the results of clinical studies focused on female patients with diagnosed ovarian cancer [125]. On the other hand, the activation of TNF-β-related signaling pathways can lead to neoplastic cell transformation in liver and prostate cancer development [126]. The histological compartment of granulosa cells within the ovarian follicle represents a cell subpopulation that is characterized by high plasticity [127,128]. Its effect is not only the differentiation of cells within the granulosa layer into mural cells, antral cells and the cells forming the cumulus oophorus but also their involvement in the formation of the corpus luteum [129]. Furthermore, human granulosa cells have been shown to display certain attributes specific to stem cells [128,130] and can exhibit capabilities to differentiate into neurons, osteocytes, chondrocytes, hepatocytes and adipocytes under appropriate in vitro culture conditions [127,131–133]. Moreover, studies conducted on granulosa cells isolated from porcine ovarian follicles demonstrated their differentiability into osteoblasts and fibroblasts [134]. In turn, bovine granulosa cells were successfully transformed into endothelial cells under in vitro culture conditions [135]. All of the aforementioned findings provide clear evidence for the enormous plasticity of granulosa cells, which also allows them to undergo neoplastic transformation [136]. One of the types that represent highly malignant and metastatic neoplasms originating from granulosa cells is ovarian granulosa-cell tumor (folliculoma) [137,138]. Therefore, taking into consideration not only the above-mentioned data justifying the potential of granulosa cells for cancer formation but also our previous investigation [35] and the results of the present research (indicating elevated expression of TNF-β and HSP27 in the presence of Ndn), it can be concluded that Ndn enhances the risk of neoplastic transformation of CCs derived from COCs subjected to IVM in a microenvironment enriched with the presence of this EDC. This scientific judgment is consistent with the results of studies by Agriesti et al. [34], who convincingly verified that Ndn increases the risk of oncogenic transformation in the cells by changing their phenotype to a stem cell-like phenotype.

CsA is a frequently used immunosuppressant [139], and due to its protective effect, it is also a factor applicable in studies focusing on the exploration of mitochondrial function [140]. A side effect of the use of CsA is a decrease in the level of GSH synthesis, which, in turn, may increase the concentration of ROS in cells [141]. Previous studies have shown

that CsA induces the processes of autophagy (self-digestion) in ex vivo expanded human tubular cells and also under in vivo conditions in the kidneys of rats. This is most likely a protective mechanism against the cytotoxicity of CsA [142–144]. The factor that stimulates autophagy is unfolded proteins, which are responsible for the activation of proteostatic stress-related events in the cisternae and tubules of the endoplasmic reticulum [145,146]. Conversely, long-term stress can induce apoptosis in a model of chronic nephropathy [147]. In our current investigation, this differential response to CsA was also identified in CCs during the IVM of porcine COCs. Protein analysis of apoptotic pathways revealed increased expression of executioner caspase 3, and RT-qPCR analysis revealed the highest level of *LC3* mRNA in COCs undergoing 3D-IVM in the presence of CsA. The intense autophagy occurring in oocytes subjected to 3D-IVM in the CsA-enriched medium was recognized by the intracellular abundance of autophagosomes observed during TEM analysis of COCs. However, despite the autophagy and apoptosis taking place in CCs, oocyte maturation was not inhibited, as was evidenced by not only the smaller number of large lipid droplets, whose diameter ranged from 1 to 3 μm, but also their perinuclear location, which is a characteristic feature of meiotically matured (i.e., MII-stage) oocytes [117].

Although CsA has been previously found to exert a protective effect on mitochondria [46,47], the detection of mitophagy in CCs originating from COCs subjected to 3D-IVM in the CsA-enriched medium implies that this endocrine disruptor prompted mitochondrial damage. In turn, the damaged mitochondria detrimentally affect intracellular metabolism by promoting the production of ROS and ultimately triggering apoptosis [148,149]. The harmful impact of CsA on the mitochondria within CCs is confirmed by the dwindling of ATP synthesis, which was identified after 3D-IVM of COCs in the presence of CsA. A similar effect was observed in breast cancer cells [150]. In addition, CsA not only reduced the mitochondrial membrane potential ($\Delta\Psi$m) that is generated by proton pumps (complexes I, III and IV) in the process of energy storage (i.e., respiratory biosynthesis of ATP) during oxidative phosphorylation but also triggered the enhancement of caspase 3 activity [151,152]. On the one hand, mitochondrial transmembrane potential is a key indicator of mitochondrial metabolic activity, because it reflects the process of electron transport and oxidative phosphorylation, the driving force behind ATP production. On the other hand, $\Delta\Psi$m represents an intermediate energy store used by ATP synthase to accumulate ATP [153]. Therefore, based on the obtained results, it can be concluded that although CsA does not interfere with the nuclear and cytoplasmic maturation of the oocyte, it may decrease the molecular quality of oocytes by diminishing ATP biosynthesis in COCs [154,155]. A similar effect that gave rise to the attenuation of the quality of oocytes due to low ATP levels was observed by Groth et al. [48] in a murine model study using CsA. These investigators demonstrated that exposure of female mice to high doses of CsA (at levels oscillating between 20 and 30 mg/kg) contributed to lessening the incidence of embryo implantation and postimplantation survival rates of conceptuses [48]. The reason for such changes was a remarkable decline in the quality of oocytes, which did not display the sufficiently abundant bioenergetic reservoirs required for the proper development of the embryo and deposited/accumulated in the intramitochondrial ATP biomachinery located within oxysomes (also known as F0-F1 particles) inside the folds of the cristae in the inner mitochondrial membrane.

One of the quite new applications of CsA is anticancer therapy for non-small cell lung cancer (NSCLC), which accounts for approximately 85–90% of all lung cancer diagnoses. In phase I/II clinical trials, CsA was administered to patients in two doses: low (1–2 mg/kg daily) and higher (3–6 mg/kg daily). Administration of a low dose has been found to increase the chance of survival by two years [156]. In turn, research undertaken by Qin and Chen [157] to explore the molecular nature of the A549 non-small cell lung cancer cell line discovered that CsA augments the proliferative activity and metabolism of glucose in neoplastic cells. In addition, the elevated lipid accumulation that was evidenced in A549 non-small cell lung cancer cells brought about the enhanced production of ROS prompted by CsA action. The aforementioned authors hypothesized that the pleiotropic

effect of CsA is dependent on cell metabolism, and its use may induce neoplastic changes in patients after organ transplantation [157]. The potential neoplastic activity may be demonstrated by the enhanced expression of TNF-β, which leads to the activation of pathways related to neoplastic transformation [126]. On the other hand, studies aimed at recognizing tumorigenic scenarios specific to prostate cancer cells have resulted in determining the predominant role of CsA both in attenuating/alleviating the capability of neoplastic cells to migrate/metastasize and in suppressing tumor growth, which can be directly elucidated by CsA-induced intensification of apoptosis occurrence [158]. Collectively, the results of a panel of studies aimed at examining the influence of CsA on oocytes undergoing 3D-IVM in its presence led to the conclusion that although CsA may stimulate cytoplasmic and nuclear maturation of the oocyte, at the same time, by reducing ATP levels, it may diminish the molecular quality of oocytes after the completion of the IVM procedure.

To sum up, recognizing the molecular mechanisms by which a triad of EACs/EDCs (Vnz, Ndn and CsA) trigger disturbances in the intracellular bioenergetic balance dependent on mitochondrial compartments is crucial for achieving satisfactory outcomes related to the extracorporeal maturation of porcine oocytes. Generating a sufficiently high percentage of porcine IVM-derived oocytes whose molecular quality has not been attenuated by EDC-prompted impairments in intramitochondrial bioenergetic homeostasis is greatly important from multiple points of view. One of them is the ability to perpetuate such availability of ex vivo–matured oocytes that might ensure abundant sources of not only ova highly capable of being fertilized by conventional IVF or ICSI but also excellent-quality nuclear recipient cells for SCNT-based cloning in pigs. The above-mentioned requirements could be fulfilled by developing the new strategy of 3D-IVM, which allowed us to improve the efficiency of the ex vivo maturation of porcine oocytes in a culture microenvironment deprived of EACs/EDCs.

The improvement of parameters related to molecular quality in recipient oocytes that have been matured in vitro under 3D culture conditions and have subsequently received donor somatic cell nuclei (DSCN) can result, among others, from retaining largely balanced biogenesis, reduplication, cytophysiological functions and distribution patterns observed for reservoirs of intraooplasmic mitochondrial compartments. The maintenance of this dynamic balance seems to be due to a remarkably diminished incidence of mitophagic and apoptotic events, which, in turn, can lead to a lack or only negligible occurrence of dysregulations in sustainable intramitochondrial ATP biosynthesis. For all of the aforementioned reasons, SCNT-mediated reconstruction of porcine enucleated oocytes that display augmented molecular quality might give rise to generating cloned embryos, in the blastomeres of which faithful and synergistic intergenomic crosstalk between nuclear and mitochondrial DNA fractions takes place. The scenario of successful transcriptional and proteomic communication between nuclear and mitochondrial compartments is undoubtedly responsible for enhancing the capabilities of DSCN to be epigenetically reprogrammed in SCNT-derived pig embryos stemming from high-quality recipient oocytes.

Furthermore, our current research contributed to successfully devising ex vivo models based on 3D-IVM of porcine oocytes undergoing treatments with a variety of EACs/EDCs (Vnz, Ndn or CsA), which might also provide promising and hopeful biomedical tools for the establishment of experimental, preclinical and clinical therapies aimed at the next-generation nonsurgical treatment modalities of acquired subfertility and fertility cases diagnosed in human female patients. In such sub-fertile or infertile women, ovarian follicles can be characterized by symptomatic failures in the in vivo maturation of oocytes due to overexposure of their reproductive systems to the selected ectopic/environmental EDCs (Vnz, Ndn and CsA), followed by the overabundant accumulation of this triad of endocrine disruptors in different ovarian tissue compartments.

Finally, in light of the results achieved in our present investigation, which suggest that Ndn not only reduces the in vitro developmental competence of pig oocytes by disturbing the metabolism of CCs, but also increases the incidence of cancerous conversion (tumorigenesis) in the cumulus oophorus compartment of porcine COCs cultured in the novel model of

3D-IVM, it is particularly important to educate young people about the risk and dangerous side effects arising from misuse of this AAS. It is worth highlighting that, according to data presented in 2021 by the Addiction Center, 1 in 50 students aged 17–18 used steroids. In turn, according to the Food and Drug Administration data, 375,000 boys and 175,000 girls abuse AASs annually (https://www.addictioncenter.com/stimulants/steroids/, accessed on 1 January 2008). The main motivation for taking AASs is the desire to improve one's own appearance in a short time, without physical exertion. For those reasons, developing new-generation ex vivo models designed using 3D-IVM-mediated culture systems of porcine COCs that have been subjected to single or combined overexposure to Vnz, Ndn and CsA might be a reliable and feasible approach to developing and optimizing anticancer treatment modalities within the framework of targeted antioncogenic therapeutics dedicated to female patients afflicted with ovarian follicle-specific oncologic diseases. The etiopathogenesis of these diseases can be related to tumorigenic transformation of cumulus oophorus-based cytological compartments stemming from EAC/EDC-overexposed ovaries into malignant and metastatic neoplasms.

4. Materials and Methods

4.1. Collection and In Vitro Maturation of Porcine Cumulus–Oocyte Complexes under 3D Culture Conditions

Ovaries that displayed the absence of corpora lutea were collected from ~4–5-month-old (i.e., prepubertal) gilts at a local abattoir under veterinarian control within 20 min of slaughter. For isolation of COCs, approximately twenty ovaries from ten female pigs were collected for each experiment. Ovaries were transported to the laboratory in sterile phosphate-buffered saline (PBS; pH 7.4, 38 °C, PAA The Cell Culture Company, Piscataway, NJ, USA) containing 1% (*v/v*) antibiotic/antimycotic solution (AASol; Thermo Fisher Scientific, Waltham, MA, USA) within ~1 h. Afterwards, ovaries were rinsed twice with sterile PBS and transferred to handling medium (HM). The latter comprised Tissue Culture Medium 199 (TCM 199; Sigma-Aldrich, St. Louis, MO, USA) supplemented with 10% (*v/v*) fetal bovine serum (FBS; Thermo Fisher Scientific) and 1% (*v/v*) AASol at a temperature of 38 °C. COCs were aspirated from morphologically normal medium-sized follicles (4–6 mm in diameter) using 28G needle having a size of 5/8" attached to a disposable syringe. For each experiment, a total of 100 COCs, which exhibited a homogenous ooplasm, and 3 to 4 compact layers of cumulus cells were selected for in vitro maturation (IVM) [49]. The procedure of IVM was performed according to the technique described by Pedersen et al. [159]. The group of COCs intended for IVM were encapsulated in fibrin-alginate hydrogel beads (FABs) according to a previously reported protocol [160]. In detail, a subpopulation ranging from 3 to 5 COCs along with a minimum volume (up to 5 μL) of maturation medium were precisely transferred (with the use of micropipette) into a drop of mixture of fibrinogen and alginate (FA: 0.5% alginate solution and 50 mg/mL fibrinogen solution mixed in a 1:1 ratio; Sigma-Aldrich). The maturation medium (MM) consisted of TCM 199 medium enriched with 10% (*v/v*) FBS, 1% (*v/v*) AAS, 10 IU/mL pregnant mare serum gonadotropin (PMSG; RayBiotech Life, Inc. Peachtree Corners, GA, USA), 5 IU/mL human chorionic gonadotrophin (hCG; Sigma-Aldrich), 0.004 mg/mL L-glutamine (Sigma-Aldrich) and 10% porcine follicular fluid (pFF). Subsequently, 7.5 μL volumes of thrombin/Ca^{2+} solution (Sigma-Aldrich) was pipetted on each FA drop. The occurring FABs were transferred to a 5% CO$_2$ incubator (38 °C, 5 to 7 min) using "incubation chambers" on the Petri dish. After this time, simultaneous gelation of fibrin and alginate was observed. In the next step, FABs with COCs inside were transferred to 96-well plates (one capsule per well, Nunc™, Thermo Fisher Scientific) containing 100 μL of MM. After 24 h of preculture, COCs were randomly allotted to a control group (CTR) and three experimental groups. For the first, second and third experimental groups, the endocrine-disrupting chemicals (EDCs) vinclozolin (Vnz; at a concentration of 10^{-7} M/mL, Sigma-Aldrich), nandrolone (Ndn; at a concentration of 10^{-5} M/mL, Sigma-Aldrich) and cyclosporine A (CsA; at a concentration of 1 μM/mL, Sigma-Aldrich) were added to the

MM, respectively. The experimental doses of the above-mentioned EDC agents used were established on the basis of literature reports and our own research [9,35,158]. Cultures were carried out for a further 48 h at 38 °C in an atmosphere of 5% CO_2 and 95% relative humidity. Following completion of IVM procedure, the maturation status of in vitro cultured COCs was initially assessed by observing them under an inverted microscope at a magnification ranging from 10× to 60× (Nikon Ti-U microscope equipped with a Nikon DS-Fi1c-U3 camera; Tokyo, Japan). The assessment of in vitro–matured COCs was accomplished not only by identifying the extrusion of the first polar body (PB) into perivitelline space but also by evaluating the extent of dispersion/expansion of CC layers surrounding each oocyte. The microscopic diagnostics of the aforementioned morphological biomarkers specific for ex vivo–matured COCs were also supported by analyzing molecular biomarkers of meiotic maturity of oocytes encompassing highly enhanced expression profiles for genes encoding MPF and the strongly reduced levels of cAMP, as described in Sections 4.3 and 4.6, respectively.

4.2. Total RNA Isolation and cDNA Synthesis

Total RNA was extracted from both COCs undergoing 3D-IVM in the presence of selected EACs and COCs cultured without addition of Vnz, Ndn or CsA. Total cellular RNA was isolated using the EZ-10 Spin Column Total RNA Mini Preps Super Kit (Bio Basic Canada Inc.; Markham, ON, Canada) according to the manufacturer's protocol. The quantity and quality of the total RNA were ascertained by measuring the absorbance at detection wavelengths λ equal to 260 nm and 280 nm with a NanoDrop ND2000 Spectrophotometer (Thermo Fisher Scientific). Moreover, RNA samples were electrophoresed on a 1% (*w/v*) denaturing agarose gel to verify the RNA quality and stored frozen at −80 °C. First-strand cDNA was prepared by reverse transcription (RT) using 1 mg of total RNA, random primers and a High-Capacity cDNA Reverse Transcription Kit (Applied Biosystems; Foster City, CA, USA) according to the manufacturer's protocol. The 20 mL total reaction volume contained random primers, dNTP mix, RNAse inhibitor and Multi Scribe Reverse Transcriptase. RT was performed in a Veriti Thermal Cycler (Applied Biosystems; Foster City, CA, USA) according to the following thermal profile: (1) 25 °C for 10 min, (2) 37 °C for 120 min and (3) 85 °C for 5 min. Genomic DNA amplification contamination was checked using control experiments, in which reverse transcriptase was omitted during the RT step. The samples were kept at −20 °C until further analysis.

4.3. Quantitative Reverse Transcriptase Real-Time Polymerase Chain Reaction (qRT-PCR)

RT-qPCR was performed according to the manufacturer's protocol. To quantitatively assess the transcriptional activities identified for each analyzed gene, the RT-qPCR reactions were successfully initiated and subsequently completed for each sample using a reaction mix prepared as follows: 1 × SYBR Select Master Mix (Thermo Fisher Scientific), 2 μL of forward and reverse primers (1 μM each) and 4 μL of 20 × diluted cDNA in a final volume of 15 μL. No-RT control run was conducted with DNase-digested RNA to verify that the digestion was successful and sufficient for selected samples. The amplification protocol included an initial preheating at 50 °C for 2 min, initial denaturation at 95 °C for 2 min and 40 cycles of amplification (15 s at 95 °C and 60 s at 60 °C). A melting curve analysis was performed at the end of each run. RT-qPCR was carried out with a Rotor-Gene Q (Qiagen, Hilden, Germany). The sequences of all RT-qPCR primers are presented in Table 1.

Table 1. Primers used for RT-qPCR.

Gene	F/R	Primer Sequence (5′→3′)	T_m (°C)	Reference
GAPDH	F	CCCACGAGCACACCTCAGAA	55.9	[161]
	R	TGCAGCCTGTACTCCCGCT	55.4	[161]
GPX4	F	ATTCTCAGCCAAGGACATCG	51.8	[162]
	R	CCTCATTGAGAGGCCACATT	51.8	[162]
FOXO3	F	GGGGAGTTTGGTCAATCAGA	51.8	[163]
	R	TGCATAGACTGGCTGACAGG	53.8	[163]
SIRT3	F	CAGCGGCATTCCAGACTTCA	53.8	[164]
	R	GTCCCAACCATCAAACTTTCCA	53.0	[164]
CASP3	F	GAGGCAGACTTCTTGTATGC	51.8	[162]
	R	CATGGACACAATACATGGAA	47.7	[162]
LC3	F	CCGAACCTTCGAACAGAGAG	53.8	[162]
	R	AGGCTTGGTTAGCATTGAGC	51.8	[162]
CDC2	F	TGGGCACTCCCAATAATGAA	49.7	[165]
	R	TCCAAGCCATTTTCATCCAA	47.7	[165]
CCNB1	F	GCTCCAGTGCTCTGCTTCTC	55.9	[165]
	R	ACAAACTTTATTAAAAGTAAATAAGTG	47.6	[165]
ATP5A1	F	AGTTGCTGAAGCAAGGACAGTAT	53.5	[161]
	R	GTGTTGGCTGATAACGTGAGAC	54.8	[161]

Alterations in the quantitative profiles (i.e., relative abundances; RAs) of relevant mRNA transcripts that were triggered by the exposure of in vitro maturing COCs to the selected EACs were rendered as the ratio of the target gene versus the reference *GAPDH* gene (coding for glyceraldehyde-3-phosphate dehydrogenase) in relation to expression in control samples using the method developed and optimized by Pfaffl [166] according to the following equation:

$$\text{Ratio} = \frac{(E_{\text{target}})^{\text{nCt}}\text{Target}^{(\text{control}-\text{sample})}}{(E_{\text{reference}})^{\text{nCt}}\text{Reference}^{(\text{control}-\text{sample})}}$$

In the above-indicated algorithmic formulation, the mathematical designation E denotes the amplification efficiency, whereas the Ct symbol is assigned to the number of RT-qPCR cycles needed for the signal to exceed a predetermined threshold value.

4.4. The Use of Apoptosis Proteome Profiler Arrays for Detailed Evaluation of Pro- and Antiapoptotic Pathways in 3D-IVM-Derived COCs Treated with the Selected Endocrine Disruptors

Analysis of the molecular mechanism that underlies the proteomic networks related to either initiation and progression or inhibition of programmed cell death in EDC-treated COCs undergoing 3D-IVM was performed using the RayBio® Human Apoptosis Antibody Array Kit (RayBiotech, Inc., Norcross, GA, USA) according to previously reported protocol [10] with additional modification. This technique detects 43 proapoptotic and antiapoptotic proteins involved in promoting or suppressing the process of programmed cell death. The COCs were washed in sterile PBS. Total protein was extracted using the cell lysis buffer contained within the kit. After lysis by freeze–thawing and subsequent homogenization, lysates were centrifuged at 14,000 rpm for 10 min at 4 °C, and supernatants were stored at −70 °C until further analyses. The protein concentration of each sample was quantified using the NanoDrop ND2000 Spectrophotometer (Thermo Fisher Scientific). Protein array membranes were immersed in the blocking buffer and incubated

with 600 mg of proteins overnight at 4 °C. After washing with the kit buffers, samples were incubated overnight with biotinylated detection antibodies at 4 °C, and after further washing, they were exposed to Alexa Fluor 555 dye-conjugated streptavidin overnight. Signals in the array membranes were detected and quantitated on a ChemiDoc chemiluminescence imaging system (Bio-Rad Laboratories Inc., GmbH, Munchen, Germany). For each protein signal, absorbance was determined using the Antibody Array Analysis Tool (RayBiotech Life, Inc., Peachtree Corners, GA, USA). Intensities of individual spots were normalized to an internal positive control (standardized amounts of biotinylated immunoglobulin G) printed directly onto the array, according to an algorithm specified by the manufacturer. The measurement for each protein was repeated twice in two independent trials ($n = 5$ for each protein in one experimental group) in each of the experimental groups. From the obtained values for each of the detected proteins, the mean value and standard deviation were obtained for each experimental group. Only the expression data of proteins that are directly involved in apoptosis and had a statistically significant increase after treatment are shown.

4.5. TUNEL-Assisted Detection of Late-Apoptotic Cells in COCs Undergoing Exposure to the Selected EACs during 3D-IVM

The In Situ Cell Death Detection Kit (Roche, Mannheim, Germany) was used to perform a terminal deoxynucleotidyl transferase (TdT)-mediated 2′-deoxyuridine-5′-triphosphate (dUTP) nick-end labeling (TUNEL) assay that was dependent on fluorescein-5-isothiocyanate (FITC) tags conjugated with dUTP nucleotides. The TUNEL assay provides a method that enables us to identify and ascertain the extent of internucleosomal DNA fragmentation arising due to the progression of apoptotic cell death to its final destructive phase. After terminating the 3D-IVM of COCs, the MM was removed from plates, and COCs were rinsed twice with sterile Ca^{2+} -and Mg^{2+}-depleted PBS (PAA The Cell Culture Company). In the next step, COCs were incubated in fixation solution composed of 4% paraformaldehyde (PFA; Santa Cruz Biotechnology Inc. Dallas, TX, USA) in PBS for 1 h at room temperature. Then, COCs were subjected to three-step washing with PBS (each step for 10 min) followed by permeabilization in 0.1% sodium citrate (Sigma-Aldrich) for 2 min on ice. Afterwards, TUNEL assay was performed according to the previously reported protocol [167]. Firstly, the COCs were treated with proteinase K (Promega Corporation, Madison, WI, USA) in a humidity chamber for 15 min at 37 °C. Secondly, COCs were rinsed twice with PBS and subsequently exposed to 3% hydrogen peroxide (H_2O_2; Sigma-Aldrich) in methanol for 10 min to block endogenous peroxidase activity. Thirdly, COCs were washed twice with PBS and deposited into the medium supplemented with 5% bovine serum albumin (fraction V; BSA-V, Sigma-Aldrich) for 20 min to block nonspecific binding. The COCs were then rinsed twice with PBS, followed by treatment with TUNEL mixture composed of TdT and FITC-tagged dUTP in a humidity chamber for 1 h at 37 °C in the dark. After the TUNEL reaction was completed, the COCs were washed thrice with PBS and counterstained with 4′,6-diamidino-2-phenylindole (DAPI) diluted in VECTASHIELD Antifade Mounting Medium (Vector Laboratories, Burlingame, CA, USA). Finally, the COCs were visually assessed, photographed and analyzed using an OLYMPUS FV1200 FLUOVIEW scanning confocal laser microscope (OLYMPUS, Tokyo, Japan) at an excitation wavelength λ_{ex} equal to 540 nm and an emission wavelength λ_{em} equal to 580 nm. Sections from each COC were evaluated under both 20× and 40× objective lenses and scored by an observer blinded to the treatment groups. For each COC section, all cross-sectional CCs profiles ($n = 100$) were counted, and the number of TUNEL-positive cells was ascertained.

4.6. Determination of cAMP Concentration in EAC-Treated COCs Subjected to 3D-IVM

The concentration of cAMP was measured using Cyclic AMP Direct ELISA (DRG MEDTek, Warsaw, Poland) in compliance with the manufacturer's protocol. Following termination of 3D-IVM and simultaneous exposure to selected endocrine disruptors, FAB-encapsulated COCs derived from all groups were washed twice with $CaCl_2$- and $MgCl_2$-

deprived PBS and placed in alginate-dissolving buffer comprising 0.055 M sodium citrate and 0.15 M NaCl for 30 min at 37 °C. Subsequently, COCs were centrifuged at 1100 rpm at 4 °C for 10 min. Supernatant was removed, and COCs were rinsed twice with PBS and centrifuged again. For protein isolation, all collected COCs (~46 COCs per experimental group) were lysed with the provided Sample Diluent. After 10 min incubation at room temperature, the suspension was sonicated. Samples were centrifuged at 1100 rpm at 4 °C for 10 min, and the supernatant was assayed directly. First Standard (150 pM/mL) was prepared by the addition of 30 μL of cAMP stock solution to 270 μL of Sample Diluent. Standards 2–6 (50, 16.67, 5.56, 1.85 and 0.617 pM/mL) were prepared by serial dilutions. The regular format of the assay protocol was used to quantitatively estimate the intracytoplasmic cAMP concentration. Prior to carrying out an assay, the Plate Primer was added to all wells that were used. Nonspecific binding (NSB) wells and Zero standard were filled with Sample Diluent (75 μL and 50 μL). All samples were run in duplicate and, before initiating an assay, were diluted four times. Afterwards, cAMP Conjugate and cAMP Antibody were added to all wells (except for NBS wells). To mix all reagents, the sides of the plate were gently tapped, and the plate was shaken at room temperature for 2 h. In the next step, all reagents were aspirated, and each well was washed four times with ELISA Wash Buffer. Then, the plate was incubated at room temperature for 30 min with 3,3′,5,5′-Tetramethylbenzidine (TMB) Substrate. To stop the reaction, to each well, Stop Solution was added. All analyses were performed in duplicate using Labtech LT-4500 Microplate Reader (Labtech International Ltd., Heathfield, East Sussex, UK) at a detection wavelength λ equal to 450 nm. Free ELISA software (elisaanalysis.com) was used to calculate cAMP concentration using built-in 4-Parameter Logistic Regression. All obtained results were multiplied by the dilution factor.

4.7. Quantitatively Ascertaining the Intracytoplasmic Glutathione Concentration in 3D-IVM-Produced COCs Exposed to the Selected Endocrine Disruptors

The Glutathione Colorimetric Detection Kit (Invitrogen™, Thermo Fisher Scientific) was used to quantify the intracellular concentration of glutathione (GSH) in Vnz-, Ndn- and CsA-treated or untreated COCs. All necessary reagents were provided by the manufacturer. To obtain the cell lysate, the pools of COCs derived from all experimental groups (at a quantity of approximately 42 COCs per group) were transferred to 1.5 mL Eppendorf tubes filled with 5% 5-sulfosalicylic acid dihydrate (SSA; Sigma-Aldrich). They were subsequently sonicated thrice for 5 s at 50 V, followed by incubation for 10 min at 4 °C. Afterwards, all samples were centrifuged at 14,000 × *g* at a temperature of 4 °C for 10 min, and the supernatants were used for further analysis. All samples were diluted 4 times in Assay Buffer, followed by de novo quadruple dilution in Sample Diluent. Standards were prepared according to the manufacturer's instructions. A total of 50 μL of the test sample or standard was consecutively added to the wells of a 96-well plate, followed by addition of 25 μL of Colorimetric Detection Reagent to each well. In the final step, 25 μL volumes of the reaction mixture, which was composed of NADPH (reduced/hydrogenated isoform of nicotinamide adenine dinucleotide phosphate) Concentrate, Glutathione Reductase Concentrate and Assay Buffer, were added. The plate was incubated for 20 min at room temperature. Measurement of intracytoplasmic GSH concentration was achieved at a detection wavelength λ equal to 405 nm using a Labtech LT-4500 Microplate Reader (Labtech International Ltd.).

4.8. Transmission Electron Microscope Analysis of Porcine COCs Undergoing 3D-IVM and Simultaneous EDC Treatment

Ultrastructural alterations in COCs were detected by transmission electron microscopy (TEM) as described previously [168]. Briefly, control, Vnz-, Ndn-, and CsA-treated COC samples were fixed with 2.5% glutaraldehyde (Polysciences Inc., Warrington, PA, USA), 0.067 M cacodylate buffer (pH 7.3) and 3 mM calcium chloride for 2 h at 4 °C. Samples were then washed in cacodylate buffer with calcium chloride at 4 °C for 2 h and post-fixed in 2% osmium tetroxide (Sigma-Aldrich) with 0.8% potassium ferrocyanide (Chempur®, Piekary

Śląskie, Poland) in the same buffer for 1 h at 4 °C. After dehydration in a series of ethanol and finally in propylene oxide, the material was embedded in PolyBed 812 epoxy resin (Polysciences Inc., Warrington, PA, USA). Ultrathin (80 nm thick) sections were contrasted with uranyl acetate and lead citrate according to standard protocols and analyzed with a Jeol JEM 2100 transmission electron microscope (TEM) (JEOL, Tokyo, Japan) at a maximum voltage output of 80 kV.

4.9. The Live Cell-Based Assay of Mitochondrial Metabolic Activity Assisted by the Seahorse XFp Analyzer

The COC bioenergetics were determined using the Seahorse XFp Analyzer (Agilent, Boston, MA, USA) kindly provided by Perlan Technologies (Poland). All assays were programmed (designed) in XF data acquisition Wave 2.6.1 software (Agilent, Boston, MA, USA). In each experiment, 3 baseline measurements were taken prior to the addition of any compound/substrate/inhibitor, and at least 3 response measurements were taken after the addition of each compound. The oxygen consumption rate (OCR) and extracellular acidification rate (ECAR) are reported as absolute rates (pM/min for OCR and mpH/min for ECAR). While sensor cartridges were hydrated (overnight) and calibrated (XF Calibrant), cell plates were incubated at 37 °C for 30 min prior to starting an assay. All experiments were performed at 37 °C in non-CO_2 conditions. Detailed protocols and their justification can be found at https://www.agilent.com/en/product/cell-analysis/how-torun-an-assay (accessed from 1 June 2020 to 1 May 2021). Additionally, detailed protocols were previously published [35,169,170].

Seahorse XF Measurement of ECAR and OCR Using Seahorse XF Cell Mito Stress Test

Following 3D-IVM under the conditions of Vnz, Ndn or CsA exposure, COCs were suspended in sterile (i.e., 0.2 μm syringe strainer-filtered) sodium bicarbonate-depleted Hank's Balanced Salt Solution ($NaHCO_3$-free HBSS; Gibco, Waltham, MA, USA). The $NaHCO_3$-free HBSS medium was enriched with 1 mM sodium pyruvate (Sigma-Aldrich), 2 mM L-Glutamine (Sigma-Aldrich), 10 mM D-glucose (Lonza Bioscience, Basel, Switzerland) and 5 mM HEPES (Sigma-Aldrich) and adjusted to pH 7.4 with 0.1 N NaOH (Sigma-Aldrich). The buffer factor of assay media was validated prior to experiments and was equal to 2.9 mM/pH. In the next step, COCs were plated (6 COCs/well) in 180 μL on Agilent Seahorse 8-well XFp Cell Culture Miniplate and allowed to settle/adhere for 30 min at 37 °C. The performance of Seahorse XF Cell Mito Stress Test resulted in real-time and noninvasive measurements of ECAR and OCR that were positively correlated with the levels of acidification stemming, to the largest extent, from such intramitochondrial metabolic activities as biochemical reactions of glycolysis and ATP biosynthesis, respectively. Measurements were continued for 1 h and consisted of (i) a sample mixing time (each 1 min long) and (ii) a data acquisition period of 57 min. The latter consisted of 3 cycles, with a waiting time before each measurement lasting for 15 min.

4.10. Assessment of Mitochondrial Distribution Pattern in 3D-IVM-Generated COCs Exposed to the Selected EDCs

MitoTracker™ Orange CM-H2TMRos (MtOR-CM; Invitrogen™, Thermo Fisher Scientific) was used to visualize mitochondria in COCs according to the method developed by Romek et al. [171]. Briefly, a 0.5 mM MtOR-CM working solution was prepared on the basis of TCM 199 medium. The MM was removed from the culture plate of COCs and replaced with 0.5 mM MtOR-CM solution. Following 30 min incubation at a temperature of 38 °C and in an atmosphere of 5% CO_2 in humidified air, COCs were washed twice in Ca^{2+}- and Mg^{2+}-deprived PBS and subsequently fixed in 4% PFA for 5 min at room temperature. Afterwards, the COCs were de novo rinsed twice with PBS and counterstained with DAPI diluted in VECTASHIELD Antifade Mounting Medium (Vector Laboratories). The images were visualized under a 60× oil objective on an OLYMPUS FV1200 FLUOVIEW confocal laser microscope with the use of an excitation wavelength of λ_{ex} = 554 nm and an emission

wavelength of λ_{em} = 576 nm. The quantification of the cell fluorescence intensity was conducted with the NIH ImageJ software.

4.11. Detection of Mitophagy Incidence in COCs Subjected to 3D-IVM and Simultaneously Treated with the Selected EACs

A Mitophagy Detection Kit® (Dojindo, Kumamoto, Japan), which was composed of Mtphagy Dye® and Lyso Dye®, was used to confirm the occurrence of mitophagy-dependent processes that were induced by exposing in vitro maturing COCs to the selected endocrine disruptors. The procedure was conducted according to the previously reported protocol [172] with an additional modification. Briefly, after 24 h preculture of porcine COCs, 100 nM Mtphagy Dye was added to the maturation medium. Following 30 min incubation (in the dark), COCs were washed twice with TCM 199 medium. Subsequently, the medium intended for 3D-IVM culture of COCs was supplemented with either Vnz, Ndn or CsA. After 3D-IVM culture for a further 48 h was terminated, the COCs were washed with TCM 199 medium, followed by treatment of ex vivo–matured COCs with the addition of 1 M Lyso Dye to each well. In the next step, the multi-well plate filled with meiotically matured COCs was incubated for an additional 30 min followed by washing with HBSS (Thermo Fisher Scientific). The oocytes and CCs that stemmed from COCs undergoing IVM under 3D culture conditions were imaged using an OLYMPUS FV1200 FLUOVIEW scanning confocal laser microscope at an emission wavelength λ_{em} equal to 650 nm, as prescribed by the manufacturer. The fluorescence intensity was quantified using the NIH ImageJ software (National Institutes of Health, Bethesda, MD, USA).

4.12. Statistical Analysis

Statistical analysis was performed using Statistica v.13.1 software (Stat-Soft, Inc., Tulsa, OK, USA). The experiments aimed at the 3D-IVM culture of porcine COCs exposed or not exposed to the selected EDCs were carried out in quintuplicate (n = 5). Brown–Forsythe test for homogeneity of variance, Bartlett's test for normality and one-way ANOVA followed by Dunnett's post hoc test were used to estimate intergroup variability not only among experimental EDC treatments but also between experimental EDC treatments and their control counterparts. All data are presented as the overall mean $\pm$ standard error of the mean (SEM), and intergroup differences were considered to be statistically significant at the 95% confidence level (* $p < 0.05$).

5. Conclusions

The objective of our current investigation was to verify an overarching research hypothesis. The results highlighted the negative impact of the selected endocrine-active compounds, which encompassed a pesticide (Vnz), an anabolic steroid (Ndn) and an immunosuppressant (CsA), on not only the developmental competences of oocytes and viability of CCs but also the molecular quality and mitochondrial metabolic activity of porcine COCs. The obtained results provide strong scientific evidence that both Vnz and Ndn decrease the developmental competence of oocytes and activate the processes of apoptosis in CCs. Furthermore, it is noteworthy that Vnz accelerates the maturation process in immature oocytes through both increased ROS production and the augmented transcriptional activity of the *CCNB1* gene encoding cyclin B1. It also triggers the onset and progression of proapoptotic events in CCs by activating the transcription factor FOXO3, which regulates the mitochondrial apoptosis pathway. In turn, Ndn inhibits the maturation of oocytes by prompting the molecular scenarios responsible for: (1) lessening the ATP synthase-mediated generation of ATP within the mitochondria; (2) enhancing the accumulation of lipid droplets and subsequently (3) intensifying the adenylate cyclase-mediated biosynthesis of cAMP from ATP and finally (4) increasing the intraooplasmic cAMP concentration. However, due to the simultaneous increase in the expression of TNF-β and HSP27 proteins in CCs, Ndn may induce the processes of their neoplastic transformation, which brings about the disruption of intercellular communication within the whole COC.

Finally, our research robustly supports that CsA does not interfere with the nuclear and cytoplasmic maturation of the oocytes. Nonetheless, the oocytes exposed to CsA are not supplied with the appropriate abundance of ATP, which would ensure the proper development of the embryo. This finding arises from a powerful scientific assessment confirmed by the high incidence of mitophagy in CCs, the direct consequence of which is insufficient ATP biogenesis within the intramitochondrial oxysomes in porcine COCs undergoing CsA treatment under 3D-IVM conditions.

Cumulatively, extensive efforts were undertaken in our present study to thoroughly decipher and quantitatively estimate a wide spectrum of molecular determinants affecting Vnz/Ndn/CsA-evoked impairments of mitochondrial activity in porcine 3D-IVM-derived oocytes intended to be used as not only meiotically matured ova able to be fertilized by standard IVF or ICSI but also nuclear recipient cells for SCNT. These efforts might allow for devising reliable and feasible approaches applied to either precisely identify or felicitously predict biomarkers correlated with the complete synchronization of the processes of meiotic, epigenomic and cytoplasmic maturation in oocytes originating from COCs grown extracorporeally in the innovative 3D culture model developed in the present research. Development and optimization of the 3D-IVM model mimicking in vivo maturation conditions that are characterized by a totally coordinated scenario of nuclear, epigenomic and ooplasmic maturation of nuclear recipient oocytes might contribute to a considerable increase in the efficiency of somatic cell cloning in pigs and other mammalian species. Furthermore, the ex vivo models designed based on 3D-IVM of porcine oocytes exposed to Vnz, Ndn or CsA might create empirical foundations to devise a panel of novel preclinical and clinical therapies aimed at ovary-specific regenerative medicine and ovarian tissue engineering strategies. The latter might be dedicated to sub-fertile or infertile female patients, whose oocytes display severe acquired insufficiency in the processes of meiotic maturation. This insufficiency can arise not only from the separate or combined intensive exposure of human ovarian follicles to Vnz, Ndn and CsA but also from the strong cytotoxic properties of these potent EACs/EDCs.

Abbreviations

ΔΨm	Mitochondrial membrane/transmembrane potential
3D	Three-dimensional
3D-IVM	Three-dimensional in vitro maturation
AAS	Anabolic androgenic steroids
ARTs	Assisted reproductive technologies
ATP	Adenosine-5′-triphosphate
ATP5A1	ATP synthase F1 subunit α
bad	Bcl2-associated agonist of cell death
Bcl-2	B-cell lymphoma 2
BIM	Bcl2-interacting mediator of cell death
cAMP	Cyclic adenosine 3′,5′-monophosphate
CCNB1	Cyclin B1 gene
CCs	Cumulus cells
CDC2	Cell division cycle 2
Cdc25	Cell division cycle 25
CDK1	Cyclin-dependent kinase 1
cg	Cortical granule
COCs	Cumulus–oocyte complexes
CsA	Cyclosporin A
DSCN	Donor somatic cell nuclei
DAPI	4′,6-Diamidino-2-phenylindole
dUTP	2′-Deoxyuridine-5′-triphosphate
EA	Early autophagosome
EACs	Endocrine-active compounds
ECAR	Extracellular acidification rate
EDCs	Endocrine-disrupting chemicals
FAB	Fibrin-alginate hydrogel bead
FasL	Fas ligand
FasR	Fas receptor
FBS	Fetal bovine serum
FITC	Fluorescein-5-isothiocyanate
FOXO3a	Forkhead box O3a
FSH	Follicle-stimulating hormone
GAPDH	Glyceraldehyde 3-phosphate dehydrogenase
GSH	Glutathione
GV	Germinal vesicle
GVBD	Germinal vesicle breakdown
hCG	Human chorionic gonadotropin
HepG2	Human hepatocarcinoma-derived cell lines
HSP27	Heat shock protein 27
ICSI	Intracytoplasmic sperm injection
IVF	In vitro fertilization
IVM	In vitro maturation
IVP	In vitro embryo production
LA	Late autophagosome
LC3	Microtubule-associated protein 1A/1B light chain 3β
LD	Lipid droplets
LH	Luteinizing hormone
MII	Metaphase II
MM	Maturation medium
MPF	Maturation/meiosis-promoting factor
mPTP	Mitochondrial permeability transition pore
MQ	Molecular quality

mRNA	Messenger RNA
mt	Mitochondria
MtOR	MitoTracker Orange
NADPH	Nicotinamide adenine dinucleotide phosphate (reduced form)
Ndn	Nandrolone
NSCLC	Non-small cell lung cancer
OCR	Oxygen consumption rate
PB	Polar body
pFF	Porcine follicular fluid
PMSG	Pregnant mare serum gonadotropin
RA	Relative abundance
qRT-PCR	Quantitative reverse transcriptase real-time polymerase chain reaction
ROS	Reactive oxygen species
RT	Reverse transcription
SCNT	Somatic cell nuclear transfer
SIRT3	Sirtuin 3
TNF-β	Tumor necrosis factor-β
TUNEL	Terminal deoxynucleotidyl transferase-mediated dUTP nick-end labelling
Vnz	Vinclozolin
ZP	Zona pellucida

References

1. Gore, A.C.; Chappell, V.A.; Fenton, S.E.; Flaws, J.E.; Nadal, A.; Prins, G.S.; Toppari, J.; Zoeller, R.T. EDC-2: The Endocrine Society's Second Scientific Statement on Endocrine-Disrupting Chemicals. *Endocr. Rev.* **2015**, *36*, E1–E150. [CrossRef] [PubMed]

2. Combarnous, Y.; Nguyen, T.M.D. Comparative Overview of the Mechanisms of Action of Hormones and Endocrine Disruptor Compounds. *Toxics* **2019**, *7*, 5. [CrossRef] [PubMed]

3. van Ravenzwaay, B.; Kolle, S.N.; Ramirez, T.; Kamp, H.G. Vinclozolin: A case study on the identification of endocrine active substances in the past and a future perspective. *Toxicol. Lett.* **2013**, *223*, 271–279. [CrossRef] [PubMed]

4. Kavlock, R.; Cummings, A. Mode of action: Inhibition of androgen receptor function–vinclozolin-induced malformations in reproductive development. *Crit. Rev. Toxicol.* **2005**, *35*, 721–726. [CrossRef]

5. Kiparissis, Y.; Metcalfe, T.L.; Balch, G.C.; Metcalfe, C.D. Effects of the antiandrogens, vinclozolin and cyproterone acetate on gonadal development in the Japanese medaka (*Oryzias latipes*). *Aquat. Toxicol.* **2003**, *63*, 391–403. [CrossRef]

6. Dang, Z.; Kienzler, A. Changes in fish sex ratio as a basis for regulating endocrine disruptors. *Environ. Int.* **2019**, *130*, 104928. [CrossRef]

7. Nilsson, E.E.; Anway, M.D.; Stanfield, J.; Skinner, M.K. Transgenerational epigenetic effects of the endocrine disruptor vinclozolin on pregnancies and female adult onset disease. *Reproduction* **2008**, *135*, 713–721. [CrossRef]

8. Buckley, J.; Willingham, E.; Agras, K.; Baskin, L.S. Embryonic exposure to the fungicide vinclozolin causes virilization of females and alteration of progesterone receptor expression in vivo: An experimental study in mice. *Environ. Health* **2006**, *5*, 4. [CrossRef]

9. Knet, M.; Tabarowski, Z.; Slomczynska, M.; Duda, M. The effects of the environmental antiandrogen vinclozolin on the induction of granulosa cell apoptosis during follicular atresia in pigs. *Theriogenology* **2014**, *81*, 1239–1247. [CrossRef]

10. Knet, M.; Wartalski, K.; Hoja-Lukowicz, D.; Tabarowski, Z.; Slomczynska, M.; Duda, M. Analysis of porcine granulosa cell death signaling pathways induced by vinclozolin. *Theriogenology* **2015**, *84*, 927–939. [CrossRef]

11. Wartalski, K.; Knet-Seweryn, M.; Hoja-Lukowicz, D.; Tabarowski, Z.; Duda, M. Androgen receptor-mediated non-genomic effects of vinclozolin on porcine ovarian follicles and isolated granulosa cells: Vinclozolin and non-genomic effects in porcine ovarian follicles. *Acta Histochem.* **2016**, *118*, 377–386. [CrossRef] [PubMed]

12. Gorczyca, G.; Wartalski, K.; Tabarowski, Z.; Duda, M. Effects of vinclozolin exposure on the expression and activity of SIRT1 and SIRT6 in the porcine ovary. *J. Physiol. Pharmacol.* **2019**, *70*, 153–165.

13. Kicman, A.T. Pharmacology of anabolic steroids. *Br. J. Pharmacol.* **2008**, *154*, 502–521. [CrossRef]

14. Llewellyn, W. Part III: Drug profiles. In *Anabolics*; Llewellyn, W., Ed.; Molecular Nutrition LLC: Jupiter, FL, USA, 2011; pp. 739–780.

15. Basaria, S.; Wahlstrom, J.T.; Dobs, A.S. Clinical review 138: Anabolic-androgenic steroid therapy in the treatment of chronic diseases. *J. Clin. Endocrinol. Metab.* **2001**, *86*, 5108–5117. [CrossRef] [PubMed]

16. Johnson, C.A. Use of androgens in patients with renal failure. *Semin. Dial.* **2000**, *13*, 36–39. [CrossRef]

17. Karbalay-Doust, S.; Noorafshan, A. Stereological study of the effects of nandrolone decanoate on the rat prostate. *Micron* **2006**, *37*, 617–623. [CrossRef]

18. Arlt, W. Androgen therapy in women. *Eur. J. Endocrinol.* **2006**, *154*, 1–11. [CrossRef]

19. Evans, N.A. Current concepts in anabolic-androgenic steroids. *Am. J. Sports Med.* **2004**, *32*, 534–542. [CrossRef]

20. Bahrke, M.S.; Yesalis, C.E. Abuse of anabolic androgenic steroids and related substances in sport and exercise. *Curr. Opin. Pharmacol.* **2004**, *4*, 614–620. [CrossRef]

21. Sjöqvist, F.; Garle, M.; Rane, A. Use of doping agents, particularly anabolic steroids, in sports and society. *Lancet* **2008**, *371*, 1872–1882. [CrossRef]

22. Kanayama, G.; Pope, H.G., Jr. History and epidemiology of anabolic androgens in athletes and non-athletes. *Mol. Cell. Endocrinol.* **2017**, *464*, 4–13. [CrossRef] [PubMed]

23. Fink, J.; Schoenfeld, B.J.; Hackney, A.C.; Matsumoto, M.; Maekawa, T.; Nakazato, K.; Horie, S. Anabolic-androgenic steroids: Procurement and administration practices od doping athletes. *Phys. Sportsmed.* **2019**, *47*, 10–14. [CrossRef] [PubMed]

24. Iriart, J.A.; Chaves, J.C.; Orleans, R.G. Body cult and use of anabolic steroids by bodybuilders (Article in Portuguese). *Cad. Saude Publica* **2009**, *25*, 773–782. [CrossRef] [PubMed]

25. Hall, R.C.W.; Hall, R.C.W. Abuse of supraphysiological doses of anabolic steroids. *South. Med. J.* **2005**, *98*, 550–555. [CrossRef] [PubMed]

26. Cannavò, S.; Curtò, L.; Trimarchi, F. Exercise-related female reproductive dysfunction. *J. Endocrinol. Investig.* **2001**, *24*, 823–832. [CrossRef]

27. Tripathi, A.; Tekkalaki, B.; Saxena, S.; Himanshu, D. Iatrogenic dependence of anabolic-androgenic steroid in Indian non-athletic women. *BMJ Case Rep.* **2014**, *2014*, bcr2013202472. [CrossRef]

28. Belardin, L.B.; Simão, V.A.; Leite, G.A.A.; Chuffa, L.G.A.; Camargo, I.C.C. Dose-dependent effects and reversibility of the injuries caused by nandrolone decanoate in uterine tissue and fertility of rats. *Birth Defects Res. B Dev. Reprod. Toxicol.* **2014**, *101*, 168–177. [CrossRef]

29. Kam, P.C.A.; Yarrow, M. Anabolic steroid abuse: Physiological and anaesthetic considerations. *Anaesthesia* **2005**, *60*, 685–692. [CrossRef]

30. Groot, M.J.; Biolatti, B. Histopathological effects of boldenone in cattle. *J. Vet. Med. A Physiol. Pathol. Clin. Med.* **2004**, *51*, 58–63. [CrossRef]

31. Patanè, F.G.; Liberto, A.; Maria Maglitto, A.N.; Malandrino, P.; Esposito, M.; Amico, F.; Cocimano, G.; Li Rosi, G.; Condorelli, D.; Di Nunno, N.; et al. Nandrolone Decanoate: Use, Abuse and Side Effects. *Medicina* **2020**, *56*, 606. [CrossRef]

32. Elks, J.; Ganellin, C.R. *The Dictionary of Drugs: Chemical Data: Chemical Data, Structures and Bibliographies*, 1st ed.; Springer: Berlin/Heidelberg, Germany, 2014.

33. Handelsman, D.J. Androgen physiology, pharmacology and abuse. In *Endocrinology-E-Book: Adult and Pediatric*, 6th ed.; Jameson, J.L., De Groot, L.J., Eds.; Elsevier Health Sciences: Amsterdam, The Netherlands, 2010; pp. 2469–2498.

34. Agriesti, F.; Tataranni, T.; Pacelli, C.; Scrima, R.; Laurenzana, I.; Ruggieri, V.; Cela, O.; Mazzoccoli, C.; Salerno, M.; Sessa, F.; et al. Nandrolone induces a stem cell-like phenotype in human hepatocarcinoma-derived cell line inhibiting mitochondrial respiratory activity. *Sci. Rep.* **2020**, *10*, 2287. [CrossRef]

35. Gorczyca, G.; Wartalski, K.; Wiater, J.; Samiec, M.; Tabarowski, Z.; Duda, M. Anabolic steroids-driven regulation of porcine ovarian putative stem cells favors the onset of their neoplastic transformation. *Int. J. Mol. Sci.* **2021**, *22*, 11800. [CrossRef] [PubMed]

36. Mobini Far, H.R.; Agren, G.; Lindqvist, A.S.; Marmendal, M.; Fahlke, C.; Thiblin, I. Administration of the anabolic androgenic steroid nandrolone decanoate to female rats causes alterations in the morphology of their uterus and a reduction in reproductive capacity. *Eur. J. Obstet. Gynecol. Reprod. Biol.* **2007**, *131*, 189–197. [CrossRef]

37. Chuffa, L.G.A.; Souza, R.B.; Frei, F.; Mesquita, S.F.P.; Camargo, I.C.C. Nandrolone decanoate and physical effort: Histological and morphometrical assessment in adult rat uterus. *Anat. Rec.* **2011**, *294*, 335–341. [CrossRef] [PubMed]

38. Karbalay-Doust, S.; Noorafshan, A. Stereological estimation of ovarian oocyte volume, surface area and number: Application on mice treated with nandrolone decanoate. *Folia Histochem. Cytobiol.* **2012**, *50*, 275–279. [CrossRef] [PubMed]

39. Simão, V.A.; Berloffa Belardin, L.; Araujo Leite, G.A.; de Almeida Chuffa, L.G.; Camargo, I.C.C. Effects of different doses of nandrolone decanoate on estrous cycle and ovarian tissue of rats after treatment and recovery periods. *Int. J. Exp. Pathol.* **2015**, *96*, 338–349. [CrossRef] [PubMed]

40. Vázquez-Laslop, N.; Mankin, A.S. How Macrolide Antibiotics Work. *Trends Biochem. Sci.* **2018**, *43*, 668–684. [CrossRef]

41. Maarten, N.; Kuypers, D.R.J.; Minnie, S. Calcineurin inhibitor nephrotoxicity. *Clin. J. Am. Soc. Nephrol.* **2009**, *4*, 481–508.

42. Russell, G.; Graveley, R.; Seid, J.; al-Humidan, A.K.; Skjodt, H. Mechanisms of action of cyclosporine and effects on connective tissues. *Semin. Arthritis Rheum.* **1992**, *21*, 16–22. [CrossRef]

43. Wiesner, R.H.; Goldstein, R.M.; Donovan, J.P.; Miller, C.M.; Lake, J.R.; Lucey, M.R. The impact of cyclosporine dose and level on acute rejection and patient and graft survival in liver transplant recipients. *Liver Transpl. Surg.* **1998**, *4*, 34–41. [CrossRef]

44. Efimov, S.V.; Dubinin, M.V.; Kobchikova, P.P.; Zgadzay, Y.O.; Khodov, I.A.; Belosludtsev, K.N.; Klochkov, V.V. Comparison of cyclosporin variants B–E based on their structural properties and activity in mitochondrial membranes. *Biochem. Biophys. Res. Commun.* **2020**, *526*, 1054–1060. [CrossRef] [PubMed]

45. Kim, J.S.; He, L.; Lemasters, J.J. Mitochondrial permeability transition: A common pathway to necrosis and apoptosis. *Biochem. Biophys. Res. Commun.* **2003**, *304*, 463–470. [CrossRef]

46. Sharov, V.G.; Todor, A.; Khanal, S.; Imai, M.; Sabbah, H.N. Cyclosporine A attenuates mitochondrial permeability transition and improves mitochondrial respiratory function in cardiomyocytes isolated from dogs with heart failure. *J. Mol. Cell. Cardiol.* **2007**, *42*, 150–158. [CrossRef] [PubMed]

47. Zakerkish, F.; Soriano, M.J.; Nocella-Mestre, E.; Brännström, M.; Díaz-García, C. Differential effects of the immunosuppressive calcineurin inhibitors cyclosporine-A and tacrolimus on ovulation in a murine model. *Hum. Reprod. Open* **2021**, *2021*, hoab012. [CrossRef]

48. Groth, K.; Brännström, M.; Mölne, J.; Wranning, C.A. Cyclosporine A exposure during pregnancy in mice: Effects on reproductive performance in mothers and offspring. *Hum. Reprod.* **2010**, *25*, 697–704. [CrossRef]

49. Camargo, I.C.C.; Leite, G.A.A.; Pinto, T.; Ribeiro-Paes, J.T. Histopathologycal findings in the ovaries and uterus of albino female rats promoted by co-administration of synthetic steroids and nicotine. *Exp. Toxicol. Pathol.* **2014**, *66*, 195–202. [CrossRef]

50. Mesbah, F.; Bordbar, H.; Khozani, T.T.; Dehghani, F.; Mirkhani, H. The non-preventive effects of human menopausal gonadotropins on ovarian tissues in nandrolone decanoate-treated female rats: A histochemical and ultra-structural study. *Int. J. Reprod. Biomed.* **2018**, *16*, 159–174. [CrossRef]

51. Motlik, J.; Crozet, N.; Fulka, J. Meiotic competence in vitro pf pig oocytes isolated from early antral follicles. *J. Reprod. Fertil.* **1984**, *72*, 323–328. [CrossRef]

52. Marchal, R.; Feugang, J.M.; Perreau, C.; Venturi, E.; Terqui, M.; Mermillod, P. Meiotic and developmental competence of prepubertal and adult swine oocyte. *Theriogenology* **2001**, *56*, 17–29. [CrossRef]

53. Wang, H.; Cui, W.; Meng, C.; Zhang, J.; Li, Y.; Qian, Y.; Xing, G.; Zhao, D.; Cao, S. MC1568 Enhances Histone Acetylation During Oocyte Meiosis and Improves Development of Somatic Cell Nuclear Transfer Embryos in Pig. *Cell. Reprogram.* **2018**, *20*, 55–65. [CrossRef]

54. Samiec, M.; Skrzyszowska, M. High developmental capability of porcine cloned embryos following trichostatin A-dependent epigenomic transformation during in vitro maturation of oocytes pre-exposed to *R*-roscovitine. *Anim. Sci. Pap. Rep.* **2012**, *30*, 383–393.

55. Gupta, M.K.; Heo, Y.T.; Kim, D.K.; Lee, H.T.; Uhm, S.J. 5-Azacytidine improves the meiotic maturation and subsequent in vitro development of pig oocytes. *Anim. Reprod. Sci.* **2019**, *208*, 106118. [CrossRef] [PubMed]

56. Watson, A.J. Oocyte cytoplasmic maturation: A key mediator of oocyte and embryo developmental competence. *J. Anim. Sci.* **2007**, *85* (Suppl. 13), E1–E3. [CrossRef]

57. Coticchio, G.; Dal Canto, M.; Mignini Renzini, M.; Guglielmo, M.C.; Brambillasca, F.; Turchi, D.; Novara, P.V.; Fadini, R. Oocyte maturation: Gamete-somatic cells interactions, meiotic resumption, cytoskeletal dynamics and cytoplasmic reorganization. *Hum. Reprod. Update* **2015**, *21*, 427–454. [CrossRef] [PubMed]

58. Conti, M.; Franciosi, F. Acquisition of oocyte competence to develop as an embryo: Integrated nuclear and cytoplasmic events. *Hum. Reprod. Update* **2018**, *24*, 245–266. [CrossRef]

59. Morselli, M.G.; Luvoni, G.C.; Comizzoli, P. The nuclear and developmental competence of cumulus–oocyte complexes is enhanced by three-dimensional coculture with conspecific denuded oocytes during in vitro maturation in the domestic cat model. *Reprod. Domest. Anim.* **2017**, *52*, 82–87. [CrossRef] [PubMed]

60. Ferreira, A.F.; Soares, M.; Almeida Reis, S.; Ramalho-Santos, J.; Sousa, A.P.; Almeida-Santos, T. Does supplementation with mitochondria improve oocyte competence? A systematic review. *Reproduction* **2021**, *161*, 269–287. [CrossRef]

61. Takeda, K. Functional consequences of mitochondrial mismatch in reconstituted embryos and offspring. *J. Reprod. Dev.* **2019**, *65*, 485–489. [CrossRef]

62. Lee, W.J.; Lee, J.H.; Jeon, R.H.; Jang, S.J.; Lee, S.C.; Park, J.S.; Lee, S.L.; King, W.A.; Rho, G.J. Supplement of autologous ooplasm into porcine somatic cell nuclear transfer embryos does not alter embryo development. *Reprod. Domest. Anim.* **2017**, *52*, 437–445. [CrossRef]

63. Srirattana, K.; St. John, J.C. Additional mitochondrial DNA influences the interactions between the nuclear and mitochondrial genomes in a bovine embryo model of nuclear transfer. *Sci. Rep.* **2018**, *8*, 7246. [CrossRef]

64. Eppig, J.J.; O'Brien, M.J. Development in vitro of mouse oocytes from primordial follicles. *Biol. Reprod.* **1996**, *54*, 197–207. [CrossRef] [PubMed]

65. Hunter, M.G. Oocyte maturation and ovum quality in pigs. *Rev. Reprod.* **2000**, *5*, 122–130. [CrossRef] [PubMed]

66. Cran, D.G. Qualitative and quantitative structural changes during pig oocyte maturation. *J. Reprod. Fertil.* **1985**, *74*, 237–245. [CrossRef] [PubMed]

67. Sasseville, M.; Gagnon, M.C.; Guillemette, C.; Sullivan, R.; Gilchrist, R.B.; Richard, F.J. Regulation of gap junctions in porcine cumulus-oocyte complexes: Contributions of granulosa cell contact, gonadotropins, and lipid rafts. *Mol. Endocrinol.* **2009**, *23*, 700–710. [CrossRef] [PubMed]

68. Santiquet, N.W.; Develle, Y.; Laroche, A.; Robert, C.; Richard, F.J. Regulation of gap-junctional communication between cumulus cells during in vitro maturation in swine, a gap-FRAP study. *Biol. Reprod.* **2012**, *87*, 46. [CrossRef] [PubMed]

69. Zhou, C.J.; Wu, S.N.; Shen, J.P.; Wang, D.H.; Kong, X.W.; Lu, A.; Li, Y.J.; Zhou, H.X.; Zhao, Y.F.; Liang, C.G. The beneficial effects of cumulus cells and oocyte-cumulus cell gap junctions depends on oocyte maturation and fertilization methods in mice. *PeerJ* **2016**, *4*, e1761. [CrossRef]

70. Milakovic, I.; Jeseta, M.; Hanulakova, S.; Knitlova, D.; Hanzalova, K.; Hulinska, P.; Machal, L.; Kempisty, B.; Antosik, P.; Machatkova, M. Energy Status Characteristics of Porcine Oocytes During In Vitro Maturation is Influenced by Their Meiotic Competence. *Reprod. Domest. Anim.* **2015**, *50*, 812–819. [CrossRef]

71. Tsai, T.S.; Tyagi, S.; St. John, J.C. The molecular characterisation of mitochondrial DNA deficient oocytes using a pig model. *Hum. Reprod.* **2018**, *33*, 942–953. [CrossRef]

72. Zhao, J.; Li, Y. Adenosine triphosphate content in human unfertilized oocytes, undivided zygotes and embryos unsuitable for transfer or cryopreservation. *J. Int. Med. Res.* **2012**, *40*, 734–739. [CrossRef]

73. Zuidema, D.; Sutovsky, P. The domestic pig as a model for the study of mitochondrial inheritance. *Cell Tissue Res.* **2020**, *380*, 263–271. [CrossRef]

74. Dumollard, R.; Duchen, M.; Carroll, J. The role of mitochondrial function in the oocyte and embryo. *Curr. Top. Dev. Biol.* **2007**, *77*, 21–49. [PubMed]

75. Cagnone, G.L.; Tsai, T.S.; Makanji, Y.; Matthews, P.; Gould, J.; Bonkowski, M.S.; Elgass, K.D.; Wong, A.S.; Wu, L.E.; McKenzie, M.; et al. Restoration of normal embryogenesis by mitochondrial supplementation in pig oocytes exhibiting mitochondrial DNA deficiency. *Sci. Rep.* **2016**, *6*, 23229. [CrossRef] [PubMed]

76. El Shourbagy, S.H.; Spikings, E.C.; Freitas, M.; St John, J.C. Mitochondria directly influence fertilisation outcome in the pig. *Reproduction* **2006**, *131*, 233–245. [CrossRef] [PubMed]

77. Tsai, T.S.; St John, J.C. The effects of mitochondrial DNA supplementation at the time of fertilization on the gene expression profiles of porcine preimplantation embryos. *Mol. Reprod. Dev.* **2018**, *85*, 490–504. [CrossRef]

78. Labarta, E.; de Los Santos, M.J.; Herraiz, S.; Escribá, M.J.; Marzal, A.; Buigues, A.; Pellicer, A. Autologous mitochondrial transfer as a complementary technique to intracytoplasmic sperm injection to improve embryo quality in patients undergoing in vitro fertilization-a randomized pilot study. *Fertil. Steril.* **2019**, *111*, 86–96. [CrossRef]

79. Xu, L.; Mesalam, A.; Lee, K.L.; Song, S.H.; Khan, I.; Chowdhury, M.M.R.; Lv, W.; Kong, I.K. Improves the in vitro developmental competence and reprogramming efficiency of cloned bovine embryos by additional complimentary cytoplasm. *Cell. Reprogram.* **2019**, *21*, 51–60. [CrossRef]

80. Bebbere, D.; Ulbrich, S.E.; Giller, K.; Zakhartchenko, V.; Reichenbach, H.D.; Reichenbach, M.; Verma, P.J.; Wolf, E.; Ledda, S.; Hiendleder, S. Mitochondrial DNA Depletion in Granulosa Cell Derived Nuclear Transfer Tissues. *Front. Cell Dev. Biol.* **2021**, *9*, 664099. [CrossRef]

81. Song, S.H.; Lee, K.L.; Xu, L.; Joo, M.D.; Hwang, J.Y.; Oh, S.H.; Kong, I.K. Production of cloned cats using additional complimentary cytoplasm. *Anim. Reprod. Sci.* **2019**, *208*, 106125. [CrossRef]

82. Babayev, E.; Seli, E. Oocyte mitochondrial function and reproduction. *Curr. Opin. Obstet. Gynecol.* **2015**, *27*, 175–181. [CrossRef]

83. Srirattana, K.; St John, J.C. Manipulating the mitochondrial genome to enhance cattle embryo development. *G3 (Bethesda)* **2017**, *7*, 2065–2080. [CrossRef]

84. Srirattana, K.; St John, J.C. Transmission of dysfunctional mitochondrial DNA and its implications for mammalian reproduction. *Adv. Anat. Embryol. Cell Biol.* **2019**, *231*, 75–103. [PubMed]

85. Tokumoto, T.; Tokumoto, M.; Nagahama, M.Y. Induction and inhibition of oocyte maturation by EDCs in zebrafish. *Reprod. Biol. Endocrinol.* **2005**, *3*, 69. [CrossRef] [PubMed]

86. D'Angelo, J.; Freeman, E. Effects of endocrine-disrupting chemical exposure on zebrafish ovarian follicles. *Bios* **2017**, *88*, 9–18. [CrossRef]

87. Roth, Z.; Komsky-Elbaz, A.; Kalo, D. Effect of environmental contamination on female and male gametes—A lesson from bovines. *Anim. Reprod.* **2020**, *17*, e20200041. [CrossRef] [PubMed]

88. Jeong, P.S.; Lee, S.; Park, S.H.; Kim, M.J.; Kang, H.G.; Nanjidsuren, T.; Son, H.C.; Song, B.S.; Koo, D.B.; Sim, B.W.; et al. Butylparaben Is Toxic to Porcine Oocyte Maturation and Subsequent Embryonic Development Following In Vitro Fertilization. *Int. J. Mol. Sci.* **2020**, *21*, 3692. [CrossRef] [PubMed]

89. Sobek, A.; Tkadlec, E.; Klaskova, E.; Prochazka, M. Cytoplasmic Transfer Improves Human Egg Fertilization and Embryo Quality: An Evaluation of Sibling Oocytes in Women with Low Oocyte Quality. *Reprod. Sci.* **2021**, *28*, 1362–1369. [CrossRef]

90. Do, M.; Jang, W.G.; Hwang, J.; Jang, H.; Kim, E.J.; Jeong, E.J.; Shim, H.; Hwang, S.; Oh, K.; Byun, S.; et al. Inheritance of mitochondrial DNA in serially recloned pigs by somatic cell nuclear transfer (SCNT). *Biochem. Biophys. Res. Commun.* **2012**, *424*, 765–770. [CrossRef]

91. Song, S.H.; Oh, S.H.; Xu, L.; Lee, K.L.; Hwang, J.Y.; Joo, M.D.; Kong, I.K. Effect of additional cytoplasm of cloned embryo on in vitro developmental competence and reprogramming efficiency in mice. *Cell. Reprogram.* **2020**, *22*, 236–243. [CrossRef]

92. Srirattana, K.; Kaneda, M.; Parnpai, R. Strategies to Improve the Efficiency of Somatic Cell Nuclear Transfer. *Int. J. Mol. Sci.* **2022**, *23*, 1969. [CrossRef]

93. Martinović, D.; Blake, L.S.; Durhan, E.J.; Greene, K.J.; Kahl, M.D.; Jensen, K.J.; Makynen, E.A.; Villeneuve, D.L.; Ankley, G.T. Reproductive toxicity of vinclozolin in the fathead minnow: Confirming an anti-androgenic mode of action. *Environ. Toxicol. Chem.* **2008**, *27*, 478–488. [CrossRef]

94. Makynen, E.A.; Kahl, M.D.; Jensen, K.M.; Tietge, J.E.; Wells, K.L.; Van Der Kraak, G.; Ankley, G.T. Effects of the mammalian antiandrogen vinclozolin on development and reproduction of the fathead minnow (*Pimephales promelas*). *Aquat. Toxicol.* **2000**, *48*, 461–475. [CrossRef]

95. Anway, M.D.; Skinner, M.K. Epigenetic programming of the germ line: Effects of endocrine disruptors on the development of transgenerational disease. *Reprod. Biomed. Online* **2008**, *16*, 23–25. [CrossRef]

96. Uzumcu, M.; Zachow, R. Developmental exposure to environmental endocrine disruptors: Consequences within the ovary and on female reproductive function. *Reprod. Toxicol.* **2007**, *23*, 337–352. [CrossRef] [PubMed]

97. Merviel, P.; Cabry, R.; Chardon, K.; Haraux, E.; Scheffler, F.; Mansouri, N.B.; Devaux, A.; Hikmat Chahine, H.; Bach, V.; Copin, H. Impact of oocytes with CLCG on ICSI outcomes and their potential relation to pesticide exposure. *J. Ovarian Res.* **2017**, *10*, 42. [CrossRef] [PubMed]

98. Renault, V.M.; Thekkat, P.U.; Hoang, K.L.; White, J.L.; Brad, C.A.; Kenzelmann Broz, D.; Venturelli, O.S.; Johnson, T.M.; Oskoui, P.R.; Xuan, Z.; et al. The pro-longevity gene FoxO3 is a direct target of the p53 tumor suppressor. *Oncogene* **2011**, *30*, 3207–3221. [CrossRef]

99. Sionov, R.V.; Vlahopoulos, S.A.; Granot, Z. Regulation of Bim in Health and Disease. *Oncotarget* **2015**, *6*, 23058–23134. [CrossRef]

100. Obexer, P.; Geiger, K.; Ambros, P.F.; Meister, B.; Ausserlechner, M.J. FKHRL1-mediated expression of Noxa and Bim induces apoptosis via the mitochondria in neuroblastoma cells. *Cell Death Differ.* **2007**, *14*, 534–547. [CrossRef]

101. Hagenbuchner, J.; Kuznetsov, A.; Hermann, M.; Hausott, B.; Obexer, P.; Ausserlechner, M.J. FOXO3-induced reactive oxygen species are regulated by BCL2L11 (Bim) and SESN3. *J. Cell Sci.* **2012**, *125*, 1191–1203. [CrossRef]

102. Lee, K.S.; Joo, B.S.; Na, Y.J.; Yoon, M.S.; Choi, O.H.; Kim, W.W. Clinical assisted reproduction: Cumulus cells apoptosis as an indicator to predict the quality of oocytes and the outcome of IVF–ET. *J. Assist. Reprod. Genet.* **2001**, *18*, 490–498. [CrossRef]

103. Kasof, G.M.; Gomes, B.C. Livin, a novel inhibitor of apoptosis protein family member. *J. Biol. Chem.* **2001**, *276*, 3238–3246. [CrossRef]

104. Sugihara, E.; Hashimoto, N.; Osuka, S.; Shimizu, T.; Ueno, S.; Okazaki, S.; Yaguchi, T.; Kawakami, Y.; Kosaki, K.; Sato, T.A. The Inhibitor of Apoptosis Protein Livin Confers Resistance to Fas-Mediated Immune Cytotoxicity in Refractory Lymphoma. *Cancer Res.* **2020**, *80*, 4439–4450. [CrossRef] [PubMed]

105. Aki, T.; Uemura, K. Cell Death and Survival Pathways Involving ATM Protein Kinase. *Genes* **2021**, *12*, 1581. [CrossRef] [PubMed]

106. Rueda, C.B.; Llorente-Folch, I.; Traba, J.; Amigo, I.; Gonzalez-Sanchez, P.; Contreras, L.; Juaristi, I.; Martinez-Valero, P.; Pardo, B.; Del Arco, A.; et al. Glutamate excitotoxicity and Ca^{2+}-regulation of respiration: Role of the Ca2+ activated mitochondrial transporters (CaMCs). *Biochim. Biophys. Acta* **2016**, *1857*, 1158–1166. [CrossRef] [PubMed]

107. Li, X.; Fang, P.; Li, Y.; Kuo, Y.M.; Andrews, A.J.; Nanayakkara, G.; Johnson, C.; Fu, H.; Shan, H.; Du, F. Mitochondrial reactive oxygen species mediate lysophosphatidylcholine-induced endothelial cell activation. *Arterioscler. Thromb. Vasc. Biol.* **2016**, *36*, 1090–1100. [CrossRef]

108. Mazat, J.P.; Ransac, S.; Heiske, M.; Devin, A.; Rigoulet, M. Mitochondrial energetic metabolism-some general principles. *IUBMB Life* **2013**, *65*, 171–179. [CrossRef]

109. Baines, C.P. Role of the mitochondrion in programmed necrosis. *Front. Physiol.* **2010**, *1*, 156. [CrossRef]

110. Cabon, L.; Galán-Malo, P.; Bouharrour, A.; Delavallée, L.; Brunelle-Navas, M.N.; Lorenzo, H.K.; Gross, A.; Susin, S.A. BID regulates AIF-mediated caspase-independent necroptosis by promoting BAX activation. *Cell Death Differ.* **2012**, *19*, 245–256. [CrossRef]

111. Chaube, S.K.; Prasad, P.V.; Thakur, S.C.; Shrivastav, T.G. Hydrogen peroxide modulates meiotic cell cycle and induces morphological features characteristic of apoptosis in rat oocytes cultured in vitro. *Apoptosis* **2005**, *10*, 863–874. [CrossRef]

112. Yu, Y.; Dumollard, R.; Rossbach, A.; Lai, F.A.; Swann, K. Redistribution of mitochondria leads to bursts of ATP production during spontaneous mouse oocyte maturation. *J. Cell. Physiol.* **2010**, *224*, 672–680. [CrossRef]

113. Marangos, P.; Carroll, J. The dynamics of cyclin B1 distribution during meiosis I in mouse oocytes. *Reproduction* **2004**, *128*, 153–162. [CrossRef]

114. Conti, M.; Hsieh, M.; Zamah, A.M.; Oh, J.S. Novel signaling mechanisms in the ovary during oocyte maturation and ovulation. *Mol. Cell. Endocrinol.* **2012**, *356*, 65–73. [CrossRef] [PubMed]

115. Holt, J.E.; Lane, S.I.R.; Jones, K.T. The control of meiotic maturation in mammalian oocytes. *Curr. Top. Dev. Biol.* **2013**, *102*, 207–226. [PubMed]

116. Prates, E.G.; Marques, C.C.; Baptista, M.C.; Vasques, M.I.; Carolino, N.; Horta, A.E.M.; Charneca, R.; Nunes, J.T.; Pereira, R.M. Fat area and lipid droplet morphology of porcine oocytes during in vitro maturation with trans-10, cis-12 conjugated linoleic acid and forskolin. *Animal* **2013**, *7*, 602–609. [CrossRef] [PubMed]

117. Abazarikia, A.; Ariu, F.; Rasekhi, M.; Zhandi, M.; Ledda, S. Distribution and size of lipid droplets in oocytes recovered from young lamb and adult ovine ovaries. *Reprod. Fertil. Dev.* **2020**, *32*, 1022–1026. [CrossRef]

118. He, B.; Yin, C.; Gong, Y.; Liu, J.; Guo, H.; Zhao, R. Melatonin-induced increase of lipid droplets accumulation and in vitro maturation in porcine oocytes is mediated by mitochondrial quiescence. *J. Cell. Physiol.* **2018**, *233*, 302–312. [CrossRef]

119. Bordbar, H.; Mesbah, F.; Talaei, T.; Dehghani, F.; Mirkhani, H. Modulatory effect of gonadotropins on rats' ovaries after nandrolone decanoate administration: A stereological study. *Iran. J. Med. Sci.* **2014**, *39*, 44–50.

120. Carteri, R.B.; Kopczynski, A.; Menegassi, L.N.; Rodolphi, M.S.; Strogulski, N.R.; Portela, L.V. Anabolic-androgen steroids effects on bioenergetics responsiveness of synaptic and extrasynaptic mitochondria. *Toxicol. Lett.* **2019**, *307*, 72–80. [CrossRef]

121. Nagano, M.; Katagiri, S.; Takahashi, Y. ATP content and maturational/developmental ability of bovine oocytes with various cytoplasmic morphologies. *Zygote* **2006**, *14*, 299–304. [CrossRef]

122. Duran, H.E.; Simsek-Duran, F.; Oehninger, S.C.; Jones, H.W., Jr.; Castora, F.J. The association of reproductive senescence with mitochondrial quantity, function, and DNA integrity in human oocytes at different stages of maturation. *Fertil. Steril.* **2011**, *96*, 384–388. [CrossRef]

123. Kumar, M.; Pathak, D.; Kriplani, A.; Ammini, A.C.; Talwar, P.; Dada, R. Nucleotide variations in mitochondrial DNA and supra-physiological ROS levels in cytogenetically normal cases of premature ovarian insufficiency. *Arch. Gynecol. Obstet.* **2010**, *282*, 695–705. [CrossRef]

124. Lanneau, D.; Brunet, M.; Frisan, E.; Solary, E.; Fontenay, M.; Garrido, C. Heat shock proteins: Essential proteins for apoptosis regulation. *J. Cell. Mol. Med.* **2008**, *12*, 743–761. [CrossRef] [PubMed]

125. Bodzek, P.; Damasiewicz-Bodzek, A.; Janosz, I.; Witek, L.; Olejek, A. Heat shock protein 27 (HSP27) in patients with ovarian cancer. *Ginekol. Pol.* **2021**, *92*, 837–843. [CrossRef] [PubMed]

126. Fernandes, M.T.; Dejardin, E.; dos Santos, N.R. Context-dependent roles for lymphotoxin-β receptor signaling in cancer development. *Biochim. Biophys. Acta* **2016**, *1865*, 204–219. [CrossRef] [PubMed]

127. Dzafic, E.; Stimpfel, M.; Virant-Klun, I. Plasticity of granulosa cells: On the crossroad of stemness and transdifferentiation potential. *J. Assist. Reprod. Genet.* **2013**, *30*, 1255–1261. [CrossRef]

128. Dompe, C.; Kulus, M.; Stefańska, K.; Kranc, W.; Chermuła, B.; Bryl, R.; Pieńkowski, W.; Nawrocki, M.J.; Petitte, J.N.; Stelmach, B.; et al. Human granulosa cells—stemness properties, molecular cross-talk and follicular angiogenesis. *Cells* **2021**, *10*, 1396. [CrossRef]

129. Skinner, M.K.; Schmidt, M.; Savenkova, M.I.; Sadler-Riggleman, I.; Nilsson, E.E. Regulation of granulosa and theca cell transcriptomes during ovarian antral follicle development. *Mol. Reprod. Dev.* **2008**, *75*, 1457–1472. [CrossRef]

130. Lavranos, T.C.; Rodgers, H.F.; Bertoncello, I.; Rodgers, R.J. Anchorage-independent culture of bovine granulosa cells: The effects of basic fibroblast growth factor and dibutyryl cAMP on cell division and differentiation. *Exp. Cell Res.* **1994**, *211*, 245–251. [CrossRef] [PubMed]

131. Kossowska-Tomaszczuk, K.; De Geyter, C.; De Geyter, M.; Martin, I.; Holzgreve, W.; Scherberich, A.; Zhang, H. The multipotency of luteinizing granulosa cells collected from mature ovarian follicles. *Stem Cells* **2009**, *27*, 210–219. [CrossRef]

132. Riva, F.; Omes, C.; Bassani, R.; Nappi, R.E.; Mazzini, G.; Cornaglia, A.I.; Casasco, A. In-vitro culture system for mesenchymal progenitor cells derived from waste human ovarian follicular fluid. *Reprod. Biomed. Online* **2014**, *29*, 457–469. [CrossRef]

133. Wang, J.; Chu, K.; Wang, Y.; Li, J.; Fu, J.; Zeng, Y.A.; Li, W. Procr-expressing granulosa cells are highly proliferative and are important for follicle development. *iScience* **2021**, *24*, 102065. [CrossRef]

134. Oki, Y.; Ono, H.; Motohashi, T.; Sugiura, N.; Nobusue, H.; Kano, K. Dedifferentiated follicular granulosa cells derived from pig ovary can transdifferentiate into osteoblasts. *Biochem. J.* **2012**, *447*, 239–248. [CrossRef]

135. Merkwitz, C.; Ricken, A.M.; Lösche, A.; Sakurai, M.; Spanel-Borowski, K. Progenitor cells harvested from bovine follicles become endothelial cells. *Differentiation* **2010**, *79*, 203–210. [CrossRef] [PubMed]

136. Elsherif, S.; Bourne, M.; Soule, E.; Lall, C.; Bhosale, P. Multimodality imaging and genomics of granulosa cell tumors. *Abdom. Radiol.* **2020**, *45*, 812–827. [CrossRef] [PubMed]

137. Pectasides, D.; Pectasides, E.; Psyrri, A. Granulosa cell tumor of the ovary. *Cancer Treat. Rev.* **2008**, *34*, 1–12. [CrossRef] [PubMed]

138. Sekkate, S.; Kairouani, M.; Serji, B.; Tazi, A.; Mrabti, H.; Boutayeb, S.; Errihani, H. Ovarian granulosa cell tumors: A retrospective study of 27 cases and a review of the literature. *World J. Surg. Oncol.* **2013**, *11*, 142. [CrossRef] [PubMed]

139. Wiesner, R.; Rabkin, J.; Klintmalm, G.; McDiarmid, S.; Langnas, A.; Punch, J.; McMaster, P.; Kalayoglu, M.; Levy, G.; Freeman, R.; et al. A randomized double-blind comparative study of mycophenolate mofetil and azathioprine in combination with cyclosporine and corticosteroids in primary liver transplant recipients. *Liver Transpl.* **2001**, *7*, 442–450. [CrossRef]

140. Ahlbach, C.L.; Lexa, K.W.; Bockus, A.T.; Chen, V.; Crews, P.; Jacobson, M.P.; Lokey, R.S. Beyond cyclosporine A: Conformation-dependent passive membrane permeabilities of cyclic peptide natural products. *Future Med. Chem.* **2015**, *7*, 2121–2130. [CrossRef]

141. Jimenez, R.; Galan, A.I.; Gonzalez de Buitrago, J.M.; Palomero, J.; Munoz, M.E. Glutathione Metabolism In Cyclosporine A-Treated Rats: Dose-And Time-Related Changes In Liver And Kidney. *Clin. Exp. Pharmacol. Physiol.* **2000**, *27*, 991–996. [CrossRef]

142. Pallet, N.; Bouvier, N.; Legendre, C.; Gilleron, J.; Codogno, P.; Beaune, P.; Thervet, E.; Anglicheau, D. Autophagy protects renal tubular cells against cyclosporine toxicity. *Autophagy* **2008**, *4*, 783–791. [CrossRef]

143. Pallet, N.; Bouvier, N.; Bandjallabah, A.; Rabant, M.; Flinois, J.P.; Hertig, A.; Legendre, C.; Beaune, P.; Thervet, E.; Anglicheau, D. Cyclosporine-induced endoplasmic reticulum stress triggers tubular phenotypic changes and death. *Am. J. Transplant.* **2008**, *8*, 2283–2296. [CrossRef]

144. Pallet, N.; Anglicheau, D. Autophagy: A protective mechanism against nephrotoxicant-induced renal injury. *Kidney Int.* **2009**, *75*, 118–119. [CrossRef]

145. Ogata, M.; Hino, S.; Saito, A.; Morikawa, K.; Kondo, S.; Kanemoto, S.; Murakami, T.; Taniguchi, M.; Tanii, I.; Yoshinaga, K. Autophagy is activated for cell survival after endoplasmic reticulum stress. *Mol. Cell. Biol.* **2006**, *26*, 9220–9231. [CrossRef] [PubMed]

146. Ciechomska, I.A.; Gabrusiewicz, K.; Szczepankiewicz, A.; Kaminska, B. Endoplasmic reticulum stress triggers autophagy in malignant glioma cells undergoing cyclosporine A-induced cell death. *Oncogene* **2013**, *32*, 1518–1529. [CrossRef] [PubMed]

147. Han, Z.B.; Lan, G.C.; Wu, Y.G.; Han, D.; Feng, W.G.; Wang, J.Z.; Tan, J.H. Interactive effects of granulosa cell apoptosis, follicle size, cumulus–oocyte complex morphology, and cumulus expansion on the developmental competence of goat oocytes: A study using the well-in-drop culture system. *Reproduction* **2006**, *132*, 749–758. [CrossRef] [PubMed]

148. Nunnari, J.; Suomalainen, A. Mitochondria: In sickness and in health. *Cell* **2012**, *148*, 1145–1159. [CrossRef]

149. Wang, Y.; Hekimi, S. Mitochondrial dysfunction and longevity in animals: Untangling the knot. *Science* **2015**, *350*, 1204–1207. [CrossRef]

150. Jiang, K.; He, B.; Lai, L.; Chen, Q.; Liu, Y.; Guo, Q.; Wang, Q. Cyclosporine A inhibits breast cancer cell growth by downregulating the expression of pyruvate kinase subtype M2. *Int. J. Mol. Med.* **2012**, *30*, 302–308. [CrossRef]

151. Jeon, S.H.; Piao, Y.J.; Choi, K.J.; Hong, F.; Baek, H.W.; Kang, I.; Ha, J.; Kim, S.S.; Chang, S.G. Prednisolone suppresses cyclosporin A-induced apoptosis but not cell cycle arrest in MDCK cells. *Arch. Biochem. Biophys.* **2005**, *435*, 382–392. [CrossRef]

152. Roy, M.K.; Takenaka, M.; Kobori, M.; Nakahara, K.; Isobe, S.; Tsushida, T. Apoptosis, necrosis and cell proliferation-inhibition by cyclosporine A in U937 cells (a human monocytic cell line). *Pharmacol. Res.* **2006**, *53*, 293–302. [CrossRef]

153. Zorova, L.D.; Popkov, V.A.; Plotnikov, E.Y.; Silachev, D.N.; Pevzner, I.B.; Jankauskas, S.S.; Babenko, V.A.; Zorov, S.D.; Balakireva, A.V.; Juhaszova, M.; et al. Mitochondrial membrane potential. *Anal. Biochem.* **2018**, *552*, 50–59. [CrossRef]

154. Zeng, H.T.; Ren, Z.; Yeung, W.S.; Shu, Y.M.; Xu, Y.W.; Zhuang, G.L.; Liang, X.Y. Low mitochondrial DNA and ATP contents contribute to the absence of birefringent spindle imaged with PolScope in in vitro matured human oocytes. *Hum. Reprod.* **2007**, *22*, 1681–1686. [CrossRef] [PubMed]

155. Gore-Langton, R.E. Cyclosporine differentially affects estrogen and progestin synthesis by rat granulosa cells in vitro. *Mol. Cell. Endocrinol.* **1988**, *57*, 187–198. [CrossRef]

156. Ross, H.J.; Cho, J.; Osann, K.; Wong, S.F.; Ramsinghani, N.; Williams, J.; Downey-Hurtado, N.; Slater, L.M. Phase I/II trial of low dose cyclosporin A with EP for advanced non-small cell lung cancer. *Lung Cancer* **1997**, *18*, 189–198. [CrossRef]

157. Qin, X.; Chen, Z. Metabolic dependence of cyclosporine A on cell proliferation of human non-small cell lung cancer A549 cells and its implication in post-transplant malignancy. *Oncol. Rep.* **2019**, *41*, 2997–3004. [CrossRef] [PubMed]

158. Cevik, O.; Turut, F.A.; Acidereli, H.; Yildirim, S. Cyclosporine-A induces apoptosis in human prostate cancer cells PC3 and DU145 via downregulation of COX-2 and upregulation of TGFβ. *Turk. Biyokim. Derg.* **2019**, *44*, 47–54. [CrossRef]

159. Pedersen, H.S.; Løvendahl, P.; Nikolaisen, N.K.; Holm, P.; Hyttel, P.; Nyengaard, J.R.; Chen, F.; Callesen, H. Mitochondrial dynamics in pre- and post-pubertal pig oocytes before and after in vitro maturation. *Reprod. Fertil. Dev.* **2014**, *26*, 189–190. [CrossRef]

160. Gorczyca, G.; Wartalski, K.; Tabarowski, Z.; Duda, M. Proteolytically Degraded Alginate Hydrogels and Hydrophobic Microbioreactors for Porcine Oocyte Encapsulation. *J. Vis. Exp.* **2019**, *161*, e61325. [CrossRef]

161. Pawlak, P.; Warzych, E.; Chabowska, A.; Lechniak, D. Differences in cytoplasmic maturation between the BCB+ and control porcine oocytes do not justify application of the BCB test for a standard IVM protocol. *J. Reprod. Dev.* **2014**, *60*, 28–36. [CrossRef]

162. Jia, B.Y.; Xiang, D.C.; Shao, Q.Y.; Zhang, B.; Liu, S.N.; Hong, Q.H.; Quan, G.B.; Wu, G.Q. Inhibitory effects of astaxanthin on postovulatory porcine oocyte aging in vitro. *Sci. Rep.* **2020**, *10*, 20217. [CrossRef]

163. Matsuda, F.; Inoue, N.; Maeda, A.; Cheng, Y.; Sai, T.; Gonda, H.; Goto, Y.; Sakamaki, K.; Manabe, N. Expression and function of apoptosis initiator FOXO3 in granulosa cells during follicular atresia in pig ovaries. *J. Reprod. Dev.* **2011**, *57*, 151–158. [CrossRef]

164. Jin, D.; Tan, H.J.; Lei, T.; Gan, L.; Chen, X.D.; Long, Q.Q.; Feng, B.; Yang, Z.Q. Molecular cloning and characterization of porcine sirtuin genes. *Comp. Biochem. Physiol. B Biochem. Mol. Biol.* **2009**, *153*, 348–358. [CrossRef] [PubMed]

165. Lee, S.K.; Zhao, M.H.; Kwon, J.W.; Li, Y.H.; Lin, Z.L.; Jin, Y.X.; Kim, N.H.; Cui, X.S. The association of mitochondrial potential and copy number with pig oocyte maturation and developmental potential. *J. Reprod. Dev.* **2014**, *60*, 128–135. [CrossRef] [PubMed]

166. Pfaffl, M.W. A new mathematical model for relative quantification in real-time RT-PCR. *Nucleic Acids Res.* **2001**, *29*, e45. [CrossRef] [PubMed]

167. Duda, M.; Durlej, M.; Knet, M.; Knapczyk-Stwora, K.; Tabarowski, Z.; Slomczynska, M. Does 2-hydroxyflutamide inhibit apoptosis in porcine granulosa cells?—An in vitro study. *J. Reprod. Dev.* **2012**, *58*, 438–444. [CrossRef]

168. Romek, M.; Gajda, B.; Rolka, M.; Smorąg, Z. Mitochondrial activity and morphology in developing porcine oocytes and pre-implantation non-cultured and cultured embryos. *Reprod. Domest. Anim.* **2011**, *46*, 471–480. [CrossRef]

169. De Moura, M.B.; Van Houten, B. Bioenergetic analysis of intact mammalian cells using the Seahorse XF24 Extracellular Flux analyzer and a luciferase ATP assay. In *Molecular Toxicology Protocols*; Keohavong, P., Grant, S., Eds.; Humana Press: Totowa, NJ, USA, 2014; pp. 589–602.

170. Muller, B.; Lewis, N.; Adeniyi, T.; Leese, H.J.; Brison, D.R.; Sturmey, R.G. Application of extracellular flux analysis for determining mitochondrial function in mammalian oocytes and early embryos. *Sci. Rep.* **2019**, *9*, 16778. [CrossRef]

171. Romek, M.; Kucia, M.; Gajda, B.; Krzysztofowicz, E.; Smorag, Z. Effect of high hydrostatic pressure on mitochondrial activity, reactive oxygen species level and developmental competence of cultured pig embryos. *Theriogenology* **2019**, *68*, 99–108. [CrossRef]

172. Adegoke, E.O.; Xue, W.; Machebe, N.S.; Adeniran, S.O.; Hao, W.; Chen, W.; Han, Z.; Guixue, Z.; Peng, Z. Sodium Selenite inhibits mitophagy, downregulation and mislocalization of blood-testis barrier proteins of bovine Sertoli cell exposed to microcystin-leucine arginine (MC-LR) via TLR4/NF-κB and mitochondrial signaling pathways blockage. *Ecotoxicol. Environ. Saf.* **2018**, *166*, 165–175. [CrossRef]

Article

The Induced Expression of *BPV E4* Gene in Equine Adult Dermal Fibroblast Cells as a Potential Model of Skin Sarcoid-like Neoplasia

Przemysław Podstawski [1,2,*], Marcin Samiec [3], Maria Skrzyszowska [3], Tomasz Szmatoła [1,4], Ewelina Semik-Gurgul [1] and Katarzyna Ropka-Molik [1,*]

1 Department of Animal Molecular Biology, National Research Institute of Animal Production, Krakowska 1 Street, 32-083 Balice, Poland; tomasz.szmatola@iz.edu.pl (T.S.); ewelina.semik@iz.edu.pl (E.S.-G.)
2 Department of Animal Reproduction, Anatomy and Genomics, University of Agriculture in Kraków, Mickiewicza 24/28, 30-059 Kraków, Poland
3 Department of Reproductive Biotechnology and Cryoconservation, National Research Institute of Animal Production, Krakowska 1 Street, 32-083 Balice, Poland; marcin.samiec@iz.edu.pl (M.S.); maria.skrzyszowska@iz.edu.pl (M.S.)
4 Center for Experimental and Innovative Medicine, University of Agriculture in Krakow, Rędzina 1c Street, 30-248 Kraków, Poland
* Correspondence: przemyslaw.podstawski@iz.edu.pl (P.P.); katarzyna.ropka@iz.edu.pl (K.R.-M.)

Abstract: The equine sarcoid is one of the most common neoplasias in the *Equidae* family. Despite the association of this tumor with the presence of bovine papillomavirus (BPV), the molecular mechanism of this lesion has not been fully understood. The transgenization of equine adult cutaneous fibroblast cells (ACFCs) was accomplished by nucleofection, followed by detection of molecular modifications using high-throughput NGS transcriptome sequencing. The results of the present study confirm that *BPV-E4-* and *BPV-E1^E4*-mediated nucleofection strategy significantly affected the transcriptomic alterations, leading to sarcoid-like neoplastic transformation of equine ACFCs. Furthermore, the results of the current investigation might contribute to the creation of in vitro biomedical models suitable for estimating the fates of molecular dedifferentiability and the epigenomic reprogramma-bility of *BPV-E4* and *BPV-E4^E1* transgenic equine ACFC-derived sarcoid-like cell nuclei in equine somatic cell-cloned embryos. Additionally, these in vitro models seem to be reliable for thoroughly recognizing molecular mechanisms that underlie not only oncogenic alterations in transcriptomic signatures, but also the etiopathogenesis of epidermal and dermal sarcoid-dependent neoplastic transformations in horses and other equids. For those reasons, the aforementioned transgenic models might be useful for devising clinical treatments in horses afflicted with sarcoid-related neoplasia of cutaneous and subcutaneous tissues.

Keywords: equine; dermal fibroblast cell; sarcoid; nucleofection; oncogenic/neoplastic transformation; RNA-Seq; NGS; transcriptome

1. Introduction

Sarcoid is one of the most common skin tumor types in equids. It does not belong to the metastasizing tumors but is considered to be locally invasive [1–3]. Moreover, the high severity rates that have been found to result from sarcoid-dependent oncogenic transformation of epidermal and dermal tissues seem to be low. However, sarcoids contribute to lowering the value of the animal and the overall deterioration of the animal's welfare by occurring mainly in places exposed to movement [2]. This location exposes the possibility of mechanical damage, which can lead to transformations of minor forms into severe forms characterized by ulceration [2].

So far, it has been possible to link the presence of sarcoids with the infection of bovine papillomavirus types 1 and 2 (BPV-1, BPV-2) and, less frequently, type 13 (BPV-13), which

has been confirmed at the DNA, miRNA, and protein levels [3–5]. These viruses belong to a species-specific family of *Papillomaviridae*, which means they can only infect specific species of animals. BPV is so far the only documented case of a natural species barrier breach [6]. In cattle, it typically attacks the differentiated cells stemming from epithelial and connective tissues such as epidermal keratinocytes and dermal fibroblasts [6,7], causing mainly skin lesions in the form of papillomas, warts, and various neoplasms [8]. In the family *Equidae*, the infection does not produce new virus particles [9], but leads to changes in the level of gene expression, leading to neoplastic changes.

The genome of *Papillomaviridae* is highly conserved. It consists of seven early genes (*E1–E7*), two late genes (*L1* and *L2*), and a noncoding region (NCR, also known as the upstream regulatory region or URR) containing regions that control viral replication. The early genes are responsible for the replication activities of the virus (*E1*), the regulation of transcription (*E2*), and the coding of individual viral proteins (cytoplasmic—*E3*, and transforming—*E4–E7*). Late genes encode viral capsid proteins [10,11]. Among the transforming proteins, the *E5–E7* proteins are found in the genomes of all known carcinogenic viruses [12].

There are many known treatment methods for dealing with sarcoids. Unfortunately, some of them are only effective for a specific type of sarcoid and only for a specific tumor site (such as the BCG vaccine) [13]. Surgical methods have a high probability (up to 30%) of the disease's recurrence in a more aggressive form [14]. There are also methods with good prognosis, but due to the need to apply them directly to the skin lesion, they can be very painful; also some sites, like ears, are more sensitive, which requires general anesthesia in certain cases [15]. For this reason, further efforts are needed to develop new treatments for this condition, which could be amended by the development of new models that can study that neoplasm at the molecular level.

The molecular mechanisms underlying sarcoid-dependent neoplastic transformation are not yet fully understood. Previous studies have focused on the analysis of differences in gene expression between sarcoid and normal skin tissues, comparing the transcriptional activities of genes in the cell lines established from these tissues [16,17]. Some studies have aimed to devise in vitro models of murine fibroblast-derived cancerous cell lines generated by transfection with *BPV* transgenes or to create mouse models of dermal sarcoid-related neoplasia [18]. However, so far there have been no studies that target the development of an ex vivo model of sarcoid-dependent tumorigenesis in equine adult cutaneous fibroblasts cell (ACFC) lines, whose oncogenic transformation has been accomplished by transfection with *BPV* fusion genes. Moreover, there has been a lack of data confirming which virus genes are responsible for the neoplastic transformation of ACFCs into dermal sarcoid-like cells. That model could contribute to a more comprehensive understanding of the molecular changes in equine ACFCs undergoing sarcoid-related cancerogenesis due to viral infection.

Multifaceted transcriptomic characterization of mitotically stable cancerous cell lines stemming from *BPV-E4* and *BPV-E4^E1* transgenic equine ACFCs that have undergone nucleofection-mediated neoplastic transformation into nonmalignant sarcoid-like tumor cells is a sine qua non for accomplishing somatic cell cloning. The use of ACFC-derived sarcoid-like cells as a completely new source of nuclear donor cells (NDCs) to create equine cloned embryos and progeny by somatic cell nuclear transfer (SCNT) has not yet been realized. On the other hand, efforts by Li et al. [19] and Shao et al. [20] have confirmed that successful transcriptional reprogramming and molecular dedifferentiation of genomes inherited from NDCs that originated, respectively, from such highly metastatic neoplasms as cerebellum-specific medulloblastoma and breast cancer have sustainably contributed to promoting the epigenetically controlled remission of their typically cancerous markers and malignancy-related attributes in cloned mouse embryos.

To the best of our knowledge, transgenization and simultaneous co-transfection of the ex vivo expanded equine ACFCs that have been created by nucleofection according to the approaches formerly devised and adapted by Skrzyszowska et al. [21] and Samiec et al. [22] to generate genetically modified cloned pig embryos have not yet been reported. Addi-

tionally, the aforementioned strategies have been applied, for the first time, to research targeted at not only cell culture engineering but also experimental and preclinical attempts, with the use of in vitro transgenic models designed to examine the molecular nature of sarcoid-dependent oncogenic transformation (carcinogenesis) of equine ACFCs. These extracorporeal models have also been developed to explore the genetic and epigenetic determinants of procancerous tumorigenesis of epidermal and dermal provenance in horses and phylogenetically consanguineous taxa (i.e., other equids).

Furthermore, it is also noteworthy that, thus far, approaches focused on utilizing *BPV-E4* and *BPV-E4^E1* transgenic ACFC derivatives, which have undergone oncogenic transformation into sarcoid-like cells as a result of nucleofection, have been conceptualized for the needs of SCNT-based cloning in horses and a variety of members of *Equidae* family for the first time. For all these reasons, elaborating the abovementioned approaches seems to be strongly justified by the scientific thesis assuming profound amelioration of epigenomic plasticity in the ex vivo immortalized nonmalignant cancerous derivatives of ACFCs, which are characterized by an unlimited lifespan. This, in turn, might result in the enhanced susceptibility of genetically modulated ACFC-derived sarcoid-like cell nuclei to being epigenomically dedifferentiated and transcriptionally reprogrammed in equine cloned embryos generated by SCNT-mediated assisted reproductive technologies (ARTs).

Therefore, in our current investigation, efforts were undertaken to generate equine ACFC lines that had been genetically transformed into sarcoid-like cells as a result of their nucleofection with *BPV* transgenes encoding recombinant representatives of the transforming protein family, designated as either *BPV-E4* or *BPV-E1^E4*. Our study also sought to thoroughly unravel the modifications arising in genomic signatures that have incurred sarcoid-dependent alterations in transcriptomic profiles of horse ACFC-derived neoplastic cells.

2. Results

2.1. Preliminary Validation of the Samples Used

All the harvested horse skin tissues were tested for the presence of *BPV* DNA. The presence of the viral DNA amplicon in samples intended for further procedures showed the absence of products unique for *BPV* genetic material.

2.2. Comparative Statistical Estimations Resulting from Next-Generation Sequencing (NGS) among BPV-E4 and BPV-E1^E4 Transgenic Equine ACFC-Derived Neoplastic Cells

After NGS sequencing, an average of 13 million raw reads were obtained per sample, from which 99.6% passed the quality filters. The mapping rate to reference genome ranged from 73.6% to 89.1% (average: 86.8%), which was about 11.3 million reads mapped per sample. The PCA clustering that was performed for both comparisons confirmed the group homogeneity (Figure S1). The average percent of reads mapped to genes per sample was 65.5. The data have been submitted to the Gene Expression Omnibus (GEO) database and received the accession number GSE193906.

2.3. Analysis of Differentially Expressed Genes (DEGs) in Oncogenically Transformed Equine ACFCs Expressing BPV-E4 and BPV-E1^E4 Transgenes

Transcriptome profiling allowed us to perform a comparison of the whole expression profile between the control and the *BPV-E4* and *BPV-E1^E4* groups. After the comparison of control and *BPV-E4* groups, 1640 DEGs were identified, of which 624 were upregulated and 1016 downregulated in the *BPV-E4* group. The highest numbers of 3328 DEGs were identified due to the comparison of the control and *BPV-E1^E4* groups. Among them, 1626 genes were shown to be upregulated and 1602 genes were recognized to be downregulated in the *BPV-E1^E4* group as compared to the control samples.

To establish the differences between the impacts of *BPV-E4* and *BPV-E1^E4* transgenes, the DEG sets obtained for both comparisons were combined and 910 common genes were identified. Moreover, 2318 and 730 unique DEGs were detected following sarcoid-

dependent neoplastic transformation of equine ACFCs via nucleofection with *BPV-E1ˆE4* and *BPV-E4* transgenes, respectively (Figure 1).
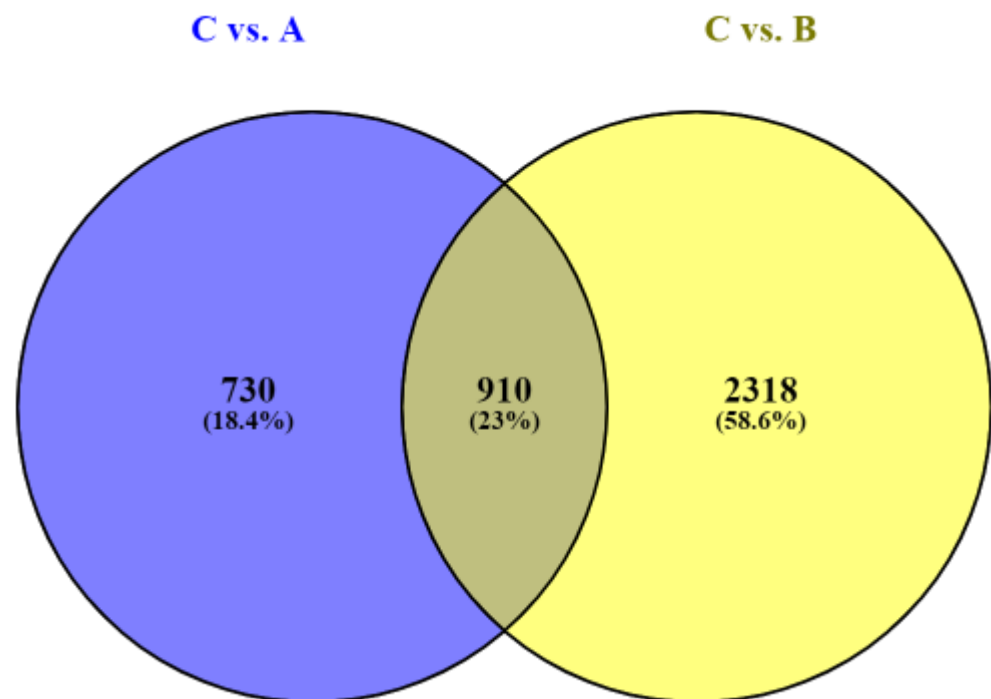
Figure 1. The Venn diagram of common and unique differentially expressed genes (DEGs) following the comparisons of *BPV-E4* (A) vs. control (C) groups, and *BPV-E1ˆE4* (B) vs. control (C) groups (Venny 2.1 BioinfoGP).

Among the DEGs identified for cells nucleofected with the *BPV-E4* transgene, six gene families were found, for which the expression of 10 or more genes was altered, and they accounted for 6% of all DEGs (Figure 2A). In the case of *BPV-E1ˆE4* transgene-mediated nucleofection, there were three times as many such families, and they accounted for 10% of all DEGs (Figure 2B). Only one family encompassing the genes encoding centromere proteins identified for *BPV-E4* transgenic samples did not occur among the gene families identified for *BPV-E1ˆE4* transgenic cell counterparts.

2.4. Gene Ontology (GO) Enrichment Analysis of BPV-E4 and BPV-E1ˆE4 Transgenic Equine ACFC-Derived Neoplastic Cells

The GO enrichment analysis performed for DEGs between control and *BPV-E4* groups allowed us to detect several significant Gene Ontology terms (Table 1). Most of those GO terms were over-represented as follows: 34 DEGs correlated to negative regulation of cell proliferation (FDR < 0.002); 24 DEGs responsible for positive regulation of cell migration (FDR < 0.0001); and 21 DEGs related to both cell adhesion and cell migration (FDR < 0.003 and FDR < 0.0005, respectively). Additionally, the overabundance of DEGs that has been shown to be significant was noticed for GOs characteristic of cell–matrix adhesion and actin cytoskeleton organization. In identified GO terms, the genes that represented two families have been found to occur frequently, as has been indicated below: the genes coding for different isotypes of integrins (*ITGs*) such as *ITGB6*, *ITGB3*, *ITGA6*, *ITGA1*, *ITGA8*, and *ITGB4*, and the genes coding for kinesin superfamily proteins (*KIFs*) such as *KIFC1*, *KIF23*, *KIF11*, *KIF20A*, and *KIF3B*.
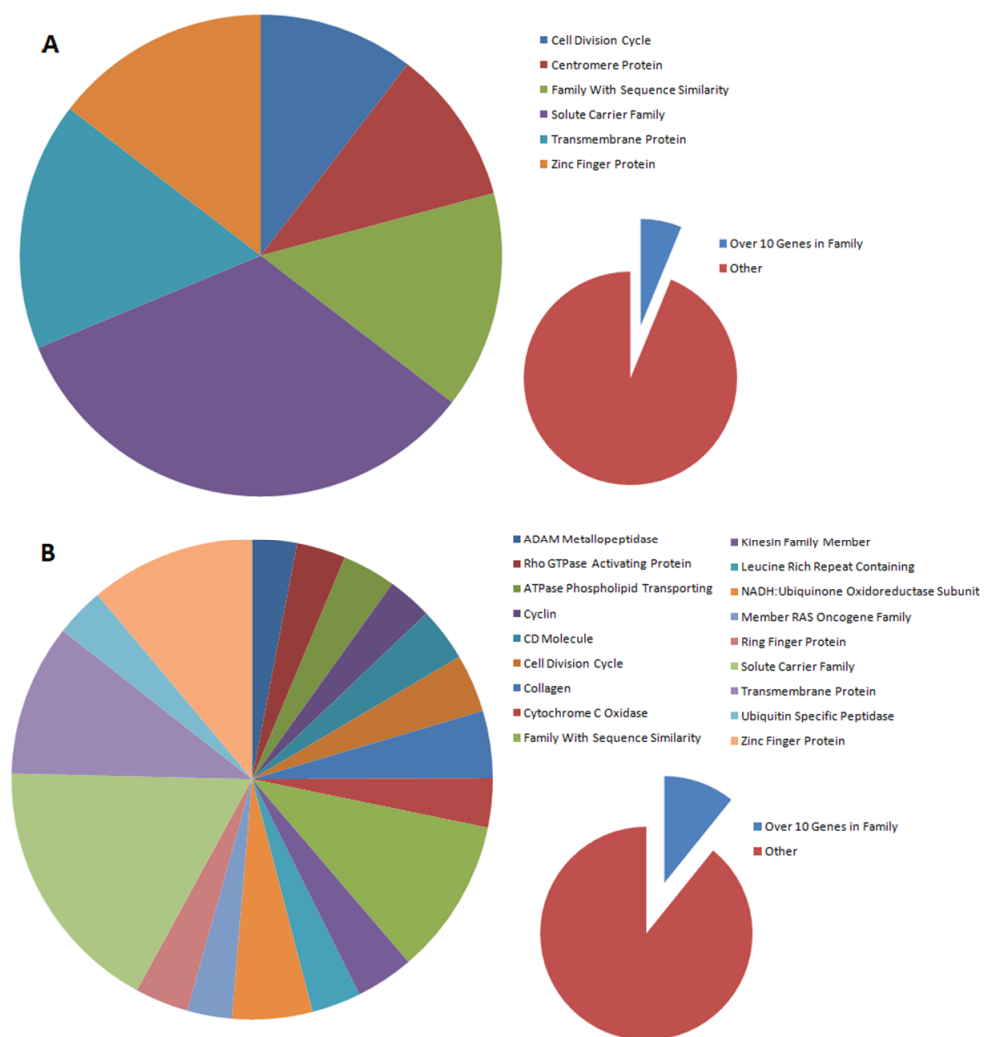
Figure 2. Pie charts that depict the contribution of families with 10 or more genes undergoing expression changes identified following the sarcoid-dependent oncogenic transformation of equine ACFCs triggered by nucleofection with either *BPV-E4* (**A**) or *BPV-E1^E4* (**B**) transgenes.

The enrichment analysis performed for the comparison of the incidence of DEGs between control and *BPV-E1^E4* samples revealed that the focal adhesion GO terms were over-represented by 99 DEGs, 65 of which were upregulated; their 34 counterparts were downregulated (FDR < 0.0001) (Table 2). The GOs, for which most of the genes were recognized as upregulated, have been shown to be related to negative regulation of extrinsic apoptotic signaling, transforming growth factor-β receptor signaling, and collagen fibril organization.

2.5. Pathway Enrichment Analysis among Oncogenically Transformed Equine ACFCs Expressing BPV-E4 and BPV-E4^E1 Transgenes

The results confirmed almost the same significantly over-represented molecular pathways, not only between *BPV-E4* and control intergroup comparisons (Table 3), but also between *BPV-E1^E4* and control intergroup comparisons (Table 4). The PI3K-Akt signaling pathways were identified with the highest numbers of DEGs–44 for *BPV-E4* and 73 for *BPV-E4^E4* transgenic cell subpopulations, respectively. In both cases, the genes encoding integrins (*ITGs*) and fibroblast growth factors (*FGFs*) were detected.

Table 1. The significant enrichment in Gene Ontology terms detected on the basis of comparative analysis of DEGs set between *BPV-E4* and the control group.

Gene Ontology	N$_{all}$	N$_u$	Upregulated Genes	N$_d$	Downregulated Genes	FDR
positive regulation of cell migration	24	14	*SEMA4D, CORO1A, INSR, F2R, DAB2, PDGFD, MMP14, SDCBP, CDH13, PIK3R1*	10	*ATP8A1, COL18A1, ARHGEF39, CCL26, HAS2, SEMA7A, BMP2, SNAI1, EGFR, TRIP6*	<0.001
negative regulation of cell proliferation	34	17	*IFIT3, SKAP2, IRF1, F2R, SMAD1, KAT2B, ZEB1, TESC, GLI3, CDH13*	17	*EREG, CER1, FEZF2, WNK2, AXIN2, HMGA1, RBPJ, PTPN14, SPRY2, BMP2*	<0.001
cell-matrix adhesion	15	5	*VCAM1, SNED1, ITGB4, CL2L11, ITGA8*	10	*EPDR1, ITGB6, TECTA, OTOA, FREM1, TNN, STRC, ITGB3, ITGA6, ITGA1*	<0.001
cell migration	21	9	*SDC4, ASAP3, RASGEF1A, JAK2, LIMD1, MMP14, CLN3, JAK1, NDE1*	12	*TNS3, DEPDC1B, TNN, HES1, CSPG4, ELMO1, SDC1, SNAI1, ABL2, FSCN1*	<0.001
mitotic spindle assembly	9	3	*KIF3B, WRAP73, ARHGEF10,*	6	*BIRC5, NEK2, MYBL2, KIFC1, KIF11, RAB11A*	0.002
mitotic cytokinesis	8	0	-	8	*NUSAP1, KIF20A, CEP55, KIF23, RACGAP1, ANLN, CKAP2, PLK1,*	0.002
chromosome segregation	11	2	*NDE1, NEK3*	9	*NEK2, HJURP, CENPT, SPC25, CENPN, KIF11, CENPW, CDCA2, RCC1*	0.002
actin cytoskeleton organization	15	8	*CDC42, EP2, CORO1A, RHOJ, SDCBP, NISCH, CLN3, WASF2, BCL6*	7	*ARHGAP26, ELMO1, DIAPH3, NUAK2, ABL2, PFN1, TMSB4X*	0.002
cell adhesion	21	5	*GPNMB, ITGA8, CERCAM, EPHB4, TNFAIP6*	16	*POSTN, TNC, TGFBI, COL18A1, NINJ1, HES1, SUSD5, HAS2, ITGA6, COL15A1*	0.003

N$_{all}$—Number of all detected DEGs; N$_u$—Number of upregulated DEGs; N$_d$—Number of downregulated DEGs; FDR—False Discovery Rate in DAVID software.

Furthermore, as has been revealed by the pathway enrichment analysis, modifications observed in the cell cycle (Figure 3), regulation of actin cytoskeleton (Figure 4), and ECM remodeling (reflected in the alterations recognized for focal adhesion and ECM-receptor interaction) have been proven among neoplastically transformed equine ACFCs exhibiting expression of either *BPV-E4* or *BPV-E1ˆE4* transgenes.

The DEGs associated with such processes as focal adhesion, regulation of actin cytoskeleton, and ECM-receptor interaction were represented mainly by integrins, lamins, collagens, and *FGF* genes (Tables 3 and 4). Taking into account these pathways, for cells transformed oncogenically via nucleofection with *BPV-E4* and *BPV-E1ˆE4* gene constructs, the most upregulated genes detected are *ITGA8* (*Integrin Subunit Alpha 8*), *XIAP* (*X-Linked Inhibitor Of Apoptosis*), *ROCK2* (*Rho Associated Coiled-Coil Containing Protein Kinase 2*), and *LAMA3* (*Laminin Subunit α3*), while such genes as *FGF12* (*Fibroblast Growth Factor 12*), *FGFR3* (*Fibroblast Growth Factor Receptor 3*), *ITGA6* (*Integrin Subunit α6*), *CCND1* (*Cyclin D1*), *CCND2* (*Cyclin D2*); *COL6A6* (*Collagen Type VI α6 Chain*), and *BAD* (*BCL2-Associated Agonist Of Cell Death*) have been allotted to their downregulated counterparts (Figure 5A,B).

Table 2. The significant enrichment in Gene Ontology terms detected on the basis of comparative analysis of DEGs set between *BPV-E1ˆE4* and control group.

Gene Ontology	N_{all}	N_u	Upregulated Genes	N_d	Downregulated Genes	FDR
negative regulation of canonical Wnt signaling pathway	33	21	*EGR1, WNT5A, DKK2, SOX9, LIMD1, GREM1, BICC1, GLI3, STK4, LATS1*	12	*NOTUM, WNT11, GPC3, DRAXIN, AXIN2, CAV1, LRP4, NPHP4, MLLT3, MAD2L2*	0.009
focal adhesion	99	65	*ITGA8, SORBS1, CNN1, MCAM, ITGA11, SYNPO2, FBLN7, NEXN, LPP, PHLDB2*	34	*CSPG4, PROCR, FLRT2, HMGA1, TNS4, TSPAN4, CAV1, FHL1, KIF22, PLAU*	
negative regulation of extrinsic apoptotic signaling pathway	15	13	*TGFBR1, COL11A1, COL1A1, LOX, COL5A1, GREM1, P4HA1, LOXL2, COL1A2, NF1*	2	*FMOD, ANXA2*	<0.001
transforming growth factor beta receptor signaling pathway	19	12	*TGFBR1, FOS, SKIL, SMAD4, SMURF1, COL1A2, SMAD9 FERMT2, TGFBR3, MTMR4,*	7	*HPGD, SMAD6, PTPRK, SMURF2, TAB1, PXN, TGFB3*	<0.001
collagen fibril organization	15	13	*TGFBR1, COL11A1, COL1A1, LOX, COL5A1, GREM1, P4HA1, LOXL2, COL1A2, NF1*	2	*FMOD, ANXA2*	<0.001

N_{all}—Number of all detected DEGs; N_u—Number of upregulated DEGs; N_d—Number of downregulated DEGs; FD—False Discovery Rate in DAVID software.

Table 3. The significant enrichment in molecular KEGG pathways detected on the basis of comparative analysis of DEGs set between *BPV-E4* and control group.

KEGG Pathways	N_{all}	N_u	N_d	FDR	Most Deregulated Genes	
					Up	Down
Focal adhesion (ecb04510)	31	11	20	0.051	*ITGB4, LAMA3, XIAP, ITGA8, PDGFD, PIK3R1, SOS2, ROCK2, LAMB2, ERBB2*	*TNC, ITGB6, CCND2, TNN, CCND1, COL6A6, SHC3, ACTN3, ITGB3, BAD*
Regulation of actin cytoskeleton (ecb04810)	34	13	21	0.008	*FGF18, ITGB4, F2R, ITGA8, ARHGEF6, PDGFD, DIAPH2, PIK3R1, SOS2, ROCK2*	*ITGB6, FGF12, BDKRB2, IQGAP3, FGFR3, ACTN3, ITGB3, DIAPH3, ITGB7, ITGA6*
ECM-receptor interaction (ecb04512)	19	5	14	0.010	*ITGB4, LAMA3, SDC4, ITGA8, LAMB2*	*TNC, ITGB6, TNN, COL6A6, HMMR, ITGB3, ITGB7, ITGA6, SDC1, ITGA1*
PI3K-Akt signaling pathway (ecb04151)	44	20	24	0.051	*FGF18, ITGB4, LAMA3, INSR, CREB3L1, BCL2L11, F2R, TGA8, NR4A1, JAK2*	*TNC, ITGB6, FGF12, CCND2, TNN, CCND1, ANGPT1, COL6A6, FGFR3, ITGB3*
Cell cycle (ecb04110)	28	9	18	0.001	*CDC14A, RB1, STAG1, CDC25B, E2F5, SMC3, RBL1, RBL2, RAD21*	*CCND2, CDC45, CCND1, MCM5, CCNB2, CCNB1, CDC20, E2F1, CDK1, BUB1*
Steroid biosynthesis (ecb00100)	9	1	8	0.008	*SOAT1*	*HSD17B7, TM7SF2, LSS, SQLE, FDFT1, SQLE, FDFT1, FAXDC2, EBP, SC5D*
Pathways in cancer (ecb05200)	52	23	29	0.010	*FGF18, LAMA3, FOS, XIAP, F2R, TGFBR2, ADCY9, MITF, RB1, ADCY3*	*CTNNA2, WNT7B, FGF12, MMP1, CXCL8, BDKRB2, TCF7, BIRC5, CCND1, AXIN2*

N_{all}—Number of all detected DEGs; N_u—Number of upregulated DEGs; N_d—Number of downregulated DEGs; FD—False Discovery Rate in DAVID software.

Table 4. The significant enrichment in molecular KEGG pathways detected on the basis of comparative analysis of DEGs set between *BPV-E1ˆE4* and control group.

KEGG Pathways	N$_{all}$	N$_u$	N$_d$	FDR	Most Deregulated Genes	
					Up	**Down**
Focal adhesion (ecb04510)	63	42	21	<0.001	*ITGA8, THBS1, ITGA11, OL11A1, XIAP, PDPK1, LAMA3, MYLK3, ROCK2, PP1R12A*	*LAMC3, SHC3, COL5A3, COL4A1, CCND1, CCND2, COL6A6, BAD, VEGFD, COL6A3*
Regulation of actin cytoskeleton (ecb04810)	57	43	14	<0.001	*FGF21, ITGA8, FGF5, ITGA11, MYLK3, ROCK2, PPP1R12A, PFN2, FGFR2, ARHGEF6*	*BDKRB2, FGFR3, ITGAX, FGF12, IQGAP2, DIAPH3, ITGA6, GSN, ITGAE, EGFR*
ECM-receptor interaction (ecb04512)	30	18	12	0.001	*ITGA8, THBS1, ITGA11, COL11A1, LAMA3, LAMA5, COL1A1, COL5A, ITGB7, FN1,*	*LAMC3, COL5A3, COL4A1, COL6A6, COL6A3, ITGA6, SDC1 CD44, AGRN, TNN, IL6*
PI3K-Akt signaling pathway (ecb04151)	73	47	26	0.019	*FGF21, ITGA8, FGF5, THBS1 ITGA11, COL11A1, CREB3L1, INSR, EFNA1, DPK1*	*LAMC3, FGFR3, COL5A3, COL4A1, CCND1, FGF12, CCND2 IL7, COL6A6,*
Cell cycle (ecb04110)	32	10	22	0.047	*GADD45B, RBL1, SMAD4, STAG1, EP300, CDC27, AD21, YWHAG, STAG2, E2F5*	*CCND1, CCND2, CCNB2, CDC20, MCM5, CCNB1, CDK1, CDC45 PKMYT1, PLK1,*
FoxO signaling pathway (ecb04068)	38	22	16	0.003	*TGFBR1, INSR, PDPK1, PRKAB2, AKT3, FBXO32, IRS2, GADD45B, SMAD4, PRKAG3*	*IL6, CCND1, CCND2, CCNB2, CCNB1, TNFSF10, S1PR1, PLK1, CDKN2B, G6PC3,*
Proteoglycans in cancer (ecb05205)	48	27	21	0.019	*ITPR1, THBS1, WNT5A, PDPK1, ROCK2, PPP1R12A, AKT3, FN1, CAMK2D, PIK3R1*	*WNT11, ERBB3, GPC3, CCND1, WNT7B, HPSE, MMP9, TIMP3 CAV1, IGF2,*
Rap1 signaling pathway (ecb04015)	49	34	15	0.035	*FGF21, FGF5, THBS1, INSR, ADCY5, EFNA1, AKT3, SIPA1L2, PFN2, ADCY9*	*RAP1GAP, FGFR3, FGF12, ID1, ADORA2A, VEGFD, ANGPT1, ANGPT4, HGF, MAP2K3,*
TNF signaling pathway (ecb04668)	29	16	13	0.047	*MAP3K8, EDN1, CREB3L1, FOS, AKT3, CREB3L2, TAB3, PIK3R1, ITCH, MAP3K5*	*CSF2, IL6, CXCL1, VCAM1, MMP9, IL15, CREB3L4, MAP2K3, CCL2, TRADD*

N$_{all}$—N$_u$—Number of upregulated DEGs; N$_d$—Number of downregulated DEGs; FDR—False Discovery Rate in Number of all detected DEGs; DAVID software.

The onset of pathways related to cancerous transformation was identified uniquely for genetically transformed cells that had been nucleofected with *BPV-E4* gene construct (Table 3). The significant overabundance in initiating of pathways associated with neoplasia has been empirically justified by the detection of 52 DEGs in *BPV-E4* transgenic equine ACFCs oncogenically transformed into sarcoid-like cells (Table 3). Only *BPV-E1ˆE4* transgenic cells were characterized by promoting and rewiring molecular programs based on the FoxO-, Rap1-, and TNF-mediated signaling pathways and molecular mechanisms dependent on proteoglycans actively functioning in cancer cells (Table 4). The switching on of procancerous mechanisms prompted by Rap1 signaling pathway and activation of proteoglycans is reflected in the presence of 49 and 48 DEGs, respectively. Crosstalk between these molecular regulatory networks in *BPV-E1ˆE4* transgenic equine ACFC-derived neoplastic cells remains under control and requires the reciprocal cooperation of the panel of genes linked to Wnt signaling pathway and coding for such proteins as fibroblast growth factors, matrix metalloproteinases (*MMP*s), and interleukins (Table 4).
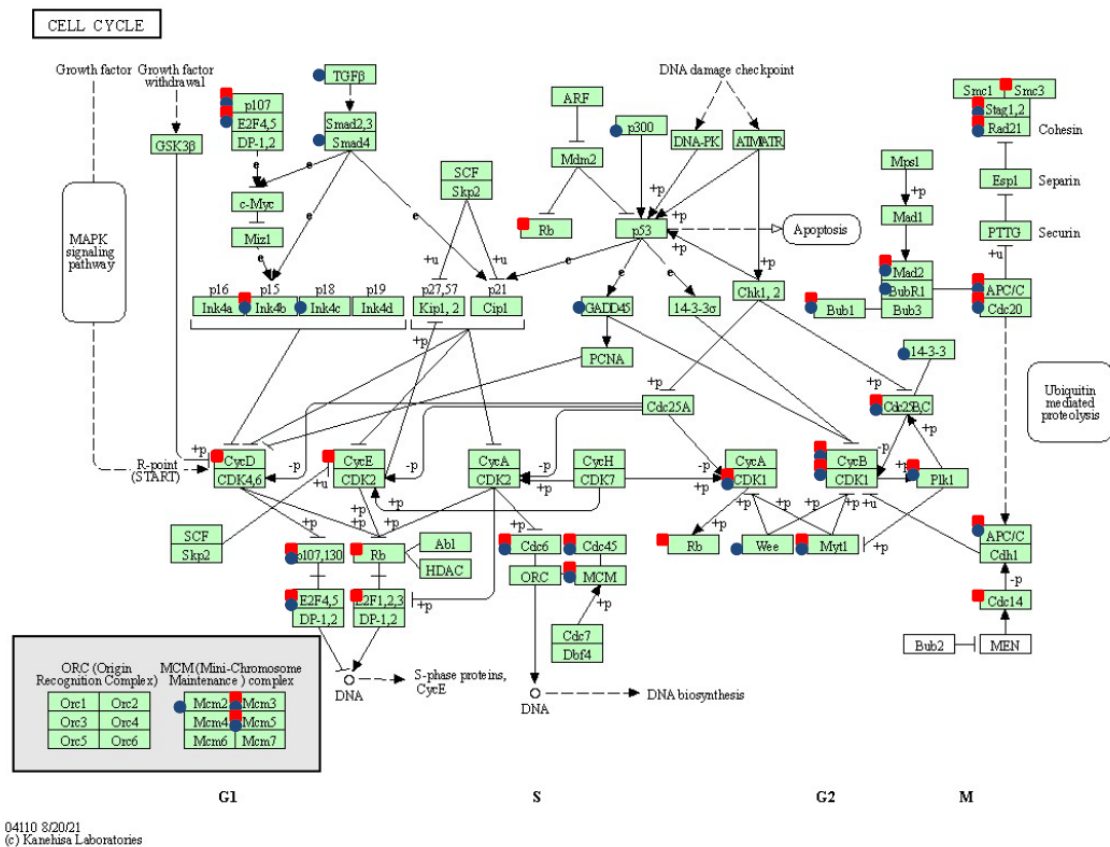
Figure 3. Cell cycle pathway (ecb 04110) over-represented following two strategies of sarcoid-dependent neoplastic transformation triggered by either *BPV-E4* or *BPV-E1ˆE4* transgenes. The red squares denote genes modified by *BPV-E4* insert, while the blue circles indicate *BPV-E1ˆE4* transgene-induced modifications; arrows present molecular interaction or relation, while dotted arrows show indirect link or unknown reaction.

2.6. Enrichment Analysis for Identification of DEGs in BPV-E4 and BPV-E1ˆE4 Transgenic ACFCs Undergoing Sarcoid-Dependent Oncogenic Transformation

The 910 genes identified as differentially expressed in both *BPV-E4* and *BPV-E1ˆE4* genetically transformed groups as compared to the control were analyzed in terms of enrichment pathways and GO terms. The results confirmed the significant incidence of DEGs associated with cell cycle control (FDR < 0.0001, 21 DEGs), regulation of actin cytoskeleton (FDR < 0.0007; 21 DEGs), and focal adhesion (FDR < 0.0009; 21 DEGs). The genes involved in these molecular networks displayed close interactions and were simultaneously characterized by the occurrence of two clusters dependent on gene association and direction of modifying/diversifying their transcriptional activities (Figure 6A). The genes with the highest number of interactions with other DEGs were either downregulated as follows: *CDK1* (*Cyclin-Dependent Kinase 1*), *EGFR* (*Epidermal Growth Factor Receptor*), *CCND1* (*Cyclin D1*), and *CCND2* (*Cyclin D2*); or upregulated as follows: *ITGA8* (*Integrin Subunit Alpha 8*) and *RLB1 gene* (Figure 6B).

2.7. qPCR-Assisted Validation Accomplished for Transcriptional Activity Levels of Genes in Neoplastically Transformed Equine ACFCs Expressing BPV-E4 and BPV-E1ˆE4 Transgenes

The qPCR validation confirmed a high and significant correlation between RNA-seq data and relative quantities/abundances of gene transcripts estimated using real-time PCR methods (Table 5). The highest correlation coefficients have been identified for *TIMP1, MMP2, MMP14,* and *MMP24* genes (R^2 from 0.814 to 0.989). The occurrence of a nonsignificant correlation coefficient between RNA-seq- and qPCR-mediated expression profiles was noticed for only one gene, *MMP17*.
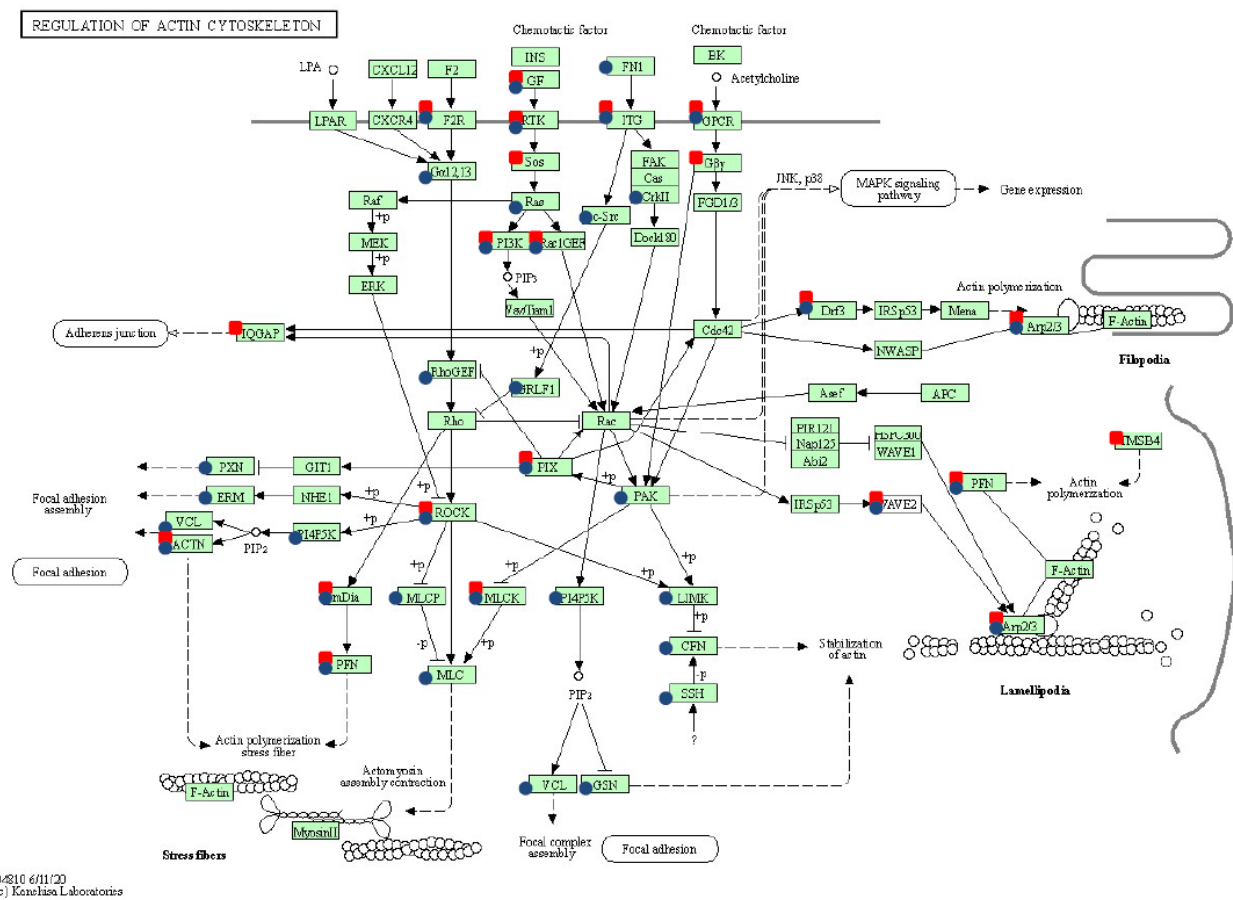
Figure 4. Regulation of actin cytoskeleton pathway (ecb04810) modifications following two strategies of sarcoid-dependent neoplastic transformation triggered either by *BPV-E4* or by *BPV-E1^E4* transgenes. The red squares denote genes modified by *BPV-E4* insert, while the blue circles indicate *BPV-E1^E4* transgene-induced modifications; arrows present molecular interaction or relation, while dotted arrows show indirect link or unknown reaction.

Table 5. The correlation coefficients and their corresponding *p*-value for qPCR validation.

Gene	Accession Number	Correlation Coefficient
MMP2	ENSECAG00000000953	0.839 ***
MMP14	ENSECAG00000008351	0.887 *
MMP9	ENSECAG00000013081	0.662 *
MMP15	ENSECAG00000000196	0.897 **
MMP17	ENSECAG00000013201	0.440 ns
MMP24	ENSECAG00000024778	0.814 *
PTGER2	ENSECAG00000009713	0.686 *
TIMP1	ENSECAG00000014259	0.989 ***
FGF10	ENSECAG00000014361	0.748 *
RECK	ENSECAG00000010426	0.688 *

* *p*-value < 0.05; ** *p*-value < 0.001; *** *p*-value < 0.0001; ns—nonsignificant.
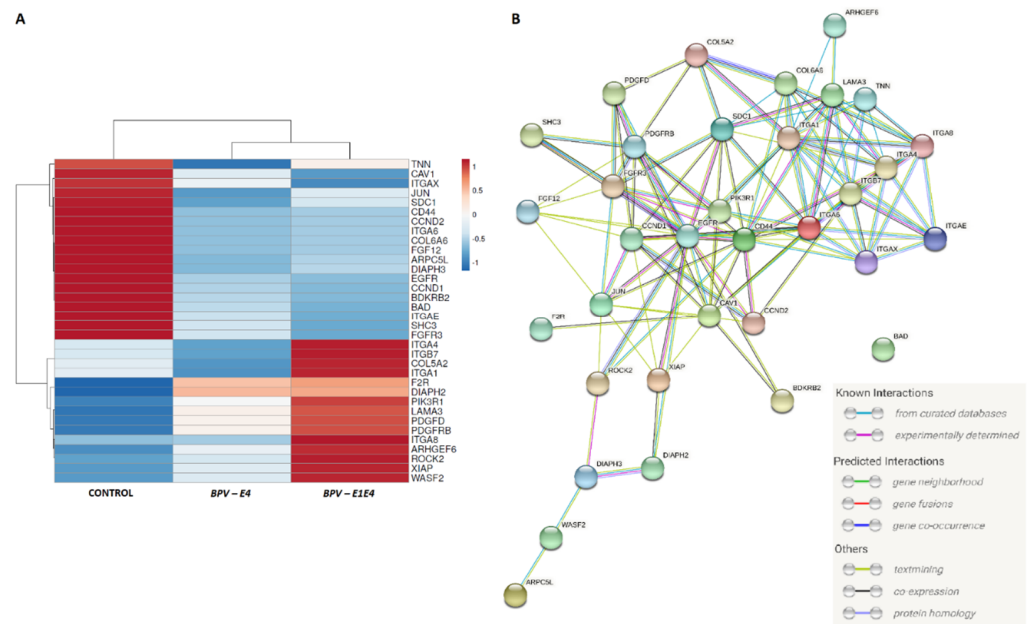
Figure 5. The interactions between 34 genes identified in both *BPV-E4* and *BPV-E1ˆE4* transgenic cells, and belonged to focal adhesion, regulation of actin cytoskeleton, and ECM-receptor interaction pathways. (**A**) the heatmap of the mean expression for groups (R package [23]); (**B**) the inter-relations between identified DEGs (String software [24]).
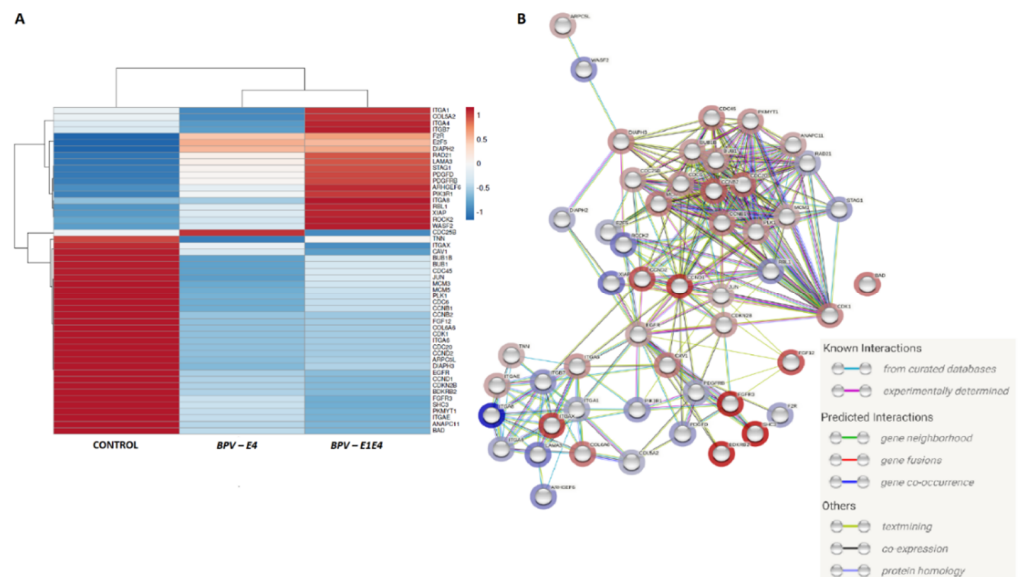
Figure 6. The interactions between 51 genes identified in both *BPV-E4* and *BPV-E1ˆE4* transgenic cells undergoing sarcoid-dependent neoplastic transformation, and belonged to molecular pathways related to procancerous intracellular conversion: (**A**) the heatmap of the mean expression for groups (R package [23]); (**B**) the interaction between identified DEGs with FC direction marked (String software [24]).

3. Discussion

To date, there is still limited information about equine sarcoid genetics as well as about the etiology of sarcoids' occurrence at the molecular level. The identification of such mechanisms related with neoplasia formation seems to be critical for prophylaxis or future treatment. Little research has been done comparing the sarcoid cell transcript with that of healthy horse skin cells. These studies were mainly performed on microarrays, so they

were limited by the selected panel of genes [16]. Transfected horse skin cells are proposed as a new model to conduct research on the effect of individual viral genes on changes inside the cell. In this study, we compared the overall transcriptome using the RNA-seq technique, which enabled the detection of DEGs on a much larger scale. We tried to answer the question of which viral genes affect the cell transcriptome, directing changes toward neoplastic transformations, and how. So far, a model of transfected skin cells has been developed in sarcoid research, but it included transfected mouse skin cells [18]. Moreover, this model was not conducted fully in vitro due to the introduction of altered cells into living organisms. An additional advantage of the present research was using two variants of the studied transcript. Such an approach made it possible to approximate the functions performed by the added fragment of the E1 protein. So far, it has been argued that the effect of the papillomavirus E4 protein is mainly related to viral replication by controlling cellular processes towards the return of differentiated cells to the cell cycle [25–27]. Our research has demonstrated that the presence of the BPV-E1ˆE4 protein also influences changes in the expression of other host cell genes and may play a role in carcinogenesis.

Following *BPV-E4* transgene-mediated nucleofection of equine ACFCs, a total of 1640 DEGs were identified, out of which 62% were found to be downregulated and 38% upregulated. In contrast, after *BPV-E1ˆE4* transgene-dependent neoplastic transformation of ACFCs into sarcoid-like cells, 3328 genes were detected, out of which 51% were shown to be downregulated and 49% upregulated. This confirms the ratio of downregulated genes to upregulated genes obtained in the microarray studies performed by Semik et al. [16] and in other cancers such as pancreatic cancer, cervical cancer, and renal cancer [28–30]. Attention should be paid to the differences in deregulated genes depending on the type of insert introduced. In the case of the fragment encoding the BPV-E4 protein alone, genes deregulated also by the splicing protein BPV-E1ˆE4 accounted for 55%, while genes common to both inserts accounted for 27% of all deregulated genes. Therefore, the conclusion is drawn that the presence of the BPV-E1 protein fragment strongly influences the change of the protein function in the process of neoplasia formation, not only by enabling modification of the expression level of new genes but also by inhibiting the deregulation of gene expression occurring in the case of the direct product of the *BPV-E4* gene.

The distribution of gene families that are differentially expressed between nontransfected and transfected cells depends on the type of gene introduced. In our studies, gene families were selected in which at least 10 genes were subject to altered expression. In the case of the introduction of the *BPV-E4* gene alone, six gene families were observed to be differentially expressed (cell division cycle, centromere protein, family with sequence similarity, solute carrier family, transmembrane protein, and zinc finger protein), while for the spliced insert, three times as many families were detected (ADAM metallopeptidase, Rho GTPase-activating protein, phospholipid-transporting ATPase, cyclin, CD molecule, cell division cycle, collagen, cytochrome c oxidase, family with sequence similarity, kinesin family member, leucine-rich repeat-containing protein, NADH:ubiquinone oxidoreductase subunit, member of RAS oncogene family, ring finger protein, solute carrier family, transmembrane protein, ubiquitin-specific peptidase, and zinc finger protein). Moreover, all families (with the exception of centromere proteins) designated for the *BPV-E4* insert were also among the families designated for the *BPV-E1ˆE4* insert. This may indicate that, despite the differences in DEGs, the major pathways regulated by this protein are not altered by the introduction of the BPV-E1 protein fragment to cells, but the number of such families is increasing.

Interesting results were obtained based on the Gene Ontology analysis. The function of the BP virus E4 protein is related to the reintroduction of the host cells into the cell cycle [27]. For the *BPV-E4* insert, 34 DEGs were identified for GO regulation of cell proliferation, 11 DEGs for chromosome segregation, nine DEGs for the mitotic spindle assembly, and eight DEGs for the mitotic cytokinesis that can be associated with this function. However, we cannot unequivocally determine whether the differences noticed in the transcriptomic profiles exert a negative or positive effect on the host cell cycle. Our research also showed that a

similar number of statistically significant changes in GO were seen for the DEGs associated with cell migration processes such as positive regulation of cell migration (24 DEGs), cell adhesion and cell migration (21 DEGs respectively), and cell–matrix adhesion (15 DEGs). This may indicate that the reasons for the nonmetastatic nature of the sarcoid [2] can be found in the analyzed gene. Among the DEGs belonging to the changed GOs, the protein families of integrins and kinesin superfamily proteins had the largest share. The high proportion of integrins may indicate the neoplasmic nature of the BPV-E4 protein. Changes in the expression level of integrins have been associated with various cancers. They act as a factor controlling the migration capacity of altered cells via extracellular matrix (ECM) remodeling and modification of cell–ECM interaction [31–33]. It has been established that integrin also plays a key role in the regulation of cancer progression through involvement in the regulation of cancer stem cells, metastasis, tumor angiogenesis, and metabolism [33]. In turn, kinesin superfamily proteins are involved in transporting many intracellular components. Additionally, they are involved in cell division and are responsible, among other things, for the assembly of microtubule spindles and the separation of chromosomes. Their expression is tightly regulated and its disturbance can lead to increased (in the case of upregulation) or decreased (downregulation) cell proliferation [34].

In the case of the *BPV-E1ˆE4* insert, the largest number of DEGs were involved in focal adhesion, with 99 genes in total, and nearly twice as many genes were upregulated. This may indicate a high involvement of the BPV-E1ˆE4 fusion protein in the processes related to cells migration. Another significant GO was the negative regulation of the canonical Wnt signaling pathway. Deregulation of this pathway is associated with the formation and metastasis of numerous cancers, such as colorectal cancer, breast cancer, and ovarian cancer [35]. An example that can be drawn from our present study is the overexpression of the *SOX9* gene, which is considered a tumor progression factor [36]. The results of the research by Aldaz et al. [36] proved that an increased level of *SOX9* can promote tumor cell proliferation in both in vitro and in vivo models throughout *BMI1* activation and *p21* inhibition. The study by Xue et al. [37] pinpointed the strong influence of the overexpression of *SOX9* on breast cancer stem cells, while in the report by Ma et al. [38], *SOX9* was designated as a "master regulator" of the processes encompassing the survival and metastasis of breast cancer cells [38].

Additionally, GOs, whose deregulation is associated with carcinogenic processes, such as apoptosis, and which are classified as related to hallmarks of cancer [39], and the *TGF-β* (transforming growth factor-β) receptor (*TGFBR*) signaling pathway, have been shown to be significant. The *TGF-β* gene is considered to be one of the most potent regulators of cell proliferation (usually negative), and it can also function as a promoter of the metastasis of TGF-β-resistant tumor cells [40]. Several previous reports indicated that upregulation of the *TGFβ1* gene is characteristic during tumorigenesis and can promote cell motility and migration [41,42]. Moreover, in vitro studies by Zhou et al. [43] have confirmed that the transfection of neoplastic (adenocarcinoma) cells derived from colonic and rectal epithelial cells (enterocytes) with the use of a *pCMV5-TGFBR1*6A-HA* gene construct brings about TGFBR1*6A (type 1 transforming growth factor β receptor)-induced activation of the p38 MAPK pathway, followed by expedited and highly malignant oncogenic modulation of these colorectal tumor cells. This, in turn, gives rise to an enhancement of the ex vivo capabilities of colorectal cancer cells to grow unchecked, invade less invasive or noninvasive subpopulations of intestinal adenocarcinoma cells, and metastasize from primary malignant lesions (i.e., primary tumor sites) to other locations (the so-called metastatic foci) of the transgenic cell culture engineering model [43]. The upregulation of the *TGFBR* gene, which was observed in our study due to the *BPV-E1ˆE4* transgene-mediated oncogenic transformation of equine ACFCs into sarcoid-like cells, may also indicate a pivotal role of TGF-β receptors in the onset and progression of the processes responsible for the migration and metastasis of neoplastic cells. The other upregulated gene, which represents the GOs related to *TGF-β* receptors, is the *c-Fos* proto-oncogene, widely recognized as one of the most important predictors determining carcinoma's progression [44]. The exact role of the

FOS gene in tumorigenesis and metastasis is still unclear, but the overexpression of this gene has been hypothesized to trigger tumorigenesis and, thereby, has been potentially found to be a poor prognostic factor for oncology patients. The increased expression of the *FOS* gene can trigger the *VEGF* (vascular endothelial growth factor) and enhance *NANOG* and *c-myc* genes in head and neck squamous cell carcinoma [45]. On the other hand, downregulation of the *Fos* proto-oncogene can be related to tumor suppression [46].

The whole transcriptome's modification under both transfection types showed the significant overexpression of genes involved in pathways related to cytoskeleton and ECM–matrix remodeling: regulation of actin cytoskeleton, focal adhesion, and ECM–receptor interaction. These results confirmed previous findings that in cancer the ECM matrix is subject to dynamic changes that reflect progression and metastasis [47,48]. Together with collagens and laminins, ECM matrix modification stimulated cancer cell activity and tumor progression [49,50]. The present study allowed us to identify the differential expression of collagens, laminin, and integrins. The detected significantly enriched GO was due to the collagen fibril organization. The collagen family is the most exposed DEG family in this analysis, in contrast to the analysis performed for the BPV-E4 protein. The integrin and kinesin superfamily proteins had the largest share. Moreover, both *BPV-E4-* and *BPV-E1^E4*-mediated nucleofection of equine ACFCs brought about the upregulation of *FGFR3* and *FGF12* (fibroblast growth factor receptor 3 and fibroblast growth factor 12), which are known as factors promoting tumor growth and metastasis [51].

Surprisingly, we have also observed differential expression of the *F2R* gene (encoding coagulation factor II thrombin receptor), which, according to the literature, can stimulate the migration and invasion of cancer cells under *SOX9* influence [52]. The other gene upregulated in nucleofected equine ACFCs was *ROCK2* (Rho associated coiled-coil containing protein kinase 2). Kaczorowski et al. [53] indicated that both *ROCK1* and *ROCK2* genes can be critical for controlling cellular motility and cancer invasiveness, while the inhibition of *ROCK2* decreased the tumor growth based on the osteosarcoma model [54].

The equine ACFCs nucleofected with the *BPV-E1^E4* gene construct displayed significant deregulation of s higher number of pathways than *BPV-E4* transgenic ACFCs, such as the FoxO signaling pathway, the PI3K-Akt and *TNF* signaling pathways, and Proteoglycans in cancer. The study by Semik et al. [16], which was focused on transcriptome differences between sarcoid and healthy skin tissues, showed significant over-representation of genes belonging to the PI3K-Akt signaling pathway, pathways in cancer, and cytokine–cytokine receptor interaction. Moreover, the abovementioned authors have observed differences in the expression of genes involved in actin cytoskeleton regulation, tight junction, and cell adhesion. Genes with differential expression such as *FGFR2* and *FGF10* have been identified in healthy and sarcoid-related tissues [16] and, analogously, in both *BPV-E1^E4* transgenic ACFCs and their control, nontransgenic counterparts. Similar to in the present study, healthy skin and sarcoids were characterized by differences with regard to collagens, integrins, and tubulin genes, which can affect the cytoskeleton arrangement and cell mobility [16].

Interestingly, in the current in vitro study, we noticed the significant downregulation of the *IGF2* (insulin-like growth factor 2) and *EGFR1* (epidermal growth factor receptor 1) genes. Such results are in contrast to the literature data, which showed overexpression of both genes in different types of cancers. The increased expression of the *IGF2* gene is strongly associated with a poor prognosis via stimulating cell proliferation [55]. Similarly, upregulation of the *EGFR1* gene, which is closely related to the tumor stage [56], and its overexpression means a poor prognosis of clinical outcome [57]. The low expression of both genes is characteristic for normal cells, but not for their neoplastic counterparts. Nonetheless, *EGFR1* can be downregulated by different factors such as decorin [58] or ubiquitin-specific peptidase 8 (*UBPY*) [59]. Such a mechanism aims to terminate cell proliferation and stop uncontrolled cell growth, which contributes to carcinogenesis. On the other hand, we observed the significant upregulation of the insulin receptor gene (*ISNR*), which is responsible for stimulation of tumor cell proliferation, migration, and

invasion [60], and can be co-expressed with the *EGFR* gene in tumors [61]. Overexpression of *INSR* is correlated with a poor prognosis for oncology patients [62] and can be used as an early tumor-related marker [63]. However, it should be highlighted that, in this study, the effect of only one gene of the *BP* virus is investigated. The aforementioned differences in the achieved gene expression levels may result from the lack of interaction with other viral proteins. Thus, neoplastic changes may occur differently.

To sum up, the results of the current investigation have confirmed that *BPV-E4-* and *BPV-E1ˆE4*-mediated nucleofection significantly affected transcriptomic alterations, leading to sarcoid-like neoplastic transformation of equine ACFCs. Nevertheless, the changes in transcriptomic signatures arising in the cells nucleofected with *BPV-E1ˆE4* fusion genes increasingly tended to resemble those that occurred in vivo in equine sarcoids. This finding may be justified by the onset and progression of modifications in crucial signaling pathways such as PI3K-Akt-mediated signal transduction pathway and a variety of closely related pathways. For this reason, we propose the strategy based on transgenically induced expression of BPV-E1ˆE4 fusion protein as a completely new ex vivo model of sarcoid-dependent oncogenic transformation in equine ACFCs. This biomedical model can be used not only to more comprehensively explore and decipher the molecular nature of dermal sarcoid-like neoplasia, but also to preclinically or clinically predict the directions and targets of anticancer therapies in specimens afflicted with epidermal and dermal sarcoids.

4. Materials and Methods

4.1. Experimental Schedule

The experimental protocol (as depicted in Figure 7) was divided into three main steps: (1) designing and preparing the transgene sequences to be expressed in equine ACFCs; (2) nucleofection-mediated neoplastic transformation of ACFCs prompted by *BPV-E4* and *BPV-E1ˆE4* transgenes; and (3) analysis of transcriptome changes in *BPV-E4* and *BPV-E1ˆE4* transgenic cells.
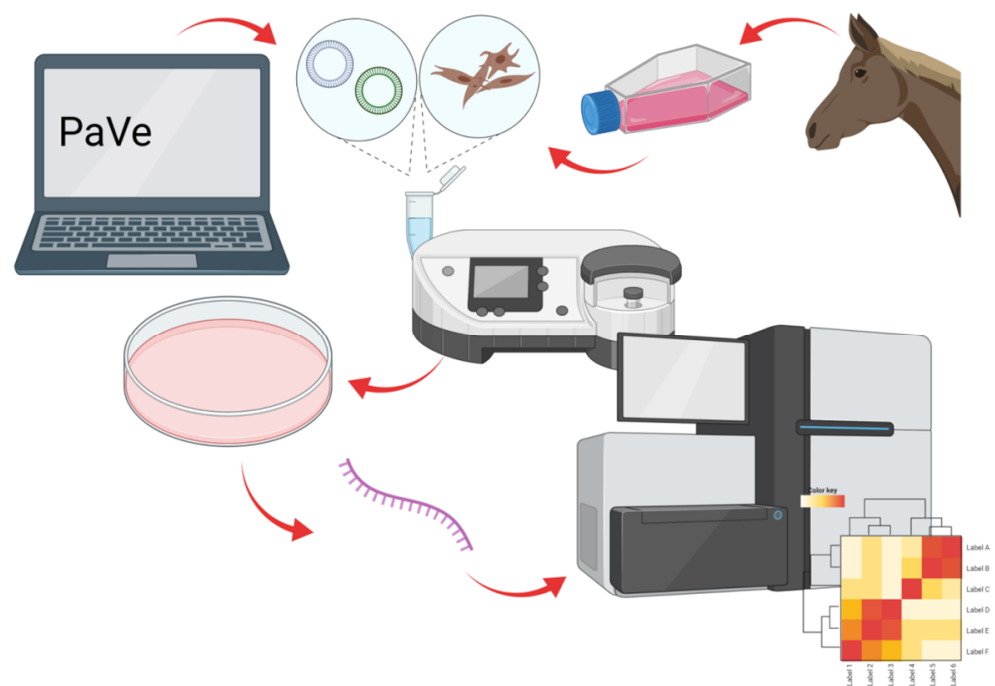
Figure 7. Experimental schedule. Created with BioRender.com [64].

In the first series of experiments, the gene sequences were designed based on information available in the biological database PaVe [65]. The sequences were cloned by the manufacturer (GeneArt Gene Synthesis, Thermo Scientific, Waltham, MA, USA) into

pMA-T plasmids, from which they were cut out with appropriately selected restriction enzymes. The excised sequences were cloned into expression plasmids (T-REx System, Invitrogen, Waltham, MA, USA, Thermo Scientific). The plasmids were propagated in competent *Escherichia coli* bacteria (strain DH5α; Invitrogen).

In the second series of experiments, the sarcoid-dependent genetic transformation of ACFCs was induced by nucleofection with the use of *BPV-E4* and *BPV-E1ˆE4* transgenes. Positively transformed nucleofectants that had acquired combined immune resistance to a cocktail of select antibiotics were expanded ex vivo and subsequently assigned to a further series of experiments.

In the third series of experiments, in order to perform a transcriptome analysis, RNA samples were isolated from the control (nontransgenic) and *BPV-E4* and *BPV-E1ˆE4* transgenic cell lines, from which cDNA libraries were then derived. The assessment of transcriptomic profiles was accomplished by next-generation sequencing (NGS) on an Illumina apparatus (Illumina, San Diego, CA, USA).

4.2. Designing Gene Inserts for Further Experiments Aimed at Nucleofection of Equine ACFCs

The inserted sequence of the *BPV-E4* gene was designed on the basis of the information available in the papillomavirus database, PaVe [65]. The sequence of the analyzed gene was designed with two variants. The first variant was based on the amino acid sequence of the *BPV1-E4* protein (gi 60965.E4) transcribed into the sequence encoding a given gene. The second variant was based on the amino acid sequence of the *BPV-E4* protein, including the amino acid sequence of the *BPV-E1* protein fragment (gi 60965), which more closely corresponds to the actual structure of the *BPV-E4* protein in vivo. In addition, the sequences were flanked with amino acid sequences characteristic of restriction enzymes (two different enzymes for each insert) enabling the creation of sticky ends. The enzymes were selected based on the MCS sequence of the plasmids of the target inserts (*pcDNA4/TO/myc-his/B*; T-REx System; Invitrogen) in such a way that the sequence ends they formed were not complementary. Such selection of enzymes prevented the formation of circular structures inside the enzymatic digestion products and also ensured that the insert sequence was placed in the correct direction concerning the target plasmid sequence. Additionally, the sequences of the inserts were enriched with the consensus KOZAK sequence (gccgccaccatgg).

4.3. The Reactions of Enzymatic Restriction and Ligation

The insert sequences provided by the manufacturer were cloned into *pMA-T* plasmids, from which they were excised using the restriction enzymes included in the design process. The reaction mixture contained a DNA template in the form of a plasmid containing the appropriate gene and a set of specific enzymes along with a buffer matched to them (for the gene: *BPV-E4*-AflII, KpnI, buffer 2.1; *BPV-E1ˆE4*-SacII, AflII, Cut Smart buffer; New England BioLabs, Ipswich, MA, USA), and digestion was carried out overnight. In addition, pcDNA plasmids from the T-REx system set (*pcDNA4/TO/myc-His/B*; Invitrogen) were also digested by restriction enzymes corresponding to the individual sequences of the inserts. The amount of template DNA was estimated to obtain 400 ng of the actual product (cut insert sequence or linear plasmid), which corresponds to the maximum amount of DNA that could be used in one sample during the gel purification method, made in the next step.

Digestion products were separated with agarose gel electrophoresis (0.8% low melting point agarose in TBE buffer, 80 V, until DNA band separation). The DNA band containing the viral gene sequence (*BPV-E4* or *BPV-E1ˆE4*) or a linear form of the digested plasmid was cut from the gel (ethidium bromide-mediated staining) and purified with a High Pure PCR Product Purification Kit (Roche, Warsaw, Poland). Purified DNA was eluted in the manufacturer's buffer, heated to 56 °C.

The obtained fragments of the corresponding gene variants were combined with the *pcDNA 4/TO/myc-His/B* plasmid in a mass ratio of 3:1. The required volumes of individual DNA were calculated using an online calculator [66]. According to the manufac-

turer's guidelines, the reaction was performed with a Rapid DNA Ligation Kit (Roche, Basel, Switzerland).

4.4. Molecular Cloning of DNA Plasmid Constructs with Inserted BPV-E4 or BPV-E1^E4 Gene Sequences

Plasmids were cloned with Subcloning Efficiency DH5α Competent Cells (Invitrogen). Ten nanograms of plasmid DNA were introduced into bacteria by the heat-shock method. After the addition of DNA, the bacteria were held at 42 °C for 20 s after 30 min of incubation on ice, and then the bacteria were put on ice again for 2 min. Transformed bacteria were incubated in 1 mL low-salt Luria-Bertani Broth (Sigma-Aldrich, Merck Life Sciences, Poznań, Poland) for 1 h at 225 rpm and 37 °C. The bacteria were seeded on a low-salt LB broth with the addition of agarose (Sigma-Aldrich) and 120 µg/mL ampicillin (Gibco, Thermo Scientific), which served as a selective antibiotic, and incubated overnight at 37 °C. The genetically transformed bacterial cells that had been found to display immune resistance to ampicillin were positive for the occurrence of plasmid DNA. Obtained bacterial colonies were tested for positive recombination with Quick Screen PCR. Fragments of picked bacterial colonies were suspended in 15 µL of 0.1% Triton X-100 (Sigma-Aldrich) in TE buffer, then incubated in 100 °C for 5 min and centrifuged ($13,000 \times g$; 10 min). The supernatant was sequenced (Sanger method; Genetic Analyzer XL, Applied Biosystems, Thermo Fisher Scientific) to confirm the presence and quality of plasmids. Bacterial colonies that were positive for plasmid presence were grown for 14 h at 37 °C (250 rpm) in 100 mL of low-salt LB broth (Sigma-Aldrich) enriched with 120 µg/mL ampicillin. Suspended bacteria were centrifuged ($4500 \times g$; 20 min; 4 °C) followed by removal of supernatants. Plasmid DNA was isolated with a Qiagen Plasmid Midi Kit (Qiagen, Wroclaw, Poland), according to the manufacturer's protocol. Plasmid DNA was eluted in 50 mL of TC-treated water.

4.5. Establishment of Primary Cultures and Mitotically Stable Lines of Equine Adult Cutaneous Fibroblast Cells (ACFCs)

Adult skin tissue-derived biopsies (*n* = 4) were collected postmortem from the lower eyelid regions of horses slaughtered in the local abattoir. Dermal tissue samples were deposited into tubes filled with Dulbecco's Modified Eagle's Medium (DMEM; Gibco) supplemented with 10% fetal bovine serum (FBS; Gibco), HEPES (Gibco) and primocin (InvivoGen, Alab, Warsaw, Poland). Tubes were stored at 4 °C for no longer than 24 h after the recovery of cutaneous tissue explants.

Primary cell cultures were generated according to the modified procedures described in the study by Tomasek et al. [67]. Briefly, dermal tissue samples were disinfected with 70% ethanol and washed thrice in a $1\times$ solution of Dulbecco's phosphate-buffered saline (DPBS; pH 7.2; Gibco), followed by cutting into smaller pieces (approximately 2 mm × 2 mm), which were placed into cell culture flasks containing DMEM (Gibco) enriched with 10% FBS and primocin. Cutaneous tissue fragments were incubated at 37 °C in an atmosphere of 5% CO_2 and 100% humidity for two weeks, until the cells spontaneously migrated from the tissue explants. The culture medium was changed two times per week and passages were performed immediately after the ex vivo proliferating cells had reached 90% confluence. The first passages were characterized by the presence of epidermal keratinocytes in culture. Therefore, during the passaging procedure, the cells were trypsinized until the adherent equine adult cutaneous fibroblast cells (ACFCs) were efficiently detached. Keratinocytes, as less detachable epidermal cells [68], were still attached to the bottom of the culture dishes. For that reason, these cell subpopulations have not been replated. The homogenous ACFC lines, in the subpopulations of which the disappearance of epidermal keratinocytes was clearly confirmed, were successfully established at the third passage.

4.6. Genetic Transformation of Equine ACFCs Mediated by Nucleofection

The approaches that were applied both to prepare the equine ACFCs prior to nucleofection and to nucleofect them were accomplished according to the methods used for the transgenization of porcine dermal fibroblast cells (NDCs for SCNT), as comprehensively

described in studies by Skrzyszowska et al. [21] and Samiec et al. [22]. Briefly, the ex vivo expanded equine ACFCs that had previously reached approximately 90% confluence were prepared for the nuclefection procedure by trypsinization and subsequent resuspension in HEPES-buffered Tissue Culture Medium 199 (TCM 199; Sigma-Aldrich) supplemented with 5% FBS (Sigma-Aldrich), followed by centrifugation at $200\times g$ for 10 min. Afterwards, the centrifugation pools of cells (each at a concentration ranging from 4×10^5 to 5×10^5) were subjected to co-transfection nucleofection using the Amaxa^{TM} Normal Human Dermal Fibroblast– Adult (NHDF-Adult) Nucleofector^{TM} Kit (Lonza, CELLLAB, Warsaw, Poland) and a mixture of two pcDNA plasmids included in the T-REx kit (Invitrogen). The aforementioned mixture of two plasmids (a total amount of 2.8 µg and in a mass ratio of 6:1) was comprised of pcDNA^{TM} *6/TR* and pcDNA^{TM} *4/TO/myc-His/B* with the appropriate transgene variant inserted (either *BPV-E4* or *BPV-E1ˆE4*). The co-transfection of equine ACFCs was carried out within the Amaxa nucleofection cuvettes inserted into the holder of the Amaxa Nucleofector^{TM} II Device (Amaxa Biosystems, Lonza, Medianus, Kraków, Poland). The nucleofection process was triggered by the U-023 program intended for transgenization of human dermal fibroblasts and resulted in high transfection efficiency. The U-023 program was delivered by Amaxa Nucleofector^{TM} Technology (Amaxa Biosystems).

4.7. Treatment of Cell Nucleofectants Leading to Positive Antibiotic-Dependent Selection of BPV-E4 or BPV-E1ˆE4 Transgenic Equine ACFCs and Their Subsequent Tetracycline-Induced Neoplastic Transformation into Sarcoid-like Cells

After nucleofection, the equine ACFCs were seeded into collagen-coated culture dishes (Greiner Bio-One GmbH, BIOKOM Systems, Janki near Warsaw, Poland) and incubated for 48 h in DMEM enriched with recombinant human basic fibroblast growth factor (rh-bFGF; Sigma-Aldrich). The culture medium was subsequently changed to a medium supplemented with 200 µg/mL zeocin (Invitrogen) and 6 µg/mL blasticidin S (Thermo Scientific, Waltham, MA, USA). As a consequence of zeocin- and blasticidin S-dependent negative selection, the nontransgenic (TG⁻) cells that had not effectively undergone *BPV-E4-* or *BPV-E1ˆE4*-induced oncogenic transformation were eliminated from subpopulations encompassing cell nucleofectants due to the lack of immune resistance to selective antibiotics (i.e., combined resistance to zeocin and blasticidin S). The ACFCs that had undergone efficient transgenization were found to display antibiotic resistance. Seven days later, the selection was complete and the remaining positively selected transgenic (TG⁺) cells were cultured under standard conditions in the medium supplemented with 10% Tet-System Approved FBS (Gibco). Plasmid expression was induced by the addition of 1 µg/mL tetracycline (Invitrogen) to the culture medium 24 h before accomplishing further procedures.

The concentrations of the individual antibiotics were selected by establishing the lowest concentrations of the antibiotics that destroyed the cell culture within a week. For this purpose, media with different concentrations of individual antibiotics were introduced into the cultures, carried out in 96-well culture plates with 100% confluence. The concentrations were 2, 4, 6, 8, 9, 10, 11, 12, and 14 µg/mL for blasticidin S and 50, 100, 200, 400, 600, 800, 1000, 1100, and 1300 µg/mL for zeocin. One week later, the number of vial cells was measured using CellTiter Blue dye (Promega, Walldorf, Germany). The culture medium was removed from each well, and then 100 µL of culture medium with dye was added to it (in a 5:1 ratio). The cultures were then incubated for 5.5 h in an incubator (37 °C, 5% CO_2, 100% humidity), protected from light. The measurement was performed on a PlateReader 2200 (Eppendorf, Warsaw, Poland) (excitation: 535 nm, emission: 595 nm). The lowest concentrations of antibiotics were selected as those for which the fluorescence level did not differ significantly from the fluorescence of empty wells.

4.8. Detection of BPV DNA in Equine ACFCs Subjected to Oncogenic Transformation with the Aid of Nucleofection

DNA was isolated with a NucleoMag Vet Kit (Macherey-Nagel, Bionovo, Legnica, Poland) according to the manufacturer's protocol. DNA was dissolved in DEPC-treated

water (Life Technologies, Ambion, Thermo Scientific, Waltham, MA, USA). The quality of isolated DNA was checked with NanoDrop 2000 (Life Technologies).

Polymerase chain reaction (PCR) was performed with AmpliTaq Gold 360 Master Mix polymerase (Applied Biosystems) with primers specific for the *BPV1* and *BPV2* consensus region [69]. The temperature profile was set with respect to the polymerase supplier's protocol and with a primer annealing temperature of 57–58 °C. PCR products were separated in agarose gel electrophoresis (3% agarose in TBE).

4.9. Isolation of RNA Samples from BPV-E4 and BPV-E1^E4 Transgenic Equine ACFC-Derived Neoplastic Cells

According to the producer's protocol, RNA was directly isolated from adherent cultures of *BPV-E4* and *BPV-E1^E4* transgenic equine ACFC-derived neoplastic cell lines that were expanded ex vivo on the bottom of culture dishes. To extract RNA samples, a PureLink™ RNA mini kit (Invitrogen) was used. The procedure was maintained, with the addition of a DNase treatment step (PureLink™ DNase Set, Invitrogen). RNA was eluted with DEPC-treated water (Thermo Fisher Scientific, Waltham, MA, USA).

The quality and quantity of RNA were measured with a 2200 TapeStation Automated Electrophoresis System (Agilent Technologies, Santa Clara, CA, USA), as well as a nanodrop 2000 spectrophotometer (Thermo Scientific) and agarose gel (2% agarose in TBE buffer) electrophoresis.

4.10. NGS Sequencing among Oncogenically Transformed Equine ACFCs Expressing BPV-E4 and BPV-E4^E1 Transgenes

All samples were sequenced using the NGS approach. High-quality RNA (RIN value from 9.3 to 9.8) was used for cDNA libraries preparation with the TruSeq RNA Kit v2 kit (Illumina, San Diego, CA, USA) according to the attached protocol. The individual cDNA libraries were ligated with different indexes to be able to pool samples during the NGS sequencing procedure. The quality and quantity of obtained libraries were assessed using Qubit 2.0 (Qubit™ dsDNA BR AssayKit, Invitrogen, Waltham, MA, USA) and TapeStation 2200 (D100 ScreenTapes, Agilent Technologies, Santa Clara, CA, USA). In the next step, the cDNA libraries were sequenced on the NextSeq 500 Illumina platform (Illumina) and NextSeq 500/550 High Output KIT v 2.5 (75 cycles) according to the protocol.

The raw data were first checked for quality with FastQC v0.11.7 software, followed by the removal of adapters and low-quality reads (Phred quality of 20 and read length of 36). Then, the filtered reads were mapped to the EquCab3 genome with STAR software. Afterwards, the mapped reads were annotated and counted to specific gene thresholds with the usage of Ensembl GTF file version 100 (via htseq-count software). Differential expression analysis was performed with the use of Deseq2 software v3.14.

Gene Ontology enrichment and over-represented Pathways analyses (KEGG, GO) were performed using David software (version 6.8) [70] based on the *Equus caballus* reference. The significance was based on the False Discovery Rate (FDR), calculated as a *p*-value after Benjamin multiple testing correction [71]. For the visualization of gene interaction, String software v11.5 [24] was applied with *Equus caballus* as a reference.

4.11. qPCR-Assisted Validation Accomplished for Transcriptional Activity Levels of Genes in Neoplastically Transformed Equine ACFCs Expressing BPV-E4 and BPV-E1^E4 Transgenes

RNA-seq validation was performed using real-time PCR. The exact transcript levels were estimated for 10 DEGs for which specific primers were designed based on Ensemble reference (Primer3 Input (version 0.4.0) software; [72]) (Table S1). The cDNA samples were synthesized from 300 ng of total RNA using a High-Capacity RNA-to-cDNA™ Kit (Applied Biosystems). The qPCR reaction was carried out in triplicate for each sample with Sensitive RT HS-PCR EvaGreen Mix (A&A Biotechnology, Gdynia, Poland) according to the manufacturer's protocol and using QuantStudio7Flex platform (Applied Biosystems). The expression was calculated using the delta–delta CT method, according to Pfaffl et al. [73],

and based on two endogenous controls, i.e., *ACTB* and *UBB* genes that encode β-actin and ubiquitin B, respectively [74].

The NGS data (normalized counts) and relative quantity (RQ) were compared using the Pearson correlation (SAS software, version 8.02).

5. Conclusions

Our research sought to unravel the transcriptomic signatures of in vitro proliferating *BPV-E4* and *BPV-E4ˆE1* transgenic equine ACFCs that have undergone sarcoid-dependent oncogenic transformation. It might contribute to further investigations focused on somatic cell cloning in domestic horses and other equids. The goal of these investigations might be determining the suitability of nonmalignant sarcoid-like derivatives of ACFCs to be used as an epigenomically plastic and dedifferentiable source of NDCs for generating equine cloned embryos and offspring by SCNT-mediated ARTs. This might be of importance for both empirically and preclinically developing novel ex vivo biomedical models. The latter will attempt to track and decipher the molecular pathways of the processes responsible for the epigenomic reprogrammability of transcriptional profiles within the nuclear DNA of transgenic equine ACFC-derived sarcoid-like cells. On the one hand, the formerly indicated processes have been found to incur at the onset and progression of sarcoid-dependent neoplasia due to nucleofection-mediated cancerous transformation under extracorporeal conditions. On the other hand, these processes might trigger the irreversible attenuation of neoplastic transformation into dermal sarcoid-like tumors and subsequent initiation of the anticancer conversion of neoplastic ACFCs as a result of SCNT-based cloning, not only in horses but also in other taxonomic representatives of the *Equidae* family.

Abbreviations

ACFC	Adult cutaneous fibroblast cell
ACTB	Actin β
ADAM	Disintegrin and metalloproteinase domain
Akt	Serine/threonine kinase
ART	Assisted reproductive technology
BAD	Bcl2-associated agonist of cell death
BCG	Bacillus Calmette–Guérin
BMI	Polycomb ring finger
BPV	Bovine Papillomavirus
CCND	Cyclin D
CD	Cluster of differentiation
CDK	Cyclin-dependent kinase
COL	Collagen
DAVID	Database for Annotation, Visualization, and Integrated Discovery
DEG	Differentially expressed gene
DMEM	Dulbecco's Modified Eagle's Medium
DPBS	Dulbecco's phosphate-buffered saline
ECM	Extracellular matrix
EGFR	Epidermal growth factor receptor
F2R	Coagulation factor II thrombin receptor
FBS	Fetal bovine serum
FDR	False discovery rate
FGF	Fibroblast growth factor
FGFR	Fibroblast growth factor receptor
FOS	Fos proto-oncogene
FoxO	Forkhead box O
GEO	Gene Expression Omnibus
GO	Gene Ontology
HEPES	4-(2-hydroxyethyl)-1-piperazineethanesulfonic acid
IGF	Insulin-like growth factor
ISNR	Insulin receptor
ITG	Integrin
ITGA	Integrin subunit α
KEGG	Kyoto Encyclopedia of Genes and Genomes
KIF	Kinesin superfamily protein
LAMA	Laminin subunit α
LB	Luria–Bertani
MAPK	Mitogen-activated protein kinase
MCS	Multiple cloning site
MMP	Matrix metalloproteinase
NANOG	Nanog homeobox
NCR	Noncoding region
NDC	Nuclear donor cell
NGS	Next generation sequencing
PCA	Principal component analysis
PCR	Polymerase chain reaction
PI3K	Phosphoinositide 3-kinase
PTGER	Prostaglandin E receptor
Rap	Ras-related protein
RECK	Reversion inducing cysteine rich protein with kazal motifs
Rho	Rhodopsin
ROCK	Rho-associated coiled-coil containing protein kinase
SCNT	Somatic cell nuclear transfer
SOX	SRY-box transcription
TBE	Tris/borate/EDTA

TCM	Tissue culture medium
TE	Tris-EDTA
TGFB	Transforming growth factor β
TGFBR	Transforming growth factor β receptor
TIMP	Tissue inhibitor of metalloproteinase
TNF	Tumor necrosis factor
UB	Ubiquitin
UBP	Ubiquitin-specific peptidase
URR	Upstream regulatory region
VEGF	Vascular endothelial growth factor
Wnt	Wingless-type MMTV integration site family
XIAP	X-linked inhibitor of apoptosis

References

1. Haralambus, R.; Burgstaller, J.; Klukowska-Rötzler, J.; Steinborn, R.; Buchinger, S.; Gerber, V.; Brandt, S. Intralesional Bovine Papillomavirus DNA Loads Reflect Severity of Equine Sarcoid Disease. *Equine Vet. J.* **2010**, *42*, 327–331. [CrossRef]
2. Knottenbelt, D.C. A Suggested Clinical Classification for the Equine Sarcoid. *Clin. Tech. Equine Pract.* **2005**, *4*, 278–295. [CrossRef]
3. Yuan, Z.; Gallagher, A.; Gault, E.A.; Campo, M.S.; Nasir, L. Bovine Papillomavirus Infection in Equine Sarcoids and in Bovine Bladder Cancers. *Vet. J.* **2007**, *174*, 599–604. [CrossRef] [PubMed]
4. Bogaert, L.; Martens, A.; Van Poucke, M.; Ducatelle, R.; De Cock, H.; Dewulf, J.; De Baere, C.; Peelman, L.; Gasthuys, F. High Prevalence of Bovine Papillomaviral DNA in the Normal Skin of Equine Sarcoid-Affected and Healthy Horses. *Vet. Microbiol.* **2008**, *129*, 58–68. [CrossRef] [PubMed]
5. Nasir, L.; Reid, S.W.J. Bovine Papillomaviral Gene Expression in Equine Sarcoid Tumours. *Virus Res.* **1999**, *61*, 171–175. [CrossRef]
6. Yuan, Z.Q.; Gault, E.A.; Gobeil, P.; Nixon, C.; Campo, M.S.; Nasir, L. Establishment and Characterization of Equine Fibroblast Cell Lines Transformed in Vivo and in Vitro by BPV-1: Model Systems for Equine Sarcoids. *Virology* **2008**, *373*, 352–361. [CrossRef] [PubMed]
7. Bogaert, L.; Martens, A.; Kast, W.M.; Van Marck, E.; De Cock, H. Bovine Papillomavirus DNA Can Be Detected in Keratinocytes of Equine Sarcoid Tumors. *Vet. Microbiol.* **2010**, *146*, 269–275. [CrossRef]
8. Bocaneti, F.; Altamura, G.; Corteggio, A.; Velescu, E.; Roperto, F.; Borzacchiello, G. Bovine Papillomavirus: New Insights into an Old Disease. *Transbound. Emerg. Dis.* **2016**, *63*, 14–23. [CrossRef] [PubMed]
9. Nasir, L.; Campo, M.S. Bovine Papillomaviruses: Their Role in the Aetiology of Cutaneous Tumours of Bovids and Equids. *Vet. Dermatol.* **2008**, *19*, 243–254. [CrossRef]
10. Lancaster, W.D.; Olson, C. Animal papillomaviruses. *Microbiol. Rev.* **1982**, *46*, 191–207. [CrossRef]
11. Rector, A.; Van Ranst, M. Animal Papillomaviruses. *Virology* **2013**, *445*, 213–223. [CrossRef] [PubMed]
12. Bravo, I.G.; Félez-Sánchez, M. Papillomaviruses. *Evol. Med. Public Health* **2015**, *2015*, 32–51. [CrossRef]
13. Knottenbelt, D.C. The Equine Sarcoid: Why Are There so Many Treatment Options? *Vet. Clin. N. Am. Equine Pract.* **2019**, *35*, 243–262. [CrossRef] [PubMed]
14. Taylor, S.D.; Toth, B.; Baseler, L.J.; Charney, V.A.; Miller, M.A. Lack of Correlation between Papillomaviral DNA in Surgical Margins and Recurrence of Equine Sarcoids. *J. Equine Vet. Sci.* **2014**, *34*, 722–725. [CrossRef]
15. Funiciello, B.; Roccabianca, P. *Equine Sarcoid*; IntechOpen: London, UK, 2020; ISBN 978-1-83962-317-2.
16. Semik, E.; Gurgul, A.; Ząbek, T.; Ropka-Molik, K.; Koch, C.; Mählmann, K.; Bugno-Poniewierska, M. Transcriptome Analysis of Equine Sarcoids. *Vet. Comp. Oncol.* **2017**, *15*, 1370–1381. [CrossRef] [PubMed]
17. Semik-Gurgul, E. Molecular Approaches to Equine Sarcoids. *Equine Vet. J.* **2021**, *53*, 221–230. [CrossRef]
18. Bogaert, L.; Woodham, A.W.; Da Silva, D.M.; Martens, A.; Meyer, E.; Kast, W.M. A Novel Murine Model for Evaluating Bovine Papillomavirus Prophylactics/Therapeutics for Equine Sarcoid-like Tumours. *J. Gen. Virol.* **2015**, *96*, 2764–2768. [CrossRef]
19. Li, L.; Connelly, M.C.; Wetmore, C.; Curran, T.; Morgan, J.I. Mouse embryos cloned from brain tumors. *Cancer Res.* **2003**, *63*, 2733–2736.
20. Shao, G.-B.; Ding, H.-M.; Gao, W.-L.; Li, S.-H.; Wu, C.-F.; Xu, Y.-X.; Liu, H.-L. Effect of Trychostatin A Treatment on Gene Expression in Cloned Mouse Embryos. *Theriogenology* **2009**, *71*, 1245–1252. [CrossRef]
21. Skrzyszowska, M.; Samiec, M.; Słomski, R.; Lipiński, D.; Mały, E. Development of porcine transgenic nuclear-transferred embryos derived from fibroblast cells transfected by the novel technique of nucleofection or standard lipofection. *Theriogenology* **2008**, *70*, 248–259. [CrossRef]
22. Samiec, M.; Skrzyszowska, M.; Lipiński, D. Pseudophysiological transcomplementary activation of reconstructed oocytes as a highly efficient method used for producing nuclear-transferred pig embryos originating from transgenic foetal fibroblast cells. *Pol. J. Vet. Sci.* **2012**, *15*, 509–516. [CrossRef] [PubMed]
23. R: The R Project for Statistical Computing. Available online: https://www.r-project.org/ (accessed on 21 January 2022).
24. STRING: Functional Protein Association Networks. Available online: https://string-db.org/ (accessed on 21 January 2022).

25. Doorbar, J.; Foo, C.; Coleman, N.; Medcalf, L.; Hartley, O.; Prospero, T.; Napthine, S.; Sterling, J.; Winter, G.; Griffin, H. Characterization of Events during the Late Stages of HPV16 Infectionin VivoUsing High-Affinity Synthetic Fabs to E4. *Virology* **1997**, *238*, 40–52. [CrossRef] [PubMed]

26. Pray, T.R.; Laimins, L.A. Differentiation-Dependent Expression of E1^E4 Proteins in Cell Lines Maintaining Episomes of Human Papillomavirus Type 31b. *Virology* **1995**, *206*, 679–685. [CrossRef]

27. Wilson, R.; Fehrmann, F.; Laimins, L.A. Role of the E1–E4 Protein in the Differentiation-Dependent Life Cycle of Human Papillomavirus Type 31. *J. Virol.* **2005**, *79*, 6732–6740. [CrossRef]

28. Boer, J.M.; Huber, W.K.; Sültmann, H.; Wilmer, F.; von Heydebreck, A.; Haas, S.; Korn, B.; Gunawan, B.; Vente, A.; Füzesi, L.; et al. Identification and Classification of Differentially Expressed Genes in Renal Cell Carcinoma by Expression Profiling on a Global Human 31,500-Element CDNA Array. *Genome Res.* **2001**, *11*, 1861–1870. [CrossRef] [PubMed]

29. Nakamura, T.; Furukawa, Y.; Nakagawa, H.; Tsunoda, T.; Ohigashi, H.; Murata, K.; Ishikawa, O.; Ohgaki, K.; Kashimura, N.; Miyamoto, M.; et al. Genome-Wide CDNA Microarray Analysis of Gene Expression Profiles in Pancreatic Cancers Using Populations of Tumor Cells and Normal Ductal Epithelial Cells Selected for Purity by Laser Microdissection. *Oncogene* **2004**, *23*, 2385–2400. [CrossRef] [PubMed]

30. Yoon, J.; Lee, J.; Namkoong, S.; Bae, S.; Kim, Y.W.; Han, S.; Cho, Y.; Nam, G.; Kim, C.-K.; Seo, J.-S.; et al. cDNA Microarray Analysis of Gene Expression Profiles Associated with Cervical Cancer. *Cancer Res. Treat.* **2003**, *35*, 451–459. [CrossRef]

31. Desgrosellier, J.S.; Cheresh, D.A. Integrins in Cancer: Biological Implications and Therapeutic Opportunities. *Nat. Rev. Cancer* **2010**, *10*, 9–22. [CrossRef]

32. Hamidi, H.; Ivaska, J. Every Step of the Way: Integrins in Cancer Progression and Metastasis. *Nat. Rev. Cancer* **2018**, *18*, 533–548. [CrossRef]

33. Valdembri, D.; Serini, G. The Roles of Integrins in Cancer. *Fac. Rev.* **2021**, *10*, 45. [CrossRef]

34. Lucanus, A.J.; Yip, G.W. Kinesin Superfamily: Roles in Breast Cancer, Patient Prognosis and Therapeutics. *Oncogene* **2018**, *37*, 833–838. [CrossRef] [PubMed]

35. Koni, M.; Pinnarò, V.; Brizzi, M.F. The Wnt Signalling Pathway: A Tailored Target in Cancer. *Int. J. Mol. Sci.* **2020**, *21*, 7697. [CrossRef] [PubMed]

36. Aldaz, P.; Otaegi-Ugartemendia, M.; Saenz-Antoñanzas, A.; Garcia-Puga, M.; Moreno-Valladares, M.; Flores, J.M.; Gerovska, D.; Arauzo-Bravo, M.J.; Samprón, N.; Matheu, A.; et al. SOX9 Promotes Tumor Progression through the Axis BMI1-P21CIP. *Sci. Rep.* **2020**, *10*, 357. [CrossRef] [PubMed]

37. Xue, Y.; Lai, L.; Lian, W.; Tu, X.; Zhou, J.; Dong, P.; Su, D.; Wang, X.; Cao, X.; Chen, Y.; et al. SOX9/FXYD3/Src Axis Is Critical for ER+ Breast Cancer Stem Cell Function. *Mol. Cancer Res. MCR* **2019**, *17*, 238–249. [CrossRef] [PubMed]

38. Ma, Y.; Shepherd, J.; Zhao, D.; Bollu, L.R.; Tahaney, W.M.; Hill, J.; Zhang, Y.; Mazumdar, A.; Brown, P.H. SOX9 Is Essential for Triple-Negative Breast Cancer Cell Survival and Metastasis. *Mol. Cancer Res. MCR* **2020**, *18*, 1825–1838. [CrossRef]

39. Hanahan, D.; Weinberg, R.A. The Hallmarks of Cancer. *Cell* **2000**, *100*, 57–70. [CrossRef]

40. Jakowlew, S.B. Transforming Growth Factor-β in Cancer and Metastasis. *Cancer Metastasis Rev.* **2006**, *25*, 435. [CrossRef]

41. Kim, W.; Kim, E.; Lee, S.; Kim, D.; Chun, J.; Park, K.H.; Youn, H.; Youn, B. TFAP2C-Mediated Upregulation of TGFBR1 Promotes Lung Tumorigenesis and Epithelial–Mesenchymal Transition. *Exp. Mol. Med.* **2016**, *48*, e273. [CrossRef]

42. Zeng, Q.; Phukan, S.; Xu, Y.; Sadim, M.; Rosman, D.S.; Pennison, M.; Liao, J.; Yang, G.-Y.; Huang, C.-C.; Valle, L.; et al. Tgfbr1 Haploinsufficiency Is a Potent Modifier of Colorectal Cancer Development. *Cancer Res.* **2009**, *69*, 678–686. [CrossRef]

43. Zhou, R.; Huang, Y.; Cheng, B.; Wang, Y.; Xiong, B. TGFBR1*6A Is a Potential Modifier of Migration and Invasion in Colorectal Cancer Cells. *Oncol. Lett.* **2018**, *15*, 3971–3976. [CrossRef]

44. Mahner, S.; Baasch, C.; Schwarz, J.; Hein, S.; Wölber, L.; Jänicke, F.; Milde-Langosch, K. C-Fos Expression Is a Molecular Predictor of Progression and Survival in Epithelial Ovarian Carcinoma. *Br. J. Cancer* **2008**, *99*, 1269–1275. [CrossRef]

45. Muhammad, N.; Bhattacharya, S.; Steele, R.; Phillips, N.; Ray, R.B. Involvement of C-Fos in the Promotion of Cancer Stem-like Cell Properties in Head and Neck Squamous Cell Carcinoma. *Clin. Cancer Res. Off. J. Am. Assoc. Cancer Res.* **2017**, *23*, 3120–3128. [CrossRef]

46. Gao, F.; Zhou, L.; Li, M.; Liu, W.; Yang, S.; Li, W. Inhibition of ERKs/Akt-Mediated c-Fos Expression Is Required for Piperlongumine-Induced Cyclin D1 Downregulation and Tumor Suppression in Colorectal Cancer Cells. *OncoTargets Ther.* **2020**, *13*, 5591–5603. [CrossRef]

47. Nallanthighal, S.; Heiserman, J.P.; Cheon, D.-J. The Role of the Extracellular Matrix in Cancer Stemness. *Front. Cell Dev. Biol.* **2019**, *7*, 86. [CrossRef] [PubMed]

48. Winkler, J.; Abisoye-Ogunniyan, A.; Metcalf, K.J.; Werb, Z. Concepts of Extracellular Matrix Remodelling in Tumour Progression and Metastasis. *Nat. Commun.* **2020**, *11*, 5120. [CrossRef] [PubMed]

49. Walker, C.; Mojares, E.; del Río Hernández, A. Role of Extracellular Matrix in Development and Cancer Progression. *Int. J. Mol. Sci.* **2018**, *19*, 3028. [CrossRef] [PubMed]

50. Xu, S.; Xu, H.; Wang, W.; Li, S.; Li, H.; Li, T.; Zhang, W.; Yu, X.; Liu, L. The Role of Collagen in Cancer: From Bench to Bedside. *J. Transl. Med.* **2019**, *17*, 309. [CrossRef] [PubMed]

51. Li, L.; Zhang, S.; Li, H.; Chou, H. FGFR3 Promotes the Growth and Malignancy of Melanoma by Influencing EMT and the Phosphorylation of ERK, AKT, and EGFR. *BMC Cancer* **2019**, *19*, 963. [CrossRef]

52. Gao, G.; Yang, M.; Wang, F.; Dang, G.; Zhang, X.; Zhao, J.; Wang, X.; Jin, B. Coagulation Factor 2 Thrombin Receptor Promotes Malignancy in Glioma under SOX2 Regulation. *Aging* **2020**, *12*, 10594–10613. [CrossRef] [PubMed]

53. Kaczorowski, M.; Biecek, P.; Donizy, P.; Pieniążek, M.; Matkowski, R.; Hałoń, A. ROCK1 and ROCK2 Are Down-Regulated in Aggressive and Advanced Skin Melanomas—A Clinicopathological Perspective. *Anticancer Res.* **2020**, *40*, 1931–1942. [CrossRef]

54. Zucchini, C.; Manara, M.C.; Cristalli, C.; Carrabotta, M.; Greco, S.; Pinca, R.S.; Ferrari, C.; Landuzzi, L.; Pasello, M.; Lollini, P.-L.; et al. ROCK2 Deprivation Leads to the Inhibition of Tumor Growth and Metastatic Potential in Osteosarcoma Cells through the Modulation of YAP Activity. *J. Exp. Clin. Cancer Res.* **2019**, *38*, 503. [CrossRef] [PubMed]

55. Dong, Y.; Li, J.; Han, F.; Chen, H.; Zhao, X.; Qin, Q.; Shi, R.; Liu, J. High IGF2 Expression Is Associated with Poor Clinical Outcome in Human Ovarian Cancer. *Oncol. Rep.* **2015**, *34*, 936–942. [CrossRef] [PubMed]

56. Spano, J.-P.; Lagorce, C.; Atlan, D.; Milano, G.; Domont, J.; Benamouzig, R.; Attar, A.; Benichou, J.; Martin, A.; Morere, J.-F.; et al. Impact of EGFR Expression on Colorectal Cancer Patient Prognosis and Survival. *Ann. Oncol. Off. J. Eur. Soc. Med. Oncol.* **2005**, *16*, 102–108. [CrossRef] [PubMed]

57. Mitsudomi, T.; Yatabe, Y. Epidermal Growth Factor Receptor in Relation to Tumor Development: EGFR Gene and Cancer. *FEBS J.* **2010**, *277*, 301–308. [CrossRef] [PubMed]

58. Csordás, G.; Santra, M.; Reed, C.C.; Eichstetter, I.; McQuillan, D.J.; Gross, D.; Nugent, M.A.; Hajnóczky, G.; Iozzo, R.V. Sustained Down-Regulation of the Epidermal Growth Factor Receptor by Decorin: A Mechanism for Controlling Tumor Growth In Vivo. *J. Biol. Chem.* **2000**, *275*, 32879–32887. [CrossRef]

59. Mizuno, E.; Iura, T.; Mukai, A.; Yoshimori, T.; Kitamura, N.; Komada, M. Regulation of Epidermal Growth Factor Receptor Down-Regulation by UBPY-Mediated Deubiquitination at Endosomes. *Mol. Biol. Cell* **2005**, *16*, 5163–5174. [CrossRef]

60. Heidegger, I.; Kern, J.; Ofer, P.; Klocker, H.; Massoner, P. Oncogenic functions of IGF1R and INSR in prostate cancer include enhanced tumor growth, cell migration and angiogenesis. *Oncotarget* **2014**, *5*, 2723–2735. [CrossRef]

61. Ma, Y.; Tang, N.; Thompson, R.C.; Mobley, B.C.; Clark, S.W.; Sarkaria, J.N.; Wang, J. InsR/IGF1R Pathway Mediates Resistance to EGFR Inhibitors in Glioblastoma. *Clin. Cancer Res. Off. J. Am. Assoc. Cancer Res.* **2016**, *22*, 1767–1776. [CrossRef]

62. Sun, J.; Lu, Z.; Deng, Y.; Wang, W.; He, Q.; Yan, W.; Wang, A. Up-Regulation of INSR/IGF1R by C-Myc Promotes TSCC Tumorigenesis and Metastasis through the NF-KB Pathway. *Biochim. Biophys. Acta BBA—Mol. Basis Dis.* **2018**, *1864*, 1873–1882. [CrossRef]

63. Roudnicky, F.; Dieterich, L.C.; Poyet, C.; Buser, L.; Wild, P.; Tang, D.; Camenzind, P.; Ho, C.H.; Otto, V.I.; Detmar, M. High Expression of Insulin Receptor on Tumour-Associated Blood Vessels in Invasive Bladder Cancer Predicts Poor Overall and Progression-Free Survival. *J. Pathol.* **2017**, *242*, 193–205. [CrossRef]

64. BioRender. Available online: https://biorender.com/ (accessed on 25 January 2022).

65. PaVE: Papilloma Virus Genome Database. Available online: https://pave.niaid.nih.gov/ (accessed on 21 January 2022).

66. NEBioCalculator. Available online: https://nebiocalculator.neb.com/#!/ligation (accessed on 21 January 2022).

67. Tomasek, J.J.; Haaksma, C.J.; Eddy, R.J.; Vaughan, M.B. Fibroblast Contraction Occurs on Release of Tension in Attached Collagen Lattices: Dependency on an Organized Actin Cytoskeleton and Serum. *Anat. Rec.* **1992**, *232*, 359–368. [CrossRef]

68. Sharma, R.; Barakzai, S.Z.; Taylor, S.E.; Donadeu, F.X. Epidermal-like Architecture Obtained from Equine Keratinocytes in Three-Dimensional Cultures. *J. Tissue Eng. Regen. Med.* **2016**, *10*, 627–636. [CrossRef]

69. Teifke, J.P.; Kidney, B.A.; Löhr, C.V.; Yager, J.A. Detection of Papillomavirus-DNA in Mesenchymal Tumour Cells and Not in the Hyperplastic Epithelium of Feline Sarcoids. *Vet. Dermatol.* **2003**, *14*, 47–56. [CrossRef] [PubMed]

70. DAVID Functional Annotation Bioinformatics Microarray Analysis. Available online: https://david.ncifcrf.gov/ (accessed on 21 January 2022).

71. Benjamini, Y.; Hochberg, Y. Controlling the False Discovery Rate: A Practical and Powerful Approach to Multiple Testing. *J. R. Stat. Soc. Ser. B Methodol.* **1995**, *57*, 289–300. [CrossRef]

72. Primer3 Input (Version 0.4.0). Available online: https://bioinfo.ut.ee/primer3-0.4.0/ (accessed on 21 January 2022).

73. Pfaffl, M.W.; Tichopad, A.; Prgomet, C.; Neuvians, T.P. Determination of Stable Housekeeping Genes, Differentially Regulated Target Genes and Sample Integrity: BestKeeper—Excel-Based Tool Using Pair-Wise Correlations. *Biotechnol. Lett.* **2004**, *26*, 509–515. [CrossRef]

74. Bogaert, L.; Van Poucke, M.; De Baere, C.; Peelman, L.; Gasthuys, F.; Martens, A. Selection of a Set of Reliable Reference Genes for Quantitative Real-Time PCR in Normal Equine Skin and in Equine Sarcoids. *BMC Biotechnol.* **2006**, *6*, 24. [CrossRef] [PubMed]

Article

Tracking the Molecular Scenarios for Tumorigenic Remodeling of Extracellular Matrix Based on Gene Expression Profiling in Equine Skin Neoplasia Models

Przemysław Podstawski [1,2,*], Katarzyna Ropka-Molik [1,*], Ewelina Semik-Gurgul [1], Marcin Samiec [3], Maria Skrzyszowska [3], Zenon Podstawski [2], Tomasz Szmatoła [1,4], Maciej Witkowski [5,6] and Klaudia Pawlina-Tyszko [1]

[1] Department of Animal Molecular Biology, National Research Institute of Animal Production, Krakowska 1 Street, Balice, 32-083 Kraków, Poland; ewelina.semik@iz.edu.pl (E.S.-G.); tomasz.szmatola@iz.edu.pl (T.S.); klaudia.pawlina@iz.edu.pl (K.P.-T.)

[2] Department of Animal Reproduction, Anatomy and Genomics, University of Agriculture in Kraków, Mickiewicza 24/28, 30-059 Kraków, Poland; zenon.podstawski@urk.edu.pl

[3] Department of Reproductive Biotechnology and Cryoconservation, National Research Institute of Animal Production, Krakowska 1 Street, Balice, 32-083 Kraków, Poland; marcin.samiec@iz.edu.pl (M.S.); maria.skrzyszowska@iz.edu.pl (M.S.)

[4] Center for Experimental and Innovative Medicine, University of Agriculture in Krakow, Rędzina 1c Street, 30-248 Kraków, Poland

[5] Institute of Veterinary Medicine, University Centre of Veterinary Medicine JU-AU, Mickiewicza 24/28, 30-059 Kraków, Poland; mawitkow@gmail.com

[6] Horse Clinic Służewiec, Puławska 266 Street, 02-684 Warsaw, Poland

[*] Correspondence: przemyslaw.podstawski@iz.edu.pl (P.P.); katarzyna.ropka@iz.edu.pl (K.R.-M.)

Abstract: An important component of tissues is the extracellular matrix (ECM), which not only forms a tissue scaffold, but also provides the environment for numerous biochemical reactions. Its composition is strictly regulated, and any irregularities can result in the development of many diseases, including cancer. Sarcoid is the most common skin cancer in equids. Its formation results from the presence of the genetic material of the bovine papillomavirus (BPV). In addition, it is assumed that sarcoid-dependent oncogenic transformation arises from a disturbed wound healing process, which may be due to the incorrect functioning of the ECM. Moreover, sarcoid is characterized by a failure to metastasize. Therefore, in this study we decided to investigate the differences in the expression profiles of genes related not only to ECM remodeling, but also to the cell adhesion pathway, in order to estimate the influence of disturbances within the ECM on the sarcoid formation process. Furthermore, we conducted comparative research not only between equine sarcoid tissue bioptates and healthy skin-derived explants, but also between dermal fibroblast cell lines transfected and non-transfected with a construct encoding the E4 protein of the BP virus, in order to determine its effect on ECM disorders. The obtained results strongly support the hypothesis that ECM-related genes are correlated with sarcoid formation. The deregulated expression of selected genes was shown in both equine sarcoid tissue bioptates and adult cutaneous fibroblast cell (ACFC) lines neoplastically transformed by nucleofection with gene constructs encoding BPV1-E1^E4 protein. The identified genes (*CD99*, *ITGB1*, *JAM3* and *CADM1*) were up- or down-regulated, which pinpointed the phenotypic differences from the backgrounds noticed for adequate expression profiles in other cancerous or noncancerous tumors as reported in the available literature data. Unravelling the molecular pathways of ECM remodeling and cell adhesion in the in vivo and ex vivo models of epidermal/dermal sarcoid-related cancerogenesis might provide powerful tools for further investigations of genetic and epigenetic biomarkers for both silencing and re-initiating the processes of sarcoid-dependent neoplasia. Recognizing those biomarkers might insightfully explain the relatively high capacity of sarcoid-descended cancerous cell derivatives to epigenomically reprogram their nonmalignant neoplastic status in domestic horse cloned embryos produced by somatic cell nuclear transfer (SCNT).

---

1. Introduction

The extracellular matrix (ECM) is an important component of every tissue, which apart from forming its scaffold, also provides an appropriate environment for a number of biochemical processes, thus enabling the maintenance of homeostasis of the organism [1,2]. Each tissue has its own ECM composition, but its basic components are water, proteins and polysaccharides [1]. These components enable the control of their behavior through their continuous interaction with cells in several processes, such as migration, adhesion, proliferation, differentiation, and survival [2,3]. In addition, the components of the ECM are tightly organized and constantly change as a result of biochemical processes within the ECM that must be carefully controlled. Any uncontrolled changes in the composition of these components may lead to disturbances in the functioning of the whole organism, thus leading to the development of disease [2,3]. In humans, these changes in the ECM are associated with many diseases, such as osteogenesis imperfecta, Marfan syndrome, coronary heart disease, hypertension, and asthma, as well as diseases of other systems (liver cirrhosis, inflammatory bowel diseases, chronic kidney diseases) [3]. Moreover, pathological changes in the composition of the ECM are considered to be one of the most important factors leading to cancer.

In equines, the most common skin tumor is the sarcoid. This neoplasia is characterized by a lack of metastatic capacity, although it may disturb the well-being of the affected animal through induced discomfort or soreness. Moreover, there is no single effective treatment for this tumor, and it has a high recurrence probability [4–7]. It has been shown that the presence of the sarcoid is associated with the presence of genetic material of bovine papillomavirus types 1 and 2 and, less frequently, 13 (*BPV-1, -2* or *-13*) [5,8,9]. This virus belongs to a species-specific family of viruses attacking skin cells, *Papillomaviridae*, and the sarcoid is the only documented case of infection of an organism other than its default host [10,11]. The genome of *BPV* consists of double-stranded DNA in which the late genes (*L1* and *L2*) and early genes (*E1–E7*) can be specified. Late genes are responsible for the production of capsid proteins, while early genes are related to replication, transcription control and encode individual viral proteins, including transforming proteins [12].

The exact mechanism responsible for the formation of the sarcoid is not fully understood. It has been shown that the mere presence of viral genetic material in skin cells is not sufficient to generate a sarcoid [9,13]. However, it has been observed that sarcoids are most often formed in places where the skin has been previously traumatized [8]. On this basis, it has been hypothesized that the sarcoid forms as a consequence of an incorrect wound healing process, which may result from disturbances in the proper ECM composition of the skin tissue due to the presence of viral DNA [14]. Therefore, in the present study, we decided to analyze selected genes related to the ECM rearrangements and affecting the process of cell adhesion, which is dependent on the alterations of ECM properties. The current investigation also broadens mechanistic insights into the molecular basis of the lack of metastatic capacity pinpointed for this neoplasia. To the best of our knowledge, thoroughly elucidating the genetic background of multifaceted etiopathogenesis of epidermal and dermal sarcoid-related neoplasia in both equine in vivo and ex vivo models has provided, for the first time, strong empirical evidence for profound alterations in the molecular phenotypes determining intracellular pathways of ECM remodeling and cell adhesion. This might be tremendously helpful for future studies that aim to extensively exploring the epigenetic mechanisms underlying either the suppression/repression or restoration/recapitulation of molecular traits positively correlated with the sarcoid-dependent tumorigenic transformation of skin-derived cells in domestic horses. Such a collection of further studies might be especially suitable for assessing the capabilities of

nuclear genomes inherited from neoplastic skin cell derivatives that can be epigenetically reprogrammed in equine somatic cell-cloned embryos and progeny. In turn, research focused on somatic cell nuclear transfer (SCNT)-based cloning might contribute to the development and optimization of the preclinical and clinical modalities of oncological treatments in domestic horses, as well as other equids afflicted with sarcoid-mediated cancerogenesis diagnosed within cutaneous and subcutaneous tissue compartments. For all the above-mentioned reasons, the present investigation sought to comprehensively compare the differences in gene expression patterns and their resultant impacts on the changes in ECM structure, not only between healthy skin tissue bioptates and the sarcoid tissue samples, but also between non-transfected dermal fibroblast cell lines and dermal fibroblast cell lines transfected with the gene encoding the BPV1-E1^E4 protein.

2. Results

2.1. Identified DEGs Belonged to ECM Remodeling and Cell Adhesion Pathways

The pathway enrichment analysis of set of differentially expressed genes (DEGs), which occurred between dermal fibroblast cell lines transfected with gene construct coding for the BPV1-E1^E4 protein and control (i.e., non-transfected) fibroblast cell lines, allowed for the identification of 30 DEGs (p-value < 0.05) that belong to ECM remodeling pathway (as indicated by the false discovery rate; FDR < 0.000012) and 27 that belong to cell adhesion pathway (FDR < 0.03). The same analysis performed for the comparison of the sarcoid tissue samples and healthy skin showed a significant involvement of 29 DEGs in ECM remodeling (FDR < 0.001) and 44 DEGs in cell adhesion (FDR < 0.0001) pathways (Figures 1–3).
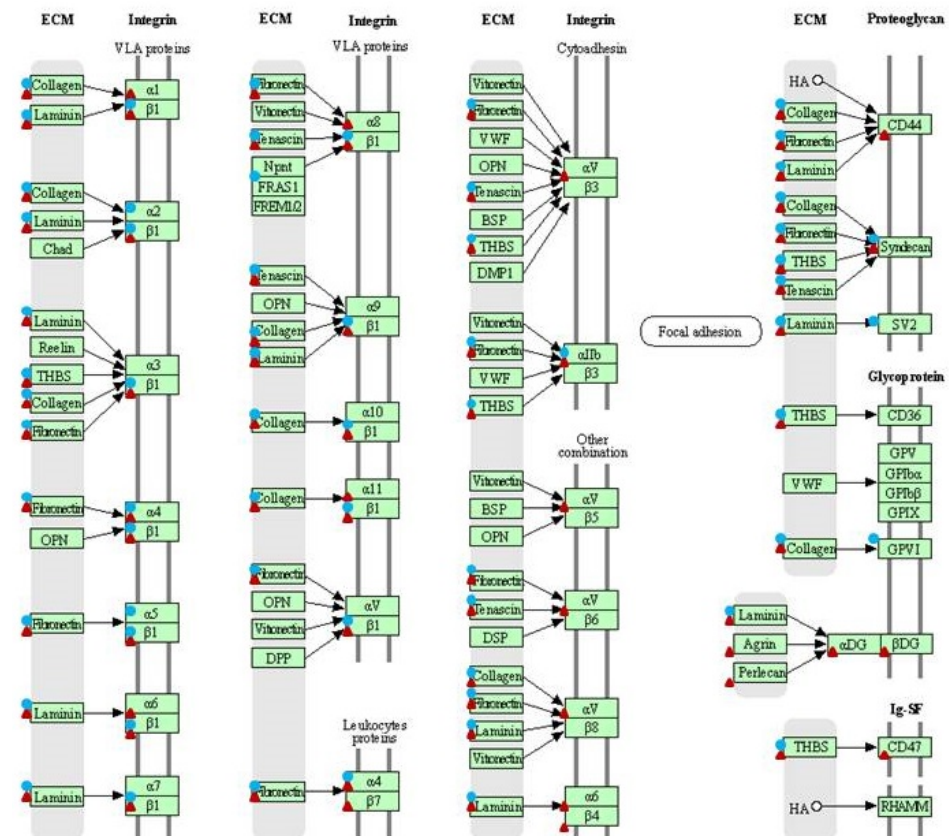

Figure 1. Differentially expressed genes (DEGs) related to ECM remodeling pathway (ecb04512). Circles—DEGs identified with the microarray analysis. Triangles—DEGs identified with the RNA-seq analysis (KEGG pathway database [15]).
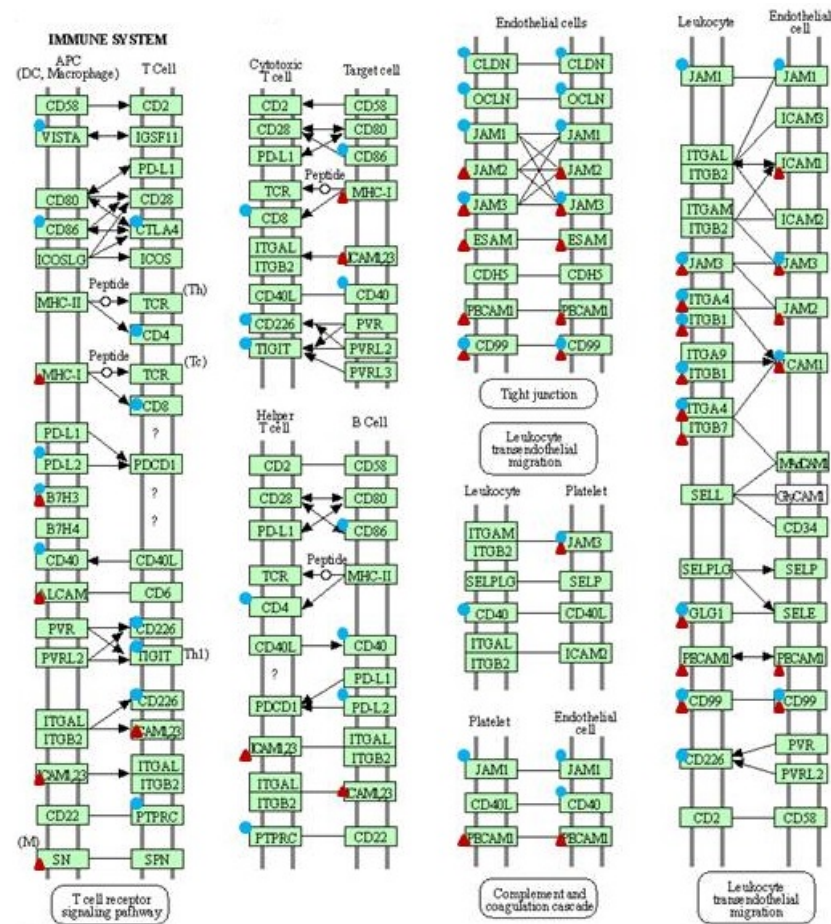
Figure 2. Differentially expressed genes (DEGs) related to cell adhesion pathway (ecb04514). Circles—DEGs identified with the microarray analysis. Triangles—DEGs identified with the RNA-seq analysis (KEGG pathway database [15]).

2.2. Selection of DEGs Potentially Involved in Sarcoids Occurrence

The most numerous DEGs detected within both pathways were genes coding collagens, integrins, laminins and claudins (Table 1). In order to identify deregulated genes common for both in vivo and in vitro comparisons, a Venn diagram was used (Figure 4). Four panels of genes were compared, and we observed DEGs that were unique to each analysis and common gene set, modified regardless of in vitro or in vivo approaches. Seven DEGs involved in the cell adhesion pathway (*CADM1*, *CD99*, *CNTNAP1*, *JAM3*, *MPZL1*, *SDC2*, *VCAM1*) were detected as significant, regardless of the analyzed model.

Similarly, six DEGs belonging to the ECM matrix remodeling pathway (*COL1A1*, *COL1A2*, *COL4A2*, *COL6A2*, *COL6A3*, *FN1*) were frequently identified in sarcoid tissue explants as compared to healthy skin samples, groups of dermal fibroblast cell lines transfected with *BPV1-E1^E4* gene constructs, and control (i.e., non-transfected) dermal fibroblast cell lines (Figure 4). Moreover, *ITGA6*, *ITGA8* and *ITGB7* genes were detected as significantly differentially expressed and belonged to the ECM matrix and cell adhesion pathways. Interestingly, three genes (*ITGA4, ITGB1* and *SDC1*), whose expressions were significantly modified in both pathways, were detected in both in vivo and in vitro models of sarcoid-related tumorigenesis.

Based on the aforementioned findings, nine DEGs (*CADM1*, *CD99*, *CNTNAP1*, *FN1*, *JAM3*, *MPZL1*, *SDC1*, *SDC2*, *VCAM1*) were selected for a further analysis using real-time PCR.
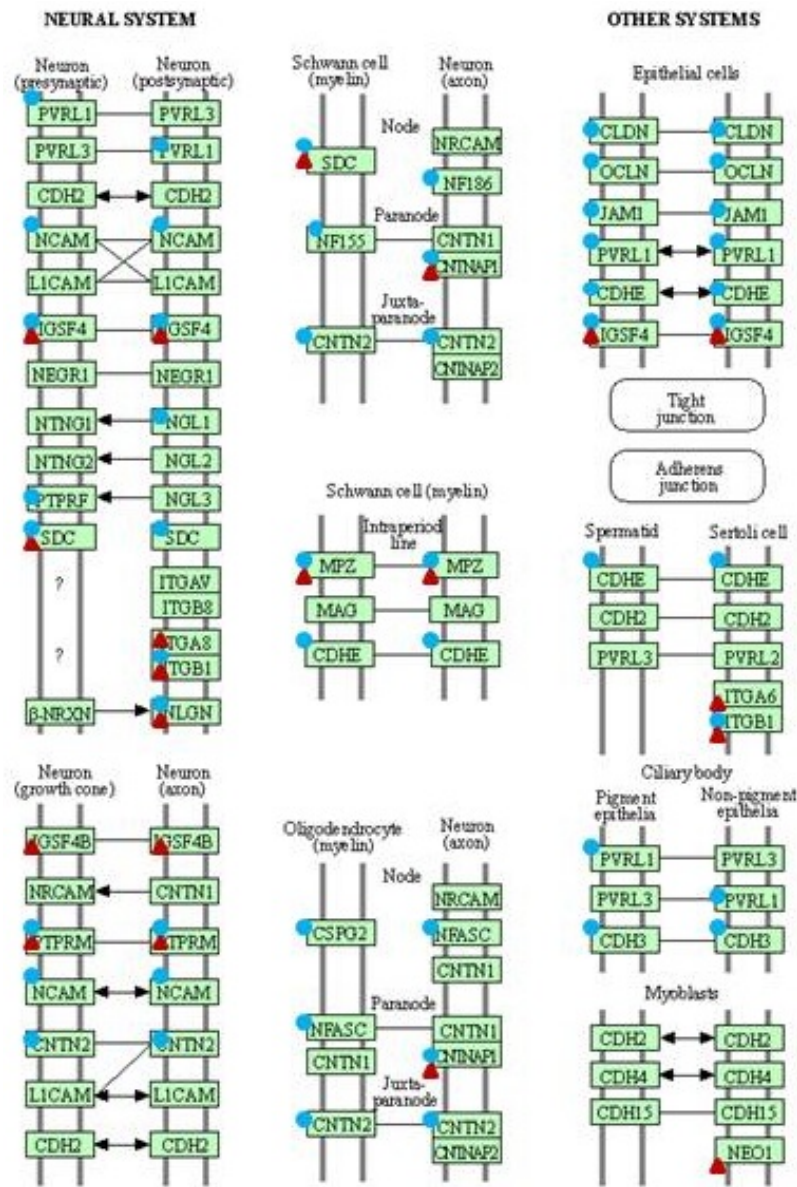
Figure 3. Differentially expressed genes (DEGs) related to cell adhesion pathway (ecb04514). Circles—DEGs identified with the microarray analysis. Triangles—DEGs identified with the RNA-seq analysis (KEGG pathway database [15]).

Table 1. Identified differentially expressed genes (DEGs) related to ECM remodeling and cell adhesion pathways.

	ECM Remodeling		Cell Adhesion	
	cell lines transfected with *BPV1-E1^E4* gene and control lines	sarcoid tissue and healthy skin	cell lines transfected with *BPV1-E1^E4* gene and control lines	sarcoid tissue and healthy skin
Collagens	*COL11A1; COL1A1; COL1A2; COL4A1; COL5A1; COL5A2; COL5A3; COL6A2; COL6A3; COL6A6*	*COL1A1; COL1A2; COL2A1; COL4A1; COL4A2; COL6A1; COL6A2; COL6A3; COL9A1; COL9A2; COL9A3*	-	-

Table 1. *Cont*.

	ECM Remodeling		Cell Adhesion	
Integrins	*ITGA1; ITGA11; ITGA4; ITGA6; ITGA8; ITGB1; ITGB7*	*ITGA2; ITGA2B; ITGA4; ITGA5; ITGB1*	*ITGA4; ITGA6; ITGA8; ITGB1; ITGB7*	*ITGA4; ITGB1*
Laminins	*LAMA3; LAMA4; LAMA5; LAMC3*	*LAMA2; LAMB1; LAMB3; LAMB4; LAMC1*	-	-
Claudins	-	-	-	*CLDN14; CLDN16; CLDN17; CLDN2; CLDN34; CLDN4; CLDN9*
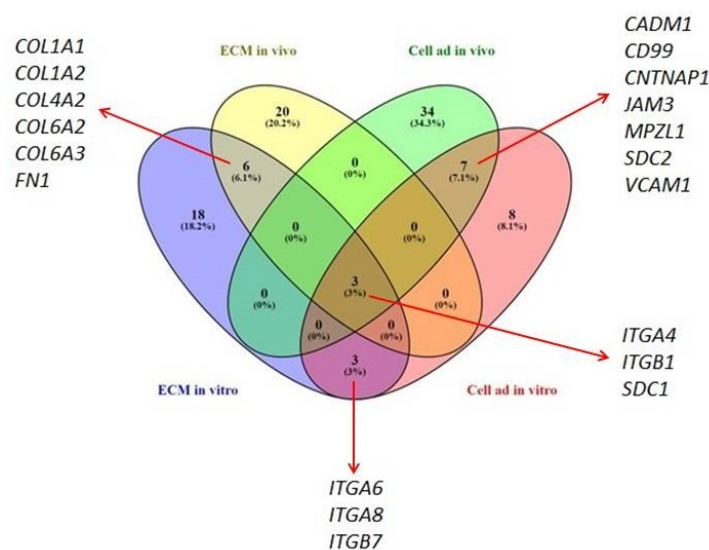
Figure 4. Venn diagram of common and unique differentially expressed genes (DEGs) following the comparisons of dermal fibroblast cell lines transfected with *BPV1-E1^E4* gene constructs and sarcoid tissue vs. control groups for ECM remodeling pathway (ECM in vitro and ECM in vivo, respectively); dermal fibroblast cell lines transfected with *BPV1-E1^E4* gene constructs and sarcoid tissue vs. their control groups for cell adhesion pathway (Cell ad in vitro and Cell ad in vivo, respectively) (Venny 2.1 BioinfoGP [16]).

2.3. Expression Patterns of Selected DEGs Evaluated Using qPCR

2.3.1. The Genes Up-Regulated in Sarcoids and *BPV1-E1^E4* Transgenic Dermal Fibroblast Cell Lines

The qPCR analysis confirmed a significant up-regulation of several genes in the sarcoid samples compared to healthy skin tissue. An increased expression level was observed for *CD99* (p-value < 0.0495); *FN1* (p-value < 0.0002); *ITGB1* (p-value < 0.0109); and *JAM3* (p-value < 0.0224). The greatest differences between the analyzed groups were detected for *FN1*, *CD99* and *JAM3* genes, as indicated by fold change (FC) at the levels of 7.43, 3.05 and 3.06, respectively (Figure 5).
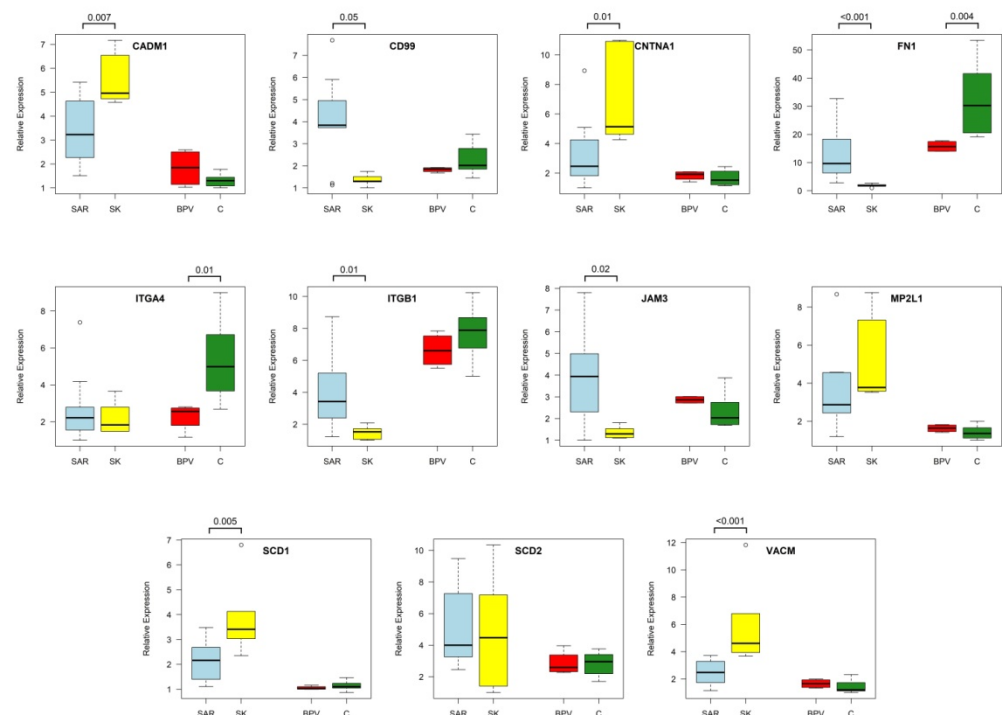
Figure 5. The differences in DEGs expression levels between analyzed groups of equine sarcoids (SAR), skin (SK) samples, control dermal fibroblast cell lines nucleofected with empty vectors (C), and dermal fibroblast cell lines nucleofected with *BPV-E4ˆE1* transgene (BPV) (R software v4.1 [17]).

2.3.2. The Genes Down-Regulated in Sarcoids and *BPV1-E1ˆE4* Transgenic Dermal Fibroblast Cell Lines

Four genes—*CADM1*; *CNTNAP1*; *SCD1*; and *VCAM1*—were significantly down-regulated in sarcoid tumors (Figure 5). The lowest transcript level in sarcoids compared to healthy tissue was identified for *VCAM1* (p-value < 0.0010; FC −2.41) and *CNTNA1* (p-value < 0.0109; FC −2.10). For the two other genes, FC values were as follows: −1.83 for *SDC1* and −1.64 for *CADM1*.

For the *FN1* gene, a significant down-regulation of the expression level was detected in *BPV1-E1ˆE4* transgenic cell lines compared to control cell lines (p-value < 0.0040). The obtained difference was a −2.04-fold change. Similarly, the expression level in control cell lines was significantly higher for the *ITGA4* gene as compared to *BPV1-E1ˆE4* transgenic cells (p-value < 0.0161).

2.4. The Functional Enrichment Analysis of the Obtained Network

The gene ontology (GO) analysis of genes that showed differential expressions confirmed their involvement in the anchoring junction (FDR < 0.0001), integrin complex (FDR < 0.0001) and protein complex involved in cell adhesion (FDR < 0.0001), as well as the paranodal junction (FDR < 0.0016), cell–cell junction (FDR < 0.0089) and integrin binding (FDR < 0.0360) (Figure 6). Among the genes involved in the most numerous GO terms were those identified as up-regulated (*JAM3* and *ITGB1*) and those identified as down-regulated (*CNTNAP1*), while *FN1* and *ITGB1* exhibited the highest number of interactions between genes. The analysis of the closest connections with other genes involved in the processes and not included in our analyzes indicated that *CD63*, *CD9*, *ITGA8* and *FLNA* genes can be candidate genes related to the ECM remodeling and cell adhesion during sarcoid growth and development. The *ITGA4* gene was also identified as strongly related to the majority of GO terms, but its differential expression was confirmed only in the in vitro model.
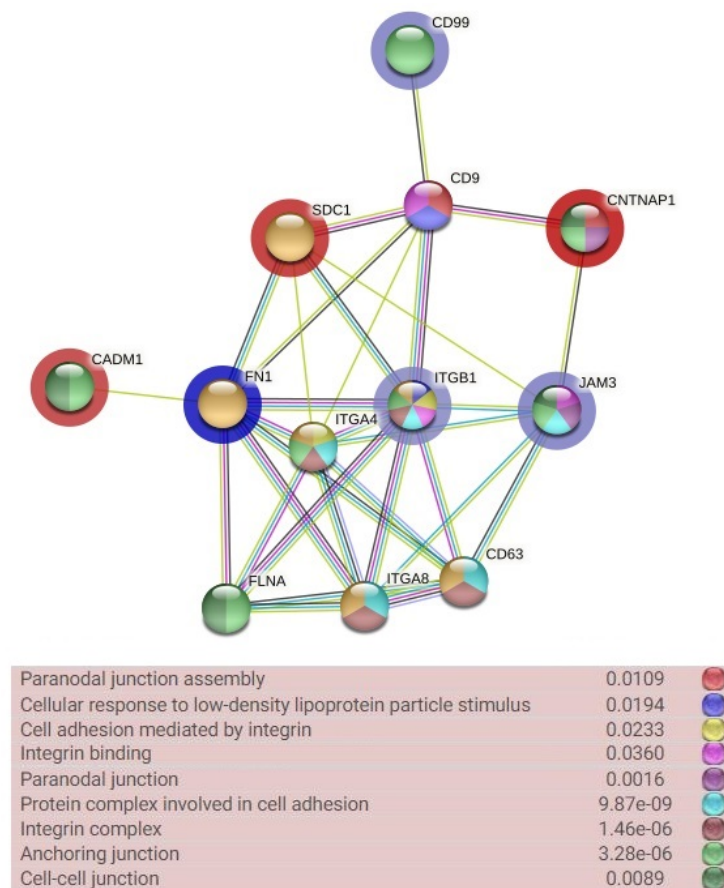
Paranodal junction assembly	0.0109	🔴
Cellular response to low-density lipoprotein particle stimulus	0.0194	🔵
Cell adhesion mediated by integrin	0.0233	🟡
Integrin binding	0.0360	🟣
Paranodal junction	0.0016	🟣
Protein complex involved in cell adhesion	9.87e-09	🔵
Integrin complex	1.46e-06	🔴
Anchoring junction	3.28e-06	🟢
Cell-cell junction	0.0089	🟢

Figure 6. The gene ontology (GO) terms and interactions between set of chosen differentially expressed genes (DEGs) and their closest connected genes (String software [18] *Equus caballus* reference). The GO terms are marked in color, as shown in the figure legend (GOs are presented with their corresponding false discovery rates; FDRs). The blue and red areolas show fold change (blue—up-regulation; red—down-regulation).

3. Discussion

ECM and cell adhesion molecules remodeling are considered as essential factors that lead to the formation, growth, and development of cancer cells. Therefore, both molecular pathways/extracellular matrix remodeling and cell adhesion were the subjects of our interest in equine sarcoid occurrence. High-throughput NGS data allowed us to narrow the searching area of candidate genes associated with molecular remodeling in horse skin cells leading to sarcoid formation. Among all identified DEGs, selected genes were either involved in both investigated pathways or belonged to one pathway. Nonetheless, they were detected not only in sarcoid tissue bioptates, but also in the ex vivo-expanded dermal fibroblast cells transfected with *BPV1-E4ˆE1* gene construct.

The detected genes with the greatest changes in expression levels were *FN1* (Fibronectin 1); *CD99* (Cluster of differentiation 99) and *JAM3* (Junctional Adhesion Molecule 3), which were all significantly up-regulated in sarcoid tissue compared to healthy skin. Fibronectin is a multifunctional extracellular matrix (ECM) glycoprotein that plays a key role in tissue repair via involvement in early and the late wound-healing responses [19]. Fibronectin, as a part of the extracellular matrix, binds a broad spectrum of other ECM proteins, including collagens, laminins, fibrinogen and fibrillins, syndecans and tenascin [20]. Thus, fibronectin regulates the composition of the extracellular matrix as well as attaching to other ECM molecules [21]. Moreover, the fibronectin matrix separates selected growth factors and related proteins, e.g., BMP1, VEGF and LTBP in order to control the cell signaling [22]. On the one hand, due to such a broad spectrum of molecular dependencies,

fibronectin plays a critical role in cell growth, adhesion, migration and differentiation. On the other hand, the disruptions of the structure or function of fibronectin can lead to remarkable changes in ECM organization and result in a number of disorders in organisms, including cancer [23]. The increased expression of *FN1* gene has been reported in many types of cancer, including gastric [24], breast [25], thyroid [26], renal [27] and ovarian [28] cancers. Furthermore, in many cases, the up-regulation of *FN1* indicates a poor prognosis for patients [24,26,28]. The elevated expression level of fibronectin 1 is strongly related to modifications of extracellular space, and it contributes and promotes the spread, migration, proliferation and differentiation of cells [29]. It has been confirmed that the over-expression of the *FN1* gene inhibited apoptosis processes and promoted cell migration by regulating the NF-κB pathway [30]. During tumorigenesis, cell migration is activated by the increased expression of *FN1*, which up-regulates both *MMP9* and *MMP2* genes [30]. In the present report, more than a 7-fold increase in *FN1* gene expression in the sarcoid tissue compared to healthy skin was observed. Such high differences can indicate that ECM remodeling occurs, as in both human cancers and equine sarcoids. Interestingly, the previous study performed on sarcoids confirmed the significant over-expression of both *MMP2* and *MMP9* genes in the tumor tissue and in cell lines transfected with *BPV-1* gene construct [31]. These findings strengthen the hypothesis that one of the main mechanisms responsible for sarcoid formation can be the *FN1*–matrix metalloproteinase axis. The increased transcript level of *FN1* and both *MMP9* and *MMP2* genes can be considered as biological markers of sarcoid formation.

The up-regulation of the expression level of *CD99* gene, which encodes cell surface glycoprotein belonging to ECM matrix and is responsible for cell–cell adhesion, was also observed in sarcoids. CD99 protein is responsible for cell migration, differentiation and apoptosis [32], but its exact function is not fully understood. In some cancers, the over-expression of *CD99* increases migration and invasion [33], while in most cases, *CD99* up-regulation enhances cell–cell adhesion and apoptosis inhibiting tumor cell migration and metastasis [34]. The second mechanism of *CD99* regulation may occur during sarcoid development, which may explain its non-metastasizing nature.

In turn, the JAM3 protein, which regulates cells adhesion and communication between cells and ECM [35], is up-regulated in variety of cancers [36,37]. The over-expression of *JAM3* promotes migration and suppresses apoptosis. The study performed on renal cell carcinoma showed that the *JAM3* gene is critical for its tumor migration ability via the regulation of genes coding for N-cadherin, integrin β1 (ITGB1) and MMP2 [36]. The presented study confirmed the sarcoid-specific increase in the expression of not only the *JAM3* gene, but also the *ITGB1* gene, whose expression is considered to be a poor outcome marker during cancer prognosis [38]. It is contrary to the nature of sarcoids, which is a non-metastasizing tumor. However, the expression patterns pinpointed for *ITGB1* and *JAM3* genes may suggest that, although these genes are over-expressed, their overall expression level may be not high enough to affect sarcoid tissue or their effect may be altered by co-expression patterns of another genes.

It is noteworthy that the *VCAM1* gene experienced the greatest down-regulation in sarcoid tissue as compared to the healthy skin control group. This gene encodes vascular cell adhesion molecule-1, whose expression is specific for epithelial cells, but under such conditions as high level inflammation or chronic diseases, its expression is also found on the surfaces of other cell types, including cancer cells [39,40]. The VCAM1 protein plays an important role in the recruitment of leukocytes and their migration to various tissues, which has numerous applications in chronic inflammation and cancerous tumorigenesis [39]. Various studies indicate a strong association of the *VCAM-1* gene with the tumor development process, where it plays a key role in angiogenesis and supports metastasis [39,40]. Its influence on metastasis has been observed in numerous neoplasms. An example is the positive correlation identified in the up-regulation of the *VCAM-1* gene with breast cancer metastases in lungs. In epithelium ovarian cancer patients, the high expression of this gene was associated with a low chance of survival. This situation is similar in the case

of colorectal cancer, where the over-expression of the *VCAM-1* gene is associated with metastasis and progression of this cancer [40]. Moreover, the over-expression of this gene has been also observed in other malignant neoplasms, such as gastric cancer, melanoma and lung cancer [39]. These data strongly facilitate the justification of our findings, revealing that the low expression profiles identified for the *VCAM-1* gene in sarcoid tissue samples are responsible for the failure of this non-malignant (benign) neoplasm to metastasize. This can be explained by the lack of activation of transcription of this important biomarker of the carcinogenesis process.

The second-most down-regulated gene is the *CNTNAP1* gene encoding the contyactin-associated protein 1 (caspr-1). This protein is an important component of paranodal junctions, and its mutations are mainly associated with neuropathies [41]. However, there are reports that this gene is related to clear-cell renal carcinoma. In this tumor, the expression of the *CNTNAP1* gene was positively associated with cancer-associated fibroblasts [42]. The detection of the deregulated expression of this gene in sarcoid tissue samples, as compared to healthy skin-derived explants, may provide the empirical evidence and mechanistic insights that, despite its mainly neurological connections, the *CNTNAP1* gene may be a valuable source of information on the molecular basis of sarcoid formation. However, the lack of more detailed studies of this gene in the context of tumors do not allow such broad conclusions to be drawn.

The *SCD1* gene that encodes the enzymatic protein designated as stearoyl CoA desaturase 1 is proven to be associated with the lipid metabolism of the cell by biocatalyzing the synthesis of monosaturated fatty acids (MUFAs) from precursors that are saturated fatty acids (SFAs) [43]. This contributes to the synthesis of the basic components of biological membranes, and signaling molecules and provides a source of energy needed for the functioning of the cell [43]. Research also shows that the *SCD1* gene is related to the positive regulation of autophagy. This gene also plays an important role in the development of various cancers. The deregulated expression of the *SCD1* gene is associated with many human neoplasms, which indicates its important role in the process of carcinogenesis [44]. It has been shown that its overexpression is related to the proliferation of neoplastic cells and metastasis. Furthermore, the positive regulation of the autophagy process does not occur in all types of neoplasms [43]. For example, the transcriptional repression of the *SCD1* gene in human hepatocellular carcinoma (HCC) cells was brought about the activation of the apoptosis processes induced by autophagy [43], and this increased the expression of *SCD1* gene in these cells, leading to a worse prognosis for patients. The differentiation of influences on the process of autophagy is explained by the heterogeneous structure of the neoplastic tissue [43]. The involvement of this gene in lipid metabolism is largely associated with the process of carcinogenesis. The participation of *SCD1* gene in the synthesis of MUFAs suggests that it has a function supporting the proliferation of cancer cells by supplying them with the energy and building components that they need. Research that was conducted on human breast cancer and murine Lewis lung carcinoma confirmed that the silencing the transcriptional activity of *SCD1* gene was related to a reduction in tumor cell proliferation [45]. The inhibition of the MUFAs synthesis process and the resulting reduction in cell proliferation may explain why sarcoids do not exhibit metastasis.

The last gene observed to have a decreased expression in sarcoid tissues relative to the control was *CADM1*. The low expression of this gene was detected in many neoplasms, with the exception of hematological tumors, in which the overexpression of this gene was observed [46,47]. It is assumed that the reduction in the expression of this gene takes place through the methylation of its promoter [46]. On this basis, it can be concluded that a similar mechanism occurs in skin cells infected with *BPV*. It was shown that the low level of expression of this gene is associated with the development of neoplasms, and can function as an indicator of poor prognosis in patients suffering from numerous neoplasms, such as those of the respiratory system, hepatocellular cancer, glioblastoma and neuroblastoma [46,48]. Moreover, it is noteworthy that, as a result of expediting/intensifying the onset and progression of proapoptotic pathways, the overexpression of the *CADM1*

gene was found to inhibit migration and metastasis in gastric cancer, colon, prostate, and ovarian cancers, as well as different skin cancers, such as malignant melanoma or cutaneous squamous cell carcinoma [46–48]. Therefore, it can be concluded that, in the process of sarcoid formation, which is characterized by a low metastasis, the level of deregulation of this gene is not high enough to lead to the migration of its cells into the body.

The last analyzed gene was integrin α4β1 (*ITGA4*), which was found to be down-regulated in dermal fibroblast cell lines oncogenically transformed via nucleofection with the *BPV1-E1ˆE4* gene construct. Its over-expression is correlated with increased metastasis in ovarian and colon cancers. Furthermore, the abundant expression of the *ITGA4* gene has been found in melanoma cells characterized by its high capabilities to metastasize. Additionally, the transcriptional suppression noticed for this gene can lead to the inhibition of metastasis [49]. Low quantitative profiles estimated in the expression of the *ITGA4* gene in *BPV1-E1ˆE4* transgenic dermal fibroblast cells support these data and could be one of the reasons for the lack of metastasis in sarcoid tissue.

To sum up, in the present study, we analyzed a panel of genes that were responsible for ECM remodeling and cell adhesion pathways. Our findings strongly support the hypothesis that ECM-related genes are correlated with sarcoid formation. The deregulated expression of selected genes was found in both equine sarcoid tissue bioptates and adult cutaneous fibroblast cell (ACFC) lines, neoplastically transformed by nucleofection with a gene construct encoding the BPV1-E1ˆE4 protein. These genes were up- and down-regulated and, in some cases (*CD99*, *ITGB1*, *JAM3* and *CADM1*), the pinpointed phenotypic background differed from the backgrounds noticed for similar expression patterns in other cancerous (malignant) or noncancerous (benign) neoplasms, as indicated according to the available literature data.

4. Materials and Methods

4.1. The Use of High-Throughput Data to Establish Genes Involved in ECM Remodeling and Cell Adhesion Pathways

To establish DEGs involved in ECM remodeling and cell adhesion pathways, two sets of data obtained from our previous investigations were used (GSE193906 and GSE83430) [31,50]. The raw data annotated as GSE193906 were generated via NGS sequencing of two groups encompassing ACFC lines transfected with the *BPV1-E1ˆE4* gene construct and control (i.e., non-transfected) ACFC lines. The raw reads were mapped to the reference genome (EquCab3; assembly 102 Ensembl) using STAR software v2.7.8. The inter-group comparative analysis of identified DEGs was accomplished with the aid of Deseq2 software v3.14. According to this statistical software, the levels of significant differences occurring between experimental groups were adjusted to p-values < 0.05 after multiple testing corrections.

In order to obtain full insights into the transcriptomic modifications that can take place during sarcoid formation, a second set of data was used: GSE83430 [50]. The data denoted as significantly different (p-value < 0.05) were analyzed in a way similar to the previous work [50]; however, without a final filtering of genes by fold change (FC). Specifically, quality control was performed by normalizing the signal strength distribution followed by a correlation analysis and principal component analysis with the aid of the GeneSpring GX software, version 14.9 (Agilent Technologies, Santa Clara, CA, USA). The presence of inter-group significant diversity in the expression of genes between each pair of sarcoid bioptates and control skin tissue explants was confirmed by both Student's t-test and FC estimation, which enables DEGs to be identified. Subsequently, the Benjamini–Hochberg procedure was used to calculate the adjusted p-values (false discovery rates; FDRs). The criteria of statistical significance were p-value < 0.05 and FC > 1.

The occurrence of significant variability between identified DEGs (at the levels of p-value < 0.05), which was proven for both comparisons (sarcoid bioptates vs. healthy skin explants and ACFC lines transfected with gene construct coding for BPV1-E1ˆE4 protein vs. control ACFC lines), was also thoroughly evaluated depending on the commitment of DEGs to and their over-representation in either ECM remodeling or cell adhesion pathways. This

statistical evaluation of inter-group variability (at the levels of FDR < 0.05) was achieved by using David software (version 6.8) [51] based on the *Equus caballus* reference and KEGG database (Fisher's exact test with Benjamini correction) [15]. String software v11.5 [18] with the *Equus caballus* reference was applied to identify protein interactions.

4.2. Collection of Tissue Samples

Skin tissue samples were collected post mortem from horses (near eye region) in a slaughter facility (n = 8). Tissue bioptates were collected in tubes filled with either RNAlater solution (Ambion; Thermo Scientific, Waltham, MA, USA) (for the purposes of RNA isolation) or cell culture medium comprised of Dulbecco's Modified Eagle's Medium (DMEM; Gibco, Thermo Scientific, Waltham, MA, USA) supplemented with 10% fetal bovine serum (FBS; Gibco, Thermo Scientific, Waltham, MA, USA) (for the purposes of establishing the primary cultures and resultant ACFC lines). Sarcoid tissues (n = 10) were collected during standard veterinary removal procedures. All procedures were approved by Polish law (The Polish Act on the Protection of Animals Used for Scientific or Educational Purposes of 15 January 2015, which implements Directive 2010/63/EU of the European Parliament on the protection of animals used for scientific purposes), and further approval by the Animal Ethics Committee was not mandatory.

4.3. Establishment of Primary Cultures and Nucleofection of Equine ACFCs

The procedures encompassing the ex vivo establishment and nucleofection of ACFC lines were comprehensively described in the study by Podstawski et al. [52]. Briefly, the primary cultures of horse skin-derived fibroblast cells followed by mitotically stable ACFC lines were established in compliance with the method developed and optimized by Tomasek et al. [53]. According to this method, the small pieces of dermal tissue explants were placed at the bottom of the culture dish filled with DMEM (Gibco, Thermo Scientific, Waltham, MA, USA) enriched with 10% FBS (Gibco, Thermo Scientific, Waltham, MA, USA) and incubated until the fibroblast cells outgrew the skin bioptates, started to spontaneously and vigorously migrate, and formed cell colonies at the bottom of the culture dish. Subsequently, the fibroblast cell lines were cultured under the conditions of 37 °C, 5% CO_2 and 100% humidity until they reached 90% confluence followed by several passages leading to cell population doublings.

As thoroughly specified in our previous investigation [52], immediately after ACFC lines had reached 90% confluence, they were trypsinized, centrifuged in Tissue Culture Medium 199 (TCM 199; Sigma-Aldrich, Merck Life Sciences, Poznań, Poland), supplemented with 5% FBS (Gibco, Thermo Scientific, Waltham, MA, USA) and then subjected to in vitro transgenization by nucleofection using the T-REx system (Invitrogen, Thermo Scientific, Waltham, MA, USA) and *BPV1-E1^E4* gene construct. The cell transfection was performed with the aid of the Amaxa Nucleofector™ II Device (Amaxa Biosystems, Lonza, Medianus, Kraków, Poland) and by using a dedicated reagent kit as follows: Amaxa™ Normal Human Dermal Fibroblast-Adult (NHDF-Adult) and Nucleofector™ Kit (Lonza, CELLLAB, Warsaw, Poland). Positive selection of transgenic (i.e., efficiently nucleofected) ACFC lines was achieved by 7-day verification of their resistance to a cocktail of antibiotics composed of 200 µg/mL zeocin (Invitrogen, Thermo Scientific, Waltham, MA, USA) and 6 µg/mL blasticidin S (Thermo Scientific, Waltham, MA, USA). The cell nucleofectants that survived the zeocin/blasticidin S-dependent selection were classified as transgenic and used for further procedures.

4.4. Gene Expression Measurements Using Real-Time PCR Approach

RNA was isolated (skin samples n = 8; sarcoids n = 10) with the PureLink™ RNA mini kit (Invitrogen, Thermo Scientific, Waltham, MA, USA) using an additional DNase treatment on the columns (PureLink™ DNase Set; Invitrogen, Thermo Scientific, Waltham, MA, USA). The quality and quantity of the obtained genetic material were validated by electrophoretic separation (2% agarose gel) and with the Nanodrop 2000 spectrophotometer

(Thermo Scientific, Waltham, MA, USA). The RIN values were estimated using TapeStation 200 (Agilent Technologies, Santa Clara, CA, USA) and scores for RINs ranged from 8.5 to 9.5. Next, 300 ng of total RNA was used to synthesize cDNA using the High-Capacity RNA-to-cDNA™ Kit (Applied Biosystems, Thermo Fisher Scientific, Waltham, MA, USA). Then, a real-time PCR reaction was performed. Each reaction was carried out in triplicate. The reactions were performed on the QuantStudio7Flex platform (Applied Biosystems, Thermo Fisher Scientific, Waltham, MA, USA), and the Sensitive RT HS-PCR EvaGreen Mix kit (A&A Biotechnology, Gdynia, Poland) was used according to the manufacturer's protocol. Two genes were used as endogenous controls: β-actin (*ACTB*) and ubiquitin B (*UBB*) [54]. The obtained results were calculated by the ΔΔCT method [55]. The real-time PCR primer sequences that were used are presented in Supplementary Table S1.

5. Conclusions and Future Goals

For further investigations, a comprehensive deciphering of the molecular scenarios that are responsible for the onset and progression of ECM remodeling and cell adhesion, in both in vivo and in vitro research models of sarcoid-dependent tumorigenic transformation, might be a useful tool. These investigations might create the biological foundations to identify a desirable source of highly reprogrammable and dedifferentiable neoplastic derivatives of dermal tissue cells. These skin-derived sarcoid cells might provide donor cell nuclei, which display a strong capability to epigenomically reprogram their transcriptomic signatures in equine embryos generated by somatic cell cloning. The production of such cloned horse embryos, which are able to develop into conceptuses and progeny, might be a powerful strategy for designing in vivo and ex vivo biomedical models. These models can be used for the preclinical and clinical exploration of genetic and epigenetic mechanisms, which underly the processes of either remission or resumption of procancerous tumorigenesis of cutaneous and subcutaneous tissue compartments into sarcoids.

Conflicts of Interest: The authors declare no conflict of interest. The funders had no role in the design of the study; in the collection, analyses, or interpretation of data; in the writing of the manuscript, or in the decision to publish the results.

Abbreviations

ACFC	Adult cutaneous fibroblast cell
BMP	Bone morphogenetic protein
BPV	Bovine papillomavirus
CADM1	Cell adhesion molecule
CD99	Cluster of differentiation 99 surface antigen
CLDN	Claudin
CNTNAP	Contactin-associated protein
CoA	Coenzyme A
COL	Collagen
DEG	Differentially expressed gene
ECM	Extracellular matrix
FC	Fold change
FDR	False discovery rate
FLNA	Filamin A
FN1	Fibronectin
GO	Gene ontology
HCC	Human hepatocellular cancer
ITGA	Integrin subunit α
ITGB	Integrin subunit β
JAM	Junctional adhesion molecule
KEGG	Kyoto Encyclopedia of Genes and Genomes
LAMA	Laminin subunit α
LTBP	Latent transforming growth factor-β-binding protein
MMP	Matrix metalloproteinase
MPZL1	Myelin protein zero-like protein 1
MUFA	Monosaturated fatty acid
NF-κB	Nuclear factor κ-light-chain-enhancer of activated B cells
NGS	Next-generation sequencing
PCR	Polymerase chain reaction
qPCR	Quantitative polymerase chain reaction
SCNT	Somatic cell nuclear transfer
SDC	Syndecan
SFA	Saturated fatty acid
VCAM	Vascular cell adhesion molecule
VEGF	Vascular endothelial growth factor

References

1. Frantz, C.; Stewart, K.M.; Weaver, V.M. The Extracellular Matrix at a Glance. *J. Cell Sci.* **2010**, *123*, 4195–4200. [CrossRef] [PubMed]
2. Bonnans, C.; Chou, J.; Werb, Z. Remodelling the Extracellular Matrix in Development and Disease. *Nat. Rev. Mol. Cell Biol.* **2014**, *15*, 786–801. [CrossRef] [PubMed]
3. Järveläinen, H.; Sainio, A.; Koulu, M.; Wight, T.N.; Penttinen, R. Extracellular Matrix Molecules: Potential Targets in Pharmacotherapy. *Pharmacol. Rev.* **2009**, *61*, 198–223. [CrossRef] [PubMed]
4. Knottenbelt, D.C. A Suggested Clinical Classification for the Equine Sarcoid. *Clin. Tech. Equine Pract.* **2005**, *4*, 278–295. [CrossRef]
5. Yuan, Z.; Gallagher, A.; Gault, E.A.; Campo, M.S.; Nasir, L. Bovine Papillomavirus Infection in Equine Sarcoids and in Bovine Bladder Cancers. *Vet. J.* **2007**, *174*, 599–604. [CrossRef]
6. Haralambus, R.; Burgstaller, J.; Klukowska-Rötzler, J.; Steinborn, R.; Buchinger, S.; Gerber, V.; Brandt, S. Intralesional Bovine Papillomavirus DNA Loads Reflect Severity of Equine Sarcoid Disease. *Equine Vet. J.* **2010**, *42*, 327–331. [CrossRef]
7. Taylor, S.D.; Toth, B.; Baseler, L.J.; Charney, V.A.; Miller, M.A. Lack of Correlation Between Papillomaviral DNA in Surgical Margins and Recurrence of Equine Sarcoids. *J. Equine Vet. Sci.* **2014**, *34*, 722–725. [CrossRef]
8. Nasir, L.; Reid, S.W.J. Bovine Papillomaviral Gene Expression in Equine Sarcoid Tumours. *Virus Res.* **1999**, *61*, 171–175. [CrossRef]

9. Bogaert, L.; Martens, A.; Van Poucke, M.; Ducatelle, R.; De Cock, H.; Dewulf, J.; De Baere, C.; Peelman, L.; Gasthuys, F. High Prevalence of Bovine Papillomaviral DNA in the Normal Skin of Equine Sarcoid-Affected and Healthy Horses. *Vet. Microbiol.* **2008**, *129*, 58–68. [CrossRef]

10. Yuan, Z.Q.; Gault, E.A.; Gobeil, P.; Nixon, C.; Campo, M.S.; Nasir, L. Establishment and Characterization of Equine Fibroblast Cell Lines Transformed in Vivo and in Vitro by BPV-1: Model Systems for Equine Sarcoids. *Virology* **2008**, *373*, 352–361. [CrossRef]

11. Bogaert, L.; Martens, A.; Kast, W.M.; Van Marck, E.; De Cock, H. Bovine Papillomavirus DNA Can Be Detected in Keratinocytes of Equine Sarcoid Tumors. *Vet. Microbiol.* **2010**, *146*, 269–275. [CrossRef] [PubMed]

12. Rector, A.; Van Ranst, M. Animal Papillomaviruses. *Virology* **2013**, *445*, 213–223. [CrossRef]

13. Bogaert, L.; Martens, A.; De Baere, C.; Gasthuys, F. Detection of Bovine Papillomavirus DNA on the Normal Skin and in the Habitual Surroundings of Horses with and without Equine Sarcoids. *Res. Vet. Sci.* **2005**, *79*, 253–258. [CrossRef] [PubMed]

14. Martano, M.; Corteggio, A.; Restucci, B.; De Biase, M.E.; Borzacchiello, G.; Maiolino, P. Extracellular Matrix Remodeling in Equine Sarcoid: An Immunohistochemical and Molecular Study. *BMC Vet. Res.* **2016**, *12*, 24. [CrossRef] [PubMed]

15. KEGG PATHWAY Database. Available online: https://www.genome.jp/kegg/pathway.html (accessed on 16 May 2022).

16. Venny 2.1.0. Available online: https://bioinfogp.cnb.csic.es/tools/venny/ (accessed on 16 May 2022).

17. R: The R Project for Statistical Computing. Available online: https://www.r-project.org/ (accessed on 18 May 2022).

18. STRING: Functional Protein Association Networks. Available online: https://string-db.org/ (accessed on 18 May 2022).

19. To, W.S.; Midwood, K.S. Plasma and Cellular Fibronectin: Distinct and Independent Functions during Tissue Repair. *Fibrogenesis Tissue Repair* **2011**, *4*, 21. [CrossRef]

20. Pereira, M.; Rybarczyk, B.J.; Odrljin, T.M.; Hocking, D.C.; Sottile, J.; Simpson-Haidaris, P.J. The Incorporation of Fibrinogen into Extracellular Matrix Is Dependent on Active Assembly of a Fibronectin Matrix. *J. Cell Sci.* **2002**, *115*, 609–617. [CrossRef]

21. Sottile, J.; Hocking, D.C. Fibronectin Polymerization Regulates the Composition and Stability of Extracellular Matrix Fibrils and Cell-Matrix Adhesions. *Mol. Biol. Cell* **2002**, *13*, 3546–3559. [CrossRef]

22. Dallas, S.L.; Sivakumar, P.; Jones, C.J.P.; Chen, Q.; Peters, D.M.; Mosher, D.F.; Humphries, M.J.; Kielty, C.M. Fibronectin Regulates Latent Transforming Growth Factor-β (TGFβ) by Controlling Matrix Assembly of Latent TGFβ-Binding Protein-1. *J. Biol. Chem.* **2005**, *280*, 18871–18880. [CrossRef]

23. Lin, T.-C.; Yang, C.-H.; Cheng, L.-H.; Chang, W.-T.; Lin, Y.-R.; Cheng, H.-C. Fibronectin in Cancer: Friend or Foe. *Cells* **2019**, *9*, 27. [CrossRef]

24. Sun, Y.; Zhao, C.; Ye, Y.; Wang, Z.; He, Y.; Li, Y.; Mao, H. High Expression of Fibronectin 1 Indicates Poor Prognosis in Gastric Cancer. *Oncol. Lett.* **2020**, *19*, 93–102. [CrossRef]

25. Nam, J.-M.; Onodera, Y.; Bissell, M.J.; Park, C.C. Breast Cancer Cells in Three-Dimensional Culture Display an Enhanced Radioresponse after Coordinate Targeting of Integrin Alpha5beta1 and Fibronectin. *Cancer Res.* **2010**, *70*, 5238–5248. [CrossRef] [PubMed]

26. Geng, Q.S.; Huang, T.; Li, L.F.; Shen, Z.B.; Xue, W.H.; Zhao, J. Over-Expression and Prognostic Significance of FN1, Correlating With Immune Infiltrates in Thyroid Cancer. *Front. Med.* **2022**, *8*, 812278. [CrossRef] [PubMed]

27. Dong, Y.; Ma, W.; Yang, W.; Hao, L.; Zhang, S.; Fang, K.; Hu, C.; Zhang, Q.; Shi, Z.; Zhang, W.; et al. Identification of C3 and FN1 as Potential Biomarkers Associated with Progression and Prognosis for Clear Cell Renal Cell Carcinoma. *BMC Cancer* **2021**, *21*, 1135. [CrossRef] [PubMed]

28. Bao, H.; Huo, Q.; Yuan, Q.; Xu, C. Fibronectin 1: A Potential Biomarker for Ovarian Cancer. *Dis. Markers* **2021**, *2021*, 5561651. [CrossRef] [PubMed]

29. Soikkeli, J.; Podlasz, P.; Yin, M.; Nummela, P.; Jahkola, T.; Virolainen, S.; Krogerus, L.; Heikkilä, P.; von Smitten, K.; Saksela, O.; et al. Metastatic Outgrowth Encompasses COL-I, FN1, and POSTN up-Regulation and Assembly to Fibrillar Networks Regulating Cell Adhesion, Migration, and Growth. *Am. J. Pathol.* **2010**, *177*, 387–403. [CrossRef] [PubMed]

30. Wang, J.; Deng, L.; Huang, J.; Cai, R.; Zhu, X.; Liu, F.; Wang, Q.; Zhang, J.; Zheng, Y. High Expression of Fibronectin 1 Suppresses Apoptosis through the NF-κB Pathway and Is Associated with Migration in Nasopharyngeal Carcinoma. *Am. J. Transl. Res.* **2017**, *9*, 4502–4511.

31. Podstawski, P.; Ropka-Molik, K.; Semik-Gurgul, E.; Samiec, M.; Skrzyszowska, M.; Podstawski, Z.; Szmatoła, T.; Witkowski, M.; Pawlina-Tyszko, K. Assessment of BPV-1 Mediated Matrix Metalloproteinase Genes Deregulation in the In Vivo and In Vitro Models Designed to Explore Molecular Nature of Equine Sarcoids. *Cells* **2022**, *11*, 1268. [CrossRef]

32. Pasello, M.; Manara, M.C.; Scotlandi, K. CD99 at the Crossroads of Physiology and Pathology. *J. Cell Commun. Signal.* **2018**, *12*, 55–68. [CrossRef]

33. Seol, H.J.; Chang, J.H.; Yamamoto, J.; Romagnuolo, R.; Suh, Y.; Weeks, A.; Agnihotri, S.; Smith, C.A.; Rutka, J.T. Overexpression of CD99 Increases the Migration and Invasiveness of Human Malignant Glioma Cells. *Genes Cancer* **2012**, *3*, 535–549. [CrossRef]

34. Manara, M.C.; Bernard, G.; Lollini, P.-L.; Nanni, P.; Zuntini, M.; Landuzzi, L.; Benini, S.; Lattanzi, G.; Sciandra, M.; Serra, M.; et al. CD99 Acts as an Oncosuppressor in Osteosarcoma. *Mol. Biol. Cell* **2006**, *17*, 1910–1921. [CrossRef]

35. Mateos-Quiros, C.M.; Garrido-Jimenez, S.; Álvarez-Hernán, G.; Diaz-Chamorro, S.; Barrera-Lopez, J.F.; Francisco-Morcillo, J.; Roman, A.C.; Centeno, F.; Carvajal-Gonzalez, J.M. Junctional Adhesion Molecule 3 Expression in the Mouse Airway Epithelium Is Linked to Multiciliated Cells. *Front. Cell Dev. Biol.* **2021**, *9*, 622515. [CrossRef] [PubMed]

36. Li, X.; Yin, A.; Zhang, W.; Zhao, F.; Lv, J.; Lv, J.; Sun, J. Jam3 Promotes Migration and Suppresses Apoptosis of Renal Carcinoma Cell Lines. *Int. J. Mol. Med.* **2018**, *42*, 2923–2929. [CrossRef] [PubMed]

37. Arias-Garcia, M.; Rickman, R.; Sero, J.; Yuan, Y.; Bakal, C. The Cell-Cell Adhesion Protein JAM3 Determines Nuclear Deformability by Regulating Microtubule Organization. *bioRxiv* **2020**. [CrossRef]

38. Liu, Q.Z.; Gao, X.H.; Chang, W.J.; Gong, H.F.; Fu, C.G.; Zhang, W.; Cao, G.W. Expression of ITGB1 Predicts Prognosis in Colorectal Cancer: A Large Prospective Study Based on Tissue Microarray. *Int. J. Clin. Exp. Pathol.* **2015**, *8*, 12802–12810. [PubMed]

39. Sharma, R.; Sharma, R.; Khaket, T.P.; Dutta, C.; Chakraborty, B.; Mukherjee, T.K. Breast Cancer Metastasis: Putative Therapeutic Role of Vascular Cell Adhesion Molecule-1. *Cell. Oncol.* **2017**, *40*, 199–208. [CrossRef] [PubMed]

40. Kong, D.H.; Kim, Y.K.; Kim, M.R.; Jang, J.H.; Lee, S. Emerging Roles of Vascular Cell Adhesion Molecule-1 (VCAM-1) in Immunological Disorders and Cancer. *Int. J. Mol. Sci.* **2018**, *19*, 1057. [CrossRef]

41. Vallat, J.-M.; Nizon, M.; Magee, A.; Isidor, B.; Magy, L.; Péréon, Y.; Richard, L.; Ouvrier, R.; Cogné, B.; Devaux, J.; et al. Contactin-Associated Protein 1 (CNTNAP1) Mutations Induce Characteristic Lesions of the Paranodal Region. *J. Neuropathol. Exp. Neurol.* **2016**, *75*, 1155–1159. [CrossRef]

42. Li, W.; Meng, X.; Yuan, H.; Xiao, W.; Zhang, X. M2-Polarization-Related CNTNAP1 Gene Might Be a Novel Immunotherapeutic Target and Biomarker for Clear Cell Renal Cell Carcinoma. *IUBMB Life* **2022**, *74*, 391–407. [CrossRef]

43. Ascenzi, F.; De Vitis, C.; Maugeri-Saccà, M.; Napoli, C.; Ciliberto, G.; Mancini, R. SCD1, Autophagy and Cancer: Implications for Therapy. *J. Exp. Clin. Cancer Res.* **2021**, *40*, 265. [CrossRef]

44. Wang, C.; Shi, M.; Ji, J.; Cai, Q.; Zhao, Q.; Jiang, J.; Liu, J.; Zhang, H.; Zhu, Z.; Zhang, J. Stearoyl-CoA Desaturase 1 (SCD1) Facilitates the Growth and Anti-Ferroptosis of Gastric Cancer Cells and Predicts Poor Prognosis of Gastric Cancer. *Aging* **2020**, *12*, 15374–15391. [CrossRef]

45. Luis, G.; Godfroid, A.; Nishiumi, S.; Cimino, J.; Blacher, S.; Maquoi, E.; Wery, C.; Collignon, A.; Longuespée, R.; Montero-Ruiz, L.; et al. Tumor Resistance to Ferroptosis Driven by Stearoyl-CoA Desaturase-1 (SCD1) in Cancer Cells and Fatty Acid Biding Protein-4 (FABP4) in Tumor Microenvironment Promote Tumor Recurrence. *Redox Biol.* **2021**, *43*, 102006. [CrossRef] [PubMed]

46. Li, H.; Gao, J.; Zhang, S. Functional and Clinical Characteristics of Cell Adhesion Molecule CADM1 in Cancer. *Front. Cell Dev. Biol.* **2021**, *9*, 714298. [CrossRef] [PubMed]

47. Sawada, Y.; Mashima, E.; Saito-Sasaki, N.; Nakamura, M. The Role of Cell Adhesion Molecule 1 (CADM1) in Cutaneous Malignancies. *Int. J. Mol. Sci.* **2020**, *21*, 9732. [CrossRef] [PubMed]

48. Hartsough, E.J.; Weiss, M.B.; Heilman, S.A.; Purwin, T.J.; Kugel, C.H.; Rosenbaum, S.R.; Erkes, D.A.; Tiago, M.; HooKim, K.; Chervoneva, I.; et al. CADM1 Is a TWIST1-Regulated Suppressor of Invasion and Survival. *Cell Death Dis.* **2019**, *10*, 281. [CrossRef]

49. Yen, C.Y.; Huang, C.Y.; Hou, M.F.; Yang, Y.H.; Chang, C.H.; Huang, H.W.; Chen, C.H.; Chang, H.W. Evaluating the Performance of Fibronectin 1 (FN1), Integrin A4β1 (ITGA4), Syndecan-2 (SDC2), and Glycoprotein CD44 as the Potential Biomarkers of Oral Squamous Cell Carcinoma (OSCC). *Biomarkers* **2013**, *18*, 63–72. [CrossRef]

50. Semik, E.; Gurgul, A.; Ząbek, T.; Ropka-Molik, K.; Koch, C.; Mählmann, K.; Bugno-Poniewierska, M. Transcriptome Analysis of Equine Sarcoids. *Vet. Comp. Oncol.* **2017**, *15*, 1370–1381. [CrossRef]

51. DAVID Functional Annotation Bioinformatics Microarray Analysis. Available online: https://david.ncifcrf.gov/ (accessed on 18 May 2022).

52. Podstawski, P.; Samiec, M.; Skrzyszowska, M.; Szmatoła, T.; Semik-Gurgul, E.; Ropka-Molik, K. The Induced Expression of *BPV E4* Gene in Equine Adult Dermal Fibroblast Cells as a Potential Model of Skin Sarcoid-like Neoplasia. *Int. J. Mol. Sci.* **2022**, *23*, 1970. [CrossRef]

53. Tomasek, J.J.; Haaksma, C.J.; Eddy, R.J.; Vaughan, M.B. Fibroblast Contraction Occurs on Release of Tension in Attached Collagen Lattices: Dependency on an Organized Actin Cytoskeleton and Serum. *Anat. Rec.* **1992**, *232*, 359–368. [CrossRef]

54. Bogaert, L.; Van Poucke, M.; De Baere, C.; Peelman, L.; Gasthuys, F.; Martens, A. Selection of a Set of Reliable Reference Genes for Quantitative Real-Time PCR in Normal Equine Skin and in Equine Sarcoids. *BMC Biotechnol.* **2006**, *6*, 24. [CrossRef]

55. Pfaffl, M.W. A New Mathematical Model for Relative Quantification in Real-Time RT–PCR. *Nucleic Acids Res.* **2001**, *29*, e45. [CrossRef]

Article

Trichostatin A-Mediated Epigenetic Modulation Predominantly Triggers Transcriptomic Alterations in the Ex Vivo Expanded Equine Chondrocytes

Tomasz Ząbek [1,*][ID], Wojciech Witarski [1][ID], Tomasz Szmatoła [1,2][ID], Sebastian Sawicki [2][ID], Justyna Mrozowicz [1] and Marcin Samiec [3,*][ID]

1   Department of Animal Molecular Biology, National Research Institute of Animal Production, Krakowska 1 Street, 32-083 Balice, Poland
2   University Centre of Veterinary Medicine, University of Agriculture in Kraków, Mickiewicza 24/28, 30-059 Kraków, Poland
3   Department of Reproductive Biotechnology and Cryoconservation, National Research Institute of Animal Production, Krakowska 1 Street, 32-083 Balice, Poland
*   Correspondence: tomasz.zabek@iz.edu.pl (T.Z.); marcin.samiec@iz.edu.pl (M.S.)

Abstract: Epigenetic mechanisms of gene regulation are important for the proper differentiation of cells used for therapeutic and regenerative purposes. The primary goal of the present study was to investigate the impacts of 5-aza-2′ deoxycytidine (5-AZA-dc)- and/or trichostatin A (TSA)-mediated approaches applied to epigenomically modulate the ex vivo expanded equine chondrocytes maintained in monolayer culture on the status of chondrogenic cytodifferentiation at the transcriptome level. The results of next-generation sequencing of 3′ mRNA-seq libraries on stimulated and unstimulated chondrocytes of the third passage showed no significant influence of 5-AZA-dc treatment. Chondrocytes stimulated with TSA or with a combination of 5-AZA-dc+TSA revealed significant expressional decline, mainly for genes encoding histone and DNA methyltransferases, but also for other genes, many of which are enriched in canonical pathways that are important for chondrocyte biology. The TSA- or 5-AZA-dc+TSA-induced upregulation of expanded chondrocytes included genes that are involved in histone hyperacetylation and also genes relevant to rheumatoid arthritis and inflammation. Chondrocyte stimulation experiments including a TSA modifier also led to the unexpected expression incrementation of genes encoding HDAC3, SIRT2, and SIRT5 histone deacetylases and the MBD1 CpG-binding domain protein, pointing to another function of the TSA agent besides its epigenetic-like properties. Based on the transcriptomic data, TSA stimulation seems to be undesirable for chondrogenic differentiation of passaged cartilaginous cells in a monolayer culture. Nonetheless, obtained transcriptomic results of TSA-dependent epigenomic modification of the ex vivo expanded equine chondrocytes provide a new source of data important for the potential application of epigenetically altered cells for transplantation purposes in tissue engineering of the equine skeletal system.

Keywords: equine chondrocytes; 5-AZA-dc and TSA epigenetic modifiers; transcriptome

1. Introduction

Aging is a common cause of immune-related disorders, in which underlying altered transcriptional and regulatory mechanisms contribute to inflammatory impairment. For instance, rheumatoid arthritis (RA) is an example of an immune-related condition that is a common cause of degeneration of the hyaline cartilage of the joints. Articular cartilage is an aneural and avascular tissue which has limited regenerative capacity. Therefore, in cases of joint defects, regenerative therapy is often the last available procedure to maintain joint function and restore the overall fitness of the limbs. One of the most effective regenerative approaches is to obtain chondrocytes from the healthy surfaces of the patient's joints and

use them in chondrocyte implantation in places with cartilage defects [1]. The basis for this is the availability of a large number of chondrocytes that will not be dedifferentiated in the course of in vitro expansion. Particularly, in the monolayer culture, which is often the choice for rapid chondrocyte expansion, rapid loss of the primary chondrogenic type of cells is observed. In order to diminish the chondrocyte dedifferentiation, a range of biological stimulants have been tested, which are able to influence the activity of transcription factors or target proteins or to modulate enzymes (COX-2), cytokines (TNF-α/β), and associated inflammatory cascades (NF-kB) that are important for the maintenance of differentiation of chondrocytes [2–5]. Moreover, it was found that epigenetic modifications such as DNA methylation of regulatory elements of genes or the histone code are able to determine the chondrocyte's fate [6]. A range of studies, including the in vivo cartilage stimulation of the joints and stimulation of pluripotent stem cells, implemented different epigenetic cures influencing the global expression pattern. These cures encompassed such treatment modalities as the strategies based on the use of either a non-selective inhibitor of DNA methyltransferases (DNMTs), one of which is designated as 5-aza-2′ deoxycytidine (5-AZA-dc) and triggers global passive DNA demethylation [7], or trichostatin A (TSA), representing a family of non-selective inhibitors of histone deacetylases (HDACs). TSA has been found to be an antifungal antibiotic primarily isolated from a culture broth of *Streptomyces platensis* [8]. Its main ability is the non-selective blockage of the class I and II mammalian HDACs, whose enzymatic activities are aimed at mitigating the incidence of acetylation levels within nucleosomal core-derived histones followed by transcriptional repression of the genes. In other words, by the onset of the mechanism of competitive inhibition of HDAC isoenzymes, TSA interferes with the HDAC-induced removal of acetyl groups from histones, and as a consequence of hyperacetylation of lysine residues within histones, it facilitates the opening of chromatin for transcriptional factors promoting the initiation of gene expression [8]. As a potent member of non-specific HDAC inhibitors (HDACIs), TSA has also been considered to be an effective anti-cancer drug used for a wide variety of anti-oncogenic treatment modalities within the framework of epigenetic oncological therapeutics [9]. Moreover, based on oncological research, TSA has been shown to correctly prompt the differentiation processes of dedifferentiated cells [10]. Studies comprising stimulation of primary chondrocytes with 5-AZA-dc showed that DNA demethylation facilitates the terminal differentiation of chondrocytes into the hypertrophic stage [11], whereas 5-AZA-dc treatment of human dedifferentiated chondrocytes from osteoarthritis (OA) patients revealed no substantial impact, despite the presence of osteogenic and adipogenic differentiation of the treated cells [12]. In turn, TSA has been found to be a promising therapeutic agent during the in vivo experimental treatment of cartilage disorders and cartilage regeneration [13] due to its anti-inflammatory properties [14] and ability to prevent cartilage degeneration [10]. However, in vitro studies implementing TSA treatment of human bone marrow mesenchymal stem cells (hBMMSCs) showed that TSA inhibited chondrogenic differentiation, making TSA probably not useful for cartilage tissue engineering using hBMMSCs [15].

Due to contradictory results affecting the efficiency of 5-AZA-dc and TSA—epigenetic modulators of chondrogenesis—the aim of our study was to describe transcriptional variation upon 5-AZA-dc and TSA stimulation of expanded equine chondrocytes in monolayer cultures. While 5-AZA-dc exerted no effect at the transcriptome level of expanded chondrocytes, TSA stimulation resulted in the expressional decline of genes encoding methyltransferases and genes which are overrepresented in a range of molecular pathways relevant to chondrogenesis. It seems that TSA stimulation of in vitro expanded chondrocytes is less beneficial regarding chondrogenic capacity in comparison to the reported intraarticular administration of TSA, where it showed a protective effect on the cartilage [13]. Although TSA- and/or 5-AZA-dc-assisted epigenetic transformation of the ex vivo expanded horse chondrocytes gives rise to a decrease in the expression of a wide variety of genes responsible for chondrogenic differentiation, efforts to characterize the genomic and epigenomic signatures of equine cartilage-derived cell lines appear to be required for exploring the

capabilities of TSA- and/or 5-AZA-dc-transformed, cartilage-derived somatic cell nuclei to be epigenetically reprogrammed in cloned horse embryos. Estimating the backgrounds pinpointed for epigenetic reprogrammability and molecular dedifferentiability of TSA- and/or 5-AZA-dc-modulated chondrocyte cell nuclei for the needs of generating and multiplying genetically identical equine cloned embryos, conceptuses, and progeny might be shown to be a viable solution that can be applied to modern assisted reproductive technologies based on somatic cell nuclear transfer (SCNT) in horses and other mammalian species.

2. Results

2.1. Efficiency Alignment of NGS Reads

Next-generation sequencing of 3' mRNA-seq libraries produced from 2,332,147 to 3,699,592 filtered reads per sample with the efficiency of 80.1–82.7% for uniquely mapped reads, using the EquCab 3.0 version of the horse genome (Table 1).

Table 1. Results of the alignment of 3' mRNA-seq reads against the EquCab 3.0 reference sequence of the horse genome.

Group	3rd Passage Chondrocyte Stimulation	3' mRNA-Seq Library	Total Reads after Filtering	Number of Uniquely Mapped Reads
I	5-AZA-dc [1]	2aza-1	3,114,172	2,541,510 (81.6%)
I	5-AZA-dc	3aza-1	2,685,011	2,216,276 (82.5%)
I	5-AZA-dc	4/DEO	2,332,147	1,913,713 (82.1%)
I	5-AZA-dc	6/DEO	2,603,715	2,137,736 (82.1%)
II	5-AZA-dc+TSA [2]	3tsaza-1	3,490,960	2,862,115 (82.0%)
II	5-AZA-dc+TSA	2tsaaza-1	2,915,748	2,336,842 (80.1%)
II	5-AZA-dc+TSA	4/Deo+TSA	3,091,055	2,548,432 (82.4%)
II	5-AZA-dc+TSA	6/DEO+TSA	2,821,472	2,329,453 (82.6%)
III	Control	2k-1	2,361,866	1,954,158 (82.7%)
III	Control	3k-1	3,062,350	2,511,373 (82.0%)
III	Control	4/K	3,312,867	2,732,432 (82.5%)
III	Control	6/K	3,207,522	2,627,829 (81.9%)
IV	TSA	3tsa-1	3,699,592	3,054,305 (82.6%)
IV	TSA	2tsa-1	2,753,414	2,261,816 (82.1%)
IV	TSA	4/TSA	3,158,031	2,620,954 (83.0%)
IV	TSA	6/TSA	2,858,574	2,361,644 (82.6%)

[1] 5-AZA-dc concentration of 25 µg/mL. [2] TSA concentration of 0.25 µg/mL.

2.2. Differentially Expressed Genes (DEGs) Obtained Using 3' mRNA-Seq

The comparison among investigated groups (Table 1) produced a list of differentially expressed genes (DEGs). The adjusted *p*-value was less than 0.05 for groups I and II (5-AZA-dc versus 5-AZA-dc+TSA) (Table S1), I and IV (5-AZA-dc versus TSA) (Table S2), II and III (5-AZA-dc+TSA versus control group) (Table S3), and III and IV (control group versus TSA) (Table S4). We found a lack of significant DEGs between cells stimulated with 5-AZA-dc and the control group (I vs. III).

From the list of 1980 DEGs showing a minimum fold change value of at least 1, two major sets of genes were characterized after the stimulation of cells. The first group was represented by 1636 genes upregulated in group I vs. group IV (5-AZA-dc versus TSA), I vs. II (5-AZA-dc versus 5-AZA-dc+TSA), II vs. III (5-AZA-dc+TSA versus control group), and III vs. IV (control group versus TSA) (Figure 1). The second set included 1655 genes which were downregulated in the mentioned comparisons (Figure 2).
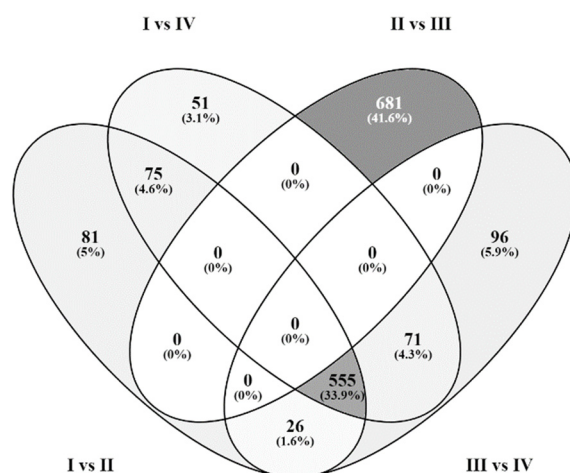
Figure 1. The Venn diagram showing the numbers of common DEGs in four comparisons when upregulated in: group I vs. group IV (5-AZA-dc versus TSA), I vs. II (5-AZA-dc versus 5-AZA-dc+TSA), II vs. III (5-AZA-dc+TSA versus control group) and III vs. IV (control group versus TSA).
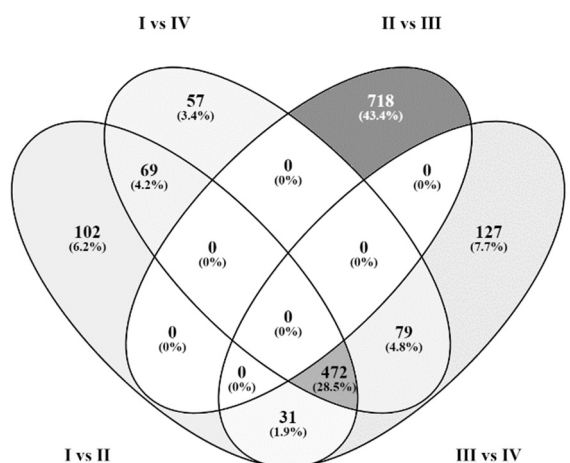

Figure 2. The Venn diagram showing the number of common DEGs in four comparisons when downregulated in: group I vs. group IV (5-AZA-dc versus TSA), I vs. II (5-AZA-dc versus 5-AZA-dc+TSA), II vs. III (5-AZA-dc+TSA versus control group), and III vs. IV (control group versus TSA).

The majority of differentially expressed genes between the investigated groups were found in comparisons that included TSA stimulation of cells. Namely, the comparison of DEG lists using the Venny integrative tool (http://bioinfogp.cnb.csic.es/tools/venny/index.html, accessed on 8 August 2022) revealed 681 exclusively upregulated and 718 downregulated genes in group II vs. group III (5-AZA-dc+TSA versus control group) and 555 exclusively upregulated and 472 downregulated genes in I vs. II, I vs. IV, and III vs. IV (5-AZA-dc versus 5-AZA-dc+TSA, 5-AZA-dc versus TSA, and control group versus TSA) (Figures 1 and 2).

2.3. General Description of Differentially Expressed Genes upon Applying Chondrocyte Stimulation in Monolayer Culture

A list of all DEGs with descriptions of their encoding proteins is included in Table S6. Variably expressed genes in this study included loci involved in the functioning of the genetic apparatus during the cell cycle, which are also important for the epigenetic control of transcriptome machinery—e.g., encoding proteins of histone acetyltransferases (HATs), acetylation readers, histone deacetylases (HDACs), histone methyltransferases (HMTs), genes encoding DNA methyltransferases and a methyl-CpG-binding domain [16], and also an equine counterpart of a gene encoding 5-azacytidine-induced protein 2 (AZI2), whose

cDNA was first detected in a human cell line after stimulation with the 5-AZA-c demethylation agent [17] (Figure 3). Genes encoding histone methyltransferases (SETD2, SETD7, KMT2E, KMT5A, KMT5B, PRMT7), the BRD1 histone acetylation reader, DNA methyltransferases (DNMT1 and DNMT3A), and AZI2 were downregulated in TSA- or 5-AZA-dc+TSA-stimulated cells in comparison to the control or to chondrocytes stimulated exclusively with 5-AZA-dc. Those encoding CREBBP and EP300 histone acetyltransferases; HDAC3, SIRT2, and SIRT5 histone deacetylases; and methyl-CpG-binding domain protein 1 (MBD1) were upregulated in TSA- or 5-AZA-dc+TSA-stimulated cells (Figure 3). Genes downregulated in TSA- or 5-AZA-dc+TSA-treated cells included also those encoding particular types of chondroproteins (Figure 3) [18]. These were genes encoding collagens (COL1A1, COL3A1, COL4A1, COL5A2, COL8A1, COL11A1, and COL12A1); non-collagenous regulatory (BMP6, MXRA5, TGFB1I1, TGFB3) and structural proteins (ECM2, EFEMP2, FNDC3B); membrane-associated proteins, such as integrins (ITGA1, -5, and -7, and ITGB5), annexin (LOC100052045), chondroitin sulfate N-acetylgalactosaminyltransferase 1 (CSGALNACT1), syndecan (SDC2), and discoidin (DDR2); and one of the proteoglycan proteins—asporin (ASPN) [18]. A set of genes which was also downregulated included those encoding transcriptional factors (TFs) important for chondrogenesis (DLX5, NFIB, NFIX, PRRX1, SOX6, TCF7L1, TRPS1, ZBTB20) [19]. Some of the genes which were upregulated in TSA- or 5-AZA-dc+TSA-stimulated cells versus control cells or cells stimulated with 5-AZA-dc alone included *COL2A1, COL9A2, ITGA2, DCBLD2, ANXA2, TGFB1, ADAMTS1, ADAMTS15*, and one gene encoding a chondrogenic transcriptional factor (STAT1) (Figure 3).

2.4. Results of Functional Overrepresentation of DEGs Using DAVID Annotation Tools

We have performed the analysis of gene enrichment in GO terms for loci with the fold change thresholds of equal to or above 1 and equal to or below −1. Implementation of a DAVID Functional Annotation Chart (https://david.ncifcrf.gov/tools.jsp, accessed on 4 July 2022) using the horse genome as the background showed significant enrichment of sets of genes involved in pathways in cancer (ecb05200), cell cycle (ecb04110), focal adhesion (ecb04510), ECM–receptor interaction (ecb04512), glycolysis/gluconeogenesis (ecb00010), proteoglycans in cancer (ecb05205), HIF-1 signaling pathway (ecb04066), PI3K-Akt signaling pathway (ecb04151), FoxO signaling pathway (ecb04068), and TGF-beta signaling pathway (ecb04350) (Table S7–S10). A variety of genes contributing to the mentioned pathways were upregulated in the 5-AZA-dc group compared to the 5-AZA-dc+TSA group or TSA group, and these were also upregulated in the control group compared to the TSA group or downregulated in the 5-AZA-dc+TSA group compared to the control group (Tables S7–S10). Moreover, DEGs between particular biological groups in this study were also enriched for the MAPK signaling pathway (ecb04010) (genes were upregulated in cells stimulated with 5-AZA-dc versus cells stimulated with the combination 5-AZA-dc+TSA or with TSA alone; they were also upregulated in controls versus cells stimulated with TSA), fluid shear stress and atherosclerosis (ecb05418) and lysine degradation (ecb00310) (genes were upregulated in cells stimulated with 5-AZA-dc versus with the combination of 5-AZA-dc+TSA, or downregulated in cells stimulated with 5-AZA-dc+TSA versus the control group), and the thyroid hormone signaling pathway (ecb04919) (genes were downregulated in cells stimulated with 5-AZA-dc+TSA versus the control group). Rheumatoid arthritis (ecb05323) and metabolic pathways (ecb01100) were the ones enriched with genes downregulated in the 5-AZA-dc group versus the 5-AZA-dc+TSA or TSA group, and these genes were also downregulated in the control group compared to the TSA group or upregulated in the 5-AZA-dc+TSA group compared to the control group (Tables S7–S10).
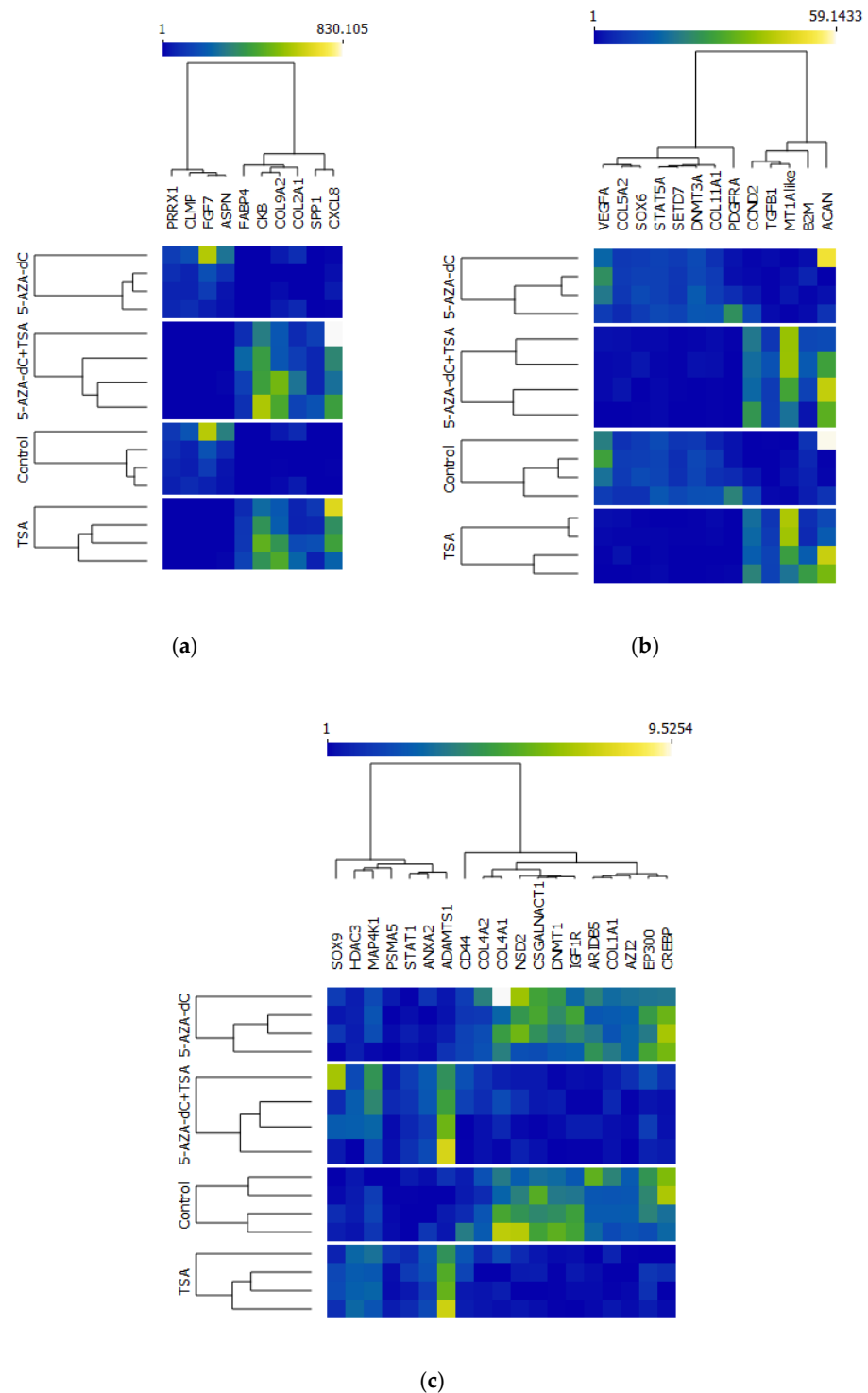
(**a**)

(**b**)

(**c**)

Figure 3. Differential expression results for 42 genes that are important for chondrogenesis and epigenetic modifications, which were validated using quantification with real-time PCR. Heat maps were generated using Orange: Data Mining web available software. Each heat map shows low expression values in blue and high expression values in yellow and white. In each figure, two major clusters are visible: the first represents genes downregulated after TSA or 5-AZA-dc+TSA treatment, and the second includes genes that were upregulated after TSA or 5-AZA-dc+TSA stimulation. (**a**) DEGs with fold changes of expression in the range from 1 to 830.1; (**b**) DEGs with fold changes of expression in the range from 1 to 59.14; (**c**) DEGs with fold changes of expression in the range from 1 to 9.5.

2.5. Validation in RNA-Seq Results

In order to check for the validity of identified transcript abundance in RNA-seq data, we selected 42 genes which were important for the biological background of the designed experiment (violin plots in Figures S1–S42 in Supplementary Figures). The tendency and significance of differential expression at the mentioned loci were confirmed using quantification via real-time PCR. In general, heat maps representing the transcriptional activity of validated genes showed two major gene clusters relevant to down- or upregulation upon TSA or 5-AZA-dc+TSA treatment of chondrocytes from the third passage (Figure 3).

Contrary to RNA-seq results, real-time PCR showed a lack of significant transcriptional variation in the *CD44* and *PSMA5* loci among all compared groups. A lack of significant differences was also found between 5-AZA-dc+TSA and the control group in *COL4A2* (Figure S15) and EP300 loci (Figure S24) (only the trend); between 5-AZA-dc, TSA, and the control group and TSA in the *STAT1* locus (Figure S38) (only the trend); between 5-AZA-dc and 5-AZA-dc+TSA and between 5-AZA-dc+TSA and the control group in the *HDAC3* locus (Figure S27); and between 5-AZA-dc and 5-AZA-dc+TSA in the *MAP4K1* locus (Figure S29). Moreover, real-time PCR using primers for *DNMT1* revealed significant differences between 5-AZA-dc+TSA and the control group, and the control and the TSA group, at this locus, which were not detected in RNA-seq data. We also checked for transcript abundance of additional markers of chondrogenic differentiation, such as *ACAN* and *SOX9*. Real-time PCR results at the *ACAN* locus revealed nonsignificant downregulation in TSA- or 5-AZA-dc+TSA-stimulated cells, showing only the trend (Figure S1). Relative quantification results of transcriptional variation between groups at the *SOX9* locus were not significant (Figure S37).

3. Discussion

5-AZA-dc and TSA are common agents used for studies on the cell cycle and cells' epigenetic alterations in in vitro systems. In this study, we observed a predominant influence of TSA treatment on transcriptome alterations of chondrocytes in monolayer cultures of the third passage. According to the observed transcriptional variation upon 5-AZA-dc and TSA treatment after the third passage of cultivated cells, the effect of 5-AZA-dc seemed to be marginal in comparison to the TSA treatment. There was a lack of significant differences in transcript abundance between 5-AZA-dc-stimulated cells and the control group. Moreover, *AZI2*, which was found to be a special marker, being upregulated under 5-azacytidine-induced demethylation [17], was underexpressed in TSA- and 5-AZA-dc+TSA-treated cells in our study. The investigated cells of the third passage were less affected by the 5-AZA-dc treatment due to a range of possible factors, such as differences in the proliferative potential between cell lines, and uneven surface coating with the applied matrigel, leading to variability in the phenotype changes due to in vitro handling. It is of note that the blockage of DNA methylation via 5-AZA-dc was reported to be more pronounced in the primary chondrocytes [20]. One possible sign of the 5-AZA-dc activity in the passaged chondrocytes might be observed upregulation of an important osteogenic marker, such as secreted phosphoprotein 1 (*SPP1*), and that of a gene relevant to adipogenic differentiation, e.g., fatty acid binding protein 4 (*FABP4*). It was previously found that human OA chondrocytes pre-cultivated with 5-AZA-dc showed signs of osteogenic and adipogenic differentiation [12]. Nonetheless, the majority of detected transcriptional variation in this study affected genes after the TSA or 5-AZA-dc+TSA treatment of equine chondrocytes. The demethylating effect of TSA seemed to be evident in our study, as genes encoding histone methyltransferases, and those encoding DNA methyltransferases, were downregulated in cells stimulated with TSA or 5-AZA-dc+TSA. However, this effect should be also checked on the DNA methylation level. Moreover, according to the literature, downregulation of DNA methyltransferases by TSA may lead to increased expression of *CREBBP* and *EP300* histone acetyltransferases and *BRD1* (histone acetylation reader), all of which occurred in our study, confirming the effect of TSA histone hyperacetylation reported elsewhere [21]. The exception was that genes encoding *HDAC3*, *SIRT2*, and

SIRT5 histone deacetylases and methyl-CpG-binding domain protein 1 (*MBD1*) belonged to a group of loci that were upregulated in chondrocytes stimulated with TSA or 5-AZA-dc+TSA. We could not find any solid explanation for this opposite effect of TSA, especially for the *HDAC3* and *MBD1* expression increases. Trichostatin A is a common inhibitor of histone deacetylases which possess a zinc-dependent active site, like HDAC3, but SIRT2 and SIRT5 histone deacetylases are in general not affected by TSA [16]. From the biological perspective, the observed expression pattern might be uncoupled from the function of histone deacetylation by *HDAC3*, *SIRT2*, and *SIRT5*, which might also have another biological role, being functionally linked with other genes induced by TSA treatment in expanded chondrocytes. For instance sirtuins themselves have been found to promote MSC chondrogenesis [22] and are important regulators of cartilage homeostasis [23]. In this regard, TSA-related *SIRT2* or *SIRT5* induction could be important for chondrocyte differentiation during expansion. In turn, methyl-CpG-binding domain protein 1 (MBD1) possesses a strong affinity to DNA methylation [24] and should be downregulated under TSA stimulation. The reason for the TSA-related *MBD1* expression increment might have been a diminished demethylation effect of chondrocytes from the third passage, which were nonsignificantly affected by 5-AZA-dc, possibly due to the factors mentioned earlier in the discussion. Therefore, TSA stimulation with an applied dose to expanded chondrocytes would seem to exert heterogeneous effects, rather than being only a demethylation or hyperacetylation agent. However, we did not find any relevant literature about the adverse effects of TSA on the activity of the above-mentioned genes. The aforementioned assumptions need to be further experimentally verified. Regarding the maintenance of the chondrogenic potential of expanded cells, the results we obtained are similar to the ones from work on chondrogenesis of human bone marrow mesenchymal stem cells (hB-MMSCs), where TSA treatment resulted in reduced expression of chondrogenesis-related genes [15]. In our study, genes downregulated after TSA or 5-AZA-dc+TSA treatment in expanded chondrocytes were those encoding numerous chondroproteins, such as collagens, non-collagenous regulatory and structural proteins, membrane-associated proteins, and proteoglycans. TSA also downregulated a group of genes encoding transcriptional factors (TFs) that are important for chondrogenesis. Some exceptions included chondral genes such as *COL2A1*, *COL9A2*, *ITGA2*, *DCBLD2*, *ANXA2*, and *TGFB1*, which were upregulated under the influence of TSA or 5-AZA-dc+TSA. *COL2A1* and *COL9A2* genes, of the six mentioned above, were highly expressed under TSA or TSA+5-AZA-dc stimulation. *COL2A1* and *COL9A2* encode components of the extracellular matrix characteristic for mature articular cartilage, which are regulated by the SOX9 master chondrogenic transcription factor in combination with SOX5 and SOX6 (TFs) [25]. In our study, we did not observe significant expression alterations of *SOX9*, despite substantial *COL2A1* and *COL9A2* TSA-related expression incrementation. Moreover, we even detected TSA-related *SOX6* downregulation, pointing to other downstream mechanisms of *COL2A1* and *COL9A2* upregulation under TSA treatment where a range of other TFs could be involved.

It is of note that the transcript abundance of *ACAN*, which is an important marker of chondrocyte differentiation regulated by SOX9 TF [25], was unaffected by TSA treatment and by 5-AZA-dc+TSA treatment of chondrocytes in our study. According to the study on the regulation of type-IX collagen gene expression in human osteoarthritic chondrocytes [26], exposure to potentially and indirectly demethylating agents such as a member of non-selective HDACIs designated as TSA might result in the activation of genes regulated by CpG differential methylation. This, however, needs to be further explored in the target loci using molecular approaches relying on bisulfite-converted DNA. In our study, we also observed TSA-related downregulation of gene groups involved in canonical molecular pathways that are important for the biology of differentiated chondrocytes, such as ECM–receptor interaction [27]; focal adhesion [28]; and HIF-1-, PI3K-Akt-, TGF-beta-, and FOXO-and MAPK signaling pathways [29–33]. Other KEGG pathways with TSA-downregulated genes in our study included glycolysis/gluconeogenesis pathways, which are relevant to glucose uptake during chondrocyte maturation [34]; the fluid shear stress pathway, a

relevant one possibly reflecting the role of mechanical loading on cartilage during chondrocyte maturation [35]; and the thyroid hormone signaling pathway, where TSH is involved in terminal differentiation of growth-plate chondrocytes [36]. Some genes which were upregulated under the influence of TSA or 5-AZA-dc+TSA are enriched in rheumatoid arthritis (RA), pointing to an alleged negative outcome of the applied means of stimulation of expanded chondrocytes in the monolayer. These loci include chemokines, matrix metallopeptidase 3 (*MMP3*), and the Fos proto-oncogene AP-1 transcription factor subunit (*FOS*); all of them contribute to molecular pathways involved in RA development [37]. Moreover, TSA- or 5-AZA-dc+TSA-related upregulation of expanded chondrocytes in this report affected other genes involved in pathophysiological remodeling and inflammation, such as those encoding for ADAMTS1 and ADAMTS15 aggrecanases [38], and STAT1, a transcription factor which inhibits chondrocyte maturation in the growth plate [19] and indirectly leads to severe chondrodysplasias [39].

In summary, it must be underlined that two-dimensional (2D) culture under monolayer conditions seems to be the fastest and least expensive method of rapid chondrocyte expansion for the purposes of regenerative and reconstructive medicine. Nevertheless, the ex vivo 2D models used for the proliferation of equine chondrocytes appear to be considered as a potential risk factor that can expedite a loss of phenotypic background specific for cartilage cells (i.e., disappearance of their chondrogenic potential) [40]. For that reason, future investigations are required to estimate the reliability and feasibility of TSA- and/or 5-AZA-dc-dependent approaches to epigenomically modulate the transcriptomic profiles pinpointed for three-dimensional (3D) models of chondrocyte expansion. The latter might provide a more conducive environment for the effective transduction of intracellular signals indispensable for perpetuating the chondrogenic differentiation of cells. Moreover, obtained results in form of transcriptome signatures of ex vivo expanded equine chondrocytes in a 2D model, subjected to TSA- and/or 5-AZA-dc-assisted epigenomic modulation, might contribute to the enhancement in biomedical applicability of epigenetically modified cartilage cells in regenerative medicine. Further, TSA- and/or 5-AZA-dc-modified chondrocyte cell lines might provide a completely new source of epigenetically altered nuclear donor cells (NDCs) usable for future studies on somatic cell cloning of horses. Such SCNT-derived horse clones might be especially suitable for studies on the treatment of a variety of histopathological changes of the skeleton. These can be pre-clinical and clinical studies designed to elaborate the negligibly intrusive procedures of reconstructive medicine and chondroplasty-mediated tissue engineering of the horse skeletal system. Such research could be applied for the treatment of chondrodystrophic and chondrodysplastic lesions evoked either by post-operative intra- and intercartilaginous connective tissue-based adhesions or by accidental and inflicted chondral defects in domestic horses [41–43]. At this point, the treatment of both degenerative abnormalities (e.g., chondromalacia patellae) in senescent chondral connective tissue and heritable malformations of the equine chondroskeletal system [44,45] could also be considered. Important pathophysiological transformations which would be another subject in this area include premalignant cartilaginous lesions in specimens afflicted with precancerous chondrocyte hypertrophy or chondrometaplasia (chondromatosis) [46–48]. Finally, other interesting ones in this matter are the oncologic disorders that are related to the carcinogenesis of cartilaginous origin such as malignant chondral neoplasms classified as metastatic chondrocyte-mediated cancers and non-malignant chondroskeletal tumors in high-genetic-merit horses displaying tremendous performance rates [49–53].

4. Materials and Methods

4.1. Short Description of the Research

The study included the setup of chondrocytes of the 1st passage and cells' adaptation to the in vitro conditions. The main stages of the experiments included the epigenetic stimulation of cultivated chondrocytes in the monolayer that reached the 3rd passage, preparation of RNA samples and RNA-seq libraries, NGS sequencing, validation of RNA-

seq results, bioinformatics, and data analysis, including genomic annotation and gene overrepresentation tests in gene ontology terms (Figure 4).
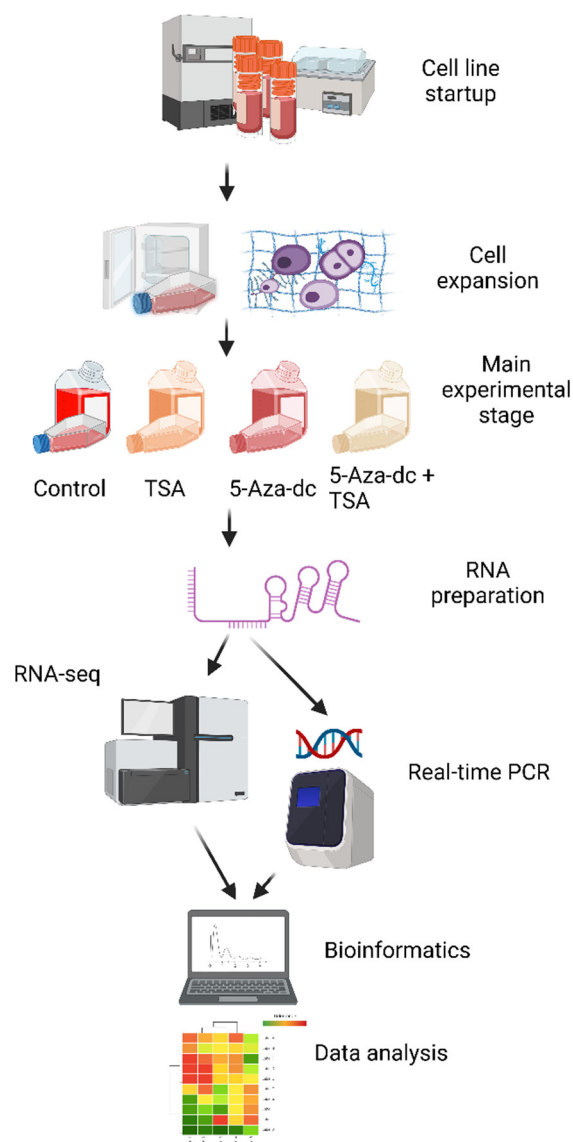

Figure 4. Scheme of the research (created with BioRender.com; license agreement *FU24GOX88E*).

4.2. Chondrocyte Culture Conditions and Applied Stimulations

The subjects of the study were equine chondrocyte cells preserved at the 1st passage of a monolayer culture stored in DMSO at −80 °C, which were previously developed from chondrocytes obtained post-mortem from the hyaline cartilage shavings of the metacarpal–phalangeal joints (by-product of slaughter material) of four unrelated cold-blood horses aged one and a half years [54]. The refrigeration stage included incubation of cells at 37 °C in DMEM high-glucose medium (Gibco, Grand Island, NY, USA) including 10% fetal bovine serum (FBS), 0.3 mg of GlutaMAX Supplement per 1 mL (Gibco Grand Island, NY, USA), and 1× Primocin (Invivogen, San Diego, CA, USA). Thereafter, chondrocytes were seeded on 10 cm Petri dishes (Eppendorf, Hamburg, Germany) previously coated with Geltrex LDEV-Free Reduced Growth Factor Basement Membrane Matrix (Thermofisher Scientific, Waltham, MA, USA). We introduced coating with Geltrex because matrigel-like compositions were characterized to be some of the most interesting solutions for preventing or delaying the dedifferentiation of cultivated chondrocytes [55]. The complex composition of Geltrex also allows chondrocytes to develop laminin-mediated effects, this

being a key component of the extracellular matrix which can promote chondrogenesis [56]. Cells were next considered suitable for further stimulation when able to regenerate from approximately 25% to almost 100% confluency within four days on the same-sized dish. Including all stages of chondrocyte adaptation to the in vitro conditions, the start of the main experiments began with the cultivation of 400,000 cells of the 3rd passage per Petri dish. Chondrocytes of the 3rd passage were subjected to epigenetic stimulation with 5-AZA-dc (Merck, Darmstadt, Germany) (group I), TSA (Merck, Darmstadt, Germany) (group IV), or a combination of both agents (5-AZA-dc+TSA) (group II). The control group included cells exclusively stimulated with DMSO (Merck, Darmstadt, Germany) (group III). The 5-AZA-dc concentration of 25 μg per 1 mL of the culture medium and the TSA concentration of 0.25 μg/mL were used as nontoxic doses in the aforementioned groups. In every experimental setting, equal amounts of DMSO were used as a solute carrier and as a negative control stimulant. Cells were cultivated for 9 days until nucleic acid isolation.

4.3. Preparation of RNA and 3′ RNA-seq Libraries, and Next-Generation Sequencing

The cell lines were the sources of RNA preparation, which was performed using an AllPrep DNA/RNA Mini Kit (Qiagen, Hilden, Germany). RNA was obtained using on average 1 million cells and additional DNase treatment. The quality of RNA samples was checked on the TapeStation system (Agilent Technologies, Inc., Santa Clara, CA, USA). The RIN values of the RNA samples were above 9.0. A colorimetric measurement using a Qubit 2.0 assay (Thermofisher Scientific, Waltham, MA, USA) was implemented to calculate the recommended amount of RNA sample to be normalized for library production using the QuantSeq 3 mRNA-seq Library Prep Kit (FWD) for Illumina (Lexogen GmbH, Vienna, Austria). The protocol of library preparation comprised first-strand cDNA synthesis with oligo(dT) priming, RNA removal, second-strand synthesis by random priming, and library enrichment by PCR using the manufacturer's recommendations, including purification steps. The quality of the produced 3′ mRNA-seq libraries was evaluated using a TapeStation system (Agilent Technologies, Inc., Santa Clara, CA, USA). The mean fragment size of the obtained libraries was 257 bp (libraries of 235 to 309 bp). Sixteen 3′ mRNA-seq libraries were pooled for the total molarity of 10 nM and were submitted for NGS comprising 50 cycles of single-read sequencing on the HiSeq Illumina platform.

4.4. Trimming, Filtering, Quantification, and Mapping of Demultiplexed NGS Reads, and Differential Analysis

Firstly, raw reads were checked for quality purposes with FastQC software (Babraham Bioinformatics, Boston, MA, USA). Then, reads were filtered to remove short ones (minimal read length set to 36) and those of low quality (Phred quality under 20). Adapter sequences were also removed (Flexbar software) [57]. After the filtration procedure, mapping to the EquCab 3.0 genome (GCA_002863925.1) was utilized with the use of Tophat2 software on default settings [58]. The successfully mapped reads were then counted in the ensemble annotation file (gtf file version 101) with the use of htseq-count software [59].

Differentially expressed genes (DEGs) were estimated using DESeq2 software [60] using default parameters. Then, genes with p-adjusted < 0.05 (Benjamini–Hochberg p-value adjustment) and fold change ≥ 1 were regarded as differentially expressed and used for further analysis.

4.5. DEGs' Functional Annotation in KEGG Pathways

In order to retrieve the biological context of the stimulatory effects of the epigenetic agents, the DEGs between biological groups were the subject of overrepresentation tests in pathways of Kyoto Encyclopedia of Genes and Genomes (KEGG) using DAVID functional annotation tools [61]. Venn diagrams [62] and heat maps [63] were produced in order to show the magnitude of differential expression for each group of genes.

4.6. Real-Time PCR

First, 200 ng of total RNA was reverse-transcribed using a High-Capacity cDNA Reverse Transcription Kit (Thermofisher Scientific, Waltham, MA, USA). RT-PCR primers were designed for regions spanning at least one intron or covering an exon junction using Primer-BLAST (Table S5). Real-time PCR was performed in triplicate for each cDNA sample with a total volume of 10 μL for each sample using Sensitive RT HS-PCR Mix EvaGreen (A&A Biotechnology, Gdynia, Poland). It was run for 45 cycles with the annealing Ta of 60 °C in a QuantStudio 7 Flex System (Thermofisher Scientific, Waltham, MA, USA). Quantification of mRNA levels was performed using the comparative ΔΔCT method [64]. The relative mRNA abundances of *RPLP0* and *SDHA* genes were applied as endogenous controls. Outliers were filtered out using Grubb's tests. The normality of the distribution was tested using the Shapiro–Wilk test, and the differences between four groups of cells were calculated as RQ values on the basis of Mann–Whitney U tests. Violin plots generated with the help of Orange data mining tools [63] were used to show the differences in fold change.

5. Conclusions and Future Goals

Although TSA-mediated epigenomic modulation of the ex vivo expanded horse chondrocyte cell lines has been mechanistically proven to bring about the diminishment in the expression of a broad spectrum of genes related to chondrogenic differentiation, comprehensively identifying genomic and epigenomic signatures in in vitro cultured equine chondrocytes that have been epigenetically transformed by exposure to TSA and/or 5-AZA-dc might still be indispensable to provide genetically and epigenetically reprogrammable/dedifferentiable cell lines of adult cartilage-derived somatic cells intended for future goals.

The latter is directed at ex situ study to protect a completely new source of epigenetically modified nuclear donor cells (NDCs) for the purposes of generating cloned horse embryos, conceptuses, and offspring by somatic cell nuclear transfer (SCNT).

To the best of our knowledge, the conceptualization of recognizing epigenetic plasticity and reprogrammability of TSA- and/or 5-AZA-dc-modulated adult chondrocytes in equine SCNT-generated embryos has been developed for the first time. This entirely novel approach might turn out to be a research model reliable and feasible for SCNT-mediated production of monogenetic and monosexual specimens not only in horses but also in other mammalian species.

In summary, determining the suitability of the above-indicated research model seems to be an excellent solution inevitable in regenerative medicine and reconstructive surgery of the equine chondroskeletal system.

Conflicts of Interest: The authors declare no conflict of interest. The funders had no role in the design of the study; in the collection, analyses, or interpretation of data; in the writing of the manuscript; or in the decision to publish the results.

References

1. Ortved, K.F.; Nixon, A.J. Cell-based cartilage repair strategies in the horse. *Vet. J.* **2016**, *208*, 1–12. [CrossRef] [PubMed]
2. He, Y.; Lipa, K.E.; Alexander, P.G.; Clark, K.L.; Lin, H. Potential Methods of Targeting Cellular Aging Hallmarks to Reverse Osteoarthritic Phenotype of Chondrocytes. *Biology* **2022**, *11*, 996. [CrossRef] [PubMed]
3. Ulivi, V.; Giannoni, P.; Gentili, C.; Cancedda, R.; Descalzi, F. p38/NF-kB-dependent expression of COX-2 during differentiation and inflammatory response of chondrocytes. *J. Cell. Biochem.* **2008**, *104*, 1393–1406. [CrossRef]
4. Buhrmann, C.; Popper, B.; Aggarwal, B.B.; Shakibaei, M. Resveratrol downregulates inflammatory pathway activated by lymphotoxin α (TNF-β) in articular chondrocytes: Comparison with TNF-α. *PLoS ONE* **2017**, *12*, e0186993. [CrossRef] [PubMed]
5. Buhrmann, C.; Brockmueller, A.; Mueller, A.L.; Shayan, P.; Shakibaei, M. Curcumin Attenuates Environment-Derived Osteoarthritis by Sox9/NF-kB Signaling Axis. *Int. J. Mol. Sci.* **2021**, *22*, 7645. [CrossRef] [PubMed]
6. Hata, K. Epigenetic regulation of chondrocyte differentiation. *Jpn. Dent. Sci. Rev.* **2015**, *51*, 105–113. [CrossRef]
7. Michalowsky, L.A.; Jones, P.A. Differential nuclear protein binding to 5-azacytosine-containing DNA as a potential mechanism for 5-aza-2′-deoxycytidine resistance. *Mol. Cell Biol.* **1987**, *7*, 3076–3083.
8. Vanhaecke, T.; Papeleu, P.; Elaut, G.; Rogiers, V. Trichostatin A-like hydroxamate histone deacetylase inhibitors as therapeutic agents: Toxicological point of view. *Curr. Med. Chem.* **2004**, *11*, 1629–1643. [CrossRef]
9. Drummond, D.C.; Noble, C.O.; Kirpotin, D.B.; Guo, Z.; Scott, G.K.; Benz, C.C. Clinical development of histone deacetylase inhibitors as anticancer agents. *Annu. Rev. Pharmacol. Toxicol.* **2005**, *45*, 495–528. [CrossRef]
10. Vigushin, D.M.; Ali, S.; Pace, P.E.; Mirsaidi, N.; Ito, K.; Adcock, I.; Coombes, R.C. Trichostatin A is a histone deacetylase inhibitor with potent antitumor activity against breast cancer in vivo. *Clin. Cancer Res.* **2001**, *7*, 971–976.
11. Haq, S.H. 5-Aza-2′-deoxycytidine acts as a modulator of chondrocyte hypertrophy and maturation in chick caudal region chondrocytes in culture. *Anat. Cell Biol.* **2016**, *49*, 107–115. [CrossRef] [PubMed]
12. Kadler, S.; Vural, Ö.; Rosowski, J.; Reiners-Schramm, L.; Lauster, R.; Rosowski, M. Effects of 5-aza-2′-deoxycytidine on primary human chondrocytes from osteoarthritic patients. *PLoS ONE* **2020**, *15*, e0234641. [CrossRef]
13. Young, D.A.; Lakey, R.L.; Pennington, C.J.; Jones, D.; Kevorkian, L.; Edwards, D.R.; Cawston, T.E.; Clark, I.M. Histone deacetylase inhibitors modulate metalloproteinase gene expression in chondrocytes and block cartilage resorption. *Arthritis Res. Ther.* **2005**, *7*, 503–512. [CrossRef] [PubMed]
14. Leoni, F.; Zaliani, A.; Bertolini, G.; Porro, G.; Pagani, P.; Pozzi, P.; Donà, G.; Fossati, G.; Sozzani, S.; Azam, T.; et al. The antitumor histone deacetylase inhibitor suberoylanilide hydroxamic acid exhibits antiinflammatory properties via suppression of cytokines. *Proc. Natl. Acad. Sci. USA* **2002**, *99*, 2995–3000. [CrossRef] [PubMed]
15. Lee, J.; Im, G.I. Effects of Trichostatin A on the Chondrogenesis from Human Mesenchymal Stem Cells. *Tissue Eng. Regen. Med.* **2017**, *14*, 403–410. [CrossRef]
16. Wan, C.; Zhang, F.; Yao, H.; Li, H.; Tuan, R.S. Histone Modifications and Chondrocyte Fate: Regulation and Therapeutic Implications. *Front. Cell Dev. Biol.* **2021**, *9*, 626708. [CrossRef] [PubMed]
17. Miyagawa, J.; Muguruma, M.; Aoto, H.; Suetake, I.; Nakamura, M.; Tajima, S. Isolation of the novel cDNA of a gene of which expression is induced by a demethylating stimulus. *Gene* **1999**, *240*, 289–295. [CrossRef]
18. Goldring, M.B. Human chondrocyte cultures as models of cartilage-specific gene regulation. *Methods Mol. Med.* **2005**, *107*, 69–95. [PubMed]
19. Liu, C.F.; Samsa, W.E.; Zhou, G.; Lefebvre, V. Transcriptional control of chondrocyte specification and differentiation. *Semin. Cell Dev. Biol.* **2017**, *62*, 34–49. [CrossRef] [PubMed]
20. Loeser, R.F.; Im, H.J.; Richardson, B.; Lu, Q.; Chubinskaya, S. Methylation of the OP-1 promoter: Potential role in the age-related decline in OP-1 expression in cartilage. *Osteoarthr. Cartil.* **2009**, *17*, 513–517. [CrossRef]
21. Rao, J.; Bhattacharya, D.; Banerjee, B.; Sarin, A.; Shivashankar, G.V. Trichostatin-A induces differential changes in histone protein dynamics and expression in HeLa cells. *Biochem. Biophys. Res. Commun.* **2007**, *363*, 263–268. [CrossRef] [PubMed]
22. Buhrmann, C.; Busch, F.; Shayan, P.; Shakibaei, M. Sirtuin-1 (SIRT1) is required for promoting chondrogenic differentiation of mesenchymal stem cells. *J. Biol. Chem.* **2014**, *289*, 22048–22062. [CrossRef] [PubMed]
23. Korogi, W.; Yoshizawa, T.; Karim, M.F.; Tanoue, H.; Yugami, M.; Sobuz, S.U.; Hinoi, E.; Sato, Y.; Oike, Y.; Mizuta, H.; et al. SIRT7 is an important regulator of cartilage homeostasis and osteoarthritis development. *Biochem. Biophys. Res. Commun.* **2018**, *496*, 891–897. [CrossRef] [PubMed]
24. Li, L.; Chen, B.F.; Chan, W.Y. An epigenetic regulator: Methyl-CpG-binding domain protein 1 (MBD1). *Int. J. Mol. Sci.* **2015**, *16*, 5125–5140. [CrossRef] [PubMed]
25. Liu, C.F.; Lefebvre, V. The transcription factors SOX9 and SOX5/SOX6 cooperate genome-wide through super-enhancers to drive chondrogenesis. *Nucleic Acids Res.* **2015**, *43*, 8183–8203. [CrossRef]
26. Imagawa, K.; de Andrés, M.C.; Hashimoto, K.; Itoi, E.; Otero, M.; Roach, H.I.; Goldring, M.B.; Oreffo, R.O. Association of reduced type IX collagen gene expression in human osteoarthritic chondrocytes with epigenetic silencing by DNA hypermethylation. *Arthritis Rheumatol.* **2014**, *66*, 3040–3051. [CrossRef]

27. Gao, Y.; Liu, S.; Huang, J.; Guo, W.; Chen, J.; Zhang, L.; Zhao, B.; Peng, J.; Wang, A.; Wang, Y.; et al. The ECM-cell interaction of cartilage extracellular matrix on chondrocytes. *Biomed. Res. Int.* **2014**, *2014*, 648459. [CrossRef]

28. Shin, H.; Lee, M.N.; Choung, J.S.; Kim, S.; Choi, B.H.; Noh, M.; Shin, J.H. Focal Adhesion Assembly Induces Phenotypic Changes and Dedifferentiation in Chondrocytes. *J. Cell Physiol.* **2016**, *231*, 1822–1831. [CrossRef]

29. Schipani, E.; Ryan, H.E.; Didrickson, S.; Kobayashi, T.; Knight, M.; Johnson, R.S. Hypoxia in cartilage: HIF-1alpha is essential for chondrocyte growth arrest and survival. *Genes Dev.* **2001**, *15*, 2865–2876. [CrossRef]

30. Kita, K.; Kimura, T.; Nakamura, N.; Yoshikawa, H.; Nakano, T. PI3K/Akt signaling as a key regulatory pathway for chondrocyte terminal differentiation. *Genes Cells.* **2008**, *13*, 839–850. [CrossRef]

31. Tekari, A.; Luginbuehl, R.; Hofstetter, W.; Egli, R.J. Transforming growth factor beta signaling is essential for the autonomous formation of cartilage-like tissue by expanded chondrocytes. *PLoS ONE* **2015**, *10*, e0120857. [CrossRef] [PubMed]

32. Rokutanda, S.; Fujita, T.; Kanatani, N.; Yoshida, C.A.; Komori, H.; Liu, W.; Mizuno, A.; Komori, T. Akt regulates skeletal development through GSK3, mTOR, and FoxOs. *Dev. Biol.* **2009**, *328*, 78–93. [CrossRef] [PubMed]

33. Stanton, L.A.; Underhill, T.M.; Beier, F. MAP kinases in chondrocyte differentiation. *Dev. Biol.* **2003**, *263*, 165–175. [CrossRef]

34. Hollander, J.M.; Zeng, L. The Emerging Role of Glucose Metabolism in Cartilage Development. *Curr. Osteoporos. Rep.* **2019**, *17*, 59–69. [CrossRef] [PubMed]

35. Zhu, F.; Wang, P.; Lee, N.H.; Goldring, M.B.; Konstantopoulos, K. Prolonged application of high fluid shear to chondrocytes recapitulates gene expression profiles associated with osteoarthritis. *PLoS ONE* **2010**, *5*, e15174. [CrossRef]

36. Wang, L.; Shao, Y.Y.; Ballock, R.T. Thyroid hormone-mediated growth and differentiation of growth plate chondrocytes involves IGF-1 modulation of beta-catenin signaling. *J. Bone Min. Res.* **2010**, *25*, 1138–1146. [CrossRef]

37. Tseng, C.C.; Chen, Y.J.; Chang, W.A.; Tsai, W.C.; Ou, T.T.; Wu, C.C.; Sung, W.Y.; Yen, J.H.; Kuo, P.L. Dual Role of Chondrocytes in Rheumatoid Arthritis: The Chicken and the Egg. *Int. J. Mol. Sci.* **2020**, *21*, 1071. [CrossRef]

38. Kelwick, R.; Desanlis, I.; Wheeler, G.N.; Edwards, D.R. The ADAMTS (A Disintegrin and Metalloproteinase with Thrombospondin motifs) family. *Genome Biol.* **2015**, *16*, 113. [CrossRef]

39. Legeai-Mallet, L.; Benoist-Lasselin, C.; Munnich, A.; Bonaventure, J. Overexpression of FGFR3, Stat1, Stat5 and p21Cip1 correlates with phenotypic severity and defective chondrocyte differentiation in FGFR3-related chondrodysplasias. *Bone* **2004**, *34*, 26–36. [CrossRef]

40. Caron, M.M.; Emans, P.J.; Coolsen, M.M.; Voss, L.; Surtel, D.A.; Cremers, A.; van Rhijn, L.W.; Welting, T.J. Redifferentiation of dedifferentiated human articular chondrocytes: Comparison of 2D and 3D cultures. *Osteoarthr. Cartil.* **2012**, *20*, 1170–1178. [CrossRef]

41. Edwards, R.B.; Lu, Y.; Cole, B.J.; Muir, P.; Markel, M.D. Comparison of radiofrequency treatment and mechanical debride-ment of fibrillated cartilage in an equine model. *Vet. Comp. Orthop. Traumatol.* **2008**, *21*, 41–48. [CrossRef] [PubMed]

42. Edwards, R.B., 3rd; Lu, Y.; Uthamanthil, R.K.; Bogdanske, J.J.; Muir, P.; Athanasiou, K.A.; Markel, M.D. Comparison of mechanical debridement and radiofrequency energy for chondroplasty in an in vivo equine model of partial thickness carti-lage injury. *Osteoarthr. Cartil.* **2007**, *15*, 169–178. [CrossRef] [PubMed]

43. Shakya, B.R.; Tiulpin, A.; Saarakkala, S.; Turunen, S.; Thevenot, J. Detection of experimental cartilage damage with acoustic. *Equine Vet. J.* **2020**, *52*, 152–157. [CrossRef] [PubMed]

44. Uthamanthil, R.K.; Edwards, R.B.; Lu, Y.; Manley, P.A.; Athanasiou, K.A.; Markel, M.D. In vivo study on the short-term effect of radiofrequency energy on chondromalacic patellar cartilage and its correlation with calcified cartilage pathology in an equine model. *J. Orthop. Res.* **2006**, *24*, 716–724. [CrossRef]

45. Ryan, A.; Bertone, A.L.; Kaeding, C.C.; Backstrom, K.C.; Weisbrode, S.E. The effects of radiofrequency energy treatment on chondrocytes and matrix of fibrillated articular cartilage. *Am. J. Sports Med.* **2003**, *31*, 386–391. [CrossRef]

46. Bodó, G.; Hangody, L.; Szabó, Z.; Peham, C.; Schinzel, M.; Girtler, D.; Sótonyi, P. Arthroscopic autologous osteochondral mosaicplasty for the treatment of subchondral cystic lesion in the medial femoral condyle in a horse. *Acta Vet. Hung.* **2000**, *48*, 343–354.

47. Bodo, G.; Hangody, L.; Modis, L.; Hurtig, M. Autologous osteochondral grafting (mosaic arthroplasty) for treatment of subchondral cystic lesions in the equine stifle and fetlock joints. *Vet. Surg.* **2004**, *33*, 588–596. [CrossRef]

48. Sparks, H.D.; Nixon, A.J.; Bogenrief, D.S. Reattachment of the articular cartilage component of type 1 subchondral cystic lesions of the medial femoral condyle with polydioxanone pins in 3 horses. *J. Am. Vet. Med. Assoc.* **2011**, *238*, 636–640. [CrossRef]

49. Smith, M.A.; Walmsley, J.P.; Phillips, T.J.; Pinchbeck, G.L.; Booth, T.M.; Greet, T.R.; Richardson, D.W.; Ross, M.W.; Schramme, M.C.; Singer, E.R.; et al. Effect of age at presentation on outcome following arthroscopic debridement of sub-chondral cystic lesions of the medial femoral condyle: 85 horses (1993—2003). *Equine Vet. J.* **2005**, *37*, 175–180. [CrossRef]

50. Frazer, L.L.; Santschi, E.M.; Fischer, K.J. The impact of subchondral bone cysts on local bone stresses in the medial femoral condyle of the equine stifle joint. *Med. Eng. Phys.* **2017**, *48*, 158–167. [CrossRef]

51. Russell, J.W.; Hall, M.S.; Kelly, G.M. Osteochondroma on the cranial aspect of the distal radial metaphysis causing teno-synovitis of the extensor carpi radialis tendon sheath in a horse. *Aust. Vet. J.* **2017**, *95*, 46–48. [CrossRef] [PubMed]

52. Olstad, K.; Østevik, L.; Carlson, C.S.; Ekman, S. Osteochondrosis Can Lead to Formation of Pseudocysts and True Cysts in the Subchondral Bone of Horses. *Vet. Pathol.* **2015**, *52*, 862–872. [CrossRef] [PubMed]

53. Secombe, C.J.; Anderson, B.H. Diagnosis and treatment of an osteochondroma of the distal tibia in a 3-year-old horse. *Aust. Vet. J.* **2000**, *78*, 16–18. [CrossRef]

54. Ząbek, T.; Witarski, W.; Semik-Gurgul, E.; Szmatoła, T.; Kowalska, K.; Bugno-Poniewierska, M. Chondrogenic expression and DNA methylation patterns in prolonged passages of chondrocyte cell lines of the horse. *Gene* **2019**, *707*, 58–64. [CrossRef]

55. Miao, Z.; Lu, Z.; Wu, H.; Liu, H.; Li, M.; Lei, D.; Zheng, L.; Zhao, J. Collagen, agarose, alginate, and Matrigel hydrogels as cell substrates for culture of chondrocytes in vitro: A comparative study. *J. Cell. Biochem.* **2018**, *119*, 7924–7933. [CrossRef] [PubMed]

56. Sun, Y.; Wang, T.L.; Toh, W.S.; Pei, M. The role of laminins in cartilaginous tissues: From development to regeneration. *Eur. Cell Mater.* **2017**, *34*, 40–54. [CrossRef]

57. Dodt, M.; Roehr, J.T.; Ahmed, R.; Dieterich, C. Flexbar—Flexible barcode and adapter processing for next-generation sequencing platforms. *Biology* **2012**, *1*, 895–905. [CrossRef]

58. Kim, D.; Pertea, G.; Trapnell, C.; Pimentel, H.; Kelley, R.; Salzberg, S.L. TopHat2: Accurate alignment of transcriptomes in the presence of insertions, deletions and gene fusions. *Genome Biol.* **2013**, *14*, R36. [CrossRef]

59. Putri, G.H.; Anders, S.; Pyl, P.T.; Pimanda, J.E.; Zanini, F. Analysing high-throughput sequencing data in Python with HTSeq 2.0. *Bioinformatics* **2022**, *38*, 2943–2945. [CrossRef]

60. Love, M.I.; Huber, W.; Anders, S. Moderated estimation of fold change and dispersion for RNA-seq data with DESeq2. *Genome Biol.* **2014**, *15*, 550. [CrossRef]

61. Dennis, G., Jr.; Sherman, B.T.; Hosack, D.A.; Yang, J.; Gao, W.; Lane, H.C.; Lempicki, R.A. DAVID: Database for Annotation, Visualization, and Integrated Discovery. *Genome. Biol.* **2003**, *4*, P3. [CrossRef] [PubMed]

62. Oliveros, J.; Venny, C. An Interactive Tool for Comparing Lists with Venn's Diagrams. 2007–2015. Available online: https://bioinfogp.cnb.csic.es/tools/venny/index.html (accessed on 8 August 2022).

63. Demsar, J.; Curk, T.; Erjavec, A.; Gorup, C.; Hocevar, T.; Milutinovic, M.; Mozina, M.; Polajnar, M.; Toplak, M.; Staric, A.; et al. Orange: Data Mining Toolbox in Python. *J. Mach. Learn. Res.* **2013**, *14*, 2349–2353.

64. Pfaffl, M.W. A new mathematical model for relative quantification in real-time RT-PCR. *Nucleic Acids Res.* **2001**, *29*, e45. [CrossRef] [PubMed]

MDPI